ARCHIVES

Investigation of Downward Facing Critical Heat Flux with Water-Based Nanofluids for In-Vessel Retention Applications

by

Gregory Lee DeWitt

B.S., Nuclear Engineering, University of California, Los Angeles, 1980
S.M., Nuclear Engineering, Massachusetts Institute of Technology, 1981
M.B.A., Finance, Boston University, 1987

SUBMITTED TO THE DEPARTMENT OF NUCLEAR SCIENCE AND ENGINEERING IN PARTIAL FULFILLMENT OF THE REQUIREMENTS FOR THE DEGREE OF

DOCTOR OF PHILOSOPHY IN NUCLEAR SCIENCE AND ENGINEERING
AT THE
MASSACHUSETTS INSTITUTE OF TECHNOLOGY

SEPTEMBER 2011

Signature of Author: _____
Department of Nuclear Science and Engineering
August 31, 2011

Certified by: _____
Jacopo Buongiorno – Thesis Supervisor
Associate Professor of Nuclear Science and Engineering

Certified by: _____
Thomas McKrell – Thesis Co-Supervisor
Research Scientist, Nuclear Science and Engineering

Certified by: _____
Lin-wen Hu – Thesis Co-Supervisor
Associate Director – MIT Nuclear Reactor Laboratory

Certified by: _____
Peter Griffith – Thesis Reader
Professor Emeritus, Mechanical Engineering

Accepted by: _____
Mujid S. Kazimi
TEPCO Professor of Nuclear Science and Engineering
Chair, Department Committee for Graduate Students

Investigation of Downward Facing Critical Heat Flux with Water-Based Nanofluids for In-Vessel Retention Applications

By

Gregory Lee DeWitt

Submitted to the Department of Nuclear Science and Engineering on August 31, 2011 in partial fulfillment of the requirements for the degree of Doctor of Philosophy in Nuclear Science and Engineering at the Massachusetts Institute of Technology

ABSTRACT

In-Vessel Retention ("IVR") is a severe accident management strategy that is power limiting to the Westinghouse AP1000 due to critical heat flux ("CHF") at the outer surface of the reactor vessel. Increasing the CHF level by altering the cooling fluid would increase the safety margin of current design power or allow for higher power. The modification to current licensed design to implement a new cooling fluid would not require significant changes to the containment and associated systems.

Previous research at MIT and other institutions has demonstrated that CHF of water on a heated metal surface can be increased from 30% to 200% with the introduction of nanoparticles. Alumina has shown the best CHF enhancement of the nanoparticles tested to date at MIT. Alumina nanoparticles and water based nanofluids have also shown long term stability in solution, which is important for the long time frame (hours to days) of IVR.

To measure the CHF of geometry and conditions relevant to IVR for the AP1000, a two-phase flow loop has been designed and built. The test section designed to have hydrodynamic similarity to the AP1000 and allows for all angles that represent the bottom surface of the reactor vessel. Research completed herein measured CHF for varied conditions of orientation angle, pressure, mass flux, fluid type, and surface material. Results for stainless steel with water based alumina 0.001% by volume nanofluid indicate an average 70% CHF enhancement with a range of 17% to 108% for geometry and conditions expected for IVR. Experiments also indicate that only about thirty minutes of boiling time is needed to obtain CHF enhancement.

Implementation could involve storage tanks of high concentration nanofluids installed in containment. Once the IVR strategy is initiated with flooding of the vessel cavity with water from the In-containment Refueling Water Storage Tank ("IRWST"), the nanofluids would be released to mix as the natural circulation flow sets up along the gap between the vessel and the insulation mounted to the concrete wall in the vessel cavity. Boiling then plates nanoparticles onto the surface enhancing CHF.

Thesis Supervisor:	Jacopo Buongiorno, PhD
Title:	Associate Professor of Nuclear Science and Engineering, Carl R. Soderberg Professor of Power Engineering
Thesis Co-Supervisor:	Thomas McKrell, PhD
Title:	Research Scientist, Center for Advanced Nuclear Engineering Systems
Thesis Co-Supervisor:	Lin-wen Hu, PhD, PE
Title:	Principal Research Scientist, Associate Director, MIT Nuclear Reactor Laboratory
Thesis Reader:	Peter Griffith, PhD
Title:	Professor Emeritus, Mechanical Engineering

ACKNOWLEDGEMENT

Many people from faculty, staff, students, friends and family have had direct positive influence on my efforts to complete my doctoral studies. I fully recognize the benefit my life has gained from their being part, as I pursued a major life ambition.

I would like to thank Professor Jacopo Buongiorno for taking me on as one of his nanofluid team members and supporting my efforts toward completion of my doctoral work. I found the experimental research stimulating and rewarding.

Thanks to Dr. Tom McKrell for your guidance and help in the green lab with all aspects of my experimental thesis. I learned a great deal working with you in the lab especially in the areas of material and electrical engineering.

Thanks to Dr. Lin-wen Hu for your support and encouragement in several areas including professional development.

Thanks to Professor Ballenger for helping me obtain a difficult to find piece of SA-508 to support my experimental matrix.

Professor Peter Griffith thanks for your efforts and advice as reader for my thesis and support for my decision to return to MIT for my PhD.

Professor Michael Driscoll thanks for being my thesis committee chairman.

Thanks to Clare Egan, Heather Barry, Linda Arduino, Dorian Cohen and all of the NSE staff for helping my experience at MIT run smoothly.

Peter Brenton thanks for your logistical support that improved my student life returning to MIT.

Rachel Morton thanks for your efforts in my office and lab with all the computer hardware and software, network and printing issues that needed help.

Thanks to Dr. Hyungdae Kim for allowing me to be a part of his post doctoral research during my first year. That experience helped me in preparing for my own thesis research.

Thanks to Dr. Rae-Joon Park of KAERI for the design and fabrication of the test section used in my thesis work during your stay at MIT and co-authoring of the associated paper presented at the ANS conference in Hollywood, Florida.

Thanks to Dr. Bao Truong for being a friend and nanofluids team member. You made my re-acclamation to student life after a long hiatus easier.

Thanks to Dr. Sung Joong Kim for sharing your experience in building a nanofluid flow loop that help me in designing my own.

Thanks to Eric Forrest for being a resource and fellow lab type who could appreciate the unexpected challenges that experimentation often involves.

Thanks to Bren Phillips for his expertise in computer software issues and help in utilizing the MIT SEM.

Thanks to Koroush Shirvan for help with RELAP access and use and an occasional talk of college football, which we both follow intently.

Special thanks to Rosie Sugrue for providing invaluable support under the MIT UROP program. I hope the connection of academic knowledge to physical reality plus the practical struggles of experimentation were valuable to you.

Thanks to classmates and fellow lab types that I had the pleasure in knowing including: Bo Feng, Dustin Langewisch, Vivek Sharma, Harry O'Hanley, Tom Conboy, Paulo Ferroni, Stefano Passerini, Tim Lucas, Stephanie Kempf, Matt Denman and any I may have inadvertently missed.

Many of my long-time friends provided encouragement to my goal of getting my PhD. When things where tough their support kept me going. Thanks Bruce & Denise Hagemeier, Chris & Amy Wilson, Peter & Debbie Avtgis, Dick & Mary Fagan, Jay & Jeanette Baldinelli, John Barry, Kevin Wenzel, Karl Weller, Brian Chaisson, Terry Murray, Bob Garrow, Lee Blaylock, and Don & Joanne Packer.

My family had to adjust quite a lot to dad going back to school. Special thanks to my wife Ann-Marie for the three plus year interruption in the normal course of our 25 years of marriage. Too many long days and nights at the institute dragged on, but our relationship held strong with her understanding and commitment. Mike and Kristen thanks for relating to dad's efforts while you two are undertaking your own academic challenges. My brother Jeff thanks for your continuing encouragement.

Thanks to Doug Spreng for your financial sponsorship of my research.

Thanks to Eric Caldwell of Northeast Water Services for providing a reduced cost Mettler Toledo/Thorton DO probe that allowed for quantification of degassing results.

Table of Contents

List of Figures

List of Tables

Nomenclature

Symbols

A_f	-	Flow area	[m^2]
A_h	-	Heated area	[m^2]
α	-	Void fraction	dimensionless
α_{th}	-	Thermal diffusivity	[m^2/s]
β	-	Volumetric flow rate	[m^3/s]
β_{exp}	-	Thermal expansion	[$(\Delta V/V)$ / °C]
Bo	-	Bond number	dimensionless
C_p	-	Heat capacity at constant pressure	[kJ/kg-C]
D	-	Diameter	[m]
D_e	-	Hydraulic diameter	[m]
δ	-	Depth or thickness	[m]
E	-	Young's modulus	[Pa]
f	-	Friction factor	dimensionless
f_{el}	-	frequency	[Hertz]
Fr	-	Froude number	dimensionless
g_c	-	Gravitational acceleration	[m/s^2]
G	-	Mass Flux	[kg/m^2-s]
H	-	Heat transfer coefficient	[W/m^2-°C]
h_{fg}	-	Heat of vaporization	[J/kg-°C]
h_f	-	Enthalpy of saturated liquid	[J/kg]
h_g	-	Enthalpy of saturated vapor	[J/kg]
h_l	-	Enthalpy of liquid	[J/kg]
h_v	-	Enthalpy of vapor	[J/kg]
h_{in}	-	Enthalpy at entrance	[J/kg]
h_{out}	-	Enthalpy at exit	[J/kg]
I	-	Current	[A]
k	-	Thermal conductivity	[W/m- °C]
K	-	Loss coefficient	dimensionless
L	-	Length	[m]
$\dot{m}$	-	Mass Flow Rate	[kg/s]
Mo	-	Morton number	dimensionless
P	-	Joule Power	[W]
P_h	-	Heated perimeter	[m]
P_{rated}	-	Rated thermal power	[MW]
P_w	-	Wetted perimeter	[m]
π	-	Pi	
π_k	-	Number of Buckingham Pi fundamental quantities	
π_n	-	Number of Buckingham Pi physical variables	
π_p	-	Number of Buckingham Pi independent dimensionless variables	
Pr	-	Pressure	[Pa]
Q	-	Thermal power	[W]

Q_{decay}	-	Decay power	[W]
q"	-	Heat flux	[W/m^2]
$q"_{CHF}$	-	Critical heat flux	[MW/m^2]
ρ	-	Density	[kg/ m^3]
ρ_{el}	-	Electrical resistivity	[Ω-m]
S	-	Slip ratio	dimensionless
t	-	Time	[s]
T_{op}	-	Time of operation	[s]
Ω	-	Electrical resistance	[Ω]
φ	-	angle in x,y plane	[degrees]
Φ_{np}	-	Nanoparticle volume fraction	dimensionless
Φ	-	Two-phase multiplier	dimensionless
θ	-	Angle in x,z plane	[degrees]
μ	-	Viscosity	[Pa-s]
σ	-	Surface tension	[N-m]
σ_{std}	-	Standard deviation	
σ_{Boltz}	-	Boltzmann constant-5.67 x 10^{-8}	[W/m^2-K^4]
χ_e	-	Equilibrium quality	dimensionless
v	-	Velocity	[m/s]
V	-	Voltage	[V]
V_{di}	-	Volume of DI water	[l]
V_{nf}	-	Volume of concentrated nanofluid	[l]
We	-	Weber number	dimensionless

Subscripts

cw	-	chilled water system
di	-	de-ionized water
e	-	equilibrium
el	-	electrical
f	-	Saturated fluid
g	-	Saturated vapor
h	-	heated
hw	-	hot water system
l	-	liquid
nf	-	nanofluids
np	-	nanoparticle
ss	-	stainless steel
ps	-	power supply
sys	-	system
v	-	vapor
w	-	wetted

Superscripts

o	-	degrees
‘	-	feet
“	-	inches

Acronyms

ARI	-	All Rods In
BFSL	-	Best Fit Straight Line
CHF	-	Critical Heat Flux
CWFM-		Chilled Water Flow Meter
DAQ	-	Data Acquisition
DAS	-	Data Acquisition System
DI	-	De-Ionized
DNB	-	Departure from Nucleate Boiling
DO	-	Dissolved Oxygen
ECCS	-	Emergency Core Cooling Systems
GPM	-	Gallons Per Minute
HWFM-		Hot Water Flow Meter
IRWST-		In-containment Refueling Water Storage Tank
LPM	-	Liters Per Minute
LOCA	-	Loss of Coolant Accident
PCS	-	Primary Coolant System
PPM	-	Parts Per Million
PPB	-	Parts Per Billion
PSU	-	Pennsylvania State University
SBLB	-	Subscale Boundary Layer Boiling facility at PSU
SSR	-	Solid-State Relay
STP	-	Standard Temperature (20 ^{o}C) and Pressure (1 atmosphere)
UCSB	-	University of California, Santa Barbara

1 Introduction

In-vessel retention ("IVR") is a severe accident management strategy employed by several advanced pressurized water reactor designs including the Westinghouse AP1000 [1]. IVR anticipates the melting and relocation of core materials into the lower vessel head, given the name "corium". The objective of IVR is to contain the corium throughout the hypothetical severe accident within the reactor pressure vessel. Success of the IVR strategy requires continuous reactor pressure vessel integrity. Reactor pressure vessel integrity avoids corium, coolant, and concrete interaction issues and maintains the second line of defense for preventing radio-nuclides from reaching the environment. The first defense is the fuel cladding, which is completely lost upon corium formation. The containment is the third and final line of defense. This scenario is of primary interest to the world given the renewed emphasis on severe accidents after the events at Fukushima Daiichi Units 1, 2 and 3, where partial core melting and corium flow to the bottom of the vessel have likely occurred.

The IVR strategy involves flooding of the reactor vessel cavity between the vessel outer surface and insulation, once it is recognized that core melt and corium development is likely. In AP1000, the coolant in the vessel cavity, originally stored in the In-containment Reactor Water Storage Tank ("IRWST"), will provide natural circulation of nearly saturated water that will boil as it removes decay heat along the vessel outer surface (see Figure 1-1). The vapor generated will mix into the containment atmosphere, be condensed by the passive cooling of the containment steel shell, and then flow back down into the vessel cavity. The pressure environment will be at or near atmospheric (1 to 3 atmospheres). This method of containing a vast majority of radio-nuclides will need to be maintained for a long period of time (days to weeks) until decay heat levels provide no danger of compromising the vessel.

Several advanced light water reactor designs have adopted IVR as a part of their design basis including: Westinghouse's AP600 and AP1000, Russian VVER-440, as well as the South Korean APR1400 [2][3]. Regulatory reviews both in the United States and Europe for the Westinghouse designs have included IVR [4].

Figure 1-1: Simplified In-Vessel Retention Diagram

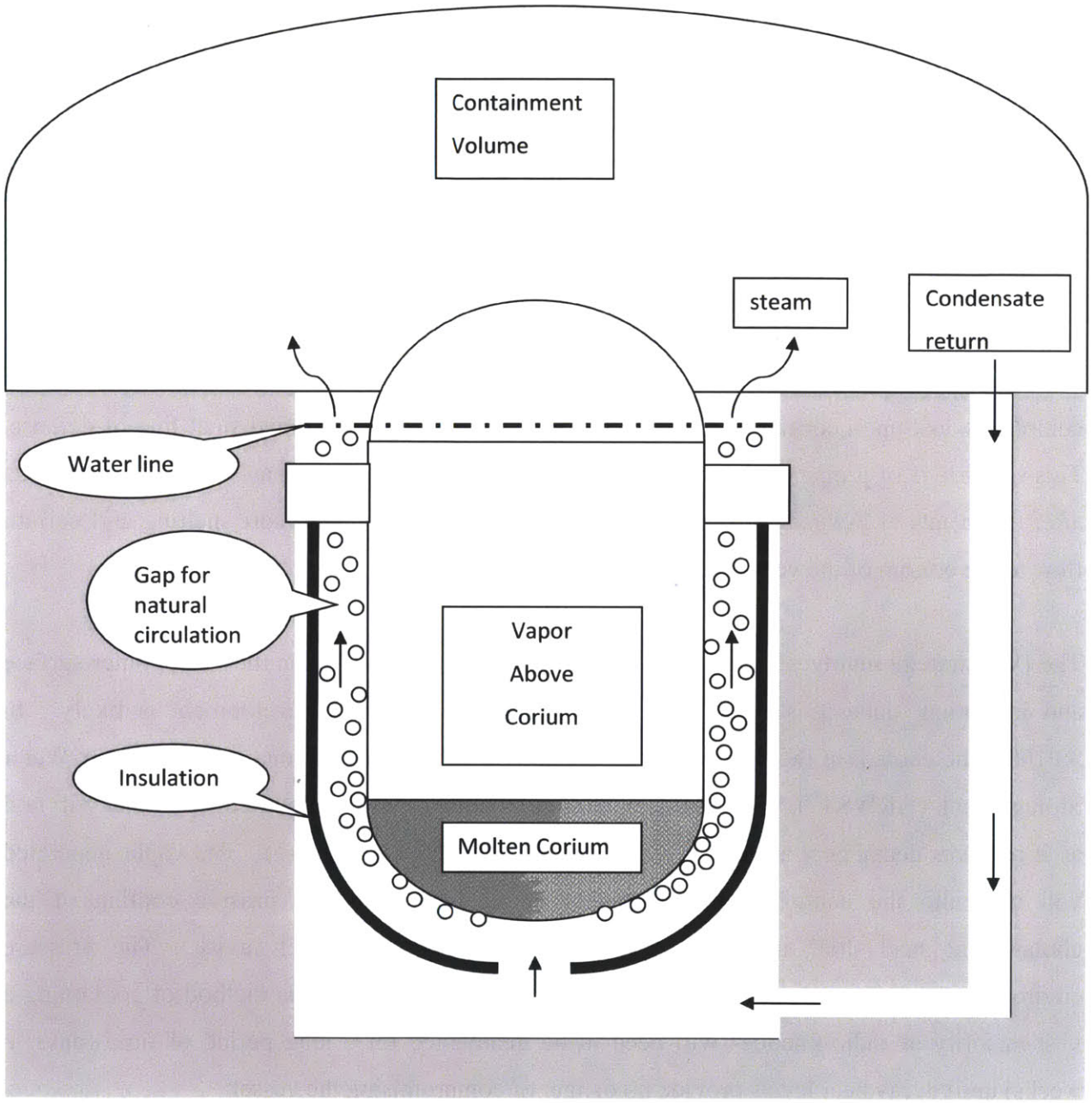

To avoid excessive temperatures, the heat transfer rate at the vessel surface needs to be sufficiently high. Since the dominant heat transfer mode at the vessel surface is flow boiling, a key design limit is then avoiding critical heat flux (CHF) along the vessel surface. CHF at any location along the vessel outer surface would result in very high temperatures to occur across the reactor pressure vessel carbon steel shell that would lower material strength and possibly allow

for creep failure of the vessel [5]. Note that though the melt temperature of carbon steel is about 1400 °C, yield strength drops significantly at temperatures above 625 °C. Pressure vessel failure would provide a migration path for highly radioactive corium materials to enter the vessel cavity and would likely induce steam explosions and concrete interactions. Uncertainties of the energetic releases of these interactions would increase risk to the primary containment [6]. Note the design limit of the primary containment for the AP1000 is about 6.1 bar gauge (60 psig).

Work previously done at MIT has investigated how utilizing nanofluids may enhance management of severe accident scenarios involving emergency core cooling systems ("ECCS") and IVR for advanced pressurized water reactors with modest modification of current design [7][8]. Chemistry and radiation effects on nanofluids have also been studied with supporting results [9]. The previous work makes the assumption that CHF enhancement measured for several nanofluids in pool and flow boiling conditions with varying geometries could be applied to IVR flow conditions and geometry [10][2]. If shown to increase CHF in the relevant conditions and geometry of downward facing with varying angle, the safety margin for the IVR strategy can be increased [11], thus opening the possibility of using the IVR approach in higher-power density reactor designs, such as the expected uprated version of the AP1000 for the Chinese market.

The experimental investigation completed herein specifically addresses geometric and flow conditions expected in IVR for the AP1000. A direct comparison is made between the CHF of water and that of nanofluids with identical flow conditions and geometry.

Results for stainless steel show a range of CHF enhancement with Alumina nanoparticles and DI water from 17% to 108% relative to DI water alone with an average of 70%.

1.1 Background

IVR strategy has been adopted by several PWR designs including: Westinghouse AP600 and AP1000, VVER-440, and South Korean APR1400 [12].

Over the past ten years a number of research efforts have demonstrated that certain nanoparticles added to water creating a nanofluid can increase CHF. CHF increases have been documented from 30% to 200% for various geometries, conditions and nanoparticle materials [13].

The surfaces analyzed to date utilizing nanofluids have involved simple geometries: spheres, plates, wires, tubes and small rods. Previous experimental conditions studied have been pool boiling or flow boiling in a vertical tube test section [14]. No work has been identified to date that investigates nanofluids on downward facing plate geometry and with conditions relevant for IVR that includes angular dependence.

Downward facing pool boiling CHF experiments have been done with water and pre-coated surfaces and have shown a strong dependence on angle [15]. Increasing angle relative to gravity lengthens bubble time at the surface. This supports vapor film development thereby lowering CHF.

Quantification of CHF enhancement with nanofluids through the range of downward facing horizontal to vertical inclinations would provide direct design criteria for the implementation of the IVR strategy. The benefits to the IVR strategy with a coolant having higher CHF include: improved safety margin and possible power up rate for design having IVR as a design limit.

1.2 Motivation

Increased CHF on the vessel surface during IVR conditions can be utilized to increase safety margin for current design power level or allow for increased power with current designs where IVR is the limiting condition [16].

Being able to quantify CHF dependence on angle, pressure and flow rate for a given working fluid can be used to identify the regions of the vessel surface most at risk. This knowledge together with an understanding of corium behavior can be coupled to better understand and

reduce the risk of vessel failure due to CHF. Additionally, design of the gap region can be optimized to maximize mass flux in the region of high corium heat flux. This and other work has shown that for conditions of interest for IVR of low pressure ($1 < Pr < 3$ atmospheres) and low quality ($-0.01 < \chi_e < 0.01$) increased mass flux increases CHF [17].

1.3 Technical Objectives

The primary objective of the work herein is to determine whether the use of nanofluids in downward facing heating and low up-flow with IVR conditions can increase CHF relative to water. The major independent variables will include: working fluid type, mass flux, and heater angle. Other variables of interest include: nanofluid concentration, pressure and surface material.

Benchmarking was accomplished by completing water-only experimental runs that range the conditions of interest [9]. Results of the water benchmarking runs are compared to IVR CHF work completed at University of California, Santa Barbara ("UCSB"), Penn State University ("PSU"), and the Sultan facility in France. These water based experiments tested ex-vessel cooling with various flow rates and low pressure on downward facing heated surfaces. Comparisons are then made between the water benchmarking and nanofluids results of analogous conditions.

A secondary objective will be to utilize the experimental results [modified CHF] to numerically model IVR with RELAP in a specified design [Westinghouse AP1000] to quantify safety margin improvement. Quantification of the results will allow for the creation of a lookup table for each working fluid. The table for each nanofluid will list CHF, mass flux, angle, and pressure. Note that quality, χ_e , is very near saturation [$-0.01 < \chi_e < +0.01$] in all IVR CHF tests performed in this thesis.

The data will also provide a basis to quantify the various independent variables influence on CHF relative to water.

2 Nanofluids

Nanofluids are liquids that have colloidal suspension of nano (10^{-9}m) scale engineered particles mixed within. The base fluids can be water, refrigerants, oils or any other. The particles are generally engineered particles with size on the size order of 20 to 200 nanometers. The base fluid used throughout the experimental matrix of this work is De-Ionized ("DI") water.

Nanotechnology has had explosive development over the past fifteen years. Today virtually any shaped structure of molecules can be assembled. Nanoparticles utilized herein were purchased from Nyacol Nano Technologies, Inc. as high concentration water based fluids. Commonly delivered concentrations are 20% by weight. These are then reduced in concentration by the addition of DI water.

Note all nanofluid concentrations described herein for the experimental matrix are by volume.

The nanofluid tested herein is alumina [Al_2O_3] with two concentrations: 0.001% and 0.01% by volume. The vendor average particle size for alumina is 20 nanometers and MIT lab DLS measurements indicate 39 nanometers [18]. Alumina was chosen because previous work at MIT has shown that this nanoparticle material has meaningful CHF enhancement and good stability in solution.

For the ultimate application of the nanofluid CHF enhancement concept with the IVR strategy the nanofluid chosen needs to have good mixing characteristics and stability in solution. Note the IVR accident time frame of interest is on the order of hours to many days. Alumina has demonstrated good mixing and stability with DI water [19].

Alumina nanofluids at concentrations of interest are Newtonian and exhibit physical properties that can be quantified and modeled by previous work at MIT for density, specific heat, viscosity, thermal conductivity, and surface tension [20]. Concentrations used herein are low ranging from 0.001% to 0.01% by volume.

Density of a nanofluid, ρ_{nf}, is determined as the volumetric average of the nanoparticle (alumina) and the base fluid (DI water).

$$\rho_{nf} = \Phi_{np} \cdot \rho_{np} + (1 - \Phi_{np}) \cdot \rho_{water} \qquad \text{Eq. 2.1}$$

For the case of alumina nanofluids with 0.01% by volume, Φ_{np}, and STP conditions the density, ρ_{nf}, is 998.41 kg/m^3 versus 998.21 kg/m^3 for DI water, ρ_{water}. This represents only a 0.02% increase from DI water, basically negligible.

Specific heat of the blended nanofluids, Cp_{nf}, assuming thermal equilibrium between the nanoparticles and water base fluid is determined by density weighting of the components.

$$Cp_{nf} = \frac{\Phi_{np} \cdot \rho_{np} \cdot Cp_{np} + (1 - \Phi_{np}) \cdot \rho_{water} \cdot Cp_{water}}{\rho_{nf}} \qquad \text{Eq. 2.2}$$

For alumina nanofluids with 0.01% by volume, and STP conditions the specific heat, Cp_{nf}, is 4,183.01 J/kg-^{o}C versus 4,184.05 J/kg-^{o}C for DI water, Cp_{water}. This represents a 0.025% decrease from DI water.

Dynamic viscosity for alumina and water based nanofluids at room temperature is estimated by the following correlation.

$$\mu_{nf} = \mu_{water} \cdot (1 + 39.11\Phi_{np} + 533.9\Phi_{np}^2) \qquad \text{Eq. 2.3}$$

For alumina nanofluids with 0.01% by volume, and STP conditions the dynamic viscosity, μ_{nf}, is 1,005.5 μPa-s versus 1,001.6 μPa-s for DI water, μ_{water}. This represents a 0.392% increase from DI water.

Thermal conductivity of alumina and water based nanofluids at room temperature is estimated by the following correlation.

$$k_{nf} = k_{water} \cdot (1 + 7.47\Phi_{np}) \qquad \text{Eq. 2.4}$$

The resulting thermal conductivity for alumina nanofluids with 0.01% by volume and STP, k_{nf}, is 0.5989 W/m-°C versus 0.5985 W/m-°C for DI water, k_{water}. This represents a 0.075% increase from DI water.

Surface tension for alumina and water based nanofluids at room temperature were measured at MIT via digital tensiometer. For alumina nanofluids with 0.01% by volume, and STP conditions the surface tension, σ_{nf} , is 0.0733 N/m versus 0.0727 N/m for DI water, σ_{water}. This represents a 0.825% increase from DI water.

Table 2-1 lists the particle size, particle density, fluid density, specific heat, viscosity, thermal conductivity, and surface tension at STP for DI water and Alumina. Note that the property deviations are within experimental errors of property measurements, thus the properties of dilute Alumina nanofluids are basically the same as water.

Table 2-1: Table of Physical Parameters at STP for Alumina

Working Fluid		DI Water	Alumina	Alumina
Concentration		n.a.	0.001%	0.01%
Particle or molecule size	nm	0.282	20 - 39	20 - 39
Particle Density	g/cm^3	n.a.	3.04	3.04
Fluid Density	kg/m^3	998.21	998.23	998.41
Specific Heat Capacity	kJ/kg-°C	4,184.05	4,183.95	4,183.01
Viscosity (dynamic)	Pa-s	1001.6×10^{-6}	1002.0×10^{-6}	1005.5×10^{-6}
Thermal Conductivity	W/m-°C	0.5985	0.5985	0.5989
Surface Tension	N/m	0.0727	0.0732	0.0733

3 CHF Enhancement with Nanofluids

Critical Heat Flux ("CHF"), also termed boiling crisis or burnout, is the condition at which with increasing surface heat flux, q", highly effective nucleate boiling ends and the transition to film boiling begins and represents the maximum heat flux in the nucleate boiling region [21]. Basically, at the surface the rate of bubble creation and coalescence becomes great enough to limit the ability of liquid to wet the surface thereby forming a vapor film. Figure 3-1 shows a boiling curve for a pool of water heated from below at atmospheric conditions.

Figure 3-1: Pool Boiling Curve

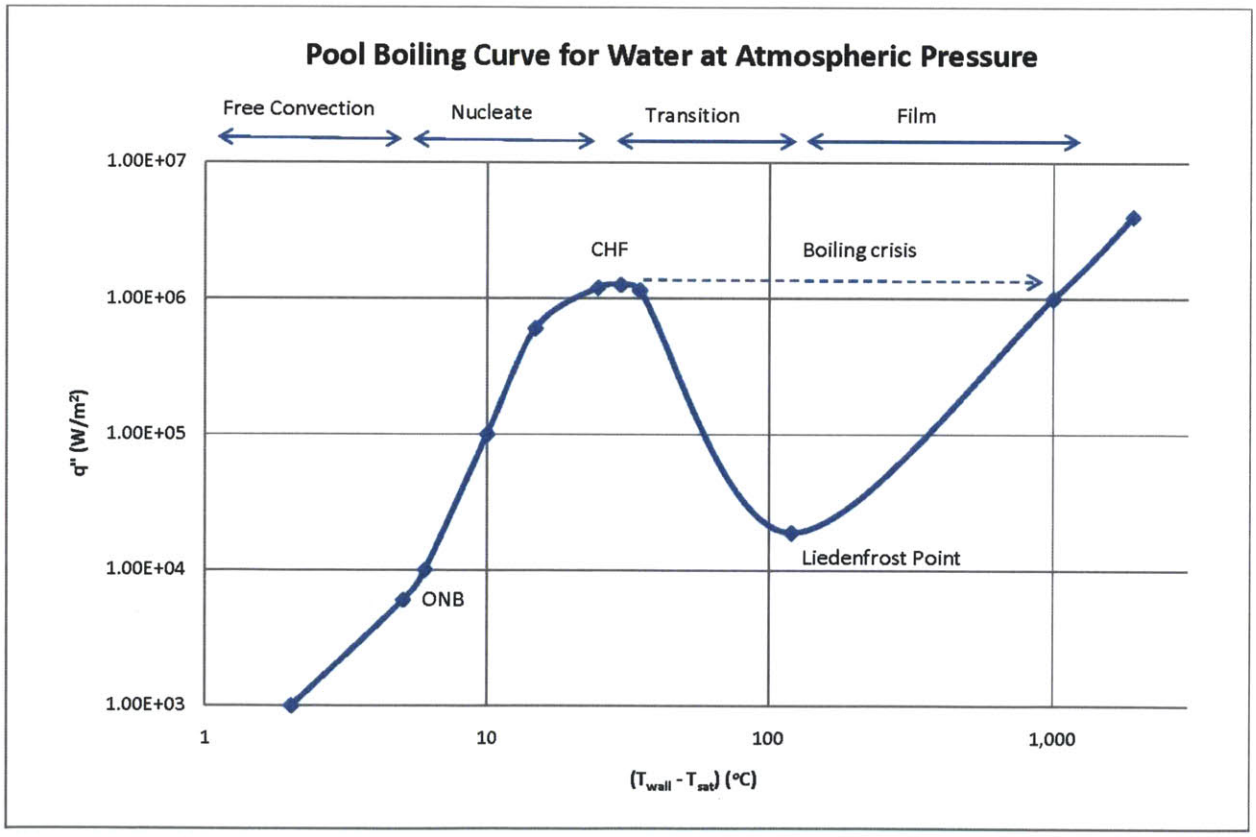

To the left of the CHF maximum, the heat transfer rates increase with increasing heat flux as the bulk fluid transitions from single phase free convection to nucleate boiling. In these regions the

wall temperature excess to saturation is modest, at less than 30 °C. To the right, post transition to film boiling, the significantly lower heat transfer coefficient to vapor causes the wall temperature to jump to over 1000 °C. The 30+ magnitude reduction in heat transfer coefficient drives the surface temperature up drastically per Newton's law of cooling.

$$q'' = h \cdot (T_{wall} - T_{bulk}) \qquad \text{Eq. 3.1}$$

Heat transfer coefficient, h, for atmospheric, pool boiling with water just before CHF is about 37 kW/m^2-°C. Heat transfer coefficient just after CHF and transition is about 1 kW/m^2-°C. With surface temperatures above 1000 °C, steels will lose their strength. Note that in about half of the CHF tests completed herein the steel sample glowed orange and then failed. Visually, the sample can be seen to develop a small orange dot that quickly grows in all directions on the surface. From orange dot to failure is generally about five (5) seconds.

With regard to IVR, pushing off CHF to higher heat flux levels will improve the likelihood of vessel integrity.

Research completed over the past ten (10) years in Sweden, Korea, Japan and the United States [22] have identified higher CHF levels for water based fluids with various nanoparticles in solution compared to DI water [23]. Geometries previously studied with nanofluids to date have included flat plates, wires, spheres, rods and tubes [24]. Conditions studied have been included pool and flow boiling with saturated and sub-cooled states [25][26][27]. Nanoparticle types studied include: gold, copper, carbon nanotubes, silica, alumina, titanium oxide, diamond, and many others [28][29].

One of the early experimental observations was done at the Royal Institute of Technology in Stockholm, Sweden in 2003[30]. The experiment took small metal spheres and quenched them in saturated and sub-cooled alumina nanofluids. It was observed that when the sphere was first quenched, the CHF behavior was basically the same as DI water. With each sequential quenching of the sphere, the CHF increased. After several quenches the film boiling nearly

disappears and transition to nucleate boiling occurs almost immediately once the sphere enters the nanofluid.

Observations at MIT for stainless steel and zircaloy spheres have identified that the boiling process modifies the surface with depositing of nanoparticles [31]. This surface change improves wettability and interferes with film layer development. Figure 3-2 depicts the center temperature of a stainless steel sphere repeatedly quenched initially in water and then alumina 0.01% by volume nanofluid. The increasing presence of nanoparticles on the surface reduces the quench time and increases CHF. In some instances, once the surface is altered, CHF level has increased more than 200% relative to DI water. Quench velocity of rods have also been seen to significantly increase from 3 cm/s to greater than 10 cm/s [32][33]. Increased CHF on the reactor vessel during IVR would increase safety margin.

Figure 3-2: Temperature Histories of a Metal Sphere with Multiple Nanofluid Quenches

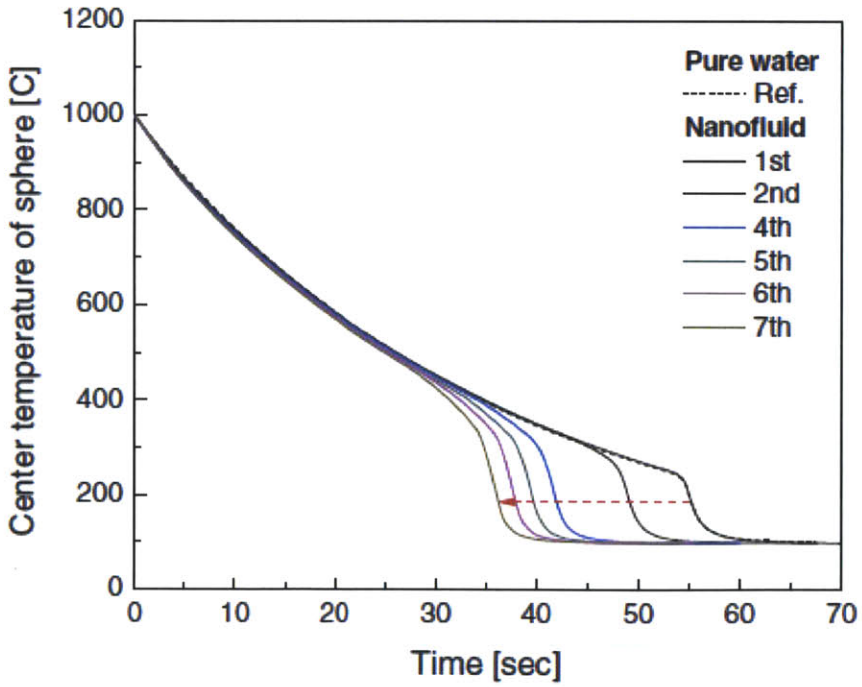

Pool boiling heat transfer and CHF with nanofluids was studied at MIT with high-speed infrared thermography by Dr. Craig Gerardi [34]. His PhD thesis work was focused on fundamentals of

boiling including: bubble departure diameter, bubble departure frequency, bubble growth and wait time, and nucleation site density.

The experimental facility allowed for visual and infrared cameras to view from below through a transparent glass heater with vapor-deposited thin films that are joule heated (see Figure 3-3). Conditions studied where: atmospheric pressure, natural convection, and both saturated and sub-cooled. The two nanofluids studied where water based with silica and diamond nanoparticle.

Figure 3-3: Schematic of Pool Boiling Facility [34]

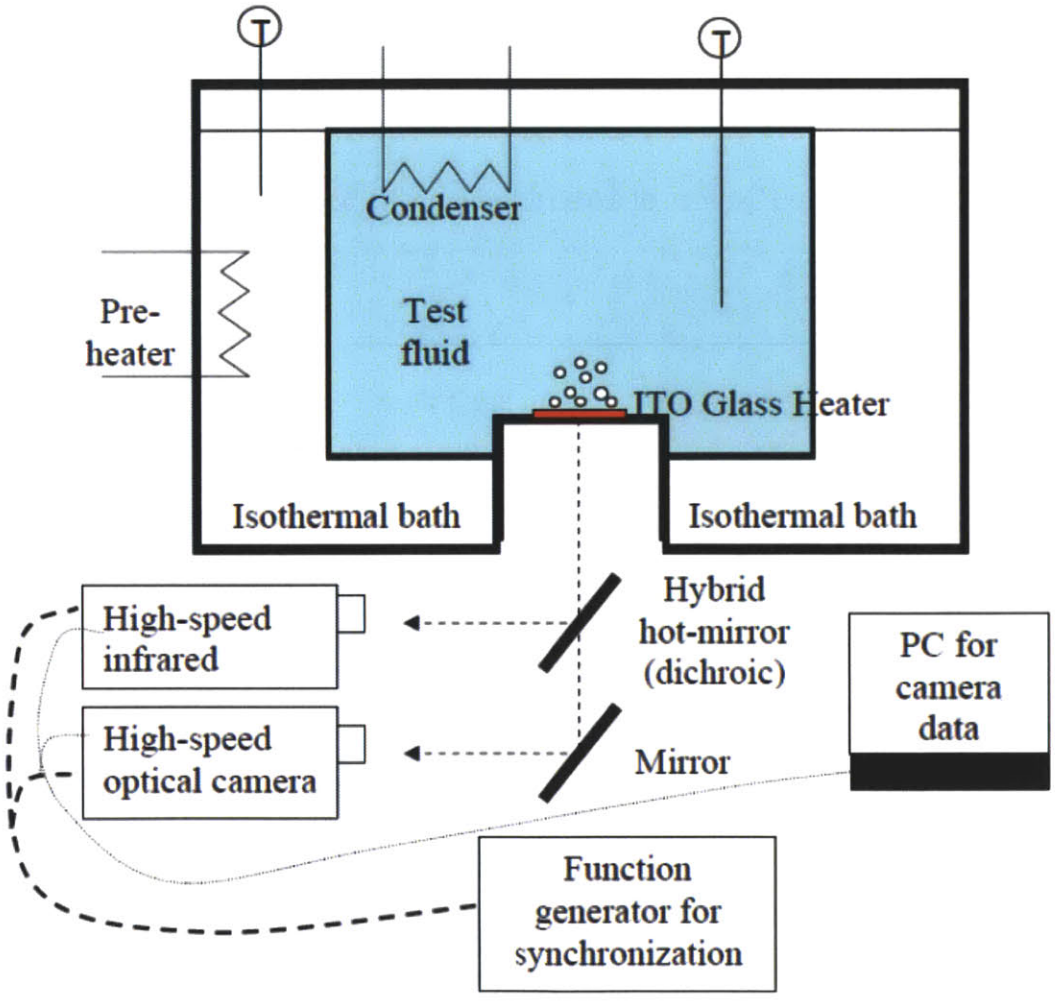

A primary conclusion related to CHF is the nanoparticle deposition on the surface increased wettability as quantified by static contact angle. Increase wettability modified the growth of

bubbles prior to CHF and promoted rewetting of hotspot at CHF. CHF enhancement relative to DI water of up to 100% was measured.

It was confirmed that boiling with nanofluids changed the surface morphology. The result was higher surface wettability. The nanoparticle deposits decreased static contact angle thereby promoting surface cooling (rewetting) and hindering hotspot growth. Hotspot quenching rate was also seen to be higher with nanofluids compared to DI water. This, in turn, slows the process of hotspots merging to cover a larger area of the heater and form a vapor film, CHF.

Highly sub-cooled flow boiling with nanofluids in tubes was studied at MIT by Dr. Sung Joong Kim for his PhD thesis. Both heat transfer coefficients and CHF were studied at atmospheric pressures [35]. Exit quality ranged from -0.05 to -0.03 representing 20 to 30 ^{o}C sub-cooling, respectively. A flow loop was built that could handle mass fluxes in the range of 1500 to 2500 kg/m^2-s through a small (10 cm length) vertically mounted tube (1/4" O.D.; 0.22" I.D.) (see Figure 3-4). Joule heating of the stainless steel tube was provided by DC supplies. Nanofluids studied included: alumina, zinc oxide and diamond. Dilute concentrations of nanofluids tested were 0.001%, 0.01% and 0.1% by volume.

Figure 3-4: Tube Boiling Flow Loop for High Sub-cooling and Mass Flux with Nanofluids [35]

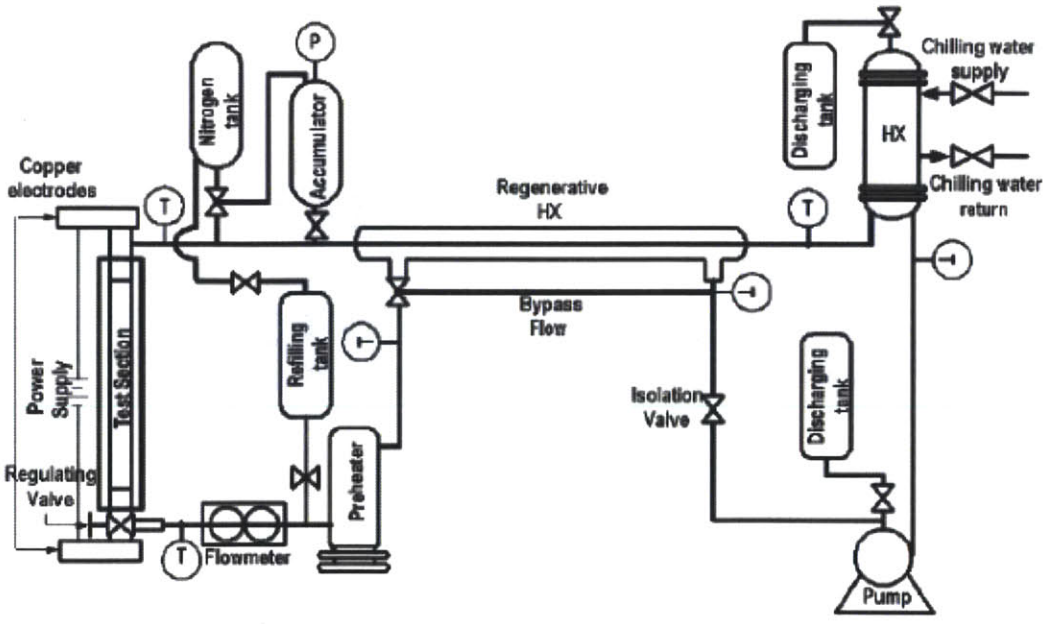

CHF was shown to be enhanced up to 50% for mass fluxes of 2000 kg/m^2-s or more. Interestingly, heat transfer coefficient was not enhanced beyond experimental uncertainty. Surface analysis of the tubes definitively showed increased wettability due to deposition of alumina and zinc oxide nanoparticles.

Pre-coated heaters utilizing nanoparticles together with DI water working fluid was studied at MIT by Dr. Bao Truong's Master's thesis work [36]. This pool boiling study first coated heaters with nanoparticle via nucleate boiling. The coated heaters were then used with DI water and joule heated to CHF. Both wires and horizontal flat heaters were used.

The test facilities built utilize an isothermal bath with pre-heater the surrounds a test cell that contains the working fluid and test heater (see Figure 3-5).

Figure 3-5: Schematic of Pool Boiling Pre-coating and CHF Facility [36]

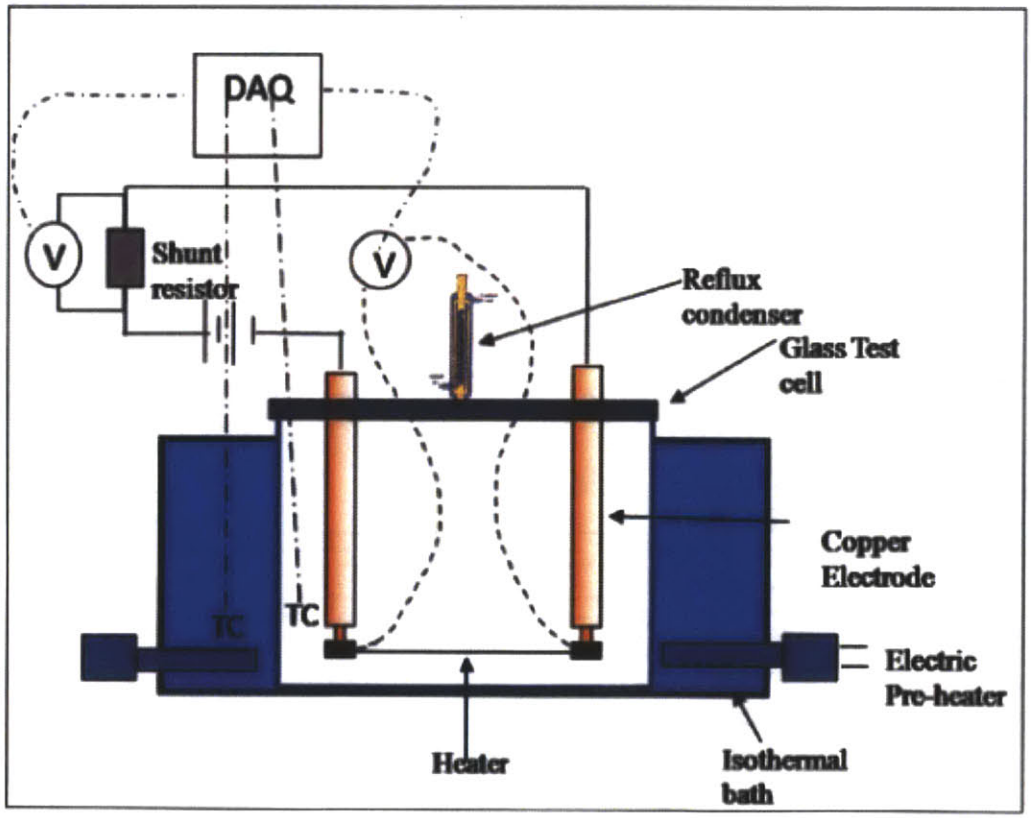

Atmospheric conditions were present and near saturation liquid temperatures. The heaters were then joule heated by DC power to CHF and measurements made. Heaters were stainless steel 316. The wire heaters had a diameter of 0.384 mm and length of 9.5 cm. The flat plates were 7.0 cm long, 0.5 cm wide and 1.2 mm thick. Flat plate tests were oriented facing up with insulation on the back and sides.

Flat plate heaters with alumina and zinc oxide pre-coating yielded CHF enhancement of 35% and 33% over bare heaters, respectively. This study also noted that within five (5) minutes of nucleate boiling with low concentration nanofluids, coating more than 1 μm thickness were measured for wire.

In the same theme and as part of his PhD work Dr. Truong studied sub-cooled flow boiling CHF with pre-coated tubing [37][38][39]. This leveraged the previously described facility built by Dr. Sung Joong Kim. For pre-coating of stainless steel tubes, a new coating loop was built (see Figure 3-6).

Figure 3-6: Schematic of Tube Coating Loop

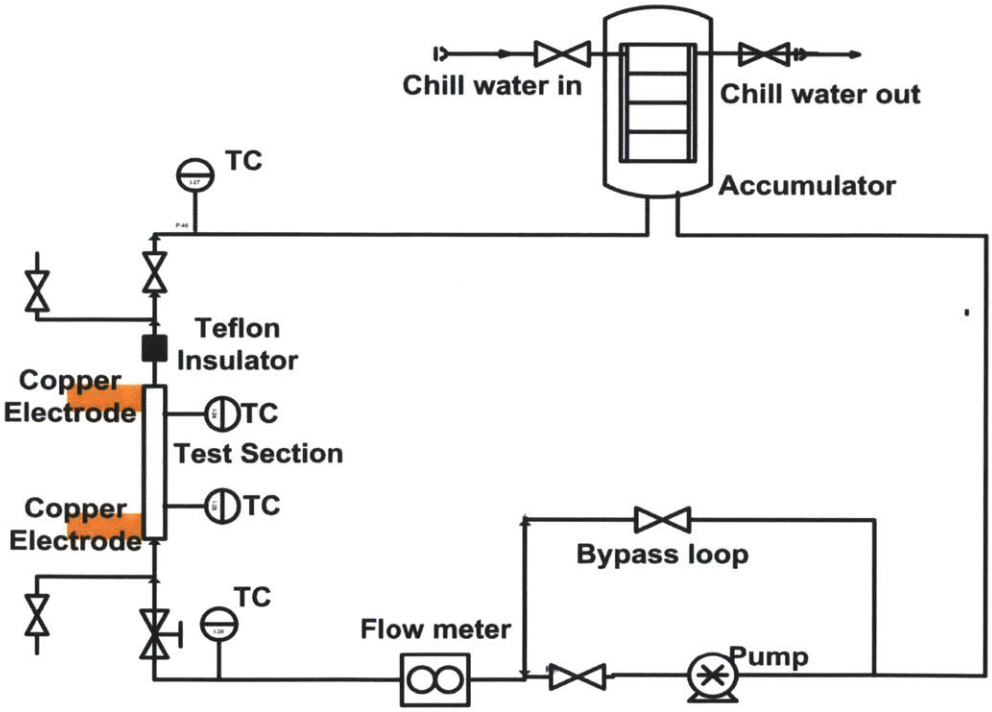

Alumina nanofluid with 0.1% by volume was chosen for this study. Bare 10 cm length stainless steel tubes (0.25"O.D.) were joule heated providing 1.0 to 1.5 MW/m^2 surface heat flux and assuring significant sub-cooled nucleate boiling. The heat exchanger on the facility allowed control of the test section inlet temperature by varying the chilled water flow rate. Inlet temperature for the tube to be coated was about 40 ^{o}C. Coating time was 1.5 to 2.0 hours.

Coated tubes were then vertically mounted onto the tube boiling flow loop (see Figure 3.4). Conditions were atmospheric pressure, 1500 or 2500 kg/m^2-s mass flux, and high sub-cooling. The range of exit qualities tested were -0.04 to -0.07.

Results indicate enhancement of 23% to 35% compared to bare tubes for 2500 kg/m^2-s mass flux cases. These measurements are somewhat lower, about 10%, than nanofluid tests by Dr. Sung Joong Kim for similar conditions. Total boiling history and related particle deposition to the sample tubes and uncertainty may be sources of explanation of the difference.

Other work, done at MIT and elsewhere, has studied numerous factors thought to influence heat transfer and CHF in the presence of nanoparticle: reduced pressure [40], use of surfactants [41], use of tri-sodium phosphate ("TSP") and boric acid [42], stability [43], copper nanoparticles [44], and low concentrations [45][46]. Additionally, extensive work has been completed to investigate the influence various promising nanoparticles have on bulk working fluid thermal conductivity and single phase heat transfer coefficient [47][48] [49] [50] [51].

Wettability, as quantified by static contact angle, has been identified as a primary contributor to CHF enhancement with nanofluids [52][53][54]. The process of boiling deposits nanoparticle onto the surface forming a porous layer [55][56][57]. This surface modification [58] increases contact angle and surface roughness [59][60] and in turn hinders vapor layer development during high bubble formation and departure rates by improving liquid rewetting.

4 Hypothesis

The hypothesis tested herein is that the use of Alumina nanofluids with 0.001% by volume can increase the CHF at all downward facing angles by 50% relative to water for SS316L in hydrodynamic conditions and time frame associated with the IVR scenario. The hypothesis test will meet one standard deviation, σ_{std}, providing 67% certainty to the conclusion. Uncertainty analyses provided in section 6.12 quantifies the error in CHF as one standard deviation, σ_{std}, equaling 4%. Note the surface condition for nearly all tests is stainless steel 316L with a sandblasted finish more fully described in chapter 10. Five (5) tests were done with SA-508 the low carbon steel used in reactor vessel fabrication.

5 IVR Description

In-Vessel Retention ("IVR") represents a severe accident mitigation strategy incorporated into procedures for several advanced light water reactor designs including: Westinghouse's AP600 and AP1000, Russian VVER-440, and South Korean APR1400. The IVR scenario is addressed in the AP1000 NRC design submittal [61]. The accident scenario assumes a full core overheat failure that causes the fuel, cladding and internals to melt [62]. Note the melting temperature of UO_2 is approximately 2850 °C. The melt relocates to the lower vessel head in a sub-critical state forming a corium pool with decay heat being generated [63]. The initiating event could be a LOCA with simultaneous failure of the ECCS. The time to relocation has been estimated between 1.7 hours to 3.7 hours depending on assumptions and methodology [64]. By the time the corium has formed, only vapor is expected to remain above the melt within the reactor vessel (see Figure 5-1). Decay heat is significant and failure to remove it can lead to reactor vessel breach [65]. This decay heat removal challenge is being lived out at Fukushima Daiichi nuclear site in Japan that suffered severe accident precipitated by an earthquake with resulting tsunami.

Vessel failure can be either by corium induced vessel wall thinning via ablation or high thermal stress [5]. Thinning could result in a local path (small hole) or general creep rupture. High thermal stress would occur if heat removal from the outer vessel low as is the case for CHF and thereby significantly increasing vessel wall temperature. Nucleate boiling heat transfer even in pool boiling is sufficient to keep vessel surface temperatures within 30 °C of saturation. For carbon steel at less than 200 °C only ~3 cm of the original 15 cm of wall thickness is needed to avoid creep rupture. Therefore as long as liquid water is in contact with the lower vessel head creep rupture is not likely to occur. The failure mode of greater concern then is CHF.

Figure 5-1: Schematic of IVR Scenario with Corium Relocation

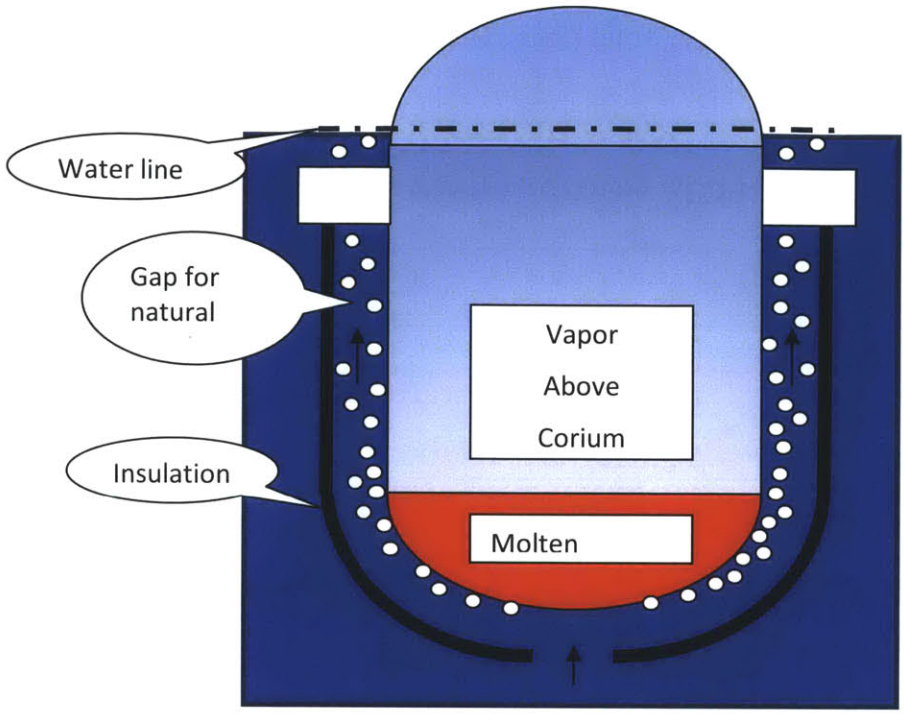

For the AP1000, starting at rated power, P_{rated}, of 3415 MWth, once the control rods have scrammed (All Roads In) the decay heat level, Q_{decay}, is expected to be 225 MWth. Over the next two (2) hours the decay heat drops to 29 MWth. After one day the decay heat level is 17 MWth. After one week the decay heat level is 12 MWth.

$$Q_{decay}(t) = 0.066 \cdot P_{rated} \cdot (t^{-0.2} - (T_{op} - t)^{-0.2}) \qquad \text{Eq. 5.1}$$

Where:
- P_{rated} = power at the time of scram = 3415 MW_{th}
- t = time from scram in seconds
- T_{op} = operating time at P_{rated} before scram in seconds

If we assume long operating time at rated power before the IVR event the last term of equation 5.1 becomes small and can be treated as zero (see Figure 5-2).

$$Q_{decay}(t) = 0.066 \cdot P_{rated} \cdot (t^{-0.2}) \qquad \text{Eq. 5.2}$$

Figure 5-2: Total Decay Heat History IVR for AP1000

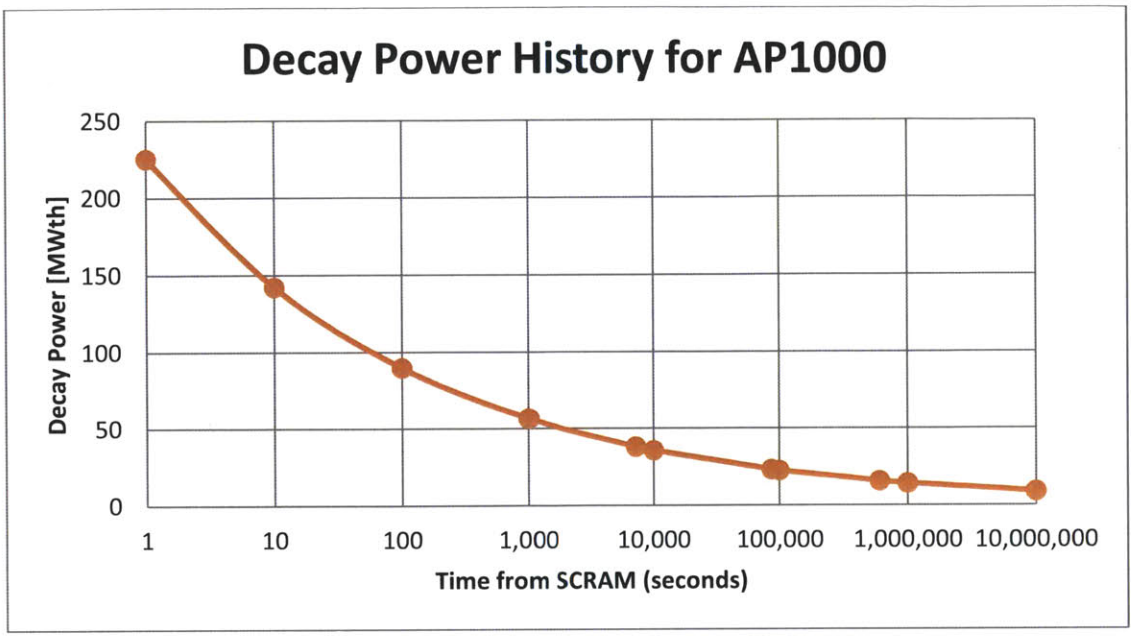

Additionally, the IVR scenario has full clad failure. Clad failure and UO_2 melt releases volatile fission product gases that are expected to escape during corium formation into the upper containment atmosphere. Decay heat from gaseous fission products represents about 25% of total decay heat [62]. The removal of the fission gas decay heat within two hours of accident initiation then reduces the amount of decay heat that needs to be extracted from the corium through the reactor vessel walls (see Figure 5-3).

$$Q_{decay}(t > 2\ hours) = 0.0495 \cdot P_{rated} \cdot (t^{-0.2}) \qquad \text{Eq. 5.3}$$

Figure 5-3: Post Fission Gas Release Decay Heat History IVR for AP1000

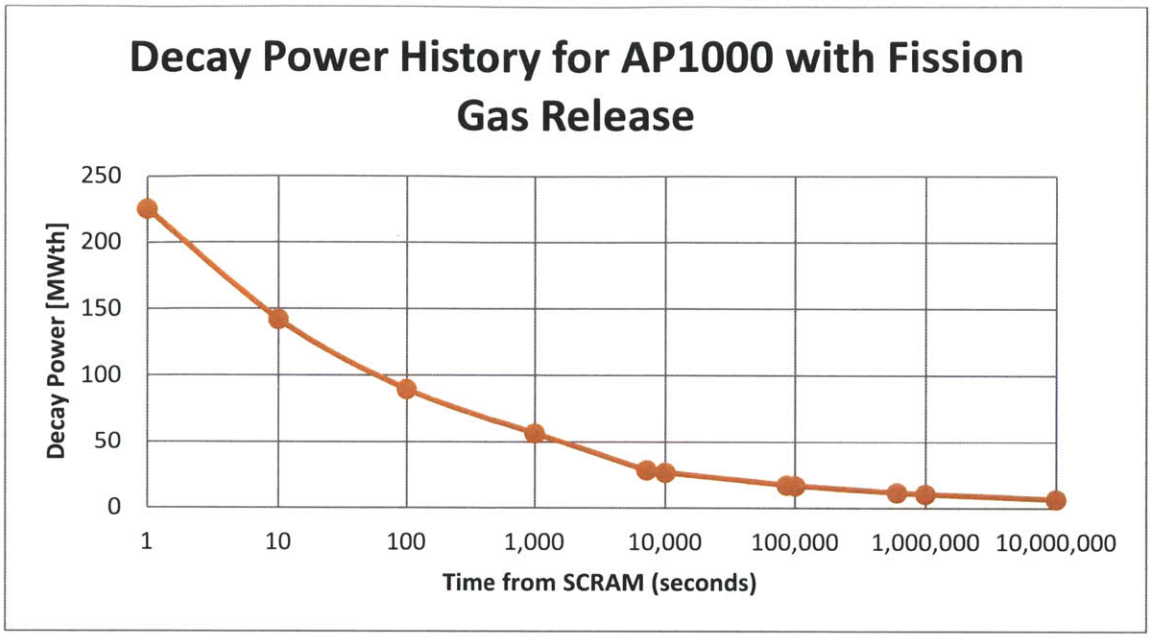

The design goal is to keep the remaining radioactive materials within the reactor vessel [6]. Achievement of the goal will prevent corium interactions with the concrete containment and the water under the vessel, and thus lower the probability of release to the environment [66]. Work by numerous investigators in the United States, France and Korea have studied in detail the IVR scenario including corium development and ex-vessel cooling [67][17].

The challenge is to remove the decay heat over many days through the reactor vessel wall without failure [68]. The IVR operating strategy is to flood the reactor cavity (and thus the lower region of the containment) once it is determined that significant core damage has occurred. Water from the IRWST tank is directed passively to the reactor vessel cavity via gravity head (no pumps). The IRWST sits above the reactor vessel cavity. Two (2) operator actuated valves, one for each feed line, do need to open for maximum flooding rate. The IRWST contains 2092.6 m^3 (552,806 gallons) of water at STP. Natural circulation sets up as the water in contact with the reactor vessel outer surface boils, thus lowering the coolant density and creating buoyancy. The

natural circulation path starts below the lower vessel head then runs up a gap between the reactor vessel and the thermal insulation, 15.24 cm (6 inches) that is attached to the concrete in the vessel cavity. The free surface liquid level is expected to be above the primary piping legs (see Figure 5-4).

Figure 5-4: Schematic of IVR Circulation with Nanofluid Injection

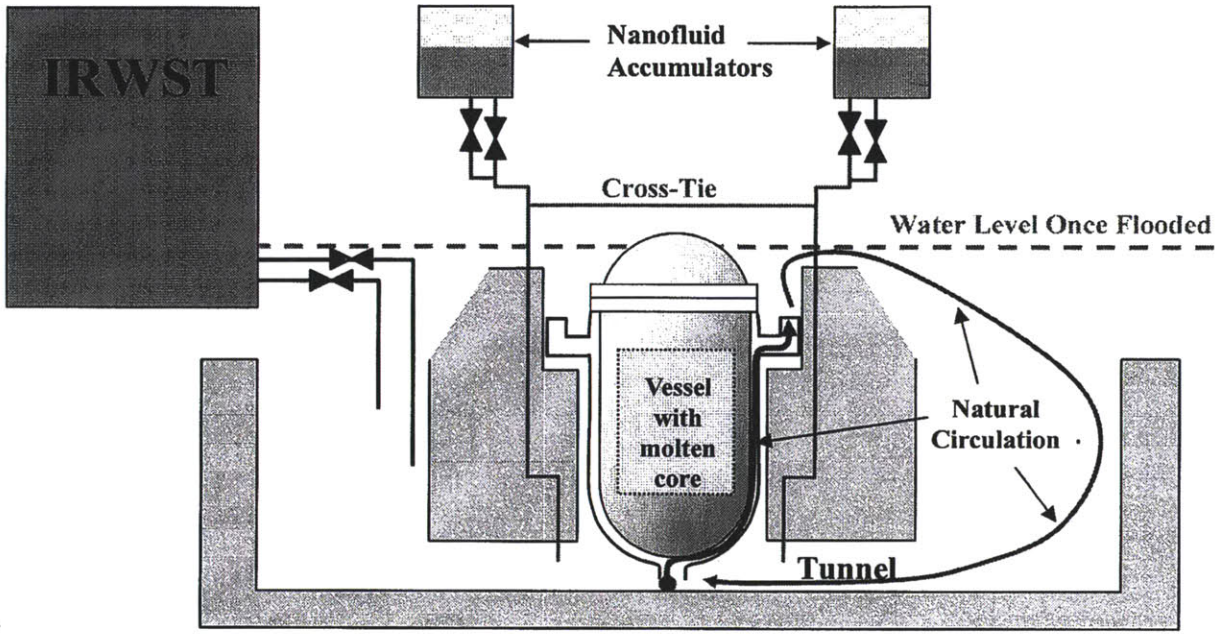

Looking down from above the reactor vessel, we see the vessel is within an octagon concrete cavity (see Figure 5-5). Between the reactor vessel outer surface and the concrete walls is a thermal insulation structure that helps protect the concrete and minimizes heat losses from the vessel under normal operation. Water from the IRWST can readily flow via natural circulation in the 15.24 cm (6 inch) annulus gap. It is in this annulus that boiling will occur along the reactor vessel surface. A smaller gap of varying size exists between the concrete and thermal insulation and is also flooded with water, thus constituting the "return line" for the natural circulation path..

Figure 5-5: Top View Schematic of Reactor Vessel Cavity During IVR

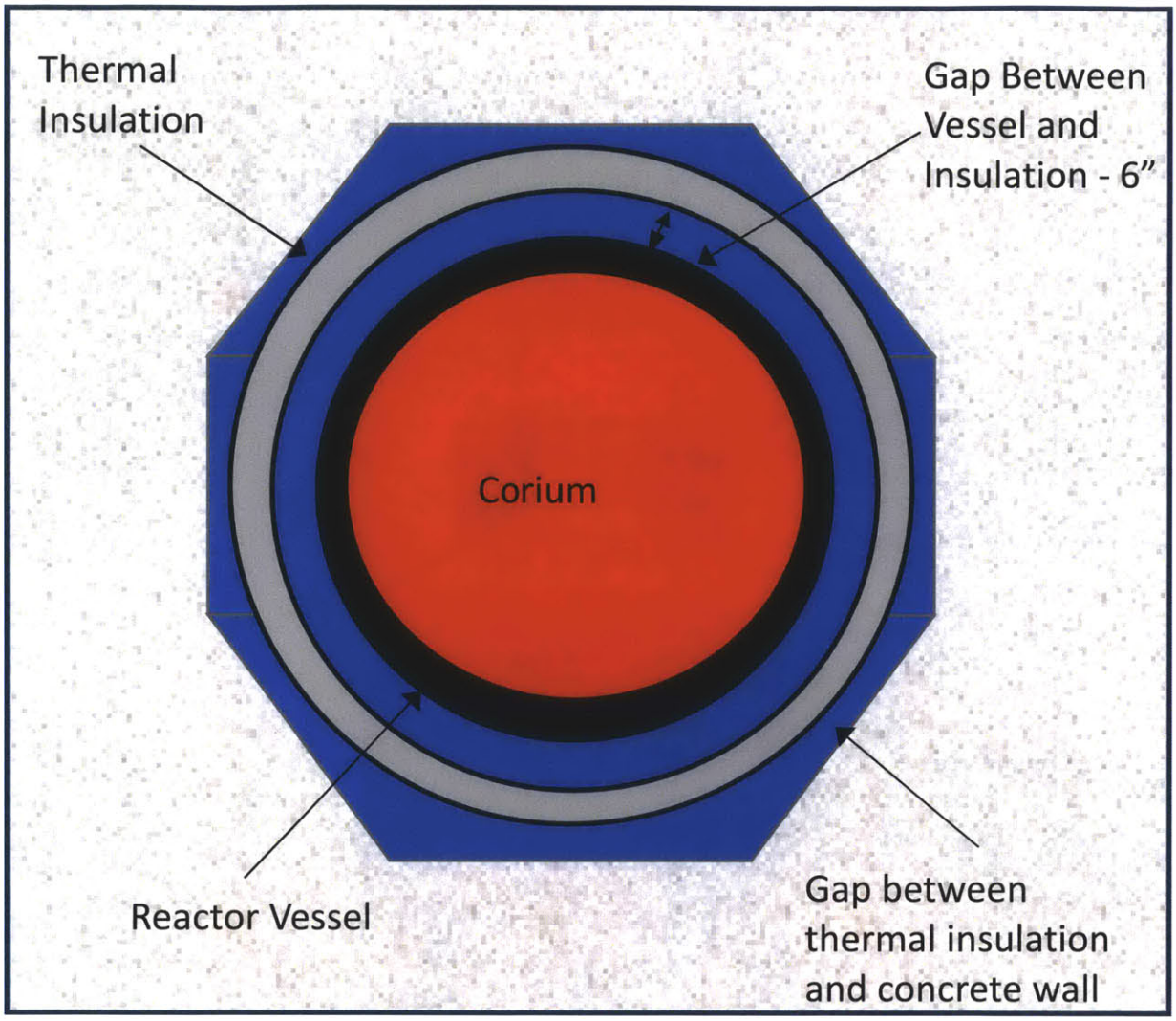

When the water from the IRWST is released it has a bulk temperature of approximately 20 °C. The bulk fluid will gain energy from the reactor vessel surface and containment atmosphere heat up due to primary system depressurization plus fission gas release. The bulk fluid is expected to become saturated and start boiling. Any saturated vapor that escapes into the air and vapor atmosphere will reach the upper containment. Steam being lighter than air will cause the vapor to circulate and be condensed via the containment cooling system. The containment cooling system involves a steel shell that has a thin film of water flowing on the environment side (see Figure 5-6). Evaporation of that film then removes heat away from the containment shell into

the environment. Evaporation on the top of the steel containment vessel is enhanced via a natural circulation path from and to the outside atmosphere (chimney effect). This represents the ultimate heat sink. The condensed liquid within the containment flows back down to the bottom of the vessel cavity. The lower density of the water/steam mixture flowing between the reactor vessel and insulation relative to the water-only return provides the buoyancy head to overcome frictional losses along the natural circulation path.

Figure 5-6: AP1000 Containment Cooling Schematic

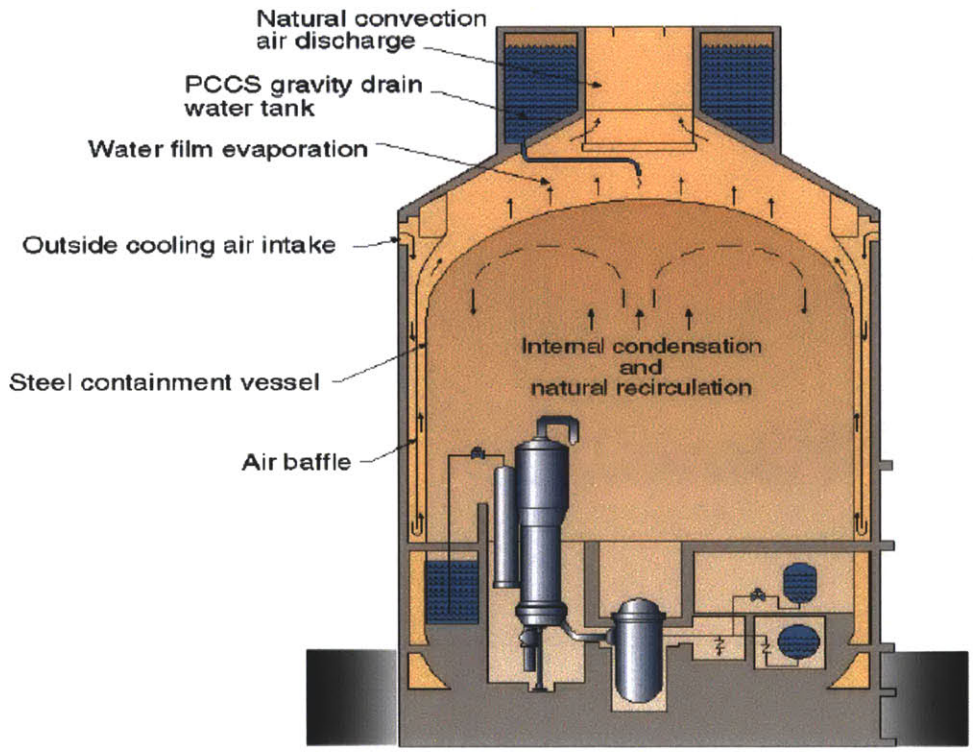

As the IVR scenario progresses the water surrounding the reactor vessel will boil. If surface heat flux is sufficiently high, CHF could occur. Near the top of the corium is of particular concern because of expected stratification of lighter metals (i.e., steel, aluminum) above the oxide decay heat source. The lighter metals above have relatively high thermal conductivity and with high heat flux from below and only thermal radiation cooling above the heat will conduct toward the vessel wall thereby acting a lens of heat, focusing effect. CHF is to be avoided at all times because of concern that the higher temperature within the reactor vessel wall associated with the

low heat transfer rate of film boiling may reduce its strength and allow creep failure. The reactor vessel lower head, upper head and belt line region are made of SA-508 low carbon steel. Note that the melting point of low carbon steel is about 1400 °C.

Pressure within the containment's upper region throughout the IVR scenario is expected to reach 3 bar, absolute (see Figure 5-7). This is well below the design limit for the containment, which is 5 bar, absolute. Pressure in the region of the lower head where the corium heat source resides has an additional 0.5 bar due to the hydraulic head of two-phase water/steam mixture.

Figure 5-7: Upper Containment Pressure History for IVR from UK Safety Report

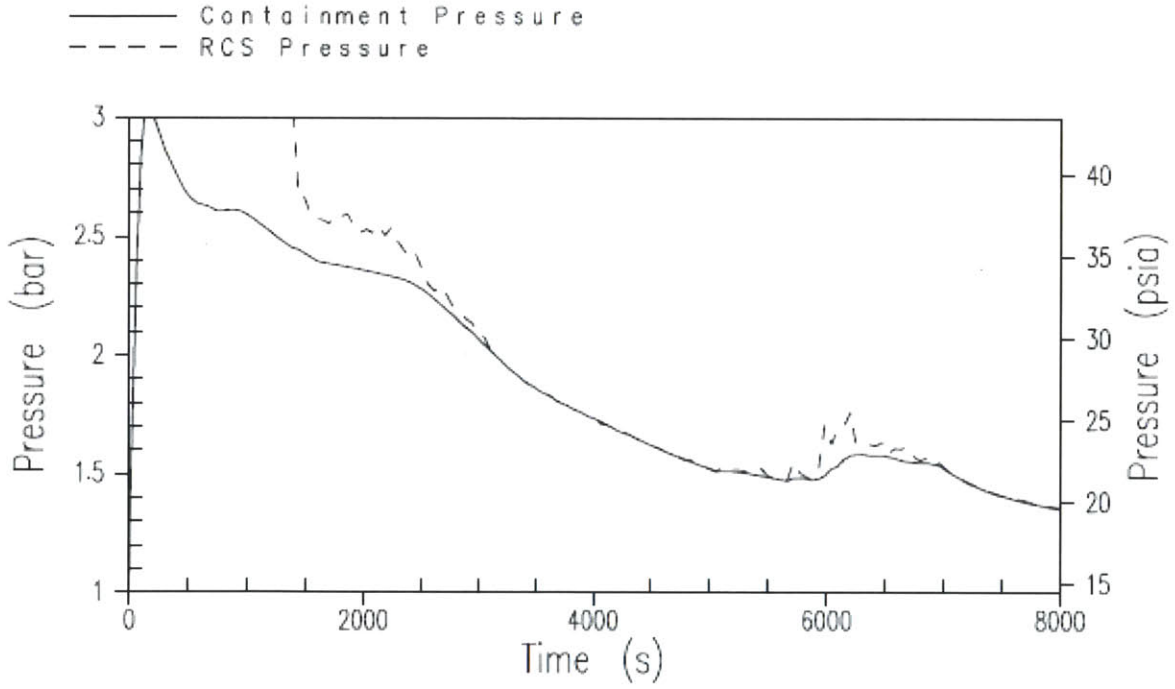

The expected containment pressure history of the IVR scenario indicates a short peak early in the event. This pressure peak is due depressurization of the primary coolant system ("PCS") and anticipated hydrogen ignition. Once the hydrogen burn occurs, containment pressure returns to less than 2 bar absolute within one (1) hour.

Work done at MIT suggests that to increase CHF for these IVR conditions on the reactor vessel outer surface, alumina nanofluids be injected to the flow from the IRWST via two accumulators

(see Figure 5-4). The identical accumulators are proposed as a safety redundancy. The higher concentration nanofluid within the accumulators would blend down to the target concentration of between 0.001% and 0.01% by volume. Then as boiling occurs on the reactor vessel outer surface the particles would deposit. The result of herein experimental work indicates CHF would be increased for all locations along the lower hemisphere by not less than 30% to an average of 70% within 30 minutes of boiling.

The reactor vessel geometry is basically a cylinder with hemispheres at top and bottom. The height of the reactor vessel from the bottom of the lower head to the top of the upper head is 12.21m (40.05 ft) (see Figure 5-8).

Figure 5-8: Simple Drawing of AP1000 Reactor Pressure Vessel

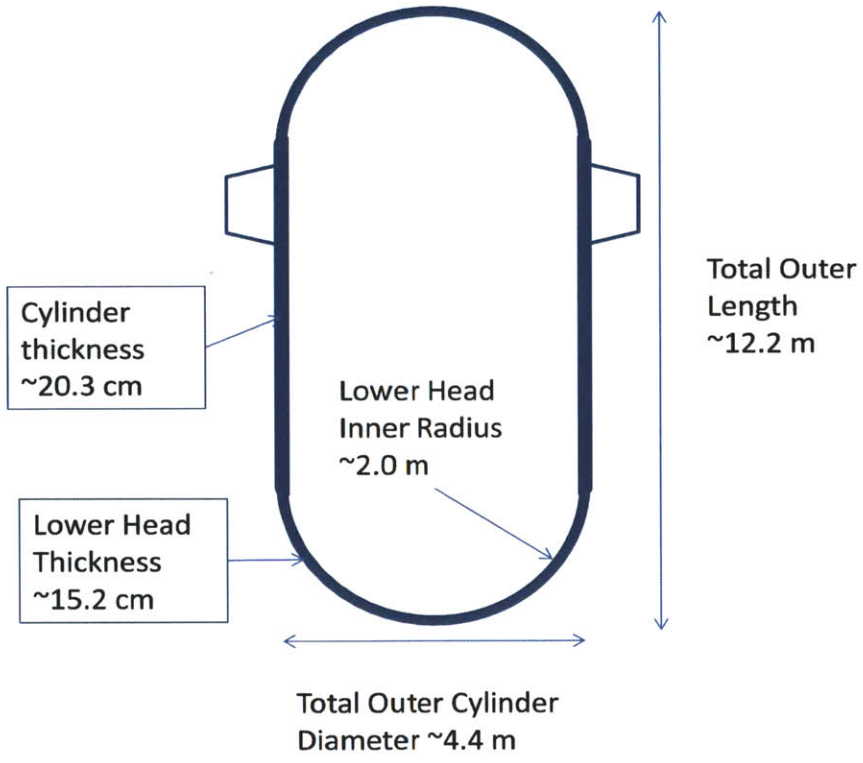

Wall thicknesses are 20.32 cm (8 inches) for the cylinder portion of the reactor vessel and 14.58 cm (6 inches) for the lower head (see Table 5-1). The outer surface area of the lower head, in

which the corium resides, is 29.35 m^2 (see Figure 5-9). The associated inner volume of the lower head is 16.98 m^3.

Figure 5-9: AP1000 Reactor Pressure Vessel, Core and Lower Internals [4]

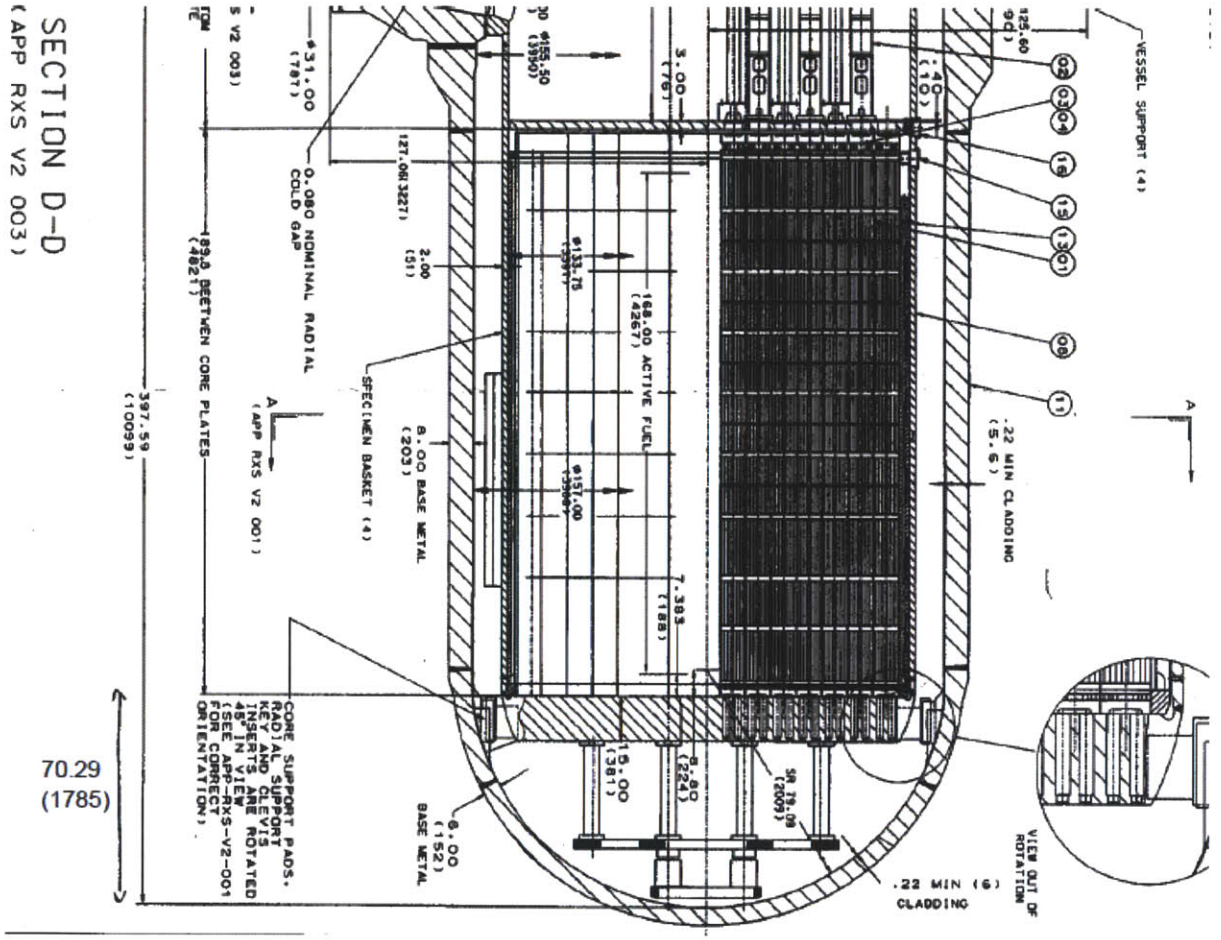

Table 5-1: AP1000 Reactor Pressure Vessel Parameters

Material	SA-508	
Cylinder shell ID	3.988 m	
Cylinder inside cross sectional area	12.49 m^2	
Cylinder shell thickness	0.203 m	8.0 in
Cylinder shell OD	4.394 m	
Cylinder shell Outside Perimeter	13.80 m	

Cylinder length	8.090 m	26.54 ft
Cylinder Outside Area	111.67 m^2	
Lower Head ID	4.02 m	401.78 cm
Lower Head Thickness	14.58 cm	6 inches
Lower Head OD	4.32 m	432.26 cm
Lower Head Outer Surface Area	29.35 m^2	
Lower Head Inner Volume	16.98 m^3	
Height of Cylinder plus upper & lower head	12.21 m	40.05 ft

Within the reactor vessel are the fuel, cladding, control rods and internals. The internals include: core support plate, core barrel, core shroud, instrumentation and other support structures. The primary materials found in the reactor vessel include: uranium oxide fuel (UO_2), stainless steel, zirconium, and control rod materials (see Table 5-2).

Table 5-2: Table of Reactor Fuel, Clad and Internal Volumes and Mass (liquid state)

Core	Mass	Volume	Density
Fuel	95,900 kg	10.97 m^3	8.74 g/cc
Active Core Cladding	17,900 kg	2.92 m^3	6.13 g/cc
Additional Zirconium	4,800 kg	0.78 m^3	6.15 g/cc
Control Rods	3,900 kg	0.58 m^3	6.72 g/cc
Core Total	122,500 kg	15.25 m^3	8.03 g/cc
Lower Internals			
Core barrel	19,000 kg	2.7 m^3	7.04 g/cc
Lower support plate	25,000 kg	3.4 m^3	7.35 g/cc
Core shroud	12,000 kg	1.7 m^3	7.06 g/cc
Shroud support structure	9,000 kg	1.3 m^3	6.92 g/cc
Control Rods	3,000 kg	0.4 m^3	7.50 g/cc
Lower Internals Total	68,000 kg	9.50 m^3	7.16 g/cc
Core + Lower Internals = Corium	190,500 kg	24.75 m^3	7.70 g/cc

As the IVR scenario unfolds. It is expected that the decay heat driven molten fuel will melt surrounding materials including the zircaloy cladding and steel internals. A fraction of the zircaloy clad is expected to react with water at high temperature in an exothermic reaction forming hydrogen gas H_2 and zirconium oxide ZrO_2.

$$Zr + 2H_2O \text{ ---> } ZrO_2 + 2H_2 + 606 \text{ kJ/mole of Zr}$$

The higher density of the oxides will stratify to the bottom of the lower head (see Figure 5-10). The ending geometry is highly uncertain and will depend on whether all or only a portion of the fuel fails and what portion of the zirconium cladding reacts with water. Additionally, due to the timing of relocation and the remaining inventory of water, blockages may form that may alter the final geometry. Blockages could form as molten fuel takes a path (i.e. toward the downcomer) that then contacts remaining water inventory or cooler internals and lowers the re–solidification. It is expected that a crust of varying thickness will form around the molten pool. Between the vessel inner surface and the molten portion of the corium, crust thickness is expected to be thickest at the bottom of the lower head, on the order of 20.3 cm (8 inches), and thin down toward the top of the corium.

Figure 5-10: Schematic of Fuel and Metal Stratification within Reactor Vessel

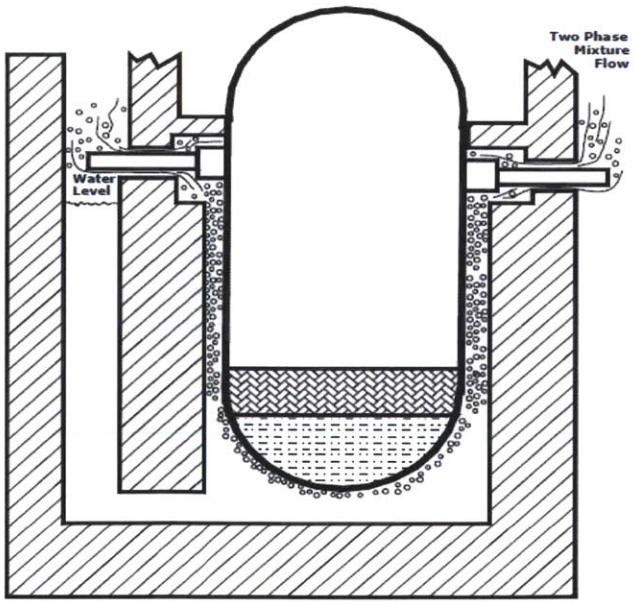

The total volume of the higher density fuel is 10.97 m^3 and once stratified will represent 65% of the 16.98 m^3 inner volume of the lower head. Cartesian coordinate relations for a circle of radius, $R^2 = x^2 + y^2$, and associated area, $A(x) = \pi y^2$, can be integrated between two points to determine the height of the UO_2 portion of the corium, 1.53 m. If we assume that ~1 m^3 of ZrO_2 is formed, the oxide portion of corium in the lower head volume increases to ~71% with an associated height of 1.61 m. The radial angle off vertical to the top of the oxide, $\theta_{oxide\ top}$, is 78.5°.

One scenario of corium development has lighter metal stratifying over heavier oxide materials (see Figure 5-11) [3]. The order of magnitude higher thermal conductivity of the liquid metal relative to oxides at the corium top could act as a focus for heat flux. The thermal conductivity of steel, k_{ss}, at temperatures above 1000 °C is on the order of 27 W/m-°C as compared to UO_2 , k_{UO2}, of 2.5 W/m-°C [69]. The molten metal layer would have a large surface area in contact with the decay heat source oxide below. The melt temperature for this layer is estimated at 1600 °K. Above the corium only superheated vapor would be available to remove heat via natural convection plus thermal radiation cooling.

Figure 5-11: Schematic of Corium with Crust and Metal Stratification

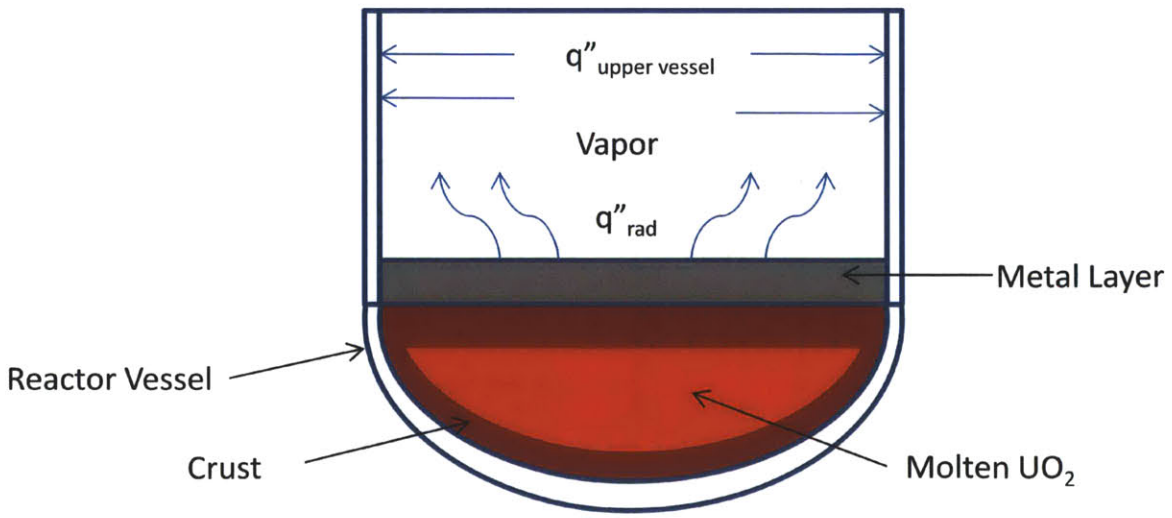

If we assume that radiation cooling dominates, one can do an energy balance of the heat flux leaving the top of the metal layer, $q"_{rad}$, and being absorbed on the inner surface of the reactor

vessel above the metal layer, $q''_{upper\ vessel}$. The area of the top of the metal layer, A_{rad}, is 12.6 m^2. The surface area of the reactor vessel above the metal layer, $A_{upper\ vessel}$, is 127.5 m^2. The average surface heat flux to the upper vessel surface is then 9.9% of what leaves the top. Applying the Stefan-Boltzmann law the surface flux can be determined. Work done by Theofanous at UCSB in the early 1990s estimated that the emissivity, ε, of the liquid metal layer would be in the range of 0.5 to 0.6.

$$q''_{rad} = \varepsilon \cdot \sigma_{boltz} \cdot (T^4_{rad} - T^4_{inner\ vessel}) \qquad \text{Eq. 5.4}$$

Where:

T_{rad}	= 1600 °K representing the top of the metal layer
ε	= 0.55
$T_{inner\ vessel}$	= 500 °K representing the average inside vessel wall

The resulting heat flux leaving the surface, q''_{rad}, is 0.2 MW/m^2. The resulting heat flux impinging the inner vessel wall above the metal layer, $q''_{inner\ vessel}$, is 0.02 MW/m^2.

Next, applying Fourier's law to the vessel:

$$q''_{inner\ vessel} = -k \cdot \frac{dT}{dx} \qquad \text{Eq. 5.5}$$

Where:

dT	= ($T_{inner\ vessel}$ – $T_{outer\ vessel}$)
$k_{carbon\ steel}$	= 40 W/m-°K for carbon steel
dx	= 20.32 cm (8 inches)

Now assume that the average outer vessel temperature above the metal layer will be 20 °C above saturated water at atmospheric pressure, $T_{outer\ vessel}$ equals 120 °C. Iterating between the heat transfer through the upper vessel wall and the thermal radiation coming off the top of the metal layer the average vessel wall inner temperature converges to 488 °K. The thermal radiation heat flux, q''_{rad}, is then 0.203 MW/m^2 and the energy leaving the corium upward is 2.55 MW.

At the earliest expected time of corium formation of ~2 hours the total decay heat from the corium is 28.6 MW (see Eq. 5.3). The thermal radiation component is then 8.9% and leaving 91.1% (26.1 MW) to go through the reactor vessel walls in contact with the corium.

Heat conducting up from the oxide layer below, less the thermal radiation loss to the upper vessel, would conduct in the radial direction out toward the reactor vessel. Depending on the thickness of the top metal layer, the radial surface heat flux leaving through the reactor vessel locally could increase significantly relative to below the metal layer. Estimates of the thickness of the metal region range from zero (0) to 0.6 m (2 feet) with large uncertainty.

If we assume all the internals melt and relocate, 24.74 m^3, a portion of the corium would be within the reactor vessel cylindrical wall, 7.72 m^3. With the inner cylinder area being 12.49 m^2 the height above the lower hemisphere would be 0.618 m. This plus the 0.483 m below the lower hemisphere plane would imply a maximum metal thickness of 1.102 m (3.62 feet).

Work at UCSB and INL developed a base case heat flux profile for the AP1000 that addresses in a conservative manner corium development that has been accepted by the NRC and UK regulators (see Figure 5-12). Generally the vessel outer surface heat flux is increasing with angle from bottom ($\theta = 0^o$) to top ($\theta = 90^o$). Crust thickness variation, temperature stratification and metal top layer focusing contribute to the shape. The minimum heat flux at the vessel bottom, 165 kW/m^2, and the maximum along the last 5° near the top, 1375 kW/m^2. Note the ~100 kW/m^2 jump in heat flux at the oxide to metal layer interface.

Figure 5-12: Base Case Corium Heat Flux Profile for the AP1000

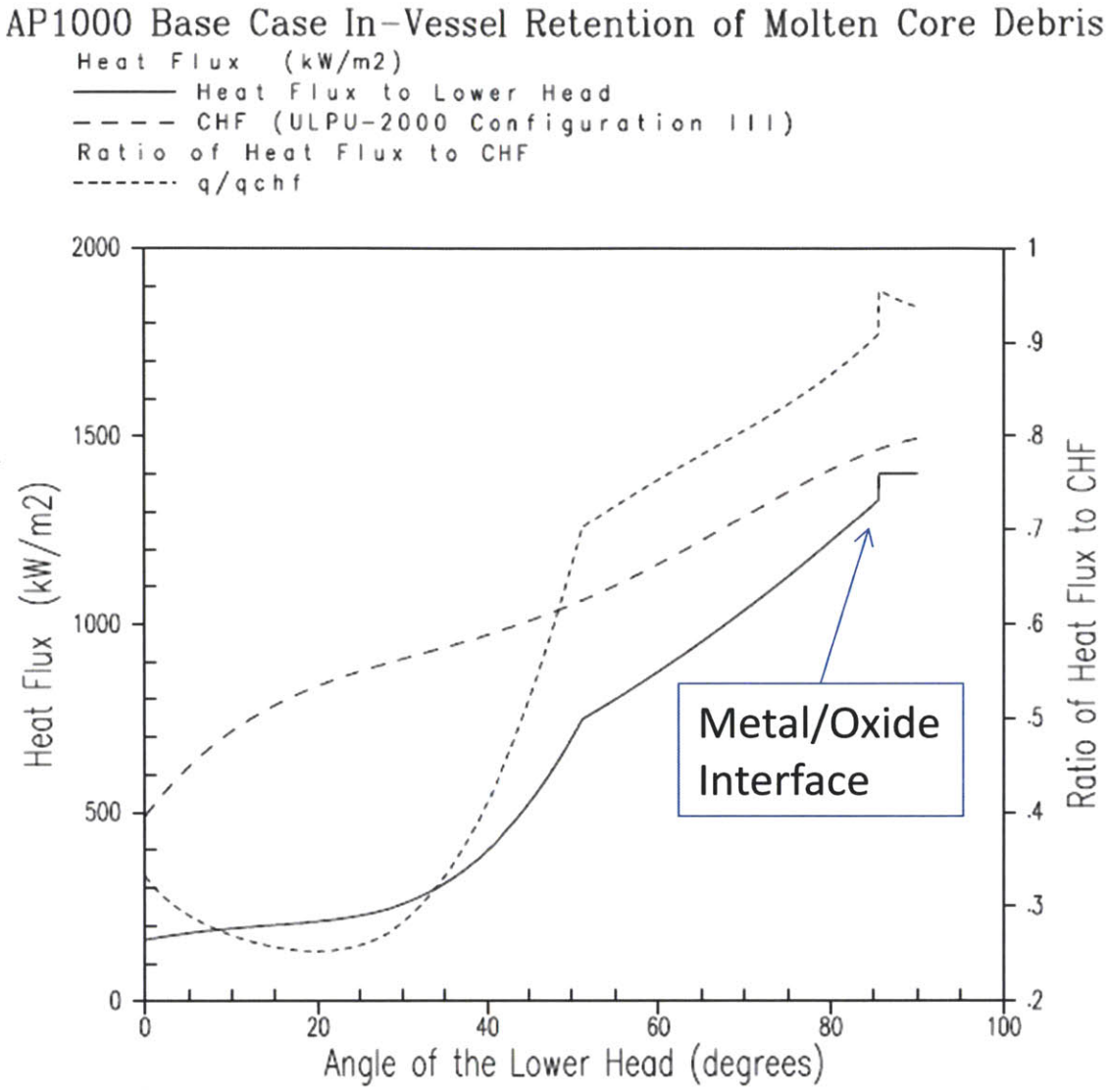

Studies at UCSB, PSU, and SULTAN in France supporting AP600 design certification indicate CHF as low as 0.5 MW/m^2 can occur at vessel bottom (see Chapter 13). The low CHF value is a result of the downward facing horizontal angle and local low flow velocity. Once the reactor vessel surface heat flux is below 0.5 MW/m^2 anywhere on the lower head there is no longer a danger of reactor vessel failure from CHF. Assuming all of the corium decay heat leaves through the lower head, water is present in the vessel cavity, and uniform heat flux, the power level with no risk of CHF would be 14.7 MW. From the decay heat formula (see Eq. 5.3) the time from scram is then just over a week, 7.2 days.

Note from the top dashed line of figure 5.12, the expected minimum CHF margin is at the bottom of the molten metal layer that sits above the oxide crusted pool. This 5% CHF margin is based on an experimentally supported correlation developed at UCSB specifically for the AP600 (see Eq. 5.6) [70]. Some of the important parameters influencing CHF along the reactor vessel from bottom moving upwards include: geometry dependent mass flux, decreasing pressure due to gravity head, increasing quality, increasing void fraction, and decreasing bubble surface residence time. Where bubble surface residence time is the time from initiation of bubble growth to departure from the surface.

$$q''_{chf}(\theta) = 490 + 30.2 \cdot \theta - 0.888 \cdot \theta^2 + 1.35x10^{-2} \cdot \theta^3 - 6.65x10^{-5} \cdot \theta^4 \quad \text{Eq. 5.6}$$

The thin 5% margin needed to be increased for the higher power of the AP1000 given that the lower head geometry was the same as the AP600. The AP600 design had a larger gap between the reactor vessel and insulation as well as high frictional losses in the area of the free water line and primary piping. As a result of additional UCSB parametric experimental study, the gap for the AP1000 was reduced to 7.62 cm (3 inches) along the lower hemisphere. Changes were also made to lower frictional losses in the region of primary pipe where steam venting to the upper containment occurs. Together these changes for the AP1000 significantly increased the flow rate and associated CHF by 30% at the metal layer thereby improving the minimum CHF margin. Details of this improvement are discussed in chapter 12.

Experimental work documented herein and previous work at MIT suggests that by adding low concentration alumina nanofluids to the reactor vessel cavity would further increase CHF margin an additional 50%. The higher margin can increase safety of current designs and allow for higher power density for future designs.

6 Two-Phase Flow CHF Loop Description

The main objective of this research is to experimentally examine CHF, with and without nanofluids, with flow conditions expected along the lower vessel head of the Westinghouse AP1000. To that end, a closed two-phase flow loop was designed and built (see Figure 6-1). The primary loop components include: pump, pre-heater, test section, accumulator, condenser, power supply, measurement instrumentation, and data acquisition system. All loop wetted metal components are stainless steel 316L or 304.

Figure 6-1: Schematic of Two-Phase Flow Loop with Downward Facing Test Section

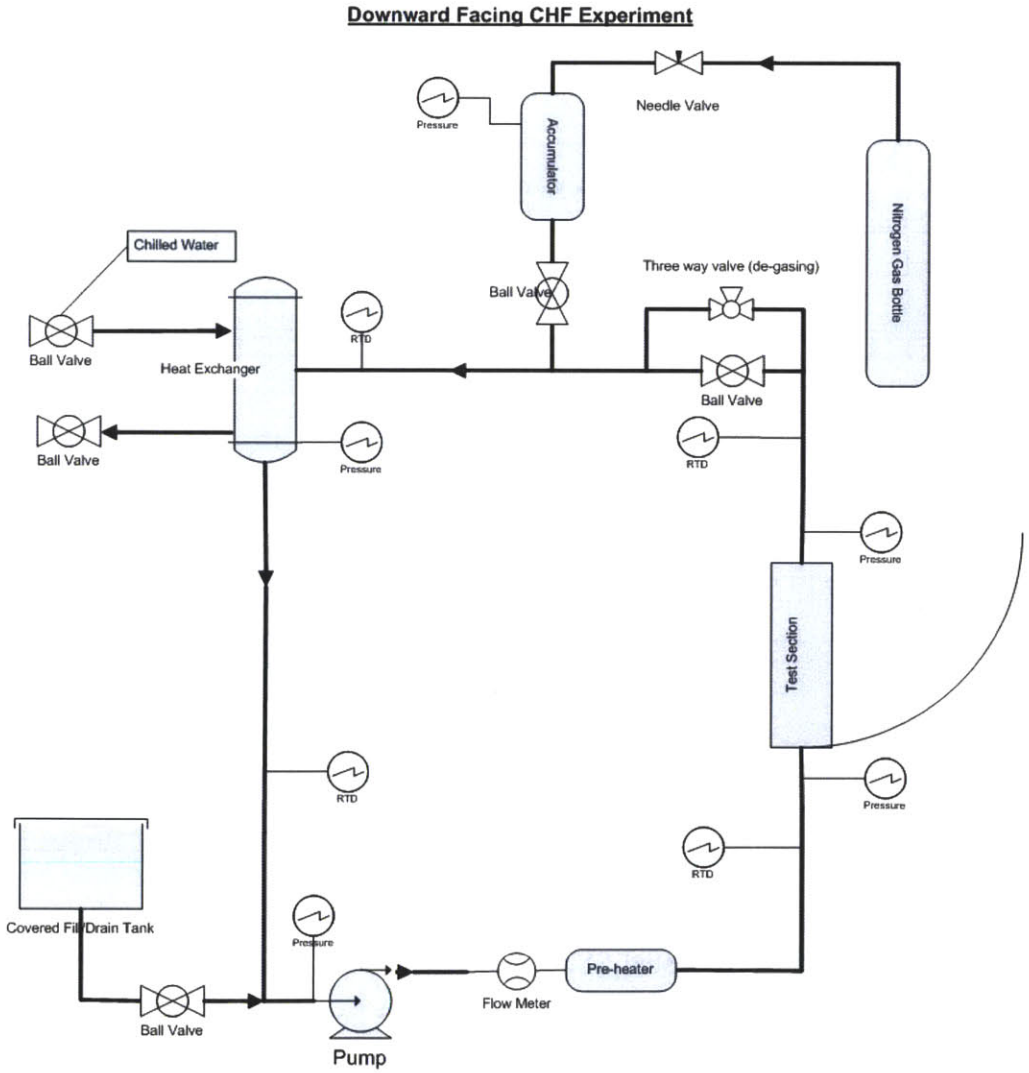

6.1 Test Section and AP1000 IVR Hydrodynamic Similarity

The test section has been fabricated with dimensions that with flow condition control provide a similar CHF environment as the lower hemisphere of the Westinghouse AP1000 vessel. Hydrodynamic similarity for CHF is quantified with the Buckingham Pi-theorem dimensionless comparison [71], as explained in Section 6.1.1.

The test section body material is stainless steel 316. The entrance and exit are 1" NPT female pipe threads. The rectangular flow channel is, 1.43 cm (0.563") wide, 2 cm (0.787") deep, and 31.75 cm (12.5") long (see Figure 6-2).

Figure 6-2: Drawing of Test Section Flow Channel

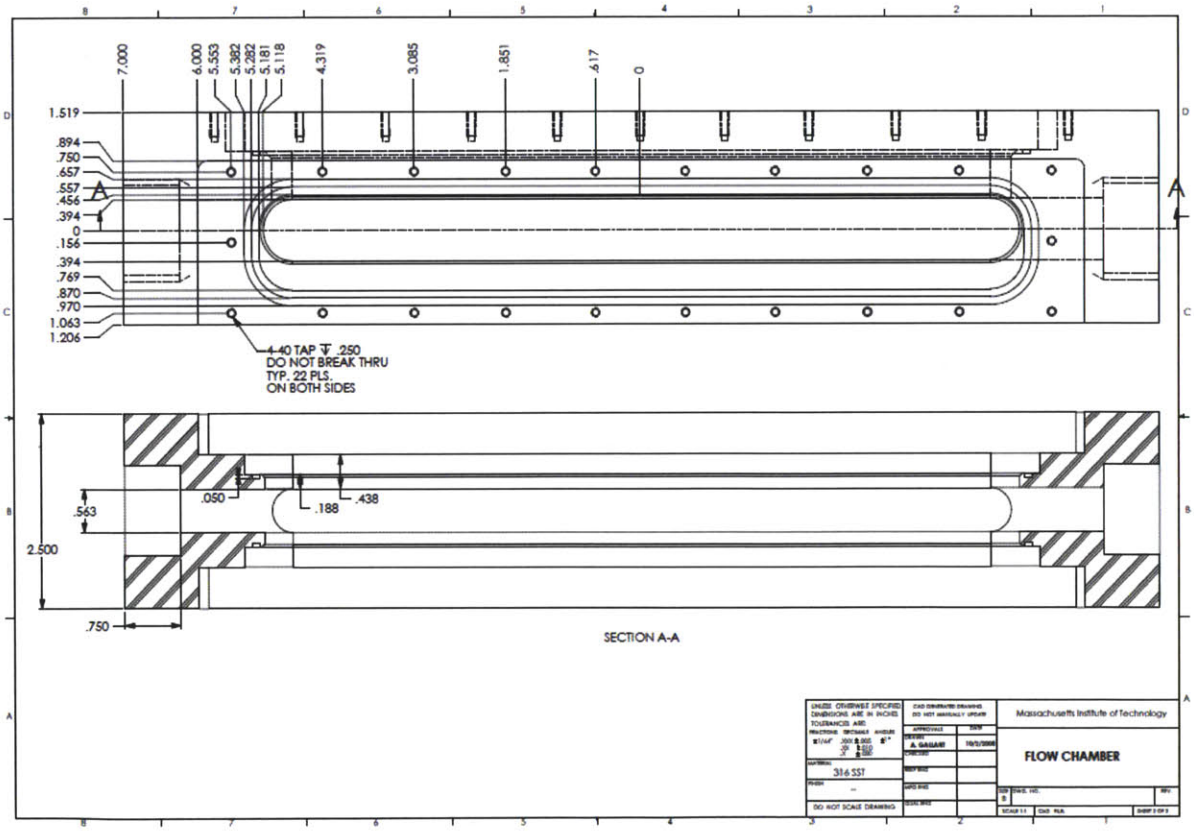

Two sample heater materials are tested SS316L and SA-508. The latter being the low carbon steel material for the AP1000 pressure vessel. The joule heated test sample is 1 cm (0.394") wide and 24 cm (9.449") total length. The heater also has two studs at each end of 2 cm (0.787")

long that copper studs thread into. The plate between the studs is 1.5 mm (0.059") thick (see Figure 6-18). The heater sits in a MACOR insulator that provides both electrical isolation and high thermal resistance to the back and sides. Forced convection is then only from the flow facing surface. Front and back windows allow for visualization.

Note that for surface heat flux calculations the heated area is 1 cm wide (0.394") and 20 cm (7.874") long between the end studs. The heat flux area, A_h, is then $2x10^{-3}$ m^2. This area is appropriate because with joule heating along the plate is significantly greater than within the two end studs (see Section 6.12). This is due to the smaller cross sectional area and larger length along the plate relative to the end studs.

6.1.1 Buckingham Pi-theorem

To establish hydrodynamic similarity of the test section and thermal hydraulic conditions relative to the AP1000 IVR conditions, the Buckingham Pi theorem is applied to the CHF phenomenon. The Buckingham Pi theorem generally states that if a physical process is known to have "n" physical parameters that influence the behavior and "k" fundamental quantities, then the original relationship has an equivalent relationship made up of p = n - k independent dimensionless variables, the π-groups, made up of the original "n" parameters. Noteworthy is the fact that the previous statement holds whether or not the original relationship is known.

CHF in the IVR situation for the AP1000 is expected to be dependent on twelve (12), n, parameters (see Table 6-1).

Table 6-1: List of Parameters Effecting CHF

Parameter	Definition	Units	IVR Range	Notation
q''_{CHF}	critical heat flux	(MW/m^2)	0.5 – 2.0	UCSB [72]
V	local fluid velocity	(m/s)	0.5 – 1.5	UCSB
x_e	local equilibrium quality	dimensionless	from -0.04 to +0.01	Near saturation
θ	Local inclination angle	degrees	0° (horizontal) to 90° (vertical)	Lower Vessel head
δ	gap thickness	(m)	0.076-0.152	3"-6" flow gap
L	channel length (m)	(m)	3.4	Lower head radius = 2.16m
ρ_f	liquid density	(kg/m^3)	940 – 960	Near saturation
ρ_g	vapor density	(kg/m^3)	0.6 – 1.1	Near saturation
σ	surface tension	(N/m)	0.055 – 0.059	Near saturation
μ_f	liquid viscosity	(Pa·s)	$2.3\times10^{-4} - 2.8\times10^{-4}$	Near saturation
h_{fg}	heat of evaporation	(kJ/kg)	2,200 – 2,260	Near saturation
G	acceleration of gravity	(m/s^2)	9.81	constant

The variation in water properties is due to the pressure variation along the vessel surface during the IVR event. Once the reactor has depressurized from the initiating event, likely LOCA, the water flooding the vessel cavity from the IRWST will provide gravity head of up to 6.1 m (~20 feet), with liquid only within the downcomer portion of the natural circulation path (see Figure 6-3). If the containment is atmospheric the bottom of the lower head pressure would then be ~1.6 bar.

Figure 6-3: AP1000 Natural Circulation Path for IVR

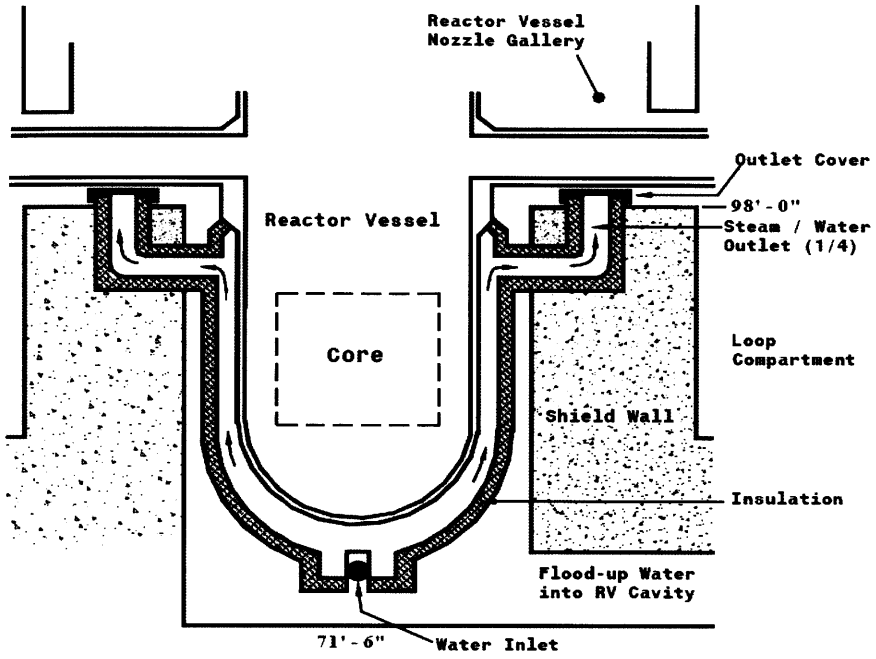

A conservative estimate of exit quality, χ_e, can be calculated by assuming the water surrounding the vessel at the earliest time of corium formation is saturated at atmospheric conditions (see Eq. 6.3) [73].

$$\chi_e = \frac{Q_{decay}(t)}{h_{fg} \cdot \dot{m}_{gap}} \qquad \text{Eq. 6.1}$$

The mass flux in the gap is estimated by taking the volumetric flow rate, β_{gap}, from the UCSB work, 0.915 m^3/s (14500 gpm), with atmospheric density and heat of evaporation from the range (see Table 6-1). This is also consistent with communications with Westinghouse [74].

$$\dot{m}_{gap} = \rho \cdot V \cdot A_{gap} = \rho \cdot \beta_{gap} \qquad \text{Eq. 6.2}$$

Where:

$$A_{gap} = \pi \cdot (r + \delta)^2_{vessel} - \pi \cdot r^2_{vessel} \qquad \text{Eq. 6.3}$$

r_{vessel}	=	2.16 m
δ	=	15.24cm (6")
ρ	=	960 kg/m^3
h_{fg}	=	2260 kJ/kg
A_{gap}	=	2.14 m^2

The resulting estimated mass flow rate is then ~878 kg/s. Next, as discussed in more detail in chapter 5 the earliest time to corium formation is about two (2) hours.

$$Q_{decay}(t = 2\ hours) = 0.0495 \cdot (3415MW) \cdot (7200^{-0.2}) \qquad \text{Eq. 6.4}$$

$$Q_{decay}(t = 2\ hours) = 28.6\ MW$$

Assuming all of Q_{decay} heats the water, exit quality, χ_e, is then estimated to be 0.014. At this relatively low level of quality the type of boiling crisis would tend to DNB type.

Next, as a quick estimate of exit void fraction, α_{exit}, can be made utilizing the Martinelli-Nelson model that covers the range of pressure and flow rates of interest (see Eq. 6.5) [75][76].

$$1 - \alpha_{exit} = \frac{X_{tt}}{\sqrt{X_{tt}+20 \cdot X_{tt}+1}} \qquad \text{Eq. 6.5}$$

With Martinelli-Nelson parameter X_{tt} equal:

$$X_{tt} = \left(\frac{\mu_f}{\mu_g}\right)^{0.1} \cdot \left(\frac{1-\chi}{\chi}\right)^{0.9} \cdot \left(\frac{\rho_g}{\rho_f}\right)^{0.5} \qquad \text{Eq. 6.6}$$

Where:

χ = χ_e , with gap exit flow at thermal equilibrium.

Substituting, results in X_{tt} equal to 1.58 and α_{exit} of 73%. Note that visual observation of void fraction near CHF and IVR conditions within the herein described test section is about 70% (see Figure 6-4). Void fraction on the order of 70%+ with mass flux less than 2000 kg/m^2-s indicates transition to annular flow regime. This level of void could be sufficient for dry-out type CHF.

Figure 6-4: Photo of Test Section Void near CHF Conditions

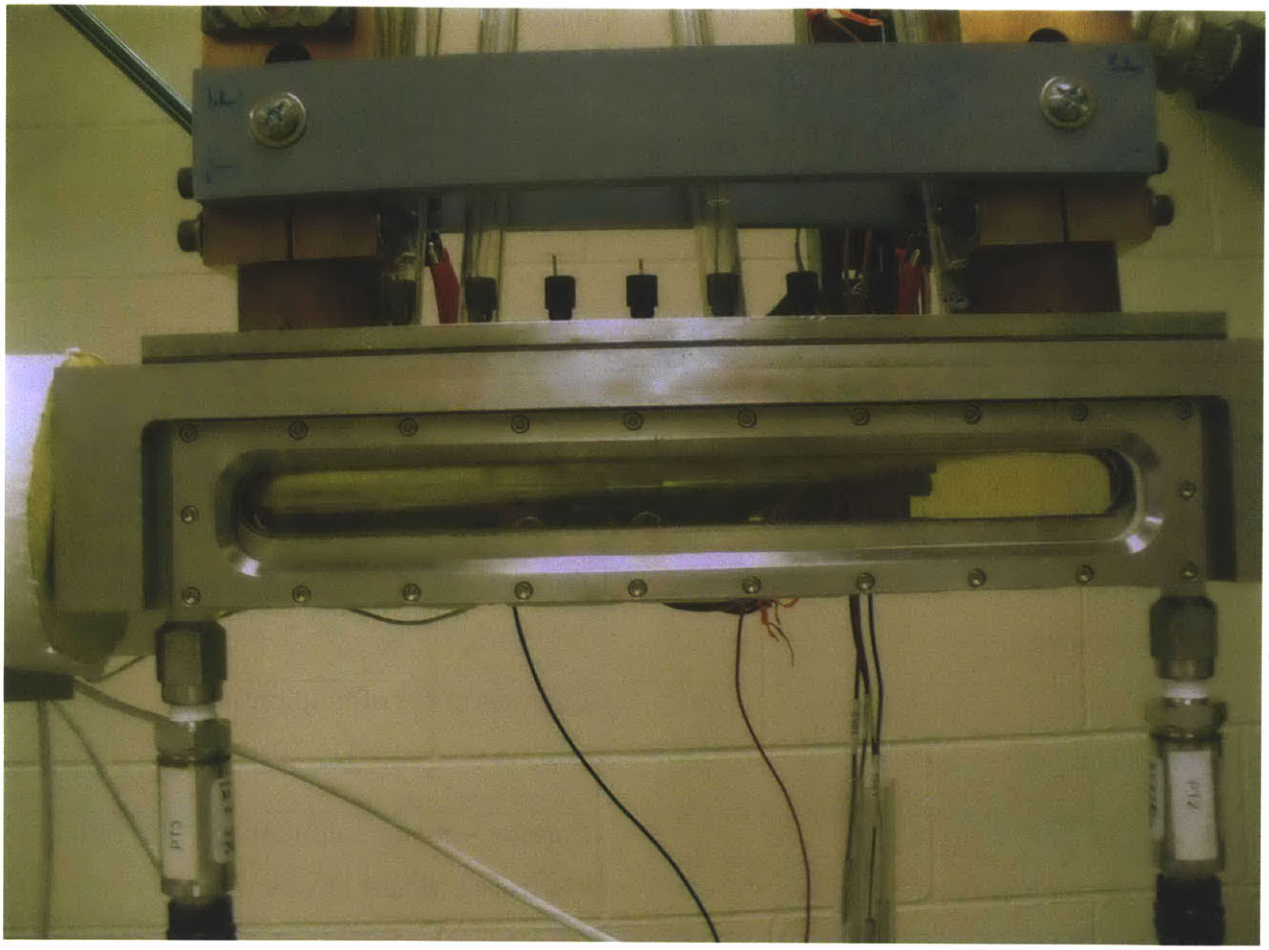

The twelve (12) listed parameters have three fundamental measures, k: time, length and mass. From the Buckingham Pi-theorem, nine (9) independent dimensionless groups, p, then need to be defined. Rigorously Buckingham Pi-theorem does not define the pi-groups or their number. From dimensional analysis, below are listed nine (9) independent groups that have physical meaning to CHF (see Table 6-2).

Table 6-2: List of Independent Dimensionless Groups Relevant to CHF

Pi Dimensionless Group	Relation	Physical meaning
Reynolds number	$Re = \frac{\rho_f V D_e}{\mu_f}$	Inertia forces to viscous forces ratio
Density ratio	$\frac{\rho_f}{\rho_g}$	Relative density
Channel aspect ratio	$\frac{L}{\delta}$	Flow development
Local equilibrium quality	χ_e	Enthalpy content of the flow
Local inclination angle	θ	Gravity influence on buoyancy
Normalized CHF	$\frac{q''_{CHF}}{\rho_f V h_{fg}}$	CHF normalized to dynamic heat of vaporization
Froude number	$Fr = \frac{V^2}{g\delta}$	Ratio of inertia to gravitational forces
Morton number	$Mo = \frac{g\mu_f^4}{\sigma^3 \rho_f}$	Captures effect of fluid properties.
nameless number	$\frac{\sigma}{\mu_f \sqrt{h_{fg}}}$	Surface tension normalized to liquid viscosity and heat of vaporization

Because of their important physical interpretation for boiling, the following two (2) pi-groups are also considered: Bond number and Weber number.

$$Bo = \frac{\rho_f g \delta^2}{\sigma}: \qquad \text{Bond number} \qquad \text{Eq. 6.7}$$

$$We = \frac{\rho_f L_b V^2}{\sigma} : \qquad \text{Weber number} \qquad \text{Eq. 6.8}$$

Where, $L_b = \sqrt{\frac{\sigma}{\rho_f g}} \approx 2.5$ mm, at the conditions of interest is the Laplace length, an intrinsic boiling scale.

It can be easily shown that the Bond number, *Bo,* and Weber number, *We,* are not independent from the other nine (9) pi-groups, as they can be obtained from combinations of *Fr*, *Re*, and *Mo*.

For the IVR application in AP1000 the typical ranges of the pi-groups are shown in the second column of Table 6-3 and compared to the test section values in the third column.

Table 6-3: Value Ranges for Pi-groups for CHF in IVR for AP1000 and Test Section

Pi-group	**AP1000 IVR range**	**Test Section**	**Comments**
$\frac{q''_{CHF}}{\rho_f V h_{fg}}$	$4.9\times10^{-4} - 9.2\times10^{-3}$	~ Same	From Buckingham Pi theorem
Re	$6.9\times10^{5} - 10.4\times10^{5}$	$2.7\times10^{4} - 7.7\times10^{4}$	Turbulent flow
$\frac{\rho_f}{\rho_g}$	825 – 1600	340 – 1600	1 to 2 atmospheres for IVR 1 to 5 atmospheres of test matrix
$\frac{L}{\delta}$	22	16	Flow not fully developed
Fr	0.17 – 0.70	1.3 – 5.1	~1 ⇒ buoyancy forces are important to bubble dynamics
Mo	$0.9\times10^{-13} - 4.5\times10^{-13}$	0.9×10^{-13}–4.5×10^{-13}	Similar bubble shape in flow
$\frac{\sigma}{\mu_f \sqrt{h_{fg}}}$	0.14 – 0.17	0.14 – 0.17	Bounded
x_e	-0.04 – +0.01	-0.04 – +0.01	DNB is the CHF mechanism
θ	0° – 90°	0° – 90°	Hemisphere
Bo	3,700 – 4,100	64 – 69	>>1 ⇒ Capillary forces are negligible
We	11 – 41	11 – 41	>>1 ⇒ Inertial forces dominate bubble dynamics

The Buckingham Pi theorem requires that the nine (9) independent pi-groups are related by a unique function:

$$\frac{q''_{CHF}}{\rho_f V h_{fg}} = f\left(\mathrm{Re}, \frac{\rho_f}{\rho_g}, \frac{L}{\delta}, Fr, Mo, \frac{\sigma}{\mu_f \sqrt{h_{fg}}}, x_e, \theta\right) \qquad \text{Eq. 6.9}$$

Therefore, to establish the CHF similarity between the IVR situation for the AP1000 and the two-phase loop experimental test section, one needs to match the values of the eight (8) pi-groups on the right hand side of Eq. 6.9.

The test section will operate from atmospheric pressure up to five (5) atmospheres, absolute. This covers the conditions expected during IVR, so the pi-groups based only on properties (i.e., $\frac{\rho_f}{\rho_g}$, M, $\frac{\sigma}{\mu_f \sqrt{h_{fg}}}$) are then matched. The IVR event is only expected to range from 1 to 2 atmospheres. The 5 atmosphere test bounds the AP1000 containment design limit.

The quality, x_e , and the angle, θ, are matched by controlling the tests section inlet sub-cooling, power, and inclination, respectively.

The pump driven mass flux range (G=500 to 1500 kg/m^2-s) driving test section fluid velocity (V = 0.5 – 1.5 m/s), gap size (δ = 2 cm) and channel length (L = 31.75 cm) insure, the remaining pi-groups (Re, L/δ, Fr, plus Bo and We) are such that the key physical phenomena are preserved. In summary, the test section flow is turbulent and not fully developed, gravity is not negligible, and capillary effects are small.

Therefore, Eq. 6.9 then suggests that the normalized CHF, ($\frac{q''_{CHF}}{\rho_f V h_{fg}}$), in the test section and in the actual IVR situation should be about the same. However, because the velocity range in the test section and IVR situation is the same, the actual value of the CHF is also expected to be about the same.

Finally, a test section flow width of at least 14.3mm and depth of 20 mm should be sufficient to eliminate edge effects, as the Laplace length is only 2.5 mm.

6.2 Flow Loop Design

A Grundfos 2 Hp centrifugal pump drives flow around the 8.8 m [29'] loop (see Figure 6-5). Mass fluxes of interest at the test section are 500, 1,000 and 1,500 kg/m^2-s and translate to velocities entering the test section of approximately 0.5, 1.0 and 1.5 m/s, respectively.

Figure 6-5: Photo of Two-Phase Flow Loop with Downward Facing Test Section

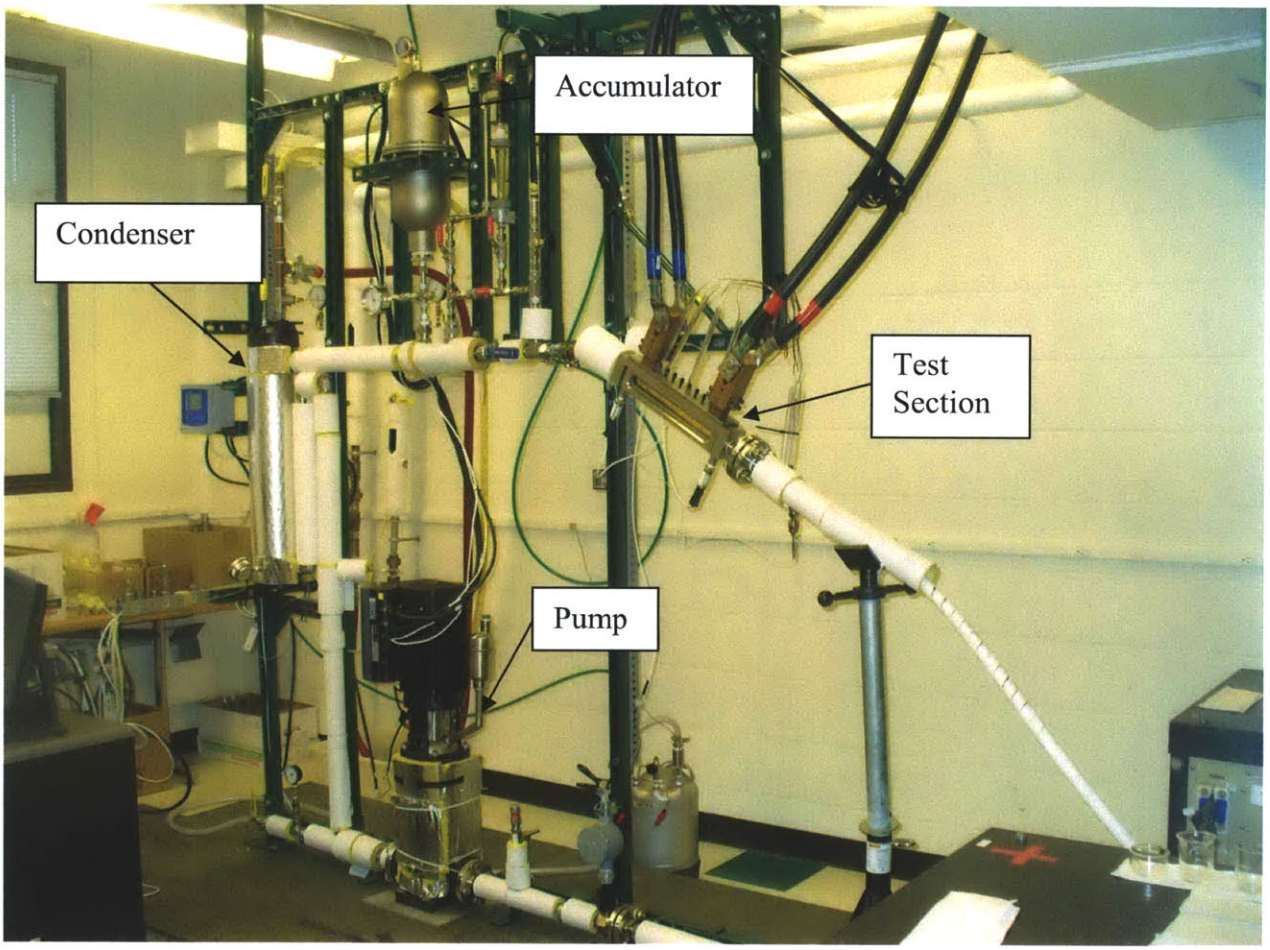

Two (2) direct current (DC) power supplies provide joule heating to the test sample within the test section. The two 18 kW power supplies made by Electronic Measurements, Inc. [Model: EMP 480] are driven by 480 Volt 3-phase and each are capable of delivering up to 30 Volts and 600 amperes of maximum current. The pair of power supplies are coupled in parallel to the test

section (see Figure 6-6). Four (4) identical locomotive cables of 3.05 cm (1.2") outer diameter, two for each DC power supply, attached to machined copper couplings (2) that in turn attach to the copper stubs (2) at each end of the test section.

Figure 6-6: Photo of Power Supply Coupling to Test Section

Downward facing angles (relative to gravity) of the heated test sample with parallel flow are accomplished with a combination of flexible tube and 90° elbow compression fittings (see Figure 6-7). All angles from horizontal ($\theta = 0^{o}$) to vertical ($\theta = 90^{o}$) are possible. The flex tube is comprised of a viton tube (3/4" OD) within a stainless steel mesh and compression to NPT adaptor fittings at both ends.

Figure 6-7: Photos of Test Section at 0°, 45° & 90°

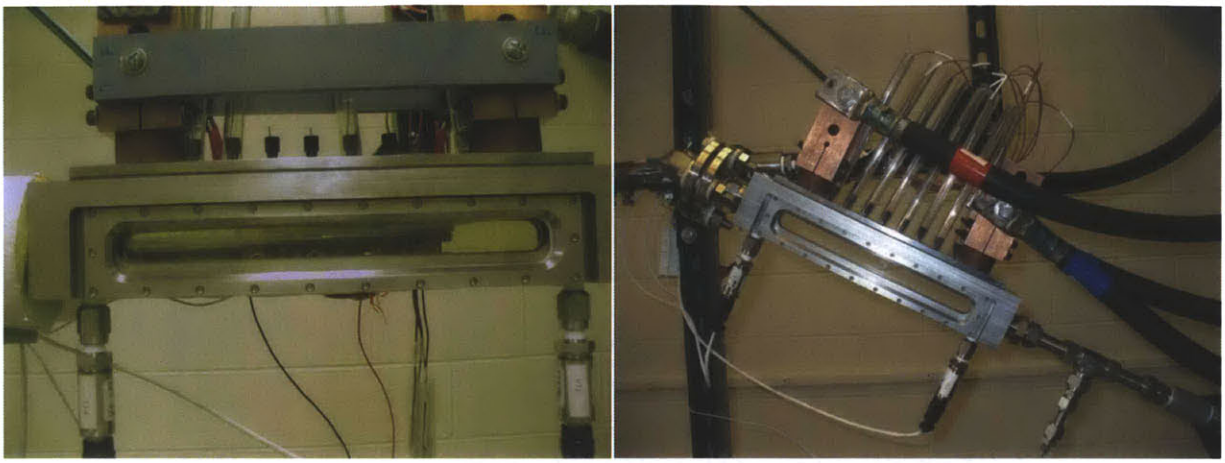

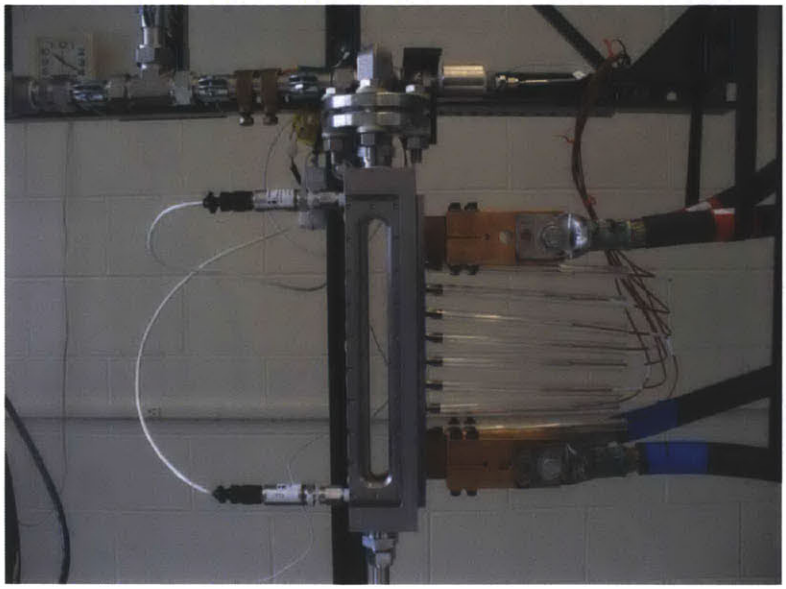

Volume expansion of the working fluid upon boiling and up to the critical heat flux limit is accommodated via an accumulator that contains a Viton bladder with nitrogen or air as the cover gas (see Figure 6-8). Total expansion volume of the accumulator is 6.1 liters (1.6 gallons). The Viton bladder material was chosen to accommodate the maximum design fluid temperature of 153 °C, which equals the saturation temperature at 5 atmospheres. The bladder type accumulator was chosen so to minimize non-condensable gas diffusion into the working fluid while not being as heavy as a bellows type.

Figure 6-8: Photo of Accumulator on Loop

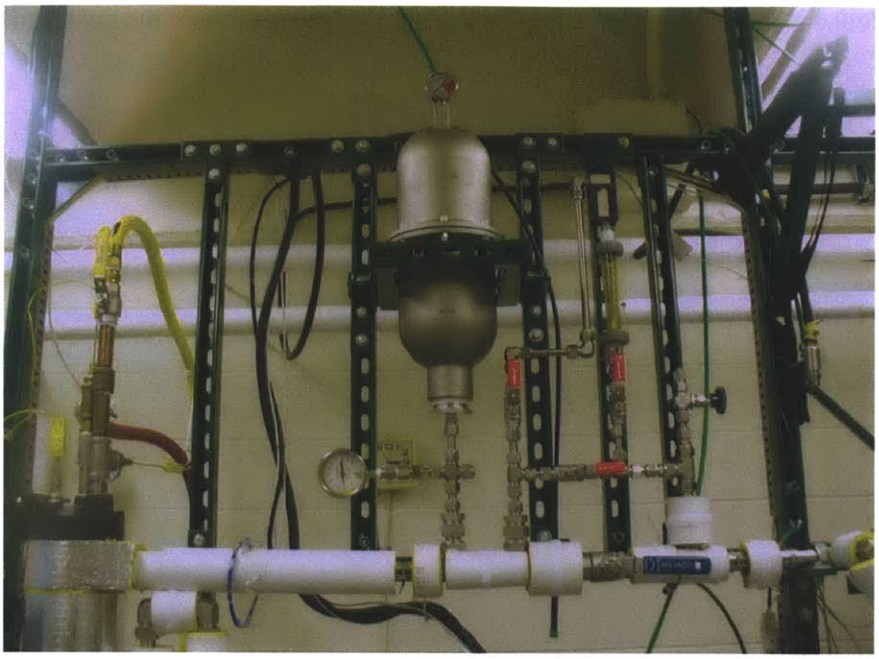

Above the bladder, gas pressure is maintained with a nitrogen gas-bottle, feed regulator, and a backpressure regulator (release) in series right to left (see Figure 6-9).

Figure 6-9: Photo of Nitrogen Gas Bottle, Feed Regulator, and Back-pressure Regulator

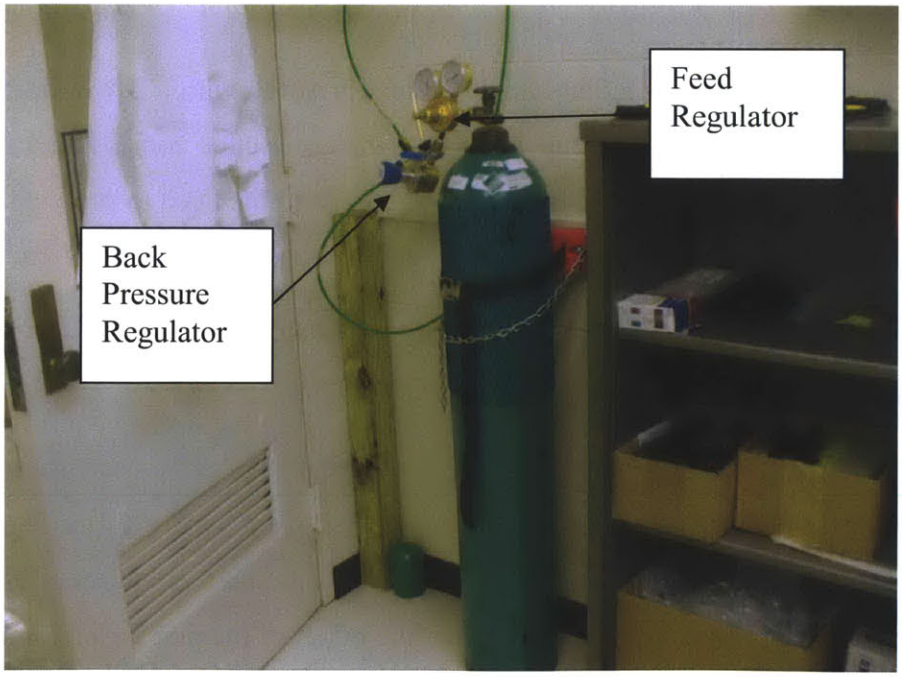

The heat sink for the loop is provided by a shell and tube condenser (see Figure 6-10). Chilled water is provided via the building cooling system and flows through the inside of the condenser stainless steel tubes. Condensation occurs within the shell on the tubes. Single phase fluid is returned to the pump.

Figure 6-10: Photo of Condenser and Chilled Water Lines

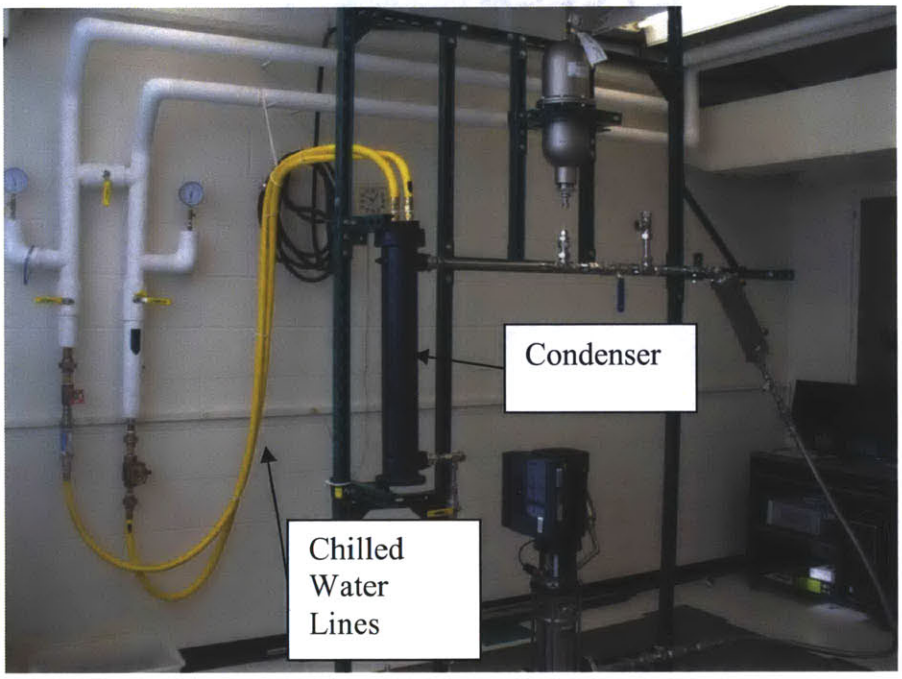

Between the pump and the test section entrance, heat is added with a 2 kW immersion heater. The need for heat addition after the pump and before the test section comes about from the desire to have the entrance conditions at or very near saturation and the need to protect the pump from cavitations. The maximum surface heat flux for the immersion heater is 9.4 W/cm^2 (61 W/in^2).

6.3 Design Parameters

The flow loop design allows for pressures up to 10 bar gauge (150 psig). The experimental matrix will only require up to 5 bar absolute (75 psia). Note that a safety relief valve with a lift setting of 14 bar gauge (140 psig) is installed near the outlet of the pump (see Figure 6-11). The maximum design temperature for the bulk fluid is 180 °C (pump limited). The experimental

matrix will only require bulk fluid temperatures up to 153 °C. The pump can deliver up to 58.4 liters per minute (15.4 gpm) with a minimum flow rate of 8.3 liters per minute (2.2 gpm). The range of interest is 8.3 to 28.4 lpm (2.2 gpm to 7.5 gpm). The chilled water system provides cold water at approximately 10 °C and with a supply pressure of ~6.6 bar gauge (100 psig) and volumetric flow rates from 7.6 to 33 liters per minute (2 to 13 gpm). Materials in contact with the working fluid are non-corrosive in the range of 4 to 10 pH for the working fluid.

Figure 6-11: Photo of Loop Pressure Relief Valve

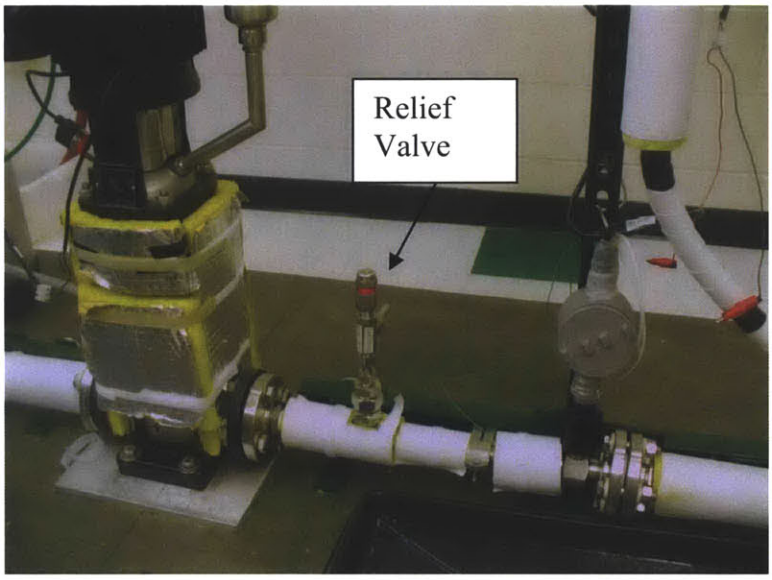

6.4 Geometry

The downward facing CHF loop is basically a rectangle that allows one side to swing via flexible tube and compression fittings. (see Figure 6-5 and Figure 6-12). The loop path length is 8.8 m [29']. The elevation change of the flow tubing is about 1.45 m [4.75'].

The flow loop components hang from a Unistrut superstructure that is attached to a (1.22 m x 2.44 m) (4'x8') raised floor and the ceiling. The raised floor allows wiring to run below without becoming a tripping hazard.

Figure 6-12: Photo of Test Loop with Vertical Test Section Orientation

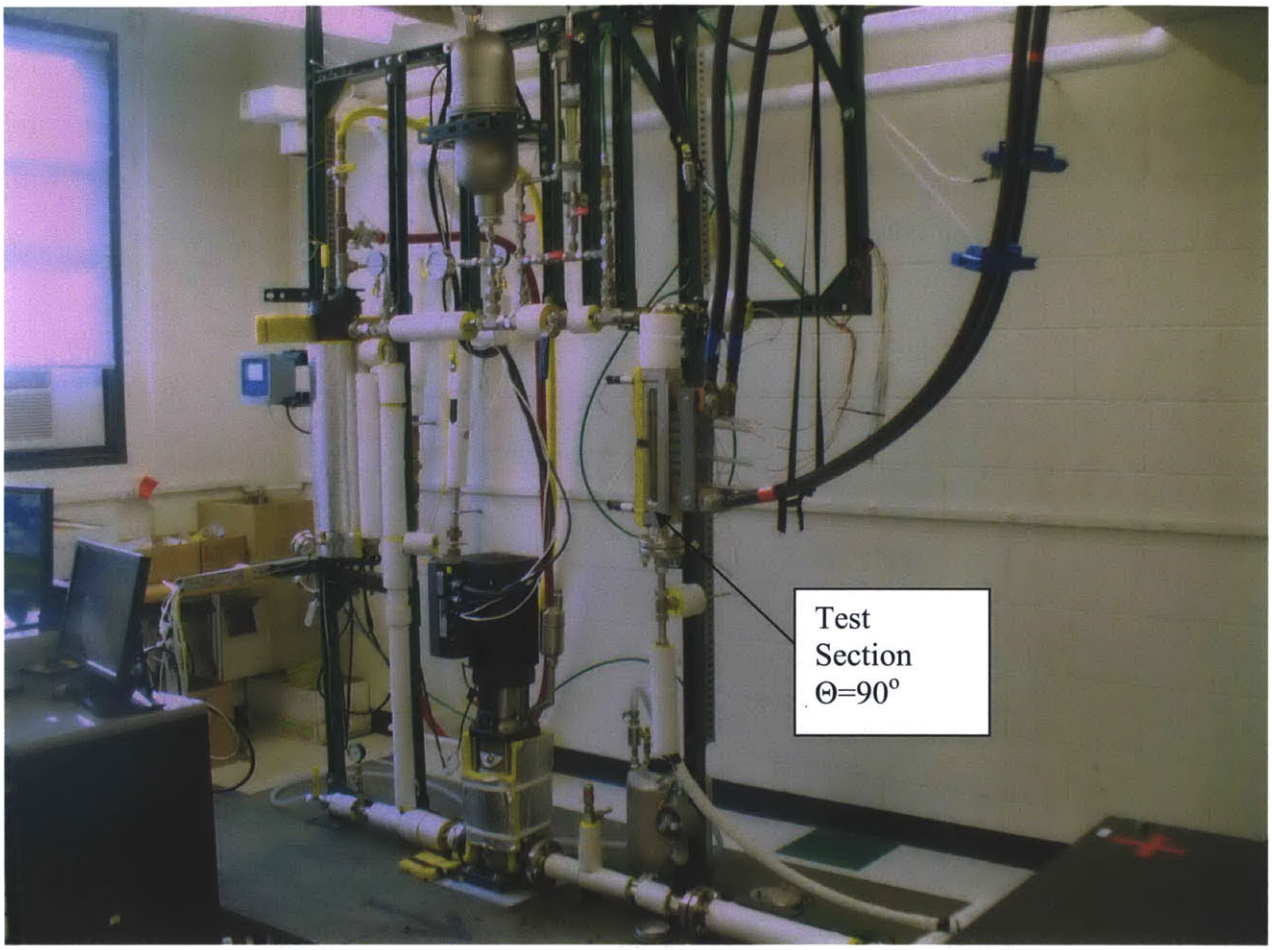

The pump is basically the bottom, center of the loop. Single-phase flow leaves the pump moving right as you face the loop with the test section to the right. The pressure relief valve sits between the pump and the turbine flow meter. Flow travels a 2.54 cm (1") stainless steel tube toward a 1" NPT turbine flow meter. Exiting the turbine flow meter the tube size is again 1". The 2 kW pre-heater piping is 1 ¼" NPT. This is next reduced to ¾" NPT to accommodate flexible tube via adapting fitting. The 2.1 m (7') flexible tube then transitions to straight tube and enters the test section.

The test section is 35.56 cm (14" inch) length with a rectangular flow channel and 1" NPT female pipe fittings on each end. The test section out fitting adapts to 2.54 cm (1") tube and couples to two 90° elbows in series that allow the test section to swing through all angles. The

1.9 cm (¾") feed to the test section and 2.54 cm (1") exit help with flow stability by acting as a relative flow restriction [77]. Visualization indicated steady flow near nearly saturated CHF conditions.

.

Along the 1.5 m (5') length of 2.54 cm (1") tube carrying the fluid from the test section exit region toward the condenser, an accumulator is tied into the loop. The accumulator stands about 0.3 m (1') above the flow loop linked with a 1.27 cm (½") stand tube that is perpendicular to loop flow.

The condenser is mounted with tubes in vertical orientation. Loop flow enters the upper portion of the shell perpendicular to the tubes. Within the 0.61 m (2') elevation drop from the center of the entrance, flow is returned to slightly sub-cooled conditions. Once out of the condenser the flow turns upward for 0.61 m (2') and then turns downward for 1.22 m (4') of elevation drop to the entrance to the pump. This provides needed Net Positive Suction Head ("NPSH") for the near saturation fluid and allows more time for conditions to equilibrate and bubbles to collapse.

Above the main loop, smaller diameter 1.27 cm (1/2") tubing provides for vacuum suction line attachment, degassing and dissolved oxygen measurement. Ball valves isolate this upper portion of the loop during the CHF portion of experiments.

6.5 Components

Five (5) major components comprise the two-phase flow loop that provide flow, thermal power, steady static system pressure, and heat removal: 1) pump, 2) pre-heater, 3) test section, 4) accumulator and 5) condenser.

6.5.1 Pump

The pressure force driving the working fluid flow is created with a Gundfos centrifugal pump [Model: CRNE3-12 X-FGJ-G-F-HQQE]. The 2 Hp pump can deliver up to 58.4 liters per minute (15.4 gpm). The experimental matrix requires volumetric flow rate range of 9.5 to 28.4 liter per minute (2.5 to 7.5 gpm). The 12 blade design allows for minimum Net Positive Suction Head ["NPSH"] of 0.61 m (2') for highly sub-cooled conditions and 1.22 m (4') for near saturation conditions. The pump also has a cooling top that allows for higher temperature operation. The maximum operating temperature with the Cool-top operating is 180 °C [356 °F].

The pump incorporates a control feedback with a downstream turbine flow meter. This allows for a volumetric flow rate to be set and maintained at the test section entrance throughout the experiment and importantly final stages of the CHF run-up where pressure drop increases as void fraction increases. As the pressure drop around the loop increases due to increased boiling the pump adjusts the pumping power to maintain a constant volumetric flow rate. Note that by operational design, single phase liquid transits the pump and enters the test section.

The pump also can be operated in a manual mode. In manual mode the pump power is altered to achieve the desired mass flux.

6.5.2 Pre-heater

A pre-heater has been incorporated into the two-phase loop design (see Figure 6-13). The requirement for a pre-heater comes about from the desire to have the working fluid enter the test section at near saturated conditions and the need to protect the pump from cavitations.

To achieve these objectives the working fluid entering the pump is kept 2 °C to 4 °C below saturation depending on flow rate. This temperature is controlled by varying the chilled water flow in the condenser. Heat is then added downstream of the turbine flow meter with either strap heaters or the immersion heater. Most tests run utilized only immersion preheating. These pre-

heaters can provide up to two (2) kilowatts of thermal energy to help bring the working fluid up to near saturated conditions at the test section entrance. At maximum, the pre-heater surface heat flux equals 94.5 kW/m^2 (61 W/in^2). This heat flux will produce little boiling even near saturated conditions and pump minimum flow.

Figure 6-13: Immersion Pre-heater on Test Loop

6.5.3 Test Section

The test section design was developed through scaling analysis to simulate the thermal and hydraulic conditions of the water flow on the outer surface of the reactor vessel of the AP1000, as discussed in chapter 6.1 above. The test section is rectangular with two windows front and back to allow for visualization of flow boiling adjacent to the heated sample (see Figure 6-14). Test section body outer dimensions are: length = 33.56 cm (14"), width = 7.62 cm (3"), and depth = 10.16 cm (4") (see Figure 6-15).

Figure 6-14: Photo of Test Section Body

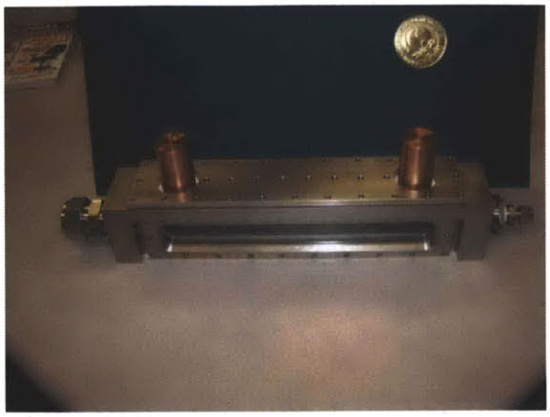

Figure 6-15: Drawing of Test Section Body

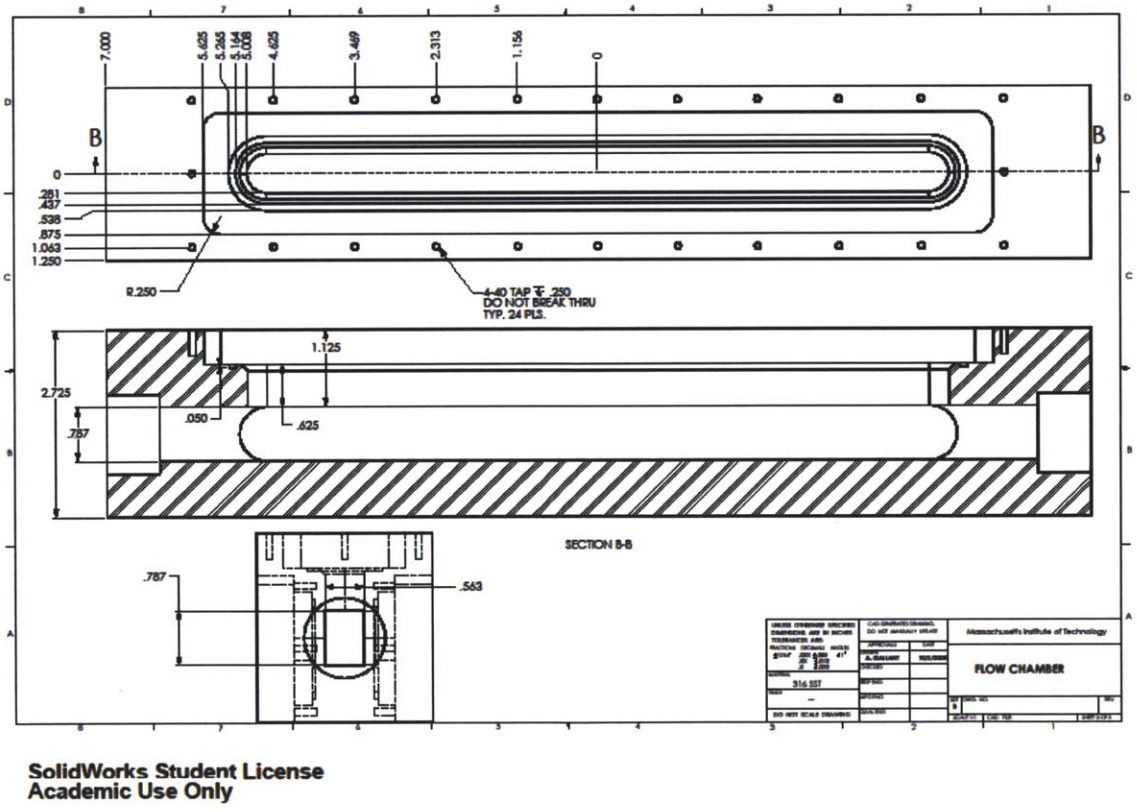

The test section material is stainless steel 316L. Machining provides for a smooth rectangular flow channel (1.43 cm x 2 cm x 31.75 cm). On one side, a test sample lays within a ceramic

insulator. The opposite side has two small (1/16") pressure taps at the entrance and exit. The two windows complete the rectangular channel (see Figure 6-16).

Figure 6-16: Photo of Test Section Assembly

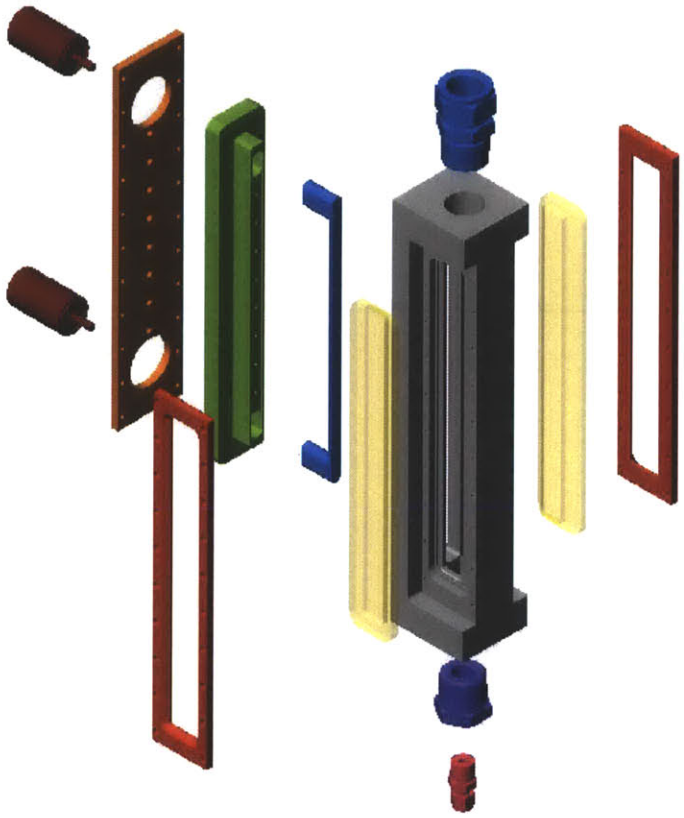

The test heater sample is basically a flat plate with studs at each end to provide for coupling to DC current (see Figure 6-17). The heater then sits within an insulator that directs heat flux out the surface exposed to the fluid flow. The heater flow facing dimensions are 1 cm width, 24 cm long, and 1.5 mm thickness (see Figure 6-18). The heated length between the studs is 20 cm. Electrical DC current flows into the test sample through two (2) copper studs with threaded leads (see Figure 6-19). O-rings on each copper stud provide a water tight seal.

Figure 6-17: Photo of Test Heater Sample

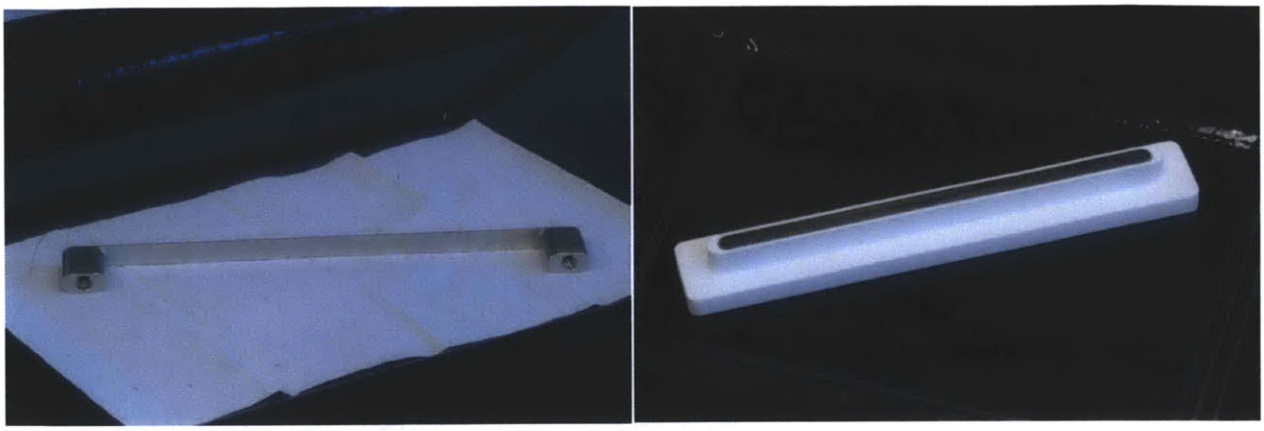

Figure 6-18: Drawing of Heater

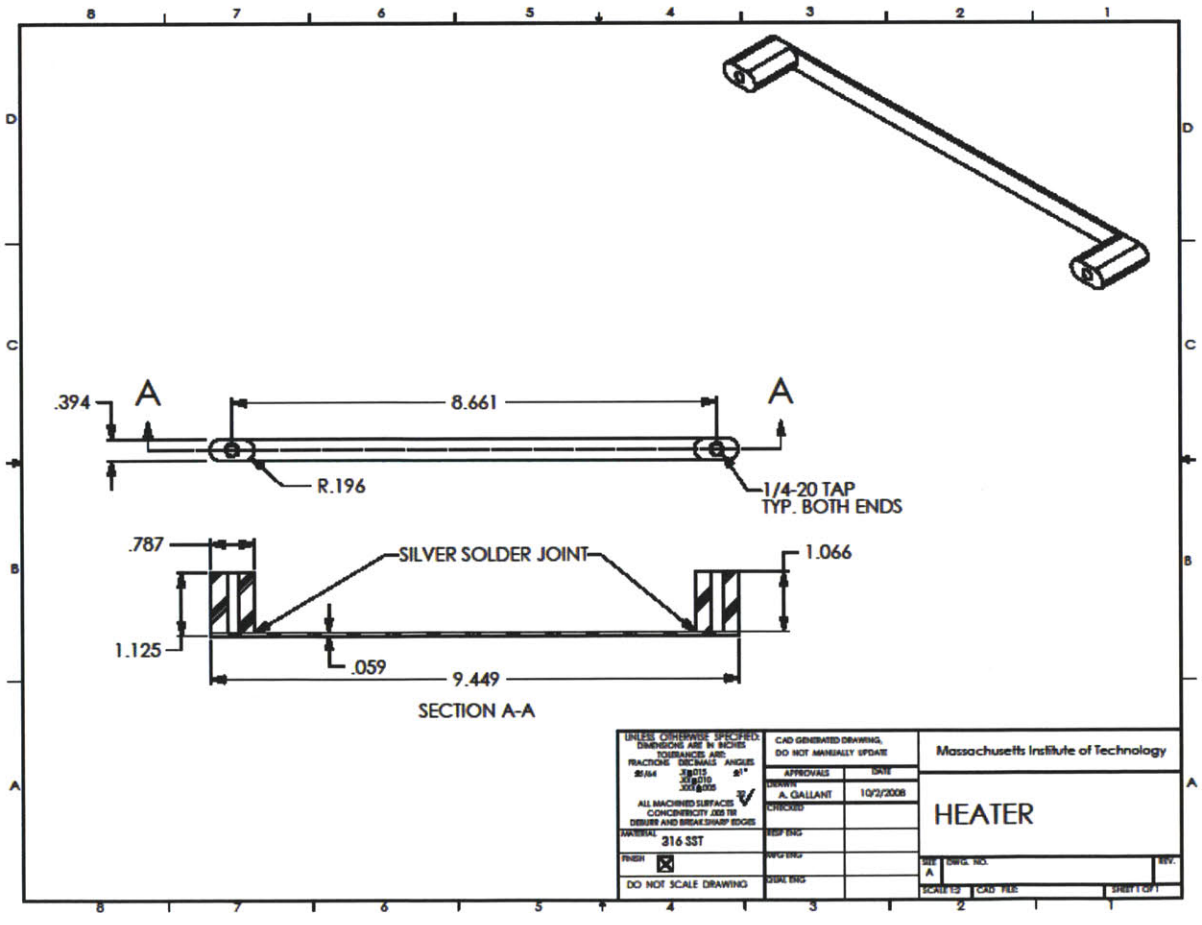

Two materials are used for test samples: stainless steel 316L and SA508. SA508 is the carbon steel used for the Westinghouse AP1000 pressure vessel. Each test sample undergoes preparation before use as more fully described in chapter 7.

Figure 6-19: Photo of Copper Stud with O-ring

The white ceramic insulating block is made of MACOR (see Figure 6-20). The insulating block provides both electric and thermal insulation between the test sample and the body of the test section. The insulating block is highly machined providing troth for the test sample that insulates the back and sides of the heater thereby focusing heat transfer out of the heater from the front surface. The insulator has eight equally spaced 2.39 cm (0.94") holes 1.6 mm that allow 1 mm OD type-K thermocouples to pass through the insulator and touch the back of the heater (see Figure 6-21). MACOR properties of interest are listed below (see Table 6-4).

Figure 6-20: Photos of MACOR Insulating Block

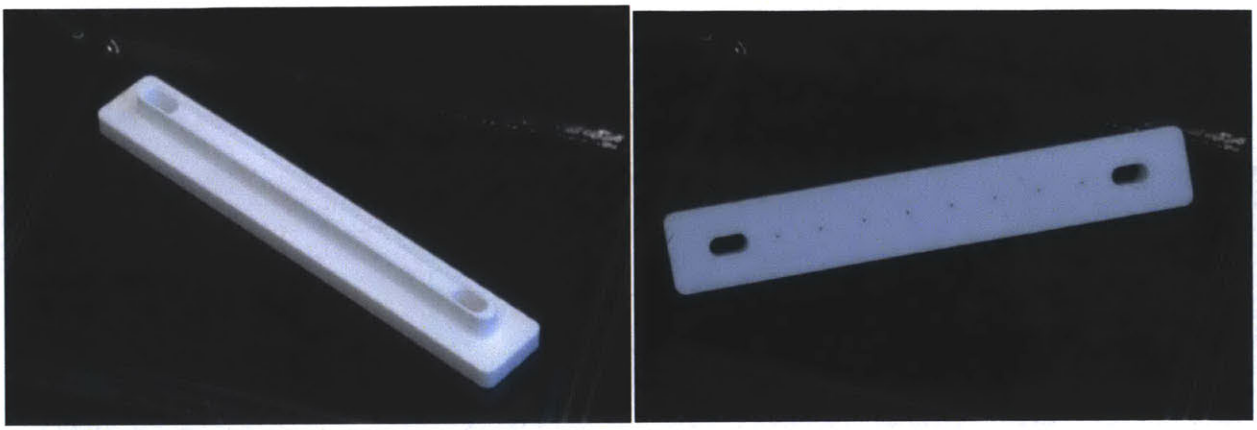

Figure 6-21: Drawing of MACOR Insulating Block

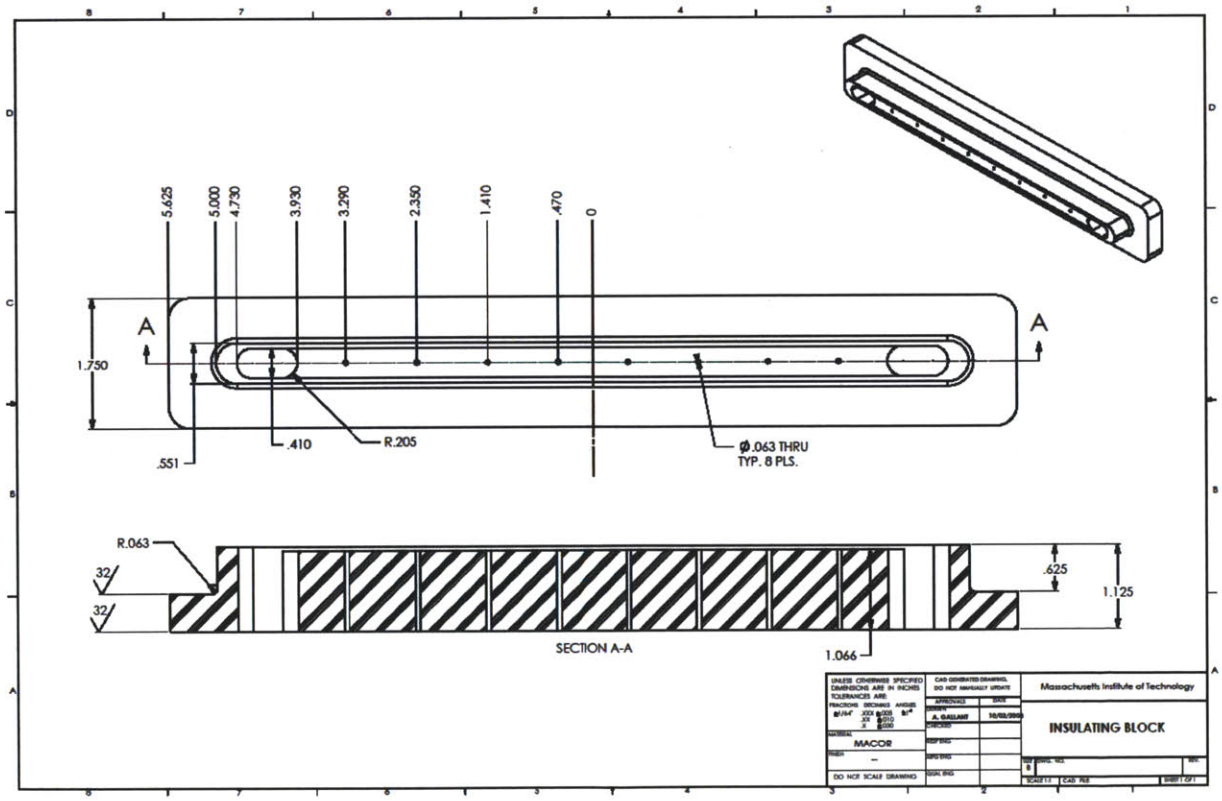

Table 6-4: MACOR Physical Properties

Density	ρ	$= 2.52\ g/cm^3$
Thermal Conductivity, 25 °C	k	= 1.46 W/m-°C
Thermal Diffusivity, 25 °C	α_{th}	$= 7.3x10^{-7}\ m^2/s$
Electrical Resistivity	ρ_{el}	$= >10^{16}\ \Omega$-cm
Expansion Coefficient (25-300 °C)	β_{exp}	$= 93x10^{-7}\ (\Delta V/V)$ / °C
Young's Modulus, 25 °C	E	= 66.9 GPa

Windows on two sides of the test section are made of either quartz or Thermalux (see Figure 6-22). The advantage of quartz is the high transparency, low thermal expansion and strength. The advantage of Thermalux is the non-brittle nature of the high temperature polymer and lower cost. Thermalux does have a yellow tint though very clear. A flat gasket and frame hold the window onto the test section body and provide a water tight seal.

Figure 6-22: Photo of Thermalux Window

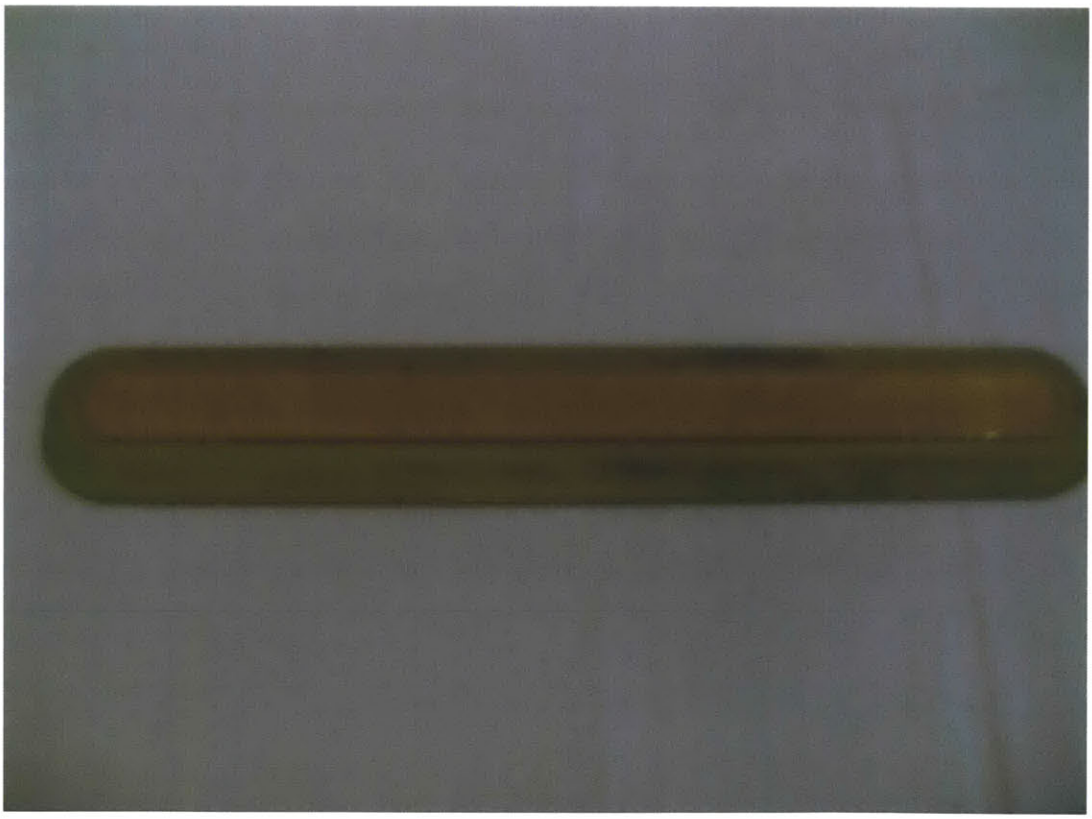

At each end of the test section body 1" NPT female taps are provided.

6.5.4 Accumulator

An accumulator [Blacoh CT2420V] is designed onto the loop to accommodate volume expansion of the working fluid from initial room temperature conditions through heavy boiling that accompanies CHF near saturated conditions (see Figure 6-23). The volume of the Blacoh accumulator allows for 6.06 liters (1.6 gallons) of expansion, which represents about half of the main two-phase loop volume (see Table 6-5). The bladder diaphragm material within the accumulator is Viton.

Table 6-5: Accumulator Dimensions

Length	50.8 cm (20")
Inner Diameter	20.32 cm (8")
Volume	6.06 liters (1.6 gallons)
Bladder Material	Viton
Shell Material:	SS316L

A bladder style accumulator was chosen to prevent the nitrogen cover gas or air (non-condensable gases) from diffusing into the working fluid, which would alter the boiling behavior of the fluid. The body is stainless steel. A ¼" NPT tap at the top of the accumulator connects the nitrogen gas system to the top side of the bladder. A visual pressure gauge mounted on top provides indication of the overhead static pressure within the balloon. The nitrogen gas system together with the accumulator are used to control the static overhead pressure that the loop experiences. The 2" NPT tap at the bottom o the accumulator is fitted with a reducing pipe fitting. The reduced ½" NPT links to 1.27 cm (½") tube via adapting coupling.

Figure 6-23: Drawing of Blacoh CT2420V Accumulator

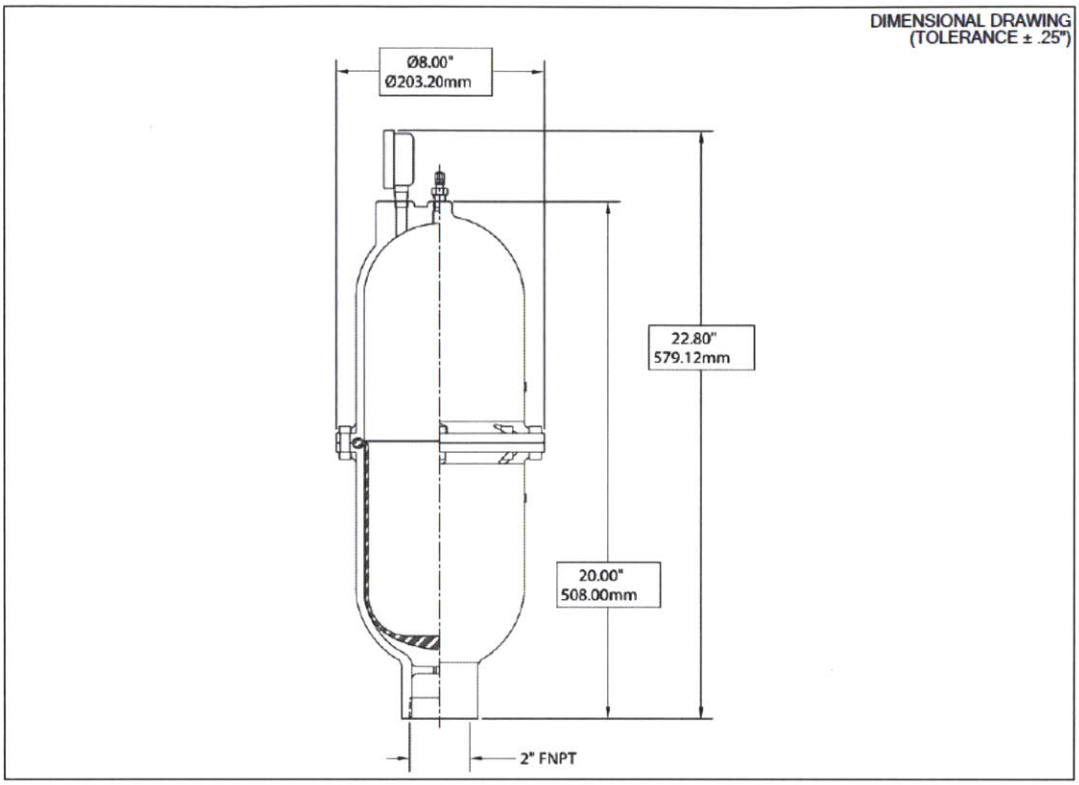

MODEL #:	CT2420V
AIR CONTROL:	CHARGE
BLADDER:	VITON
CAPACITY:	370 CUBIC INCHES/6.06 LITERS
INLET:	2" FNPT
MAXIMUM PRESSURE:	300 PSI/20 BARS
NONWETTED HOUSING:	STAINLESS STEEL
WETTED HOUSING:	STAINLESS STEEL

The viton bladder (see Figure 6-24) initially sits in the lower half of the accumulator and is held in place by a circumferential ring that is squeezed into a channel formed between the upper and lower halves. As the working fluid expands the bladder lifts until the above nitrogen pressure equals the below working fluid pressure on the bladder surface. By design the bladder can fully displace to the top allowing the full 6.06 liters (1.6 gallons) to be utilized.

Figure 6-24: Photo of Accumulator Bladder

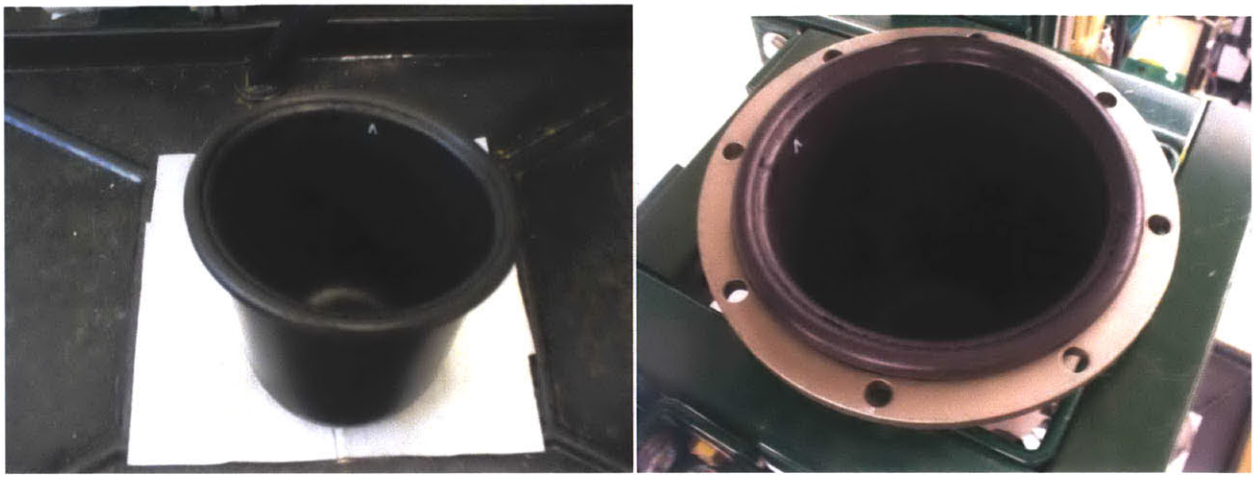

6.5.5 Condenser

The loop is fitted with a Thermasys heat exchanger [Model USSC-824-2.9-6-F-GPC] that acts as a condenser (see Figure 6-25). The shell and tube condenser is made of stainless steel with 0.9525 cm [3/8"] OD tubes also of stainless steel 316L. The tube side flow is 4-pass and eleven (11) tubes. Shell side internal diameter is 10.16 cm (4") (see Table 6-6).

Figure 6-25: Photo of Condenser

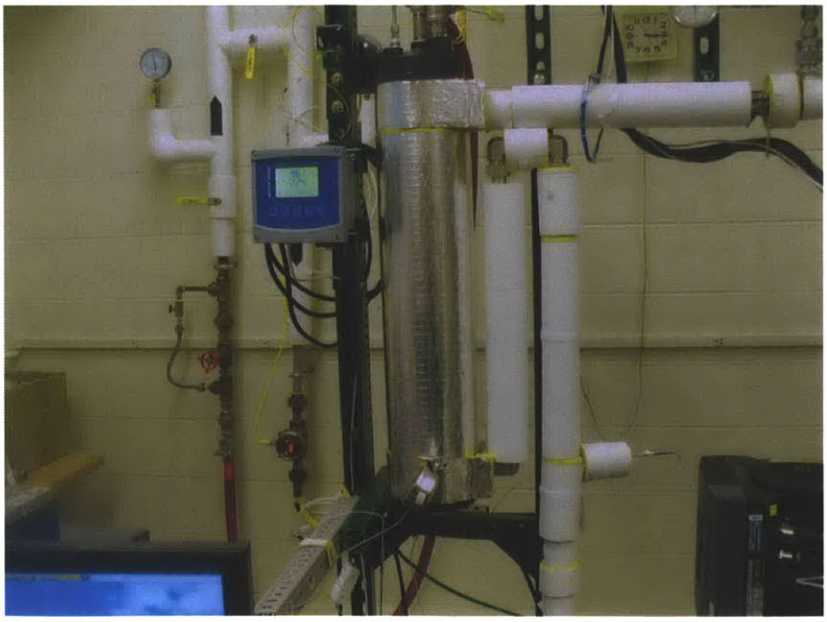

Table 6-6: Condenser Specifications

Tube Information:

Number of Tubes	=	11	
Passes	=	4	
Length, average	=	2.23 m	(7.31 feet)
Length, average/pass	=	55.74 cm	(1.829 feet)
OD	=	0.9525 cm	(3/8 inches)
Tube surface area	=	0.7339 m^2	(7.9 ft^2)
Material	=	SS316L	

Shell Information:

Length	=	0.7017 m	(27 5/8 inches)
ID	=	10.16 cm	(4 inches)
OD	=	10.795 cm	(4.25 inches)
Baffles	=	7	
Baffle separation	=	7.366 cm	(2.9 inches)

The condenser is mounted to the loop superstructure with the tubes vertical. Flow enters the top of the condenser perpendicular to the tubes and exits the bottom. Seven (7) baffles that support half the tubes in alternating left, right locations cause the flow to cross and turn back on the tubes (see Figure 6-26). The baffles are 7.37 cm (2.9") apart. The last 7.62 cm (3") at the bottom including the exit port have no tubes.

The bottom exit port, 2" NPT, is 0.61 m (2') above the entrance to the pump. Pressure and temperature are measured between the condenser exit and the pump entrance. So to provide sufficient Net Positive Suction Head ("NPSH") the temperature is managed to be 2 °C to 4 °C less than saturation, depending on flow rate.

Figure 6-26: Photo of Condenser Tubes, Flow Chamber and Baffles

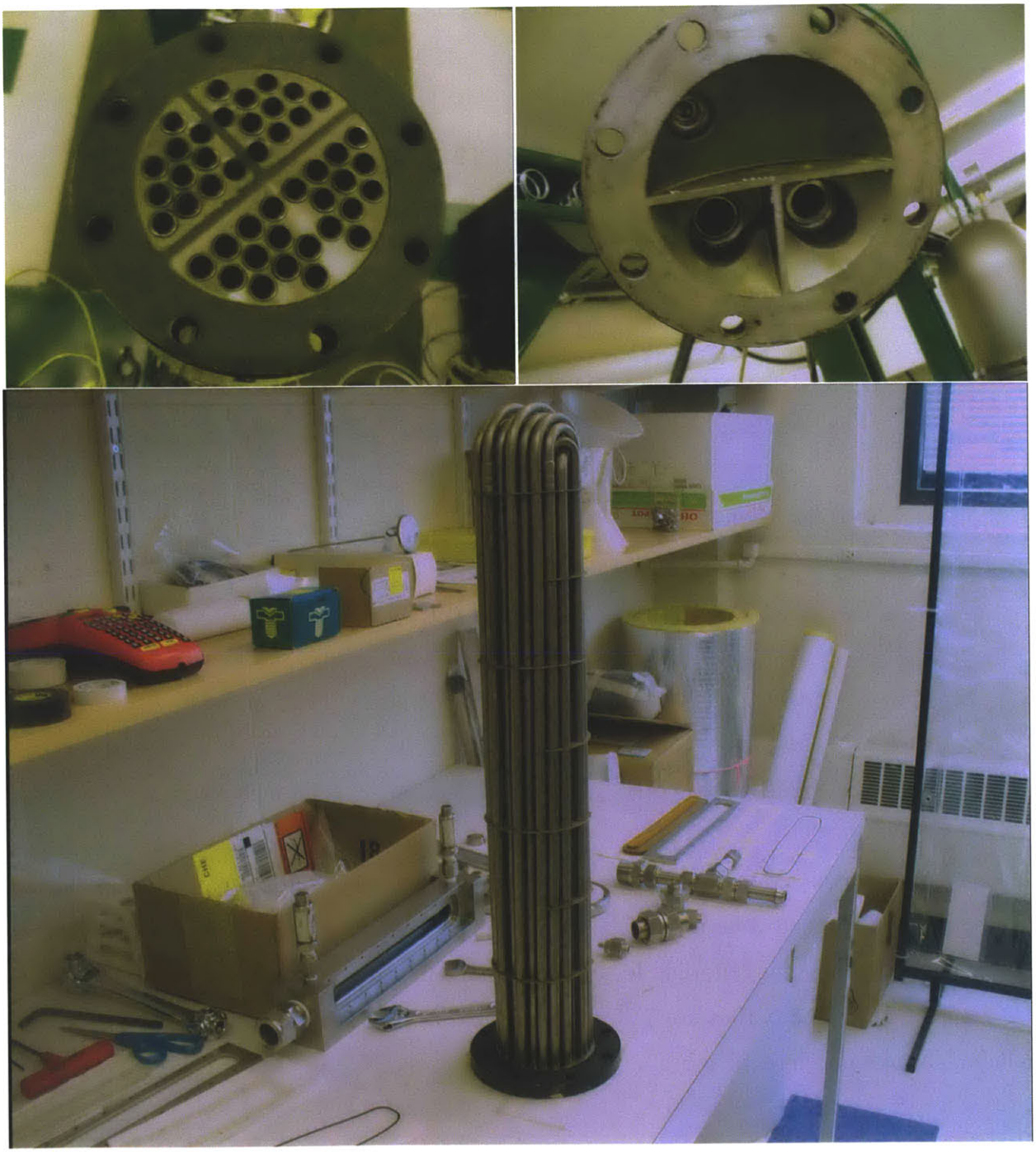

Tube side flow is provided by the university chilled water system.

6.6 Pipes, Tubes & Fittings

Loop wetted pipes, tubes and fittings are mostly stainless steel 316L and a couple of 304. Pipe is schedule 40. Tube wall thicknesses are 1.65 mm (0.065") or greater. Pipe and pipe fitting sizes used are 2", 1.5", 1.25", and ¾" standard NPT. Tube and compression fitting sizes used are 2.54 cm (1"), 1.91 cm (¾"), and 1.27 cm (½"). Stainless steel compression fitting used are all double sleeve type.

Flexible tube of 2.13 m (7') length with stainless steel mesh and fittings surrounds a 1.91 cm (¾") viton tube. The flexible tube between the pressure relief valve and test section allows for the test section to be positioned from vertical ($\theta = 90^{o}$) to horizontal ($\theta = 0^{o}$).

Lines that supply and return chilled water to the tube side of the condenser are 1.91 cm (¾") hose. The supply side hose (yellow in color) can handle pressures up to 10.2 bar gauge (150 psi) and 80 °C. The return side hose (red in color) can handle pressures up to 11.9 bar gauge (175 psi) and 200 °C. High pressure, between 6.7 bar gauge (100 psig) and 8 bar gauge (120 psig), of the chilled water system insures flow is always single phase. Note the saturation temperature of water at 6.7 bar gauge is 170 °C (338 °F) and the maximum system fluid temperature is 153 °C.

Pipe and pipe fittings on the chilled water system are mostly brass. Pipe again is schedule 40. Sizes are 1", ¾" and ¼" NPT.

6.7 Valves

Ball valves and a needle valve are utilized on the two-phase loop. Ball valves, gate valve and needle valve are used on the chilled water system. All valves on the two-phase loop are stainless steel 316L. Valves on the chilled water system are brass or stainless steel.

Ball valves are used on the two-phase loop to: (1) fill and drain the loop, (2) direct flow toward the Dissolved Oxygen Probe, and (3) isolate sections for maintenance (see Figure 6-27). The needle valve on the two-phase loop is used for degassing and vacuum isolation during fill procedures.

Figure 6-27: Photo of Two-phase Loop Valves

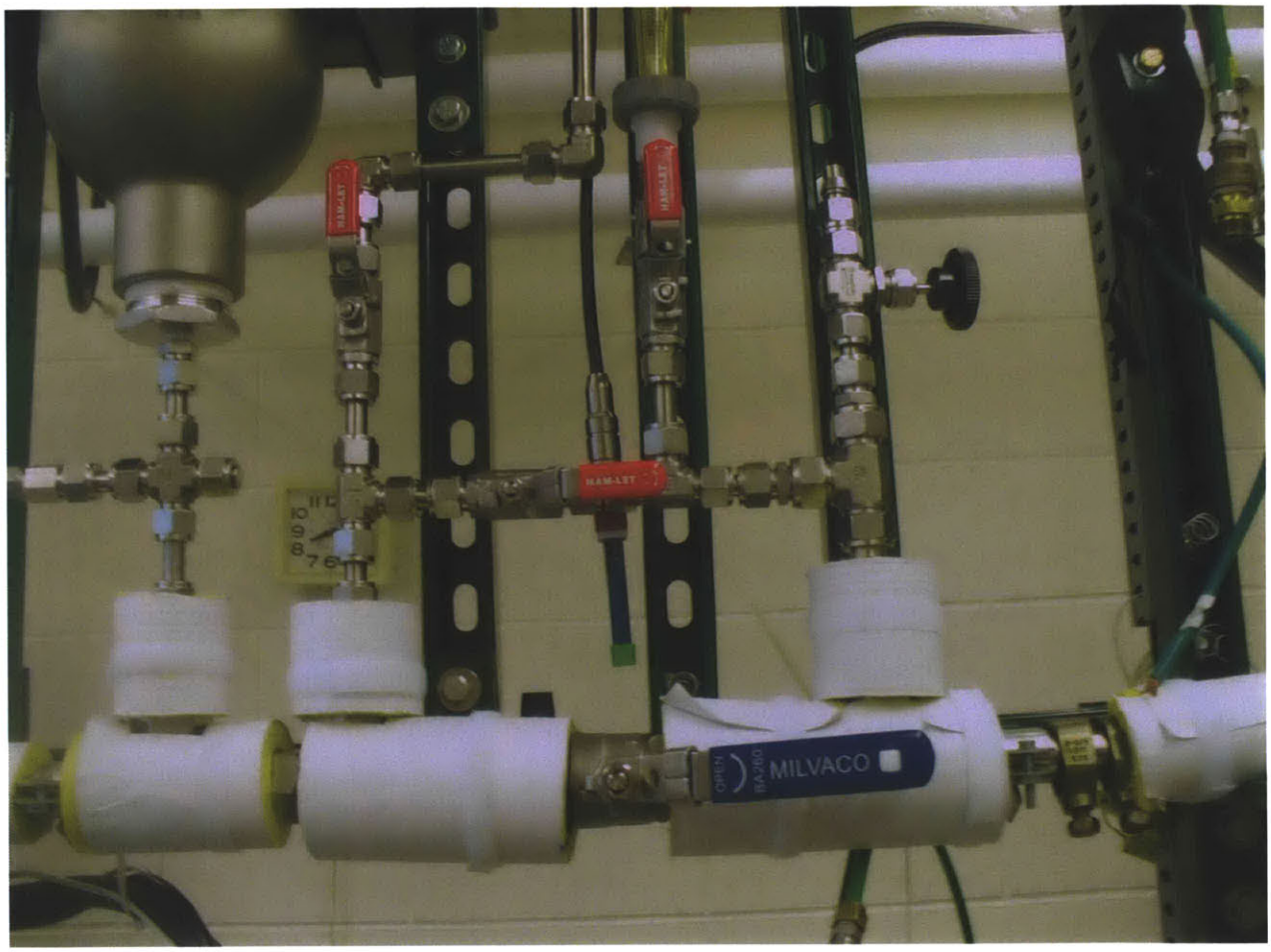

On the chilled water system ball valves are used to isolate sections for maintenance (i.e., condenser or vortex flow meter). Additionally, the chilled water system has a gate valve that is used for flow rate variation for volumetric flow rates above 7.58 lpm (2 gpm) (see Figure 6-28). The needle valve, parallel to the gate valve, on the chilled system provides flow control below 7.58 lpm (2 gpm).

Figure 6-28: Photo of Chilled Water Loop Valves

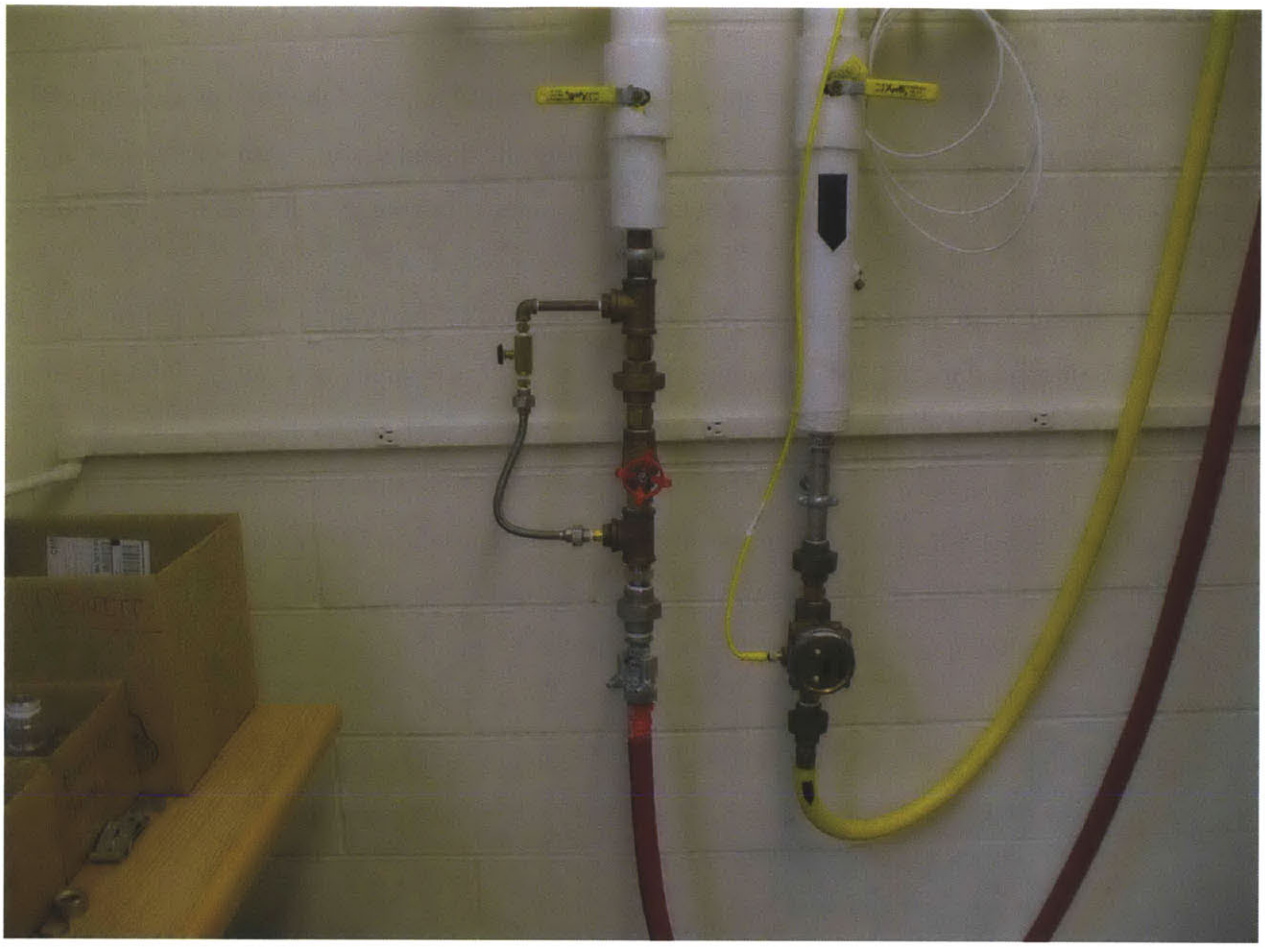

6.8 Insulation

In order to minimize the system heat loss to the environment, the two-phase flow loop is insulated with fiberglass having a reinforced paper facing. All piping, pump, and condenser are insulated. Rigid pipe and tube along with the pump and condenser have either 1.27 cm (0.5") or 2.54 cm (1") insulation. The 2.13 m (7') flexible tube length is insulated with 3.2 mm (1/8") thick and 2.54 cm (1") wide ceramic wrap insulation. The pump and condenser are insulated with 2.54 cm (1") fiberglass insulation. Additionally, the back surface of the test section away from the heater and thermocouples is also insulated with 3.81 cm (1.5") rigid insulation.

6.9 Nitrogen Gas System

A nitrogen gas system is utilized to set the system pressure at the top of the two-phase loop. The pressure communication is via the viton bladder within the accumulator. Above the bladder is plumbed to the nitrogen gas system. The bottom of bladder is in contact with the working fluid.

A nitrogen bottle with feed regulator can supply up to 117 bar gauge (1,700 psig). Static pressures of interest for the test matrix are 1, 3 and 5 atmospheres absolute. IVR accident scenarios have expected pressures within the containment from 1 atmosphere to 3 atmospheres absolute. The 5 atmosphere tests are completed to bound the containment design limit of 60 psig (75 psia, 5 atmospheres). The nitrogen system is also fitted with a GO back pressure regulator [Model BP8L-2D11D5H111]. The feed regulator and back pressure regulator work to maintain the pressure within the accumulator (see Figure 6-29).

Figure 6-29: Photo of Nitrogen Gas Feed Regulator and Backpressure Regulator

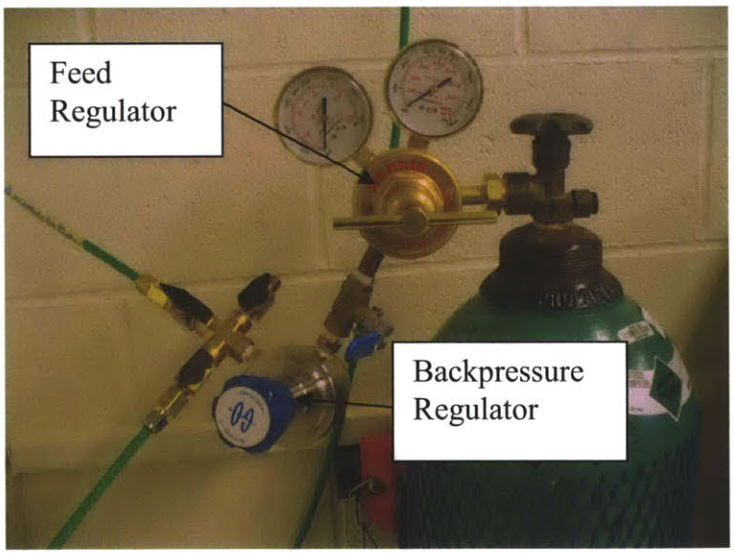

The nitrogen system is also plumbed to the fill/drain tank. Green 7.9 mm (5/16") plastic tubing runs to the top of the accumulator and the fill and drain tank. As part of the fill procedure approximately 0.34 bar (5 psig) of cover gas is used to push the working fluid to the top of the system.

6.10 Chilled Water System

Chilled water is supplied and driven by the MIT facilities chilled water system that provides building cooling throughout the university. The room was fitted with 2.54 cm (1") copper tubing together with terminating ball valves, visual pressure gauges, and surface type-K thermocouples for both the feed and return lines (see Figure 6-30).

System pressure varies with building demand and is usually about 6.7 bar to 7.7 bar gauge (100 to 115 psig) with a water temperature about 10 °C. These conditions assure signal phase flow within the chilled system for the conditions of interest herein (see Table 6-7). The copper lines are coupled to the condenser (tube side) with 1.91 cm (¾" hoses). The feed hose, yellow, is commercial grade and can handle temperature up to 75 °C. The return hose, red, is a high temperature design that is capable of carrying water temperatures of up to 200 °C.

Figure 6-30: Photo of Chilled Water Gate and Needle Valves

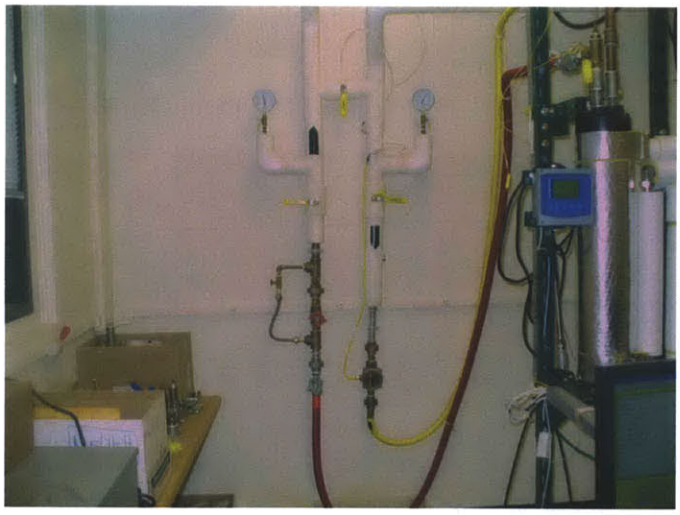

To control chilled water flow rate two (2) parallel valves are installed before the return copper tube: (1) a 1" pipe gate valve for gross flow control and (2) ¼" needle valve for fine control. Measurement of the flow is by means of a vortex flow meter that provides both a digital signal and visual output display. The vortex flow meter is mounted between the copper feed line and the feed hose to the condenser.

Table 6-7: List of Chilled Water System Parameters

Supply Temperature Range	6 °C – 10 °C	
Minimum Flow Rate	7.61 lpm	2 gpm
Maximum Flow Rate	49.3 lpm	13 gpm
Pressure Range	6.6 – 7.7 bar	100 – 115 psig
Saturation Temperature	170 °C	338 °F

6.11 Fill and Drain Tank

An 11.4 Liter (3 gallon) stainless steel tank is utilized for filling and draining the two-phase loop (see Figure 6-31). The tank is connected to the loop with reinforced nylon tube. The tank is also connected to the nitrogen gas system through the top of the tank. Nitrogen cover pressure is used to help fill the flow loop with working fluid. A needle valve is attached to the top of the tank and provides a means of de-pressurizing to the atmosphere.

Figure 6-31: Photo of Fill/Drain Tank

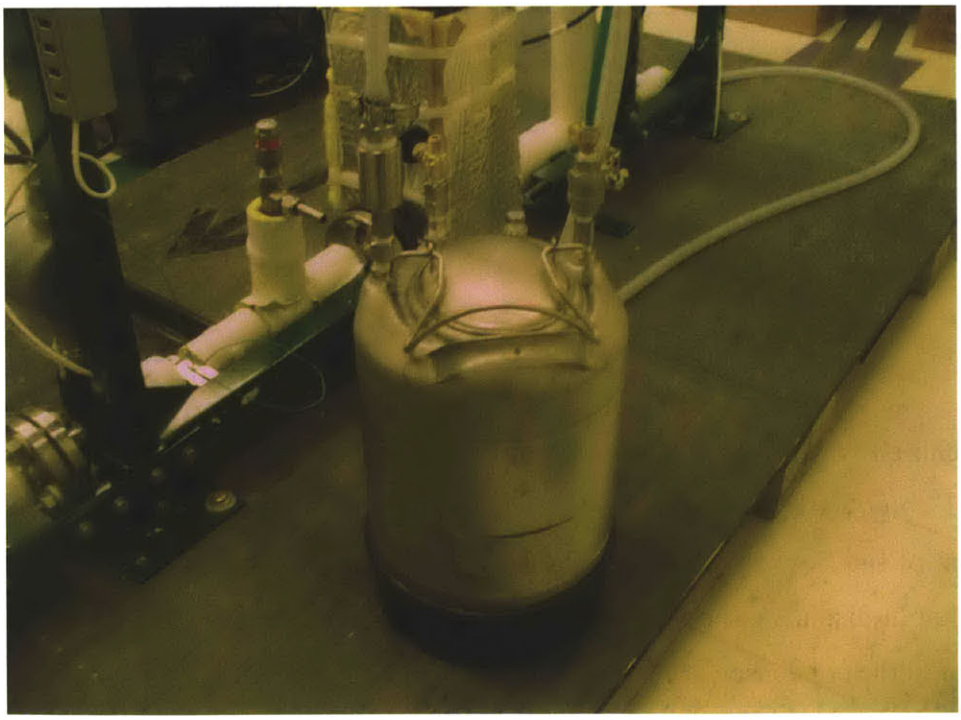

6.12 Instrumentation

Six (6) types of measurements are incorporated onto the test loop facility: (1) temperature, (2) pressure, (3) flow rate, (4) voltage drop, (5) current and (6) dissolved oxygen. A total of twenty-six (26) digital measurements are made at each scan using a DAS (see Table 6-8). Dissolved oxygen measurements are made only during the degassing portion of experiment preparation.

Table 6-8: List of Loop Measurements

Item		Description	Type	Label
1	-	Bulk loop fluid temperature at condenser exit	RTD	RTD1
2	-	Bulk loop fluid temperature at test section entrance	RTD	RTD2
3	-	Bulk loop fluid temperature at test section exit	RTD	RTD3
4	-	Bulk loop fluid temperature at condenser entrance	RTD	RTD4
5	-	Test Sample rear surface temperature (#1)	Type-K	TSK1
6	-	Test Sample rear surface temperature (#2)	Type-K	TSK2
7	-	Test Sample rear surface temperature (#3)	Type-K	TSK3
8	-	Test Sample rear surface temperature (#4)	Type-K	TSK4
9	-	Test Sample rear surface temperature (#5)	Type-K	TSK5
10	-	Test Sample rear surface temperature (#6)	Type-K	TSK6
11	-	Test Sample rear surface temperature (#7)	Type-K	TSK7
12	-	Test Sample rear surface temperature (#8)	Type-K	TSK8
13	-	Chilled water temperature on feed line	Type-K	CW1
14	-	Chilled water temperature entrance to condenser	Type-K	CW2
15	-	Chilled water temperature condenser tube middle	Type-K	CW3
16	-	Chilled water temperature condenser exit	Type-K	CW4
17	-	Chilled water temperature on return line	Type-K	CW5
18	-	Pump pressure	Danfoss	PT1
19	-	Pressure at test section entrance	Omega	PT2
20	-	Pressure at test section exit	Omega	PT3
21	-	Pressure at the exit of the condenser	Ashcroft	PT4
22	-	Flow rate in loop	Omega	FM1

23	-	Flow rate in chilled water system	Omega	FM2
24	-	Voltage drop across test section	Agilent	TSVD
25	-	Current from Power Supply (#1)	LEM	PS1
26	-	Current from Power Supply (#3)	LEM	PS3

Additionally, visual only pressure gauges are mounted on top of the accumulator, below the accumulator, near the pump inlet, on the nitrogen gas bottle regulator, and on both the feed and return lines of the chilled water system.

Temperature measurements are made with two device types: RTD and Type-K thermocouple.

6.12.1 RTDs

The four (4) RTDs are used to measure bulk fluid temperature in the two-phase loop. The first ["RTD1"] is located between the condenser outlet and pump inlet. The second ["RTD2"] is located just before the test section inlet and well after the inline heater section. The third ["RTD3"] is located just downstream of the test section. The fourth ["RTD4"] is located just before the condenser entrance. The end of each RTD is located well within the flow and away from the tube wall.

The two RTDs nearest the test section are utilized in heat balance calculations for the test section for sub-cooled conditions. The RTDs located before and after the condenser can also be used for heat balance determination on the heat exchanger during single phase operation. The specifications of the RTDs are provided below (see Table 6-9).

$$Q_{Test\ Section} = \dot{m}_{hw} \cdot Cp_{hw} \cdot (T_{RTD3} - T_{RTD2}) \qquad \text{Eq. 6.10}$$

$$Q_{Heat\ Exchanger} = \dot{m}_{hw} \cdot Cp_{hw} \cdot (T_{RTD4} - T_{RTD1}) \qquad \text{Eq. 6.11}$$

Table 6-9: List of Specifications of RTD

Manufacture:	Omega
Type:	4-wire
Model #:	PR-11-3-100-1/8-6-E
Operating Range:	-200 to 600 °C
Length:	15.24 cm (6 inches)
Sheath Diameter:	3.175mm (1/8 inch)
Sheath Material:	Stainless steel
Stated accuracy:	+/- 0.35 °C at 100 °C

6.12.2 Thermocouples

Type-K thermocouples are used for two types of measurement: (1) the temperature of the back of the test heater (see Table 6-10), and (2) the bulk temperature measurement of the chilled water flow through the tube side of the condenser (see Table 6-11). There are eight (8) locations on test sample insulating block and five (5) locations on the chilled water system.

Table 6-10: List of Specifications of Type-K Thermocouples on Test Section Heater

Manufacture:	Omega
Type:	Type-K
Model #:	KMQXL-125U-6
Operating Range:	-200 – 1250 °C
Length:	15.24 cm (6 inches)
Sheath Diameter:	1.5875 mm (1/16 inch)
Sheath Material:	Stainless steel
Stated accuracy:	+/- 1.1 °C

Table 6-11: Specifications of Type-K Thermocouples on Chilled Water Side of Heat Exchanger

Manufacture:	Omega
Type:	Type-K
Model #:	TJC36-CAIN-040U-6
Operating Range:	-200 °C to 1250 °C
Length:	15.24 cm (6 inches)
Sheath Diameter:	3.175 mm (1/8 inch) or
	6.23 mm (1/4 inch)
Sheath Material:	Stainless steel
Stated accuracy:	+/- 1.1 °C

The test section has penetrations that allow for up to eight (8) measurements of the back of the test heater. Each is spaced 2.22 cm (7/8") apart. The outer diameter of these eight thermocouples is 1.59 mm (1/16"). Most experiments only use four (4) of these measurement locations: 1) 1st - entrance location, 4th - mid location and last two 7th and 8th exit locations.

The chilled water system has five (5) bulk measurements. First, a surface type-K ["CW1"] is mounted on the 2.54 cm (1") OD copper feed line into the room. Second, the next type-K ["CW2"] is mounting into the flow just before the entrance to the condenser. Third, a type-K in mounted into the mixing box on the heat exchanger ["CW3"] and represents the temperature midway through the 4-pass flow path. Note that CW3 has a sheath diameter of 0.623 cm (¼"). Fourth ["CW4"], a type-K is mounted into the flow just after the condenser exit. Fifth, a surface type-K ["CW1"] is mounted on the 1" OD copper return line out of the room.

Note that when measureable flow exists in the chilled water system a heat balance calculation can be done on the condenser tube side.

$$Q_{Heat\ Exchanger} = \dot{m}_{cw} \cdot Cp_{cw} \cdot (T_{CW4} - T_{CW2}) \qquad \text{Eq. 6.12}$$

6.12.3 Pressure Transducers

Nine (9) pressure measurement devices are utilized to manage the hot and chilled water loops. Four (4) provide digital readings that are scanned by the Agilent DAQ. Five (5) visual gauges provide additional information for control of the chilled water system, loop and nitrogen gas system (see Table 6-12).

Table 6-12: List of Pressure Measurement Devices

Name	Location	Output
PT1	Pump exit	mA
PT2	Test section entrance	volts
PT3	Test section exit	volts
PT4	Condenser exit	mA/visual
Visual1	Before pump	psig
Visual2	Top of accumulator	psig
Visual3	Bottom of accumulator	psig
Visual4	Chilled water feed line	psig
Visual5	Chilled water return line	psig

The pressure transducer ["PT1"] on the pump is integrated with the pump electrical design and is supplied by Danfoss (see Table 6-13). This measurement is the system maximum pressure.

Table 6-13: List of Specifications of PT1

Manufacturer:	Danfoss
Model#:	MBS3000
Material:	SS316L
Range:	0 – 16 bar (0 – 232 psis)
Output:	4- 20 mA
Accuracy:	+/- 1% Full Scale
Supply:	9 – 32 VDC

The two pressure transducers mounted onto the test section, labeled PT2 and PT3, are from Omega. These two pressure measurements are made at the two ends of the heater through two 1.58 mm (1/16") holes (see Table 6-14). These pressure measurements and the RTDs before and after the heater are used to determine water properties entering and leaving the test section.

Table 6-14: List of Specifications of PT2 and PT3

Manufacturer:	Omega
Model#:	PX329 -200A5V
Material:	SS316L
Range:	0 – 13.8 bar (0 – 200 psig)
Output:	0 – 5 Volts
Accuracy:	+/- 0.25% FS (+/-0.5 psig)
Supply:	9 – 30 VDC

The pressure transducer on the condenser, PT4, provides both digital output and visual indication (see Table 6-15).

Table 6-15: List of Specifications of PT4

Manufacturer:	Ashcroft
Model#:	Xmitr 25 X 1009 SD 02L 1FL
Material:	SS316L
Range:	0 – 1000 psi
Output:	1 – 5 Volts
Accuracy:	+/- 1% BFSL (100 – 1000 psig)
	+/- 1.5% BFSL, otherwise
Supply:	10 – 24 VDC

The visual pressure gauge at the bottom of the accumulator ["Visual 3"] also measures vacuum. The vacuum information is used during the fill procedure (see Section 17.4).

6.12.4 Flow Meters

Two digital flow meters are utilized on the experimental apparatus: one turbine type flow meter, labeled HWFM, on the hot water loop and a vortex type, labeled CWFM, on the chilled water loop. The vortex type was chosen because it is not affected by particulate matter that is often found in the chilled water system.

A visual rotameter is also used and is part of the dissolved oxygen measurement system mounted above the hot side flow loop. During DO measurement the probe requires a flow rate of between 200 – 1,000 mL/minute (see Figure 6-32).

Figure 6-32: Photo of Dissolved Oxygen System with Rotameter

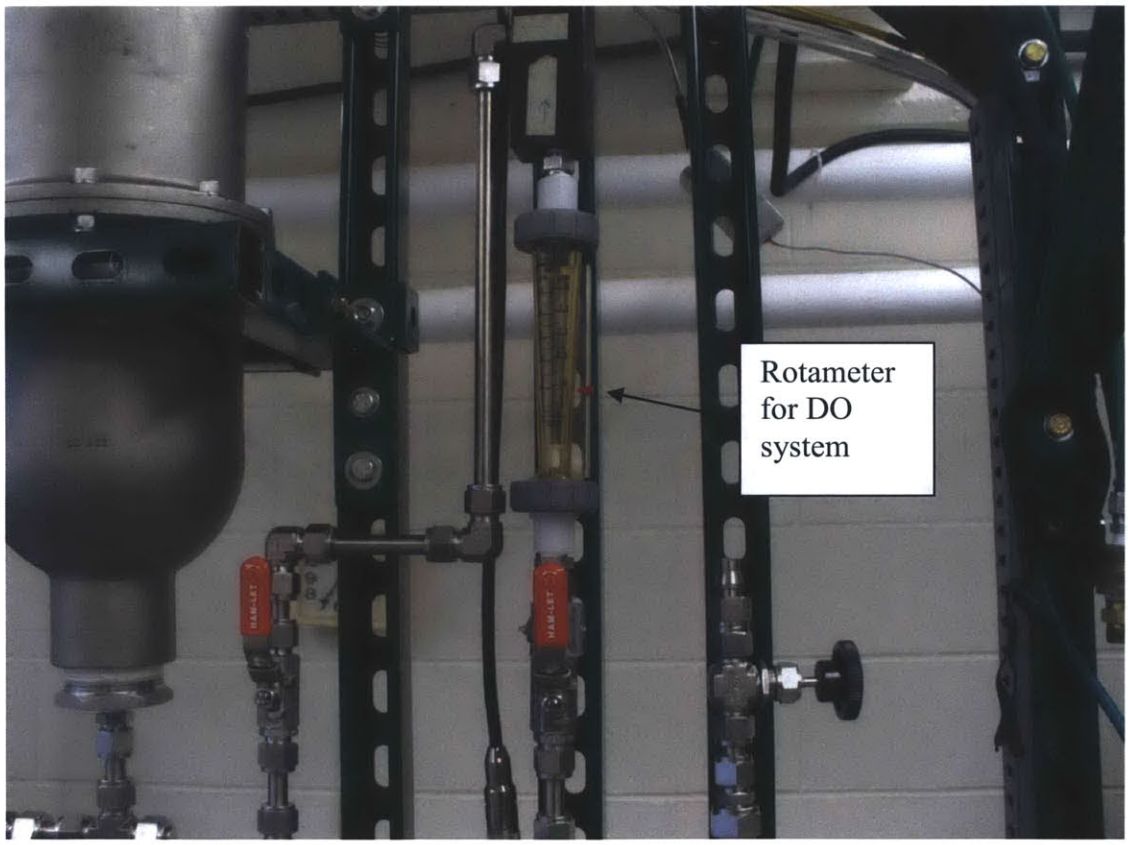

Omega is the manufacturer of both the turbine meter and the vortex meter. The turbine meter is mounted downstream of the pump and upstream of the pre-heater. The turbine meter has 1" NPT male fittings and requires 20.54 cm (10") undisturbed flow length before and 10.27 cm (5") after (see Figure 6-33). The volumetric flow rate range for the turbine flow meter is 2.8 lpm (0.75 gpm) to 28 lpm (7.5 gpm). This represents 165 to 1651 kg/m^2-s in the test section at STP. The stated flow measurement uncertainty is +/- 1% of reading (see Table 6-16).

The output of the turbine flow meter is frequency. The frequency is read by the Agilent DAQ and then in-turn to LabVIEW. The frequency is correlated to volumetric flow rate (see Section 6.11). The frequency signal is also sent through a signal conditioner. The signal conditioner converts the frequency to a voltage that is in turn sent to the pump for control.

Figure 6-33: Photo of Turbine Flow Meter and Signal Conditioner

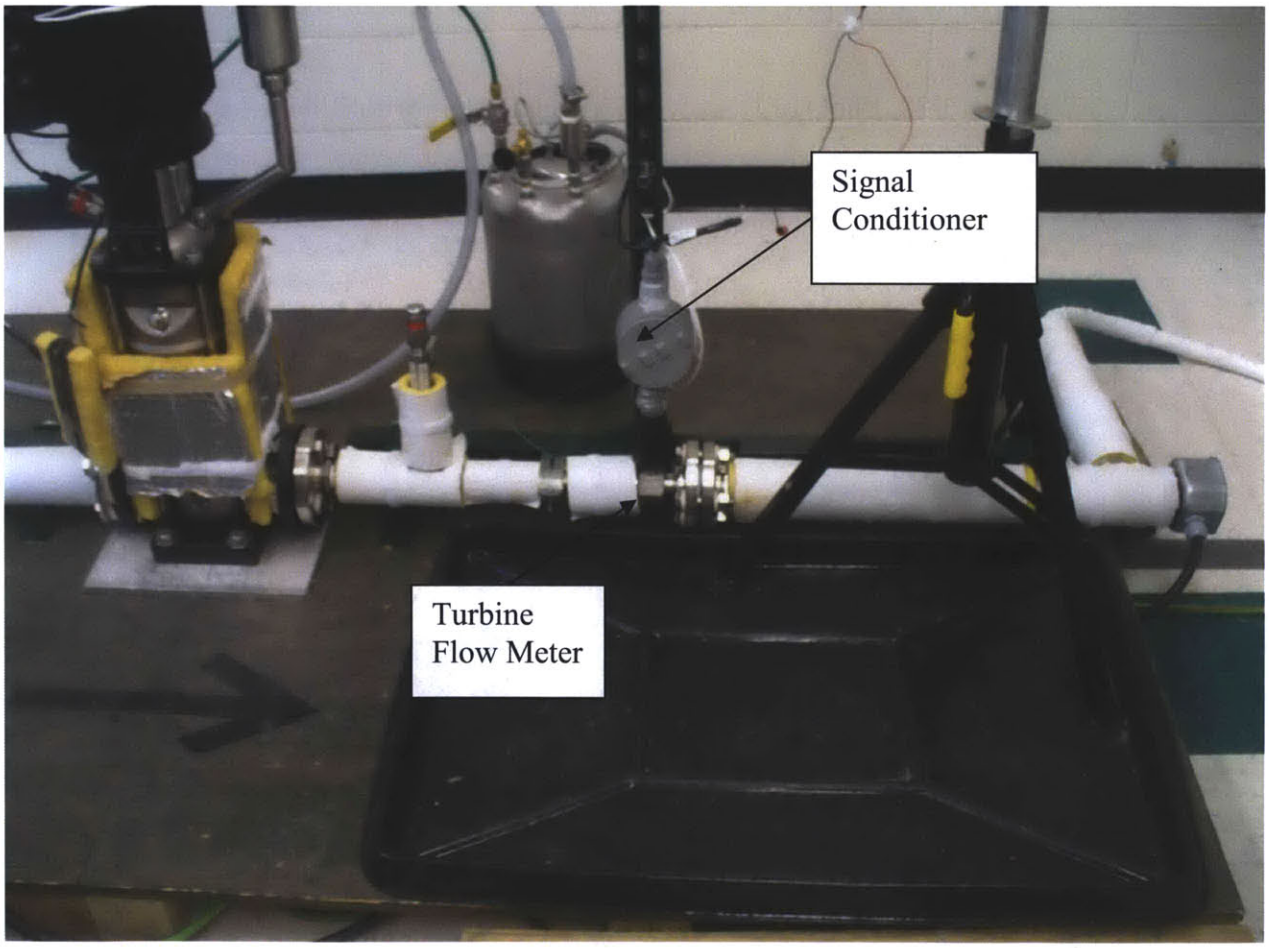

Table 6-16: Turbine Flow Meter Specifications

Manufacturer:	Omega
Model:	FTB-1422
Type:	Turbine
Output:	frequency [Hertz]
Size:	1.27 cm (1/2")
Couplings:	1" NPT male
Material:	Stainless Steel 316L
Range:	2.8 – 28 lpm (0.75 – 7.5 gpm)
Accuracy:	+/- 1.0% of reading

The vortex meter is mounted on the chilled water feed line and upstream of the condenser tube side. The vortex meter has 3/4" NPT female fittings and does not require flow stabilization either before or after (see Figure 6-34). The volumetric flow rate range for the vortex flow meter is 9.5 lpm (2.5 gpm) to 95 lpm (25 gpm). The stated flow measurement uncertainty is +/- 2% of full scale representing 0.5 gpm (see Table 6-17).

Table 6-17: Vortex Flow Meter Specifications

Manufacturer:	Omega
Model:	FV103
Type:	Vortex
Size:	3/4"
Couplings:	¾" NPT female
Output:	4 – 20 mA
Range:	9.5 – 95 lpm (2.5 – 25 gpm)
Accuracy:	+/- 2.0% full scale

Figure 6-34: Photo of Vortex Flow Meter

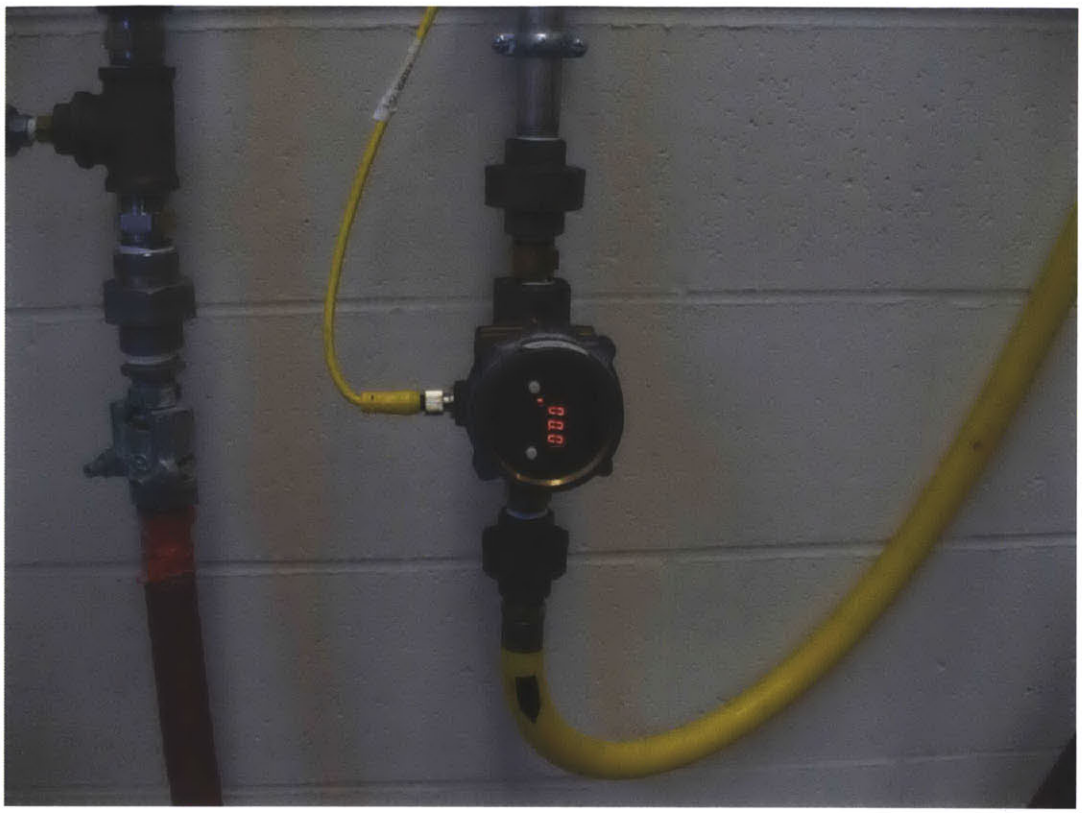

6.12.5 Current

The current from the two 18 kW DC power supplies to the test section is measured on the two [negative] locomotive cables (see Figure 6-35). The two current measurement devices are about 1.8 m (6') from the test section. Note that these two power supplies are operated in tandem.

The method is induction field measurement due to current flow. The current transducers cover up to 800 Amps per device and output a voltage signal from 0 – 10 Volts. These instruments are highly accurate at +/- 1% of full scale (see Table 6-18).

Figure 6-35: Photo of Current Measurement Devices for Each DC Power Supply

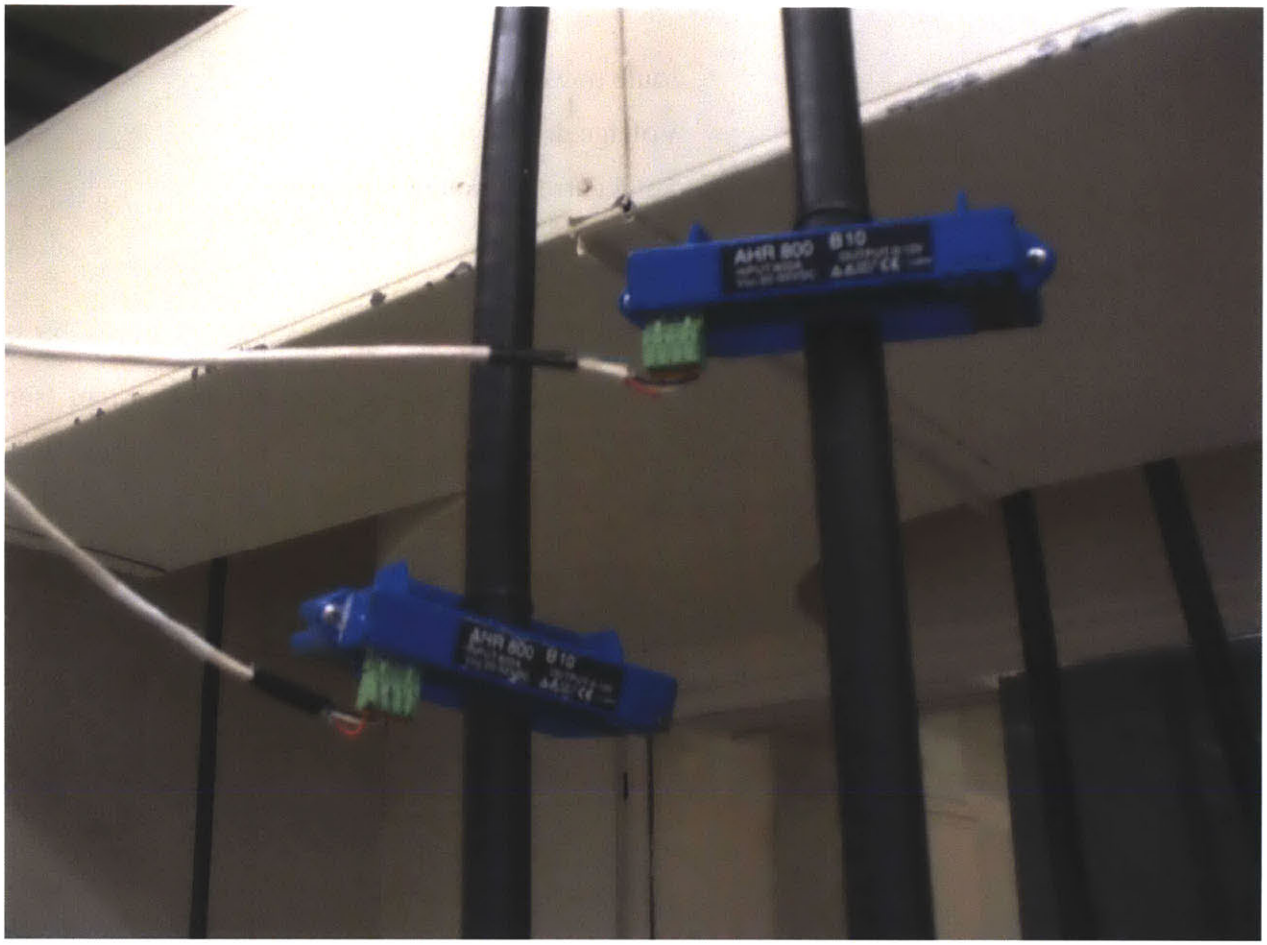

Table 6-18: Current Measurement Specifications

Make:	LEM
Model:	AHR 800 B10
Range:	0 – 800 Amps
Output:	0 – 10 Volts
Accuracy:	+/- 1.0% Full Scale

The sum of the two current measurements along with the measurement of voltage drop across the heater is utilized to calculate joule power.

$$P_{test\ section} = V_{test\ section} \cdot I_{total} \qquad \text{Eq. 6.13}$$

Where:

$P_{test\ section}$	=	Joule power to the test section
$V_{test\ section}$	=	Voltage drop across the test heater
I_{total}	=	Total current through test heater

6.12.6 Voltage Drop

Voltage drop across the test sample is measured by the Agilent data acquisition system (see Table 6-19). The leads are attached to the bolts that clamp the copper block from the locomotive cables to the copper electrodes (see Figure 6-36).

Table 6-19: Specification of Voltage Measurement by DAQ

Make:	Agilent
Model:	34980A
Range:	0 - 300 Volts
Accuracy:	+/- 0.004%

Figure 6-36: Photo of Leads for Voltage Drop Measurement

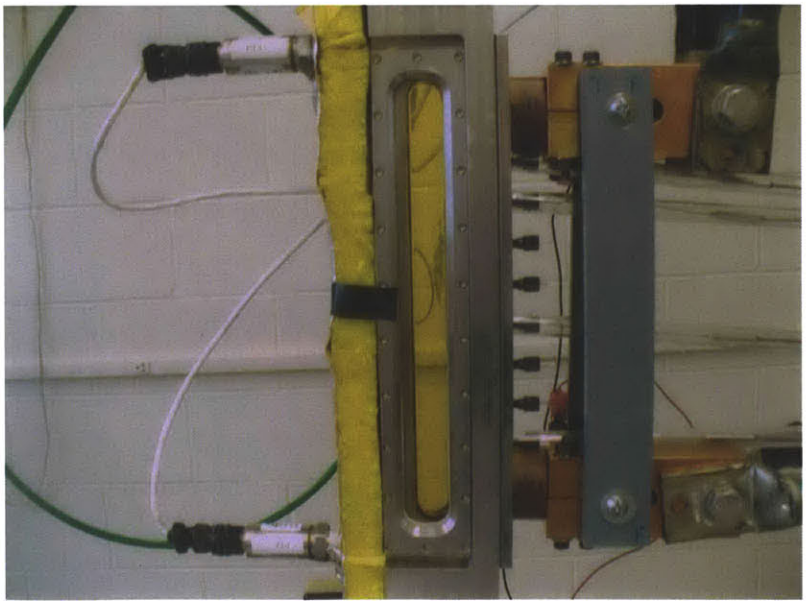

Measured voltage drop and total current are used to determine the joule heating of the test sample and electrical resistance (see Eq. 6.13). For each scan they are also used to calculate sample heater resistance. A rapid increase in sample resistance is used to help identify CHF.

$$\Omega_{test\ section} = \frac{V_{test\ section}}{I_{total}} \qquad \text{Eq. 6.14}$$

6.12.7 Dissolved Oxygen

Dissolved Oxygen ("DO") is measured after the degassing procedure is complete (see Appendix C). This quantifies a consistent (low) level of dissolved oxygen in the fluid (see Table 6-20). Dissolved oxygen is used as an indicator of the presences of non-condensable gases in the fluid. The objective is to have a consistent fluid with similar dissolved non-condensable gas levels for all tests.

The probe is located above the main loop (see Figure 6-37). Ball valves are located before and after the probe in order to isolate the probe once DO measurement is completed. This is needed to protect the probe from high temperatures.

DO measurement requires a small flow over the probe in the range of 200 mL/minute to 1,000 mL/minute. The upstream ball valve is positioned with the visual rotameter to achieve and measure the required flow.

As a target, degassing is continued until DO measurement is 4 ppm in the temperature range of 60 °C to 65 °C.

Table 6-20: Specification of DO Measurement Device

Make:	Mettler Toledo
Model:	Thornton M300
Output:	PPM of O_2 and Temperature (visual)
Accuracy:	+/- 1.0% of reading

Figure 6-37: Photo of DO Measurement Probe and Digital Meter

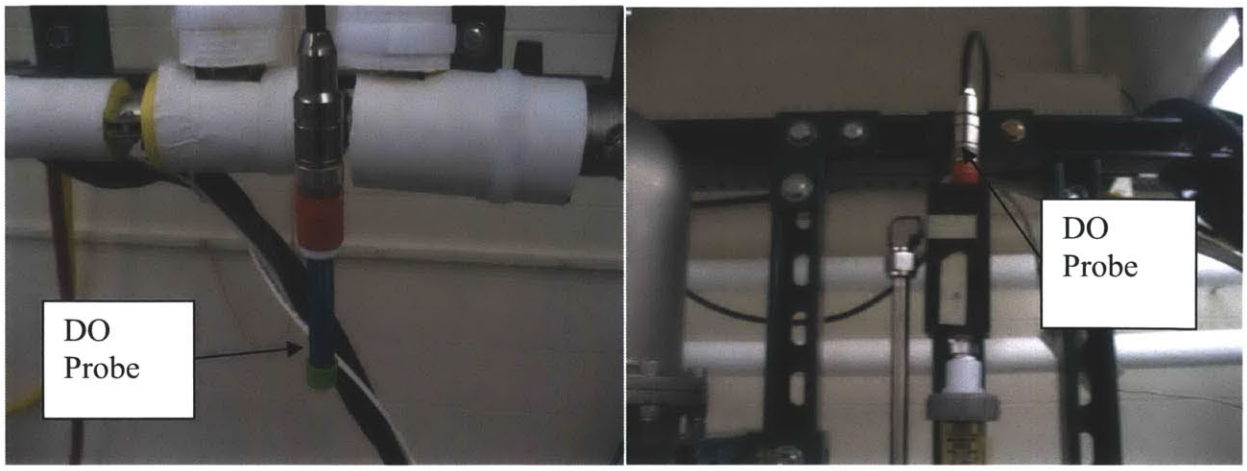

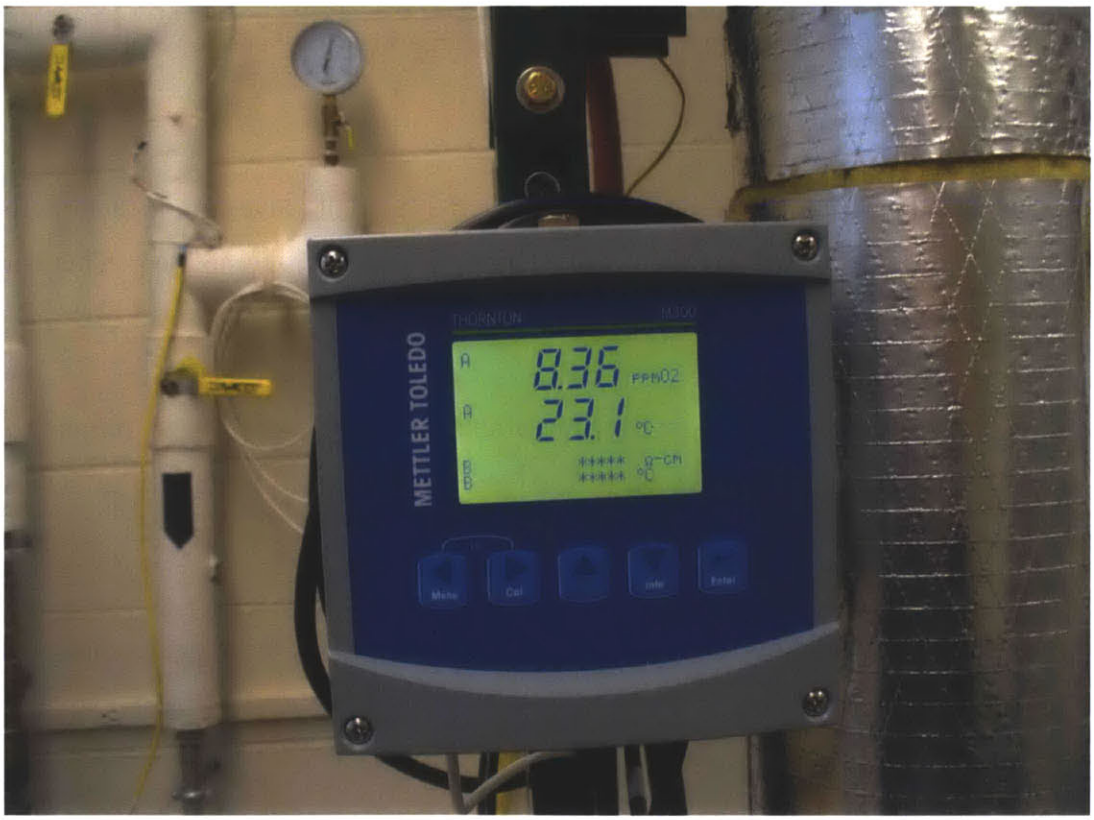

6.13 Calibration

Calibrations were completed for temperature, pressure, flow rate, current, and DO measurement instrumentation. Initial calibrations and follow-up calibrations were completed.

6.13.1 Temperature

Two types of temperature measurement devices are utilized: 1) 4-wire RTDs and 2) Type-K thermocouples. All were purchased from Omega. The temperature range of interest for the experimental matrix is 5 °C to 185 °C. The low end addresses the chilled water flow system. The high end is covers the saturation temperature at 5 atmospheres of overhead pressure (153 °C) plus wall superheat.

Calibration of temperature measurement devices was accomplished with three measurements for each device: 1) ice water [0 °C], 2) boiling water [100 °C], and 3) boiling propylene glycol [188.2 °C]. Cross calibration was accomplished with a hand held mercury or alcohol thermometer.

Digital output was recorded at each condition. Data was then processed to determine averages and standard deviations (see Table 6-21). All measurements are consistent with hand held thermometer measurements and within manufacturers stated accuracy. The Omega stated accuracy for the 4-wire RTDs is +/- 0.35 °C. The Omega stated accuracy for the Type-K thermocouples is +/- 1.1 °C. These manufacturer temperature measurement accuracies are utilized for overall uncertainty analyses.

As part of the experimental procedure the RTDs are checked before each run. One of two methods where used: (1) ice water or (2) loop flow with no heat. For the ice water check each of the RTDs was removed and placed in an ice bath and the output recorded. Loop flow check involved allowing the loop to flow with no heat addition and RTD output recorded. The loop flow check was favored once it was noted that the removal and re-installation of the RTDs with

associated compression fittings caused two RTDs to develop shorts that required replacement. The RTDs are known to be very consistent with age. These RTD checks basically confirm that no short has developed.

Table 6-21: Calibration Results of RTDs and Type-K thermocouples

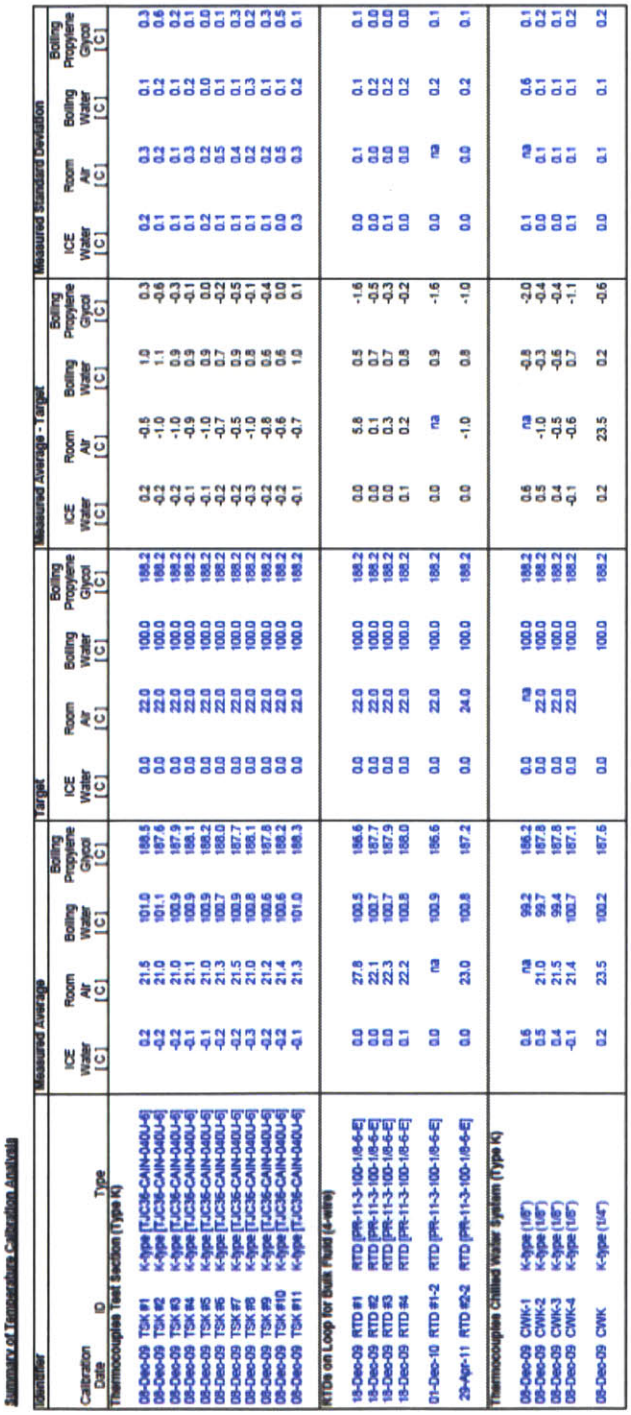

Summary of Temperature Calibration Analysis

Identifier		Measured Average				Target				Measured Average - Target				Measured Standard Deviation			
Calibration Date	ID	Type	ICE Water [C]	Room Air [C]	Boiling Water [C]	Boiling Propylene Glycol [C]	ICE Water [C]	Room Air [C]	Boiling Water [C]	Boiling Propylene Glycol [C]	ICE Water [C]	Room Air [C]	Boiling Water [C]	Boiling Propylene Glycol [C]	ICE Water [C]	Room Air [C]	Boiling Water [C]	Boiling Propylene Glycol [C]
Thermocouples Test Section (Type K)																		
09-Dec-09	TSK #1	K-type [TJC36-CAIN-040U-6]	0.2	21.5	101.0	188.5	0.0	22.0	100.0	188.2	0.2	-0.5	1.0	0.3	0.2	0.3	0.1	0.3
09-Dec-09	TSK #2	K-type [TJC36-CAIN-040U-6]	-0.2	21.0	101.1	187.6	0.0	22.0	100.0	188.2	-0.2	-1.0	1.1	-0.6	0.1	0.2	0.2	0.6
09-Dec-09	TSK #3	K-type [TJC36-CAIN-040U-6]	-0.2	21.0	100.9	187.9	0.0	22.0	100.0	188.2	-0.2	-1.0	0.9	-0.3	0.1	0.1	0.1	0.2
09-Dec-09	TSK #4	K-type [TJC36-CAIN-040U-6]	-0.1	21.1	100.9	188.1	0.0	22.0	100.0	188.2	-0.1	-0.9	0.9	-0.1	0.1	0.3	0.2	0.1
09-Dec-09	TSK #5	K-type [TJC36-CAIN-040U-6]	-0.1	21.0	100.9	188.2	0.0	22.0	100.0	188.2	-0.1	-1.0	0.9	0.0	0.2	0.2	0.0	0.0
09-Dec-09	TSK #6	K-type [TJC36-CAIN-040U-6]	-0.2	21.3	100.7	188.0	0.0	22.0	100.0	188.2	-0.2	-0.7	0.7	-0.2	0.1	0.5	0.1	0.1
09-Dec-09	TSK #7	K-type [TJC36-CAIN-040U-6]	-0.2	21.5	100.9	187.7	0.0	22.0	100.0	188.2	-0.2	-0.5	0.9	-0.5	0.1	0.4	0.1	0.3
09-Dec-09	TSK #8	K-type [TJC36-CAIN-040U-6]	-0.3	21.0	100.8	188.1	0.0	22.0	100.0	188.2	-0.3	-1.0	0.8	-0.1	0.1	0.2	0.3	0.2
09-Dec-09	TSK #9	K-type [TJC36-CAIN-040U-6]	-0.2	21.2	100.6	187.8	0.0	22.0	100.0	188.2	-0.2	-0.8	0.6	-0.4	0.1	0.2	0.1	0.3
09-Dec-09	TSK #10	K-type [TJC36-CAIN-040U-6]	-0.2	21.4	100.6	188.2	0.0	22.0	100.0	188.2	-0.2	-0.6	0.6	0.0	0.0	0.5	0.1	0.5
09-Dec-09	TSK #11	K-type [TJC36-CAIN-040U-6]	-0.1	21.3	101.0	188.3	0.0	22.0	100.0	188.2	-0.1	-0.7	1.0	0.1	0.3	0.3	0.2	0.1
RTDs on Loop for Bulk Fluid (4-wire)																		
19-Dec-09	RTD #1	RTD [PR-11-3-100-1/8-6-E]	0.0	27.8	100.5	186.6	0.0	22.0	100.0	188.2	0.0	5.8	0.5	-1.6	0.0	0.1	0.1	0.1
19-Dec-09	RTD #2	RTD [PR-11-3-100-1/8-6-E]	0.0	22.1	100.7	187.7	0.0	22.0	100.0	188.2	0.0	0.1	0.7	-0.5	0.0	0.0	0.2	0.0
19-Dec-09	RTD #3	RTD [PR-11-3-100-1/8-6-E]	0.0	22.3	100.7	187.9	0.0	22.0	100.0	188.2	0.0	0.3	0.7	-0.3	0.1	0.0	0.2	0.0
19-Dec-09	RTD #4	RTD [PR-11-3-100-1/8-6-E]	0.1	22.2	100.8	188.0	0.0	22.0	100.0	188.2	0.1	0.2	0.8	-0.2	0.0	0.0	0.2	0.0
01-Dec-10	RTD #1-2	RTD [PR-11-3-100-1/8-6-E]	0.0	na	100.9	186.6	0.0	22.0	100.0	188.2	0.0	na	0.9	-1.6	0.0	na	0.2	0.1
29-Apr-11	RTD #2-2	RTD [PR-11-3-100-1/8-6-E]	0.0	23.0	100.8	187.2	0.0	24.0	100.0	188.2	0.0	-1.0	0.8	-1.0	0.0	0.0	0.2	0.1
Thermocouples Chilled Water System (Type K)																		
09-Dec-09	CWK-1	K-type (1/8")	0.6	na	99.2	186.2	0.0	na	100.0	188.2	0.6	na	-0.8	-2.0	0.1	na	0.6	0.1
09-Dec-09	CWK-2	K-type (1/8")	0.5	21.0	99.7	187.8	0.0	22.0	100.0	188.2	0.5	-1.0	-0.3	-0.4	0.0	0.1	0.1	0.2
09-Dec-09	CWK-3	K-type (1/8")	0.4	21.5	99.4	187.8	0.0	22.0	100.0	188.2	0.4	-0.5	-0.6	-0.4	0.0	0.1	0.1	0.1
09-Dec-09	CWK-4	K-type (1/8")	-0.1	21.4	100.7	187.1	0.0	22.0	100.0	188.2	-0.1	-0.6	0.7	-1.1	0.1	0.1	0.1	0.2
09-Dec-09	CWK	K-type (1/4")	0.2	23.5	100.2	187.6	0.0		100.0	188.2	0.2	23.5	0.2	-0.6	0.0	0.1	0.1	0.2

6.13.2 Pressure

Pressure measurement devices were calibrated over a range of 0 bar [vacuum] to 13.8 bar (200 psia), which bounds the design limit of the loop 10.3 bar (150 psi). The pressure range of the experimental matrix is 1 to 5 atmospheres, absolute.

The calibrations were accomplished in a pressure vessel designed and built by nanofluid team member Eric Forrest and fitted with a NIST calibrated pressure transducer, nitrogen gas line and vacuum pump [78]. Scanned digital output was recorded. The resulting data was then regressed to determine linear fitting coefficients. Comparison was made to manufacturer recommended coefficients. Recommended coefficients are then programmed into LabVIEW.

Cross calibration was also completed on some pressure measurement devices. The procedure involved using nitrogen gas within the loop without fluid. Here the previously calibrated pressure transducers along with the feed gas regulator were compared to new pressure transducers.

6.13.2.1 PT1 on Pump

The first pressure transducer, PT1, is positioned on the pump and represents maximum loop pressure. This device was added to the loop on August 26, 2010. As a result the labels of the downstream pressure transducers where increased one. Calibration of the Danfoss MBS3000 was accomplished by cross calibration to PT2, which had been previously calibrated to a NIST certified transducer.

Nitrogen gas was brought into the otherwise empty loop. Visual measurements were also made with the gas regulator and the visual gauge below the accumulator. Scans were taken every three (3) seconds (see Figure 6-38). Averages at each pressure level are then determined (see Table 6-22)

Figure 6-38: Pressure History for PT1 Cross Calibration to PT2

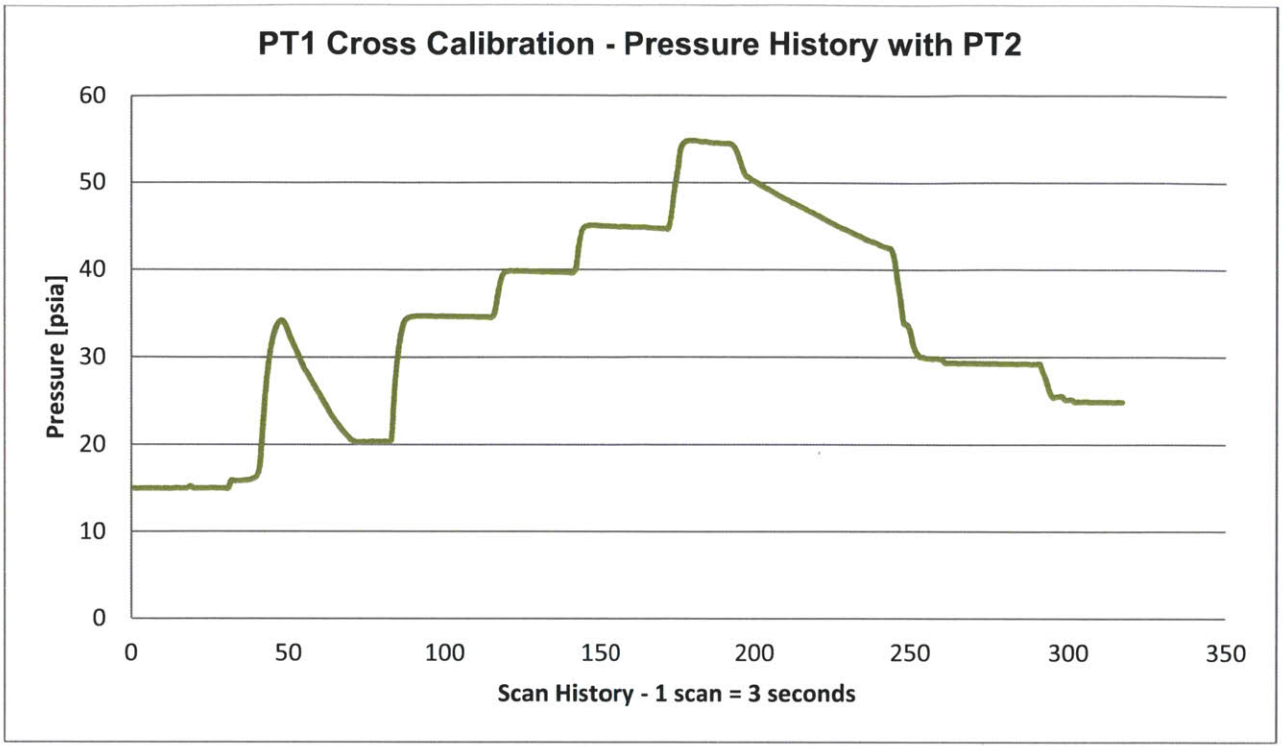

Table 6-22: Averaged Pressure History for PT1 Output to PT2

# of Scans	Notation	PT1 [mA]	PT2 [psia]
31	1 atmosphere	3.96	15.0
27	~ 20 psi – visual gauge	5.33	34.6
23	~ 25 psi – visual gauge	5.68	39.8
28	~ 30 psi – visual gauge	6.04	44.9
30	~ 15 psi – visual gauge	5.05	29.3

Figure 6-39: Graph of Averaged Pressure History for PT1 Output to PT2

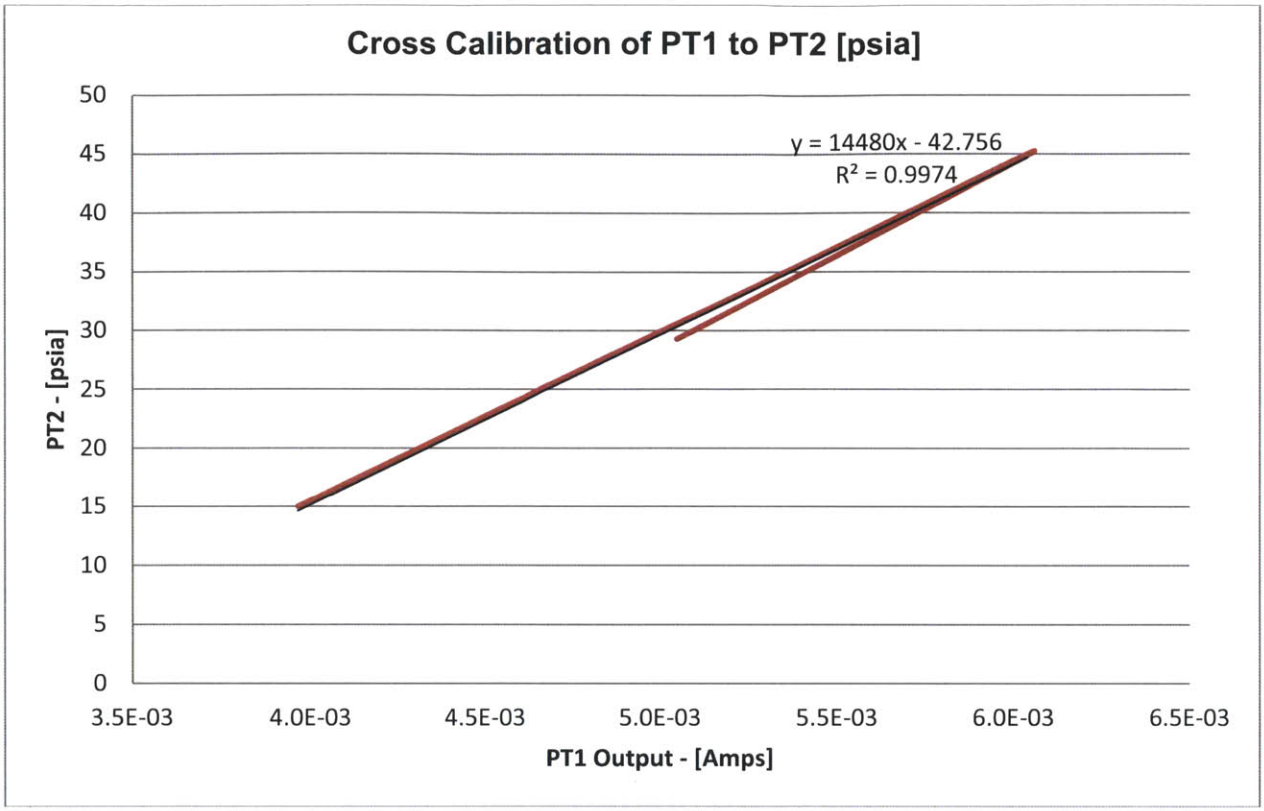

The form of the vendor recommended formula to convert transducer output [Amps] to pressure [psia] is given below (see Eq. 6.15). Note that instrument range is 232 psi with output cutoff of 4 mA.

$$Pr_{PT1} = \left(\frac{(S \cdot 1000) - 4}{16}\right) \cdot 232 + 14.7 \qquad \text{Eq. 6.15}$$

Where:

S = PT1 output [Amps]

Pr_{PT1} = PT1 pressure [psia]

To better match the correlation from above the cutoff was reduced to 3.98 from 4 (see Figure 6-39). The recommended formula is then:

$$Pr_{PT1} = \left(\frac{(S \cdot 1000) - 3.98}{16}\right) \cdot 232 + 14.7 \qquad \text{Eq. 6.16}$$

The fit was very good with correlation coefficient, R^2, above 99.7%.

6.13.2.2 PT2 – Test Section Entrance

The Omega pressure transducer at the entrance to the test section, PT2, was calibrated against a NIST certified pressure measurement device. At each pressure level the device was allowed to settle (see Figure 6.37). Scanned voltage from PT2 and pressure reading (psia) from the NIST were recorded each second. At each pressure level, averages were determined (see Table 6-23). A linear regression was then done on PT2 voltage output versus NIST pressure (see Figure 6-41).

Figure 6-40: Pressure History for PT2 Calibration to NIST Pressure Transducer

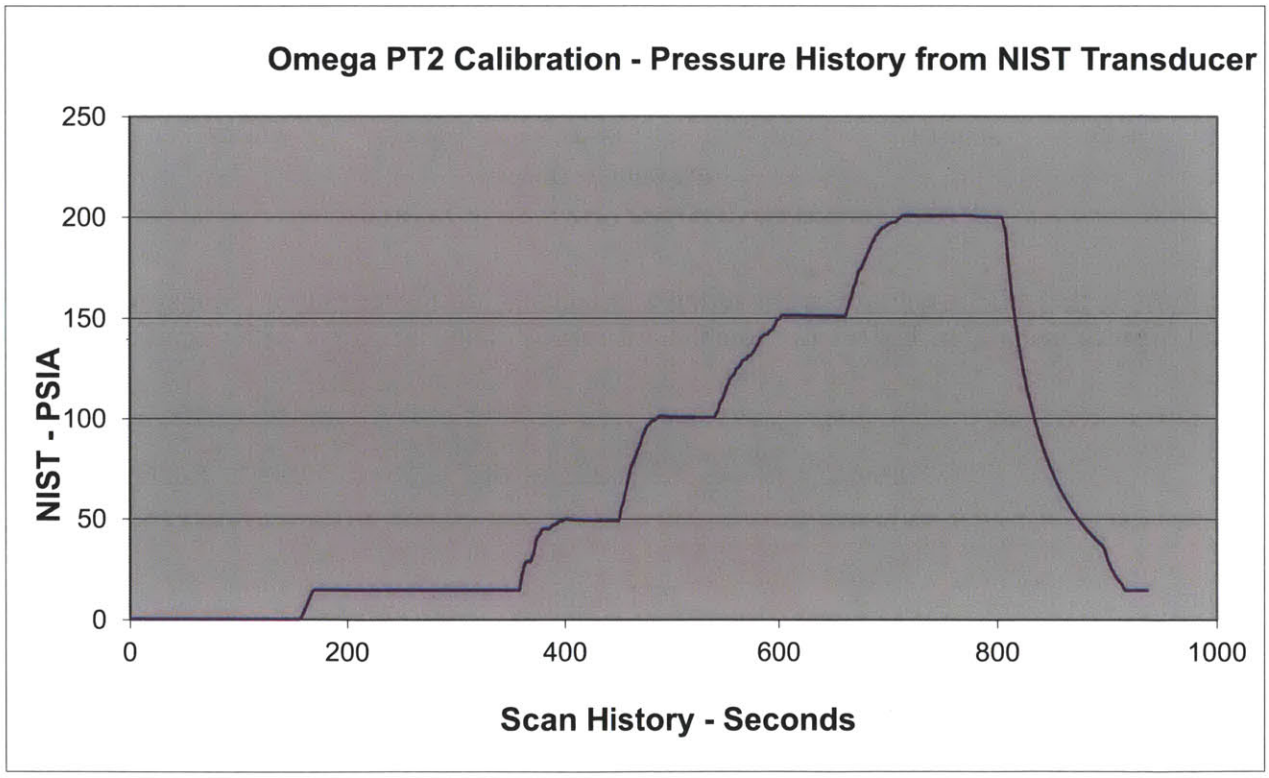

Table 6-23: Averaged Pressure History for PT2 Output to NIST Pressure Transducer

# of Scans	Notation	PT2 [Volts]	NIST [psia]
154	Vacuum	0.006	0.175
189	1 atmosphere	0.370	14.694
52	~ 50 psia	1.236	49.256
64	~ 100 psia	2.525	100.658
60	~ 150 psia	3.789	151.106
92	~ 200 psia	5.026	200.492
21	1 atmosphere	0.371	14.707

Figure 6-41: Graph of Averaged Pressure History for PT2 Output to NIST Pressure Transducer

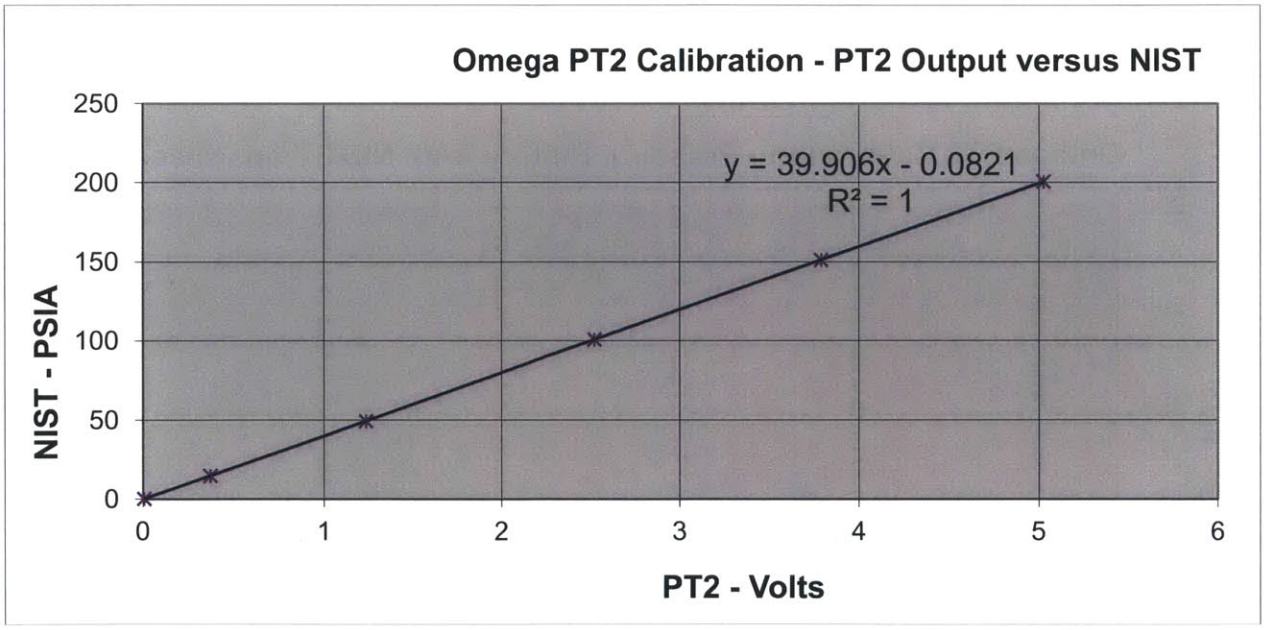

The linearity is excellent with correlation coefficient, R^2, of 99.99%. The stated accuracy of the Omega PT is +/-0.25% of full scale, which represents +/- 0.5 psi. This calibration result is within the stated instrument accuracy. As a result the manufacturer conversion from voltage output to pressure is taken (see Eq.6.17).

$$Pr_{\mathrm{PT2}} = 40 \cdot PT2_{output} \qquad \text{Eq. 6.17}$$

Where: $\mathrm{Pr_{PT2}}$ = pressure reading [psia]

$\mathrm{PT2_{output}}$ = output [Volts]

Note that PT2 needed to be replaced in April 2010. Cross calibration successfully done.

6.13.2.3 PT3 – Test Section Exit

The Omega pressure transducer at the exit to the test section, PT3, was calibrated in the same manner as PT2 (see Figure 6-42, Table 6-24, and Figure 6-43).

Figure 6-42: Pressure History for PT3 Calibration to NIST Pressure Transducer

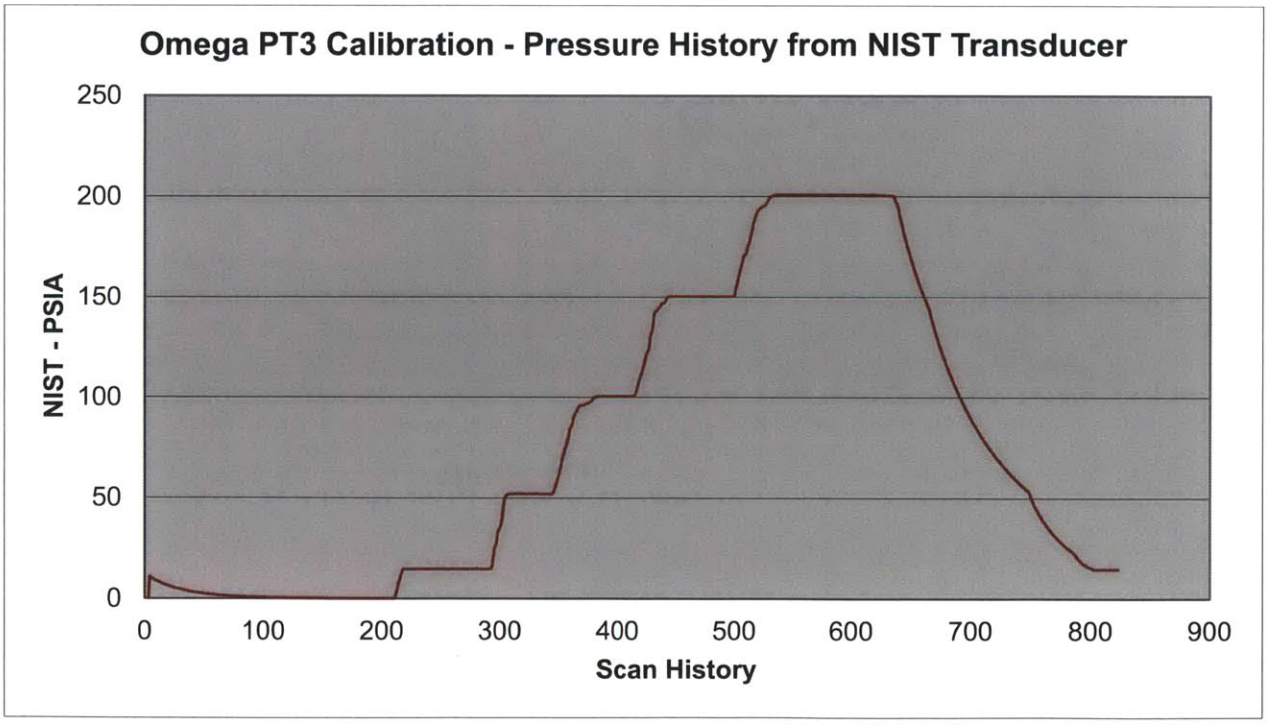

Table 6-24: Averaged Pressure History for PT3 Output to NIST Pressure Transducer

# of Scans	Notation	PT3 [Volts]	NIST [psia]
54	Vacuum	0.008	0.178
74	1 atmosphere	0.373	14.694
39	~ 50 psia	1.305	51.983
34	~ 100 psia	2.521	100.425
56	~ 150 psia	3.770	150.231
104	~ 200 psia	5.037	200.761
22	1 atmosphere	0.373	14.726

Figure 6-43: Graph of Averaged Pressure History for PT3 Output to NIST Pressure Transducer

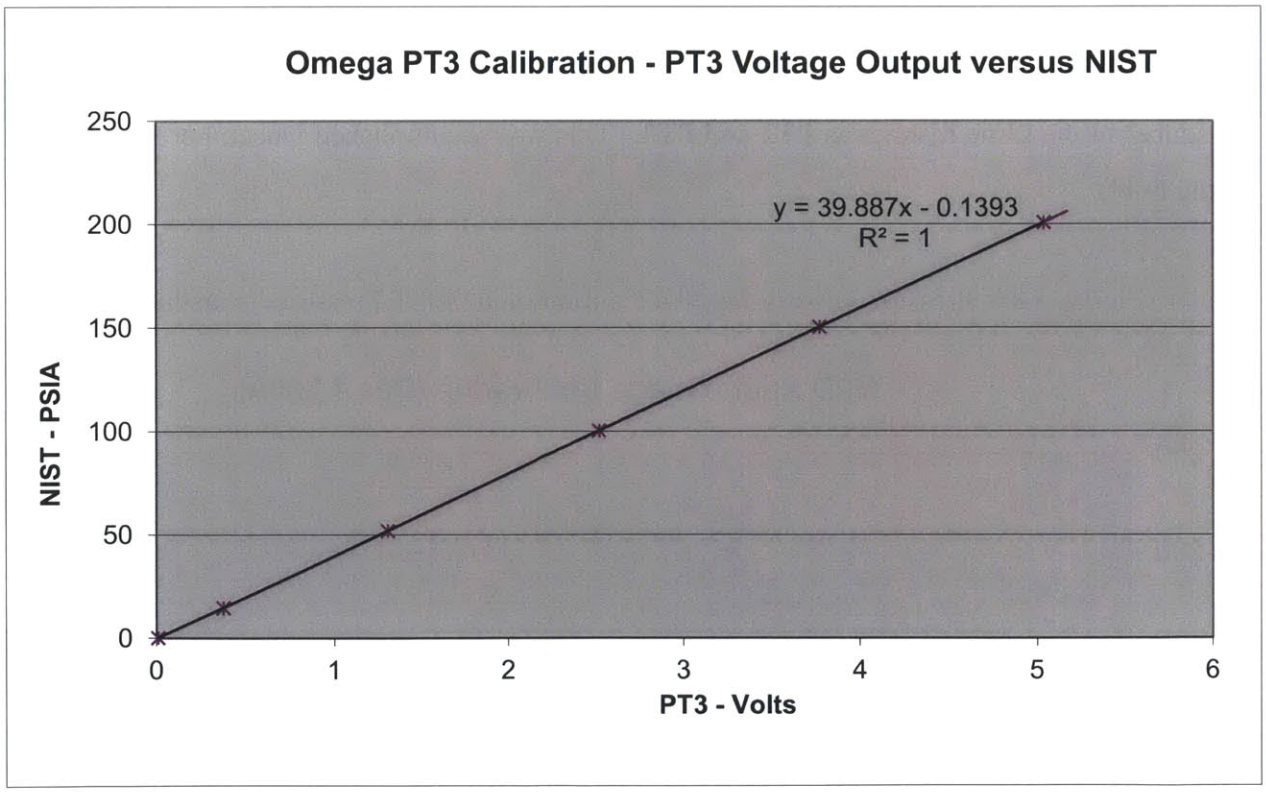

Like PT2, the linearity is excellent with correlation coefficient, R^2, greater than 99.99%. The stated accuracy of the Omega PT is +/-0.25% of full scale, which represents +/- 0.5 psi. This

calibration result is within the stated instrument accuracy. Again the manufacturer conversion from voltage output to pressure is taken (see Eq. 6.18).

$$Pr_{\mathrm{PT3}} = 40 \cdot PT3_{output} \qquad \text{Eq. 6.18}$$

6.13.2.4 PT4 – Condenser Exit

The fourth digital pressure measurement device, PT4, is mounted near the bottom of the condenser. Output range from the Ashcroft Xmitr is 1 to 5 volts. The manufacture represents linear response for the ideal conversion to pressure (psia) (see Eq. 6.19)

$$Pr_{\mathrm{PT4}} = \left(250 \cdot PT4_{output}\right) - 235.3 \qquad \text{Eq. 6.19}$$

Two calibrations were completed. The first was a cross calibration to a NIST certified pressure transducer in the same manner as PT2 and PT3. This was accomplished December 9, 2010 (see Figure 6-44).

Figure 6-44: Pressure History for PT4 Calibration to NIST Pressure Transducer

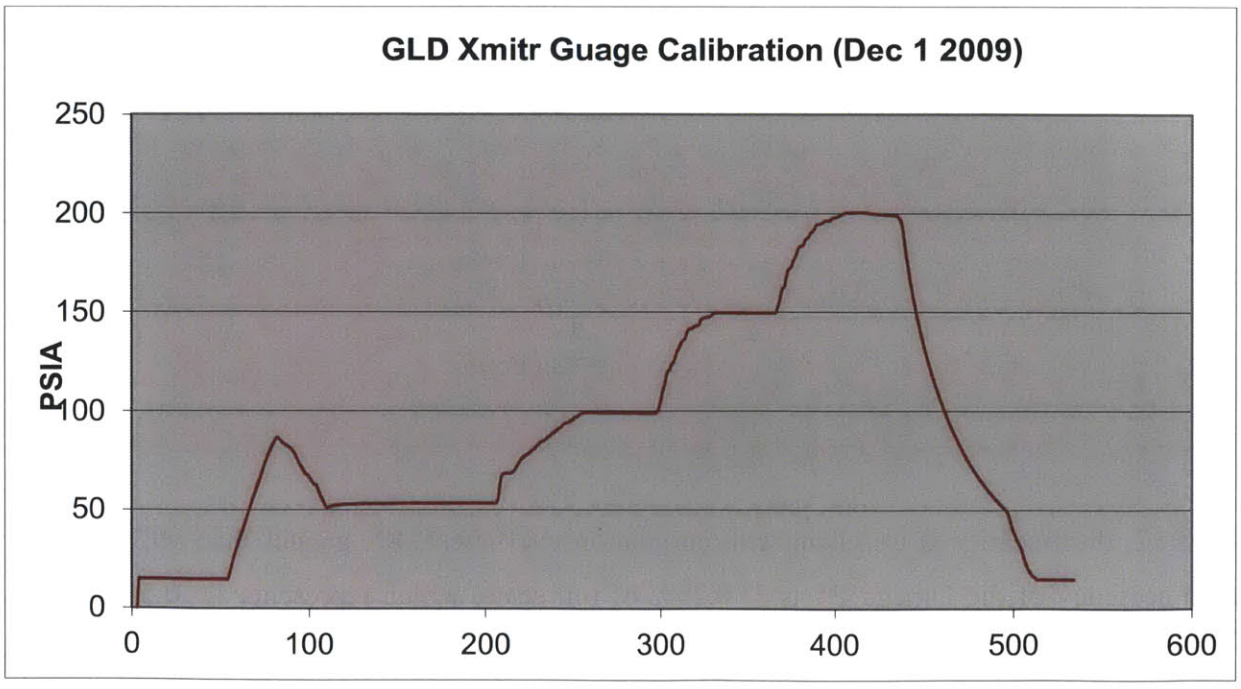

A linear regression was then done on PT4 voltage output (see Table 6-25) versus NIST pressure (see Figure 6-45).

Table 6-25: Averaged Pressure History for PT4 Output to NIST Pressure Transducer

# of Scans	Notation	PT4 [Volts]	NIST [psia]
1	Vacuum	0.948	0.1
1	1 atmosphere	1.003	14.7
51	1 atmosphere	0.966	14.714
75	~ 50 psia	1.118	53.177
42	~ 100 psia	1.29	98.916
35	~ 150 psia	1.49	149.435
26	~ 200 psia	1.69	199.812
21	1 atmosphere	0.981	14.718

Figure 6-45: Graph of Averaged Pressure History for PT4 Output to NIST Pressure Transducer

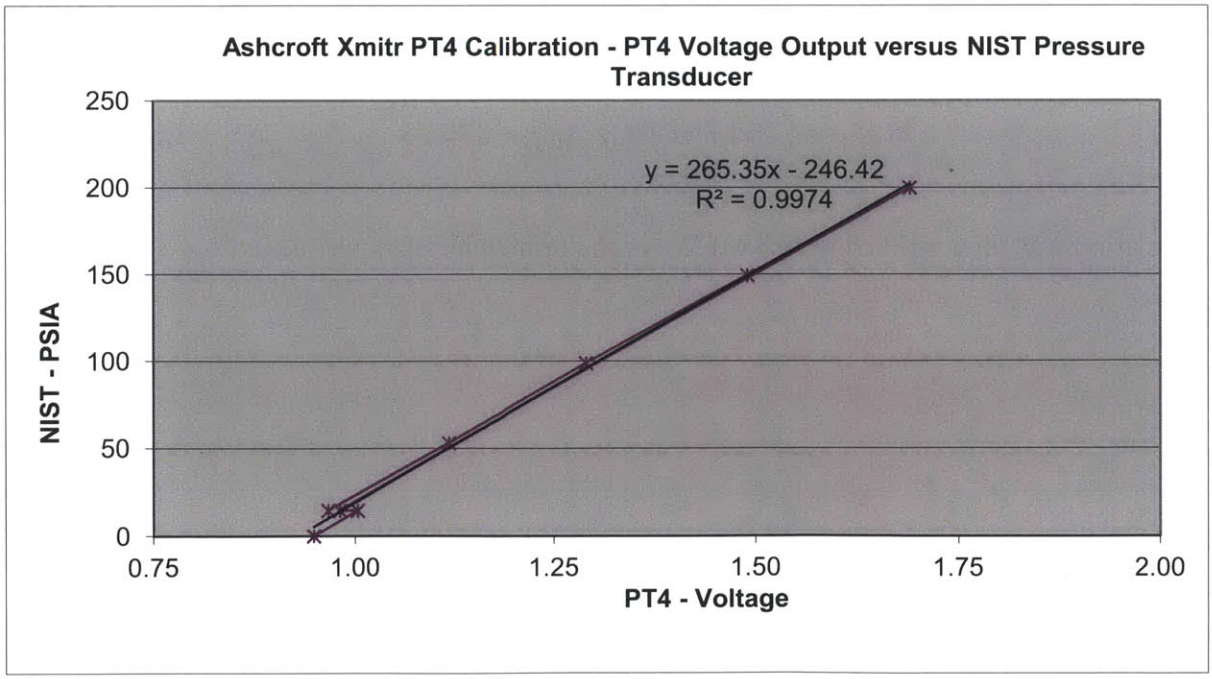

The correlation constants were taken from the linear regression. The recommended formula is then:

$$Pr_{\mathrm{PT4}} = \left(265.35 \cdot PT4_{output}\right) - 246.42 \qquad \text{Eq. 6.20}$$

The fit was very good with correlation coefficient, R^2, above 99.7%.

A second calibration was done in July 19, 2010. This calibration was accomplished by cross calibration of PT4 to PT2 and visual nitrogen gas regulator. The range calibrated was from 0 psi to 80 psi. As a result the coefficients were slightly changed and improved the R^2, above 99.97% (see Eq. 6.21).

$$Pr_{\mathrm{PT4}} = \left(266.53 \cdot PT4_{output}\right) - 253.56 \qquad \text{Eq. 6.21}$$

Some inconsistent low pressure reading justified a third calibration of PT4 done August 13, 2010. This calibration was accomplished by cross calibration to the visual nitrogen gas regulator (see Figure 6-46). The range calibrated was from 0 psi to 60 psi. As a result the coefficients were again changed (see Eq. 6.22).

$$Pr_{\mathrm{PT4}} = \left(263.7 \cdot PT4_{output}\right) - 235.73 \qquad \text{Eq. 6.22}$$

This relation was then utilized in LabVIEW for the remainder of experimentation.

Figure 6-46: Graph of Averaged Pressure History for PT4 Output to Ni Regulator Gauge

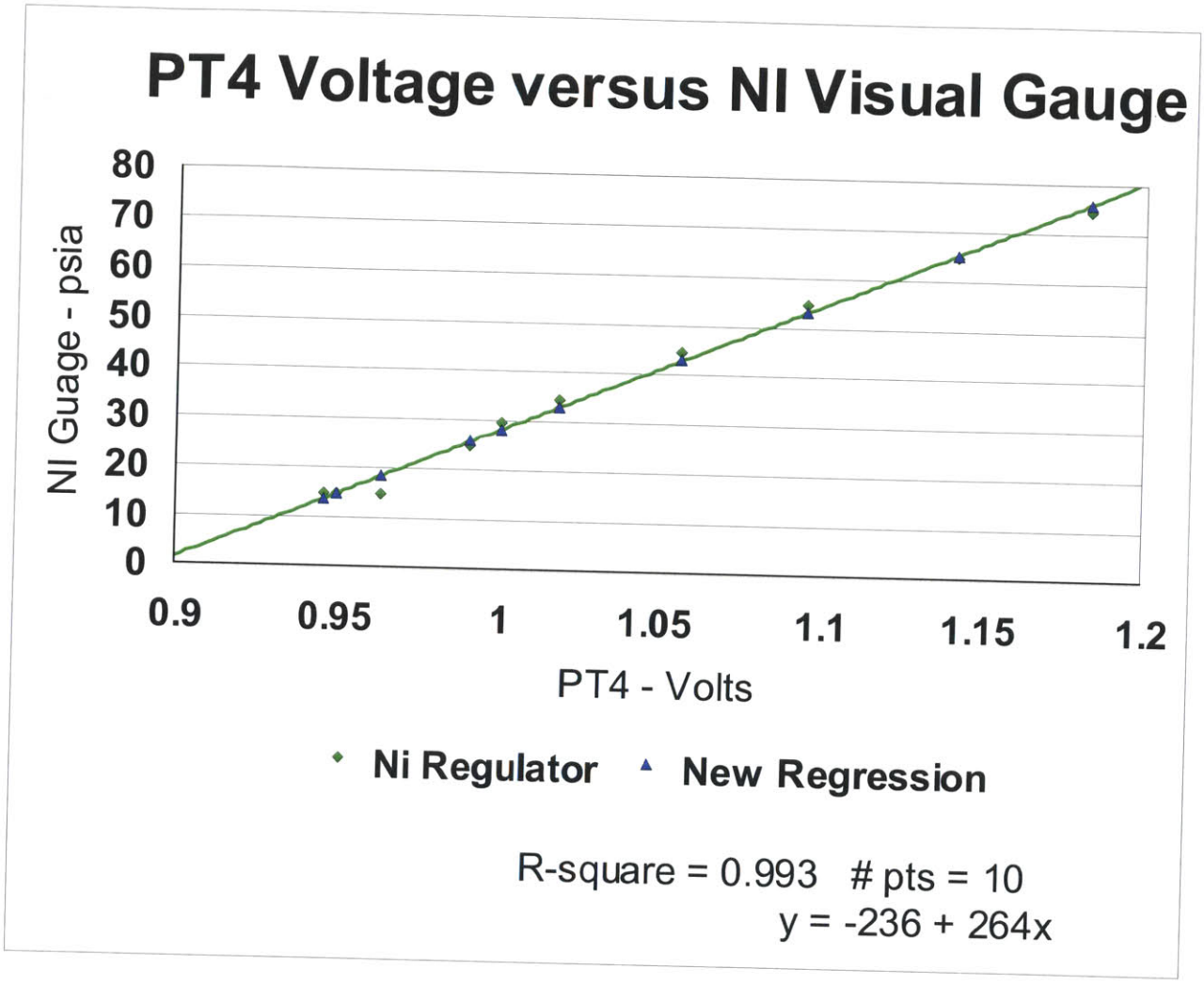

All pressure transducers provide results that are within manufacture stated accuracy. The Danfoss stated accuracy for PT1 is +/-1% of full scale. The Omega stated accuracy for PT2 and PT3 is +/- 0.25% of full scale. The stated accuracy for the pressures of interest for the Ashcroft Xmitr PT4 is +/- 1.5% of linear fit.

Note that all digital pressure transducers are checked before each experiment. This is accomplished when the loop is empty and open to the atmosphere. The initial pressure readings are recorded.

6.13.3 Flow Rate

The two flow meter devices where calibrated with a known volume and stop watch technique. Follow-up cross calibration of the turbine and vortex flow meter was also completed when deemed appropriate due to maintenance issues.

6.13.3.1 Turbine Flow Meter

The turbine flow meter was calibrated over a range of 7.6 lpm to 30.2 lpm (2 gpm to 8 gpm) with room temperature water. This range bounds the mass flux range of 500 to 1,500 kg/m^{2}s. The turbine flow meter is located downstream of the pump and upstream of the pre-heater. The Omega turbine flow meter also came with a calibration certificate (see Table 6-26). The lab calibration was compared to that provided by Omega.

Table 6-26: Omega Turbine Flow Meter Certified Calibration Data

Case	GPM	Frequency (Hertz)
1	7.51	1416
2	4.22	805
3	2.37	454
4	1.33	249
5	0.76	138

The calibration procedure took advantage of two 500 gallon tanks in the Green laboratory that have calibrated markings every 50 gallons [79]. The pump and turbine meter were set and then

timed via a stop watch over 50 gallons. The turbine meter outputs frequency which was recorded. Six flow rates were competed and are summarized below (see Table 6-27).

Table 6-27: Turbine Flow Meter Stop Watch Calibration

Test	Gallons	Time (minutes)	GPM	Frequency (Hertz)
1	25	13.85	1.80	341
2	25	10.97	2.28	430
3	25	6.70	3.73	704
4	50	12.28	4.07	788
5	25	4.45	5.62	1075
6	50	7.28	6.87	1300
7	50	6.96	7.18	1372
8	50	6.44	7.77	1507
9	50	65.37	9.32	1823

The data for both the Omega certified calibration and the lab measurements are plotted (see Figure 6-47) with volumetric flow rate [GPM] versus frequency. Note the range of interest is 2.5 gpm to 7.5 gpm.

Figure 6-47: Graph of Volumetric Flow Rate versus Frequency for Turbine Meter

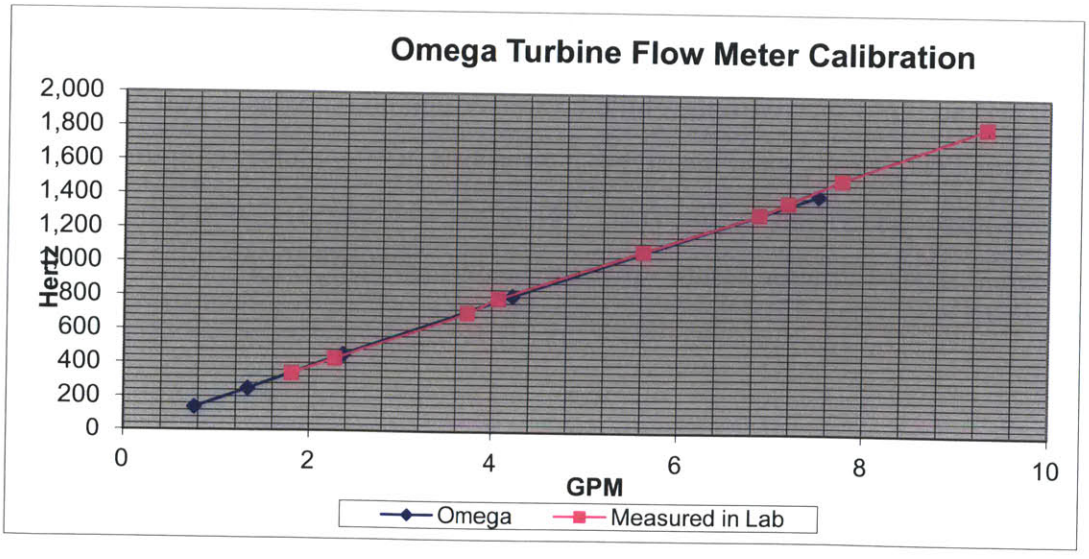

Agreement of the measured results in the lab and the Omega calibration data in the range of interest is excellent. The Omega data was taken and regressed to determine the linear coefficients to relate flow meter frequency to volumetric flow rate (gpm).

$$\beta_{\text{hw gpm}} = (f_{el} + 0.25)/189.22 \qquad \text{Eq. 6.23}$$

Where:

f_e = Frequency output of turbine meter

$\beta_{\text{hw gpm}}$ = Volumetric flow rate [gpm]

The loop hot water volumetric flow rate, β_{hw}, then is converted to metric units [m^3/s].

$$\beta_{hw} = (\beta_{\text{hw gpm}})/15852 \qquad \text{Eq. 6.24}$$

The constants are then programmed into LabVIEW to convert the frequency signal from the turbine flow meter into volumetric flow rate. Calibration results for the turbine flow meter are consistent with the manufacturers, Omega, stated accuracy of +/- 1% of reading.

6.13.3.2 Vortex Flow Meter

Chilled water flow rate on the tube side of the condenser is measured with an Omega Vortex Flow meter. The vortex flow meter is located upstream of the condenser tube side.

Calibration was accomplished with the chilled water system pressure head, two 50 gallon barrels, and stop watch. The barrels were measured and markets at 40 gallons. Output from the vortex flow meter is mA and is read by the DAQ. Note that the vortex flow meter has a threshold output of 4 mA. The calibration results are show below (see Table 6-28).

Table 6-28: Omega Vortex Flow Meter Stop Watch Calibration

Test	Gallons	Time (minutes)	GPM	Output (mA)
1	40	16.74	2.39	5.63
2	40	8.34	4.80	7.19
3	40	4.85	8.24	9.40
4	40	4.19	9.54	10.23

The resulting data is plotted with volumetric flow rate versus mA. The results are linearly fit (see Figure 6-48). The agreement between the measured results and the ideal linear behavior from Omega is excellent.

Figure 6-48: Graph of Volumetric Flow Rate [GPM] versus Output [mA] for Vortex Meter

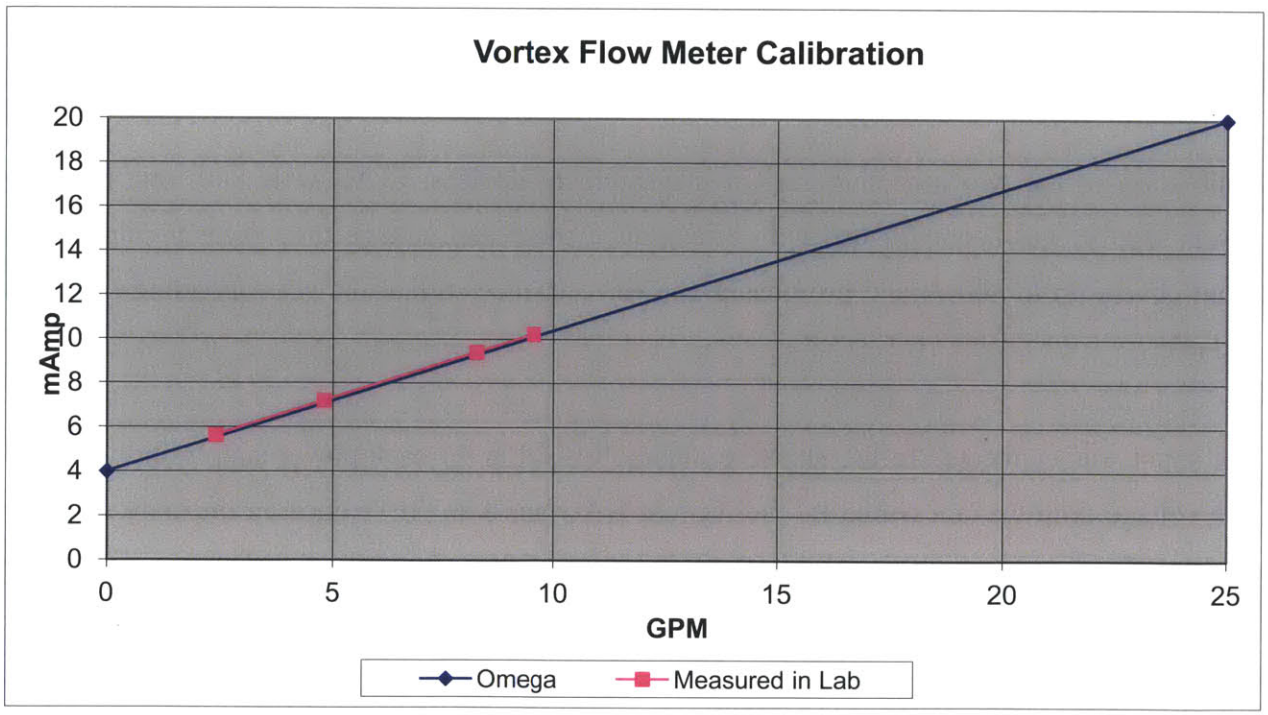

The Omega constants are accepted and then programmed into LabVIEW to convert the frequency signal from the turbine flow meter into volumetric flow rate. Omega, stated accuracy of +/- 2% of full scale.

$$\beta_{cw\,gpm} = (CWFM \cdot 1000 - 4)/0.64 \qquad \text{Eq. 6.25}$$

Where:

CWFM	=	Output of Vortex [mA]
$\beta_{cw\,gpm}$	=	Volumetric flow rate [gpm]

The loop hot water volumetric flow rate, β_{hw}, then is converted to metric units [m^3/s].

$$\beta_{cw} = (\beta_{cw\,gpm})/15852 \qquad \text{Eq. 6.26}$$

Periodically, cross calibration tests were done. These tests involved running the turbine flow meter and vortex flow meter in series on the loop with pump driven flow. No justification was found to change calibration constants for either the turbine or vortex flow meter.

6.13.4 Current

Calibration of the two inductive current measurement devices, LEM AHR 800, one for each power supply, was accomplished with a resistance shunt and voltage drop measurement. The shunt covers up to 800 A and provides a known resistance so that the corresponding output is 100 mV.

The shunt was connected to the negative locomotive cable for each power supply individually. The voltage drop was measured by the Agilent DAQ and LabVIEW once an intensity signal is given to the power supply (see Table 6-29 and Table 6-30). Intensity signals were sent to the power supply starting at zero and increasing by 10% up to 100%. The voltage drop and current measurement from the inductive meter was recorded. The shunt resistance is then divided into the measured voltage drop to calculate the current. The two currents are compared (see Figure 6-49 and Figure 6-50).

Table 6-29: Table of Shunt Calibration for PS1

Control Voltage	Count	PS1 [A]	Shunt{mV]	Shunt[A}
0	28	0.373565	0	0
1	28	30.9	4.3	34.4
2	10	91.6	11.8	94.4
3	13	152.5	19.3	154.4
4	13	213.6	26.7	213.6
5	9	274.5	34.0	272.0
6	8	335.6	41.8	334.4
7	10	396.7	49.0	392.0
8	7	457.7	57.0	456.0
9	6	518.7	64.0	512.0
10	5	579.8	71.0	568.0

Figure 6-49: Graph of Current Measured by PS1 Inductive Device versus Determined by Shunt

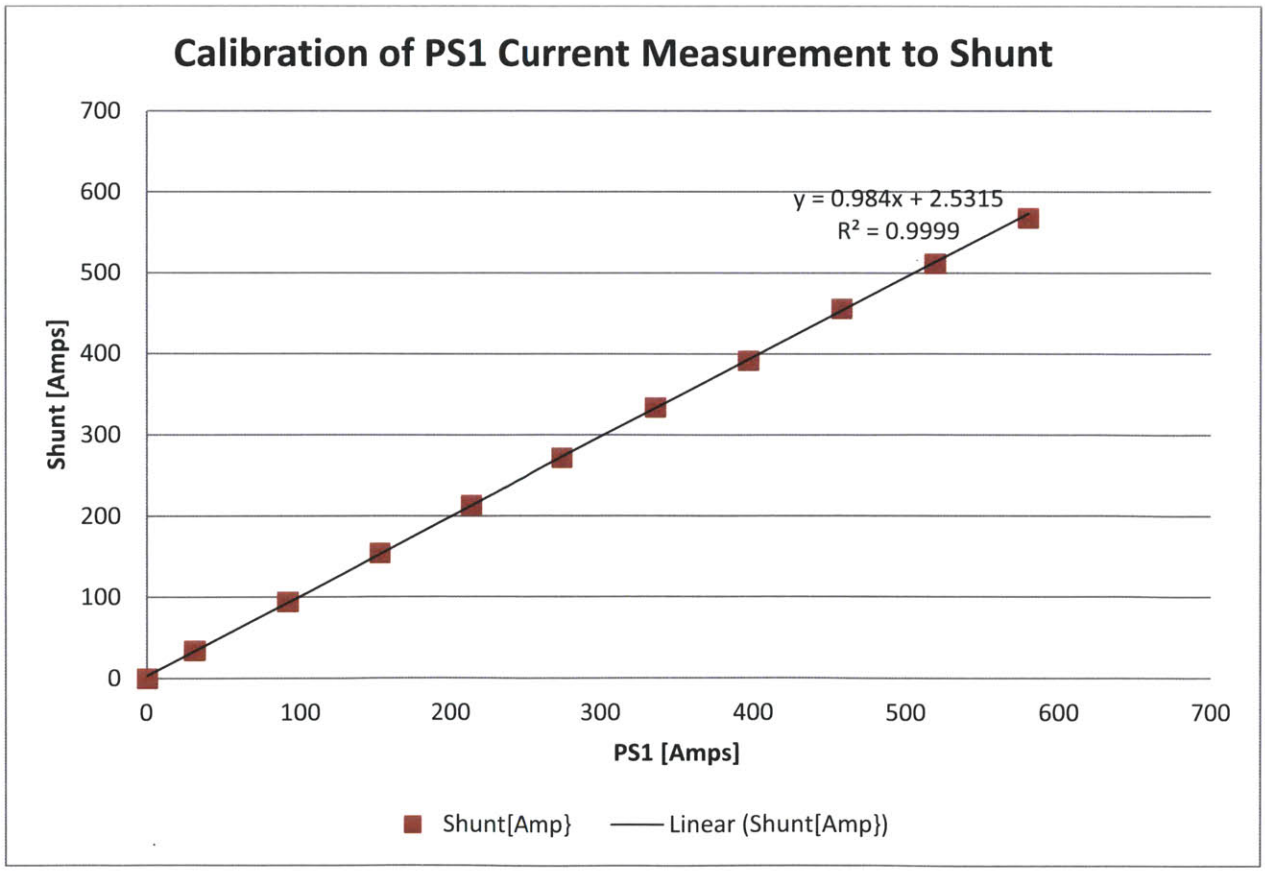

Table 6-30: Table of Shunt Calibration for PS3

Voltage	Count	PS1 [A]	Shunt{mV]	Shunt[A]
0	8	-0.77	0.00	0.00
1	10	34.8	4.6	36.8
2	7	95.7	12.0	96.0
3	6	156.7	19.0	152.0
4	6	217.8	27.0	216.0
5	6	279.0	34.0	272.0
6	6	340.1	42.0	336.0
7	7	401.3	49.0	392.0
8	6	462.4	57.0	456.0
9	5	523.6	64.0	512.0
10	5	584.8	72.0	576.0

Figure 6-50: Graph of Current Measured by PS3 Inductive Device versus Determined by Shunt

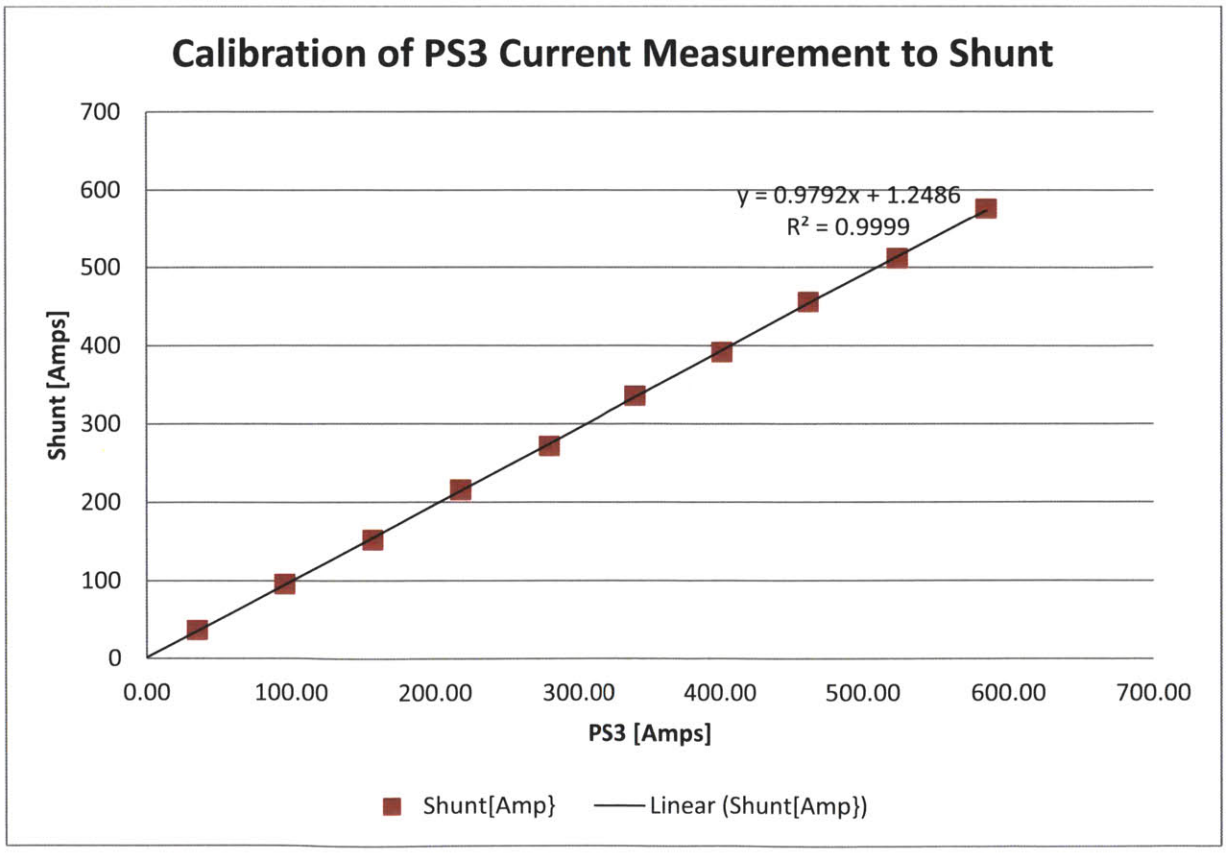

Linear fit of the current data measured by the LEM AHR 800 to that measured by shunt was completed. Agreement was excellent. Note the manufacture stated accuracy of PS1 and PS3 inductive current measurement is +/- 1% of full scale (8 A).

The linear relationship used is that recommended by the manufacturer, LEM (see Eq. 6.27).

$$I_{ps} = \left(PS_{output} \cdot 80\right) \qquad \text{Eq. 6.27}$$

Where: PS_{output} = AHR 800 Output [V]

I_{ps} = Power Supply Current [A]

6.13.5 Voltage Drop

The voltage drop across the test section is measured directly by the Agilent DAQ. The accuracy of voltage measurement is very high, +/- 0.004% and was accepted.

6.13.6 DO Measurement

Calibration of the DO probe is accomplished with reference to air at STP. The calibration and coefficient determination and implementation are internal to the device. The device has internal measurement and adjustment for temperature and barometric pressure. Basically once the calibration menu choice is made and the probe let to stand in air the device and probe to the rest. DO measurement in air at STP is about 8 ppm.

Generally, the DO probe is calibrated monthly.

Manufacturer measurement accuracy is +/- 1% of reading or about +/- 0.1 ppm at levels of interest.

6.13.7 Sample Resistance

The electrical resistance of a typical test heater was measured utilizing a 4-wire technique. For the SS316L test heater the measured resistance was 0.01033 Ohm. SA-508 has about one-third the electrical resistivity, $\rho_{el,\ SA508}$ equal to 2.7 μΩ-m, compared to SS316L $\rho_{el,\ Ss316L}$ equal to 7.49 μΩ-m at STP [80]. For the SA-508 the measured resistance was 0.00365 Ohm. The accuracy of these measurements is +/- 0.001 Ohms.

Electrical resistivity, ρ_{el}, of steel is temperature dependent (see Eq. 6.28). Resistance for both heater materials, SS316L and SA508, increase with temperature [81]. This relation is utilized to help identify the beginning of CHF. The sharp reduction in heat transfer with CHF causes a fast and dramatic increase in sample surface temperature. The increase in temperature then quickly increases the test heater resistance. Nearly half of the CHF experiments run end with the sample breaking do to the thermally induced stresses.

$$\Omega_{test\ section} = \rho_{el} \cdot \left(\frac{L}{A}\right) \qquad \text{Eq. 6.28}$$

Where:

L	=	Joule heating length (20 cm)		
A	=	Cross section area (0.15 cm^2)		
$\rho_{el,\ ss316}$	=	$7.49x10^{-7} + 5.35\ x10^{-10} * T$	[Ω-m]	
T	=	Heater Temperature	[°C]	

These inferred resistance calculations from the measurement of voltage drop and current are reviewed from the scanned data to help identify the moment that the CHF event starts (see Eq. 6.5). When the heated surface is subject to effective heat transfer conditions from either single phase liquid convection or forced nucleate boiling the temperature of the heater is generally within 30 °C of saturation temperature. For the conditions of interest herein the stable maximum heater temperature is less than 185 °C for the 5 atmosphere cases.

During heat up to CHF the resistance is highly stable. At the point of CHF the poor heat transfer rate of the vapor film causes rapid temperature rise and associated electrical resistance (see

Figure 6-51). The orange color of the heater at the location of CHF indicates a local temperature of approximately 1100 °C. The resistance then calculated from the current and voltage drop spikes up (see Figure 6.45).

Figure 6-51: Example Histogram of Test Heater Resistance

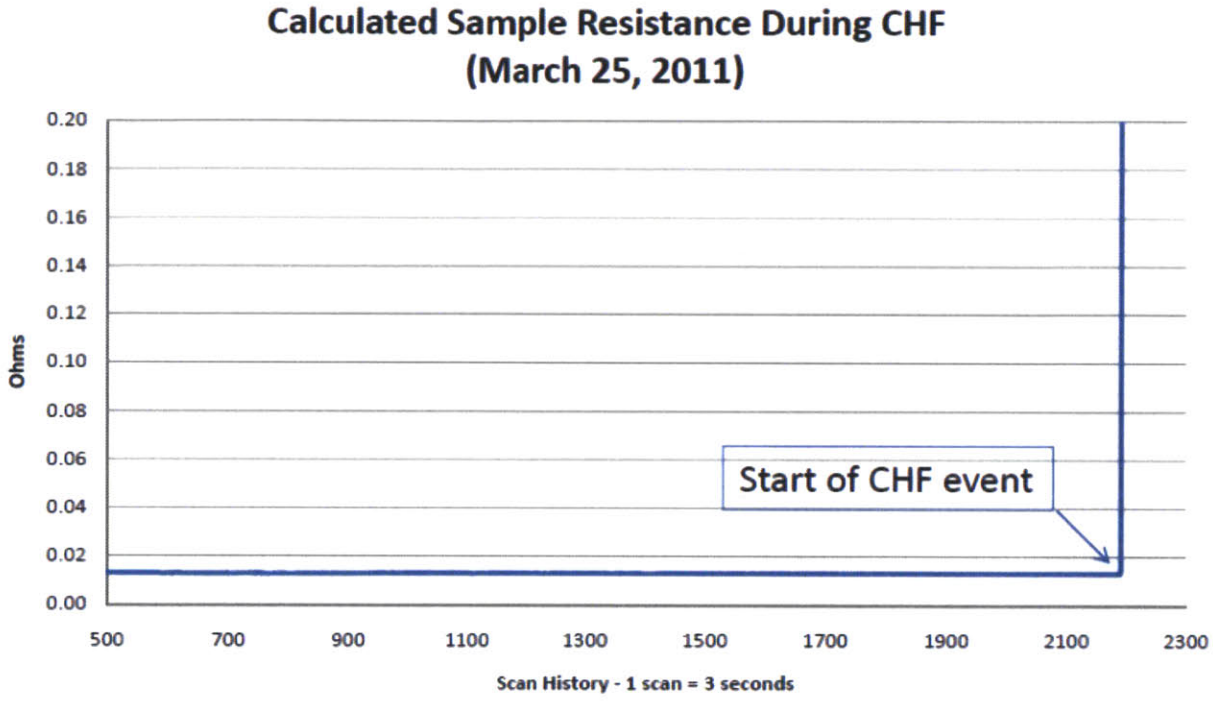

6.13.8 Downward Facing Angle

For each experiment the downward facing angle is measured with a digital goniometer. The orientation is downward horizontal ($\theta = 0^{o}$) to vertical ($\theta = 90^{o}$). The Wixey visual display provides 0.1^{o} reading accuracy. The Green Lab at MIT has a precision optical table that is used to zero the Wixey digital angle gauge before each experimental setup.

6.14 Measurement Uncertainties and Analyses

Manufacture's provided uncertainties are supported by calibrations completed. The accuracy of each instrument is taken to be that reported by the manufacturer (see Table 6-31). Accuracy is defined as the 95% confidence interval (2 σ_{std}), or better.

Table 6-31: Summary of Manufacturer Instrument Accuracy

Measurement	Manufacturer	Instrument Label	Accuracy
Temperature	Omega	RTDs	+/- 0.35 °C
Temperature	Omega	Type Ks	+/- 1.1 °C
Pressure	Omega	PT2 & PT3	+/- 0.25% full scale (0.5 psi)
Pressure	Danfoss	PT1	+/- 1.0% full scale (2 psi)
Pressure	Ashcroft	PT4	+/- 1.5% BFSL (psi)
Turbine Flow Meter	Omega	FM1	+/- 1.0% of reading (0.075 gpm)
Vortex Flow Meter	Omega	FM2	+/- 2.0% full scale (0.5 gpm)
Current	LEM	PS1 & PS3	+/- 1% of FS (8 A)
Voltage Drop	Agilent	TSVD	+/- 0.004% of reading (V)
DO	Mettler	DO	+/- 1% of reading (~ 0.1 PPM)
Angle	Wixey	θ	+/- 0.1°

Analysis of the propagation of measurement uncertainties is accomplished with two methods: (1) monte carlo and (2) propagation of error method [82].

CHF is determined by dividing the joule power delivered to the test section by the heat transfer surface area (Eq. 6.29). With CHF being a local phenomenon it is assumed that at the moment before the event starts the heat flux along the heater length is uniform due to joule heating through a constant area. The heater sits in a troth of machined MACOR insulator such that only the front surface is exposed to forced convective flow.

$$q''_{chf} = \left(\frac{V_{heater} \cdot I_{total}}{L_{heater} \cdot W_{heater} \cdot C_{bowing}}\right) \qquad \text{Eq. 6.29}$$

Where:				
	V_{heater}	=	Test section voltage drop	[V]
	I_{total}	=	$I_{PS1} + I_{PS2}$	[A]
	L_{heater}	=	$L_{total} - (2*L_{Stud})$	[0.20 m]
	W_{heater}	=	Heated surface width	[0.01 m]
	C_{bowing}	=	Area adjustment from bowing	[dimensionless]

Note that the relevant length, L_{heater}, does not include the studs at each end of the sample. This is due to the fact that the cross sectional area to current flow of the stud [2 cm^2] and total two stud length [5.715 cm] make the electrical resistance 47x smaller than the between stud length of 20 cm having 1 cm width, and 0.15 cm depth (see Eq. 6.28). Substituting Ohms Law (see Eq. 6.30), joule power is then directly proportional to resistance (see Eq. 6.31).

$$V = I \cdot \Omega \qquad \text{Eq. 6.30}$$

$$P_{test\ section} = I^2_{total} \cdot \Omega_{test\ section} \qquad \text{Eq. 6.31}$$

Where:			
	$P_{test\ section}$	=	Joule power to the test section
	$\Omega_{test\ section}$	=	Resistance across the test heater
	I_{total}	=	Total current through test heater

Additionally, it is assumed that near CHF heat conduction losses back into the MACOR insulator or back through the copper studs is negligible. This is reasonable given that the temperatures of the MACOR insulating block and attached copper couplings are near the saturation temperature of the working fluid thereby providing a small differential temperature, ~30 °C representing nucleate boiling surface temperature excess to saturation, from the heater surface to the MACOR for conduction. Additionally, MACOR is a good thermal insulator, k_{MACOR}=1.46 W/m-°C. Experiments are done in a quasi steady-state manner with incremental power changes with time between for the system to approach equilibrium.

Monte Carlo approach to error propagation was accomplished with the Excel add-in @RISK. For each right hand side component of determination of CHF (see Eq. 6.19) an uncertainty is modeled. Most of the uncertainties are assumed to be described by normal distribution (see Table 6-32). Dimensional uncertainty is from the fabrication drawing tolerances and equal to 0.0127 cm (0.005").

Table 6-32: Table of Uncertainty Parameters for CHF Calculation

Description	Symbol	Units	Uncertainty Type	Mean	Standard Deviation
Voltage Drop Across heater	V	Volts	Normal	6	0.004%
Current – PS1	I_{PS1}	Amperes	Normal	200	1.33%
Current – PS3	I_{PS3}	Amperes	Normal	200	1.33%
Total length of sample heater	L_{total}	meters	Normal	0.24	0.05%
Length of stud	L_{stud}	meters	Normal	0.02	0.65%
Width of heater	W_{heater}	meters	Normal	0.01	1.27%
Bowing area adjustment factor	C_{bowing}	dimensionless	Triangular	1.045	Min = 1.00 Max = 1.15 3.2%

An attempt is made to include in the surface area determination the influence of sample bowing. As the sample heats up all dimensions elongate. The expansion can be determined by:

$$\Delta L = \beta_{exp} \cdot L \cdot \Delta T \qquad \text{Eq. 6.32}$$

Where

β_{exp} = 16.2×10^{-6} /°C

L = 24 cm

ΔT = $T_{final} - T_{initial}$

$T_{initial}$ = 20 °C, room temperature

T_{final} = 183 °C, which represents T_{sat} at 5 atmospheres + 30 °C superheat

The resulting elongation of 0.634 mm (0.025") is less than the allowed expansion of 0.072 mm (0.0284"). The MACOR geometry therefore does provide sufficient room for the growth. Note the gap tolerance is actually larger because the MACOR also expands, but less than the steel sample.

The issue of bowing arises because the copper coupling into the heater is made water tight to the MACOR insulator via o-rings (see Figure 6-19). This contact point resists movement of the sample. Bowing is mitigated by preheating the MACOR and heater to about 110 °C before the o-ring is set. Nevertheless, some bowing can occur. Visually, bowing lifts the center of the sample less than the 1.5 mm, which is the sample width. If bowing does occur, most often the center life is less than 1 mm. Some experiments show almost no bowing.

To capture the added uncertainty to surface area a bowing area correction factor, C_{bowing}, is defined.

$$C_{bowing} = \frac{A_{heater} - A_{bow}}{A_{heater}} \qquad \text{Eq. 6.33}$$

Where:

A_{heater} = $L_{heater} * W_{heater}$ (20 cm^2)

A_{bow} = $2 * (1/2 * L_{heater} * \delta_{heater})$

δ_{heater} = Heater depth (1.5 mm)

The bow is basically a triangle. The bow area is twice the implied triangle for both sides. The minimum bow area is zero. The maximum is 3 cm^2 where the center is up 1.5 mm. This is conservative because the fact that the heater is pinned at the ends causes the side area showing to generally only occur in the middle 60% of the length. Therefore the minimum value of C_{bowing} is 1.0 and the maximum value is 1.15. To define a probability distribution an expected C_{bowing} is 1.045 and addresses visual experience.

The @RISK monte carlo simulation of 10,000 latin hypercube type samples resulted in (see Figure 6-52):

$$q''_{chf} = 1{,}126{,}921 \text{ W/m}^2$$

$$\sigma_{std} = 37{,}582 \text{ W}$$

$$\sigma_{q''} = 3.33\%$$

Figure 6-52: @RISK Monte Carlo of CHF

@RISK Output Report for Heat Flux [watts/m^2]
Performed By: Nuclear Science & Engineering
Date: Thursday, March 10, 2011 5:22:06 PM

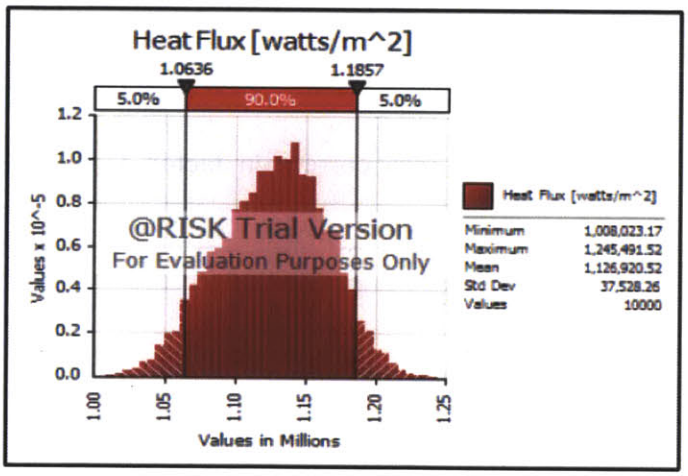

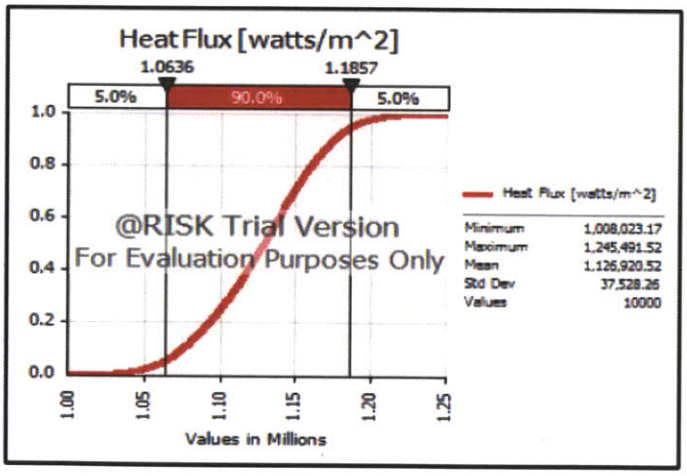

Simulation Summary Information	
Workbook Name	Uncertainty Analyses.xlsx
Number of Simulations	1
Number of Iterations	10000
Number of Inputs	7
Number of Outputs	3
Sampling Type	Latin Hypercube
Simulation Start Time	3/10/11 17:21:55
Simulation Duration	00:00:08
Random # Generator	Mersenne Twister
Random Seed	1022027594

Summary Statistics for Heat Flux [watts/m^2]			
Statistics		Percentile	
Minimum	1,008,023	5%	1,063,618
Maximum	1,245,492	10%	1,075,588
Mean	1,126,921	15%	1,084,997
Std Dev	37,528	20%	1,093,407
Variance	1408370236	25%	1,100,271
Skewness	-0.137275673	30%	1,106,958
Kurtosis	2.596901196	35%	1,113,115
Median	1,129,013	40%	1,118,319
Mode	1,139,159	45%	1,123,659
Left X	1,063,618	50%	1,129,013
Left P	5%	55%	1,133,637
Right X	1,185,667	60%	1,138,764
Right P	95%	65%	1,143,294
Diff X	122,050	70%	1,148,582
Diff P	90%	75%	1,153,837
#Errors	0	80%	1,159,893
Filter Min	Off	85%	1,167,072
Filter Max	Off	90%	1,174,531
#Filtered	0	95%	1,185,667

The propagation of error method assumes that all the contributors to uncertainty are independent and normal (see Eq. 6.34).

$$\frac{U_{q"chf}}{q"chf} = \sqrt{\left(\frac{U_v}{V}\right)^2 + 2\cdot\left(\frac{U_{Ips1}}{I_{ps1}}\right)^2 + \left(\frac{U_{L_{total}}}{L_{total}}\right)^2 + 2\cdot\left(\frac{U_{L_{stub}}}{L_{stud}}\right)^2 + \left(\frac{U_w}{W}\right)^2 + \left(\frac{U_{C_{bowing}}}{C_{bowing}}\right)^2} \quad \text{Eq. 6.34}$$

$$\frac{U_{q"chf}}{q"chf} = \sqrt{(0.004\%)^2 + 2\cdot(1.33\%)^2 + (0.05\%)^2 + 2\cdot(0.65\%)^2 + (1.27\%)^2 + (3.2\%)^2}$$

$$\frac{U_{q"chf}}{q"chf} = 4.02\%$$

The propagation of error method yields the larger heat flux uncertainty (σ_{chf} =4.02%) and is accepted.

6.15 Agilent DAQ

Analog instrumentation output and control are provided by the Agilent 34980A data acquisition system (see Figure 6-53). The Agilent DAQ has two cards: (1) 34921T data card and (2) the 34952T control card.

Figure 6-53: Photo of Agilent 34980A DAQ

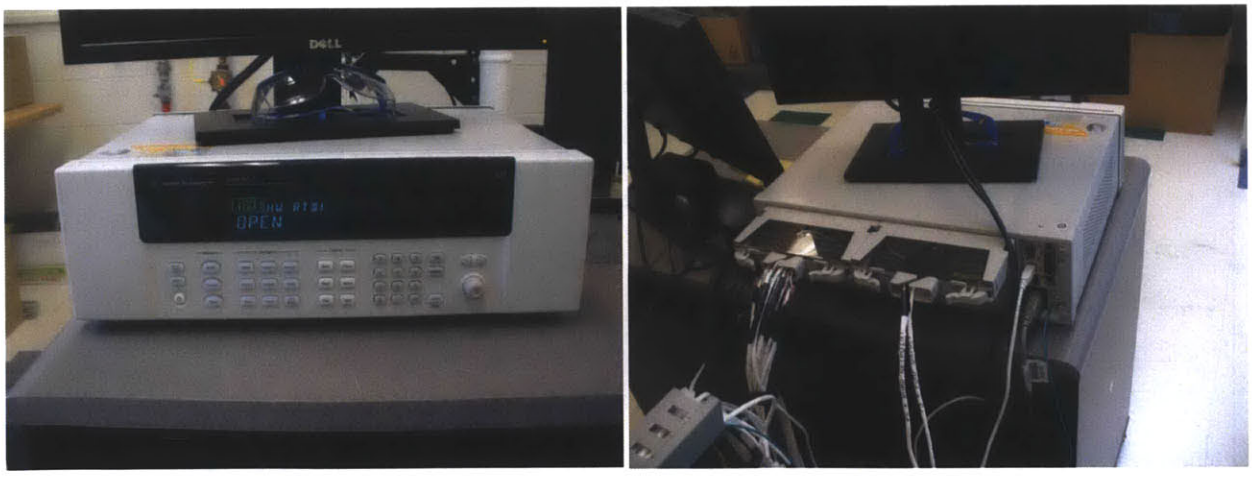

The Agilent DAQ scans all instruments at a set scan interval that is user input. Generally three (3) seconds is utilized through the experimental matrix. Analog signals from instrumentation, like voltage, frequency, or amps, are then converted to digital and recorded. For control, digital input from the user is converted to volts and transmitted to the device to be controlled. The pump and the power supplies are also controlled through the Agilent DAQ.

6.15.1 Agilent Data Card

Twenty-six (26) instruments occupy thirty (30) of the forty-four (44) channel slots of the Agilent 34921T measurement card are used (see Figure 6-54 and Figure 6-55). Three types of signals are measured from the digital instrumentation: voltage, current and frequency. The frequency measurement is from the turbine flow meter. The frequency of the rotating turbine is linearly related to the volumetric flow rate (see Eq. 6.23). Current measurement is output from the Omega vortex flow meter mounted on the chilled water system and the Danfoss pressure transducer mounted on the pump. All other instruments including: RTDs, type-K thermocouples, pressure transducers and locomotive cable current measurement provide voltage signal outputs.

Figure 6-54: Figure of Agilent 34921T Data Card Channels

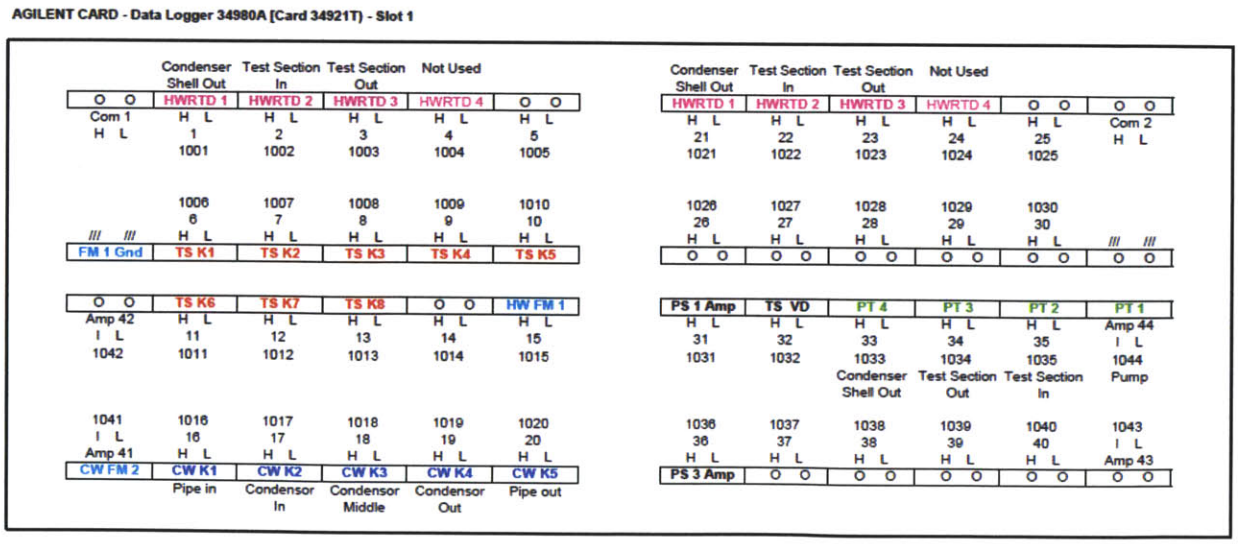

Figure 6-55: Photo of Agilent 34921T Data Card

6.15.2 Control Card

Four (4) of seven (7) channels of the Agilent 34952T control card are used (see Figure 6-56 and Figure 6-57). Channel 1 turns on or off the two (2) DC power supplies. These two are operated in tandem. Channel 2 turns on or off the pump. Channel 6 sends a [0 – 10] voltage signal to the pump to set flow intensity. Channel 7 sends a [0 – 10] voltage signal to both power supplies to set DC current intensity.

Figure 6-56: Figure of Agilent 34952T Control Card Channels

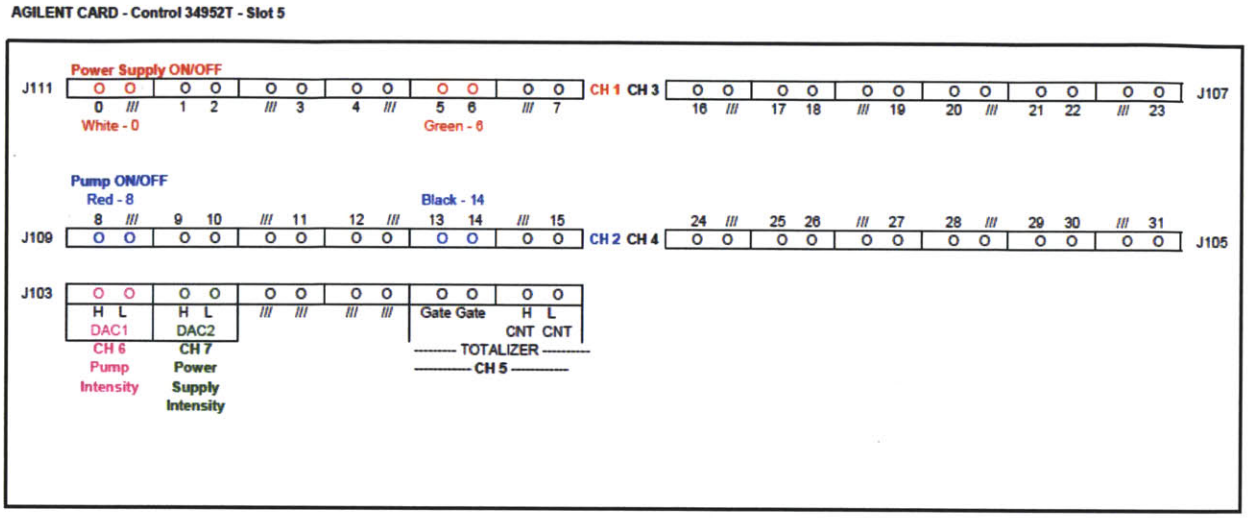

Figure 6-57: Photo of Agilent 34952T Control Card

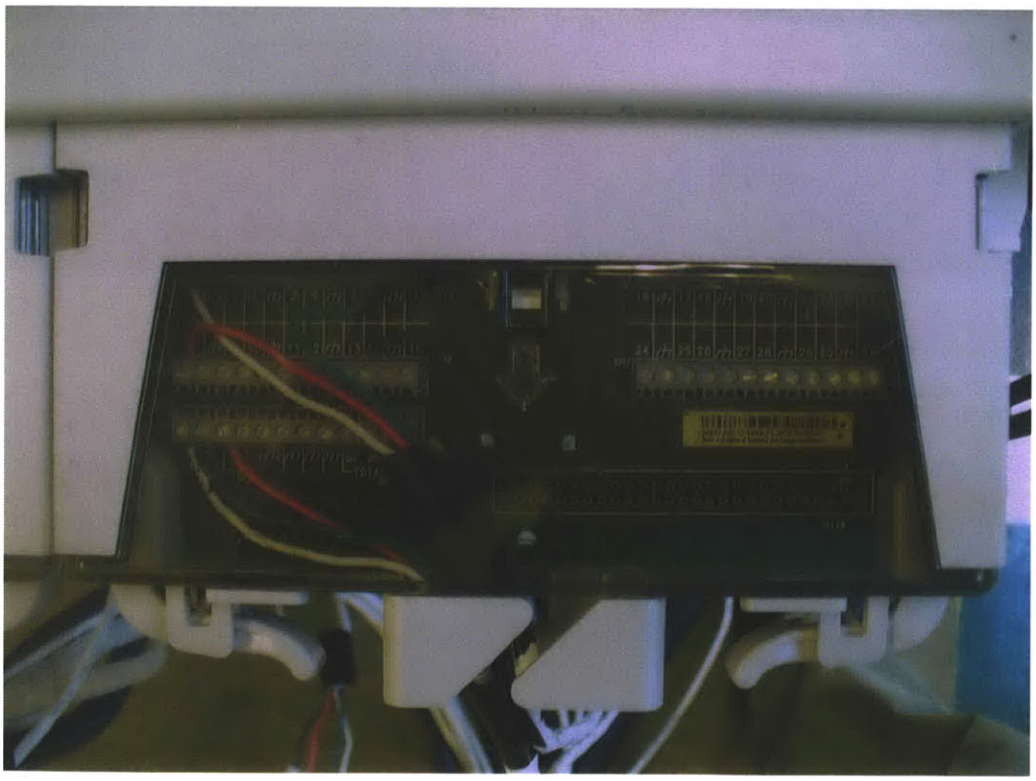

Signals sent to the power supplies and pump together with the Agilent DAQ and LabVIEW virtual instrument software allow for control of the experiment from a signal computer (see Figure 6-58).

Figure 6-58: Photo of Computer Running LabVIEW

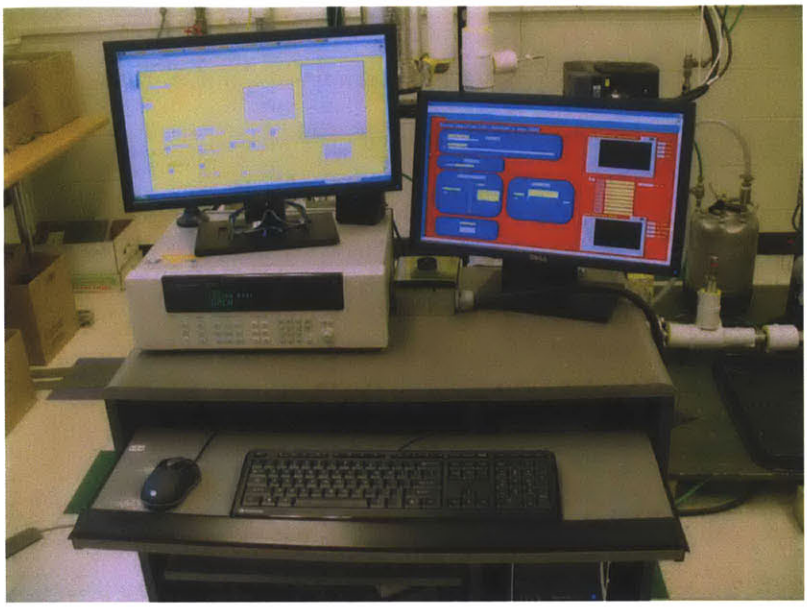

6.15.3 Control Box

A control box was designed and assembled to provide: (1) power to instruments, (2) control switches for the large power supplies, (3) control switches for the pump, and (4) an emergency stop (see Figure 6-59).

Figure 6-59: Photo of Control Box

Several instruments require DC supply including: RTDs, pressure transducers, and flow meters. The control box incorporates a 24 volt DC power supply and associated wiring and grounding. The power to the DC supply is provided by a 110 volt AC room outlet (see Figure 6-60). A green indicator light on the outside of the control box is on when power to the control box is on.

Figure 6-60: Photo of Internals of Control Box

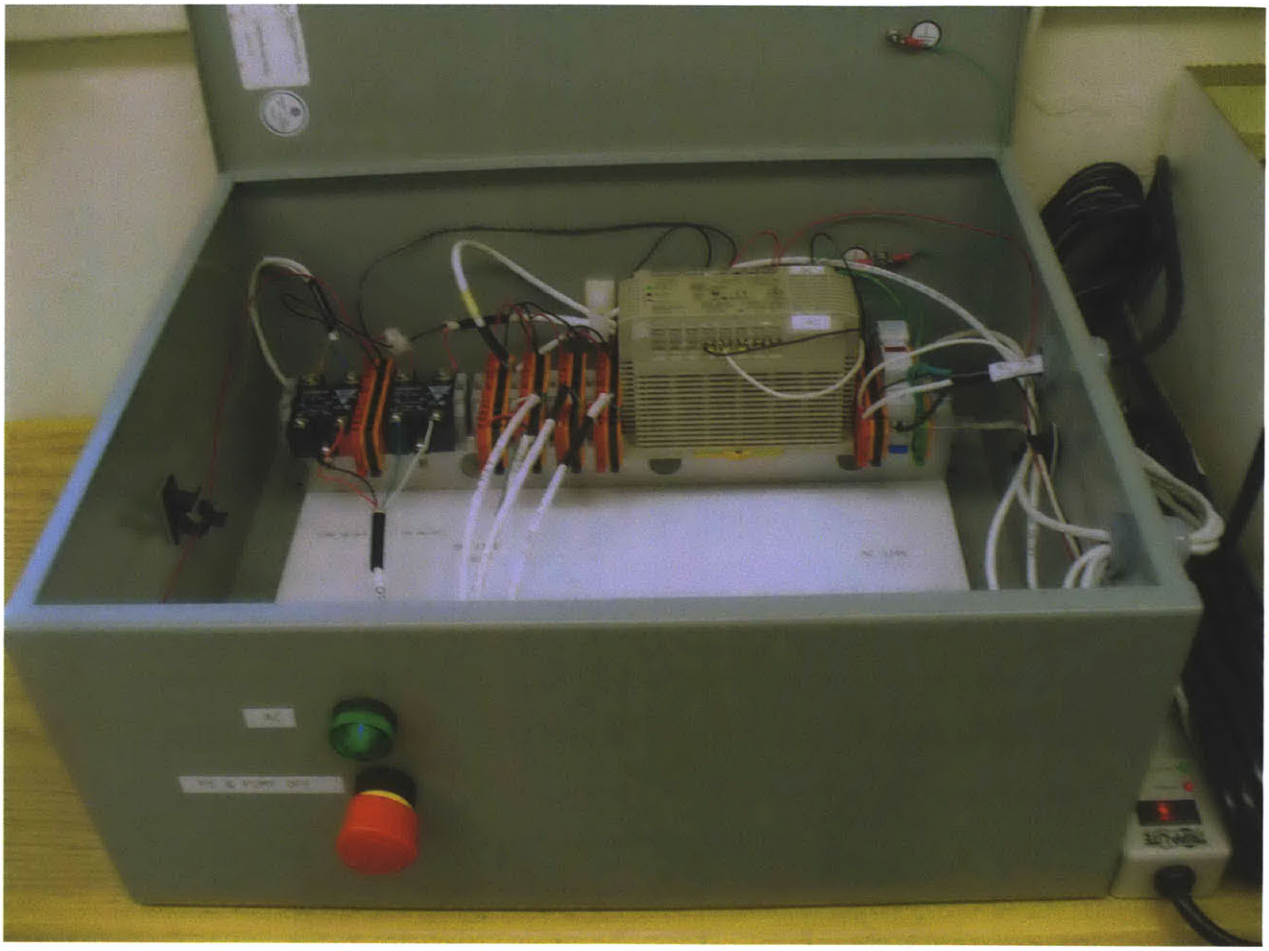

One solid-state relay ("SSR") acts as an ON/OFF switch for the two (2) large power supplies. These large power supplies are used in tandem. Functionally, the user toggles the power supplies on in LabVIEW which then directs the Agilent control card to output a voltage to the SSR thereby opening the relay. In a similar way a second, adjacent SSR acts as an ON/OFF switch for the pump.

An emergency stop button is incorporated into the control box.

6.16 LabVIEW Control & Measurement Program

LabVIEW, version 8.5, by National Instruments was chosen to: acquire data, process data for real time calculations of parameters of interest, present real time data, store both acquired data and calculated parameters and control operation of the loop and components through the Agilent system. LabVIEW is an object oriented control language specially developed for scientific data acquisition and process control.

Generally, LabVIEW provides a user interface called a front panel (see Figure 6-61). The front panel allows the user to send signals to devices to be controlled and to present data acquired and processed. Data can be presented graphically, digitally or both.

Data acquired from the Agilent system is periodic and set by choice of the user. Most experiments run herein had scan rates of once every three (3) seconds. The scan of all channels takes less than a second. Once the data is scanned, downstream processing of the data occurs including presentation routines for tables or graphs. Finally, data and processed variables are saved in spreadsheet comma separated value ("csv") format.

Figure 6-61: Photo of LabVIEW Front Panel

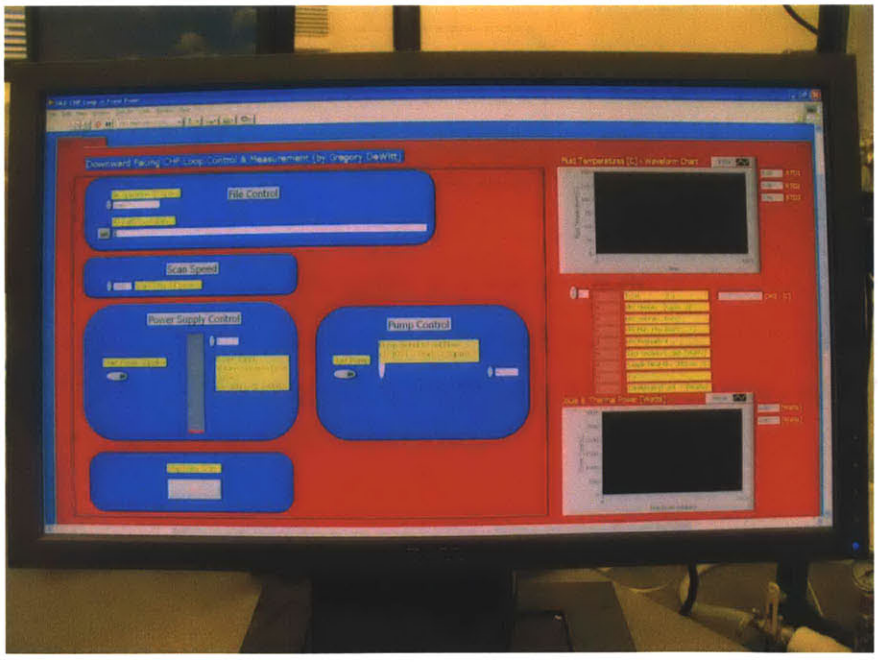

The logic of the LabVIEW program is visualized on the simplified block diagram (see Figure 6-62).

Figure 6-62: Simplified LabVIEW Block Diagram

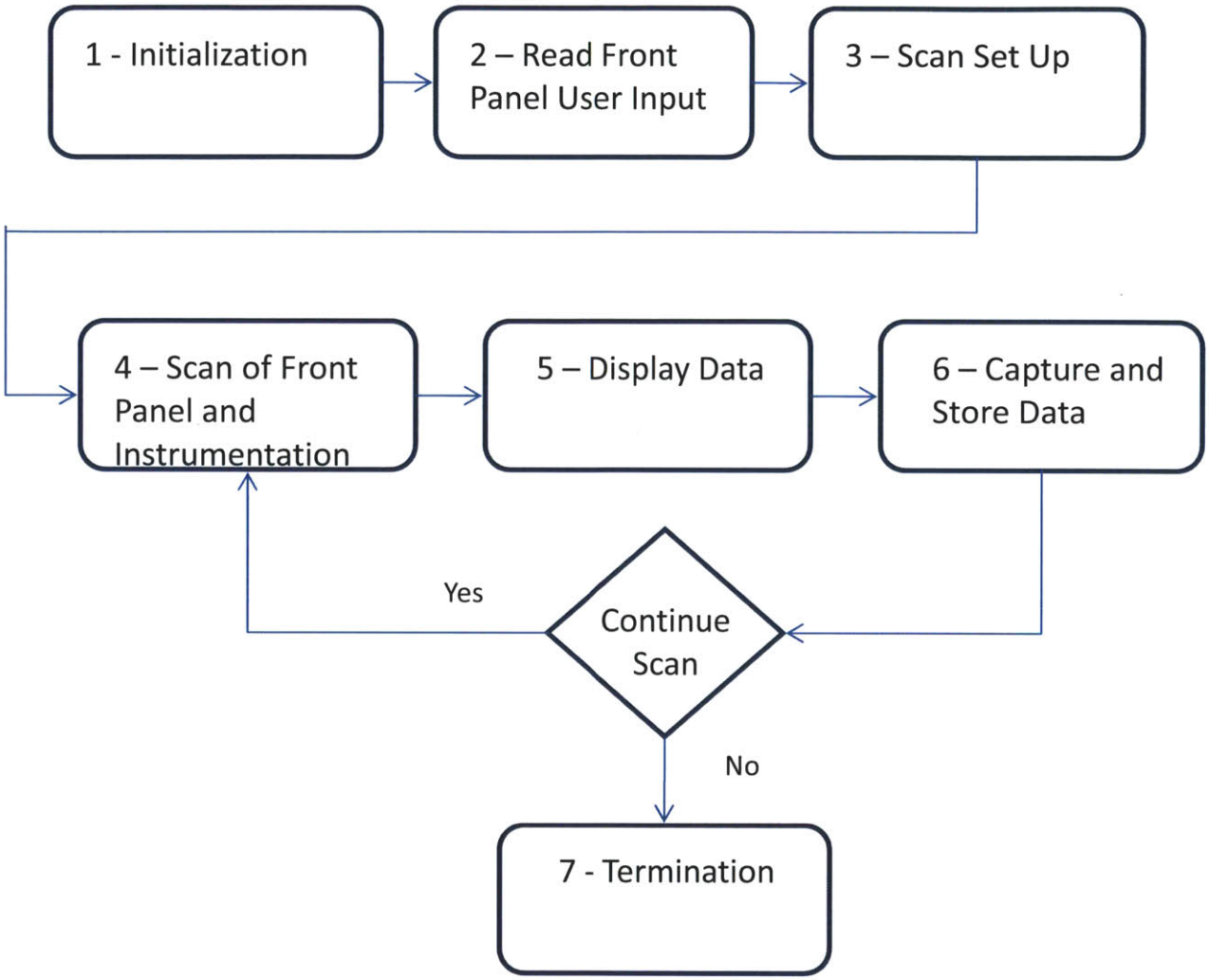

The program has seven (7) main elements: (1), initialization, (2) reading of front panel user input, (3) scan set up, (4) scan of front panel and instrumentation, (5) post scan calculations, (6) display data, (7) data capture, and (8) termination (see Appendix F).

6.16.1 Initialization

Initialization defines the DAQs device that LabVIEW is to interface with, Agilent 34980A, and how the interface is to occur. This first phase of the LabVIEW program also sets up the data flow and error handling.

6.16.2 Read Front Panel

LabVIEW reads parameters input by the user on the front panel (see Figure 6-61). First, the data file to be written is identified and then how the data is to be managed. Data can create a new file, overwrite an old file, or append what is already in a file. The file is then opened.

Second, the scan rate is input by the user on the front panel in milliseconds. Most tests were run with one scan every 3,000 msec (3 seconds).

Next, ON/OFF buttons are provided for the pump and power supplies. Green indicates on. The power supplies operate in tandem so one button signals both. The intensity level for both the pump and the power supplies are then read within the scan. The intensity scale is 0 to 10.

6.16.3 Scan set up

Scan set up portion of the LabVIEW program involves identifying the channels to be read from each the Agilent 34921T data card and the Agilent 34952T control card. Descriptive labels for each are then associated (see Table 6-33). Next, a clock is defined and initiated. The clock captures date and time information to the second for each scan.

Table 6-33: Instrument Scan List and Labels

Label	Source	Channel
DATE	LabVIEW	na
TIME	LabVIEW	na
HWRTD1	Agilent	1001
HWRTD2	Agilent	1002
HWRTD3	Agilent	1003
HWRTD4	Agilent	1004
TSK1	Agilent	1006
TSK2	Agilent	1007
TSK3	Agilent	1008
TSK4	Agilent	1009
TSK5	Agilent	1010
TSK6	Agilent	1011
TSK7	Agilent	1012
TSK8	Agilent	1013
HWFM	Agilent	1015
CWK1	Agilent	1016
CWK2	Agilent	1017
CWK3	Agilent	1018
CWK4	Agilent	1019
CWK5	Agilent	1020
PS1	Agilent	1031
TSVD	Agilent	1032
PT4	Agilent	1033
PT3	Agilent	1034
PT2	Agilent	1035
PS3	Agilent	1036
CWFM	Agilent	1041
PT1	Agilent	1044

6.16.4 Scan

Each scan has three main components: (1) get the time stamp, (2) fetch the instrument data to be scanned, (3) read the front panel input from user, (4) calculated parameters of interest from scanned data, (5) write and store array of fetched and calculated data and (6) present data to user front panel via table or graph.

Time stamp includes date and time and is written as two fields: (1) date and (2) time. Date includes month, day and year. Time is formatted to include: hour, minutes, and seconds.

Next, fetch of the twenty-six (26) Agilent channels utilized occurs in channel number order. A one dimensional array is created with all the fetched data. The initial array is only of the Agilent data and the time stamp.

Next, the base array will be appended with calculated parameters and front panel user input data. LabVIEW allows for various calculations to be executed and results stored. Calculations completed for each scan are detailed in the following section.

6.16.5 Post Scan Calculations

Conversions of instrument signals to physical parameters are done with a formula node within LabVIEW. A total of five (5) conversion types are done (see Table 6-34). Omega digital pressure transducers voltage output [Volts] is converted to pressure [psia]. Danfoss digital pressure transducers output [mA] is converted to pressure [psia]. Turbine flow meter frequency [Hertz] is converted to volumetric flow rate [gpm]. Vortex flow meter current output [mA] is converted to volumetric flow rate [gpm]. Induction current device output [Volts] is converted to current [Amps]. All temperature measurements from either type-K thermocouples or RTDs are automatically converted to ^{o}C by LabVIEW with not additional user programming.

Table 6-34: Table of LabVIEW Instrument Output Conversions

Type	Label	Channel	Output Type	Conversion	Equation
Pressure	PT1	1044	Amp	psia	Eq. 6.16
Pressure	PT2	1035	Volt	psia	Eq. 6.17
Pressure	PT3	1034	Volt	psia	Eq. 6.18
Pressure	PT4	1033	Amp	psia	Eq. 6.19
Flow	HWFM	1015	Hertz	gpm	Eq. 6.23
Flow	CWFM	1041	Amp	gpm	Eq. 6.25
Current	PS1	1031	Volt	Ampere	Eq. 6.27
Current	PS3	1036	Volt	Ampere	Eq. 6.27

All of the conversions are accomplished within the formula node of the LabVIEW program (see Appendix F). Formula node is designed to handle relatively simple algebraic operations. Several additional calculations are completed within this node and are described below.

Total current is determined and is the sum of the current delivered by the two DC power supplies [A].

$$I_{Total} = I_{PS1} + I_{PS3} \qquad \text{Eq. 6.35}$$

Joule power, P, is then calculated with the total current and voltage drop [W].

$$P = I_{Total} \cdot TSVD \qquad \text{Eq. 6.36}$$

Volumetric for rate for both loop side flow and chilled water flow, which are in units of GPM, are converted to metric [m^3/s].

$$\beta_{hw} = (\beta_{hw\,gpm})/15852 \qquad \text{Eq. 6.24}$$

$$\beta_{cw} = (\beta_{cw\,gpm})/15852 \qquad \text{Eq. 6.26}$$

Resistance of the sample is calculated with Ohms law, total current and voltage drop [Ohms].

$$\Omega_{test\ section} = \frac{V_{test\ section}}{I_{total}} \qquad \text{Eq. 6.14}$$

Where: $V_{test\ section}$ = TSVD [Volts]
Test Section Voltage Drop

Results of formula node calculations are appended and stored for each scan cycle.

Next, within a MATLAB node, a number of additional calculations are accomplished for each scan. Note that a set of MATLAB functions that interpolate steam table properties are utilized (see Table 6-35 and Appendix A-8).

Table 6-35: Table of MATLAB Functions Utilized for Water/Steam Properties

Function Name	Description	Input	Output Units
Ts	Saturation temperature	Pressure [bar]	°C
vf	Fluid specific volume	Temperature [°C]	m^3/kg
vg	Gas specific volume	Temperature [°C]	m^3/kg
muf	Fluid dynamic viscosity	Temperature [°C]	$N\text{-}s/m^2$
hfg	Heat of vaporization	Temperature [°C]	kJ/kg
Cpf	Fluid specific heat at constant pressure	Temperature [°C]	kJ/kg-°C
hf	Fluid enthalpy	Temperature [°C]	kJ/kg

The first data element calculated in the MATLAB node is the saturation temperature for the test section exit. This is accomplished by referencing the MATLAB "Ts" function with the pressure from PT3, which is located at the exit end of the heater. Note that PT3 output [psia] is converted to bar. The result is recorded each scan [°C].

$$T_{sat,exit} = ts(PT3 * 0.0689476) \quad \text{Eq. 6.37}$$

Next, the test section entrance liquid density is determined and recorded each scan [kg/m^3]. This is accomplished by referencing the MATLAB "vf" function with the temperature from RTD2, which is located just before the test section.

$$\rho_{f,entrance} = 1/vf(RTD2) \quad \text{Eq. 6.38}$$

Next, fluid velocity at the entrance is determined and recorded [m/s]. Entrance conditions are single phase liquid. This is accomplished by referencing the loop volumetric flow rate and dividing by the flow cross sectional area along the heater.

$$v_{f,entrance} = \beta_{hw}/A_f \quad \text{Eq. 6.39}$$

Where:

β_{hw}	=	Volumetric flow rate from Eq. 6.14	
A_f	=	$w_{channel} * \delta_{channel}$	[m^2]
$w_{channel}$	=	channel width	[1.43 cm]
$\delta_{channel}$	=	channel depth	[2.0 cm]

Test section mass flux is next determined and recorded [kg/m^2-s]. This is accomplished by referencing the entrance fluid velocity multiplying by the entrance fluid density. Conservation of mass and constant area require that mass flux remain constant along the rectangular heater flow channel.

$$G_{test\ section} = v_{f,entrance} \cdot \rho_{f,entrance} \quad \text{Eq. 6.40}$$

Where:

$v_{f,entrance}$	=	Flow velocity from Eq. 6.27
$\rho_{f,entrance}$	=	Fluid density from Eq. 6.26

To get an indication of the level of turbulence entering the test section, the dimensionless Reynolds number is next determined and recorded. Dynamic viscosity is determined by the MATLAB "muf" function with temperature from RTD2.

$$Re_{f,entrance} = \frac{G_{test\ section} \cdot D_e}{\mu_{f,entrance}} \qquad \text{Eq. 6.41}$$

Where:

D_e	=	$4 * A_f / P_w$	[m]
P_w	=	$(w_{channel} + \delta_{channel}) * 2$	[m]
$\mu_{f,\ entrance}$	=	muf(RTD2)	[N-s/m^2]

Now a thermal heat balance on the test section is determined and recorded [W]. This calculation is only appropriate for single phase fluid flow. The specific heat of water at constant pressure is determined by the MATLAB "Cpf" function and referencing the average bulk fluid temperature in the test section.

$$Q_{test\ section} = \dot{m}_{hw} \cdot Cp_{f,average} \cdot (T_{exit} - T_{entrance}) \qquad \text{Eq. 6.42}$$

Where:

$$\dot{m}_{hw} = \beta_{hw} \cdot \rho_{f,entrance} \qquad \text{Eq. 6.43}$$

$Cp_{f,\ average}$	=	$Cpf(T_{avg})*1000$	
		MATLAB function for fluid specific heat	[J/kg-^{o}C]
T_{avg}	=	$(T_{entrance} + T_{exit}) / 2$	[^{o}C]
T_{exit}	=	Bulk temperature RTD3 after test section	[^{o}C]
$T_{entrance}$	=	Bulk temperature RTD2 before test section	[^{o}C]

Next, surface heat flux is calculated assuming all joule power exits the heater from the surface parallel to flow and between the end studs [MW/m^2]. It is also assumed that the heat flux along the heater length is constant. The assumption is reasonable for joule heating because the cross sectional area along the length is constant and the surface temperatures are highly similar as

identified by the type-K thermocouples on the back of the heater. The heater sits in a troth of MACOR so to insulate the back and sides.

$$q''_{heater} = \frac{P}{A_{heated\,surface} \cdot 1000000} \qquad \text{Eq. 6.44}$$

Where:				
	P	=	Joule Power	[W]
	$A_{heated\ surface}$	=	$L_{heated} * W_{heated}$	[m^2]
	L_{heated}	=	0.20 m	
	W_{heated}	=	0.01 m	

From the entrance and exit conditions for the test section plus the joule power added, a calculation of exit quality is next made and recorded [83]. Heat of vaporization is determined by the MATLAB "hfg" function and referencing the saturation temperature at the exit of the test section.

$$x_{exit} = \frac{h_{f,entrance} + (P/(1000 \cdot \dot{m}_{hw})) - h_{f,exit}}{h_{fg}} \qquad \text{Eq. 6.45}$$

Where:				
	$h_{f,\,entrance}$	=	hf(RTD2)	
			MATLAB function for fluid enthalpy	[J/kg]
	P	=	Joule power	[Watts]
	$\dot{m}_{hw}$	=	Mass flow rate	[kg/s]
	$h_{f,\,exit}$	=	hf(RTD3) * 1000	
			MATLAB function for fluid enthalpy	[kJ/kg]
	h_{fg}	=	$hgf(T_{sat,exit})$	
			MATLAB function for fluid enthalpy	[kJ/kg]

Condenser heat balance based on tube side data is next calculated and recorded [Watts] [84]. This calculation is only appropriate for single phase fluid flow, which is fine for the high pressure chilled water system. The specific heat of water at constant pressure is determined by

the MATLAB "Cpf" function and referencing the average bulk fluid temperature in the condenser.

$$Q_{condenser} = \dot{m}_{cw} \cdot Cp_{f,cw\ average} \cdot (T_{cond,exit} - T_{cond,entrance}) \quad \text{Eq. 6.46}$$

Where:

$$\dot{m}_{cw} = \beta_{cw} \cdot \rho_{f,cond\ entrance} \quad \text{Eq. 6.47}$$

$$\rho_{f,cond\ entrance} = 1/vf(T_{cond,entrance}) \quad \text{Eq. 6.48}$$

$Cp_{f,\ cw\ average}$	=	$Cpf(T_{avg})*1000$	
		MATLAB function for fluid specific heat	[J/kg-°C]
T_{avg}	=	CWK3 at condenser middle	[°C]
$T_{cond,\ exit}$	=	Chilled water bulk temperature	[°C]
		CWK4 at condenser exit	
$T_{cond,\ entrance}$	=	Chilled water bulk temperature	[°C]
		CWK2 condenser entrance	

Shell side condenser heat balance is next calculated and recorded [Watts]. This calculation is only appropriate for single phase fluid flow during loop heat up toward saturation cool-down. The specific heat of water at constant pressure is taken at the same as for the test section. Reasonable given that the fluid temperature changes along the loop are generally less than 10 °C.

$$Q_{shell} = \dot{m}_{hw} \cdot Cp_{f,average} \cdot (T_{shell,exit} - T_{shell,entrance}) \quad \text{Eq. 6.49}$$

Where:

$T_{shell,\ exit}$	=	Bulk water temperature	[°C]
		RTD1 at condenser shell	
$T_{shell,\ entrance}$	=	Bulk water temperature	[°C]
		RTD4 condenser shell entrance	

Last, the pre-heater heat balance is calculated and recorded [Watts]. This calculation is only appropriate for single phase fluid flow during loop heat up toward saturation cool-down. The specific heat of water at constant pressure is taken at the same as for the test section. Reasonable given that the fluid temperature changes along the loop are generally less than 10 °C.

$$Q_{preheater} = \dot{m}_{hw} \cdot Cp_{f,preheater\ average} \cdot (T_{preheater,exit} - T_{preheater,entrance}) \quad \text{Eq. 6.50}$$

Where:

$T_{preheater,\ exit}$	=	Bulk water temperature RTD2 after pre-heater	[°C]
$T_{preheaterl,\ entrance}$	=	Bulk water temperature RTD1 before pre-heater	[°C]
$Cp_{f,\ preheater\ average}$	=	$Cpf(T_{avg})*1000$ MATLAB function for fluid specific heat	[J/kg-°C]
T_{avg}	=	$(T_{preheater,\ entrance} + T_{preheater,\ exit}) / 2$	[°C]

The results of these eleven (11) calculations are then appended to the data array.

The last two fields added to each scan record are the power supply intensity signal and pump intensity signal. Each record then has fifty-four (54) fields (see Table 6-36).

Table 6-36: Table of LabVIEW Scan Record Fields

LabVIEW Output Array

LabVIEW Index #	Name	Source	Channel	MatLAB Index #
0	DATE	LabVIEW	na	1
1	TIME	LabVIEW	na	2
2	HWRTD1	Agilent	1001	3
3	HWRTD2	Agilent	1002	4
4	HWRTD3	Agilent	1003	5
5	HWRTD4	Agilent	1004	6
6	TSK1	Agilent	1006	7
7	TSK2	Agilent	1007	8
8	TSK3	Agilent	1008	9
9	TSK4	Agilent	1009	10
10	TSK5	Agilent	1010	11
11	TSK6	Agilent	1011	12
12	TSK7	Agilent	1012	13
13	TSK8	Agilent	1013	14
14	HWFM	Agilent	1015	15
15	CWK1	Agilent	1016	16
16	CWK2	Agilent	1017	17
17	CWK3	Agilent	1018	18
18	CWK4	Agilent	1019	19
19	CWK5	Agilent	1020	20
20	PS1	Agilent	1031	21
21	TSVD	Agilent	1032	22
22	PT4	Agilent	1033	23
23	PT3	Agilent	1034	24
24	PT2	Agilent	1035	25
25	PS3	Agilent	1036	26
26	CWFM	Agilent	1041	27
27	PT1	Agilent	1044	28
28	HWFM [GPM]	Formula Node	na	29
29	PS1 [Amps]	Formula Node	na	30
30	PT4 [PSIA]	Formula Node	na	31
31	PT3 [PSIA]	Formula Node	na	32
32	PT2 [PSIA]	Formula Node	na	33
33	PT1 [PSIA]	Formula Node	na	34
34	PS3 [Amps]	Formula Node	na	35
35	CWFM [GPM]	Formula Node	na	36
36	Total Current [Amps]	Formula Node	na	37
37	Power [Watts]	Formula Node	na	38
38	HW_VFRate [m^3/s]	Formula Node	na	39
39	CW_VFRate [m^3/s]	Formula Node	na	40
40	R_ts	Formula Node	na	41
41	T_sat [C]	MATLAB Node	na	42
42	rho_l [Kg/m^3]	MATLAB Node	na	43
43	Vel_HW [m/s]	MATLAB Node	na	44
44	G_HW [Kg/m^2-s]	MATLAB Node	na	45
45	Re_HW	MATLAB Node	na	46
46	Q_ts [Watts]	MATLAB Node	na	47
47	QQ_ts [MW/m^2]	MATLAB Node	na	48
48	Xe	MATLAB Node	na	49
49	Q_cond [Watts]	MATLAB Node	na	50
50	Q_cond_shell [Watts]	MATLAB Node	na	51
51	Q_preht [Watts]	MATLAB Node	na	52
52	PS Signal	Front Panel Input	na	53
53	Pump Signal	Front Panel Input	na	54

6.16.6 Data Display

All data, captured or calculated, is displayed numerically within defined arrays (see Figure 6-63).

Figure 6-63: Photo of Front Panel Tab Data Array

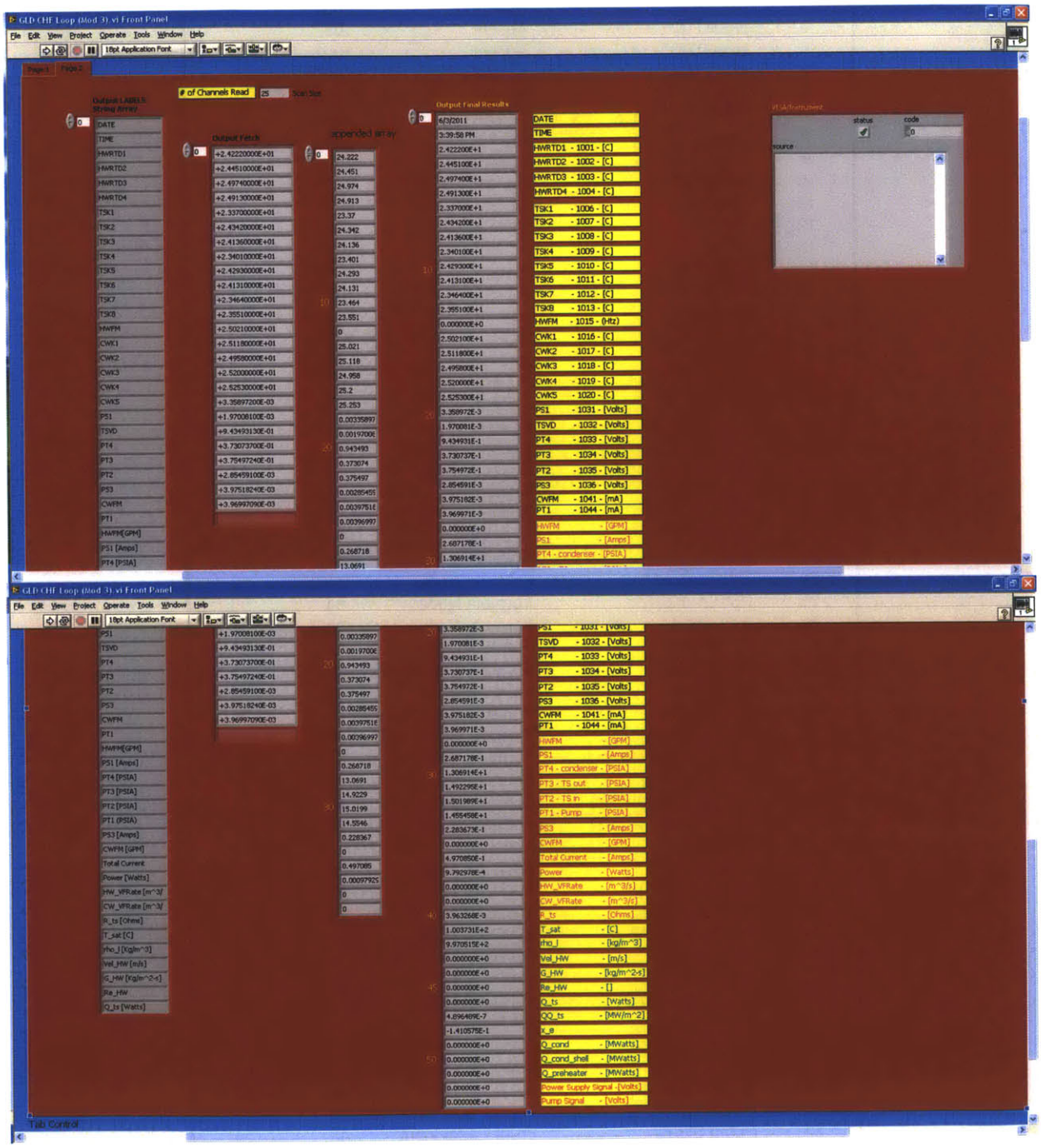

A number of graphs are programmed including: pressure transducers, RTDs, and test heater thermocouples, mass flux, and power (see Figure 6-64).

Figure 6-64: Photo of Front Panel Data Graphs

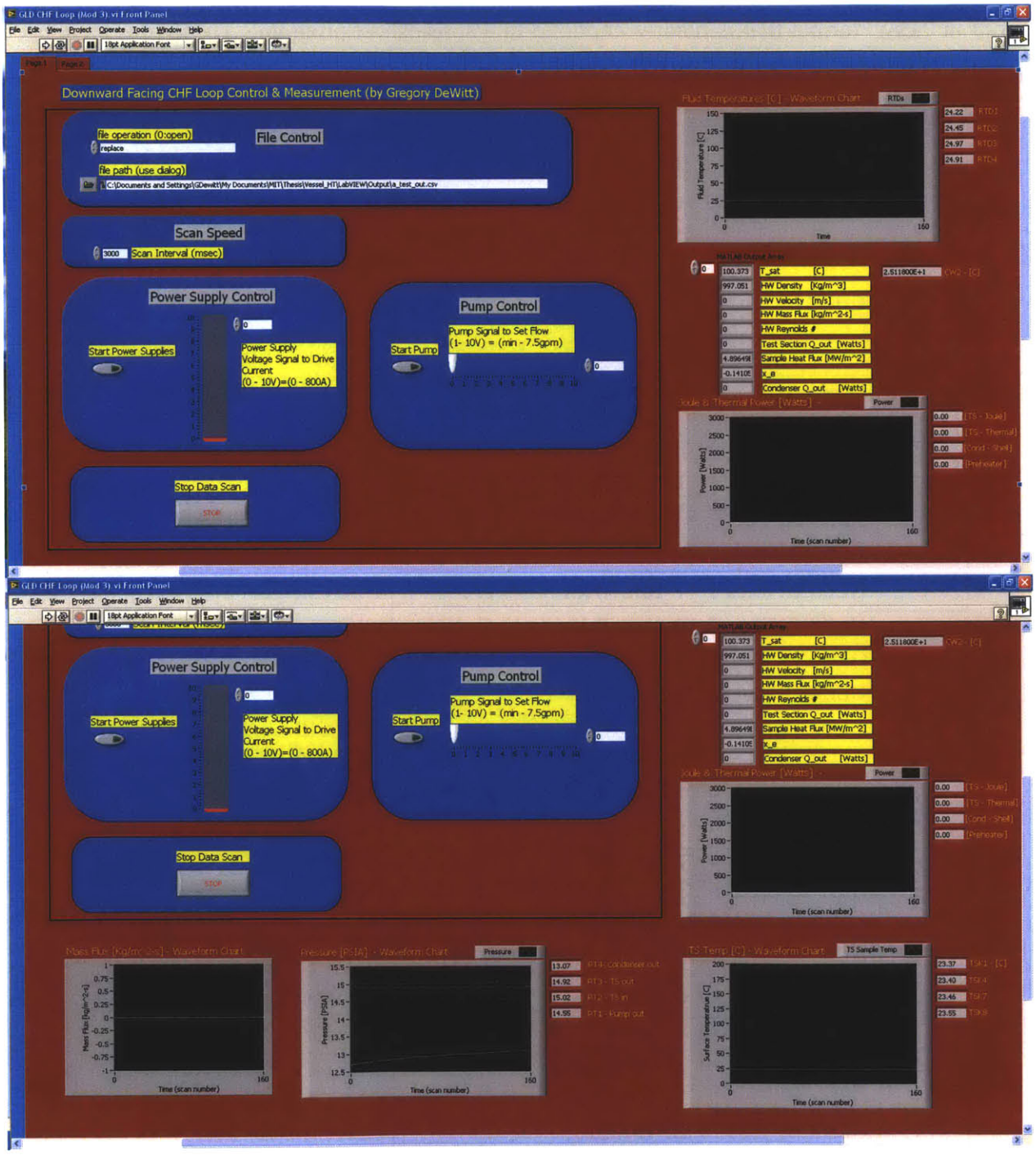

6.16.7 Data Capture

After each scan and associated calculations are complete a record is written to the data file. This method ensures that if a computer disruption occurs the data to that point is saved. The file is saved in ".csv" format that is readily imported to a spreadsheet program. These files have been imported into Excel for data capture, analysis and graphics (see Table 6-37). Note for the vast majority of experiments the data was processed with LabVIEW. For a couple early experiments Benchlink was used as a part of the Agilent system.

Table 6-37: List of CHF Data Files from LabVIEW or Benchlink

Test ID#	CHF Test File Name	Test ID#	CHF Test File Name
1	GLD_CHF_test_Mar_18_2010.xls	44	GLD CHF Data 1_21_2011.xls
2	GLD CHF Test Data_4_6_2010.xls	45	GLD CHF Data 1_24_2011.xlsx
3	GLD_CHF_Test_Data_4_8_2010.xls	46	GLD CHF Data 1_25_2011.xls
4	GLD CHF Data 4_20_2010.xls	47	GLD CHF Data 1_26_2011.xls
5	GLD CHF Data 7_15_2010.xls	48	GLD CHF Data 1_28_2011.xls
6	GLD CHF Data 7_20_2010_b.xls	49	GLD CHF Data 1_31_2011.xlsx
7	GLD CHF Data 7_26_2010_b.xls	50	GLD CHF Data 2_2_2011.xls
8	GLD CHF Data 8_11_2010_B.xls	51	GLD CHF Data 2_2_2011_b.xls
9	GLD CHF Data 8_30_2010_B.xls	52	GLD CHF Data 2_7_2011.xls
10	GLD CHF Data 9_1_2010_B.xls	53	GLD CHF Data 2_8_2011.xls
11	GLD CHF Data 9_3_2010_B.xls	54	GLD CHF Data 2_9_2011.xls
12	GLD CHF Data 9_7_2010_B.xls	55	GLD CHF Data 2_11_2011.xls
13	GLD CHF Data 9_9_2010.xls	56	GLD CHF Data 2_15_2011.xls
14	GLD CHF Data 9_10_2010_b.xls	57	GLD CHF Data 2_16_2011.xls
15	GLD CHF Data 9_15_2010.xls	58	GLD CHF Data 2_17_2011.xls
16	GLD CHF Data 9_17_2010.xls	59	GLD CHF Data 2_18_2011.xls
17	GLD CHF Data 9_21_2010.xls	60	GLD CHF Data 2_22_2011.xls
18	GLD CHF Data 9_24_2010.xls	61	GLD CHF Data 2_23_2011.xls
19	GLD CHF Data 10_1_2010.xls	62	GLD CHF Data 2_24_2011.xls
20	GLD CHF Data 10_6_2010.xls	63	GLD CHF Data 2_25_2011.xls
21	GLD CHF Data 10_8_2010.xls	64	GLD CHF Data 3_2_2011.xls
22	GLD CHF Data 10_21_2010.xls	65	GLD CHF Data 3_4_2011.xls
23	GLD CHF Data 10_21_2010_2.xls	66	GLD CHF Data 3_9_2011.xls
24	GLD CHF Data 10_22_2010.xls	67	GLD CHF Data 3_22_2011.xls
25	GLD CHF Data 10_26_2010.xls	68	GLD CHF Data 3_25_2011.xls
26	GLD CHF Data 10_29_2010.xls	69	GLD CHF Data 4_1_2011.xls

27	GLD CHF Data 11_2_2010_B.xls	70	GLD CHF Data 4_15_2011.xls
28	GLD CHF Data 11_5_2010.xls	71	GLD CHF Data 4_19_2011.xls
29	GLD CHF Data 11_11_2010.xls	72	GLD CHF Data 4_20_2011.xls
30	GLD CHF Data 11_12_2010.xls	73	GLD CHF Data 4_22_2011.xls
31	GLD CHF Data 11_16_2010.xls	74	GLD CHF Data 4_25_2011.xlsx
32	GLD CHF Data 11_19_2010.xls	75	GLD CHF Data 4_27_2011.xls
33	GLD CHF Data 11_19_2010(second).xls	76	GLD CHF Data 5_4_2011.xls
34	GLD CHF Data 12_15_2010_B.xls	77	GLD CHF Data 7_13_2011.xls
35	GLD CHF Data 12_16_2010.xls	78	GLD CHF Data 7_15_2011.xls
36	GLD CHF Data 12_20_2010.xls	79	GLD CHF Data 7_19_2011.xls
37	GLD CHF Data 12_23_2010.xls	80	GLD CHF Data 7_21_2011.xls
38	GLD CHF Data 1_7_2011_B.xls	81	GLD CHF Data 7_22_2011.xls
39	GLD CHF Data 1_10_2011.xls	82	GLD CHF Data 7_26_2011.xls
40	GLD CHF Data 1_11_2011.xls	83	GLD CHF Data 7_28_2011.xls
41	GLD CHF Data 1_14_2011.xls	84	GLD CHF Data 9_6_2011.xls
42	GLD CHF Data 1_18_2011.xls	85	GLD CHF Data 9_7_2011.xls
43	GLD CHF Data 1_20_2011.xls	HS1	GLD Highly Subcooled 12_6_2010.xlsx

6.16.8 Termination

Once the "STOP" button is triggered the file is closed, power supplies and pump are turned off.

6.16.9 Joule Power and Thermal Power Tracking

Joule power (Eq. 6.36) and thermal power (Eq. 6.42) calculated by LabVIEW can be compared to insure that instrumentation is working properly during highly sub-cooled conditions. Once voiding reaches the test section exit RTD the relation no longer holds because the heat of vaporization is not addressed.

A high sub-cooling test was run that held the exit fluid temperature at ~50 °C (see Figure 6-65). The graph shows the tracking of joule power and thermal power as energy is stepwise increased. From the time history, a graph of the average percent difference of thermal power to joule power is plotted for each steady-state power level (see Figure 6-66). Flow rate was set at 1000 kg/m^2-s and atmospheric pressure. One scan is three (3) seconds.

Figure 6-65: Graph of Joule Power and Thermal Power for High Sub-cooling Test

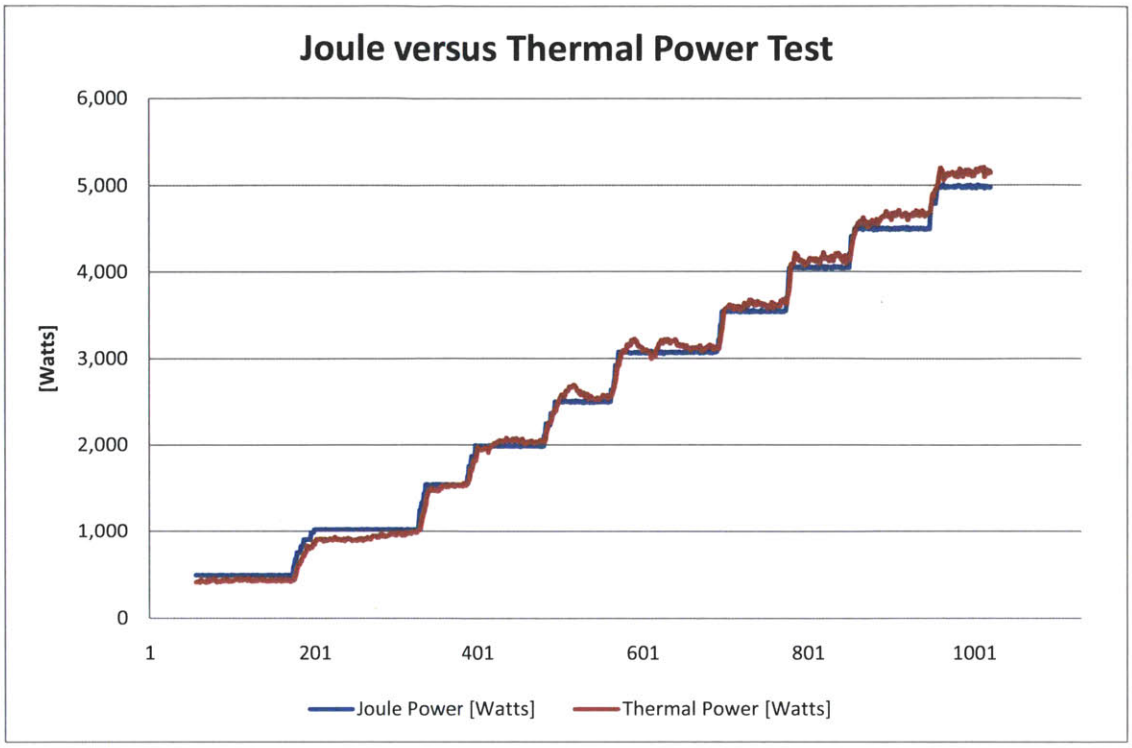

Figure 6-66: Graph of Percent Difference Thermal Power to Joule Power

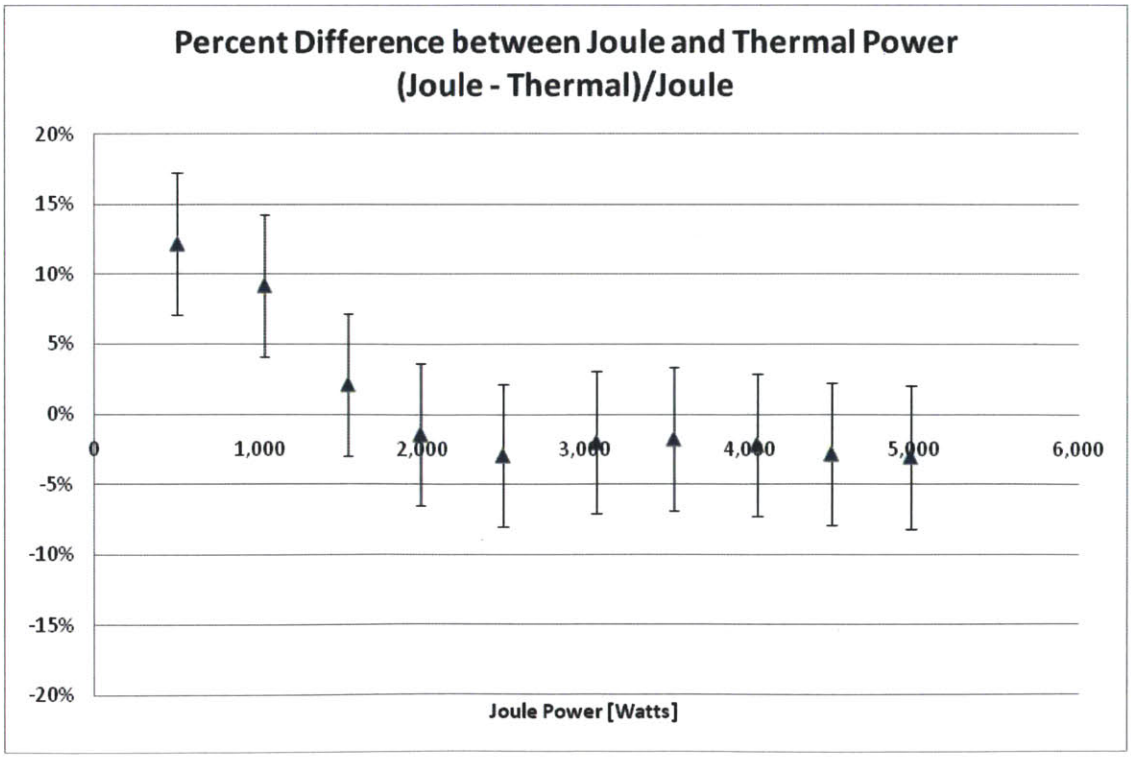

At power at below 2 kW and steady-state the thermal power calculation is less than joule power. At powers above 2 kW thermal calculated power is somewhat greater than joule. The difference trends down with increasing power to well below 5%. Note the instrument uncertainty for thermal power determination is +/- 5.1% and represents the error bar. The maximum surface heat flux for this high sub-cooling test was 2.5 WM/m^2.

7 Heater Surfaces & Preparation

Two materials are tested as sample heaters: (1) stainless steel 316L and (2) carbon steel SA-508. SA-508 carbon steel is the reactor vessel material used for the Westinghouse AP1000. Table 7-1 below lists the relevant material properties.

Since the properties of the alumina nanofluid are not significantly different than water-only, the CHF enhancement measured seems to be a surface influence. Reactor vessel SA-508 being a low carbon steel with a relatively rough surface compared to stainless steel 316L tested, the deposition of nanoparticles to the surface may be difference. Though both SS316L and SA-508 are dominated by iron, Fe, the other relative composition materials may change the surface affinity to alumina. A reduction of nanoparticle deposition may also reduce the improved wettability seen for SS316L, once boiled with alumina nanofluid.

The differences in composition may also yield differing micro-cavity geometry from the surface preparation. If the geometry of the micro-cavities for SA-508 on average are different than SS316L, the relative enhancement of CHF may be different. Wettability improvement seems to be a driver for CHF enhancement. Micro-cavity geometric and chemistry differences compared to SS316L may change wettability improvement.

Table 7-1: Material Properties of SS316L and SA-508 at STP

Parameter	Units	SS316L	SA-508
Density	[kg/m^3]	8000	7850
Melting Point	[^oC]	1400	1325
Resistivity	[ohm/m]	7.49×10^{-7}	1.74×10^{-7}
Expansion Coefficient	[$\Delta m/m$]	16.0×10^{-6}	13.0×10^{-6}
Thermal Conductivity	[$W/m\text{-}^oC$]	16	38
Specific Heat	[$kJ/kg\text{-}^oC$]	0.50	0.29

Surface preparation of the Westinghouse AP1000 reactor pressure vessel includes heat treatment and polishing to a roughness of 250 micro-inches (6.35 microns) [85]. Note that one of the results of the work at UCSB was that the paint that normally protects the vessel needs to be removed [72]. It should be noted that other vendor surface finishes could be meaningfully different.

7.1 Test Sample Preparation

The test samples are cleaned, sand blasted, and heat treated before use. Cleaning to remove particulates and oils is done before and after sand blasting. Cleaning is accomplished with DI water and acetone rinses. Sand blasting is done with silicon oxide, SiO, bead sizes ranging 210 to 305 μm (see Figure 7-1). The sample heater is sand blasted with 4 to 6 sweeps of the particle nozzle. Attention is given to assure the sandblast finish is even along the entire fluid facing surface. This provides an even finish on the surface in contact with the working fluid (see Figure 7-2). Note the top heater has a mirror shine with some swirl markings and the bottom sandblaster heater has a dull and even finish.

Figure 7-1: Photo of Sandblasting Setup

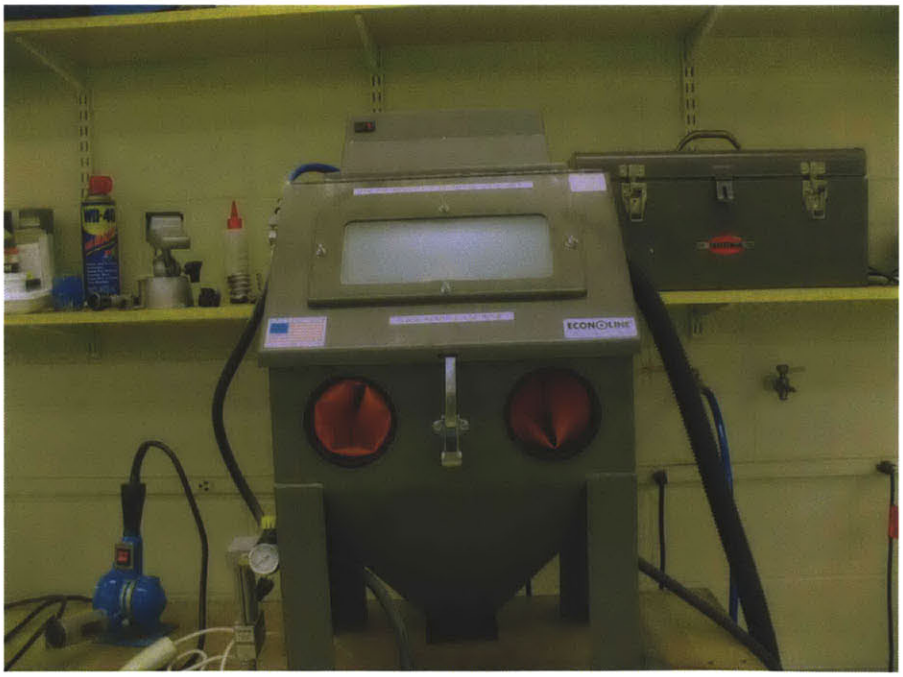

Figure 7-2: Photos of Sample Heater Before (top) and After (bottom) Sandblasting

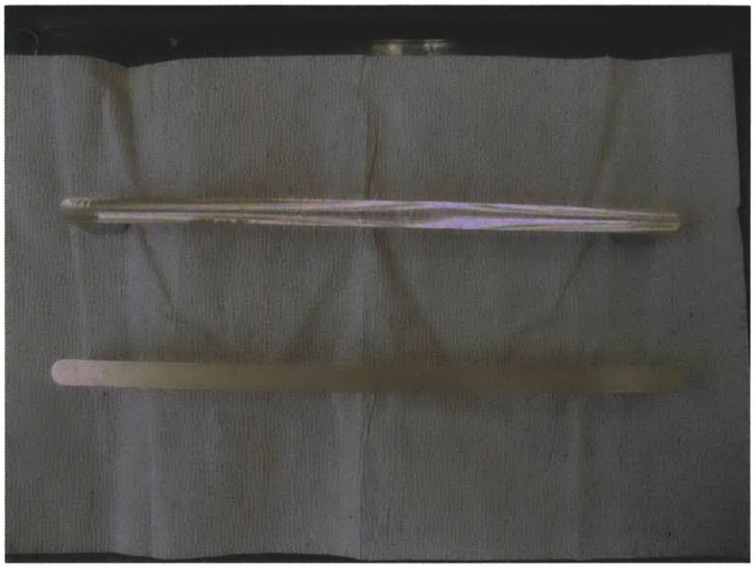

Heat treatment is accomplished with a box furnace (see Figure 7-3). The furnace temperature is raised to 10 °C above the expected saturation temperature for the experiment. For example, if saturation is expected to be 100 °C then the furnace is set for 110 °C. The heat treatment helps the o-ring on the electrode to set in the proper location for test conditions and thereby helping to avoid bowing of the sample heater. Once the heater is prepared and mounted onto the MACOR insulator block, the fit is visually examined to assure that the surface sits flat.

Figure 7-3: Photo of Box Furnace

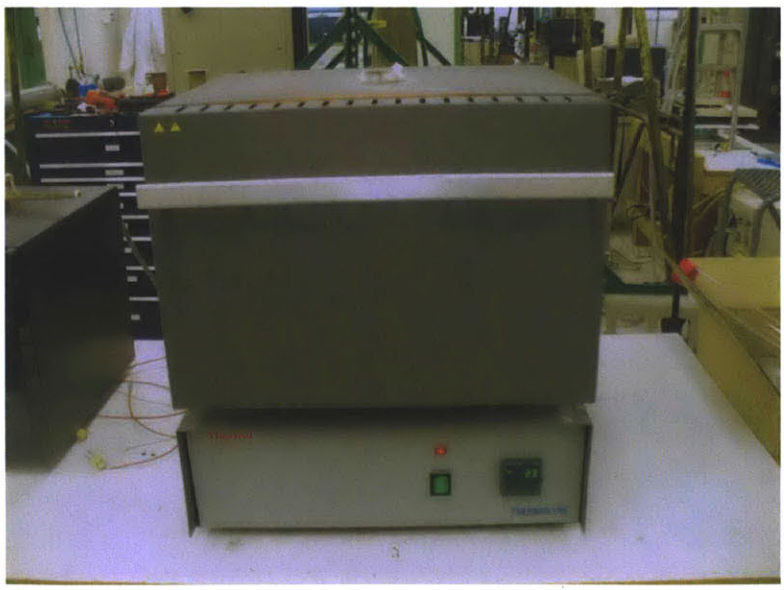

8 Surface Characterization

Four types of surface measurement have been completed to better understand nanofluid deposition during boiling in IVR conditions and the resulting influence on CHF: Scanning Electron Microscopy ("SEM"), Energy Dispersive Spectroscopy ("EDS"), confocal microscopy and contact angle measurement. It should be noted that the physical properties of the nanofluids at the low concentrations tested herein are nearly identical, within measurement uncertainty, of plain water. Therefore any significant CHF enhancement must be from surface influences, either chemical or physical.

Scanning electron microscopy ("SEM") allows for visualization of surface morphology. Energy dispersive spectroscopy ("EDS") identifies surface element composition. Confocal microscopy measures surface roughness and provides another means of visualization of fine surface details. Contact angle measurement measures the wettability of a fluid. Higher wettability improves the rate of dry spot recovery during high heat flux boiling contributing to CHF enhancement.

Several samples from SS316L and SA-508 heaters were analyzed. SS316L samples analyzed for surface characterization include: (1) unused heater with surface preparation, (2) prepared heater used for water-only CHF, (3) prepared heater used with alumina for 0.001% by volume concentration CHF test, (4) prepared heater used with alumina for 0.01% by volume concentration CHF test, (5) unused, prepared with oxidized surface, and (6) prepared with oxidized surface used for water-only CHF.

SA-508 samples analyzed for surface characterization include: (1) plain unused heater with surface preparation, (2) prepared heater used for water-only CHF, and (3) prepared heater used for alumina with 0.001% by volume concentration CHF test.

8.1 Scanning Electron Microscopy ("SEM")

Scanning electron microscopy is used to better understand surface morphology (see Table 8-1). During boiling, alumina nanoparticles can plate out onto the sample surface. This then changes the surface chemistry and geometry of the micro-cavity, from which each bubble is born. SEM and EDS analyses were completed at the Harvard Science Center for normally prepared SS316L heaters. For SA-508 and oxidized SS316L the SEM and EDS were completed at MIT.

Several levels of magnification were done for each surface including: 40 kX, 20 kX, 10 kX, 1000 X, and 250 X. Additionally, for the samples from CHF experiments two locations were analyzed: (1) below the CHF location and (2) at the CHF location, which is generally blackened in color.

Table 8-1: Summary of Samples Analyzed with SEM

Surface Material	Description
SS316L	Unused Heater - Sandblast Preparation
SS316L	Used in Water - Sandblast Preparation – before CHF location
SS316L	Plain Heater used with Water - Sandblast Preparation – Point of CHF Blackened
SS316L	Heater with Alumina 0.001% - Sandblast Preparation – before CHF location
SS316L	Heater used with Alumina 0.001% - Sandblast Preparation – blackened CHF location
SS316L	Heater used with Alumina – 0.01% - Sandblast Preparation – before CHF
SS316L	Heater used with Alumina – 0.01% - Sandblast Preparation – blackened CHF
SA-508	Unused Heater - Sandblast Preparation
SA-508	Used in Water - Sandblast Preparation – before CHF location
SA-508	Used in Water - Sandblast Preparation – blackened CHF location

SA-508	Heater with Alumina 0.001% - Sandblast Preparation – before CHF location
SA-508	Heater used with Alumina 0.001% - Sandblast Preparation – blackened CHF location
SS316L - Oxidized	Unused Heater - Sandblast Preparation
SS316L - Oxidized	Used in Water - Sandblast Preparation – before CHF location
SS316L - Oxidized	Used in Water - Sandblast Preparation – blackened CHF location

8.1.1 SEM of SS316L

Figure 8-1: SEM of SS316L Unused Heater - Sandblast Preparation - Various Magnification [40,000X]

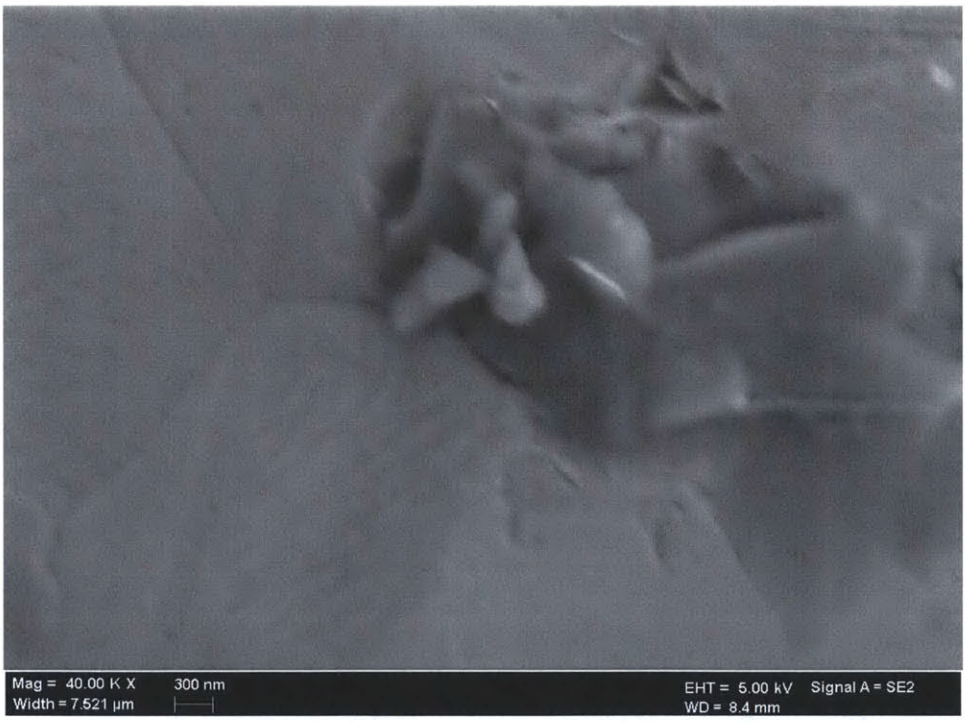

[19,930X]

[10,030X]

[1,010X]

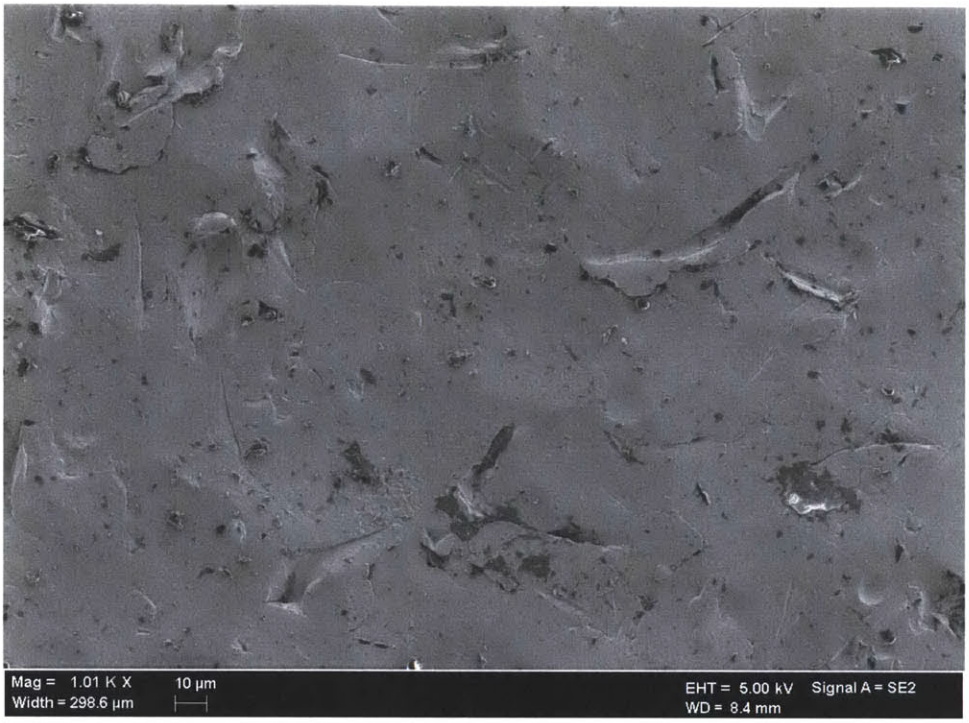
Mag = 1.01 K X
Width = 298.6 µm
10 µm
EHT = 5.00 kV
WD = 8.4 mm
Signal A = SE2

[250X]

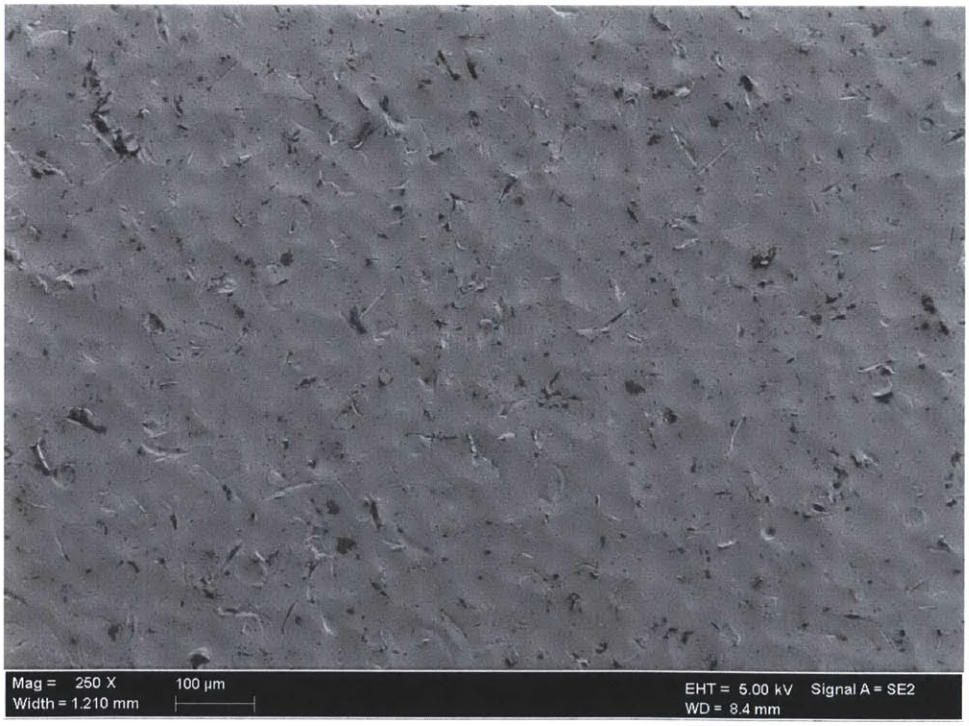
Mag = 250 X
Width = 1.210 mm
100 µm
EHT = 5.00 kV
WD = 8.4 mm
Signal A = SE2

Figure 8-2: SEM of SS316L Heater used in Water CHF - Sandblast Preparation – before CHF location – Various Magnifications

[40,060X]

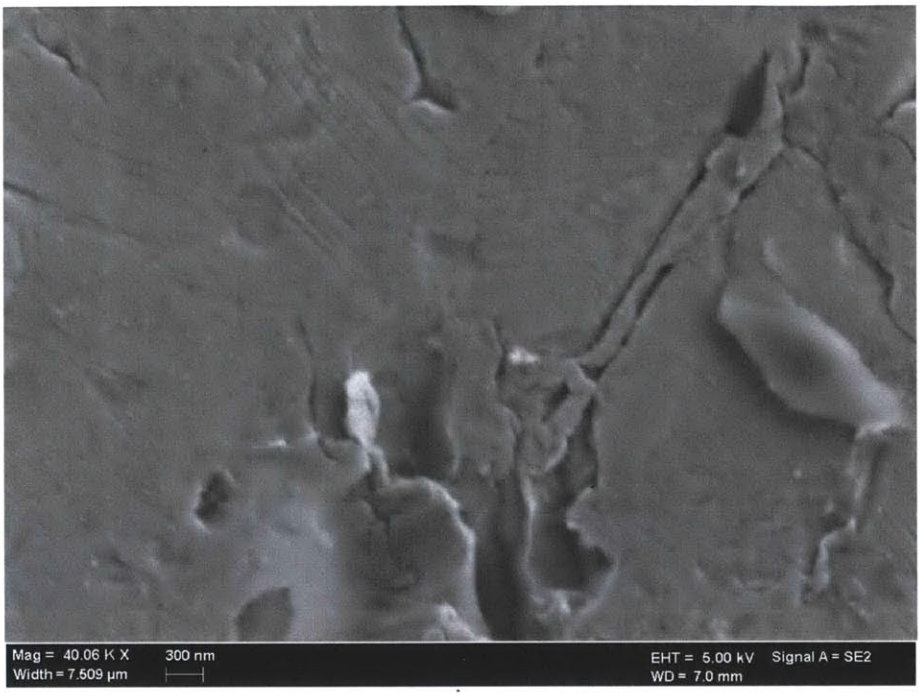

[19,950X]

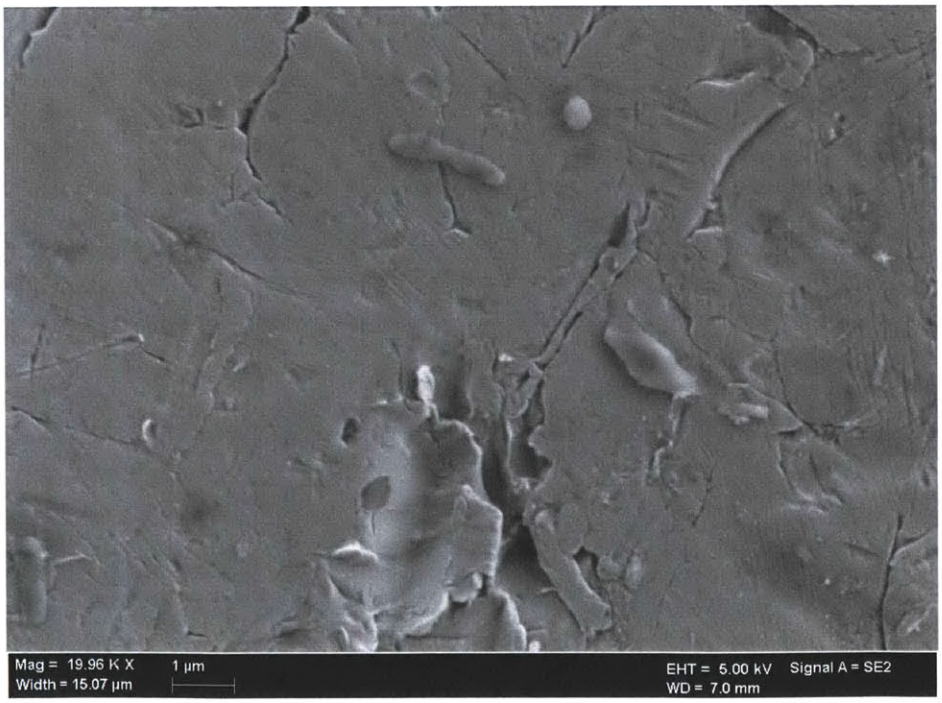

[10,050X]

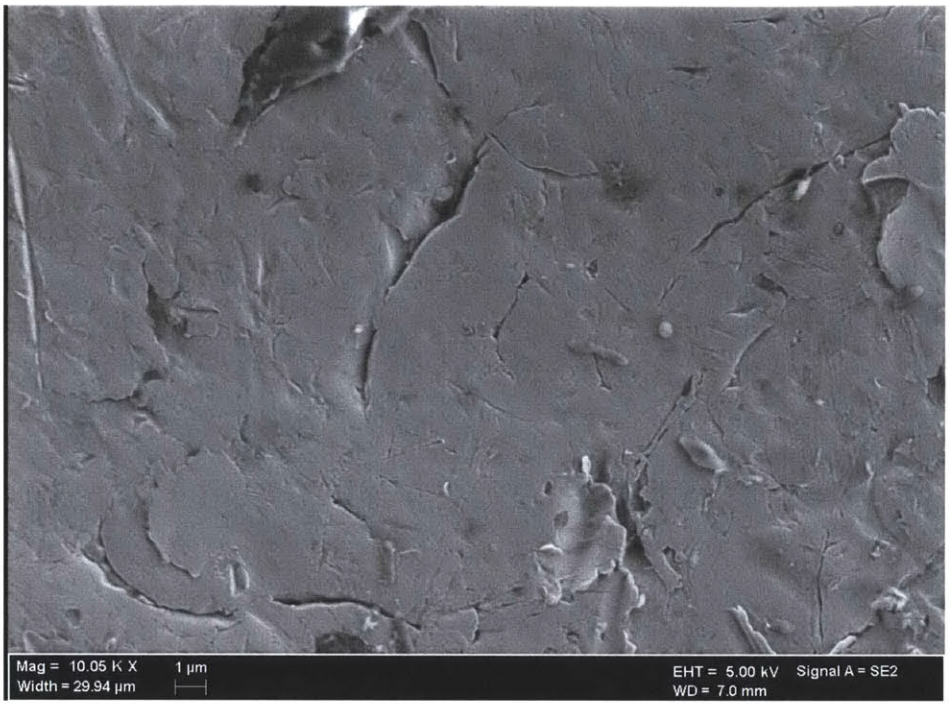
Mag = 10.05 K X
Width = 29.94 µm
1 µm
EHT = 5.00 kV
WD = 7.0 mm
Signal A = SE2

[999X]


Mag = 999 X
Width = 301.6 µm
10 µm
EHT = 5.00 kV
WD = 7.0 mm
Signal A = SE2

[248X]

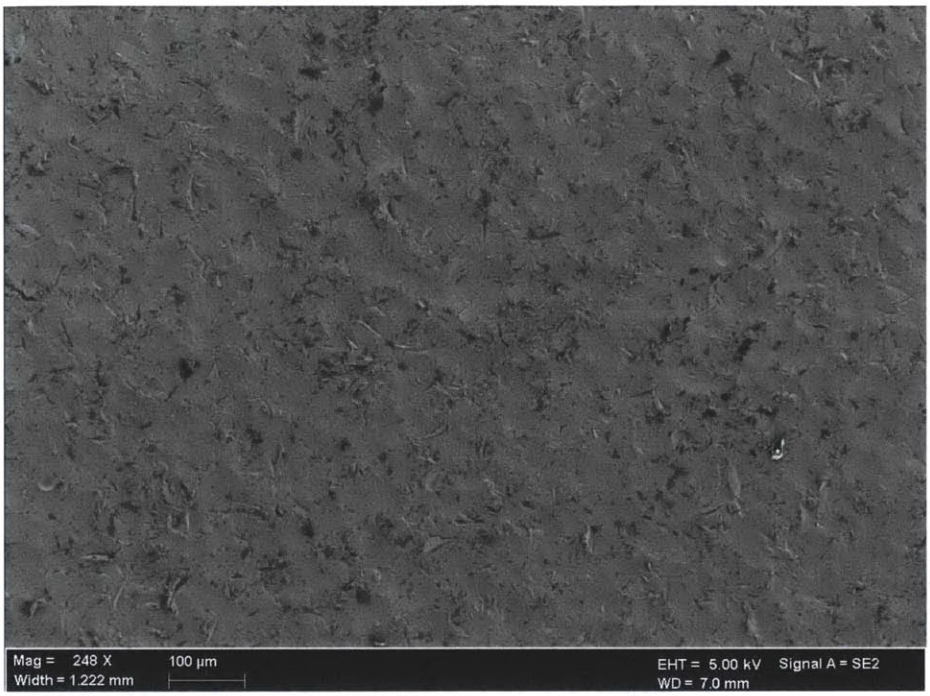

Figure 8-3: SEM of SS316L Plain Heater used with Water - Sandblast Preparation – Point of CHF Blackened - Various Magnifications

[50,280X]

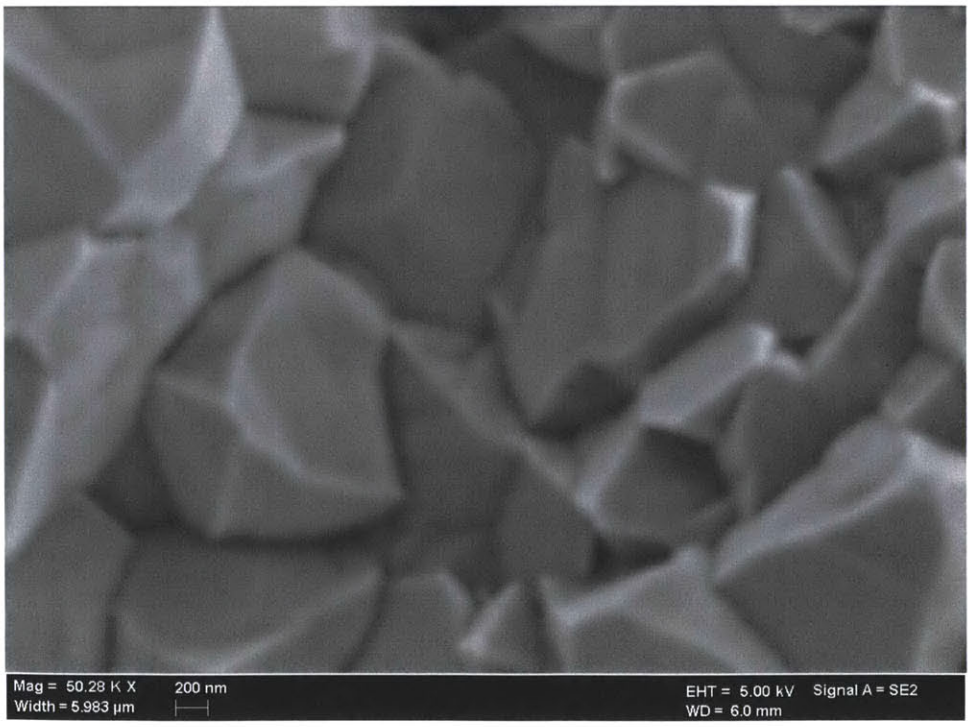

[40,000X]

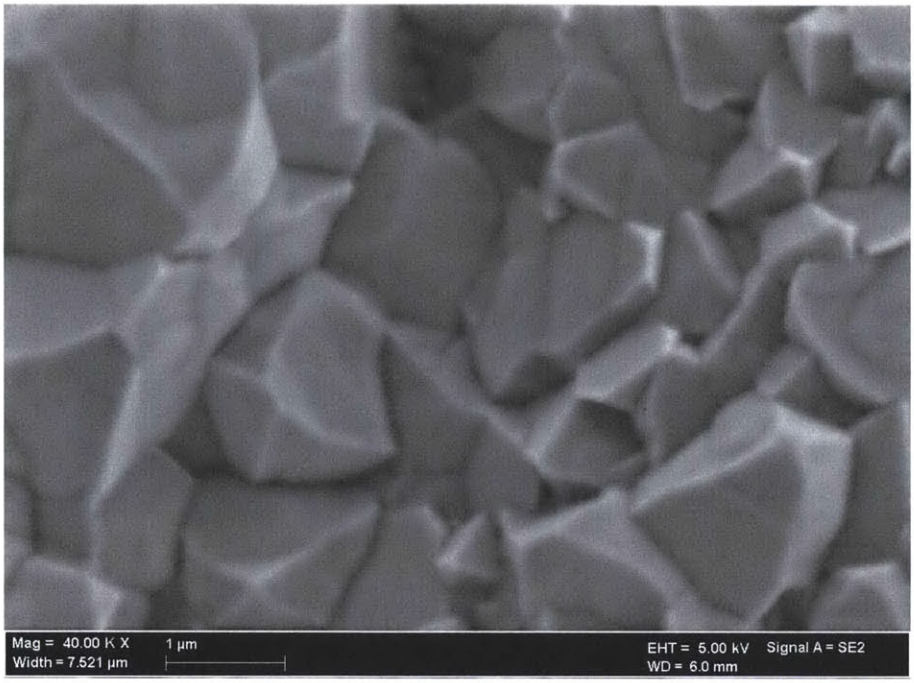

[10,030X]

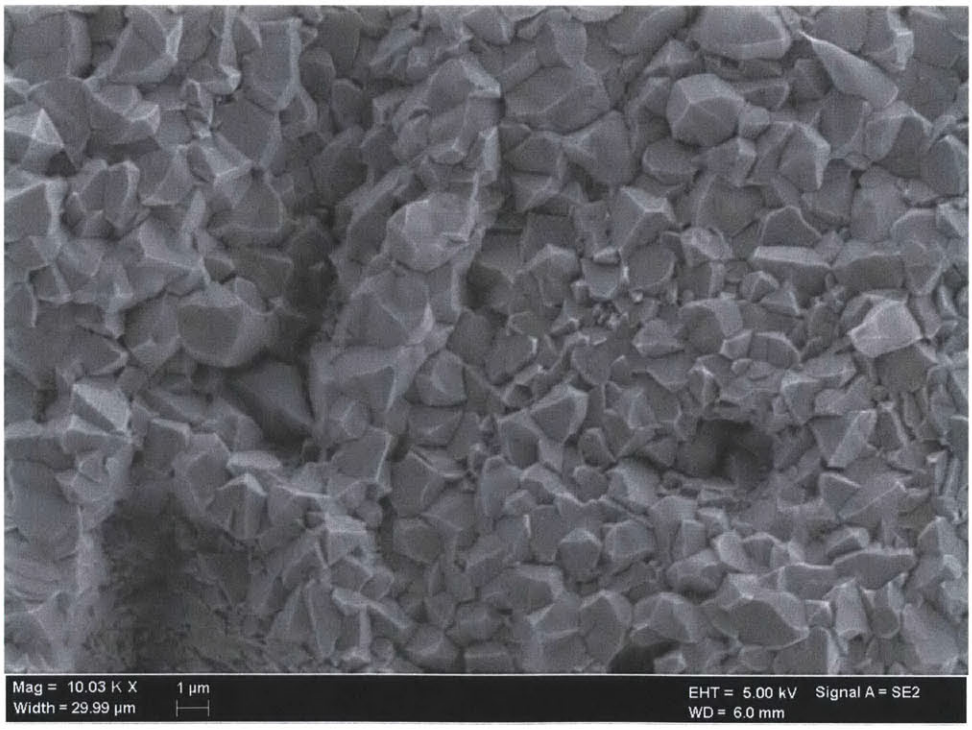

[998X]


Mag = 998 X
Width = 301.6 µm
10 µm
EHT = 5.00 kV
WD = 6.0 mm
Signal A = SE2

[250X]


Mag = 250 X
Width = 1.210 mm
100 µm
EHT = 5.00 kV
WD = 6.0 mm
Signal A = SE2

Figure 8-4: SEM of SS316L Heater used with Alumina 0.001% - Sandblast Preparation – before CHF location– Various Magnifications

[41,160X]

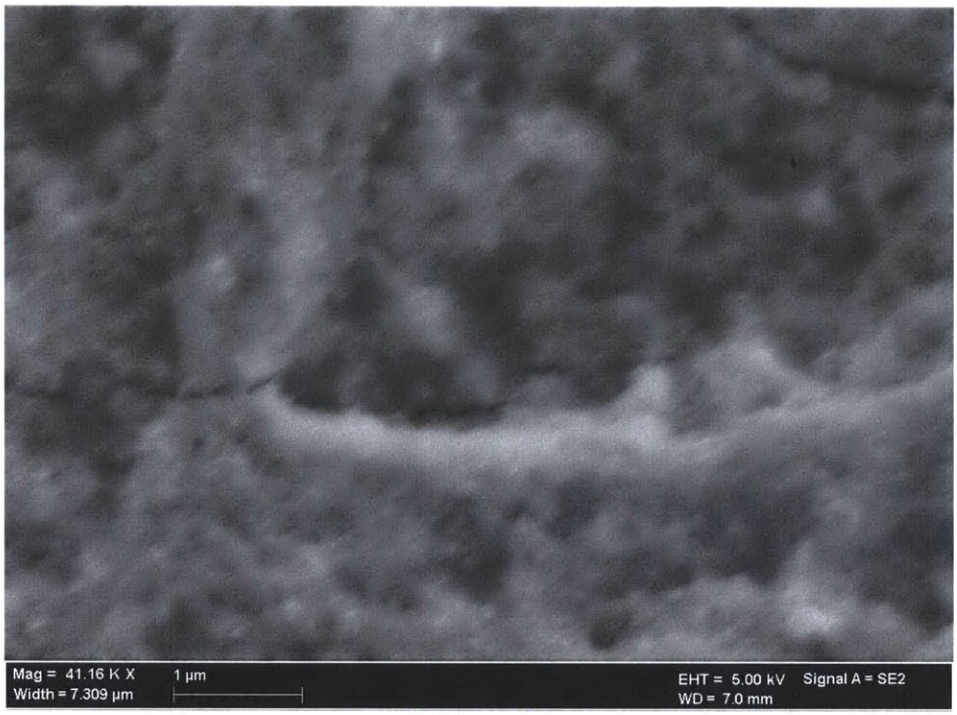

[20,090X]

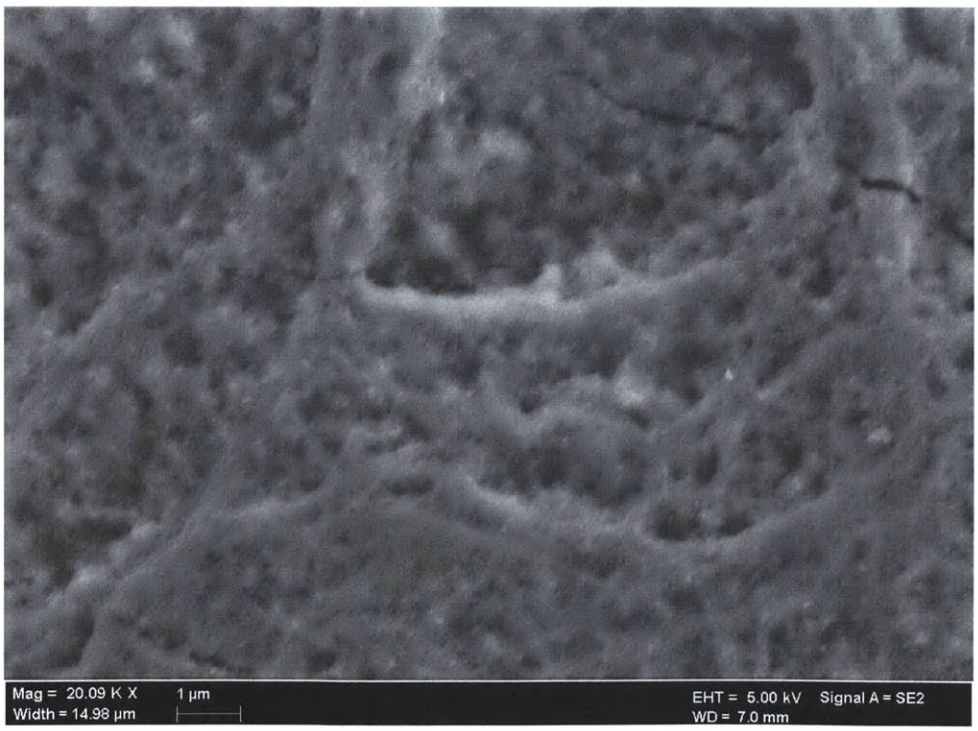

[9,900X]

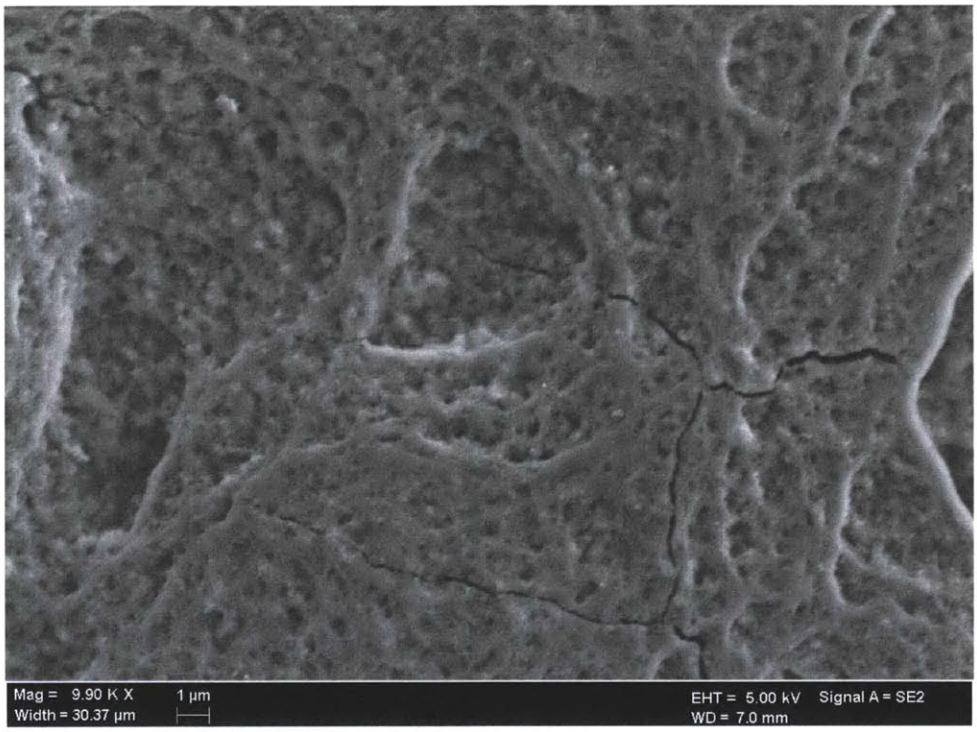
Mag = 9.90 K X
Width = 30.37 µm
1 µm
EHT = 5.00 kV
WD = 7.0 mm
Signal A = SE2

[1,010X]

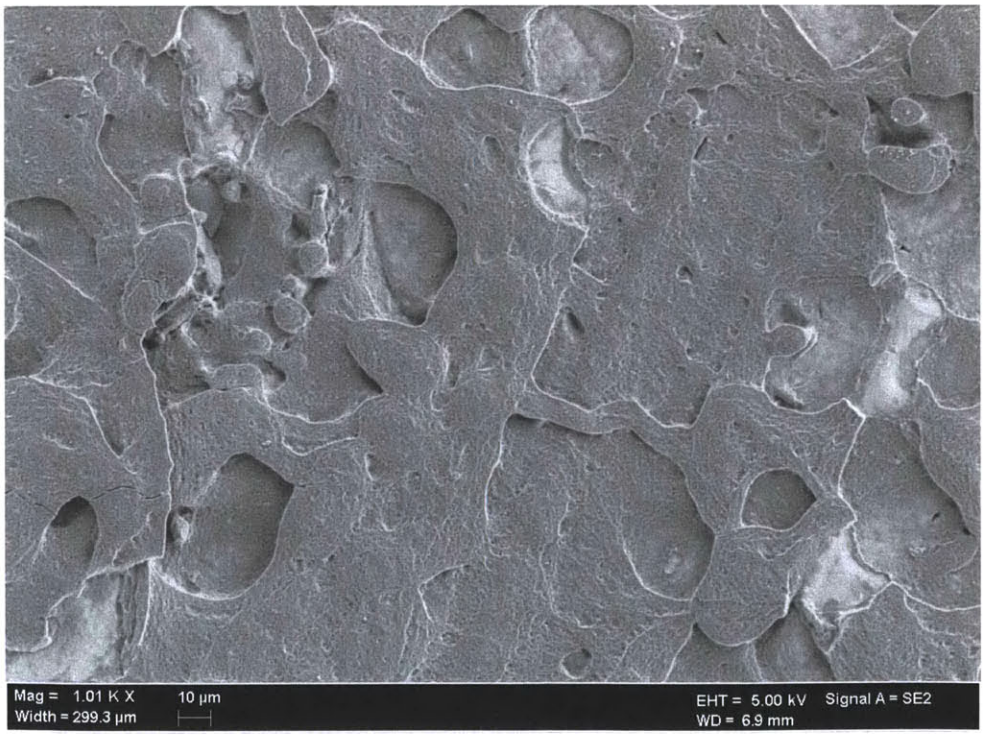
Mag = 1.01 K X
Width = 299.3 µm
10 µm
EHT = 5.00 kV
WD = 6.9 mm
Signal A = SE2

[250X]

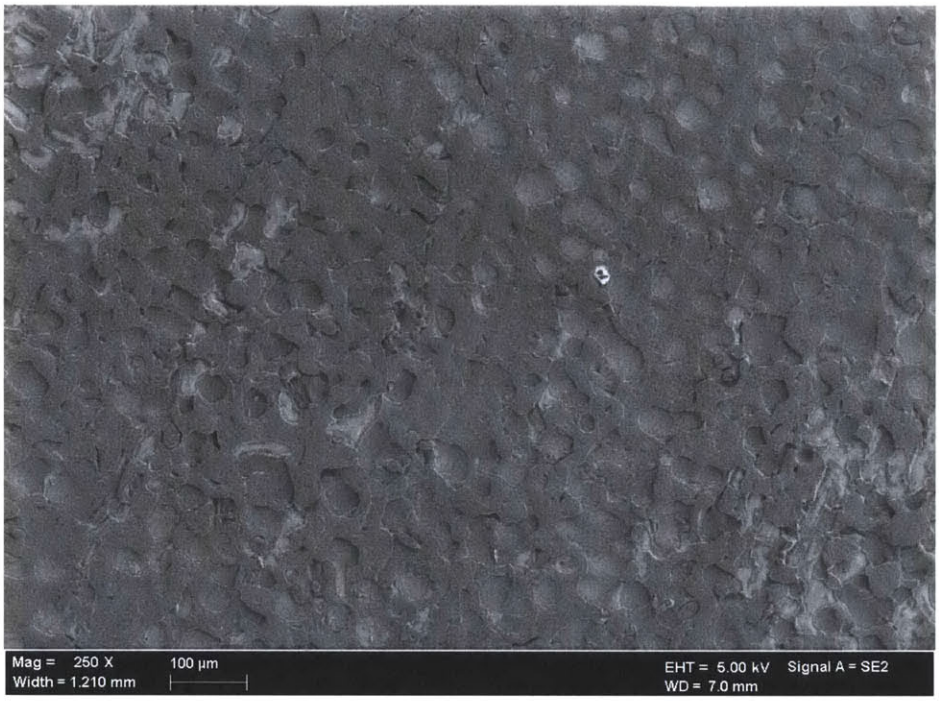

Figure 8-5: SEM of SS316L Heater used with Alumina 0.001% - Sandblast Preparation – blackened CHF location – Various Magnifications

[4,690X]

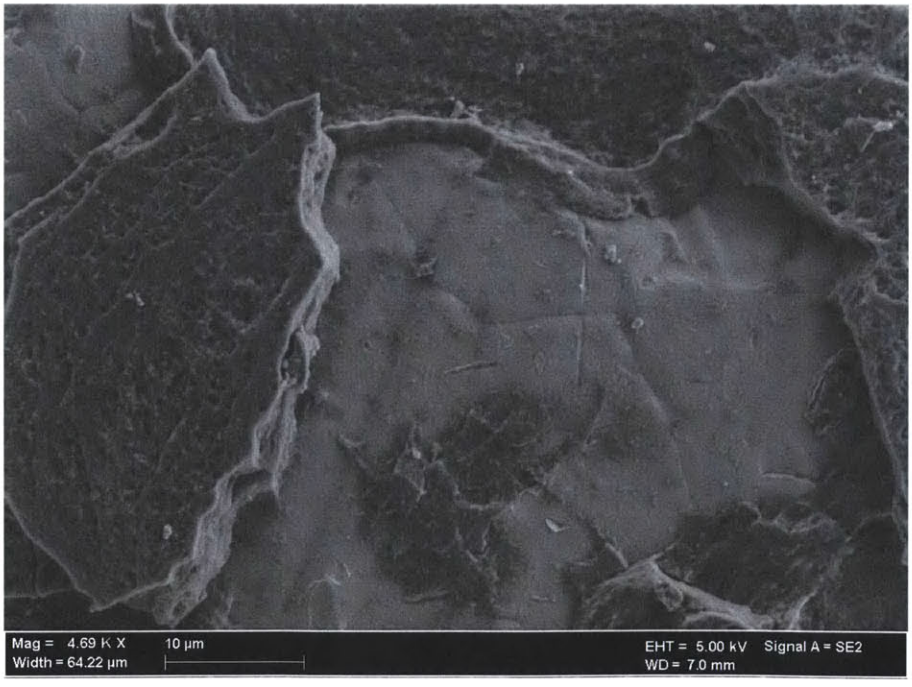

[825X]

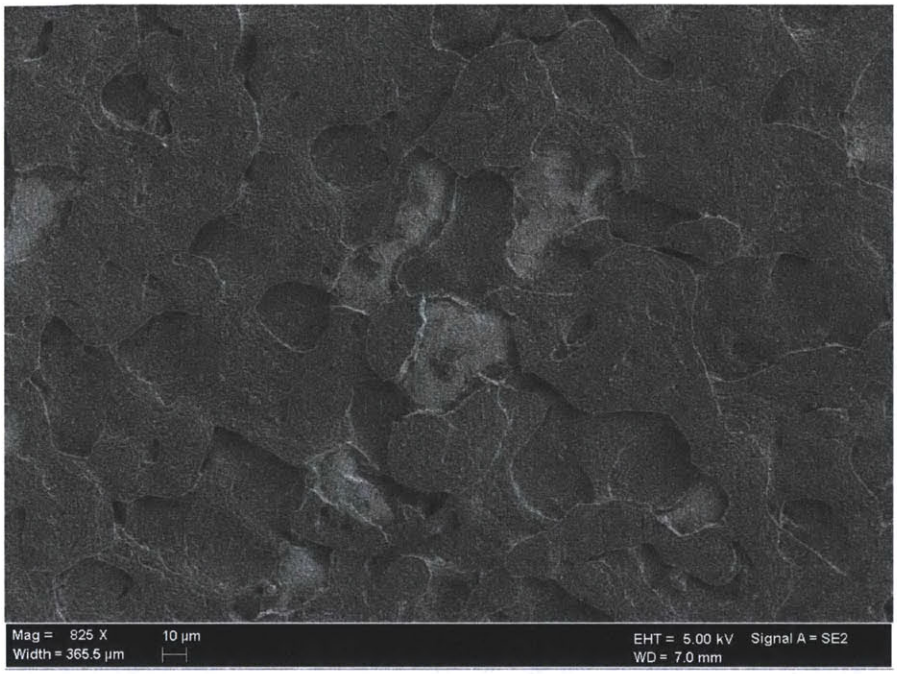

Figure 8-6: SEM of SS316L Heater used with Alumina – 0.01% - Sandblast Preparation – before CHF location – Various Magnifications

[40,000X]

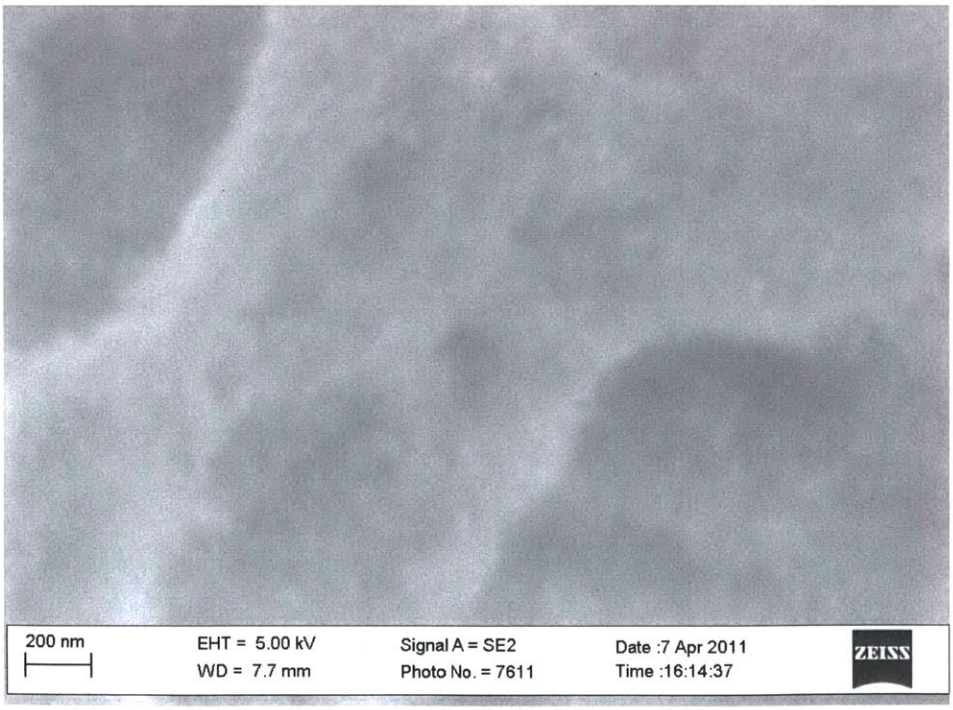

[25,000X]

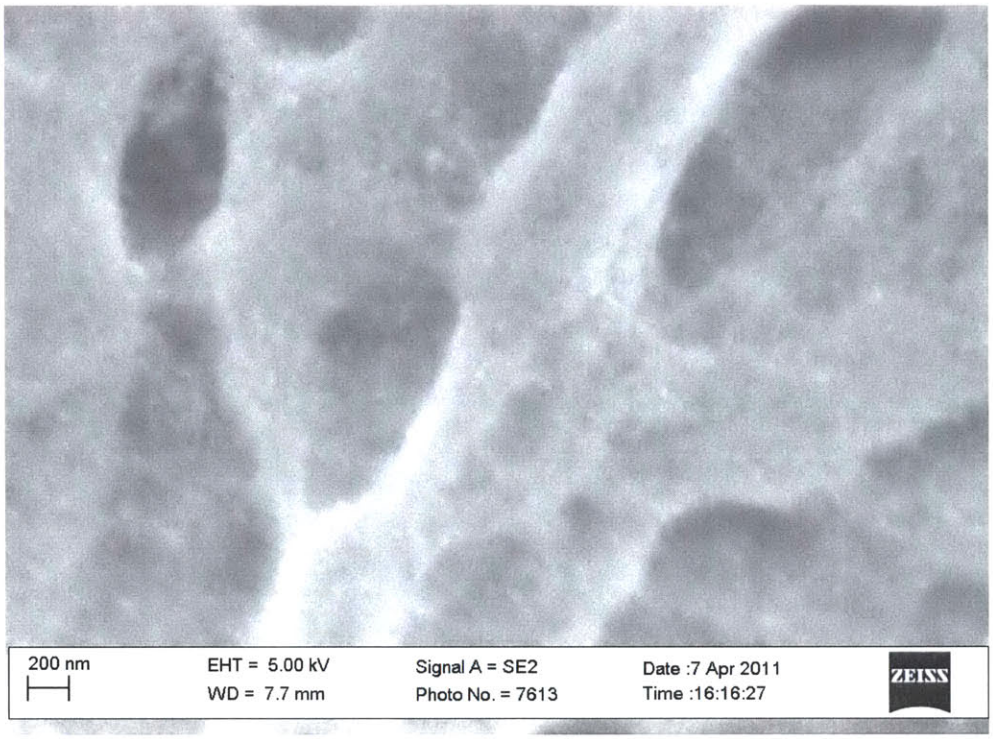

[11,000X]

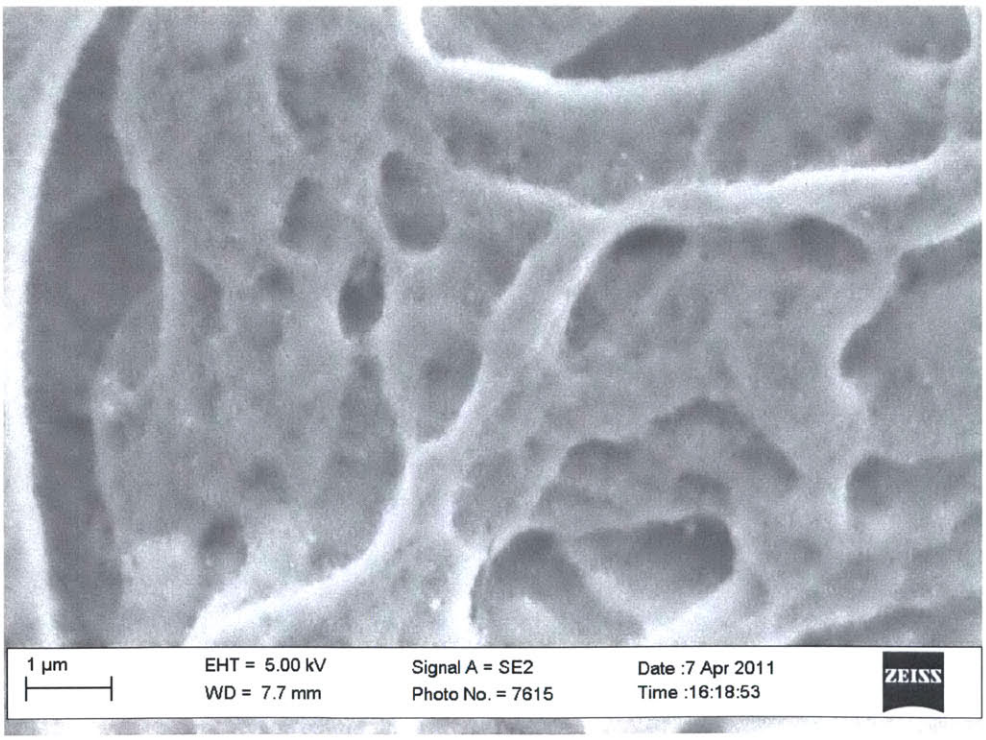

[6,000X]

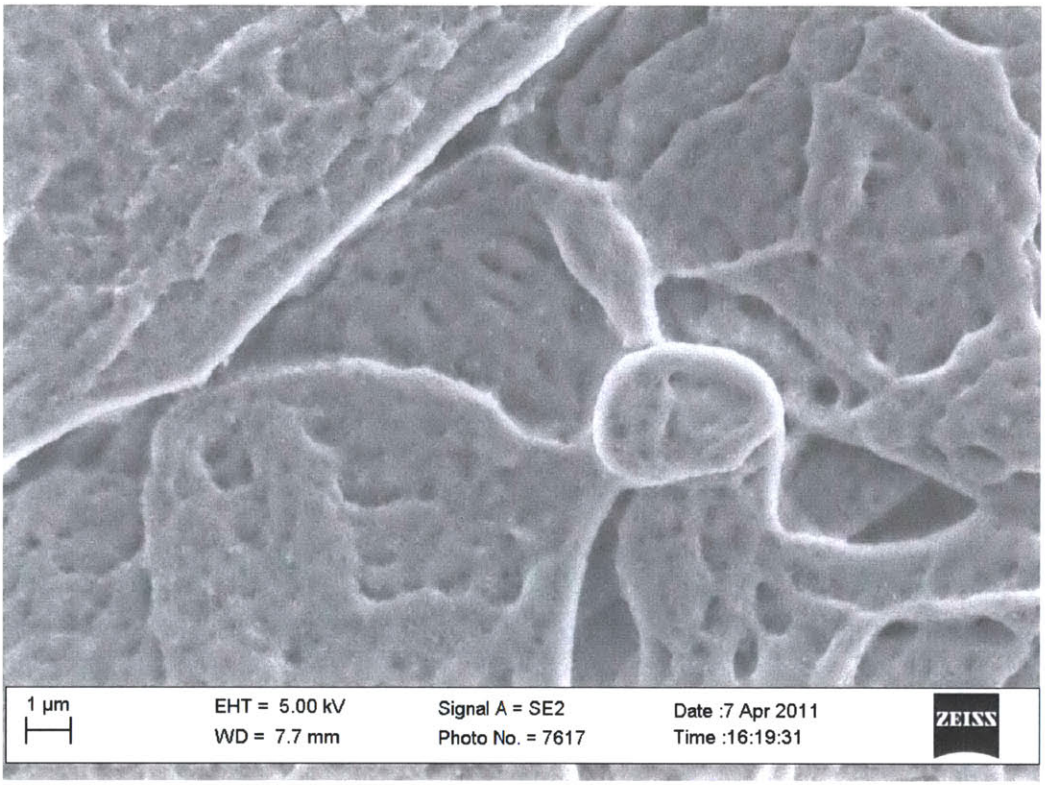
1 µm
EHT = 5.00 kV
WD = 7.7 mm
Signal A = SE2
Photo No. = 7617
Date :7 Apr 2011
Time :16:19:31
ZEISS

[1,100X]

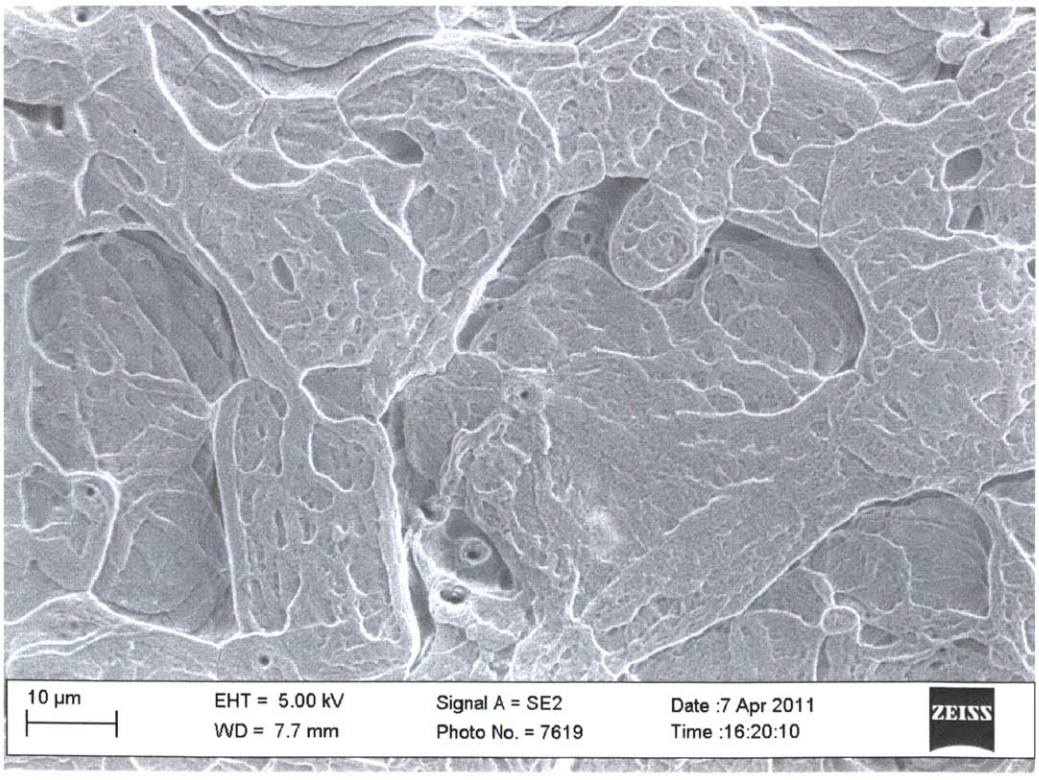
10 µm
EHT = 5.00 kV
WD = 7.7 mm
Signal A = SE2
Photo No. = 7619
Date :7 Apr 2011
Time :16:20:10
ZEISS

[300X]

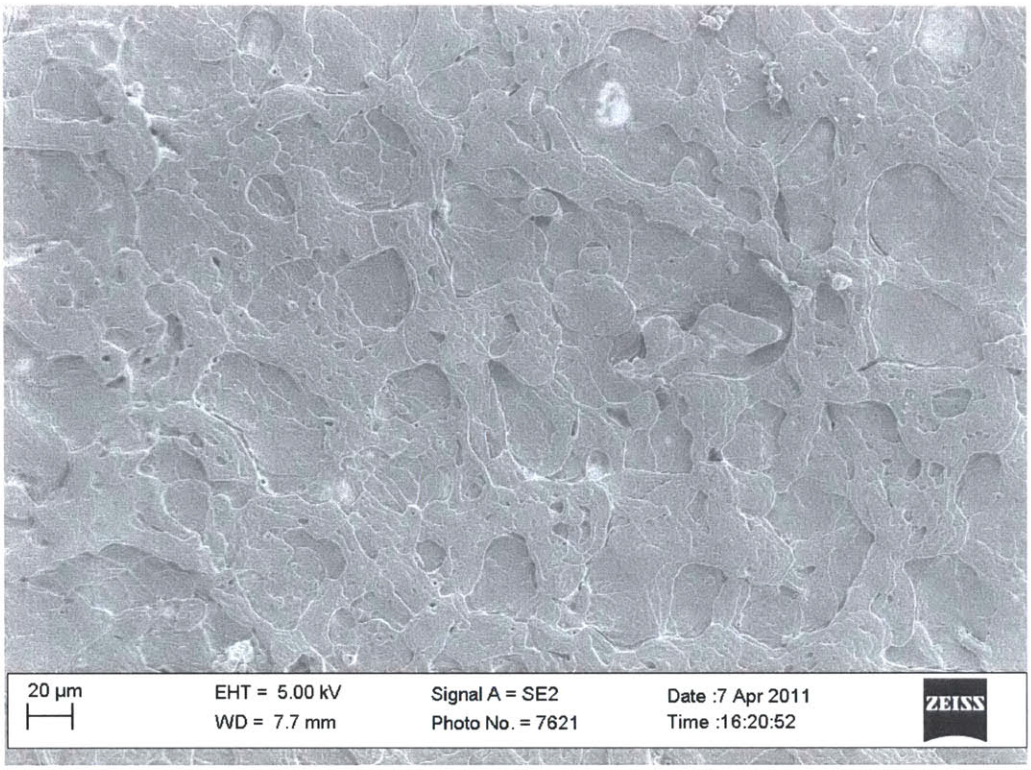
20 µm
EHT = 5.00 kV
WD = 7.7 mm
Signal A = SE2
Photo No. = 7621
Date :7 Apr 2011
Time :16:20:52
ZEISS

[65X]

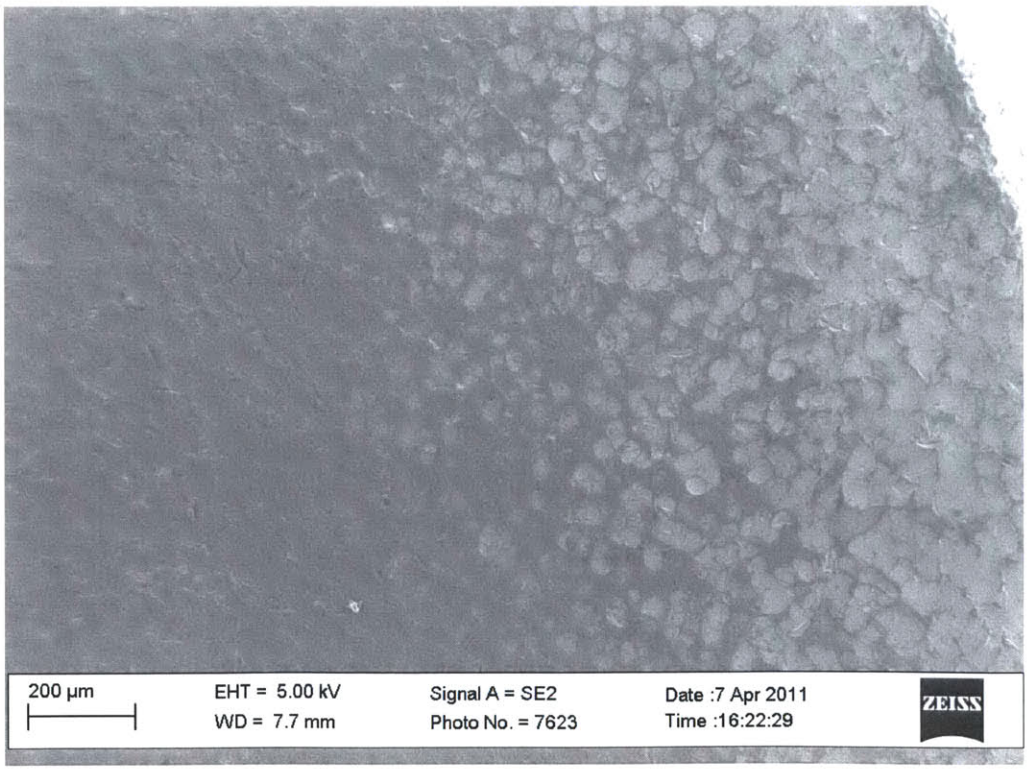
200 µm
EHT = 5.00 kV
WD = 7.7 mm
Signal A = SE2
Photo No. = 7623
Date :7 Apr 2011
Time :16:22:29
ZEISS

Figure 8-7: SEM of SS316L Heater used with Alumina – 0.01% - Sandblast Preparation – blackened CHF location – Various Magnifications

[22,500X]

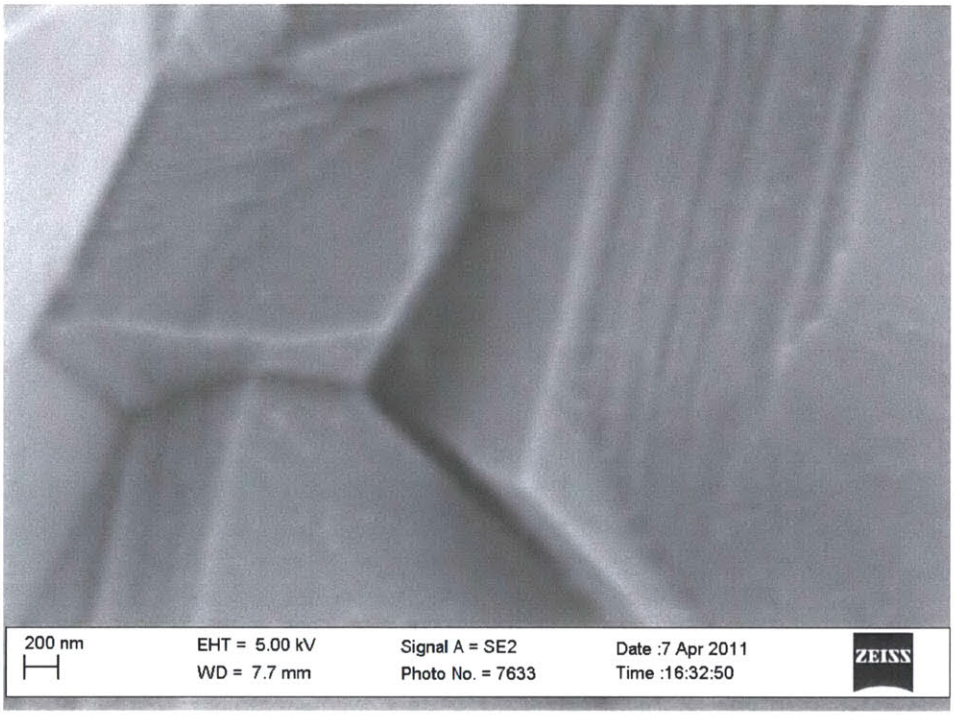

[11,000X]

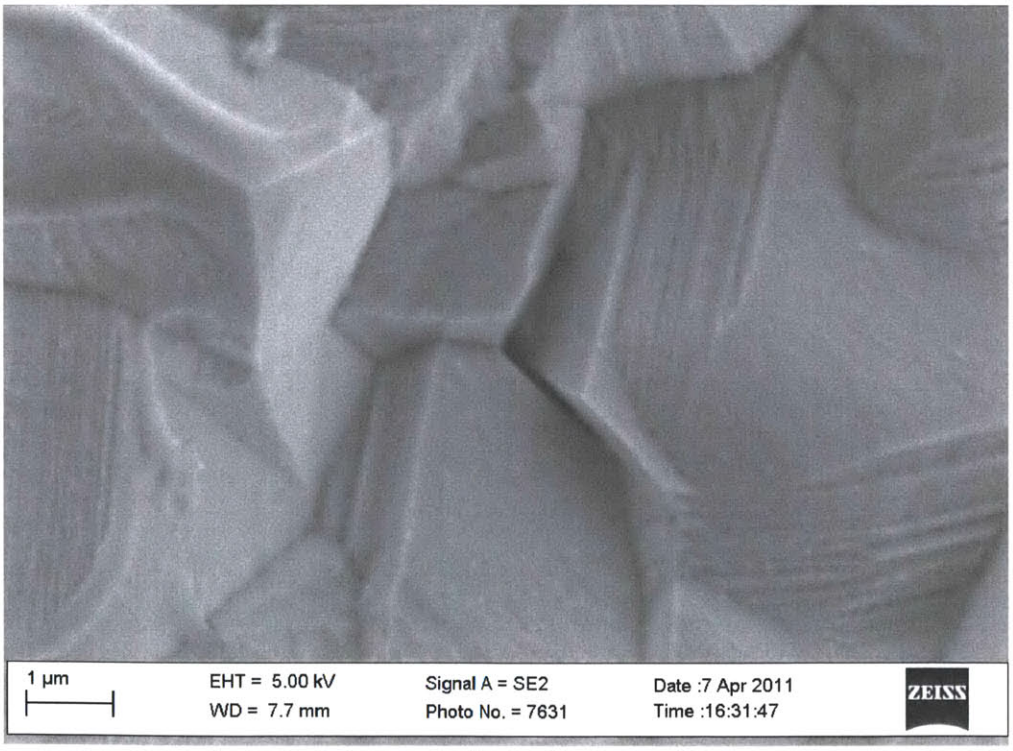

[5,500X]

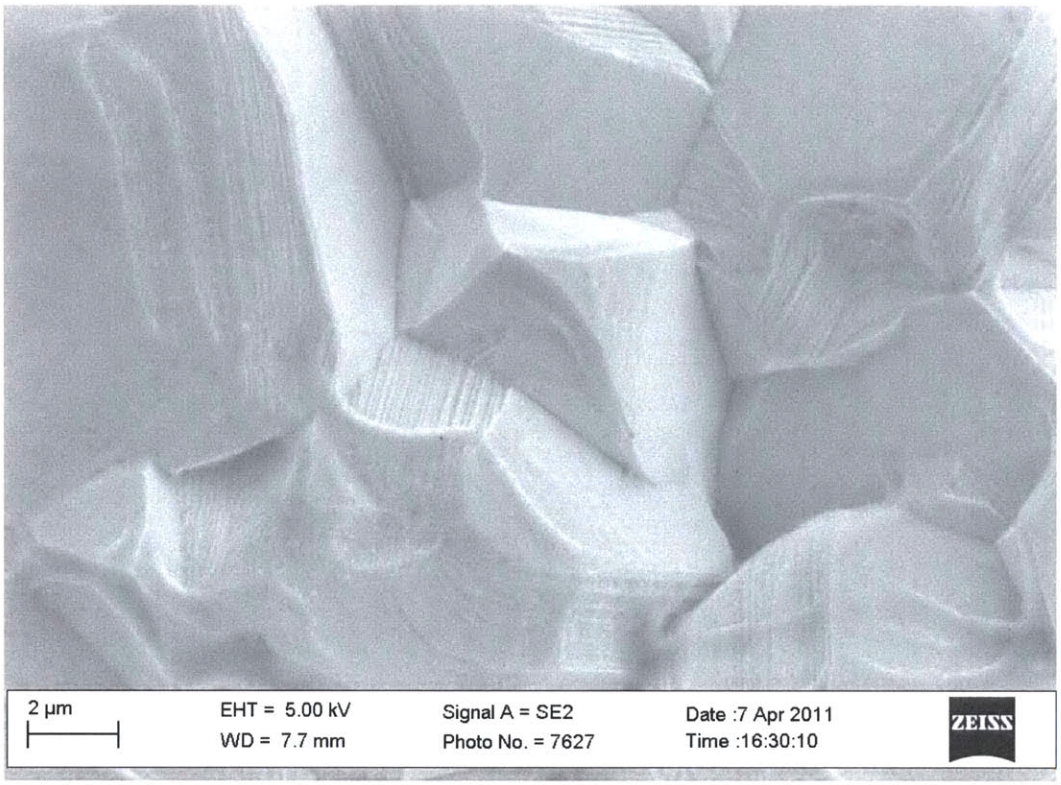
2 µm
EHT = 5.00 kV
WD = 7.7 mm
Signal A = SE2
Photo No. = 7627
Date :7 Apr 2011
Time :16:30:10
ZEISS

[1,100X]

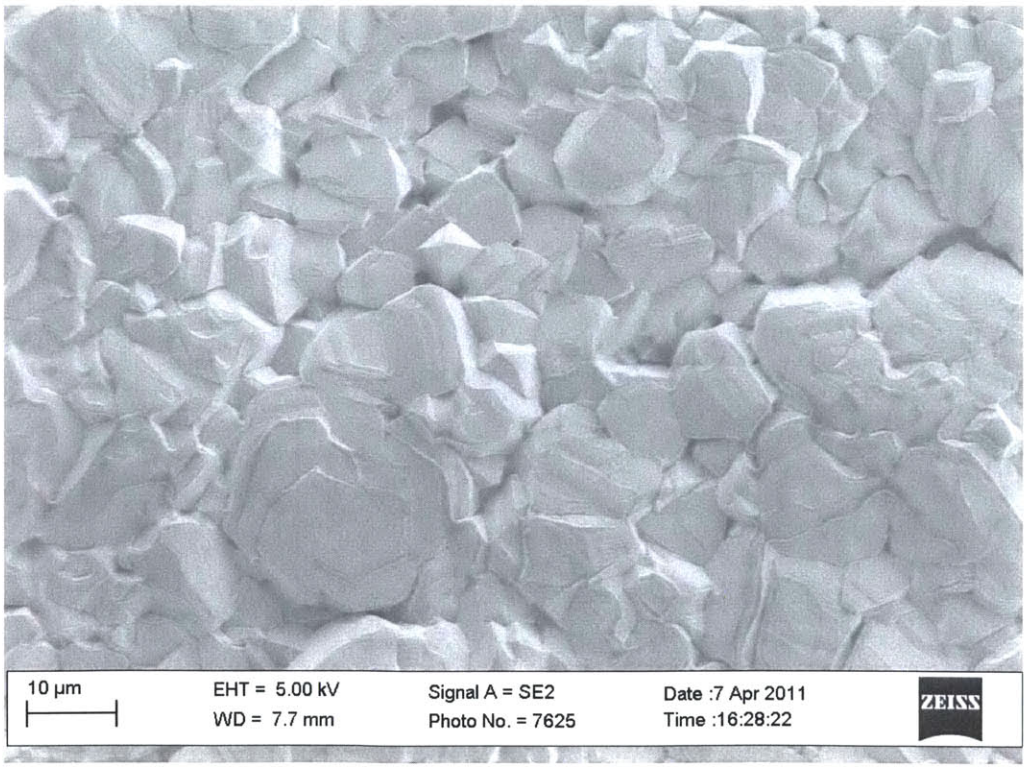
10 µm
EHT = 5.00 kV
WD = 7.7 mm
Signal A = SE2
Photo No. = 7625
Date :7 Apr 2011
Time :16:28:22
ZEISS

[250X]

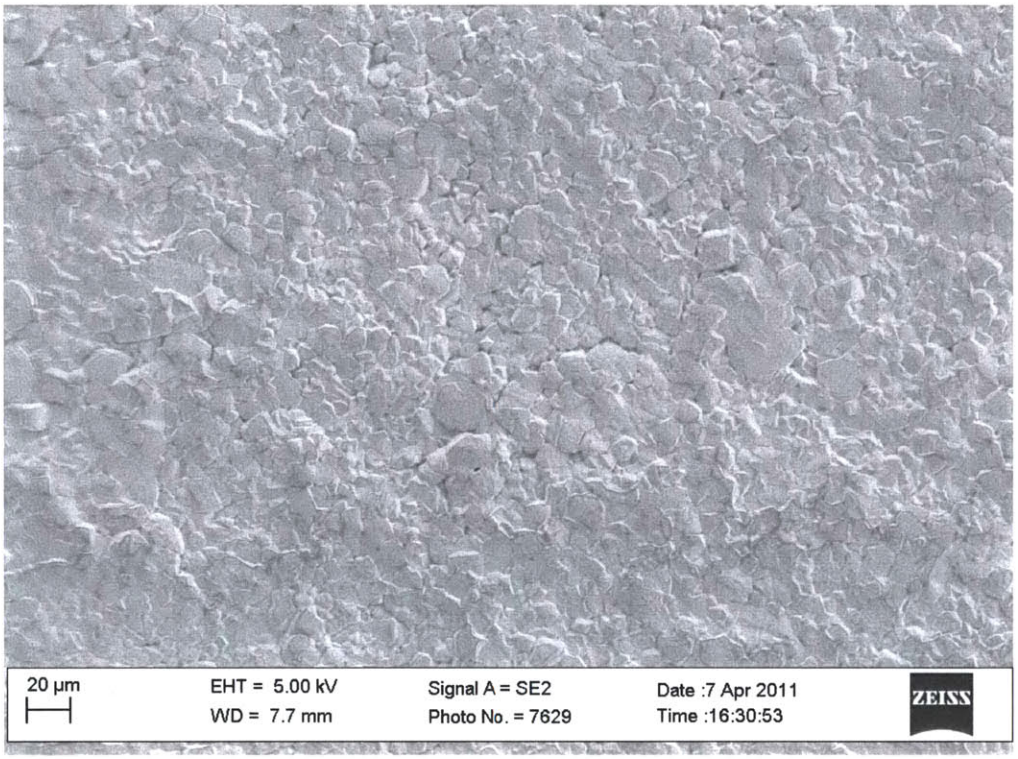
20 µm
EHT = 5.00 kV
WD = 7.7 mm
Signal A = SE2
Photo No. = 7629
Date :7 Apr 2011
Time :16:30:53
ZEISS

[50X]

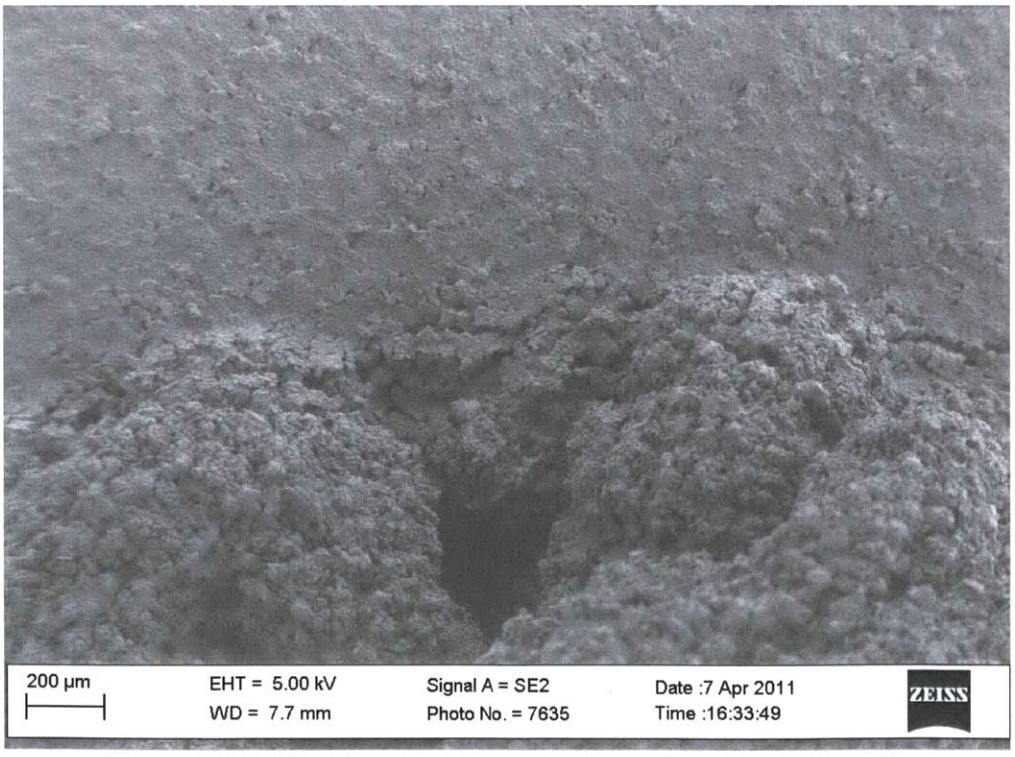
200 µm
EHT = 5.00 kV
WD = 7.7 mm
Signal A = SE2
Photo No. = 7635
Date :7 Apr 2011
Time :16:33:49
ZEISS

The first set of images (see Figure 8-1) for the SS316L unused heater with preparation shows a regular smooth surface with some imperfections from machining and sandblasting. The second set of images (see Figure 8-2), of a prepared heater used in a CHF test, are basically the same as the unused heater for before the CHF location. This surface is also basically smooth with spaced features. One can conclude that the boiling process alone with water only does little to modify the surface. At the point of CHF, blackened area, for the same heater the surface is very different with a granular structure (see Figure 8-3). This morphology is from the melting and cooling from the CHF event. The melting point of SS316L is approximately 1,370 °C. Note the orange color visualized for all CHF events herein implies a temperature above 1,000 °C.

The first sample with alumina nanofluid with 0.001% by volume concentration shows how boiling deposits the nanoparticle across the surface changing the surface morphology. The set before the point of CHF shows a surface that has many more features relative to water only (see Figure 8-4). The number of surface cavities from which boiling might arise is greater. The morphology is visually also more porous. The visualized coverage is fairly complete with no noted breaks to the underlying metal and are consistent to previous MIT findings [14][39].

The two SEM images at the point of CHF, blackened area, for the alumina 0.001% show a broken layer of alumina on the heater surface (see Figure 8-5). The CHF event with its high temperature rise and geometry change most likely dislocated the nanoparticle layer. About half of the time in CHF testing the sample actually breaks.

Comparing the alumina 0.01% images from the before CHF location (see Figure 8-6) to the previous 0.001% the morphology is very similar. The coverage of the surface and the general features are not distinguishable. The same can be said for the CHF location, blackened area, images. These observations are consistent with the measurements of CHF enhancement that are nearly the same for both 0.001% and 0.01%.

For convenience to the reader the SEM images nearest 1000X for each set are assembled (see Figure 8-8). The images show that nanoparticles deposit onto the surface during the boiling process thereby changing the morphology. The chemical and geometric change to the surface will impact wettability, which is quantified by contact angle measurement.

Figure 8-8: Side-by-Side of ~1,000X SEM Images for each Set

Unused Prepared [1,010X]

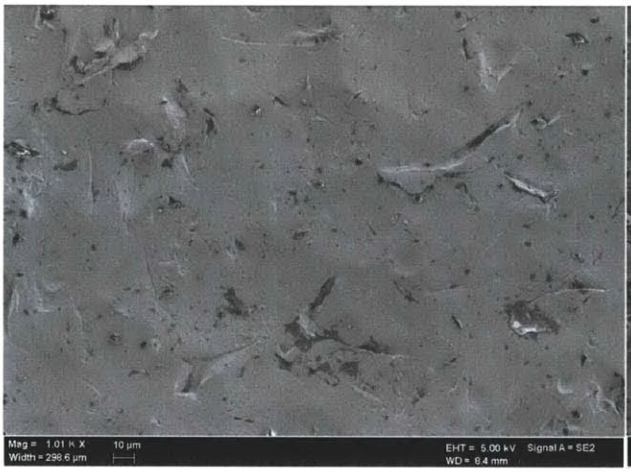

Water-only, before CHF location [999X]

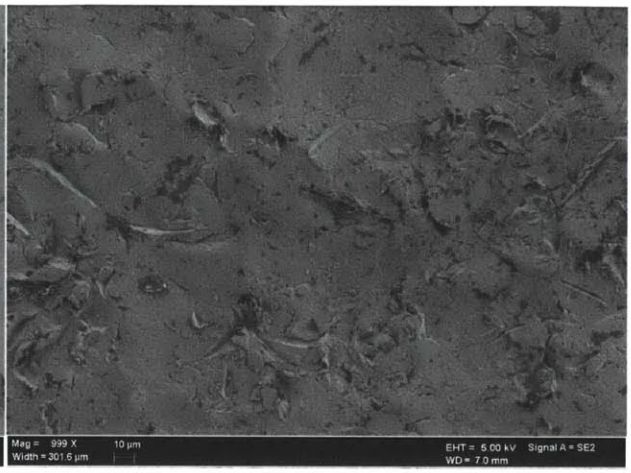

Water-only, CHF location [998X]

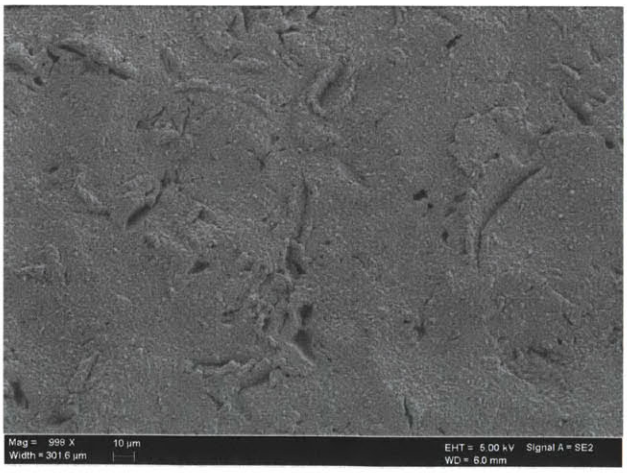

Alumina 0.001%, before CHF location [1,010X]

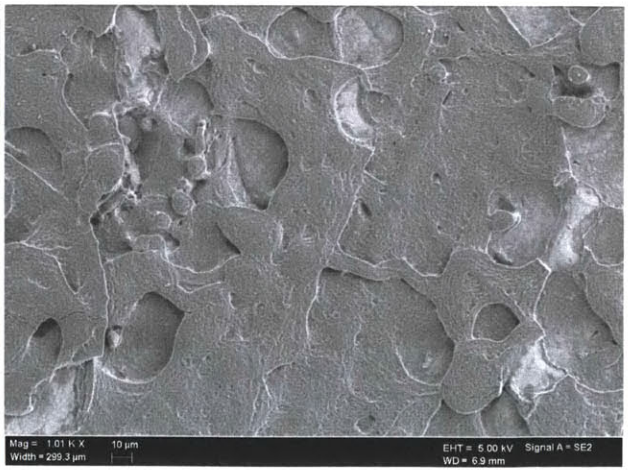

Alumina 0.001%, CHF location [825X]

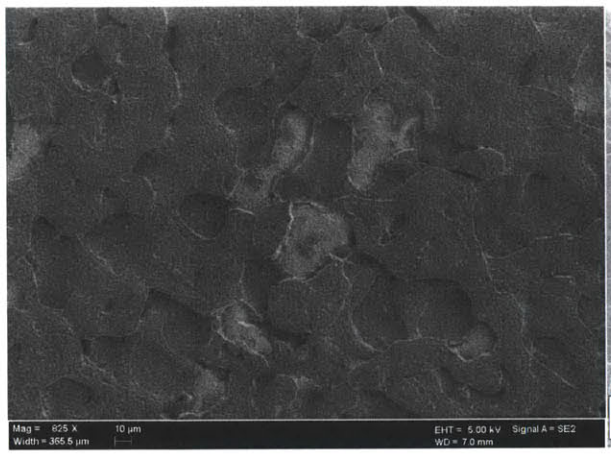

Alumina 0.01%, before CHF location [1,100X]

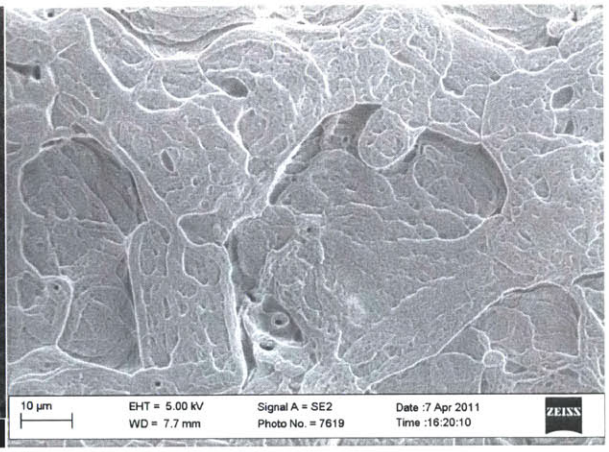

Alumina 0.01%, CHF location [1,100X]

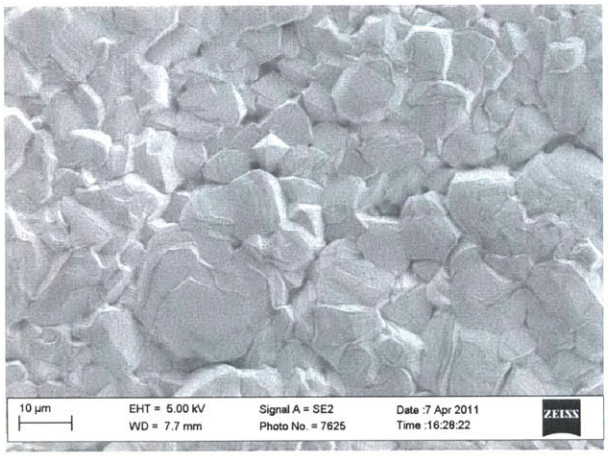

8.1.2 SEM of SA-508

Figure 8-9: SEM of SA-508 - Unused Heater - Sandblast Preparation – Various Magnifications

[40,000X]

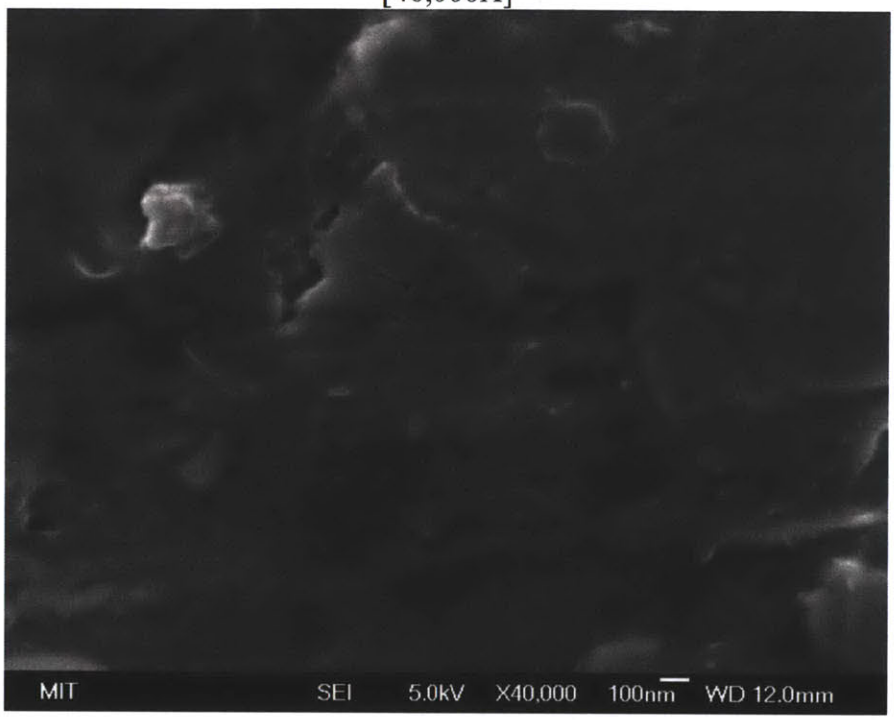

[20,000X]

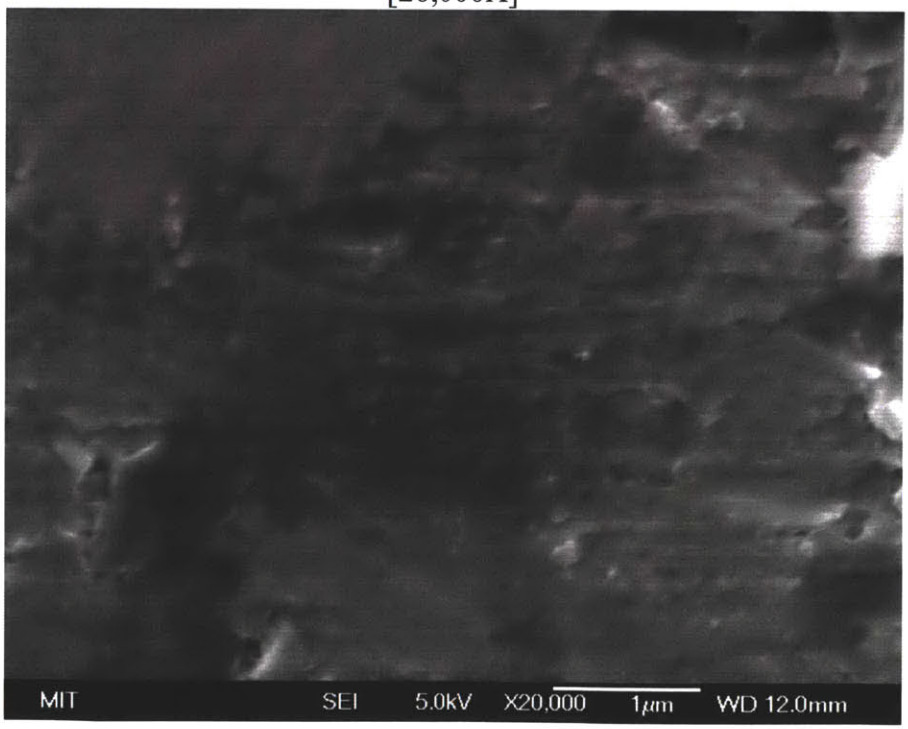

[10,000X]

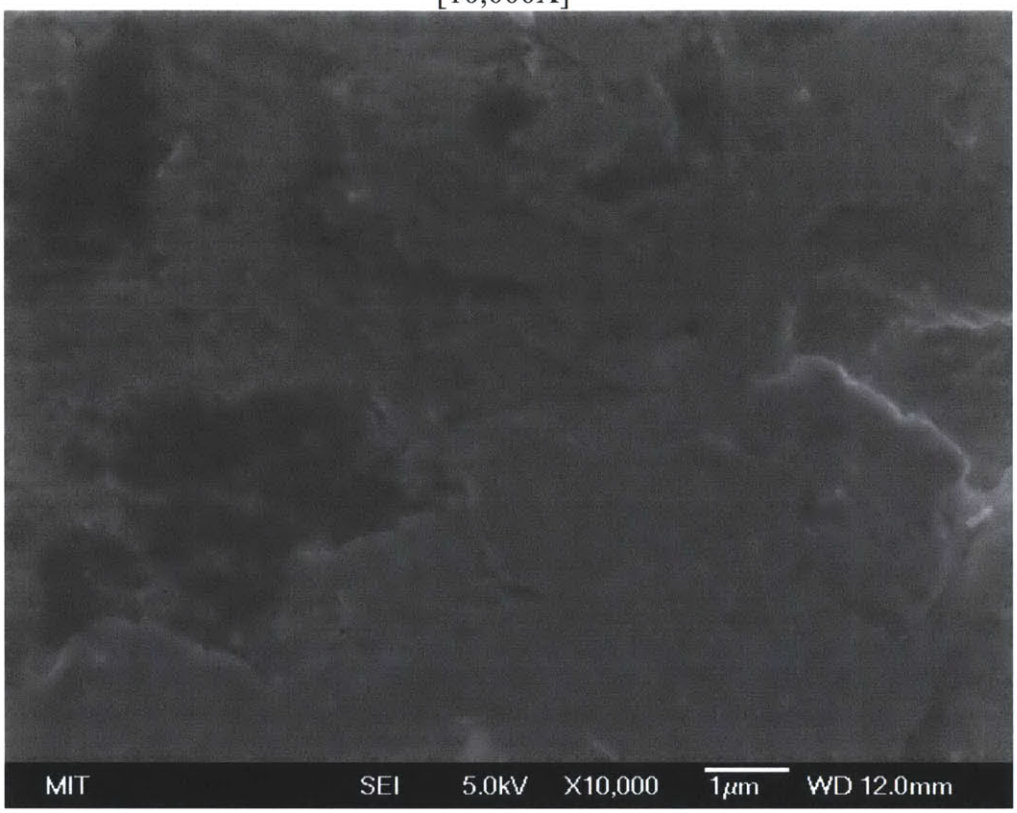

[1,000X]

[250X]

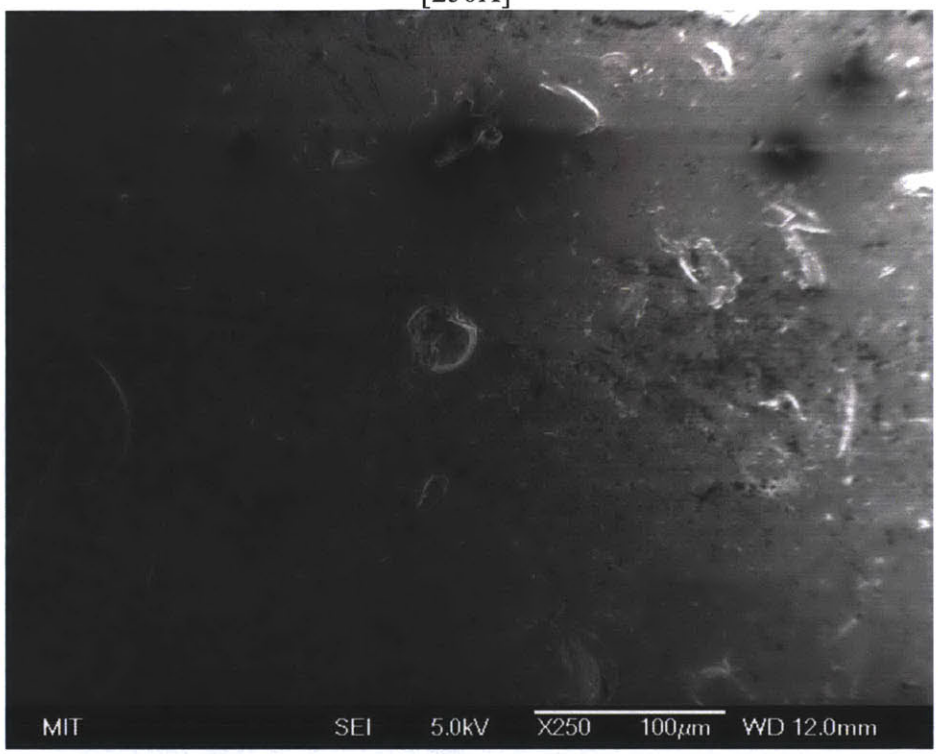

Figure 8-10: SEM of SA-508 - Used in Water - Sandblast Preparation – before CHF location – Various Magnifications

[40,000X]

[20,000X]

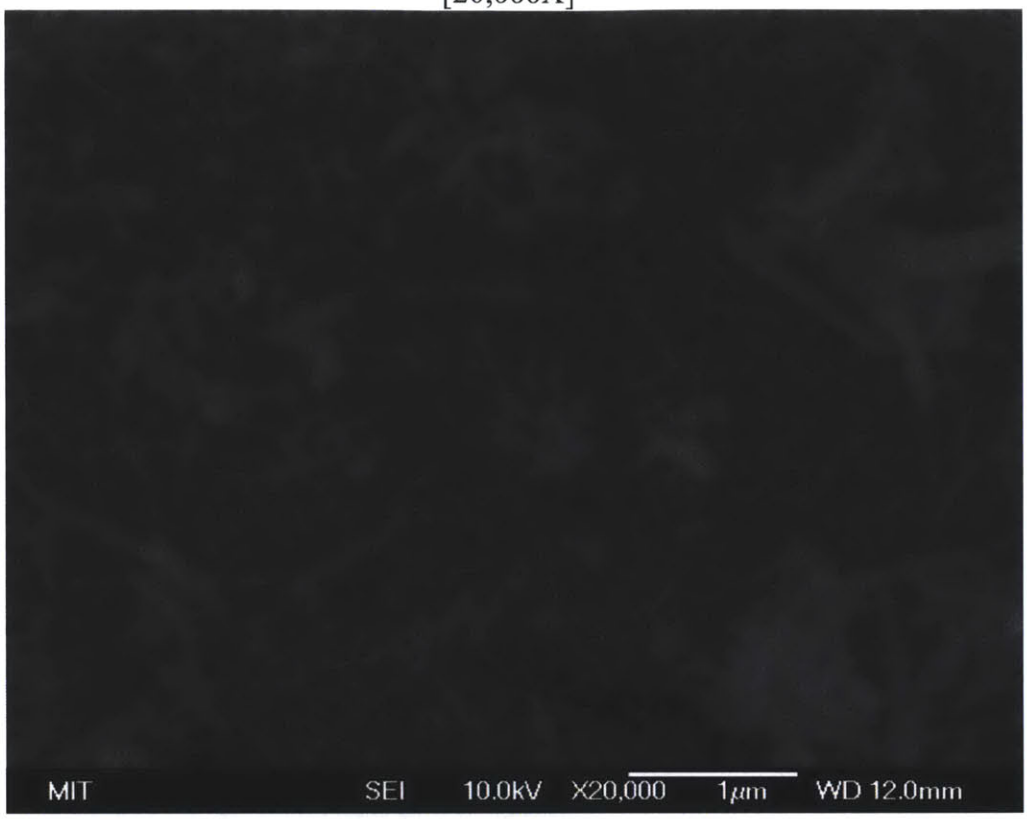

[10,000X]

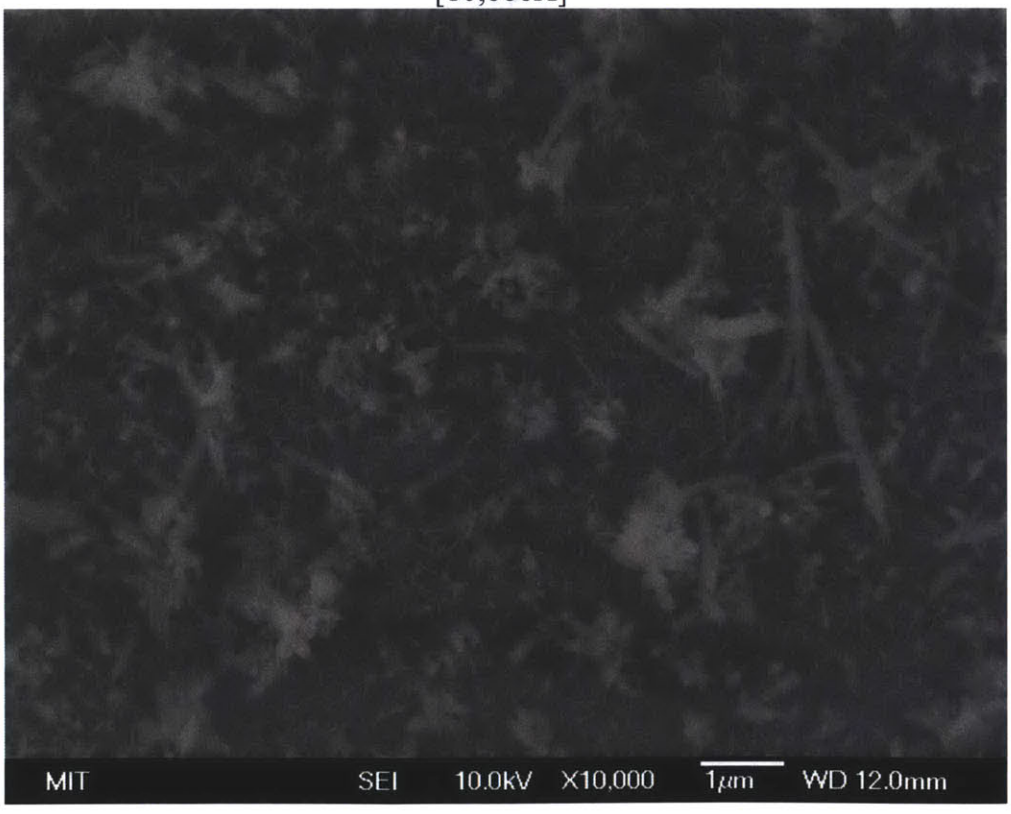

[1,000X]

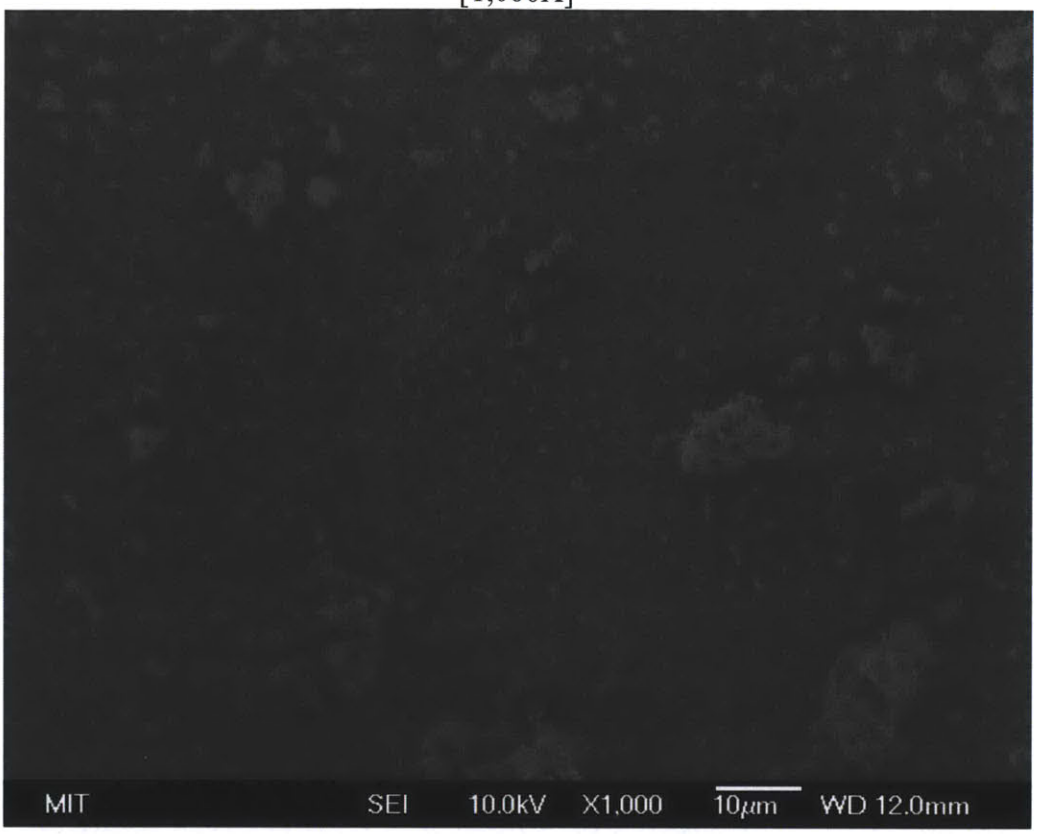
MIT
SEI
10.0kV
X1,000
10μm
WD 12.0mm

[250X]

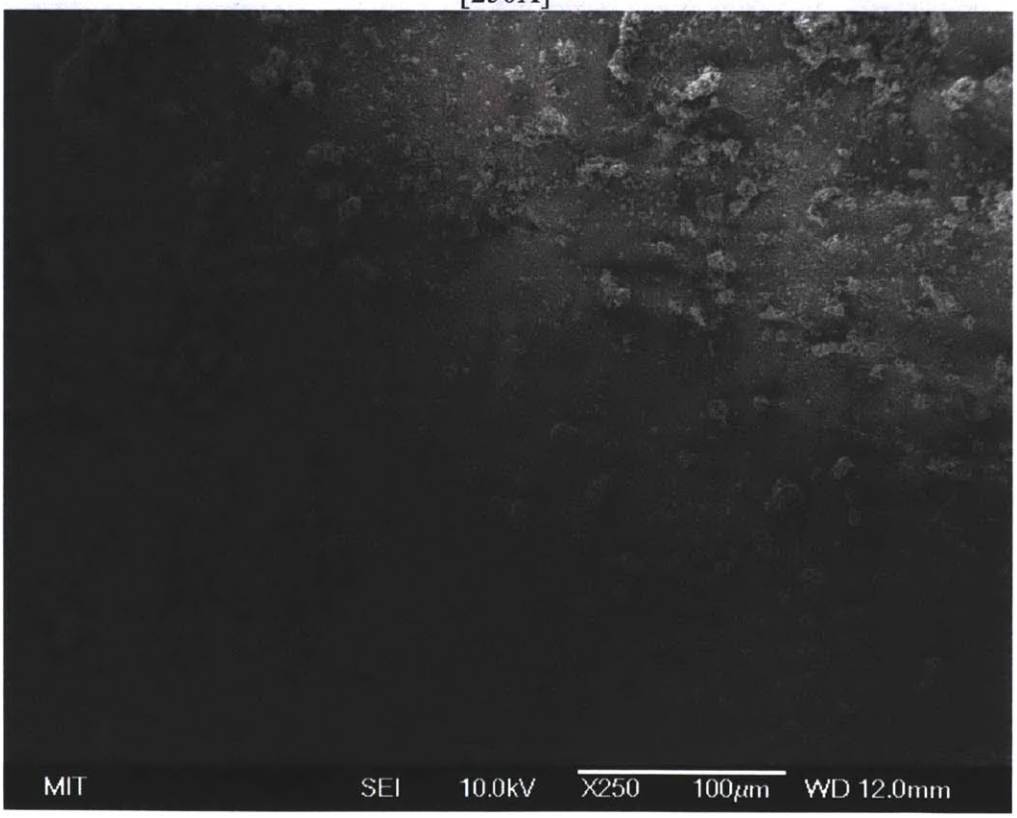
MIT
SEI
10.0kV
X250
100μm
WD 12.0mm

Figure 8-11: SEM of SA-508 - Used in Water - Sandblast Preparation – blackened CHF location – Various Magnifications

[40,000X]

[20,000X]

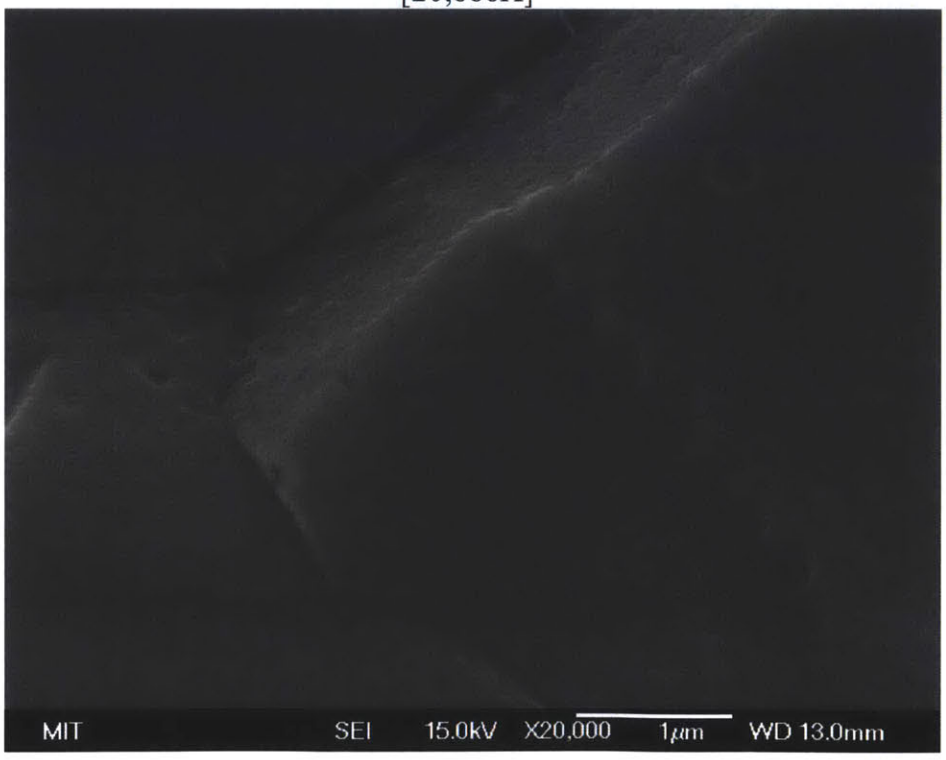

[10,000X]

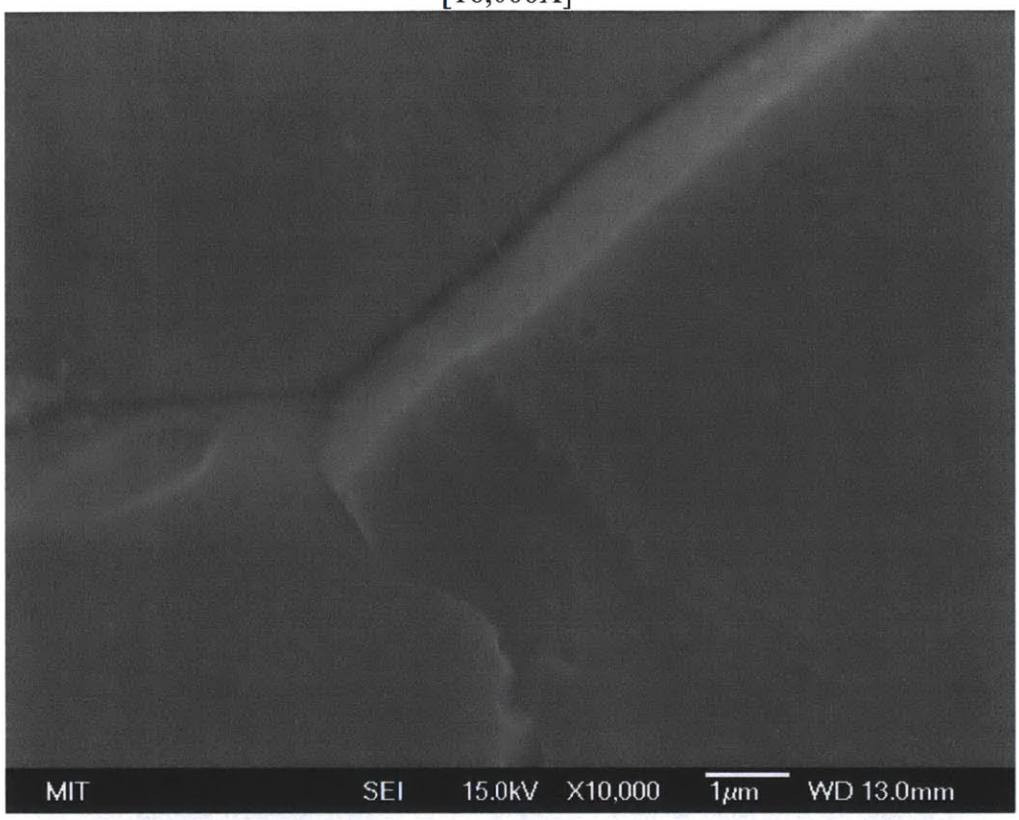

[1,000X]

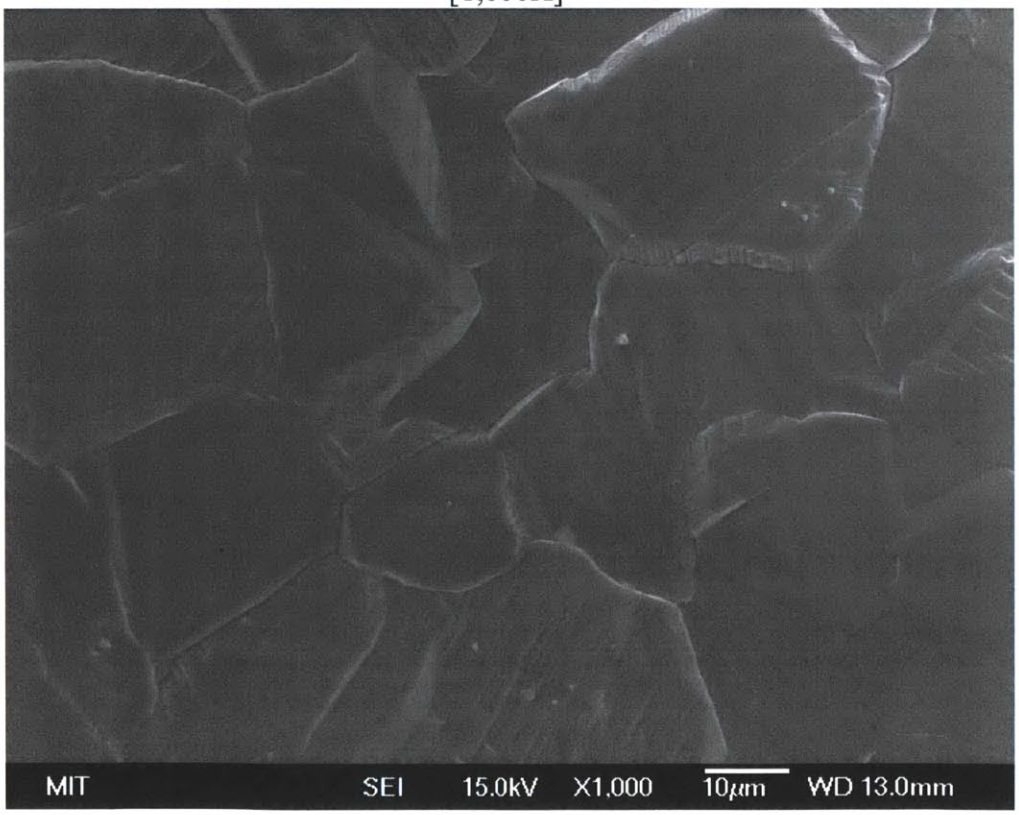

[250X]

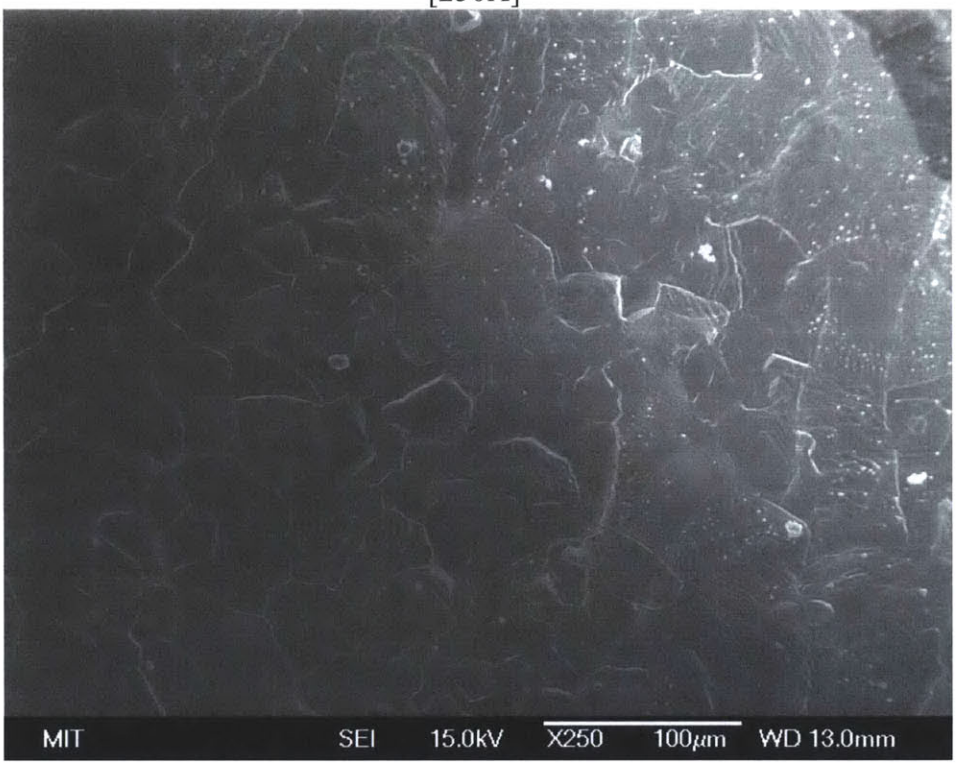

Figure 8-12: SEM of SA-508 - Heater with Alumina 0.001% - Sandblast Preparation – before CHF location – Various Magnifications

[40,000X]

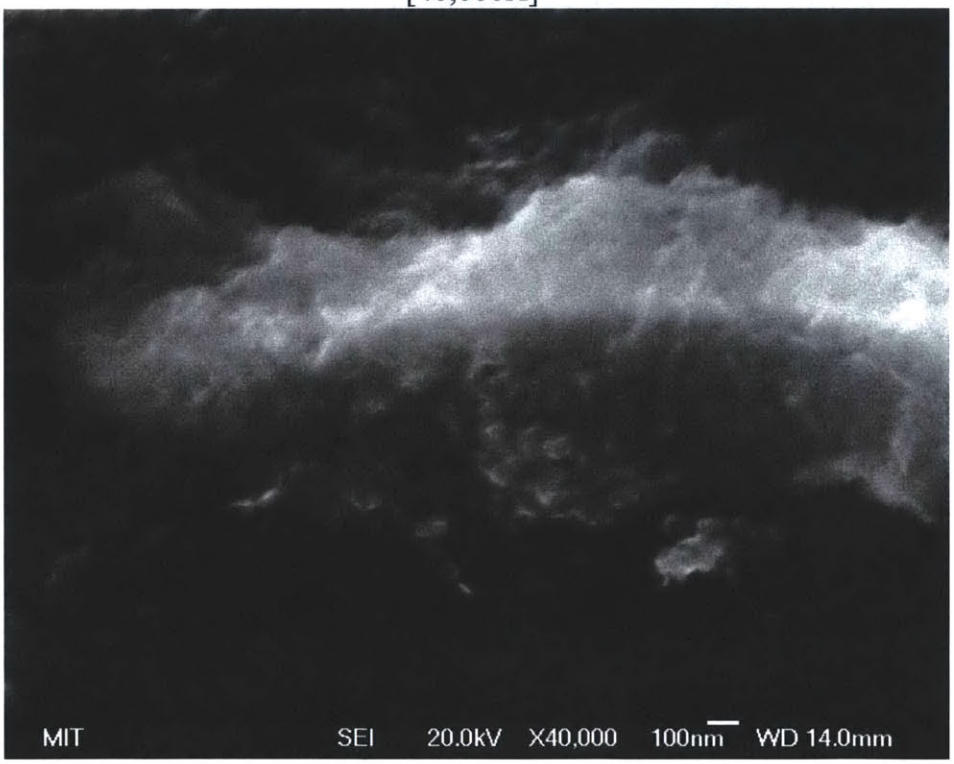

[20,000X]

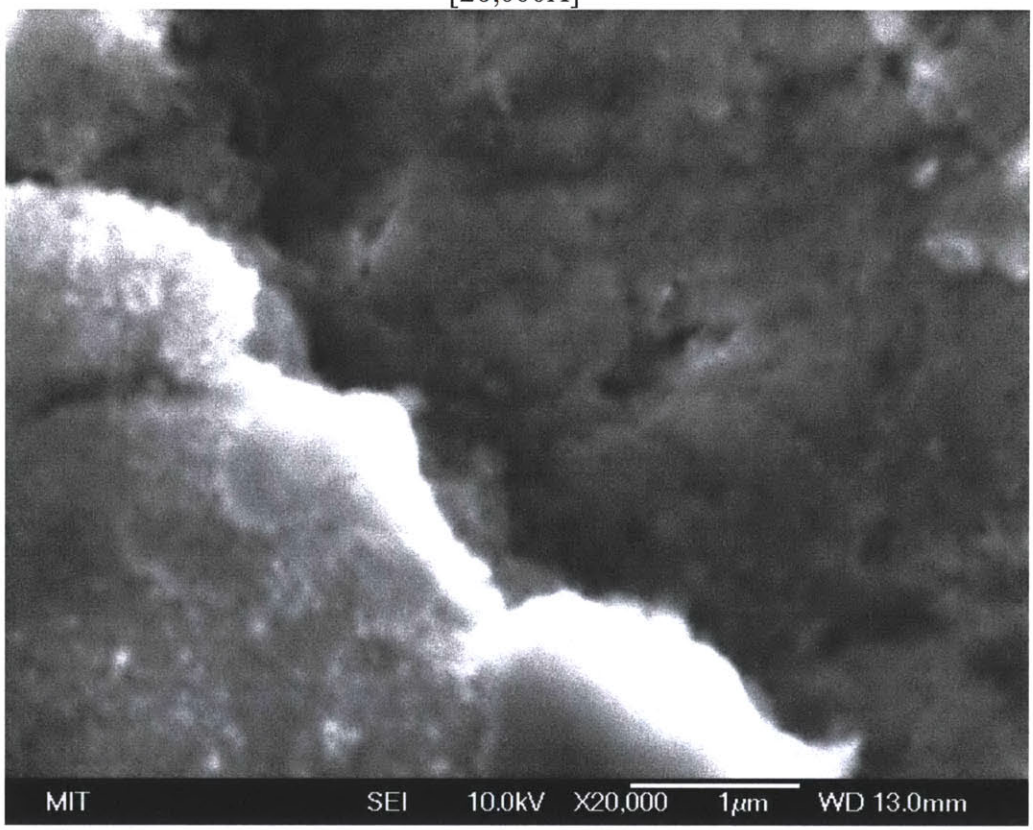

[10,000X]

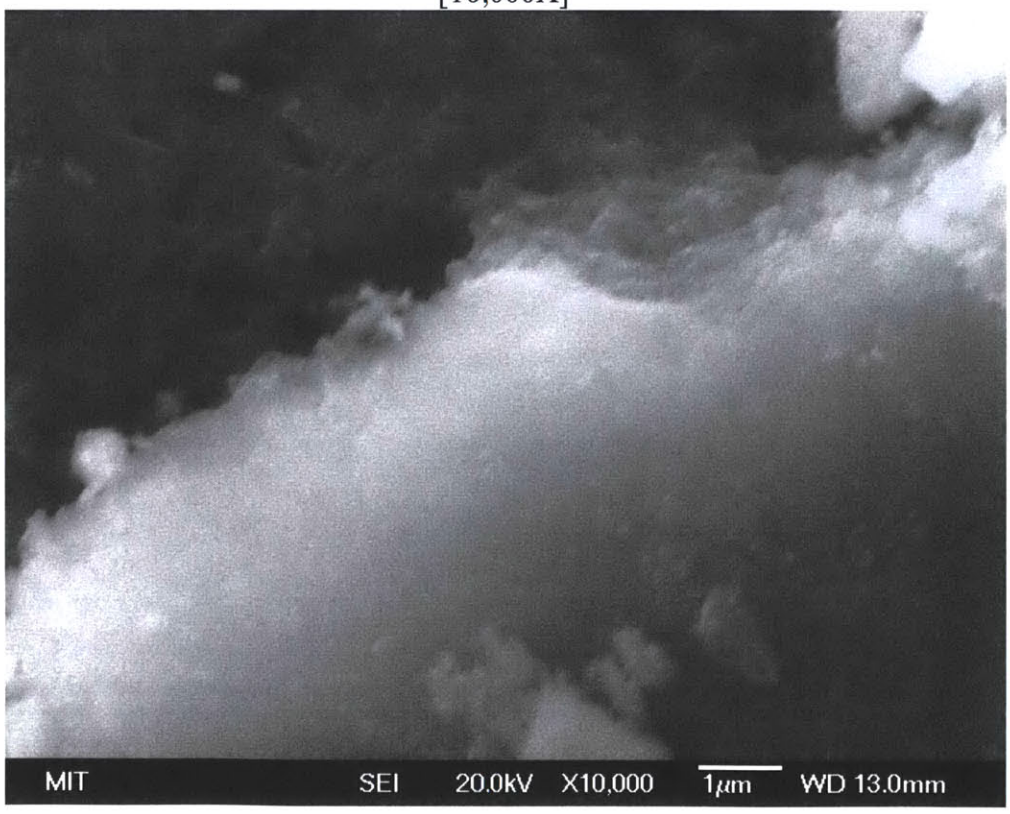

[1,000X]

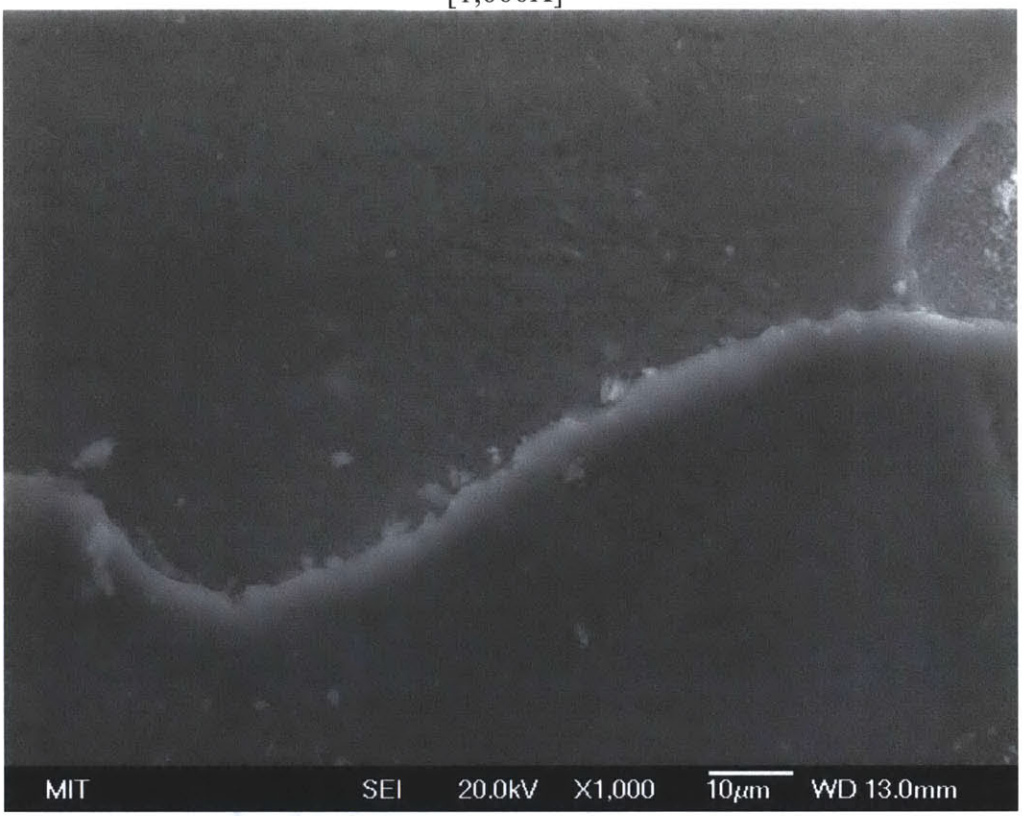
MIT SEI 20.0kV X1,000 10μm WD 13.0mm

[250X]

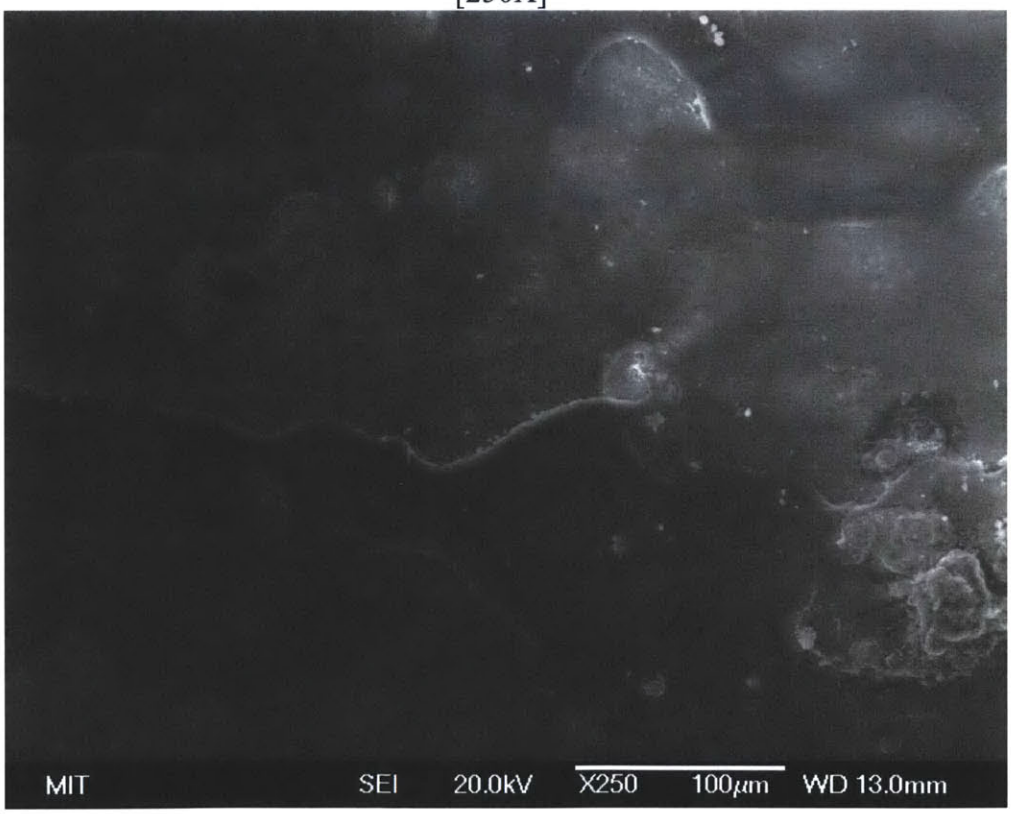
MIT SEI 20.0kV X250 100μm WD 13.0mm

Figure 8-13: SEM of SA-508 - Heater used with Alumina 0.001% - Sandblast Preparation – blackened CHF location – Various Magnifications

[40,000X]

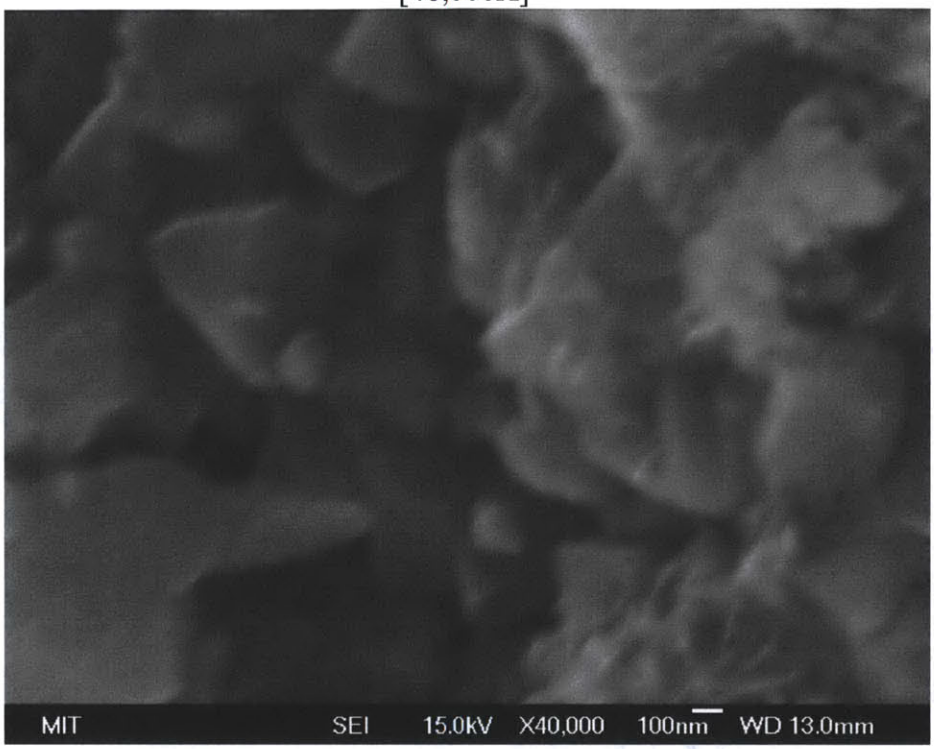

[20,000X]

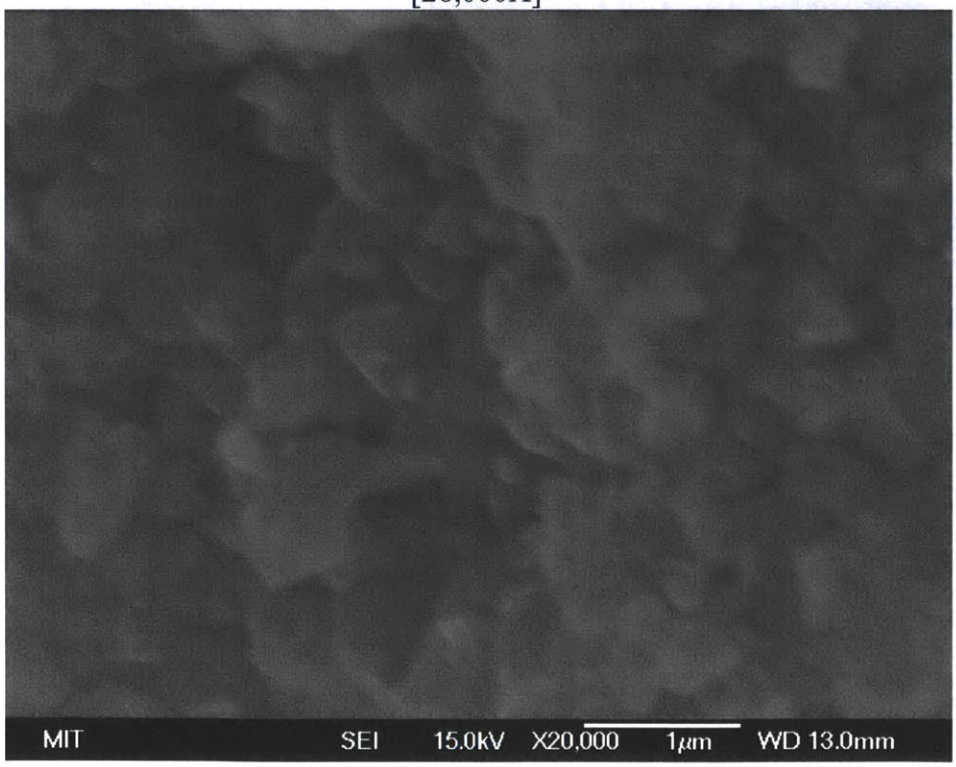

[10,000X]

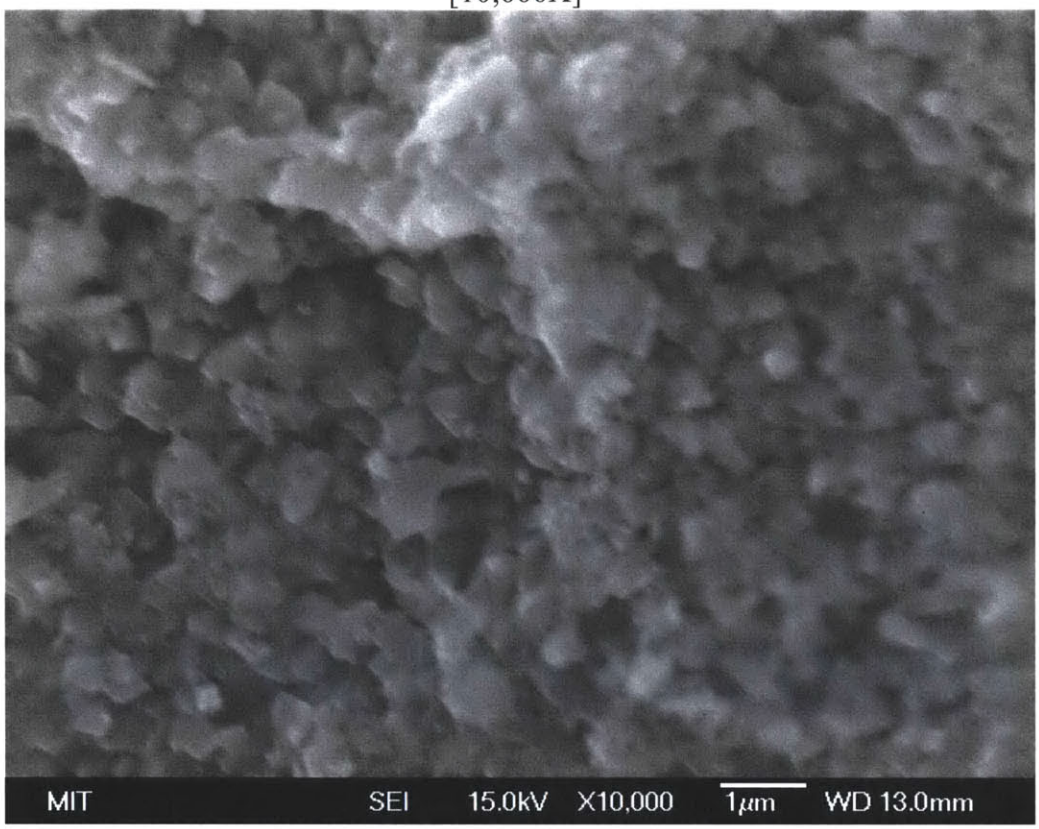

[1,000X]

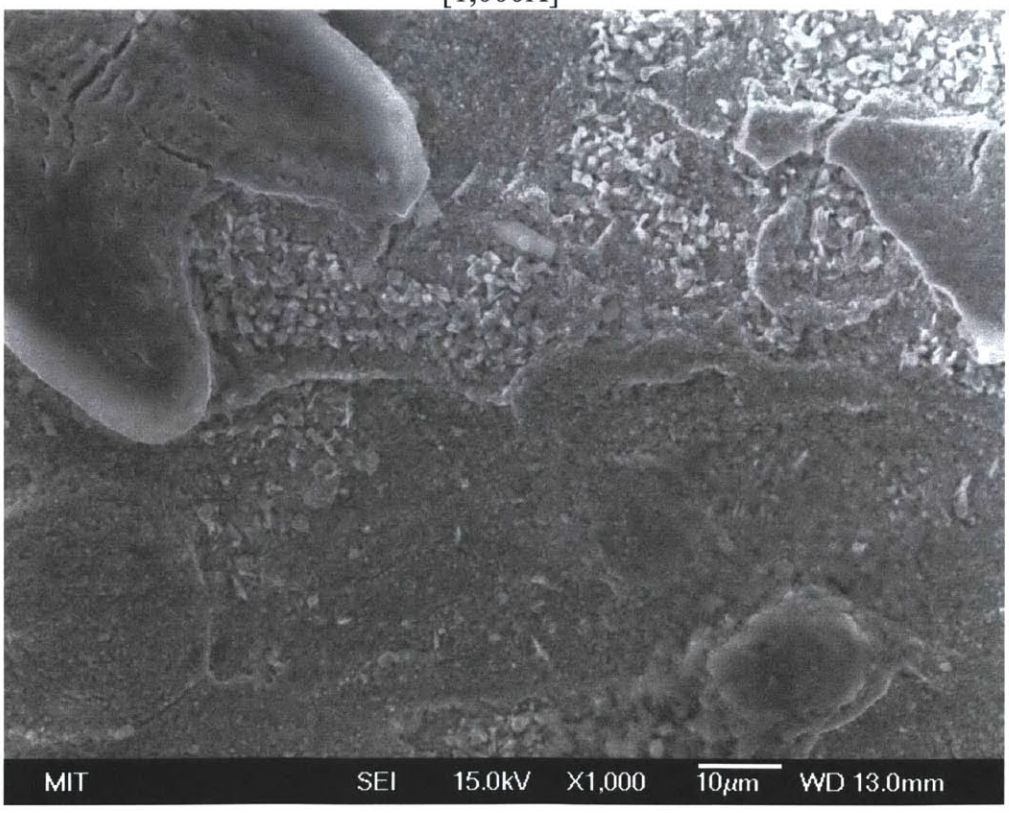

[250X]

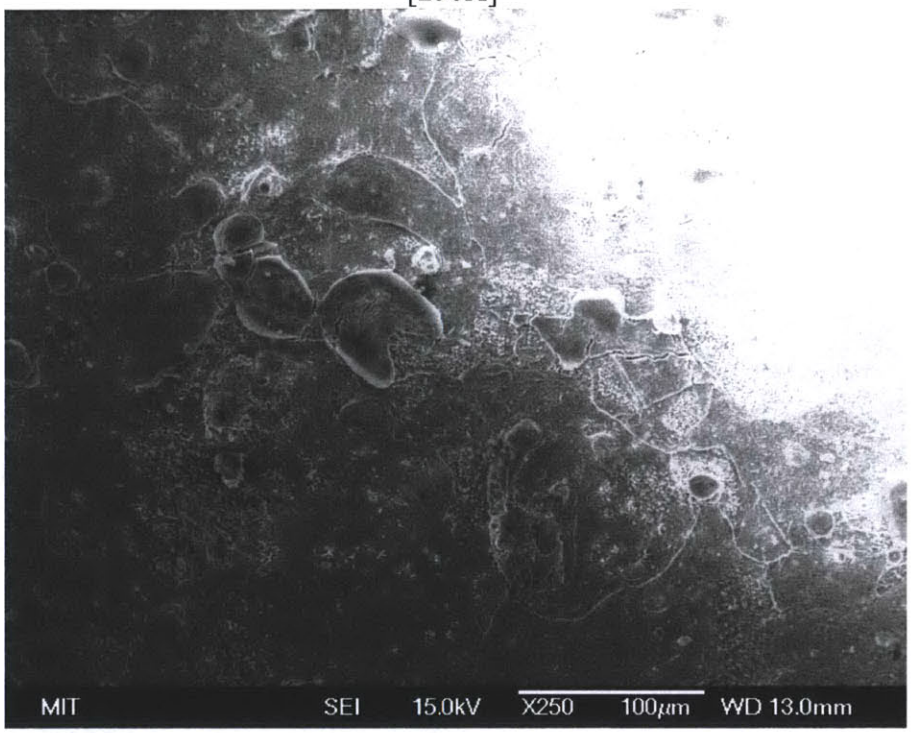

For SA508, the first set of SEM images show a reasonably smooth surface with occasional features (see Figure 8-9). The surface does not appear as smooth as the unused and prepared SS316L.

SA-508 heater used during CHF with DI water shows significant thread-like features at higher magnifications (see Figure 8-10). The lower magnifications are visually more of a spotty featured morphology. Visual observations of the unused heater indicate heavy rust like oxidation on the surface. The blackened area for the same sample has a completely different visual texture that seems more crystalline in structure (see Figure 8-11).

The SA-508 heater used with alumina 0.001% nanofluid away from the burnout area has a sponge like morphology with no sign of the thread-like features mentioned above for DI water (see Figure 8-12). The differing surface may be the presence of alumina nanoparticles. On the blackened CHF region the features are very similar to the DI water sample at a similar position (see Figure 8-13).

8.1.3 SEM of Oxidized SS316L

Figure 8-14: SEM of Oxidized SS316L - Unused Heater - Sandblast Preparation – Various Magnifications

[40,000X]

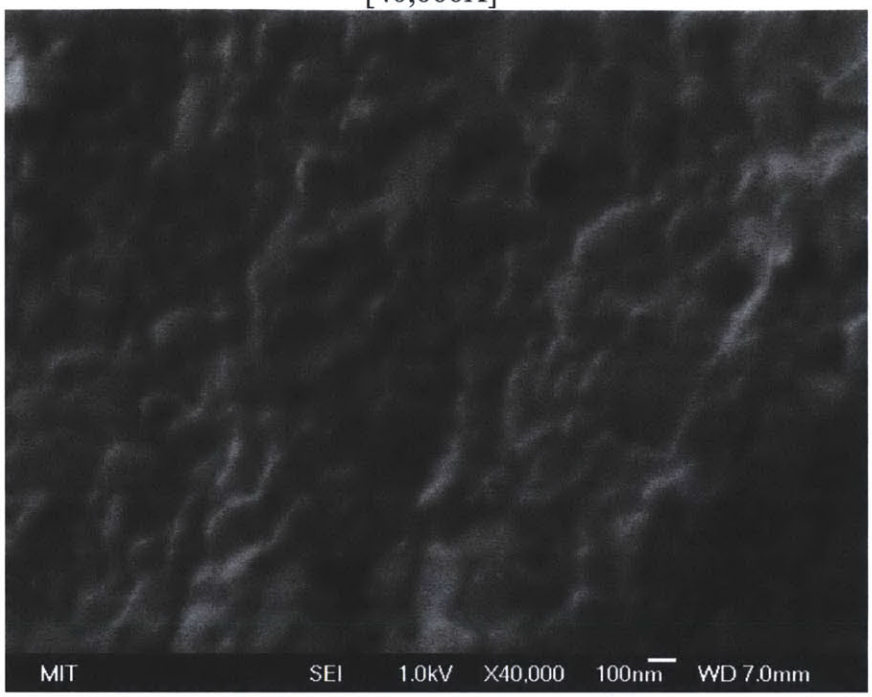

[20,000X]

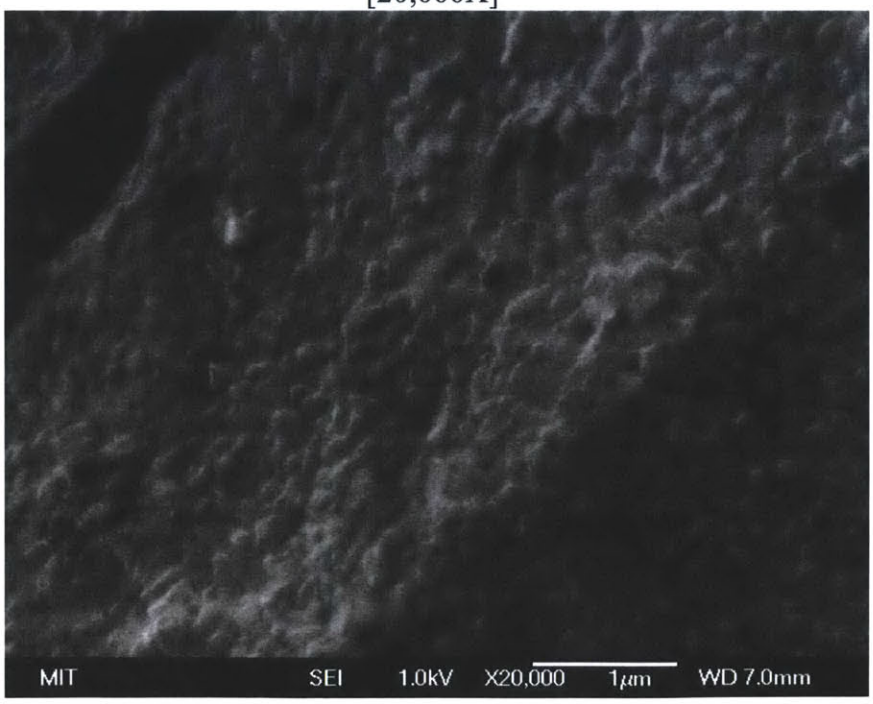

[10,000X]

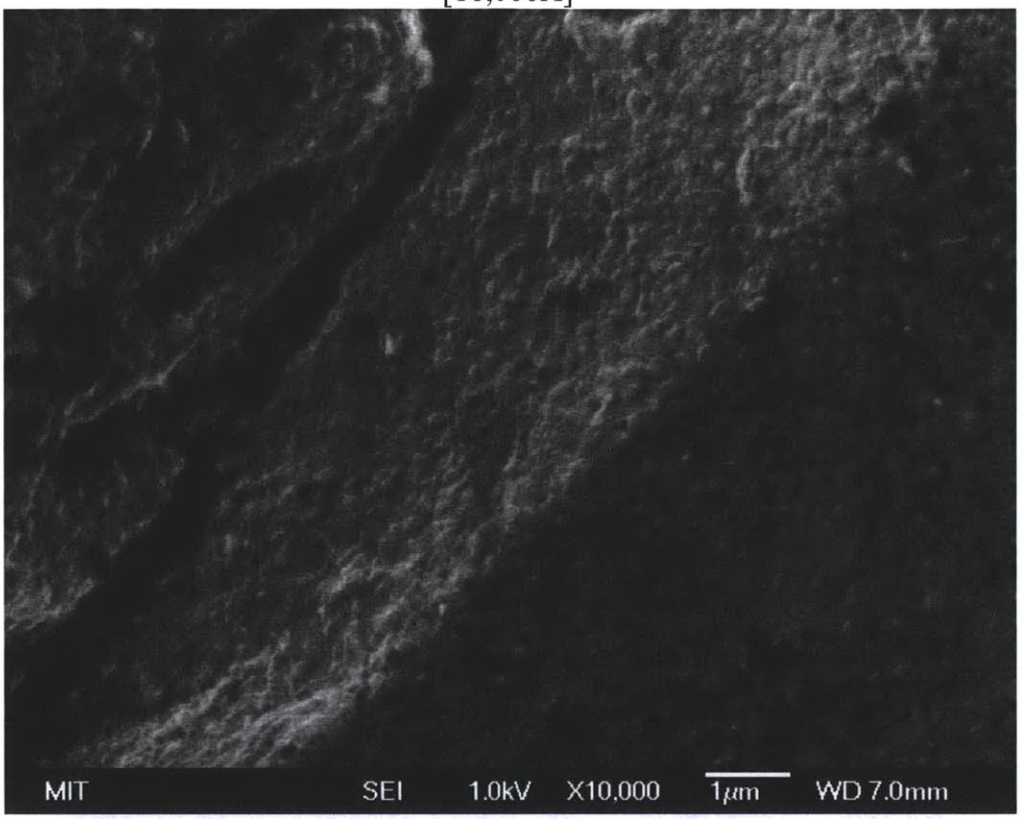

[1,000X]

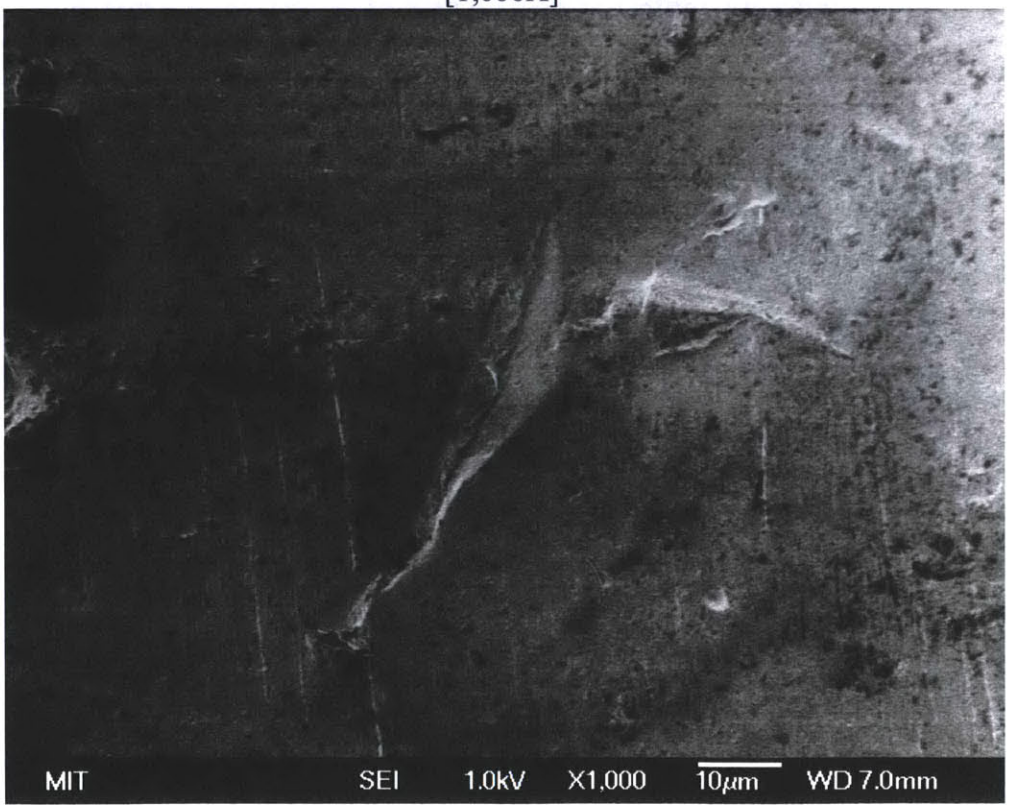

[600X]

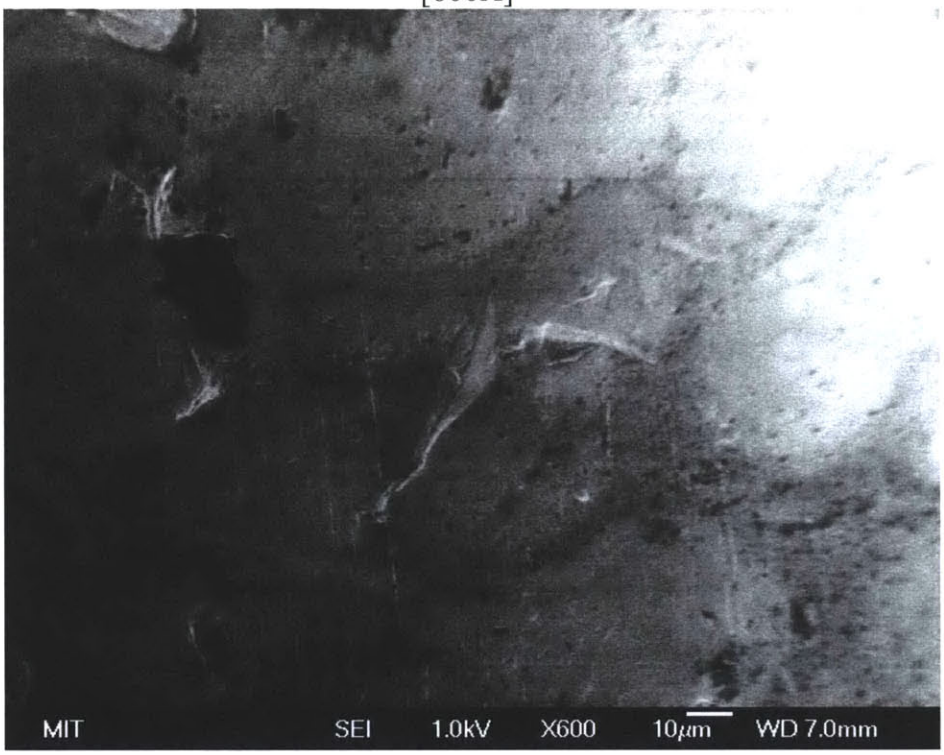

Figure 8-15: SEM of Oxidized SS316L - Used in Water - Sandblast Preparation – before CHF location – Various Magnifications

[40,000X]

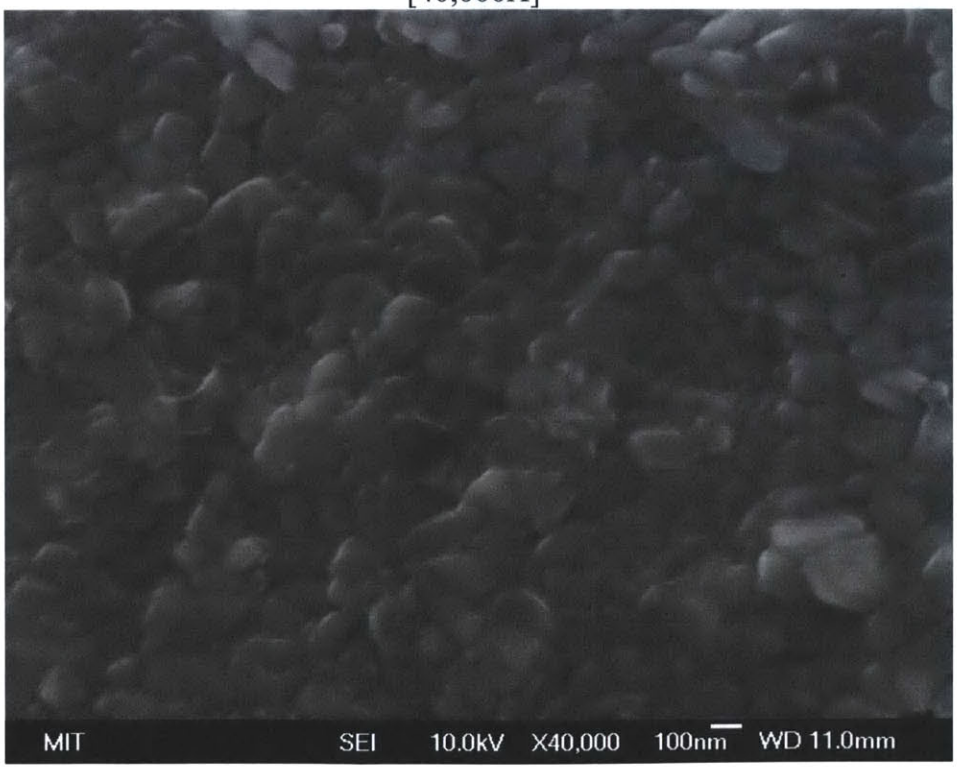

[20,000X]

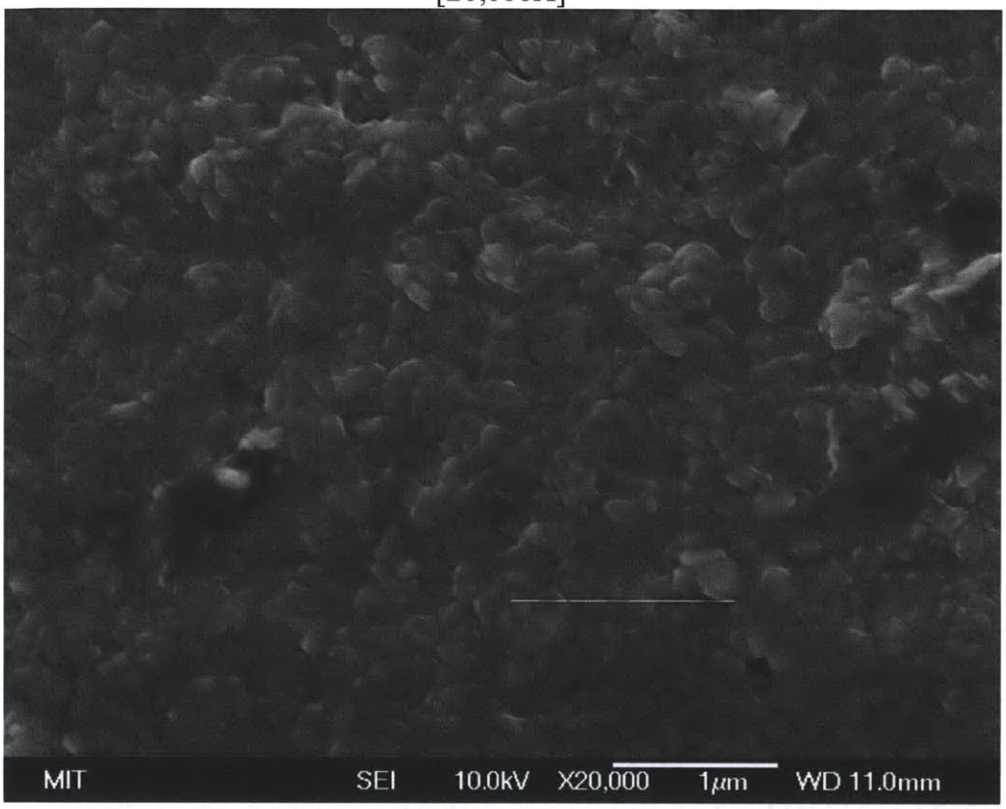

[10,000X]

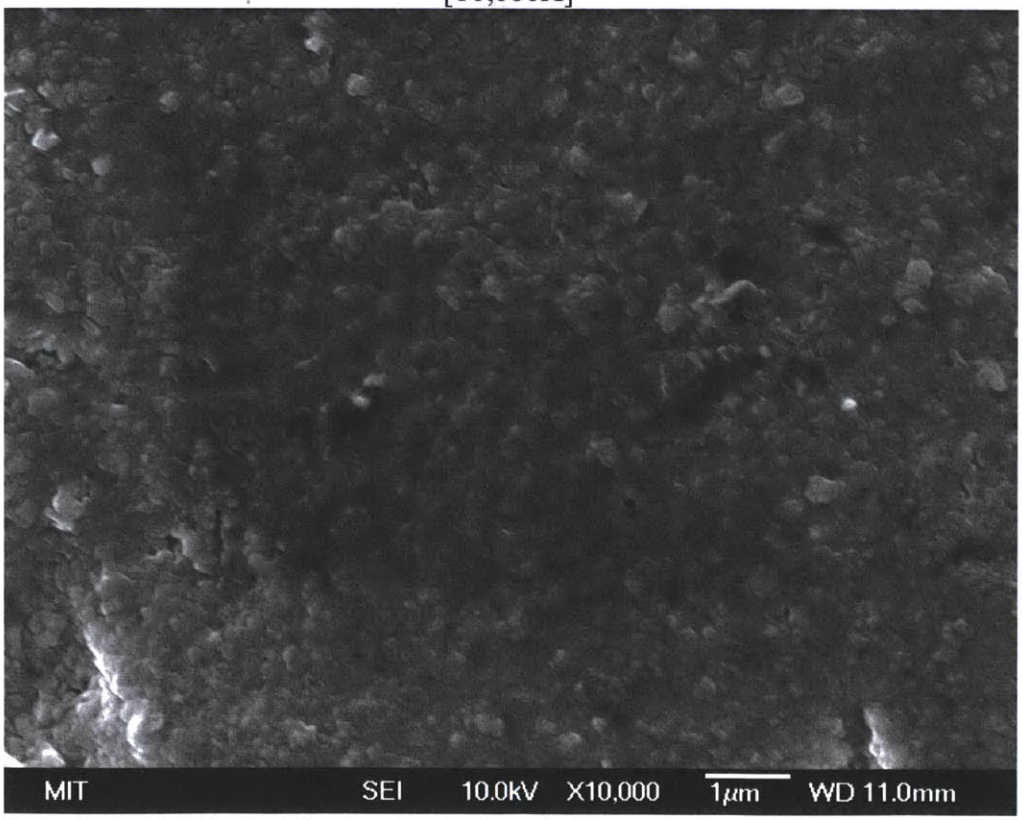

[1,000X]

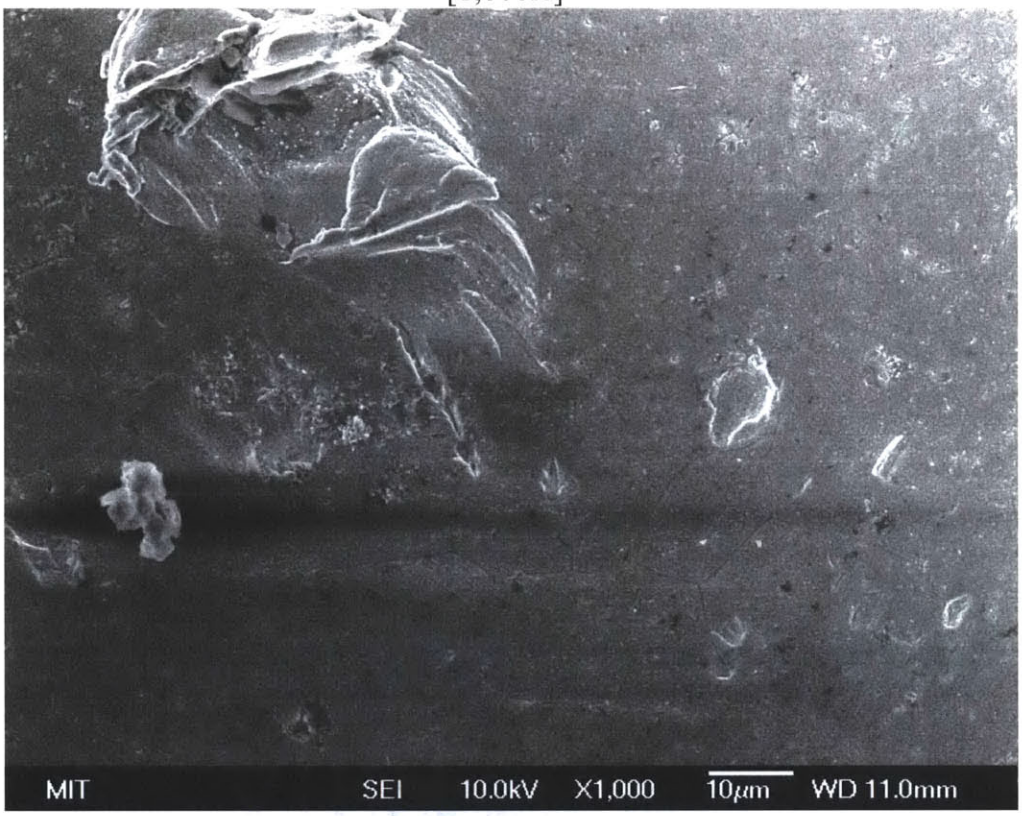
MIT SEI 10.0kV X1,000 10μm WD 11.0mm

[350X]

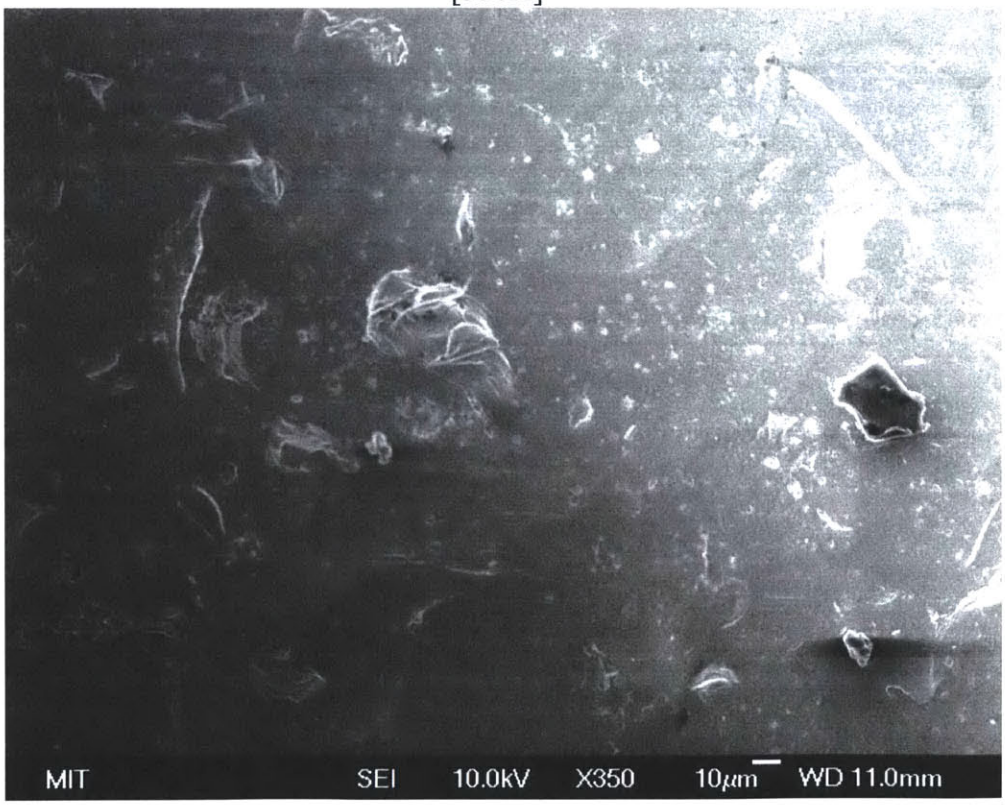
MIT SEI 10.0kV X350 10μm WD 11.0mm

Figure 8-16: SEM of Oxidized SS316L - Used in Water - Sandblast Preparation – blackened CHF location – Various Magnifications

[40,000X]

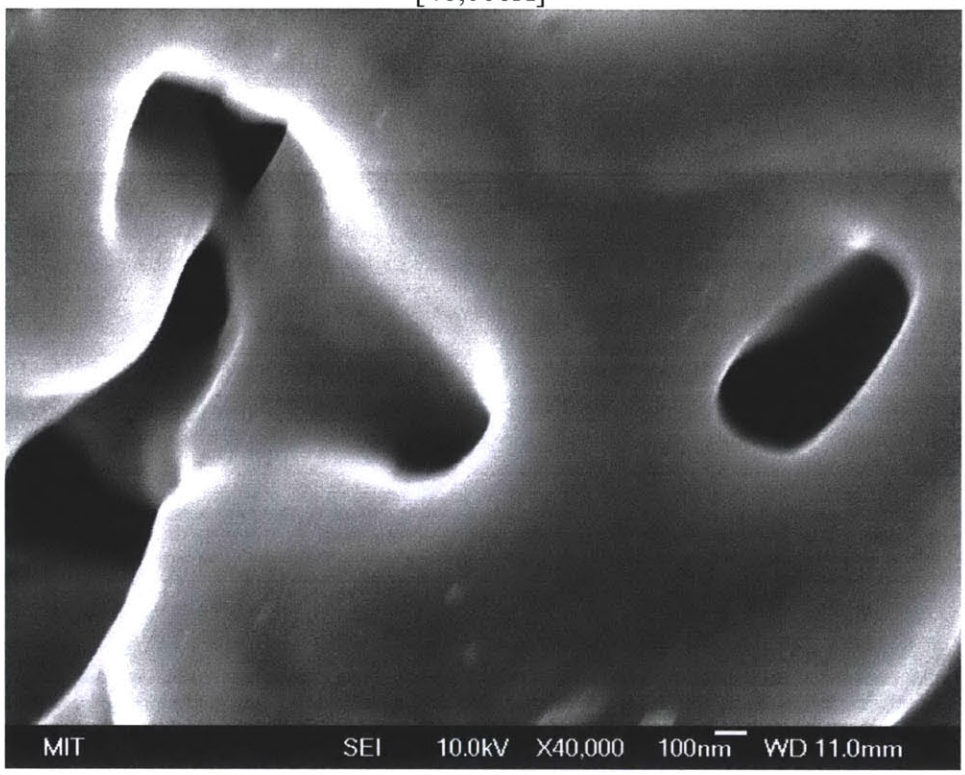

[20,000X]

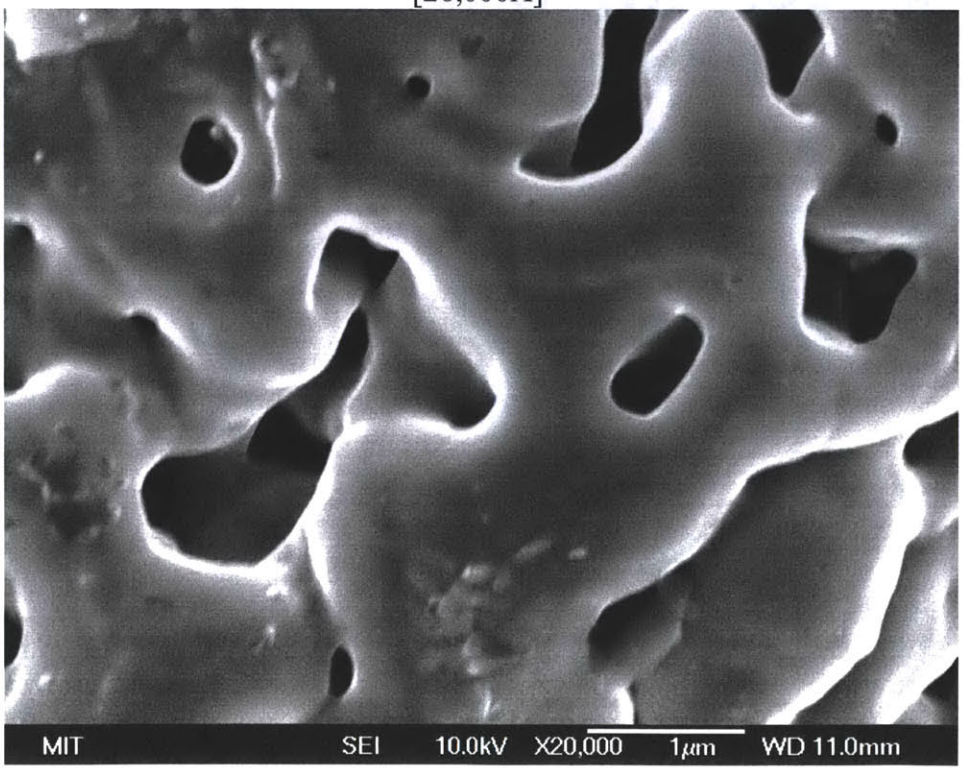

[10,000X]

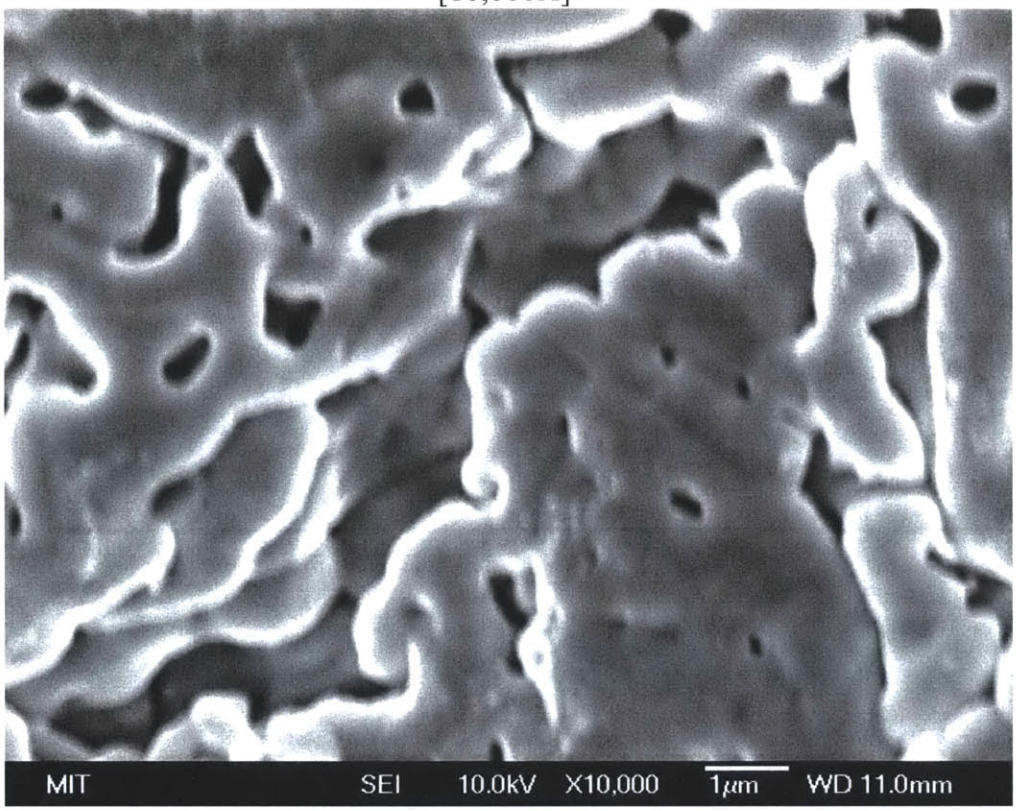

[1,000X]

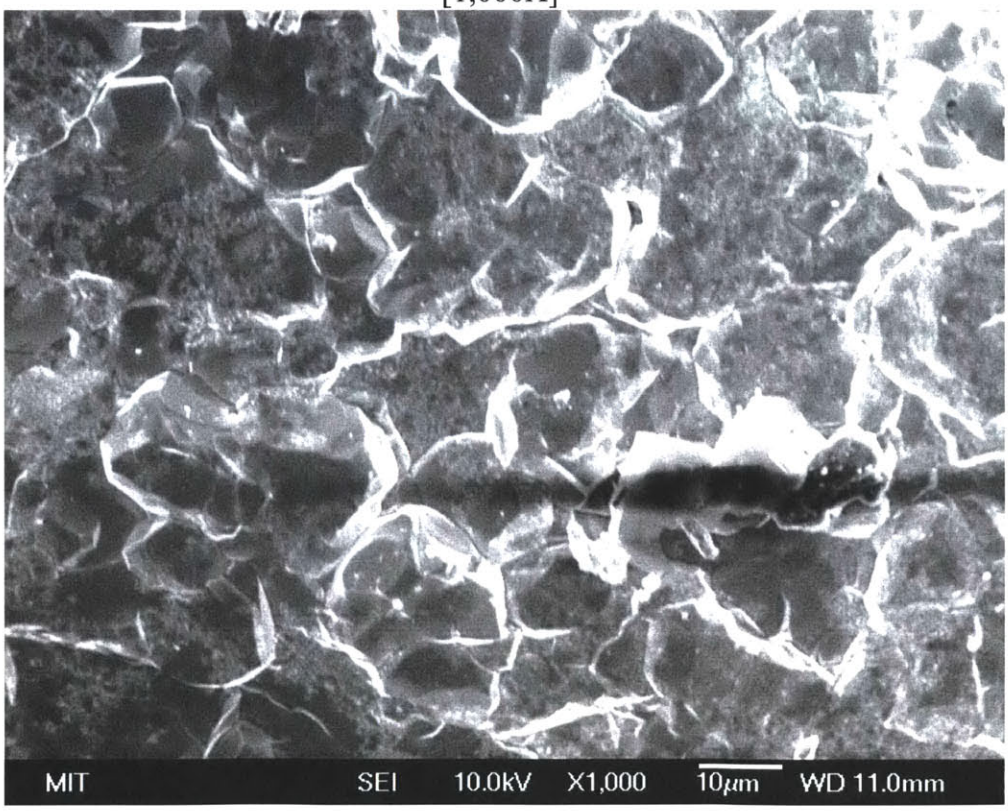

[350X]

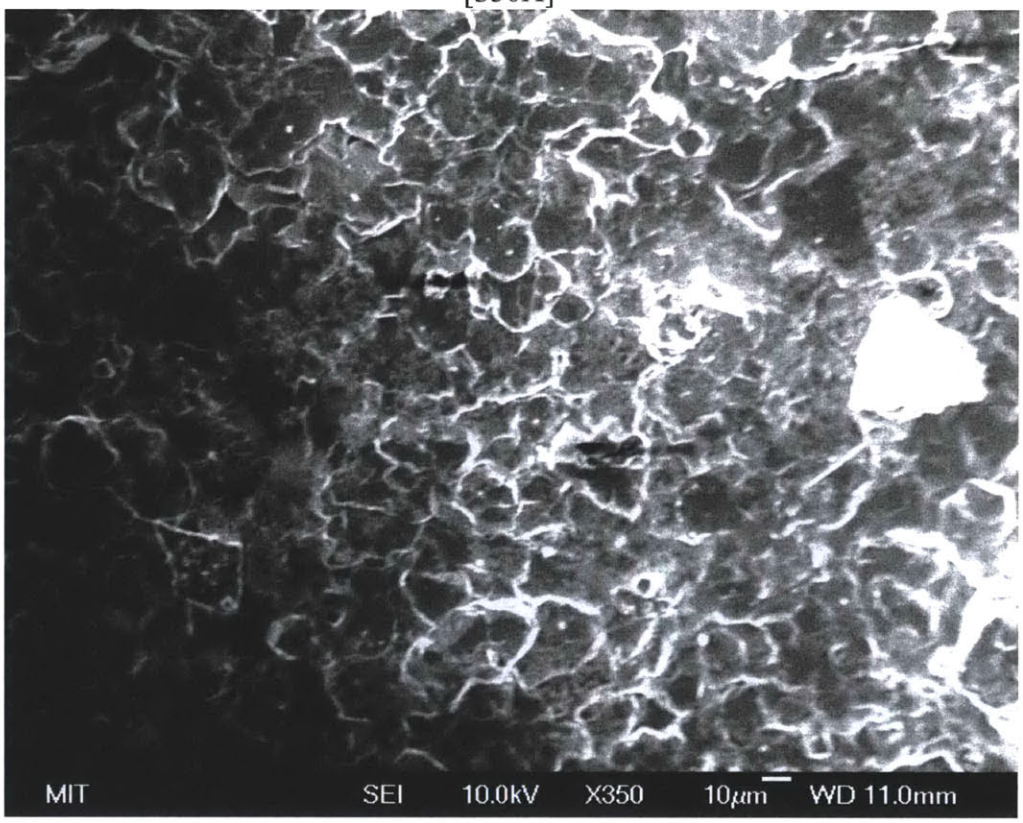

The oxidized SS316L unused and prepared heater shows a highly textured surface at high magnification (see Figure 8-14). This morphology is likely due to the oxide layer that formed from baking at 800 °C for an hour.

The oxidized SS316L heater used in the DI water CHF test shows a similar texture to the unused heater in the region before the CHF location (see Figure 8-15). At the blackened CHF region of the sample a highly porous morphology is observed (see Figure 8-16).

8.2 *Energy Dispersive X-ray Spectroscopy ("EDS")*

EDS is used to identify the components of the surface. The EDS device takes advantage of unique energy spectrum response of X-rays emitted from constituent elements from stimulation from a high energy electron beam. The same samples used for SEM are analyzed with EDS. Peaks are dominated by iron [Fe] being the main component of all steel. Small silica [Si] peaks are present from the sandblasting.

Figure 8-17: EDS of SS316L Unused Plain Heater with Sandblast Preparation

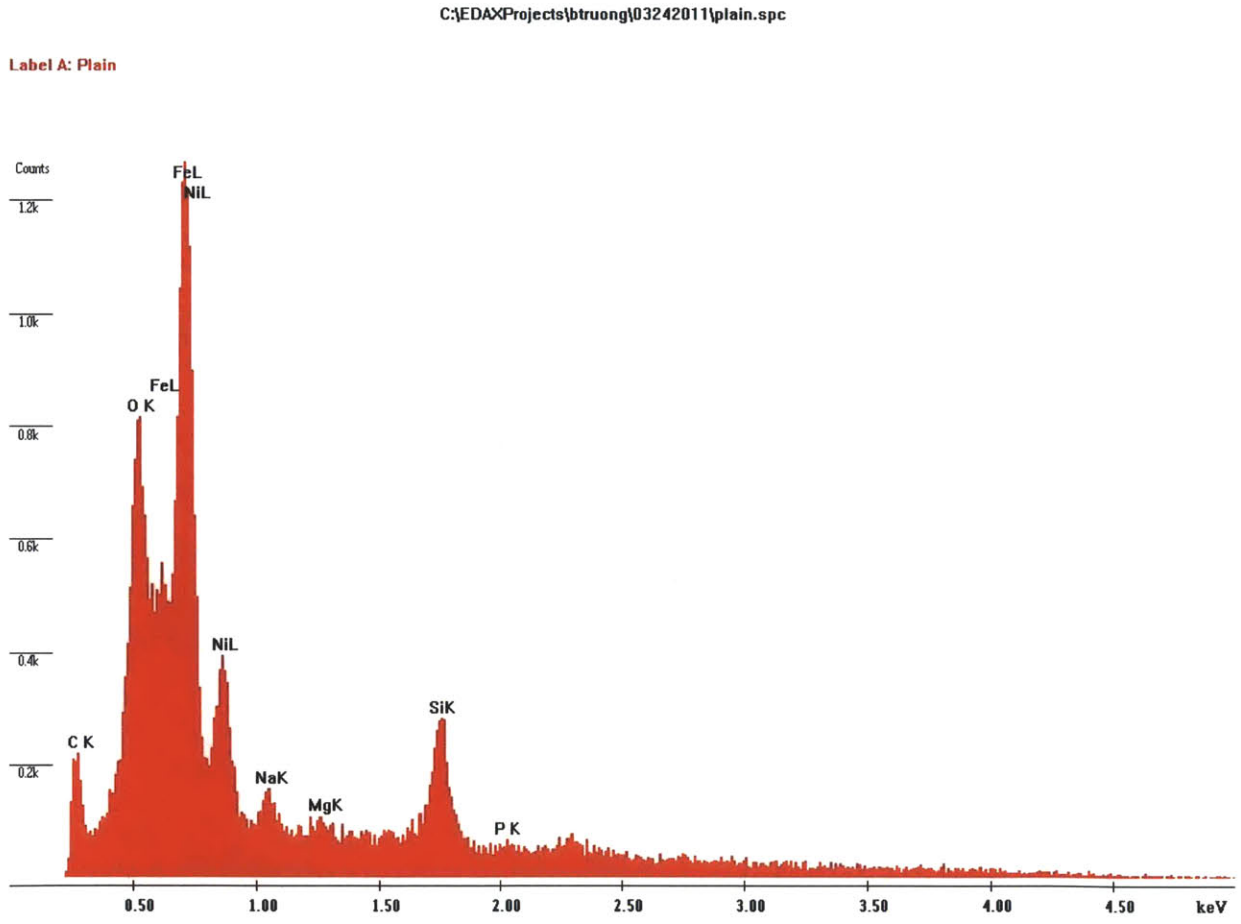

Figure 8-18: EDS of SS316L Plain Heater with Sandblast Preparation – water test – below CHF location

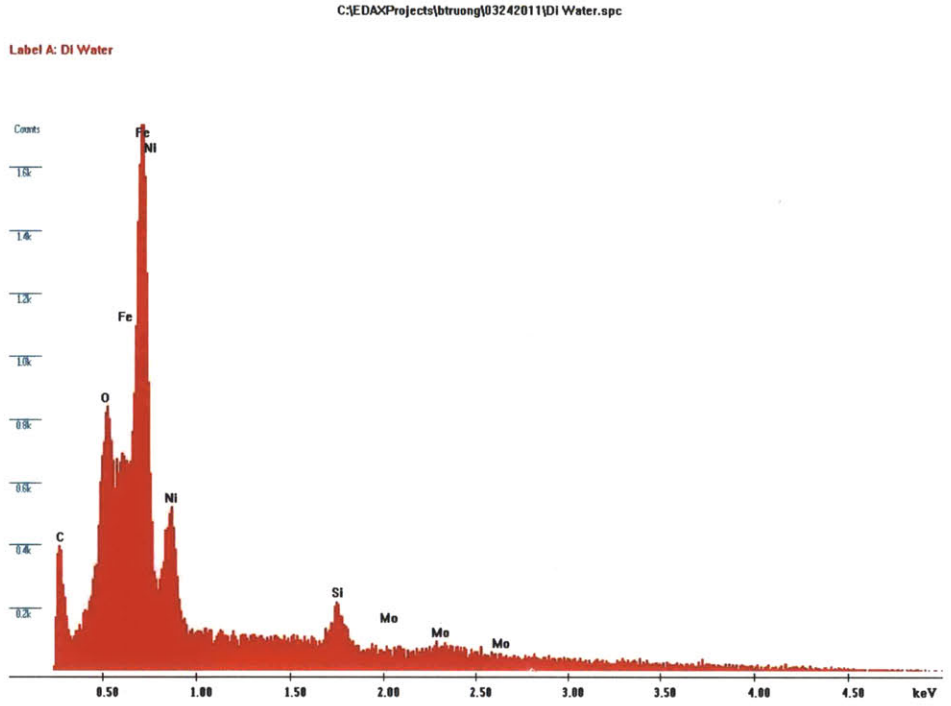

Figure 8-19: EDS of SS316L Plain Heater with Sandblast Preparation – water test – CHF location

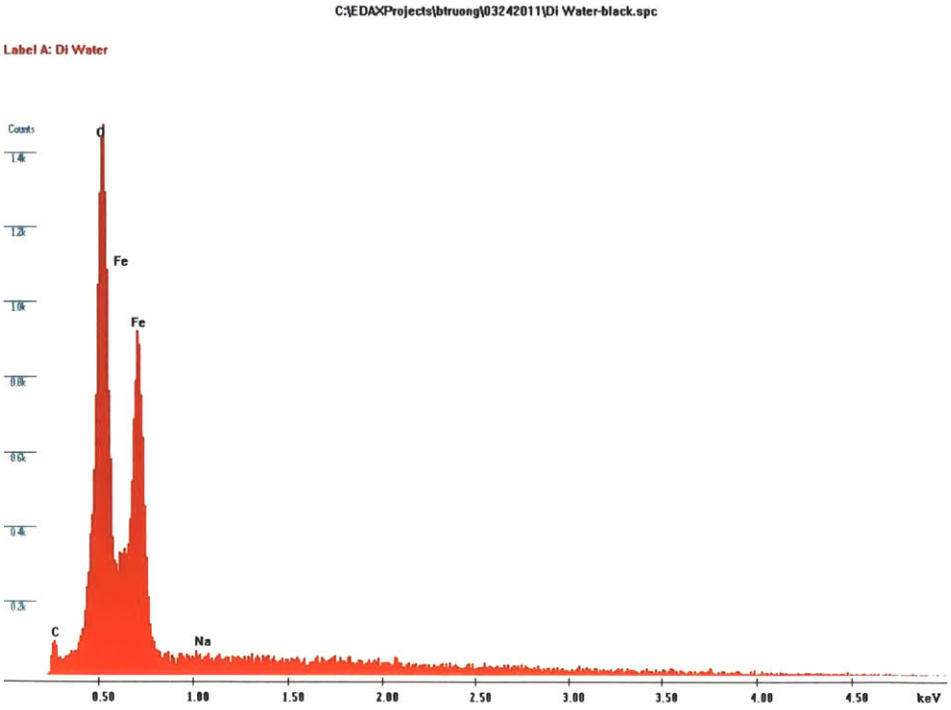

Figure 8-20: EDS of SS316L Plain Heater with Sandblast Preparation – Alumina 0.001% test – below CHF location

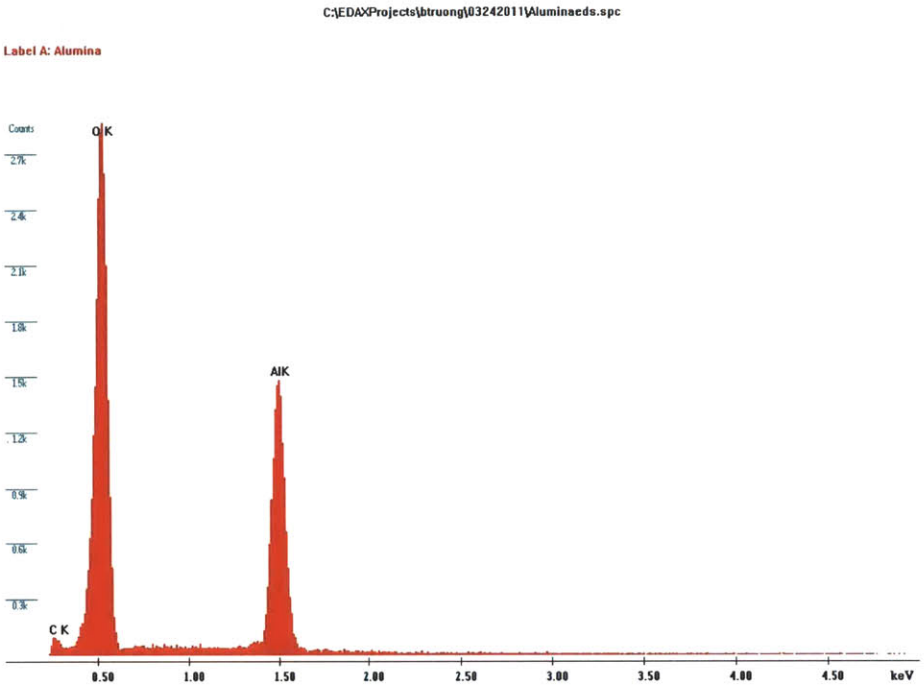

Figure 8-21: EDS of SS316L Plain Heater with Sandblast Preparation – Alumina 0.001% test – below CHF location

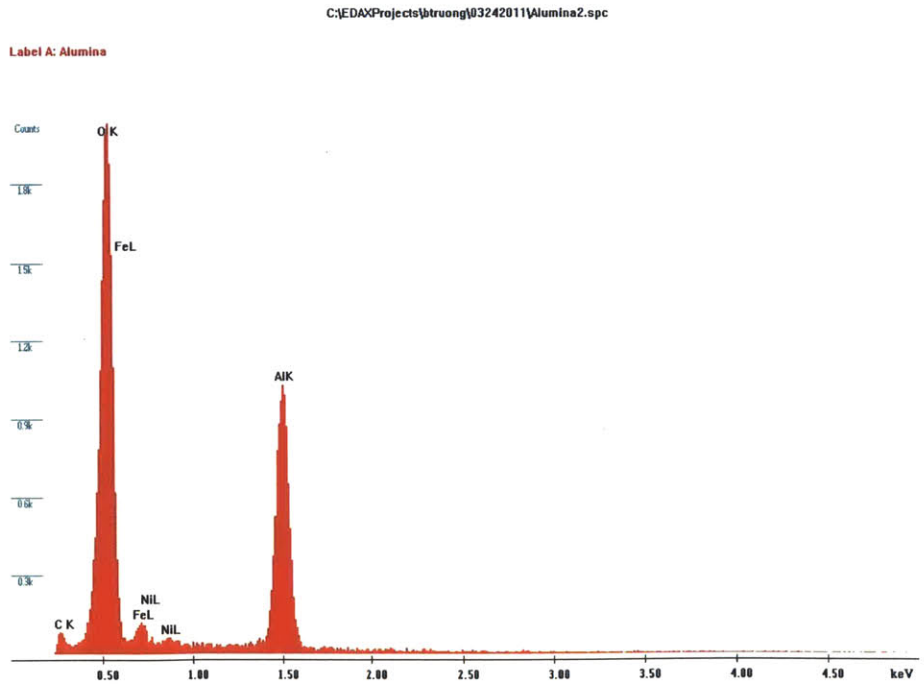

Figure 8-22: EDS of SS316L Plain Heater with Sandblast Preparation – Alumina 0.01% test – below CHF location

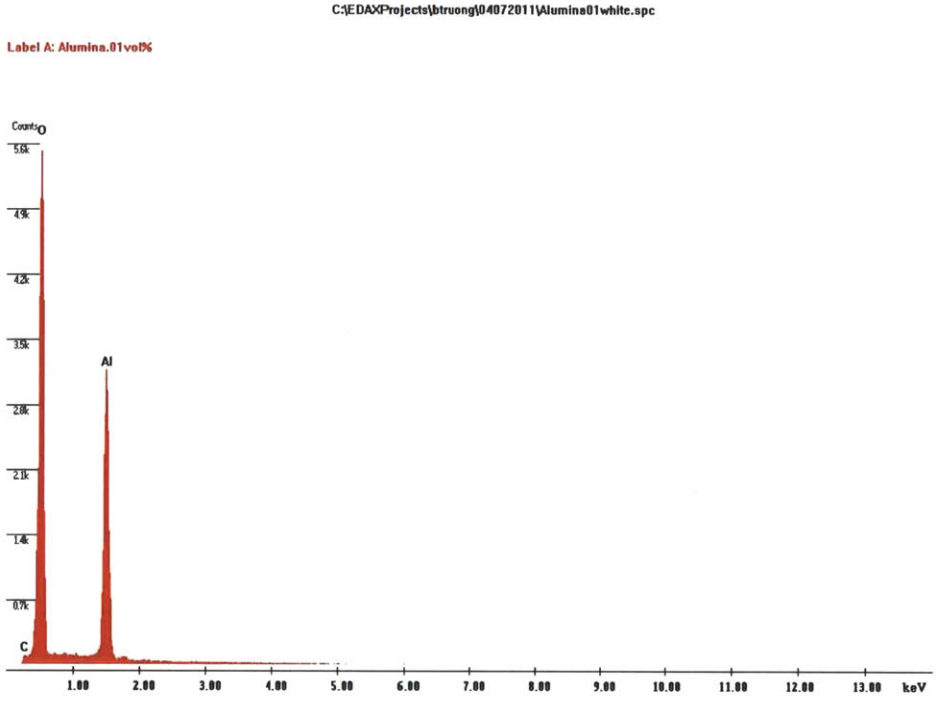

Figure 8-23: EDS of SS316L Plain Heater with Sandblast Preparation – Alumina 0.01% test – below CHF location - edge

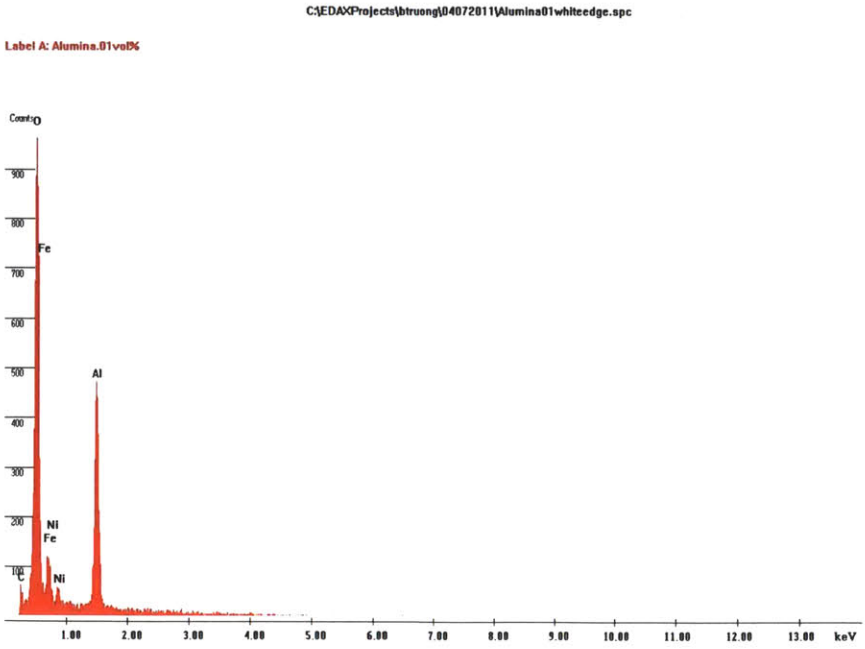

Figure 8-24: EDS of SS316L Plain Heater with Sandblast Preparation – Alumina 0.01% test – CHF location

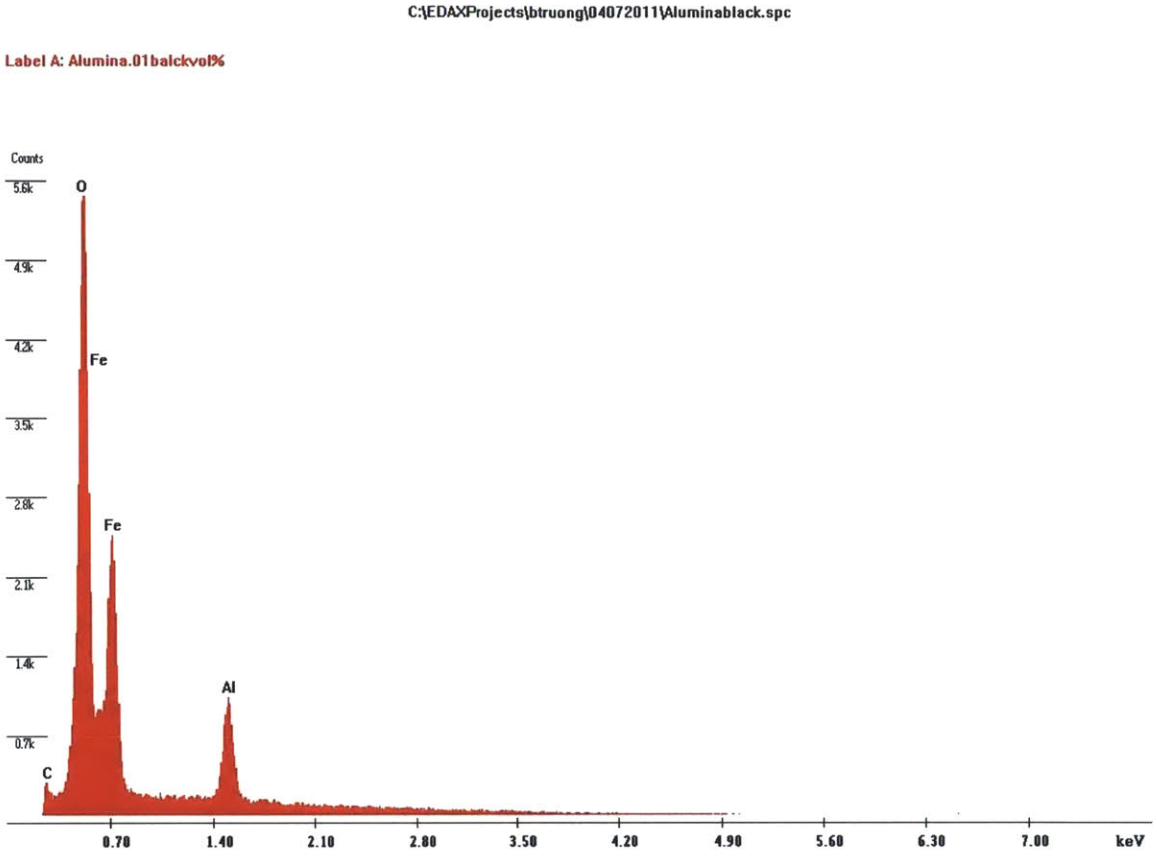

Figure 8-25: EDS of SA-508 Unused Heater with Sandblast Preparation

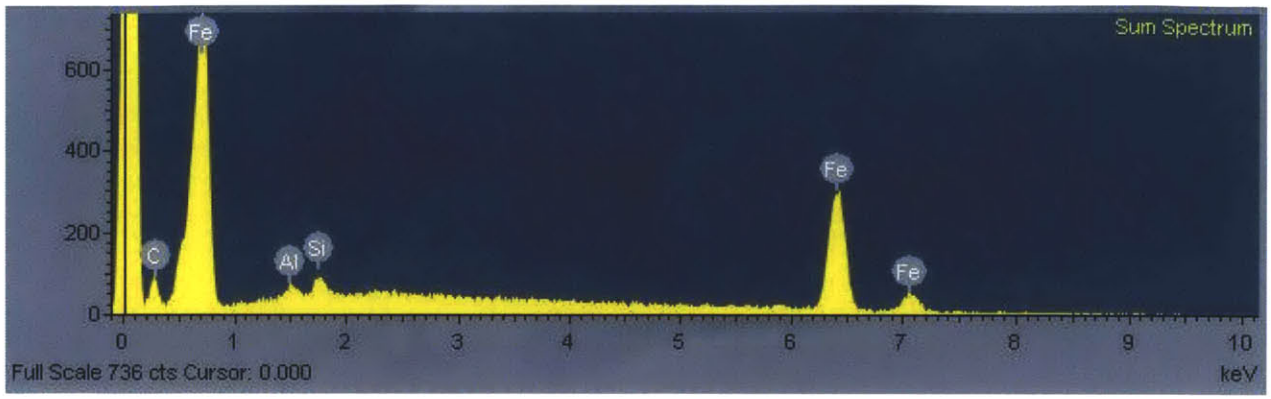

Figure 8-26: EDS of SA-508 Heater with Sandblast Preparation – DI water - below CHF location

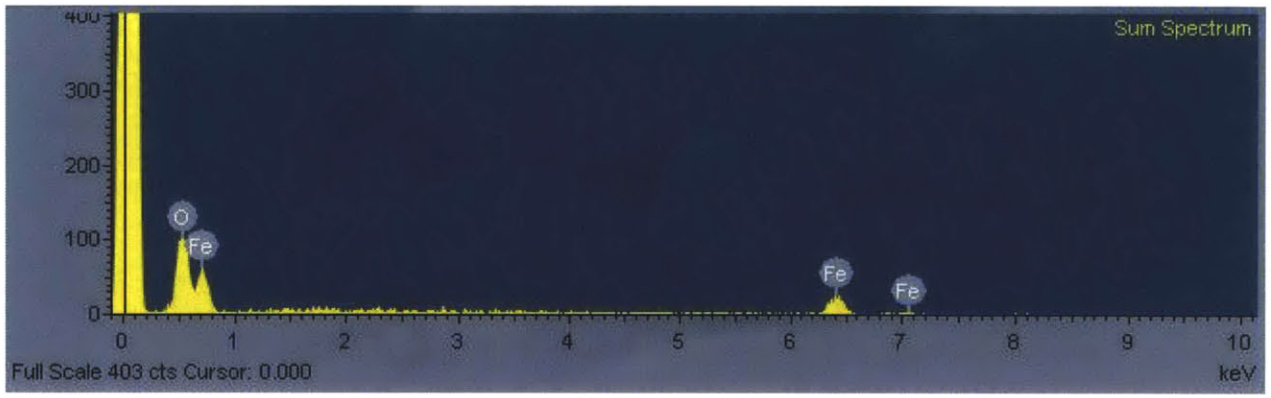

Figure 8-27: EDS of SA-508 Heater with Sandblast Preparation – Alumina 0.001% - below CHF location

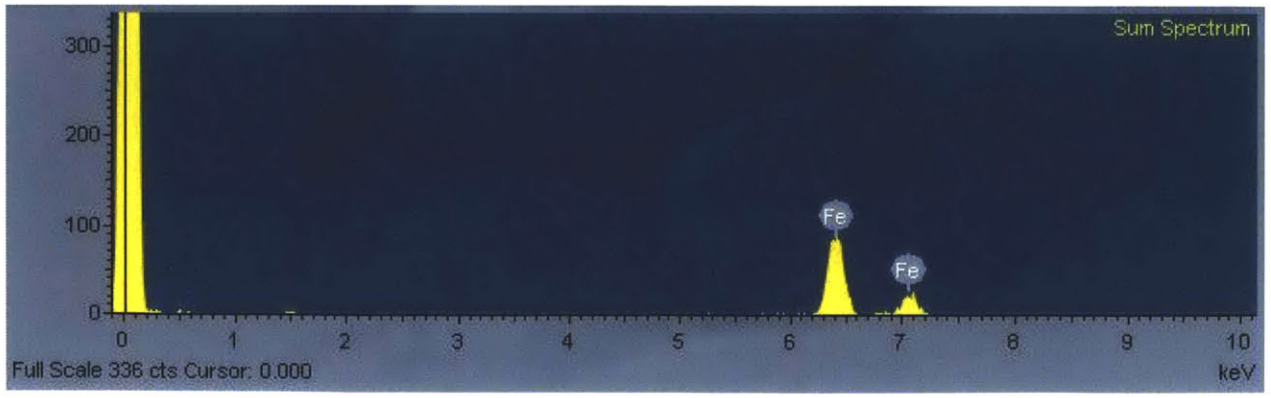

Figure 8-28: EDS of Oxidized SS316L Unused Heater with Sandblast Preparation

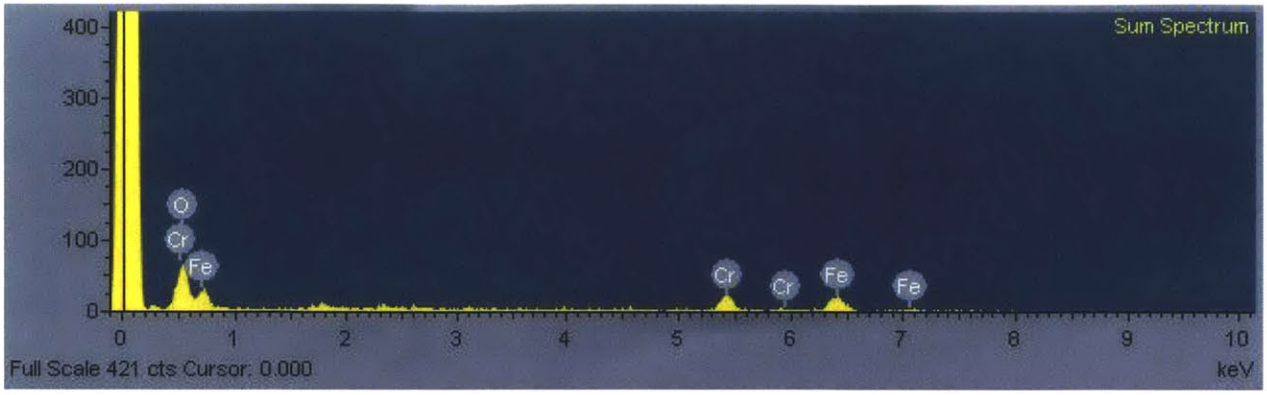

Figure 8-29: EDS of Oxidized SS316L Heater with Sandblast Preparation – DI water - below CHF location

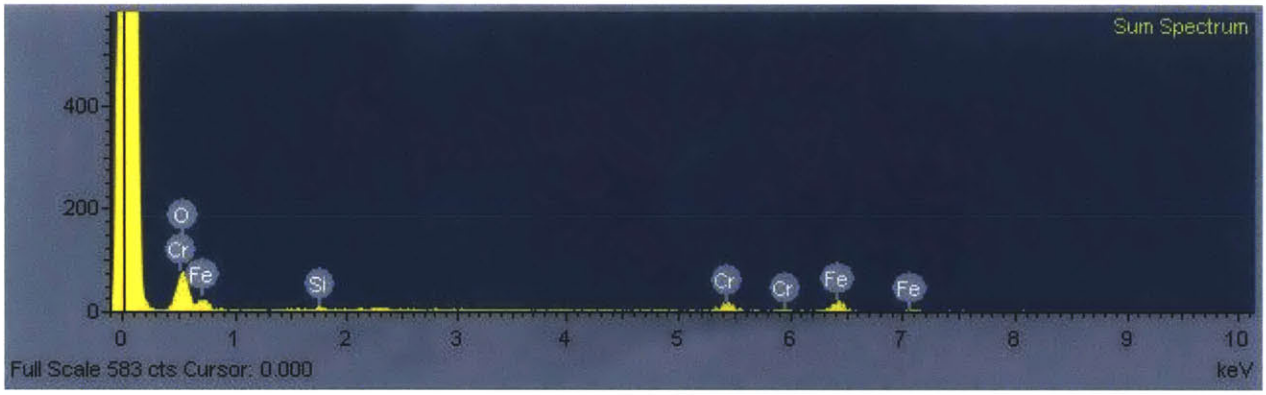

A few observations of the EDS follow for the three surface types: SS316L, SA-508 and oxidized SS316L.

First, for normally prepared SS316L, aluminum [Al] peaks of significance are only present for samples that were boiled with alumina nanofluid. Second, for both alumina concentration of 0.001% and 0.01%, EDS taken below the CHF area the coverage of nanoparticles were sufficient to not show iron [Fe]. Third, for EDS at the CHF location, the oxygen [O] and iron [Fe] peaks overlap with similar amplitude, likely due to oxidation.

For SA-508, there is a small aluminum [Al] peak in the EDS for the unused sample from the base composition of 0.02%. Additionally, SA-508 heaters used in CHF tests have oxygen [O] as

a significant peak due to oxidation of iron [Fe]. Notably, for the SA-508 CHF test with 0.001% alumina nanofluid, no aluminum [Al] is measured. This fact is likely due to the oxidation of iron dominating the surface chemistry thereby hindering the deposition of Alumina [Al_2O_3].

The oxidized SS316L heaters measure oxygen [O], which could be from sandblasting or oxidation.

8.3 Confocal Microscopy

Confocal microscopy was completed on a number of sample heaters. Confocal analysis provides a second means of understanding surface topography and provides a method to quantify surface parameters including roughness, SRa, and surface roughness ratio. The measure for surface roughness, SRa, is the arithmetic average of surface peak to valley amplitude (see Table 8-2). Surface roughness ratio directly influences contact angle for a fluid and thereby wettability. In general two locations were measured for each sample. Used samples measured are before the CHF location.

The five (5) SS316L prepared heaters analyzed are: (1) unused heater with sandblast preparation, (2) heater used in a DI water CHF test, (3) heater used in an alumina CHF test with 0.001% concentration, (4) heater used in an alumina CHF test with 0.01% concentration, and (5) heater used in a DI water CHF test after the loop was cleaned from previous use of nanofluids. The last heater was analyzed to help quantify that the loop was clean of nanoparticles before DI water tests resumed.

The measurements were taken at the Schlumberger Research Center in Cambridge, Massachusetts. The confocal microscope is an Olympus LEXT OLS3000. The confocal microscope uses a scanning laser coordinated with lenses, mirrors and light detectors to topographically map in 3D the surface. This is accomplished by setting the laser and associated components for a set focal plane, scanning that x-y plane, and recording the detector data. The focal plane is changed, z-direction, in a set increment and the scan repeated. Altering the focal plane and scanning is repeated until all planned focal planes are completed. Resulting data is analyzed to determine 3D topography (see Figure 8-30). The resolution specification is 0.01 μm.

The two (2) DI water samples and the unused sample result in roughness measures that range from 1.17 μm to 1.22 μm, less than 4% different. The post loop cleaning DI water sample is about 2% different from the case #2. This supports the conclusion that the loop cleaning was successful in removing residual alumina nanoparticles. Additionally, heavy boiling in DI water does not change the surface much relative to unused.

The two alumina cases have average surface roughness ranging from 1.41 μm to 1.495 μm, a 6% spread and about 20% greater than DI water cases.

Table 8-2: Surface Roughness Confocal Measurements

#	Description	Experiment Date	Position 1 SRa [m]	Position 2 SRa [m]	Average SRa [m]
1	Unused Heater with sandblasted surface	24-Mar-11	1.13	1.31	1.22
2	DI water CHF case	24-Sep-10	1.20	1.13	1.17
3	Alumina - 0.001% CHF case	24-Jan-11	1.30	1.69	1.50
4	Alumina - 0.01% CHF case	22-Mar-11	1.51	1.31	1.41
5	DI water CHF case - post system cleaning	20-Apr-11	1.29	1.10	1.19

The second measure, surface roughness ratio, is the actual area to projected area (see Table 8-3). Again two (2) locations for each sample are averaged.

Though the two DI water cases show a difference in surface roughness ratio of 25%, the Area2 of position 1 measurement is an anomaly. The three other DI water area measures range from 1.114 to 1.135, less than 2% different. Taken together with the SRa data, it is concluded that the post loop cleaning DI water sample is basically the same as the previous DI water sample, case #2.

The two (2) alumina cases with concentrations of 0.001% and 0.01% have average surface roughness ratio range of 1.162 to 1.172, less than 1% different. This indicates that even though 10X the concentration of alumina nanoparticles were suspended in the working fluid, a similar surface geometry resulted from the deposition of those nanoparticles by boiling. This is also consistent with the finding that the CHF for the two concentrations were similar.

Table 8-3: Confocal Data and Analysis for Surface Roughness Ratio

#	Description	Experiment Date	Position 1 Projected Area [μm²]	Position 1 Actual Area2 [μm²]	Surface Roughness Ratio	Position 2 Projected Area [μm²]	Position 2 Actual Area2 [μm²]	Surface Roughness Ratio	Average Surface Roughness Ratio
1	Unused Heater with sandblasted surface	24-Mar-11	n.a.	n.a.		n.a.	n.a.		
2	DI water CHF case	24-Sep-10	67,880	77,030	1.135	68,014	76,820	1.129	1.132
3	Alumina - 0.001% CHF case	24-Jan-11	67,815	78,941	1.164	67,881	78,674	1.159	1.162
4	Alumina - 0.01% CHF case	22-Mar-11	67,880	80,602	1.187	67,880	78,526	1.157	1.172
5	DI water CHF case - post system cleaning	20-Apr-11	67,747	106,389	1.570	67,880	75,625	1.114	1.342

The Confocal determined 3D image also provides a vertical z-scale. The range of z-scale maximum for all cases and positions is 13.0 μm to 16.3 μm. The general feature density and amplitude are very similar when visually comparing the unused heater and DI water heaters, cases #1, #2, and #5, respectively. The two alumina heaters, cases #3 and $4, show more distinctive features with higher amplitude compared to the unused and DI water heaters. Between the two alumina concentrations the 3D images are very similar.

Figure 8-30: Confocal 3D Surface Images with Imbedded Photo at with 50X Lens

Case #1 – Unused Heater with Sandblast Preparation (Position 1)

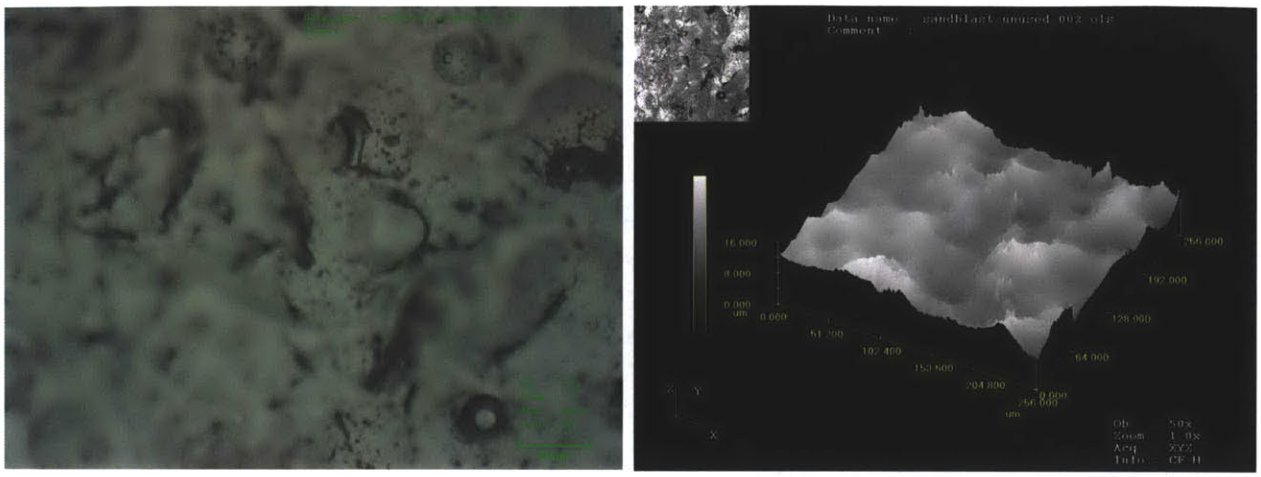

Case #1 – Unused Heater with Sandblast Preparation (Position 2)

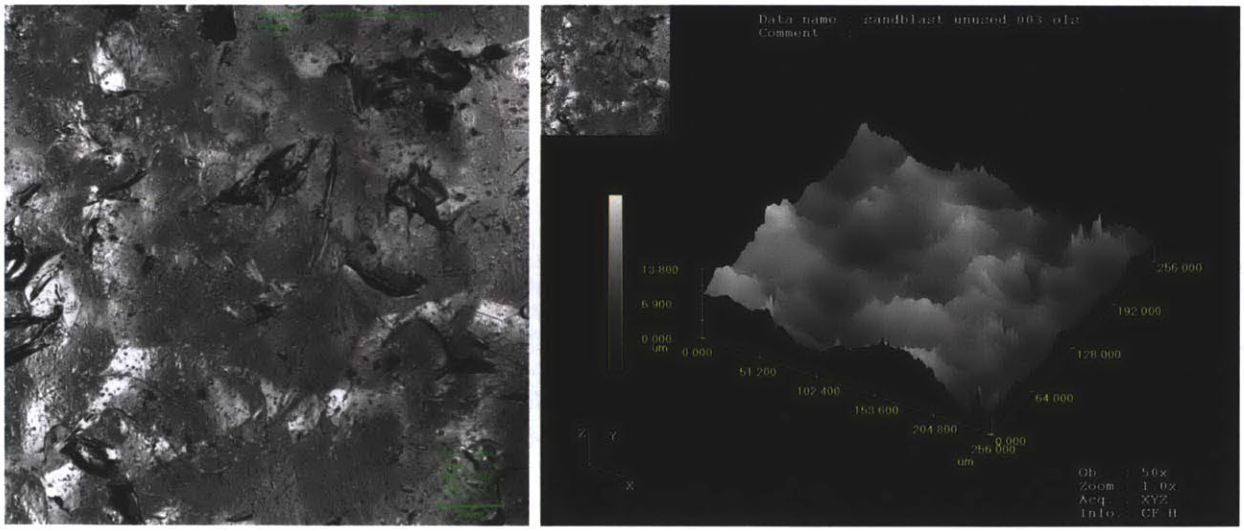

Case #2 – DI Water CHF Heater – before CHF location (Position 1)

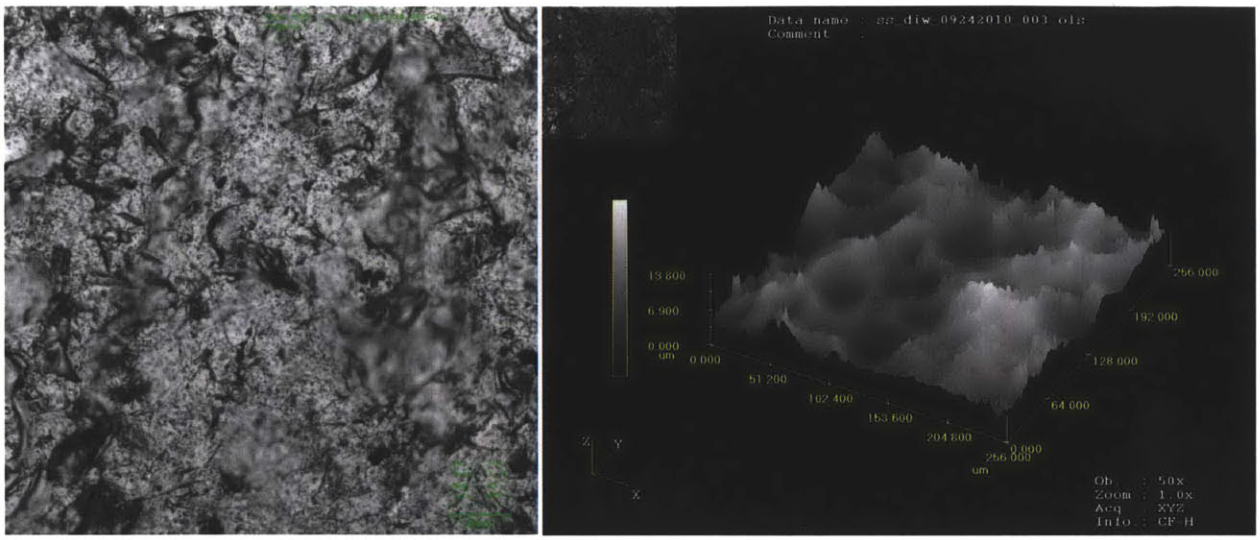

Case #2 – DI Water CHF Heater – before CHF location (Position 2)

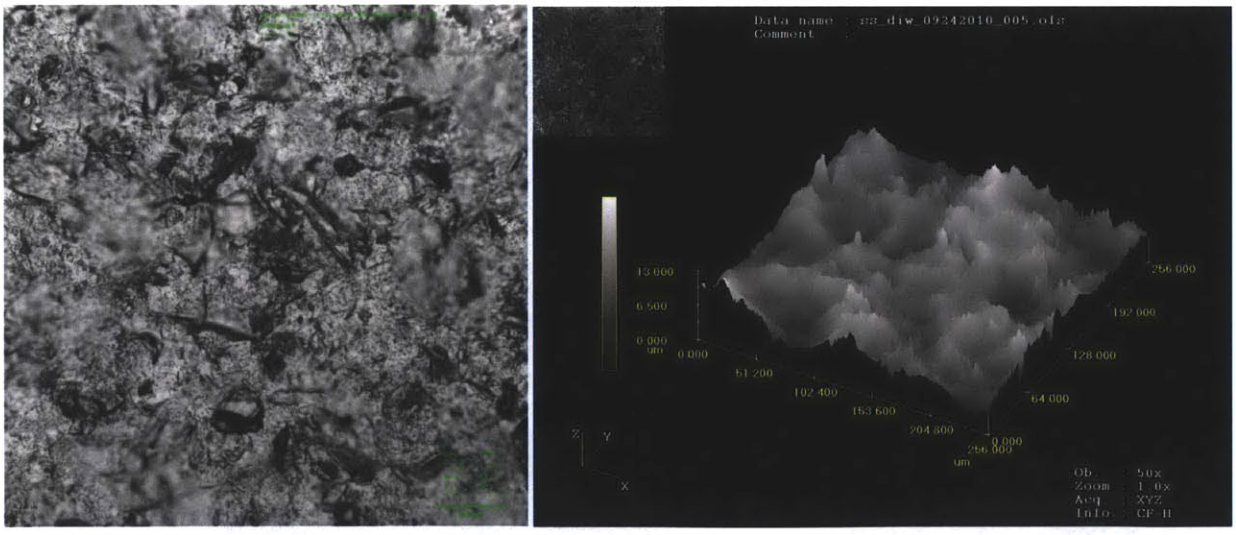

Case #3 – Alumina 0.001% CHF Heater – before CHF location (Position 1)

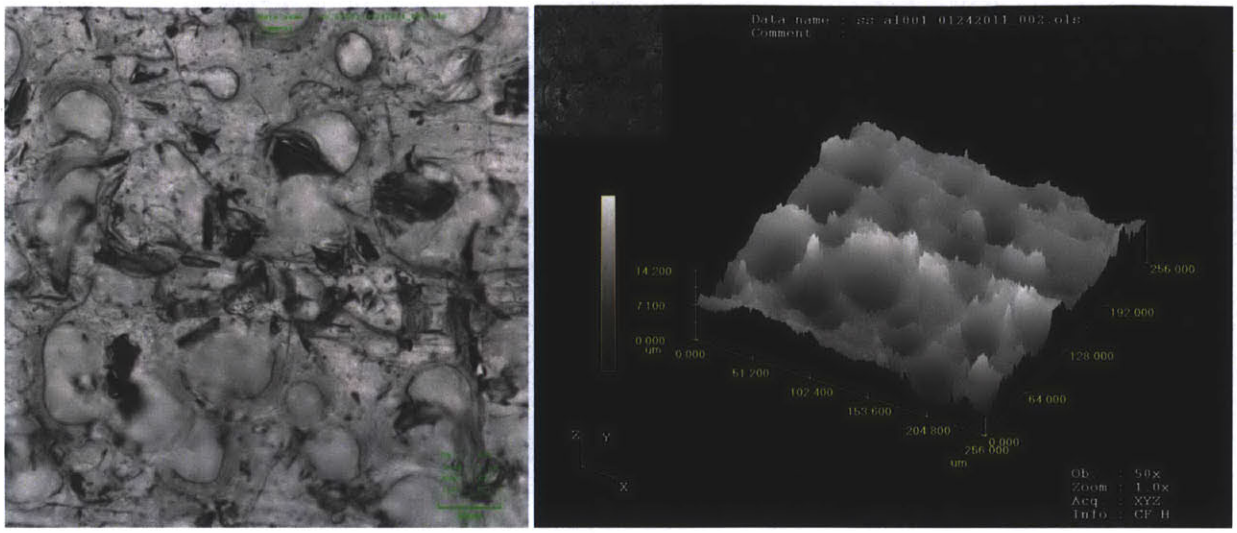

Case #3 – Alumina 0.001% CHF Heater – before CHF location (Position 2)

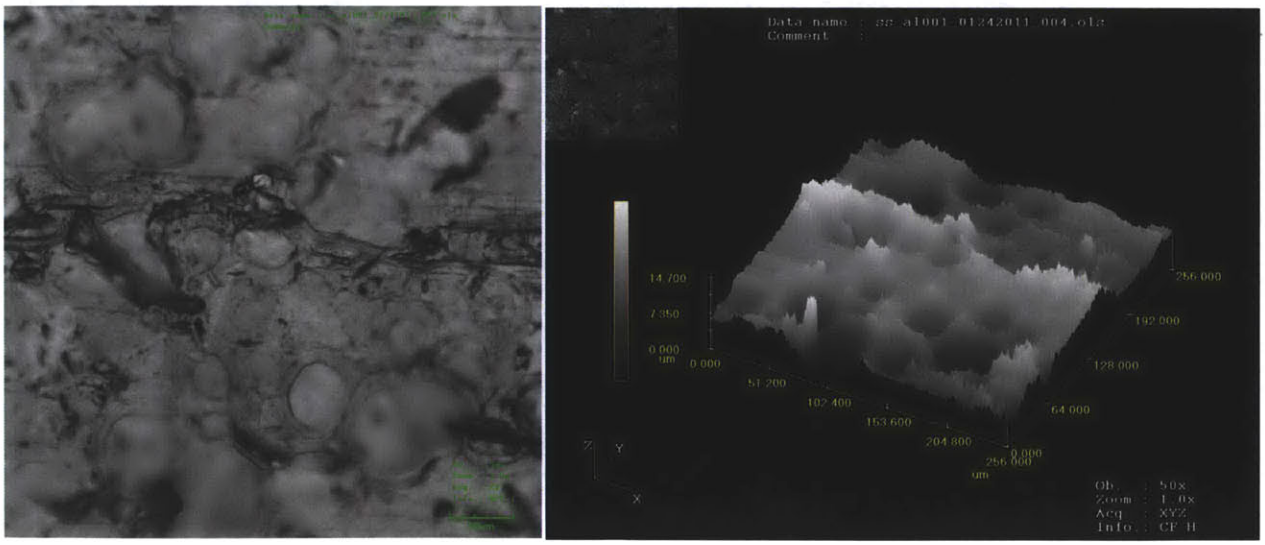

Case #4 – Alumina 0.01% CHF Heater – before CHF location (Position 1)

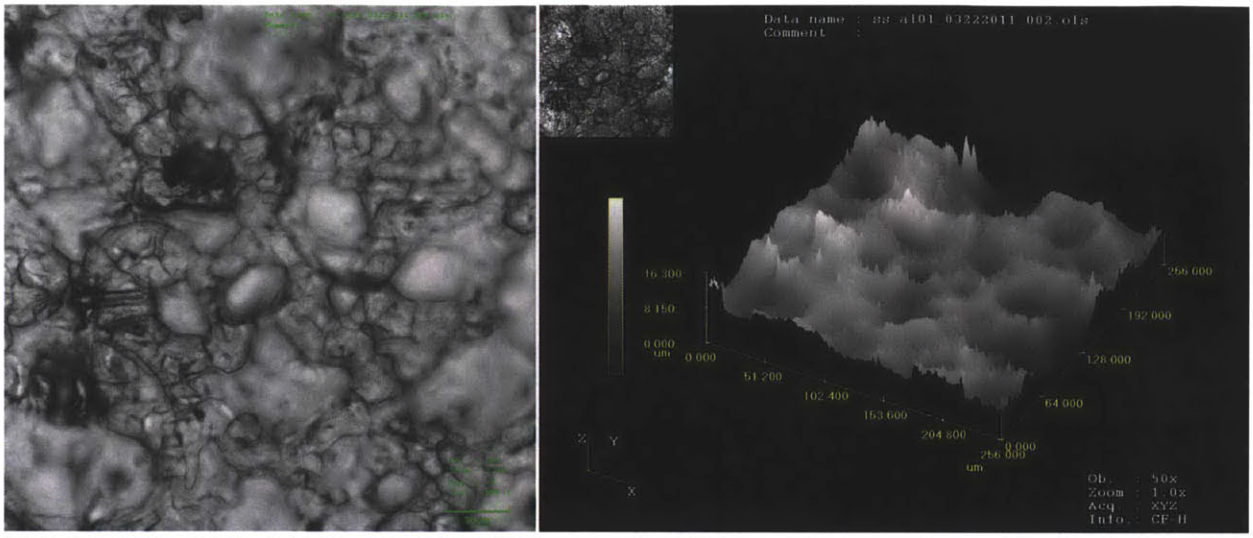

Case #4 – Alumina 0.01% CHF Heater – before CHF location (Position 2)

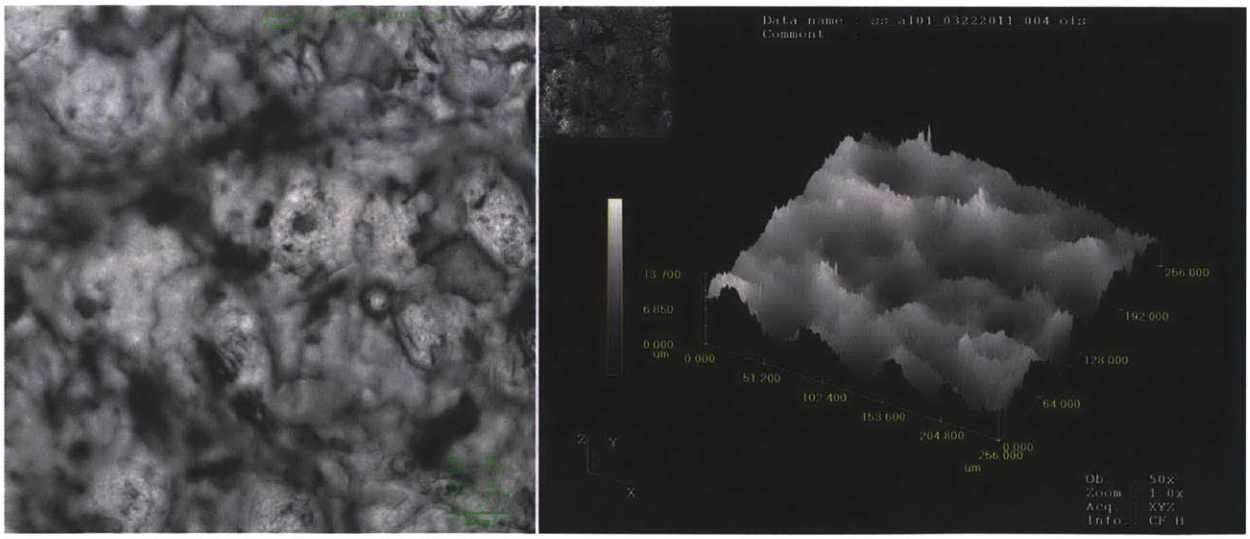

Case #5 – DI Water CHF Heater – before CHF location (Position 1)

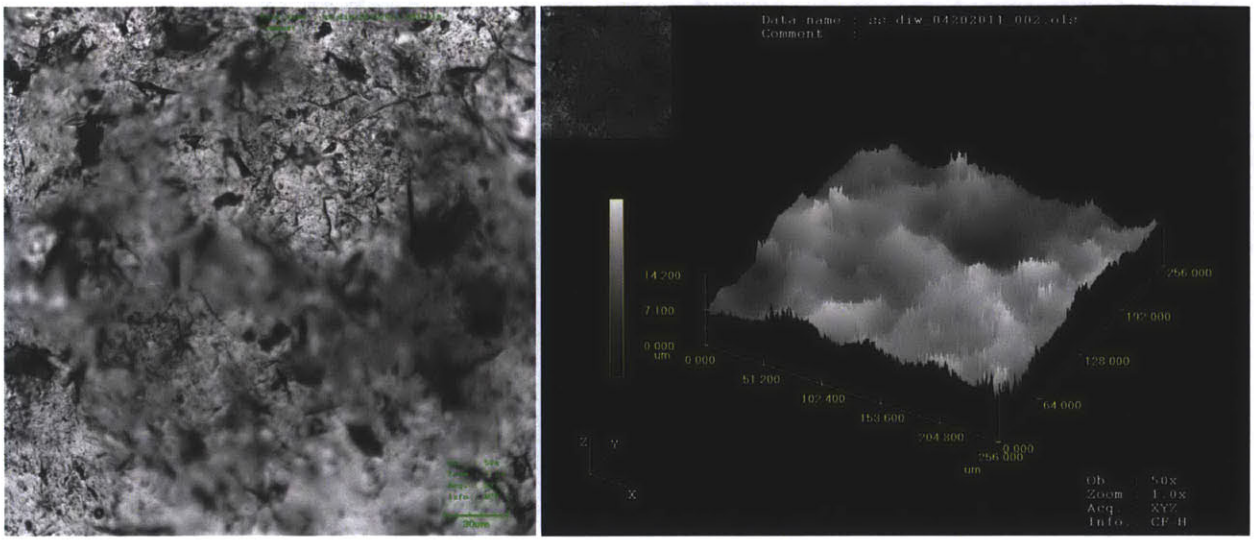

Case #5 – DI Water CHF Heater – before CHF location (Position 2)

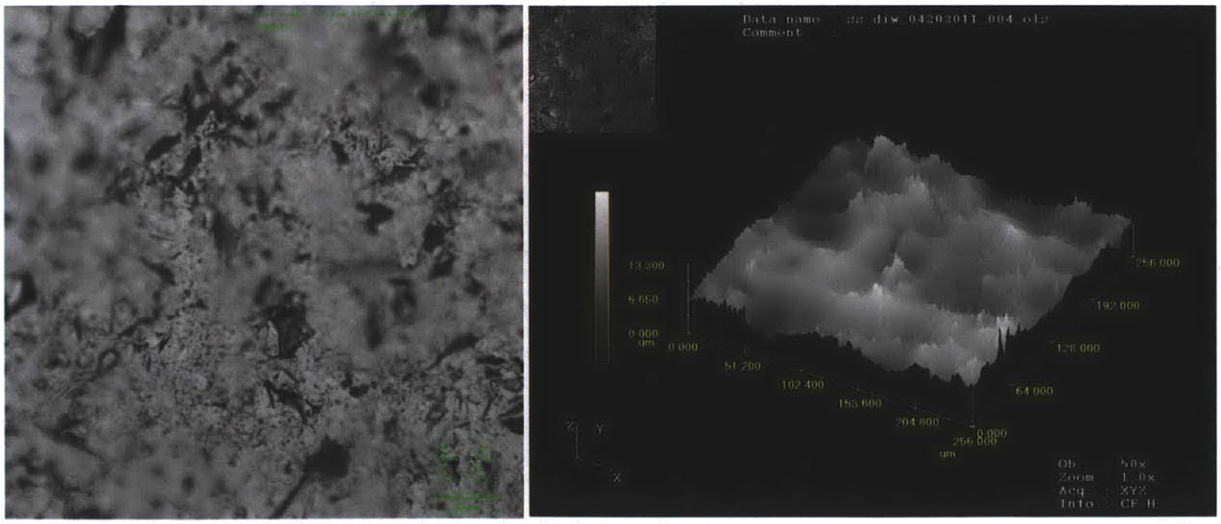

8.4 Contact Angle Measurement

Research recently completed at MIT has demonstrated the importance that surface wettability has on boiling heat transfer and CHF [86]. Wettability is a measure of the affinity a liquid has to a solid surface. The higher the wettability (lower contact angle) the faster liquid will retouch an uncovered spot. With the high boiling rate at CHF the creation and departure of bubbles creates momentary spots where only vapor is in contact with the surface. Rewetting hinders the growth in area of dry stops and merging. As a result higher wettability will likely increase the point of CHF.

To quantify wettability on surfaces used herein contact angle measurements were made. Two types of contact angle measurement were completed: static and dynamic. Static contact angle measurement involves a single drop that is still on a surface. Dynamic contact angle again is a single drop, but with a moving surface liquid interface. Two types of dynamic contact angle measurements were done: advancing and receding. To achieve dynamic angle measurement fluid within a static drop is added (advancing) or removed (receding) with a fine syringe (see Figure 8-31). Note that static contact angle should be between advancing and receding measures.

Figure 8-31: Dynamic Contact Angle Measurement Technique [54]

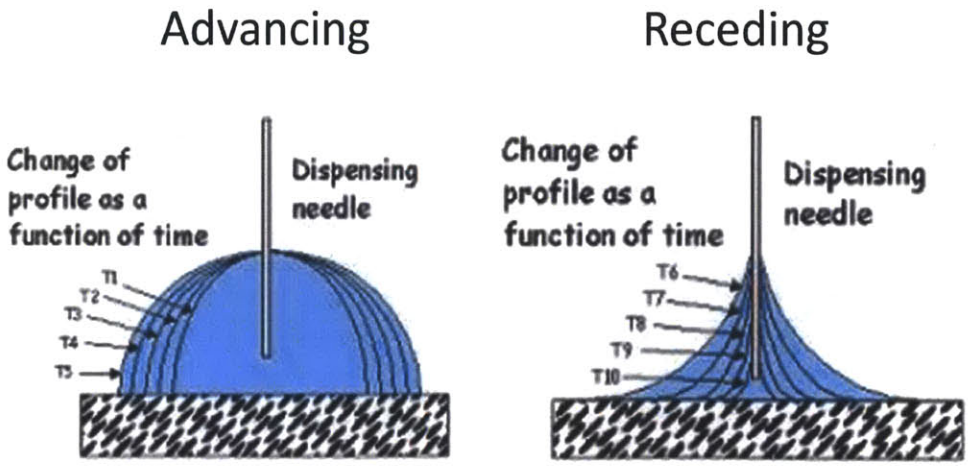

As the fluid is added or removed from the drop a film is taken. Each frame of the film is reviewed to note the first movement of the solid to liquid interface. Once the frame is identified the dynamic contact angle can be determined. Note that the receding contact angle measurement is somewhat challenging due to the low angle that results.

A KSV Instrument Ltd. Model CAM101 contact angle and optical measurement device was used for contact angle measurements and creating related images. Contact angle is determined by the software by taking a still image and fitting a curve along the droplet interface. Uncertainty for contact angle measurement is +/- 5°. All contact angle measurements were done at room temperature with DI water. Both SS316L and SA-508 samples were measured (see Table 8-4 and Table 8-5).

Table 8-4: Static Contact Angle Measurement Results

Description	Experiment Date	Surface Material	Static Left	Static Right	Static Average	Static Curve Fitting
Unused, plain	n.a.	SS316L	117.96°	same	same	Circle
Unused, sandblasted	n.a.	SS316L	103.51°	same	same	Circle
Once used, no CHF #1	n.a.	SS316L	91.09°	same	same	Circle
Once used, no CHF #2	n.a.	SS316L	88.74°	same	same	Circle
Once used, no CHF #3	n.a.	SS316L	92.76°	same	same	Circle
DI water CHF	7-Sep-10	SS316L	89.39°	same	same	circle
DI water CHF – post loop cleaning	15-Apr-11	SS316L	82.71°	77.62°	80.17°	Young/Laplace
Alumina 0.001% CHF	21-Jan-11	SS316L	36.89°	35.44°	36.17°	Young/Laplace
Alumina 0.01% CHF	22-Mar-11	SS316L	36.14°	same	same	circle
Unused, plain	n.a.	SA-508	94.56°	same	same	circle
Unused, sandblasted	n.a.	SA-508	88.58	same	same	circle
Unused, sandblasted #2	n.a.	SA-508	105.98°	same	same	circle
DI water CHF	13-Jul-11	SA-508	36.85	same	same	circle

DI water CHF	15-Jul-11	SA-508	40.48°	same	same	circle
Alumina 0.001% CHF	26-Jul-11	SA-508	21.12°	same	same	circle
Unused, sandblasted, baked	n.a.	Oxidized - SS316L	69.40°	same	same	circle
DI water CHF	21-Jul-11	Oxidized - SS316L	93.67°	same	same	circle
Alumina 0.001% CHF	6-Sepl-11	Oxidized - SS316L	<10°	same	same	circle

Table 8-5: Dynamic Contact Angle Measurement Results

Description	Experiment Date	Surface Material	Dynamic Advancing Left	Dynamic Advancing Right	Dynamic Receding Left	Dynamic Receding Right
Unused, plain	n.a.	SS316L	115.39°	same	31.47°	same
Unused, sandblasted	n.a.	SS316L	90.63°	same	8.03°	same
Once used, no CHF #1	n.a.	SS316L	114.99°	same	10.64°	same
DI water CHF	7-Sep-10	SS316L	95.77°	same	9.34°	8.92°
DI water CHF – post loop cleaning	15-Apr-11	SS316L	79.72°	same	17.92°	24.15°
Alumina 0.001% CHF	21-Jan-11	SS316L	28.61°	n.a.	8.95°	7.50°
Alumina 0.01% CHF	22-Mar-11	SS316L	28.83°	24.15°	13.26°	n.a.
Unused, plain	n.a.	SA-508	n.a.	n.a.	n.a.	n.a.
Unused, sandblasted	n.a.	SA-508				
Unused, sandblasted	n.a.	SA-508	111.89°	same	9.63°	n.a.
DI water CHF	13-Jul-11	SA-508				
DI water CHF	15-Jul-11	SA-508	90.57°	n.a.	9.54°	n.a.
Alumina 0.001% CHF	26-Jul-11	SA-508	41.96°	n.a.	4.05°	n.a.
Unused, sandblasted, baked	n.a.	Oxidized - SS316L	75.51°	79.83°	13.78°	n.a.
DI water CHF	21-Jul-11	Oxidized - SS316L	n.a.	91.53°	n.a.	29.78°

One important result of these measurements is the significant decrease in contact angle both static and dynamic contact angles for alumina CHF test samples compared to DI water with stainless steel. On average static contact angle for DI water CHF test heaters is 89°. Average static contact angle for alumina is 36°. This represents about a 60% decrease in contact angle. The associated increase in wettability supports higher CHF.

A second observation is that for SA-508 in a DI water CHF test the contact angle is about the same as for the alumina tests for stainless steel. This implies that the SA-508 surface during boiling is modified, likely from oxidation, such that contact angle is significantly reduced. This may explain the high CHF value obtained relative to stainless for similar conditions.

The following other observations can be made from the contact angle measurements. First, sandblast preparation lowers static contact angle somewhat, 118° to 103°, for stainless steel. Boiling with water also lowers static contact angle relative to unused a bit to about 89°. Whether or not the sample got to CHF does not seem to matter. For the two alumina concentrations of 0.001% and 0.01% by volume the contact angle is basically identical.

The plain SA-508 case and unused sandblasted cases have static contact angles that are somewhat lower than analogous stainless heaters. For the plain unused heaters the static contact angle is 118° for stainless and 95° for SA-508, about 23° lower.

An oxidized SS316L heater that was unused had a somewhat lower static contact angle of 69.4° compared to 102.51° for a prepared, unused SS316L heater. The oxidized SS316L heater used in DI water CHF test had a higher contact angle of 93.67° than unused. In no other example did the CHF test heater have a contact angle greater than unused.

Note that in some of the droplet images (see Figure 8-32) the surface interface is visually misleading due to tilt. The fit for contact angle determination is at the line for liquid to solid interface.

Figure 8-32: Static Contact Angle Images

SS316L – Plain, Unused Heater

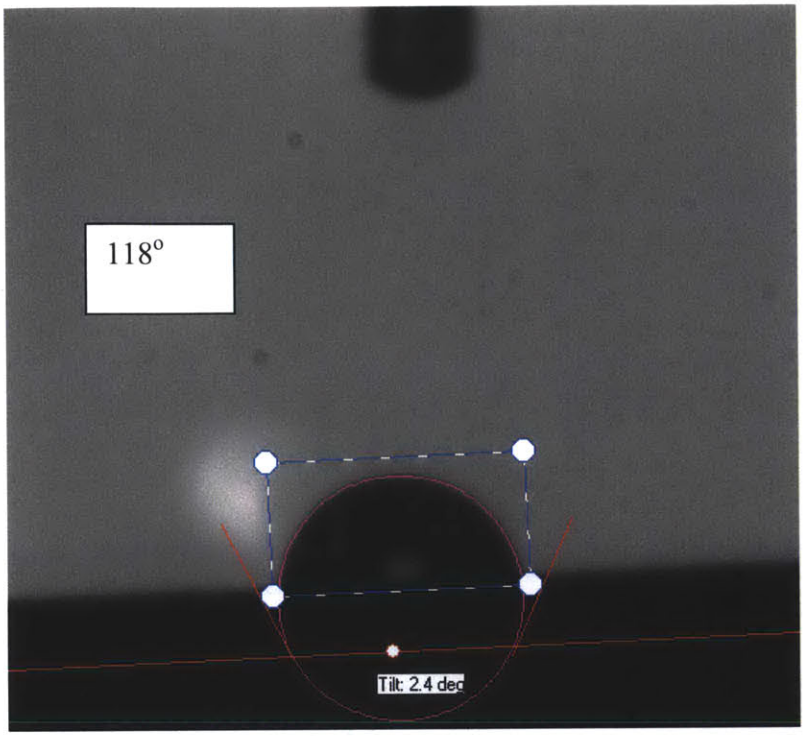

SS316L - Unused Sandblasted Heater

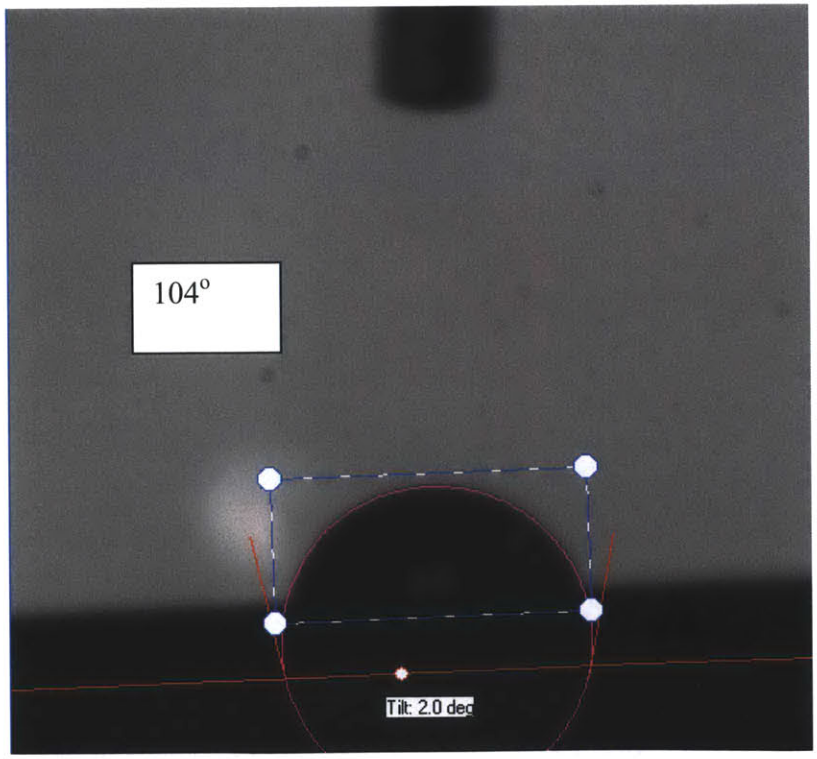

SS316L - Once used (no CHF) Heater #1

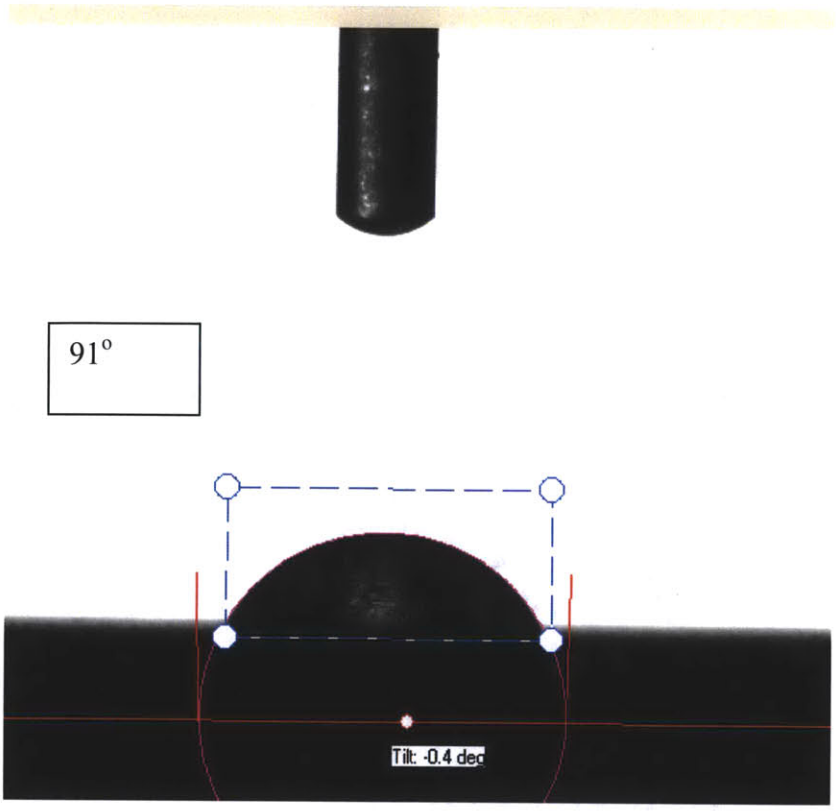

91°

SS316L - Once used (no CHF) Heater #2

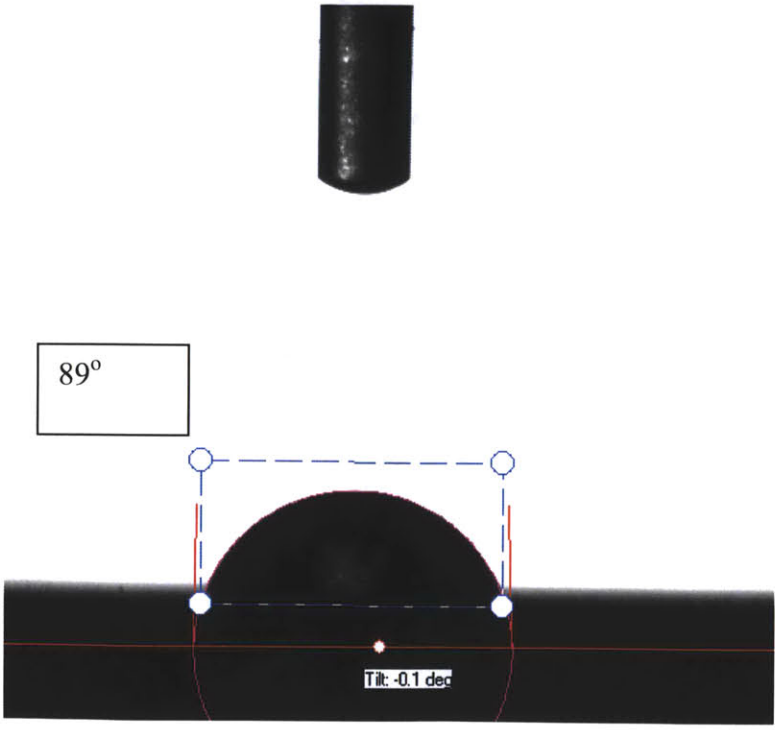

89°

SS316L - Once used (no CHF) Heater #3

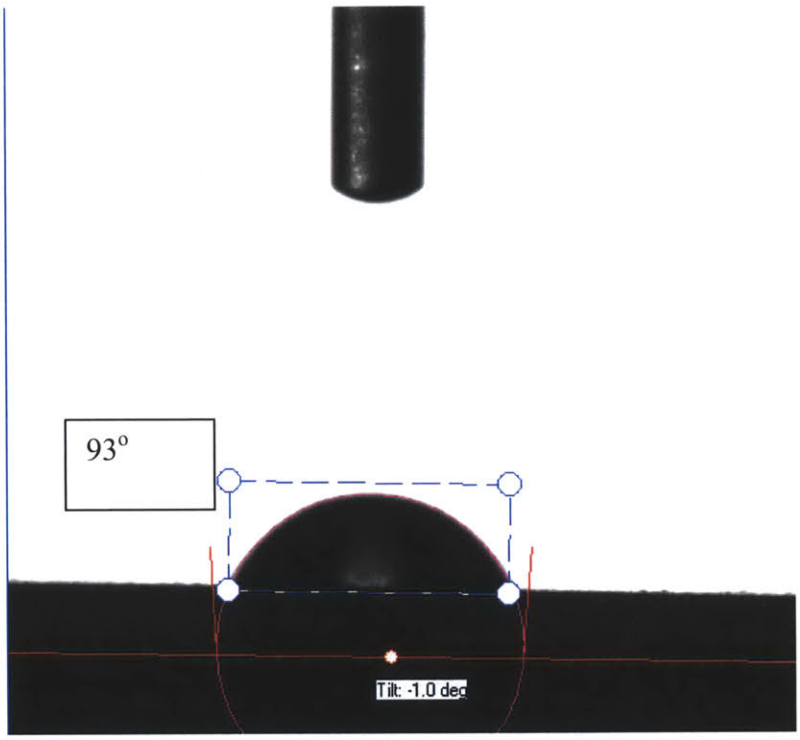

SS316L - CHF Test (Sep 7 2010) with DI Water

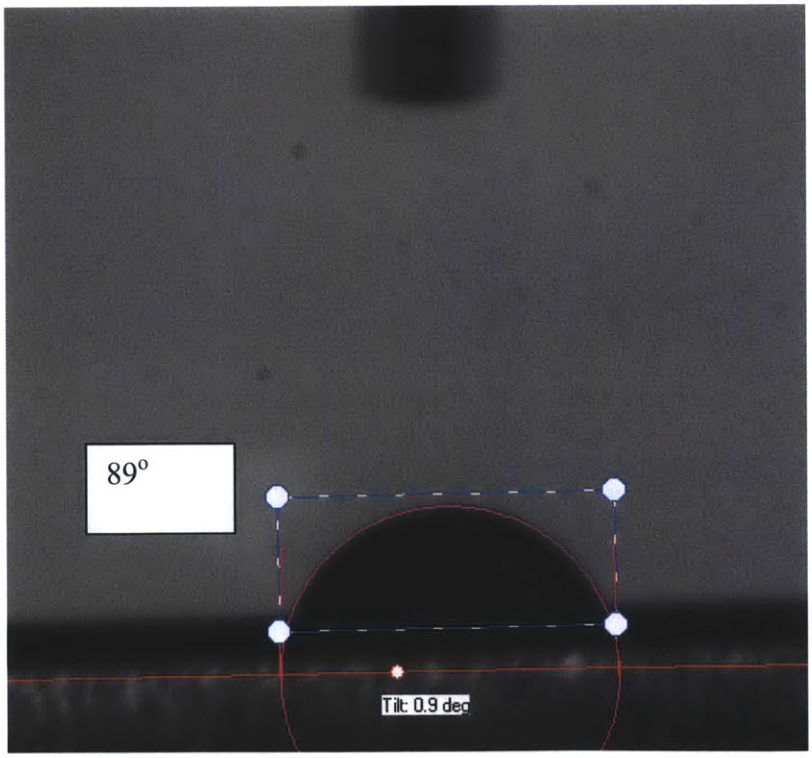

SS316L - CHF Test (Apr 15 2011) with DI Water

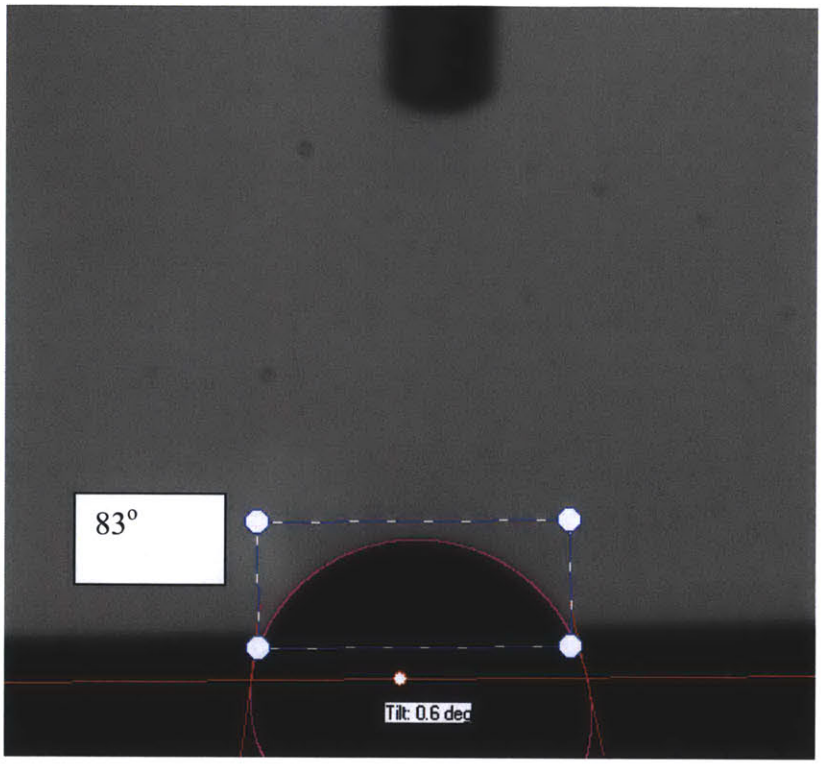

SS316L - CHF Test (Jan 21 2011) with Alumina 0.001%

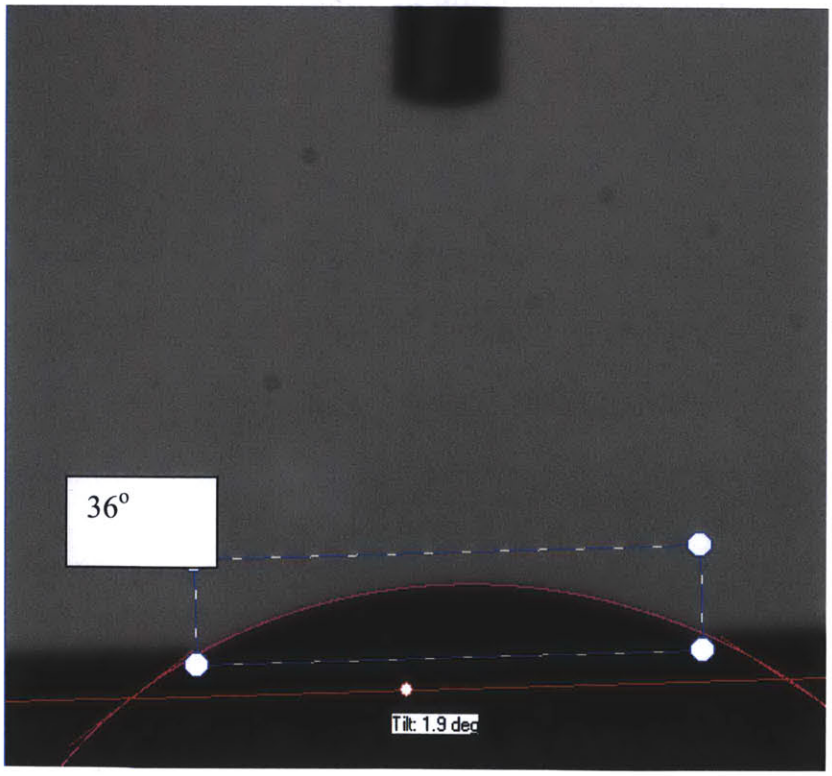

SS316L - CHF Test (Mar 22 2011) with Alumina 0.01%

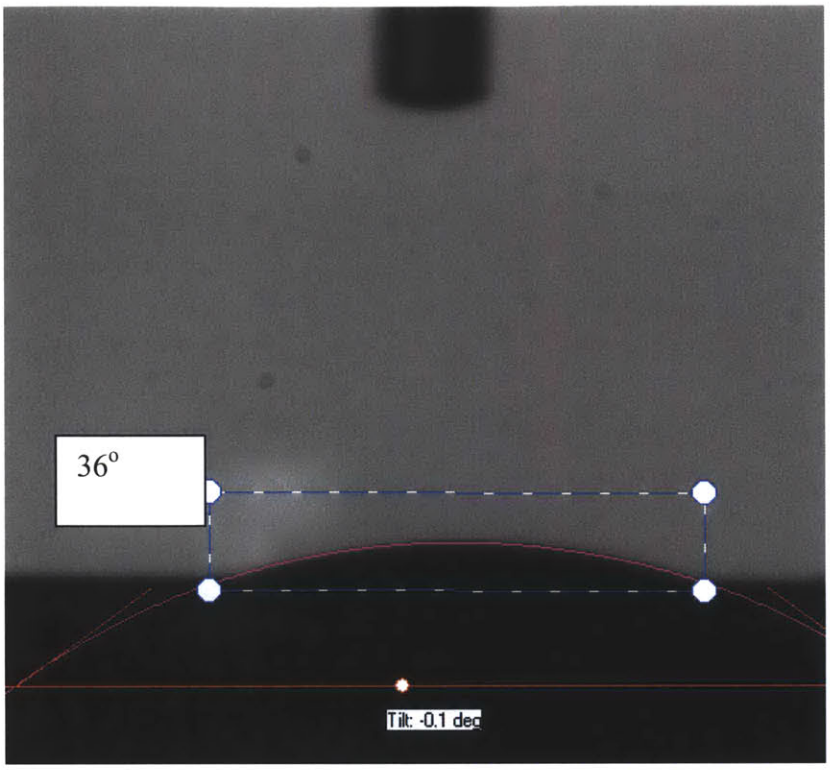

SA-508 - Plain and Unused Heater

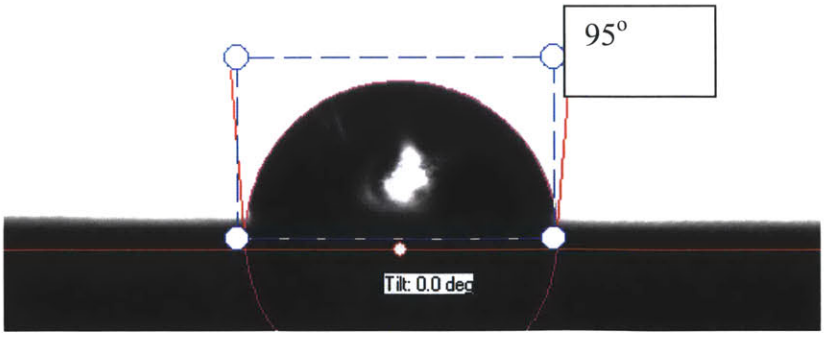

SA-508 - Sandblasted and Unused Heater

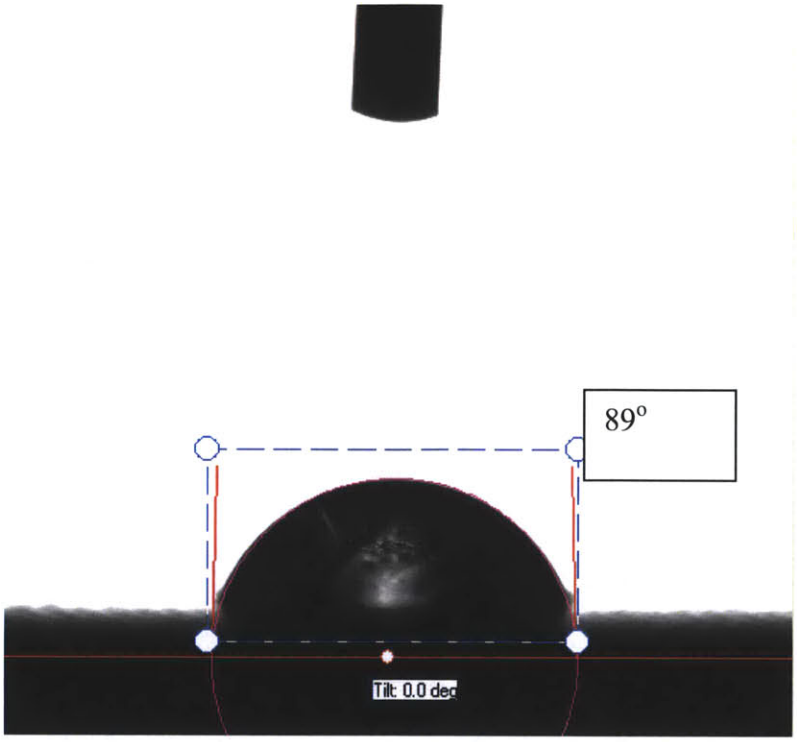

SA-508 - Sandblasted and Unused Heater #2

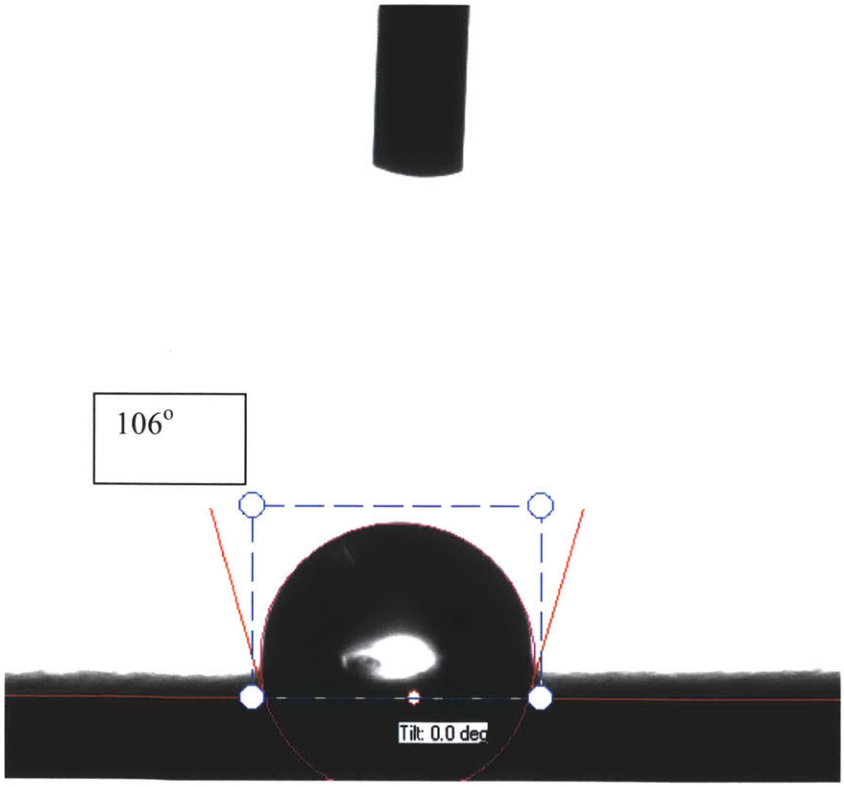

SA-508 - CHF Test with DI Water (July 13, 2011)

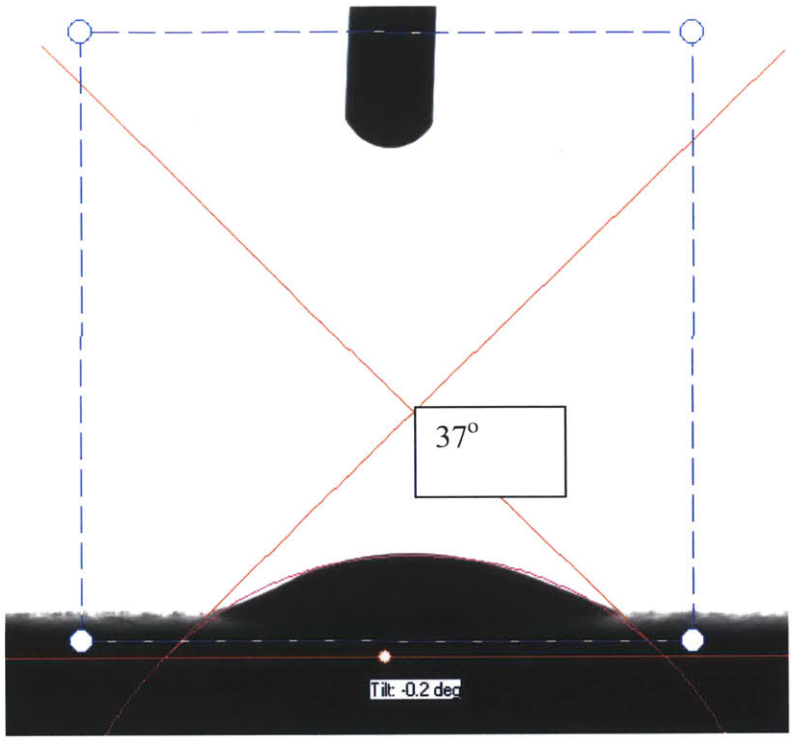

SA-508 - CHF Test with DI Water (July 15, 2011)

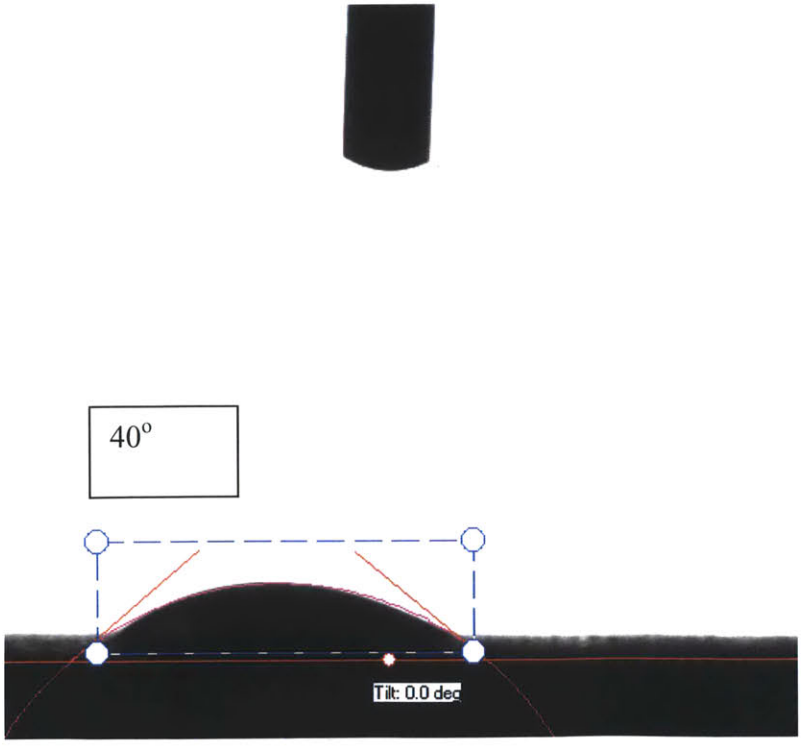

SA-508 - CHF Test with Alumina 0.001% (July 26, 2011)

21°

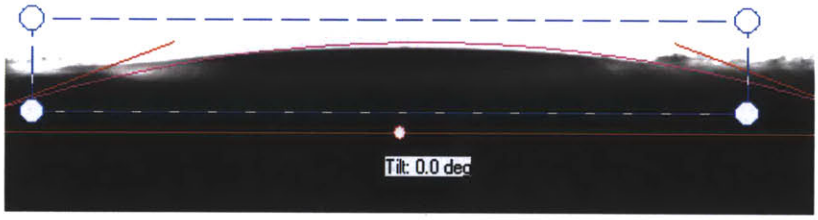

Oxidized SS316L - Unused, Prepared

69°

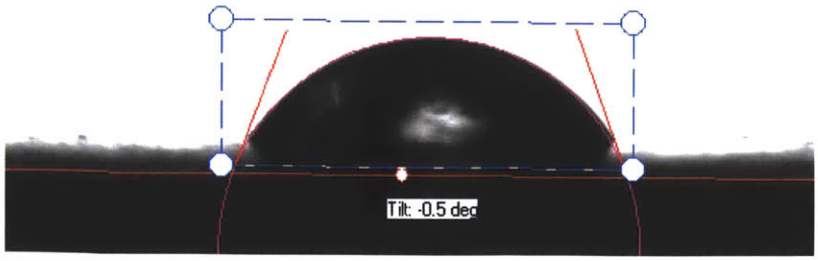

Oxidized SS316L - CHF Test with DI Water (July 21, 2011)

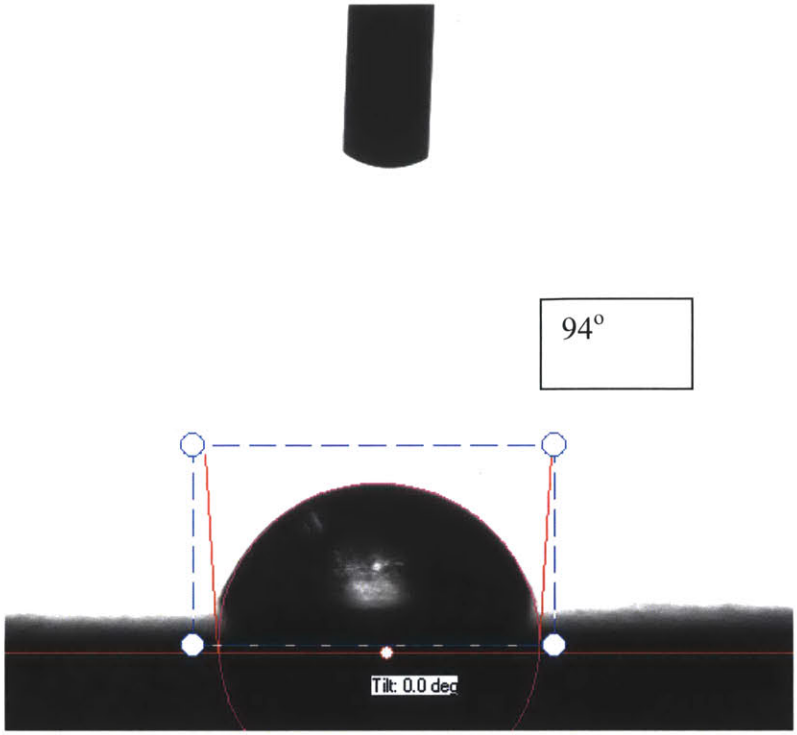

Oxidized SS316L - CHF Test with Alumina 0.001% (Sept 6, 2011)

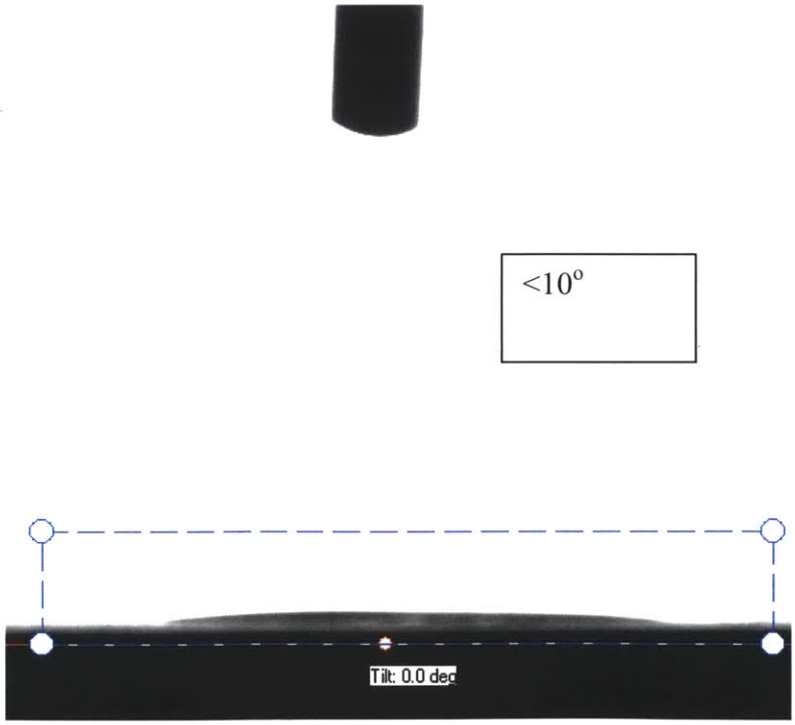

9 Nanofluids

Two concentrations of DI water based nanofluids with alumina nanoparticles are analyzed: alumina [AL_2O_3] at 0.001% and 0.01% by volume. Alumina was chosen because of previous work completed indicating that each has shown significant improvement in CHF for geometry and conditions tested [14]. Additionally, these nanofluids have exhibited good colloidal stability [18]. As noted in chapter 2, at these low concentrations, the thermo-physical properties of the working fluid are not meaningfully different than DI water (i.e., density, specific heat [87], etc.).

The vendor used for the water based alumina is Nyacol Nano Technologies, Inc. The supply in the Green Lab is 20% by weight. Visually the supplied fluid is a milky white, opaque color. Once blended down to either 0.01% or 0.001% by volume the nanofluid is clear as DI water. Note that all experiments with alumina done herein use the same Nyacol batch.

Table 9-1: Alumina Solution as Delivered from Vendor

Vendor	Nyacol Nano Technologies, Inc.	
Chemical Formula	AL_2O_3	
Density	3.04	[gm/cc]
Average particle size	20	[nm]
Lot number	104041	
Nanoparticle fraction	20%	By weight
Color as delivered	Milky white, Opaque	

Samples of nanofluids, 30 ml vials, were taken before and after nanofluid tests. The two before test samples were taken out of the fill tank before drawing into the loop. The two after test samples were also taken from the fill/drain tank, but after the system was cooled then drained. For a number of samples pH and electrical resistivity were measured.

Experiments with fluid samples taken covered several months. None of the clear glass vials show any indications of sedimentation.

9.1 Nanofluid Preparation

Preparation of nanofluid solution targets to blend between 10 and 11 liters [~2.6 gallons] of DI water and nanofluid at room temperature and represents the amount needed to fill the test loop. This base DI water is then mixed with a measured amount of high concentration nanofluid. The target concentration is by volume. The weight of the nanoparticles within the purchased solution is reported by the vendor and confirmed by volume and weight measurement in the Green lab.

To dilute down the vendor delivered alumina and convert to volume percent the following relation is used [34].

$$V_{di} = V_{nf} \cdot \left[\frac{\left(\frac{1+\Phi_{nf}}{\Phi_{nf}}\right)+\left(\frac{1-X_{nf}}{X_{nf}}\right)\cdot\left(\frac{\rho_{nf}}{\rho_{di}}\right)}{1+\left(\frac{1+X_{nf}}{X_{nf}}\right)\cdot\left(\frac{\rho_{nf}}{\rho_{di}}\right)} \right] \qquad \text{Eq. 9.1}$$

Where:

V_{di}	=	Volume of DI water needed for dilution.
V_{nf}	=	Volume of concentrated nanofluid.
Φ_{nf}	=	Target volume percent for diluted nanofluid.
X_{nf}	=	Weight percent of concentrated nanofluid.
ρ_{nf}	=	Density of nanoparticles.
ρ_{di}	=	Density of DI water at STP, 1 gm/mL.

For a 0.01% by volume target concentration for each 10.6 Liters of DI water, 14 mL of 20% by weight nanofluid is added. Delivered alumina solution from Nyacol is 20% by weight. Therefore for the concentrated alumina solution, one (1) liter weighs 1000 gm and is comprised of 200 gm alumina and 800 gm of water.

For a 0.001% by volume target concentration for each 10.6 Liters of DI water, 1.4 mL of 20% by weight nanofluid is added. Most nanofluid experiments completed herein where done at this lower concentration of 0.001% by volume.

9.2 Nanofluid pH and Electrical Conductivity Measurements

A number of samples were measured for pH and electrical conductivity in the Green Lab. The measurement device was a ExTech Instrument model EC510. For most samples from CHF experiment runs both before and after test vials are measured.

Three pH standards are provided to by ExTech and were successfully verified (see Table 9-2).

Table 9-2: ExTech pH Standards and Verification

Description	Standard pH	Measured pH
pH standard 4	4.0	4.0
pH standard 7	7.0	6.95
pH standard 10	10.0	9.97

Electrical conductivity measurement by the EC510 has three scales ranges: 0 to 199.9 μS/cm (low), 200 to 1,999 μS/cm (medium), and 2 to 19.99 mS/cm (high). Note that unit siemens, S, is the inverse of ohm, Ω.

For water only cases the pH measured ranged from 6 to 7 (see Table 9-3). Fresh DI water had an average pH of 6, a little lower than samples introduced to the two-phase loop.

For alumina with 0.001% concentration the pH measurements ranged from 6.4 to 8.3. These samples were pretty similar to DI water used in the loop.

Table 9-3: pH and Electrical Conductivity of Samples

#	Description	Measure Date	Sample Date	Sample ID	Conductivity µS/cm	Resistance MΩ	°C	pH	Notation
1	DI Water	4/16/2011	4/18/2011	n.a	0.0	> 18	22.8	5.7	unused
2	DI Water	4/16/2011	4/18/2011	n.a	0.0	> 18	21.9	6.2	unused
3	Tap Water	4/16/2011	4/18/2011	n.a	533.0	0.00	22.5	8.6	unused
4	DI Water	4/16/2011	4/15/2011	B1	26.0	0.04	22	6.7	CHF test
5	DI Water	4/16/2011	4/15/2011	E1 & E2	26.1	0.04	22	7.2	CHF test
6	DI Water	4/16/2011	4/12/2011	B1	38.7	0.03	22.2	6.2	post loop cleaning
7	DI Water	4/16/2011	4/12/2011	E1	24.5	0.04	21.6	6.8	post loop cleaning
8	Al2O3 - 0.001%	4/16/2011	4/1/2011	B1	6.5	0.15	21.5	8	CHF test
9	Al2O3 - 0.001%	4/16/2011	4/1/2011	E1	7.4	0.14	21.2	7.5	CHF test
10	Al2O3 - 0.001%	4/16/2011	2/24/2011	B1	6.0	0.17	22.1	8.3	CHF test
11	Al2O3 - 0.001%	4/16/2011	2/24/2011	E1	3.6	0.28	22	7.7	CHF test
12	Al2O3 - 0.01%	4/16/2011	3/9/2011	B1	46.1	0.02	21.4	4.6	CHF test
13	Al2O3 - 0.01%	4/16/2011	3/9/2011	B2	17.1	0.06	21.3	4.7	CHF test
14	Al2O3 - 0.01%	4/16/2011	3/9/2011	E1	15.8	0.06	21.8	4.5	CHF test
15	Al2O3 - 0.01%	4/16/2011	3/22/2011	B1	77.4	0.01	22	4.4	CHF test
16	Al2O3 - 0.01%	4/16/2011	3/22/2011	B2	32.2	0.03	21.3	4.4	CHF test
17	Al2O3 - 0.01%	4/16/2011	3/22/2011	E1	17.8	0.06	22	4.5	CHF test
18	Al2O3 - 0.001%	4/18/2011	1/10/2011	E1	11.6	0.09	21.9	6.4	CHF test
19	Al2O3 - 0.001%	4/18/2011	1/10/2011	E2	9.4	0.11	21.9	6.6	CHF test
20	Al2O3 - 0.001%	4/18/2011	12/15/2010	B1	10.1	0.10	22.2	6.9	CHF test
21	Al2O3 - 0.001%	4/18/2011	12/15/2010	E1	0.0	> 18	22.2	6.7	CHF test
22	DI Water	4/18/2011	4/13/2011	B1	5.8	0.17	21	7.3	post loop cleaning
23	DI Water	4/18/2011	4/13/2011	E1	10.0	0.10	21.6	7	post loop cleaning
24	Al2O3 - 0.001%	4/18/2011	3/4/2011	B1	5.2	0.19	21.4	6.8	CHF test
25	Al2O3 - 0.001%	4/18/2011	3/4/2011	E1	5.7	0.18	21	7	CHF test
26	Al2O3 - 20% wt.	7/16/2011	n.a	n.a	2,760.0	0.00	20	4.1	Nyacol - 20% by wt.

For alumina with 0.01% concentration the pH measurements were consistent in a tight range from 4.4 to 4.7. These samples were significantly lower than DI water and alumina 0.001%. Note that the as-delivered pH was 4.1 from Nyacol.

For the alumina pH measurements there is no noted measurement trend between before test and after test samples. The consistency then indicates that the concentration of the working fluid and general chemistry do not change during the course of the CHF test. The DI water CHF test samples are similar with two sets showing a modest increase and one set showing a modest decrease in pH going from before and after samples.

Electrical resistivity of unused DI water was > 18MΩ indicating high quality. Once introduced to the loop the electrical conductivity increases with a measured range of 5.8 μS/cm to 38.7 μS/cm for the samples taken.

For alumina with 0.001% concentration samples, the measured electrical conductivity range was 0.0 μS/cm to 11.6 μS/cm. There was no noted trend in conductivity between samples taken before or after CHF tests.

For alumina with 0.01% concentration samples, the measured electrical conductivity was higher and ranged from 15.8μS/cm to 77.4μS/cm. Differently, there was a trend in conductivity between samples taken before or after CHF tests. Samples taken after CHF tests were lower than samples taken before.

10 Test Procedure

Test procedure for downward CHF experimentation has seven (7) main steps:

1) Fluid preparation,
2) Heater sample preparation,
3) Initial readings,
4) Loop set-up,
5) Degassing,
6) Warm-up to CHF, and
7) Shutdown and disassemble.

Detailed step-by-step procedure is provided in Appendix C.

10.1 Fluid Preparation

Fluid preparation starts with about 11 liters [~2.9 gallons] of DI water placed into the fill and drain tank. A 1 kW cartridge heater is place into the fill and drain tank and the working fluid temperature brought up to about 70 °C (see Figure 10-1). This is not a necessary step, but helps reduce total experimentation time. The working fluid can be bought into the system at STP and then heated within the loop. Once at the desired fluid temperature the cartridge heater is removed from the tank. Next, when applicable, nanofluids are added via pipette to blend down the concentration from the supplier, 20% by weight, to the desired volume percent. The fill and drain tank on the loop is used to mix the DI water and nanofluids. Two formulations of alumina nanofluid used herein, 0.001% and 0.01% by volume, are more fully described in chapter 9.

Next, two 30 mL vials of the nanofluids are taken. After the CHF experiment is complete and the system cooled and drained, two more vial samples are taken.

Figure 10-1: Photo of 1 kW Cartridge Heater

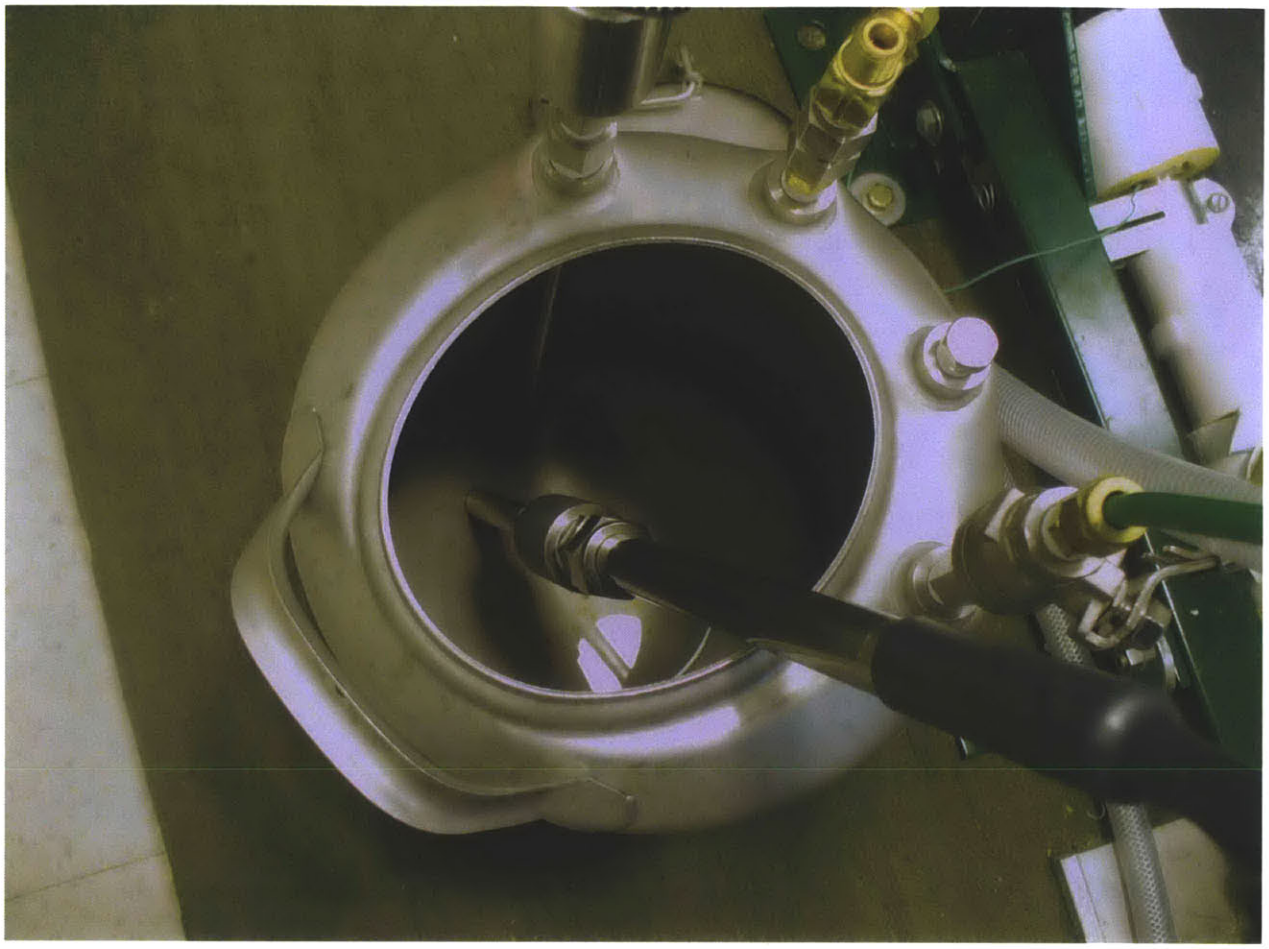

10.2 Heater Sample Preparation

Heater sample preparation starts with cleaning a new heater with DI water and acetone. The fabricator of the heaters is RAMCO. Next, the heater is sandblasted to provide the desired finish. Generally, three to five sweeps of the sandblasting nozzle are sufficient. One sweep being back and forth (see Figure 7-1). Sandblasting material is silicone beads of 210 to 305 micron size. Before the sandblasting the heater has a shiny look and swirl marks visible. Sandblasting makes the finish very even, dull looking and with no swirl marks (see Figure 7-2). After sandblasting the heater is cleaned again with DI water and acetone.

Next, the heater is mounted into the MACOR insulator. The insulator, heater and copper electrodes are then heated to about 10 °C above expected saturation temperature. The copper electrodes with o-rings are next screwed into the heated sample. The objective is to set the o-rings in a position that incorporates the expected growth of the heater. This heating step helps prevent bowing of the heater during heat up.

Additional details on heater surface preparation are described in chapter 7.

10.3 Initial Readings

Initial readings are made for the RTDs and pressure transducers. For the three RTDs an ice bath or flowing water in the loop with no heat being added is used and initial measurements taken. The pressure transducers are also read while the loop is empty and open to air. These readings mainly ensure that the instruments are functioning properly. Initial readings are recorded. At this point room temperature and general weather conditions including barometric pressure are also noted.

10.4 Loop Set-up

Loop set-up starts with loading the MACOR insulator with sample heater into the test section. A cover plate holds the insulator and heater in place. Next, the Type-K thermocouples along the back of the test section are screwed into place. Most often only four (4) of the eight (8) thermocouple locations are used (see Figure 6-4: Photo of Test Section Void near CHF Conditions). The four positions most often used are the first (nearest the fluid entrance), forth (near the middle of the test heater length), and the last two positions, seven and eight (nearest the exit).

The test section is then placed at the desired angle relative to gravity. The angle is confirmed with a digital goniometer which is accurate to 0.1°.

Figure 10-2: Photo of Thermocouple Holes on Test Section Back Plate

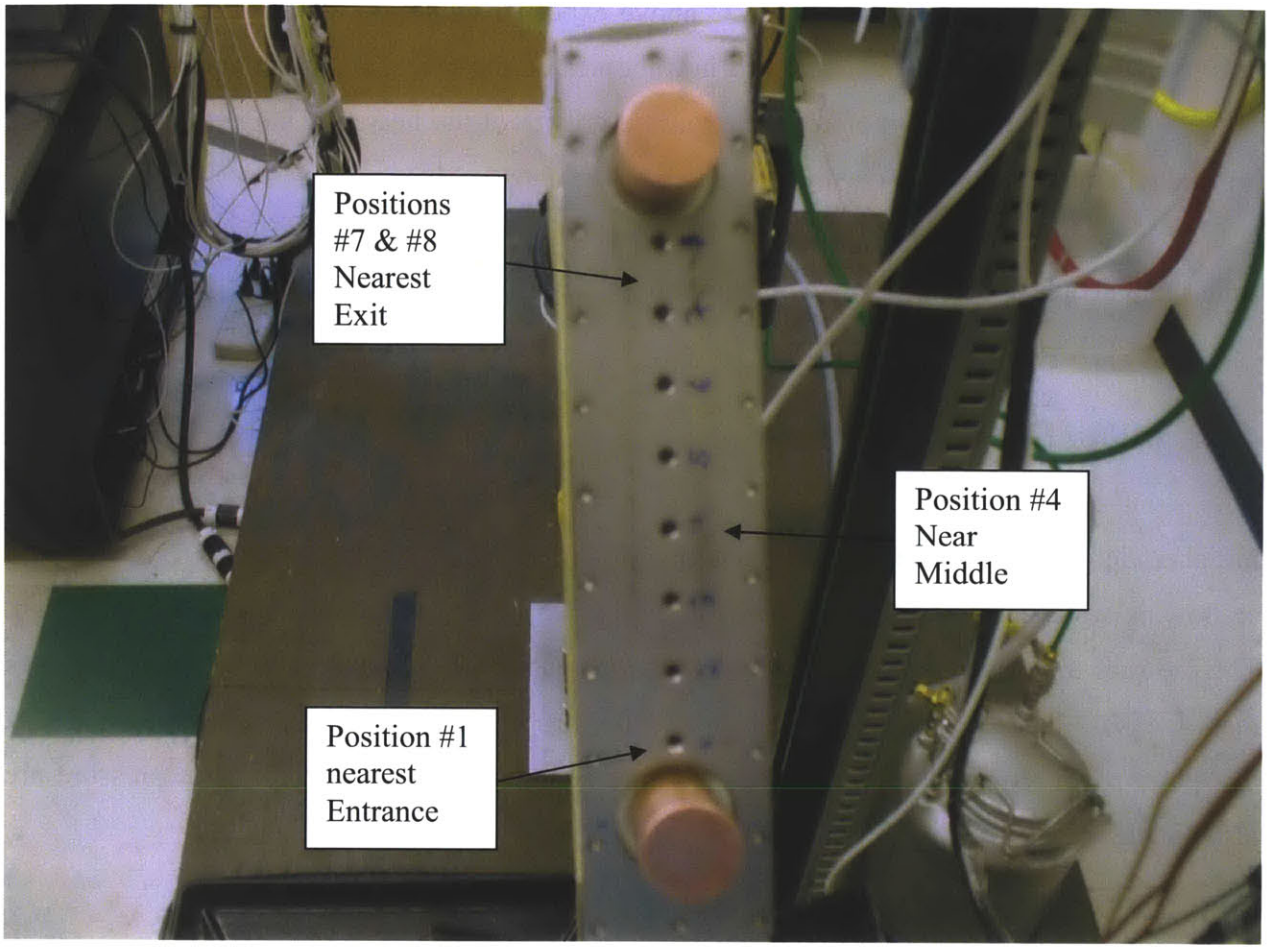

The copper blocks that electrically connect the locomotive wires from the power supplies to the heater are next mounted to the electrodes together with spacer collars (see Figure 6-6). Safety bars are then attached to the copper block to prevent contact in the event of failure of the copper stud thread.

Fluid is brought into the system in two steps. First, utilizing a vacuum pump gases are removed from the system (see Figure 10-3).

Figure 10-3: Photo of Vacuum Pump and Line to Loop

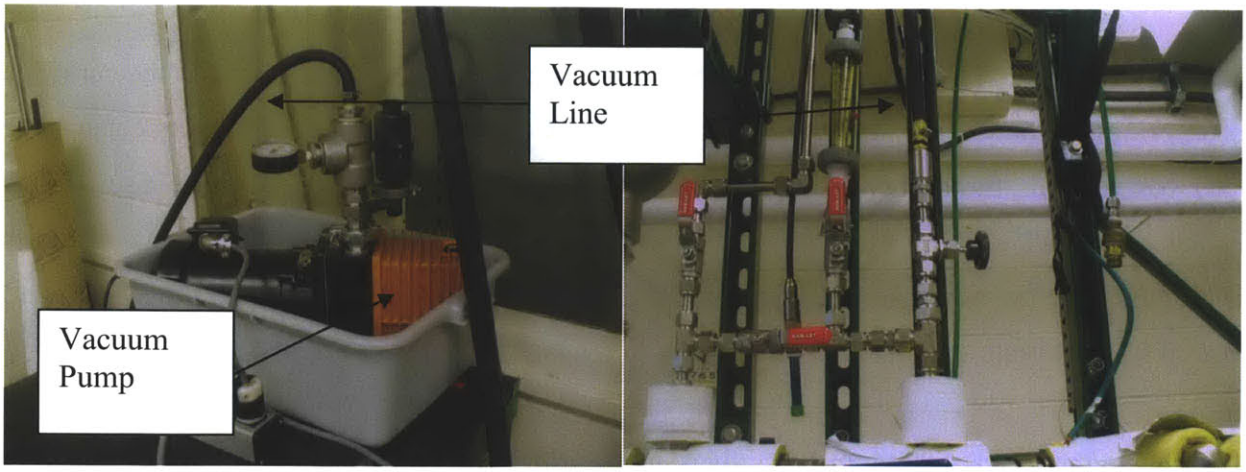

Next, a ball valve between the loop and the fill and drain tank is opened to allow the fluid to be drawn into the loop. This procedure helps reduce non-condensable gases from being trapped. The vacuum to atmosphere pressure difference will bring the fluid level up above the main loop and near the highest point, which is the location of the DO probe. To push the fluid up to the DO probe level, the fill tank is closed and about 5 psi of nitrogen gas added above the fluid. Usually several inches of fluid remains in the fill tank after the loop is filled. Again, the ball valve between the loop and the fill tank is opened. The rubber stopper at the top of the DO probe mount is slightly opened to allow gases to exit. Sometimes it is convenient to just use a small glass beaker of working fluid and just pour into the DO probe holder to complete filling. With the system full the ball valve between the loop and the fill tank is closed.

The main pump is then started at minimum flow rate for a couple minutes. The main loop ball valve is closed. This will bring whatever gases remain to the top of the system and be removed. Pump is then stopped and the DO probe screwed into place.

To test for system leaks the pump power is increased. For an atmospheric test the pump is increased until the system pressure is two atmospheres, absolute. The system valves can also be partially closed to increase pressure. Once the loop is checked for leaks the pump power is reduced to minimum and valve set to normal position.

10.5 Degassing

Degassing of the fluid starts once the DI water is put into the fill and drain tank. As the cartridge heater brings up the working fluid temperature with the tank lid open some degassing occur. For water based fluids the ability of the fluid to hold gasses declines as temperature rises. This heating occurs while the test section and cabling are being completed. Note that nanofluid is only added after the cartridge heater is removed. Once the fluid is brought into the system and allowed to equilibrate the system is usually about 39 °C.

Mass flux is then set at 500 kg/m^2-s. Valves are positioned such that bubbles are likely to gather near the degassing line. Joule heating to the test section is applied at a heat flux level such that sub-cooled nucleate boiling can be seen along the surface. The 2 kW pre-heater can also be used to help heat up the bulk fluid. Once bulk temperature of 60 °C is achieved the needle valve to the green degassing line is opened until bubbles no longer come out. The opposite end of the degassing line is under the remaining fluid in the fill tank.

Sub-cooled nucleate boiling is continued for ten (10) minutes. Again, the needle valve to the degassing line is opened and bubbles observed. These steps are repeated with ten (10) minute intervals until no further bubbles appear. Generally, only two openings of the needle valve are needed.

Valves again are changed to allow a small amount of flow (200 – 1,000 mL/min) to pass the DO probe. Once the DO probe measures a temperature of around 60 °C, a reading is made and recorded. A value of 4 ppm or less is expected.

10.6 Warm-up to CHF

To begin warming up to CHF the loop valves are changed to direct all flow within the main loop. Joule heating of the test section and the pre-heater are used to bring the bulk fluid temperature from about 60 °C toward saturation. Chilled water flow to the condenser is off at this point.

Once the bulk temperature is within 10 °C of saturation the chilled water flow to the condenser is started.

Care needs to be taken to assure the pump inlet temperature and pressure is such that cavitations are avoided. The pre-heater, 2 kW, downstream of the pump is used to bring the slightly sub-cooled flow to saturation in the test section (see Figure 6-13: Immersion Pre-heater on Test Loop). A dimmer like controller is for the pre-heater is located at the computer station (see Figure 10-4).

Figure 10-4: Photo of Pre-heater Variable Controller

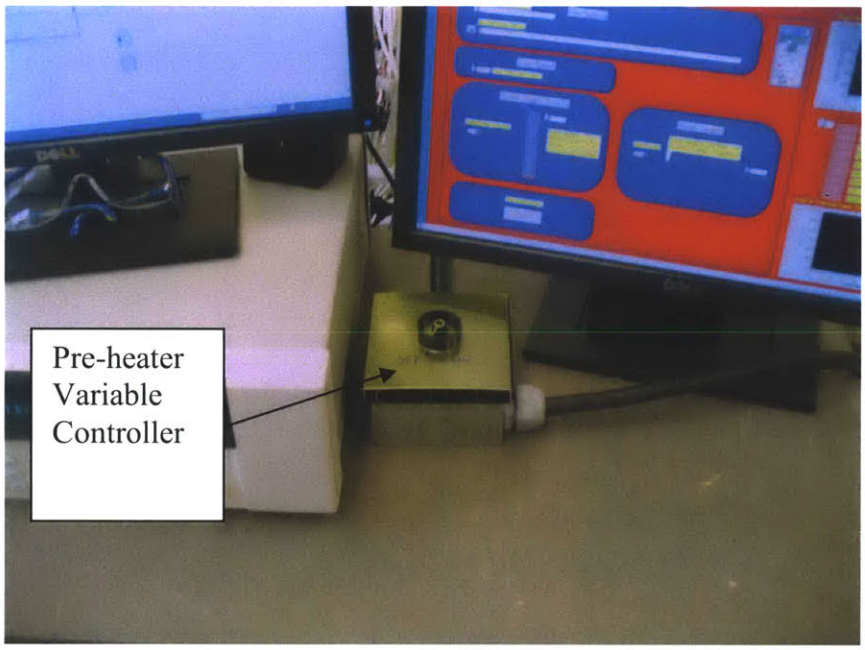

Power changes are small and gradual as CHF conditions approach. Power changes are often followed by a small chilled water flow adjustment so to maintain 2 to 3 °C sub-cooling at the pump entrance.

CHF is visualized by a bright orange dot on the sample heater. The OFF button on the LabVIEW front panel is clicked to stop the power supplies. Note if all else fails there is a red panic button on the control box. The chilled water flow is then fully opened.

At this step it is important to change the filename that LabVIEW uses so not to overwrite test data. The pump is set to minimum flow (2 gpm). The system is allowed to cool until the bulk temperature reduces to below 20 °C.

10.7 Shutdown and Disassemble

Shutdown is initiated when the bulk fluid temperature is below 20 °C. LabVIEW STOP button is clicked to stop the pump. The system is drained into the fill and drain tank. Two post experiment samples (30 mL) of nanofluid are taken, labeled, and stored

The test section is then disassembled. The burnt out heater is stored in a zip-lock bag and labeled with the date and description of the experiment. About half of the CHF experiments result in the sample breaking into pieces, usually two.

11 EXPERIMENTAL MATRIX & RESULTS

To quantify the affect that nanofluids have on CHF for conditions relevant to IVR, a series of experiments where run utilizing the two-phase flow loop facility described in chapter 6. Generally, the experimental matrix matched conditions of pressure, flow rate, inclination angle, exit quality, and surface material and changed only the working fluid: DI water and alumina nanofluid. This differential method then isolated the relative effect of nanofluid on CHF. Exit condition for this series was saturated with near zero quality, χ_e. A few additional experiments were done to quantify the influence boiling time had on nanofluid CHF. Additionally, taking advantage of the facility capabilities, a high sub-cooling experiment was also completed to visualize CHF and reported herein.

11.1 Experimental Test Matrix

Eighty-four (84) experiments were completed to analyze CHF enhancement with nanofluids. Parameters that varied included: sample material, fluid type, system pressure, mass flux, and test section angle (see Table 11-1).

Table 11-1: List of Parameters Varied in Experimental Matrix

Parameter	Range of Types
Sample Material:	SS316L; SA508
Fluids:	DI water; Water-based nanofluids with Alumina nanoparticles at 0.01% and 0.001% concentration.
Pressure:	1; 3; 5 atm
Mass Flux:	500; 1,000; 1,500 kg/m^2-s
Angle:	0 °; 30 °; 45 °; 60 °; 90°

Two (2) surface types were used: stainless steel 316L and SA-508. Stainless steel was studied because of its common use and for comparison to previous CHF enhancement work done at MIT. SA-508 was tested because it is the reactor pressure vessel material used for the AP1000. The SA-508 heaters used herein were fabricated from material from an actual pressure vessel that was used for destructive testing.

Alumina nanofluids were chosen from previous CHF research done at MIT indicating the possibility of strong CHF enhancement for IVR conditions. Forty (40) CHF runs were completed with alumina nanofluids. Of these nanofluid tests thirty-eight (38) had a concentration of 0.001% by volume and two (2) a concentration of 0.01% by volume.

The forty-four (44) DI water experiments are the bases of relative CHF enhancement and allow for comparison to other CHF investigations (i.e., UCSB and Sultan; see chapter 12).

Three (3) absolute system pressures were done: 1 atm, 3 atm, and 5 atm. These pressures bound the range of expected pressures during IVR along the lower vessel head (~ 2 atm) and the containment design limit for the Westinghouse AP1000 (5 atm).

Three (3) target mass fluxes were tested: 500; 1,000; and 1,500 kg/m^2-s. These mass fluxes bound the range of natural-circulation flow expected along the lower reactor vessel head for the AP1000 once the reactor cavity is flooded and corium development drives meaningful heat flux through the surface.

Five (5) downward facing angles are tested: 90^o (vertical), 60^o, 45^o, 30^o, and 0^o (horizontal).

To address the question as to how long it takes for boiling to deposit nanoparticles onto a SS316L surface and still get CHF enhancement a series of eight (8) reduced boiling times were completed: six (6) with alumina at 0.001% and two (2) with DI water. The limited boiling time ranged from just less than 1 hour down to about 20 minutes. These were chosen to contrast against the 1 ½ hours or more of boiling on the test heater that a normal test experiences. Note

that the IVR strategy has a time frame of hours. Corium development is expected to take at least 2 hours (see chapter 5).

Generally, all tested conditions were tested twice. If the resulting CHF measured was different by more than 10%, a third case was completed. Limited boiling tests were each unique. Not all combinations from the listed parameters were completed. The table below lists the experiments completed with target conditions (see Table 11-2).

Table 11-2: List of Experiments Completed with Target Conditions

ID #	Test Date	Working Fluid	Surface Material	Pressure [Bar]	Mass Flux [kg/m^2-s]	Angle [°]
2	06-Apr-10	DI water	SS316L	1	500	90
3	08-Apr-10	DI water	SS316L	1	500	90
4	20-Apr-10	DI water	SS316L	1	500	90
76	04-May-11	DI water	SS316L	1	500	90
32	19-Nov-10	DI water	SS316L	1	500	60
33	19-Nov-10	DI water	SS316L	1	500	60
9	30-Aug-10	DI water	SS316L	1	500	45
10	01-Sep-10	DI water	SS316L	1	500	45
13	09-Sep-10	DI water	SS316L	1	500	30
14	10-Sep-10	DI water	SS316L	1	500	30
15	15-Sep-10	DI water	SS316L	1	500	0
16	17-Sep-10	DI water	SS316L	1	500	0
5	15-Jul-10	DI water	SS316L	1	1,000	90
6	20-Jul-10	DI water	SS316L	1	1,000	90
26	29-Oct-10	DI water	SS316L	1	1,000	90
29	11-Nov-10	DI water	SS316L	1	1,000	60
30	12-Nov-10	DI water	SS316L	1	1,000	60
31	16-Nov-10	DI water	SS316L	1	1,000	60
11	03-Sep-10	DI water	SS316L	1	1,000	45
12	07-Sep-10	DI water	SS316L	1	1,000	45
70	15-Apr-11	DI water	SS316L	1	1,000	45
71	27-Apr-11	DI water	SS316L	1	1,000	45
17	21-Sep-10	DI water	SS316L	1	1,000	30
18	24-Sep-10	DI water	SS316L	1	1,000	30
19	01-Oct-10	DI water	SS316L	1	1,000	0
20	06-Oct-10	DI water	SS316L	1	1,000	0
21	08-Oct-10	DI water	SS316L	1	1,000	0

7	26-Jul-10	DI water	SS316L	1	1,500	90
25	26-Oct-10	DI water	SS316L	1	1,500	90
27	02-Nov-10	DI water	SS316L	1	1,500	30
28	05-Nov-10	DI water	SS316L	1	1,500	30
22	21-Oct-10	DI water	SS316L	1	1,500	0
23	21-Oct-10	DI water	SS316L	1	1,500	0
24	22-Oct-10	DI water	SS316L	1	1,500	0
8	11-Aug-10	DI water	SS316L	2	1,000	45
72	19-Apr-11	DI water	SS316L	3	1,000	45
73	20-Apr-11	DI water	SS316L	3	1,000	45
74	22-Apr-11	DI water	SS316L	5	1,000	45
75	25-Apr-11	DI water	SS316L	5	1,000	45
66	09-Mar-11	Al2O3 - 0.01%	SS316L	1	1,000	45
67	22-Mar-11	Al2O3 - 0.01%	SS316L	1	1,000	45
34	15-Dec-10	Al2O3 - 0.001%	SS316L	1	500	90
35	16-Dec-10	Al2O3 - 0.001%	SS316L	1	500	90
55	09-Feb-11	Al2O3 - 0.001%	SS316L	1	500	60
56	11-Feb-11	Al2O3 - 0.001%	SS316L	1	500	60
36	20-Dec-10	Al2O3 - 0.001%	SS316L	1	500	45
37	23-Dec-10	Al2O3 - 0.001%	SS316L	1	500	45
39	07-Jan-11	Al2O3 - 0.001%	SS316L	1	500	45
40	10-Jan-11	Al2O3 - 0.001%	SS316L	1	500	0
41	11-Jan-11	Al2O3 - 0.001%	SS316L	1	500	0
42	14-Jan-11	Al2O3 - 0.001%	SS316L	1	1,000	90
43	18-Jan-11	Al2O3 - 0.001%	SS316L	1	1,000	90
44	20-Jan-11	Al2O3 - 0.001%	SS316L	1	1,000	45
45	21-Jan-11	Al2O3 - 0.001%	SS316L	1	1,000	45
60	18-Feb-11	Al2O3 - 0.001%	SS316L	1	1,000	45
61	22-Feb-11	Al2O3 - 0.001%	SS316L	1	1,000	45
62	24-Feb-11	Al2O3 - 0.001%	SS316L	1	1,000	45
63	25-Feb-11	Al2O3 - 0.001%	SS316L	1	1,000	45
64	02-Mar-11	Al2O3 - 0.001%	SS316L	1	1,000	45
65	04-Mar-11	Al2O3 - 0.001%	SS316L	1	1,000	45
46	24-Jan-11	Al2O3 - 0.001%	SS316L	1	1,000	0
47	25-Jan-11	Al2O3 - 0.001%	SS316L	1	1,000	0
50	31-Jan-11	Al2O3 - 0.001%	SS316L	1	1,500	90
51	02-Feb-11	Al2O3 - 0.001%	SS316L	1	1,500	90
52	02-Feb-11	Al2O3 - 0.001%	SS316L	1	1,500	45
53	07-Feb-11	Al2O3 - 0.001%	SS316L	1	1,500	45
54	08-Feb-11	Al2O3 - 0.001%	SS316L	1	1,500	45
48	26-Jan-11	Al2O3 - 0.001%	SS316L	1	1,500	0
49	28-Jan-11	Al2O3 - 0.001%	SS316L	1	1,500	0
59	16-Feb-11	Al2O3 - 0.001%	SS316L	3	500	45

57	15-Feb-11	Al2O3 - 0.001%	SS316L	3	1,000	45
58	17-Feb-11	Al2O3 - 0.001%	SS316L	3	1,000	45
68	25-Mar-11	Al2O3 - 0.001%	SS316L	5	1,000	45
69	01-Apr-11	Al2O3 - 0.001%	SS316L	5	1,000	45
38	07-Jan-11	Al2O3 - 0.001%	SS316L	1	500	45
77	13-Jul-11	DI water	SA-508	1	1,000	45
78	15-Jul-11	DI water	SA-508	1	1,000	45
79	19-Jul-11	DI water	SA-508	1	1,000	45
82	26-Jul-11	Al2O3 - 0.001%	SA-508	1	1,000	45
83	28-Jul-11	Al2O3 - 0.001%	SA-508	1	1,000	45
80	21-Jul-11	DI water	Oxidized - SS316L	1	1,000	45
81	22-Jul-11	DI water	Oxidized - SS316L	1	1,000	45
84	6-Sepl-11	Al2O3 - 0.001%	Oxidized - SS316L	1	1,000	45
85	7-Sepl-11	Al2O3 - 0.001%	Oxidized - SS316L	1	1,000	45

Seventy-five (75) of the CHF tests were done with SS316L as the surface material with normal preparation. An additional four (4) SS316L tests where completed with an oxidized preparation to identify the impact on CHF. Five (5) CHF tests utilized SA-508 to determine the influence that the material has on CHF relative to SS316L: three (3) with DI water and two (2) with alumina at 0.001%.

Forty-four (44) experiments were completed with de-ionized water ("DI'). These tests represent the benchmark to which change of CHF due to the introduction of nanofluids is compared. Thirty-eight (38) experiments were done with 0.001% alumina. Two (2) tests with 0.01% alumina were done to identify the influence of higher weight percent of alumina nanoparticles.

Seventy-four (74) experiments were completed with atmospheric conditions in the overhead gas region of the accumulator. One (1) experiment was done at two (2) atm. Five (5) experiments were done at three (3) atm. Four (4) experiments were done at 5 atm to determine if the trends identified at lower pressure continued at the design limit of the AP1000 containment.

Twenty-three (23) experiments were completed at the lowest mass flux, 500 kg/m^2-s, entering the test section. Forty-seven (47) experiments were completed at the middle mass flux, 1,000

kg/m^2-s, entering the test section. Fourteen (14) experiments were completed at the highest mass flux, 1,500 kg/m^2-s, entering the test section.

Angle of the downward facing sample is referenced to gravity. Angle of 90° is vertical and parallel to gravity. Angle of 0° is horizontal and perpendicular to gravity. Fifteen (15) tests were completed with the test sample vertical (θ=90°). Fourteen (14) tests were done in the downward facing horizontal orientation (θ=0°). Fifty-five (55) tests spanned the intermediate angles: six (6) at 30°, forty (40) at 45°, and seven (7) at 60°.

11.2 Results for Experimental Test Matrix

The below table lists the eighty-five (85) measured conditions and CHF results inclusive of the experimental matrix of eighty-four (84) (see Table 11-3). Note the run #1 had higher sub-cooling and is shown for completeness.

Table 11-3: Measured Results of CHF Experimental Test Matrix for IVR Conditions [1atm=1.10418 bar]

				Test Section							
Run #	Experiment Date	Fluid	Surface Material	Exit Pressure [Bar]	Mass Flux [Kg/m^2-s]	Angle [Degrees]	Exit T_sat [C]	Exit T-bulk [C]	Exit Quality	Measured CHF [MW/m^2]	Notes
1	18-Mar-10	DI water	SS316L	1.28	492	90	106.6	83.6	-0.042	2.72	highly subcooled
2	06-Apr-10	DI water	SS316L	1.07	481	90	101.5	94.0	-0.012	1.11	ok
3	08-Apr-10	DI water	SS316L	1.08	540	90	101.8	97.5	-0.006	1.57	ok
4	20-Apr-10	DI water	SS316L	1.14	537	90	102.0	100.1	-0.004	1.08	ok
76	04-May-11	DI water	SS316L	1.03	509	90	100.4	100.5	0.005	1.46	ok
										1.31	Average
5	15-Jul-10	DI water	SS316L	1.16	1,011	90	103.5	102.1	-0.002	1.35	ok
6	20-Jul-10	DI water	SS316L	1.10	996	90	102.0	101.5	-0.001	1.70	ok
										1.53	Average

7	26-Jul-10	DI water	SS316L	1.11	1,532	90	102.3	99.2	-0.007	1.50	ok
										1.50	Average
8	11-Aug-10	DI water	SS316L	2.26	1,003	45	123.8	123.2	0.002	1.53	saturation, ok
9	30-Aug-10	DI water	SS316L	1.09	483	45	100.7	100.6	0.001	0.97	saturation, ok
10	01-Sep-10	DI water	SS316L	1.06	498	45	101.1	100.6	0.003	0.88	saturation, ok
										0.93	Average
11	03-Sep-10	DI water	SS316L	1.04	1,023	45	100.6	100.2	0.001	1.28	saturation, ok
12	07-Sep-10	DI water	SS316L	1.06	985	45	101.1	100.5	0.001	1.33	saturation, ok
										1.31	Average
13	09-Sep-10	DI water	SS316L	1.05	501	30	100.9	100.4	0.001	0.70	saturation, ok
14	10-Sep-10	DI water	SS316L	1.05	544	30	100.8	99.8	-0.001	0.72	ok
										0.71	Average
15	15-Sep-10	DI water	SS316L	1.06	581	0	101.1	98.2	-0.005	0.58	little sub-cooled
16	17-Sep-10	DI water	SS316L	1.06	658	0	101.2	99.4	-0.003	0.53	little sub-cooled
										0.56	Average
17	21-Sep-10	DI water	SS316L	1.14	1,039	30	103.1	102.2	-0.001	1.31	ok
18	24-Sep-10	DI water	SS316L	1.09	1,040	30	101.8	100.8	-0.001	1.28	ok
										1.30	Average
19	01-Oct-10	DI water	SS316L	1.11	1,010	0	102.4	101.9	0.001	1.32	ok
20	06-Oct-10	DI water	SS316L	1.15	1,037	0	103.3	102.0	-0.002	1.11	ok
21	08-Oct-10	DI water	SS316L	1.09	1,021	0	101.9	101.3	0.000	1.15	ok
										1.19	Average
22	21-Oct-10	DI water	SS316L	1.12	1,498	0	102.5	101.4	-0.002	1.28	ok
23	21-Oct-10	DI water	SS316L	1.10	1,493	0	102.0	101.8	0.001	1.60	ok
24	22-Oct-10	DI water	SS316L	1.11	1,496	0	102.3	101.9	0.000	1.50	ok
										1.46	Average
25	26-Oct-10	DI water	SS316L	1.11	1,476	90	102.3	102.0	0.000	1.50	Ok
26	29-Oct-10	DI water	SS316L	1.13	982	90	102.9	103.1	0.002	1.74	Ok
27	02-Nov-10	DI water	SS316L	1.13	1,507	30	102.7	102.0	-0.001	1.60	ok
28	05-Nov-10	DI water	SS316L	1.10	1,505	30	102.1	101.9	0.001	1.63	ok
										1.62	Average

29	11-Nov-10	DI water	SS316L	1.14	978	60	103.1	102.7	0.001	1.42	ok
30	12-Nov-10	DI water	SS316L	1.15	982	60	103.2	103.0	0.001	1.65	ok
31	16-Nov-10	DI water	SS316L	1.13	1,000	60	102.9	102.5	0.002	1.54	ok
										1.54	Average
32	19-Nov-10	DI water	SS316L	1.11	508	60	102.6	102.2	0.002	1.22	ok
33	19-Nov-10	DI water	SS316L	1.17	513	60	103.8	102.7	0.000	1.28	ok
										1.25	Average
34	15-Dec-10	Al2O3 - 0.001%	SS316L	1.06	512	90	101.2	101.9	0.010	1.78	ok
35	16-Dec-10	Al2O3 - 0.001%	SS316L	1.07	508	90	101.3	101.5	0.006	1.76	ok
										1.77	Average
36	20-Dec-10	Al2O3 - 0.001%	SS316L	1.15	512	45	103.3	103.3	0.006	1.50	ok
37	23-Dec-10	Al2O3 - 0.001%	SS316L	1.14	623	45	103.0	102.7	-0.004	1.25	ok
38	07-Jan-11	Al2O3 - 0.001%	SS316L	1.00	500	45	n.a	n.a	n.a	1.40	ok, morning
39	07-Jan-11	Al2O3 - 0.001%	SS316L	1.15	507	45	103.2	101.7	-0.001	1.35	ok, afternoon
										1.38	Average
40	10-Jan-11	Al2O3 - 0.001%	SS316L	1.15	547	0	103.2	102.7	0.001	1.06	ok
41	11-Jan-11	Al2O3 - 0.001%	SS316L	1.17	574	0	103.8	103.3	0.000	1.12	ok
										1.09	Average
42	14-Jan-11	Al2O3 - 0.001%	SS316L	1.17	1,037	90	103.8	103.6	0.002	2.73	ok
43	18-Jan-11	Al2O3 - 0.001%	SS316L	1.16	1,062	90	103.5	103.4	0.002	2.76	ok
										2.75	Average
44	20-Jan-11	Al2O3 - 0.001%	SS316L	1.18	1,025	45	104.1	103.5	0.002	2.55	ok
45	21-Jan-11	Al2O3 - 0.001%	SS316L	1.16	992	45	103.5	103.5	0.003	2.51	ok
										2.53	Average
46	24-Jan-11	Al2O3 - 0.001%	SS316L	1.14	1,038	0	103.1	103.0	0.002	2.16	Ok
47	25-Jan-11	Al2O3 - 0.001%	SS316L	1.16	1,015	0	103.6	102.9	0.001	2.08	ok
										2.12	Average

48	26-Jan-11	Al2O3 - 0.001%	SS316L	1.14	1,537	0	103.0	102.5	0.001	2.92	ok
49	28-Jan-11	Al2O3 - 0.001%	SS316L	1.14	1,565	0	103.1	102.6	0.001	2.80	ok
										2.86	Average
50	31-Jan-11	Al2O3 - 0.001%	SS316L	1.12	1,552	90	102.7	102.6	0.002	3.16	ok
51	02-Feb-11	Al2O3 - 0.001%	SS316L	1.14	1,531	90	103.0	102.9	0.001	3.09	ok
										3.13	Average
52	02-Feb-11	Al2O3 - 0.001%	SS316L	1.13	1,526	45	102.8	102.4	0.000	2.61	ok, afternoon
53	07-Feb-11	Al2O3 - 0.001%	SS316L	1.17	1,511	45	103.7	102.7	0.000	3.10	ok
54	08-Feb-11	Al2O3 - 0.001%	SS316L	1.12	1,565	45	102.6	102.4	0.001	2.82	ok, 3d
										2.84	Average
55	09-Feb-11	Al2O3 - 0.001%	SS316L	1.17	516	60	103.8	102.6	0.001	1.64	ok
56	11-Feb-11	Al2O3 - 0.001%	SS316L	1.16	516	60	103.5	103.5	0.002	1.73	ok
										1.69	Average
57	15-Feb-11	Al2O3 - 0.001%	SS316L	3.07	973	45	134.0	134.3	0.006	3.42	ok
58	17-Feb-11	Al2O3 - 0.001%	SS316L	3.02	960	45	133.5	133.5	0.003	3.25	ok
										3.34	Average
59	16-Feb-11	Al2O3 - 0.001%	SS316L	3.17	503	45	135.1	135.1	0.010	2.59	ok
60	18-Feb-11	Al2O3 - 0.001%	SS316L	1.12	1,006	45	102.5	102.2	0.001	2.32	Boiling ~1hr = 54min
61	22-Feb-11	Al2O3 - 0.001%	SS316L	1.09	999	45	101.9	101.4	-0.003	2.21	Boiling ~1hr = 40min
										2.27	Average
62	24-Feb-11	Al2O3 - 0.001%	SS316L	1.07	1,036	45	101.2	101.5	0.003	1.86	Boiling - 28 min
63	25-Feb-11	Al2O3 - 0.001%	SS316L	1.15	903	45	103.2	102.9	0.003	2.13	Boiling - 31 min
										2.00	Average
64	02-Mar-11	Al2O3 - 0.001%	SS316L	1.18	1,022	45	103.9	103.2	0.001	2.43	Boiling - 29 min
65	04-Mar-11	Al2O3 - 0.001%	SS316L	1.20	1,014	45	104.5	103.9	0.001	2.64	Boiling - 20 min
										2.54	Average

66	09-Mar-11	Al2O3 - 0.01%	SS316L	1.17	966	45	103.7	102.6	0.000	2.53	ok
67	22-Mar-11	Al2O3 - 0.01%	SS316L	1.13	1,022	45	102.8	102.5	0.001	2.68	ok, cut for SEM & EDS
										2.61	Average
68	25-Mar-11	Al2O3 - 0.001%	SS316L	5.14	966	45	152.7	153.0	0.011	4.61	ok
69	01-Apr-11	Al2O3 - 0.001%	SS316L	5.10	983	45	152.4	152.3	0.006	4.25	ok
										4.43	Average
70	15-Apr-11	DI water	SS316L	1.09	839	45	101.9	101.4	0.001	1.37	Boiling - 36 min
75	27-Apr-11	DI water	SS316L	1.07	982	45	101.4	100.3	-0.001	1.31	Boiling - 29 min
										1.34	Average
71	19-Apr-11	DI water	SS316L	3.12	997	45	134.6	134.6	0.003	2.36	ok
72	20-Apr-11	DI water	SS316L	3.07	914	45	134.0	134.1	0.004	2.49	ok
										2.43	Average
73	22-Apr-11	DI water	SS316L	5.02	1,006	45	151.8	151.7	0.003	2.94	ok
74	25-Apr-11	DI water	SS316L	5.11	986	45	152.4	152.4	0.003	3.13	ok
										3.04	Average
77	13-Jul-11	DI water	SA-508	1.20	997	45	104.4	104.4	0.002	2.03	ok
78	15-Jul-11	DI water	SA-508	1.19	998	45	104.0	104.0	0.002	2.42	ok
79	19-Jul-11	DI water	SA-508	1.20	1,008	45	104.4	104.1	0.001	2.41	ok
										2.29	Average
80	21-Jul-11	DI water	SS316L - Oxidized	1.16	1,015	45	103.4	103.3	0.001	2.00	Ok
81	22-Jul-11	DI water	SS316L - Oxidized	1.11	959	45	102.3	100.7	-0.001	1.95	Ok
										1.98	Average
82	26-Jul-11	Al2O3 - 0.001%	SA-508	1.14	987	45	103.1	102.5	0.001	2.41	Ok
83	28-Jul-11	Al2O3 - 0.001%	SA-508	1.18	997	45	104.0	104.0	0.002	2.40	Ok
										2.41	Average
84	6-Sep-11	DI water	SS316L - Oxidized	1.09	998	45	101.9	102.0	-0.002	2.45	Ok
85	7-Sep-11	DI water	SS316L - Oxidized	1.09	1,015	45	101.7	100.2	-0.002	2.36	Ok
										2.41	Average

11.2.1 Summary of Enhancement of Downward Facing CHF

To quantify the CHF enhancement between DI water and alumina nanofluid, sets of experimental tests that represent target conditions are grouped and averaged. Sets are at least two (2) tests. If a test result is deemed an outlier to the overall data, it is excluded from the average and noted in the table. The averaged values are then compared to determine relative enhancement (ratio) and absolute (difference) CHF enhancement (see Table 11-4). Nineteen (19) paired sets representing eighty (80) tests are reviewed. Sixteen (16) sets address SS316L with normal preparation and SA-508 and oxidized SS316L are the remaining.

For the data related to normally prepared SS316L the following are the general statistics for relative CHF enhancement:

- Minimum 17%
- Maximum 108%
- Average 70%
- Standard Deviation 28%

The minimum CHF enhancement is 17% for: atmospheric pressure, mass flux of 500 kg/m^2-s, and vertical (θ=90^o) inclination. The maximum CHF enhancement is 108% for: atmospheric pressure; mass flux of 1,500 kg/m^2-s, and vertical (θ=90^o) inclination.

For the data related to normally prepared SA-508 the conditions tested were: atmospheric pressure; mass flux of 1,000 kg/m^2-s, and downward facing inclination of 45^o. The DI water CHF average was ~2.4 MW/m^2, which is very near the value for SS316L with nanofluid of ~2.5 MW/m^2. No CHF enhancement with alumina nanofluid was measured, also at ~2.4 MW/m^2.

Oxidized SS316L had the same conditions as the SA-508. The DIW average CHF of ~2.0 MW/m^2 is 51% higher than normally prepared SS316L in DI water. The alumina 0.001% average CHF of ~2.4 MW/m^2 is 83% higher than normally prepared SS316L in DI water. The additional 32% enhancement can be attributed to the alumina nanofluid.

Table 11-4: CHF Enhancement from Pairing of Sets

Run #	Fluid	Surface Material	Exit Pressure [Bar]	Mass Flux [Kg/m^2-s]	Angle [Degree]	Measured CHF [MW/m^2]	Notes	Run #	Exit Pressure [Bar]	Mass Flux [Kg/m^2-s]	Angle [Degree]	Measured CHF [MW/m^2]	Notes	Relative CHF Enhancment	Absolute CHF Enhancement [MW/m^2]
								2	1.07	481	90	1.11	ok, not in avg		
								3	1.08	540	90	1.57	ok		
34	Al2O3 - 0.001%	SS316L	1.06	512	90	1.78	ok	4	1.14	537	90	1.08	ok, not in avg		
35	Al2O3 - 0.001%	SS316L	1.07	508	90	1.76	ok	76	1.03	509	90	1.46	ok		
						1.77	Average					1.52	Average	1.17	0.26
36	Al2O3 - 0.001%	SS316L	1.15	512	45	1.50	ok								
37	Al2O3 - 0.001%	SS316L	1.14	623	45	1.25	ok								
38	Al2O3 - 0.001%	SS316L	1.00	500	45	1.40	ok, morning	9	1.09	483	45	0.97	ok		
39	Al2O3 - 0.001%	SS316L	1.15	507	45	1.35	ok, afternoon	10	1.06	498	45	0.88	ok		
						1.38	Average					0.93	Average	1.49	0.45
40	Al2O3 - 0.001%	SS316L	1.15	547	0	1.06	ok	15	1.06	581	0	0.58	ok		
41	Al2O3 - 0.001%	SS316L	1.17	574	0	1.12	ok	16	1.06	658	0	0.53	ok		
						1.09	Average					0.56	Average	1.96	0.54
								5	1.16	1,011	90	1.35	ok		
42	Al2O3 - 0.001%	SS316L	1.17	1,037	90	2.73	ok	6	1.10	996	90	1.70	ok		
43	Al2O3 - 0.001%	SS316L	1.16	1,062	90	2.76	ok	26	1.13	982	90	1.74	ok		
						2.75	Average					1.60	Average	1.72	1.15
44	Al2O3 - 0.001%	SS316L	1.18	1,025	45	2.55	ok	11	1.04	1,023	45	1.28	ok		
45	Al2O3 - 0.001%	SS316L	1.16	992	45	2.51	ok	12	1.06	985	45	1.33	ok		
						2.53	Average					1.31	Average	1.94	1.23
								19	1.11	1,010	0	1.32	ok		
46	Al2O3 - 0.001%	SS316L	1.14	1,038	0	2.16	ok	20	1.15	1,037	0	1.11	ok		
47	Al2O3 - 0.001%	SS316L	1.16	1,015	0	2.08	ok	21	1.09	1,021	0	1.15	ok		
						2.12	Average					1.19	Average	1.78	0.93
								22	1.12	1,498	0	1.28	ok		
48	Al2O3 - 0.001%	SS316L	1.14	1,537	0	2.92	ok	23	1.10	1,493	0	1.60	ok		
49	Al2O3 - 0.001%	SS316L	1.14	1,565	0	2.80	ok	24	1.11	1,496	0	1.50	ok		
						2.86	Average					1.46	Average	1.96	1.40
50	Al2O3 - 0.001%	SS316L	1.12	1,552	90	3.16	ok	7	1.11	1,532	90	1.50	ok		
51	Al2O3 - 0.001%	SS316L	1.14	1,531	90	3.09	ok	25	1.11	1,476	90	1.50	ok		
						3.13	Average					1.50	Average	2.08	1.63
52	Al2O3 - 0.001%	SS316L	1.13	1,526	45	2.61	ok, afternoon								
53	Al2O3 - 0.001%	SS316L	1.17	1,511	45	3.10	ok	27	1.13	1,507	30	1.60	ok		
54	Al2O3 - 0.001%	SS316L	1.12	1,565	45	2.82	ok, 3d	28	1.10	1,505	30	1.63	ok		
						2.84	Average					1.62	Average	1.76	1.23

Run #	Fluid	Surface Material	Exit Pressure [Bar]	Mass Flux [Kg/m^2-s]	Angle [Degree]	Measured CHF [MW/m^2]	Notes	Run #	Exit Pressure [Bar]	Mass Flux [Kg/m^2-s]	Angle [Degree]	Measured CHF [MW/m^2]	Notes	Relative CHF Enhancment	Absolute CHF Enhancement [MW/m^2]
55	Al2O3 - 0.001%	SS316L	1.17	516	60	1.64	ok	32	1.11	508	60	1.22	ok		
56	Al2O3 - 0.001%	SS316L	1.16	516	60	1.73	ok	33	1.17	513	60	1.28	ok		
						1.69	Average					1.25	Average	1.35	0.44
57	Al2O3 - 0.001%	SS316L	3.07	973	45	3.42	ok	72	3.12	997	45	2.36	ok		
58	Al2O3 - 0.001%	SS316L	3.02	960	45	3.25	ok	73	3.07	914	45	2.49	ok		
						3.34	Average					2.43	Average	1.38	0.91
60	Al2O3 - 0.001%	SS316L	1.12	1,006	45	2.32	Boiling = 54min	11	1.04	1,023	45	1.28	saturation, ok		
61	Al2O3 - 0.001%	SS316L	1.09	999	45	2.21	Boiling = 40min	12	1.06	985	45	1.33	saturation, ok		
						2.27	Average					1.31	Average	1.74	0.96
62	Al2O3 - 0.001%	SS316L	1.07	1,036	45	1.86	Boiling - 28 min	70	1.09	839	45	1.37	Boiling - 36 min		
63	Al2O3 - 0.001%	SS316L	1.15	903	45	2.13	Boiling - 31 min	75	1.07	982	45	1.31	Boiling - 29 min		
						2.00	Average					1.34	Average	1.49	0.66
64	Al2O3 - 0.001%	SS316L	1.18	1,022	45	2.43	Boiling - 29 min	70	1.09	839	45	1.37	Boiling - 36 min		
65	Al2O3 - 0.001%	SS316L	1.20	1,014	45	2.64	Boiling - 20 min	75	1.07	982	45	1.31	Boiling - 29 min		
						2.54	Average					1.34	Average	1.89	1.20
66	Al2O3 - 0.01%	SS316L	1.17	966	45	2.53	ok	11	1.04	1,023	45	1.28	ok		
67	Al2O3 - 0.01%	SS316L	1.13	1,022	45	2.68	ok	12	1.06	985	45	1.33	ok		
						2.61	Average					1.31	Average	2.00	1.30
68	Al2O3 - 0.001%	SS316L	5.14	966	45	4.61	ok	74	5.02	1,006	45	2.94	ok		
69	Al2O3 - 0.001%	SS316L	5.10	983	45	4.25	ok	75	5.11	986	45	3.13	ok		
						4.43	Average					3.04	Average	1.46	1.40
								77	1.20	997	45	2.03	ok, not in avg		
82	Al2O3 - 0.001%	SA-508	1.14	987	45	2.41	ok	78	1.19	998	45	2.42	ok		
83	Al2O3 - 0.001%	SA-508	1.18	997	45	2.40	ok	79	1.20	1,008	45	2.41	ok		
						2.41	Average					2.42	Average	1.00	-0.01
80	DI water	SS316L - Oxidized	1.16	1,015	45	2.00	ok	11	1.04	1,023	45	1.28	ok		
81	DI water	SS316L - Oxidized	1.11	959	45	1.95	ok	12	1.06	985	45	1.33	ok		
						1.98	Average					1.31	Average	1.51	0.67
84	Al2O3 - 0.001%	SS316L - Oxidized	1.09	998	45	2.45	ok	11	1.04	1,023	45	1.28	ok		
85	Al2O3 - 0.001%	SS316L - Oxidized	1.09	1,015	45	2.36	ok	12	1.06	985	45	1.33	ok		
						2.41	Average					1.31	Average	1.84	1.10

Number of Sets	19	SS - Maximum	2.08	1.63
Number of Test	80	SS - Minmum	1.17	0.26
		SS - Average	1.70	0.98
		SS - Standard Deviation	0.28	0.41

Three tests where characterized as outliers and not included in averages that are used for determination of CHF enhancement: Run #2, Run #4, and Run #77.

Run #2 and #4 resulted in CHF values that were not only significantly less than Run #3 and #76 of the same conditions of DI water, SS316L surface material, atmospheric pressure, 500 kg/m^2-s mass flux, and 90^o, but also less than the tests at 60^o with the same conditions (see Figure 11-2: CHF versus Downward Facing Angle (G=500 kg/m^2-s)). Overall test data support increasing CHF with inclination angle. For these reasons the two tests were deemed not indicative and characterized as outliers.

Run #77 has conditions of SA-508 surface material, DI water, atmospheric pressure, 1000 kg/m^2-s mass flux, and downward facing angle of 45^o. The measured CHF of 2.03 MW/m^2 was significantly less than Run #78 and #79 that averaged 2.42 MW/m^2 and sits on the Peirce's criterion for exclusion and deemed an outlier [88].

11.2.2 Influence of Mass Flux on Downward Facing CHF

To visualize CHF and mass flux dependence, SS316L data at atmospheric condition is plotted. The scatter of the DI water and alumina data represent variance in angle that is discussed in more detail in the next section (see Figure 11-1).

Figure 11-1: Graph of CHF [q''_{chf}] Plotted against Mass Flux [G]

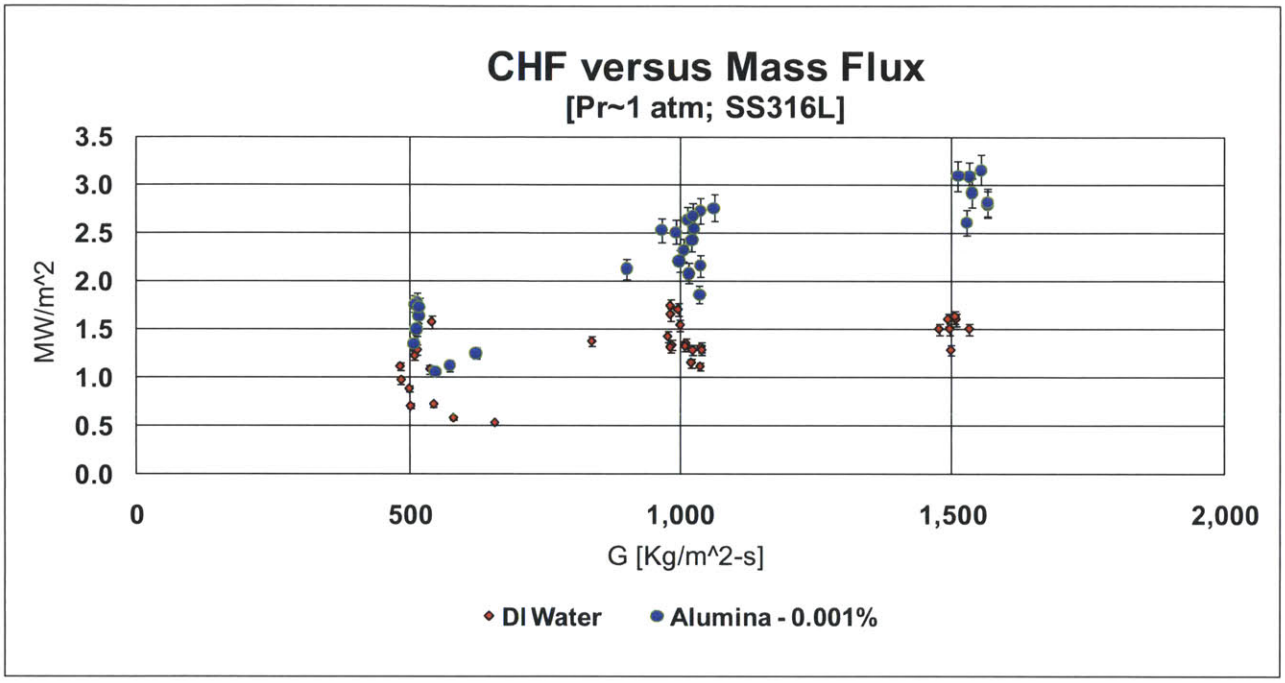

As expected CHF increases with mass flux for both water and alumina. Note a previous MIT study by Dr. S.J. Kim also measured higher CHF enhancement with increased mass flux for tube geometry [14]. Enhancement of CHF is noted for all matched conditions. Further discussion of theory, previous studies, and correlations is found in the following chapter 12.

11.2.3 Influence of Angle on Downward Facing CHF

To visualize CHF and downward facing angle, θ, dependence, SS316L data at atmospheric condition is plotted for all mass fluxes tested (see Figure 11-2, Figure 11-3, and Figure 11-4). For all three mass flux levels the variation of CHF with downward facing angle, θ, is smooth.

Figure 11-2: CHF versus Downward Facing Angle (G=500 kg/m^2-s)

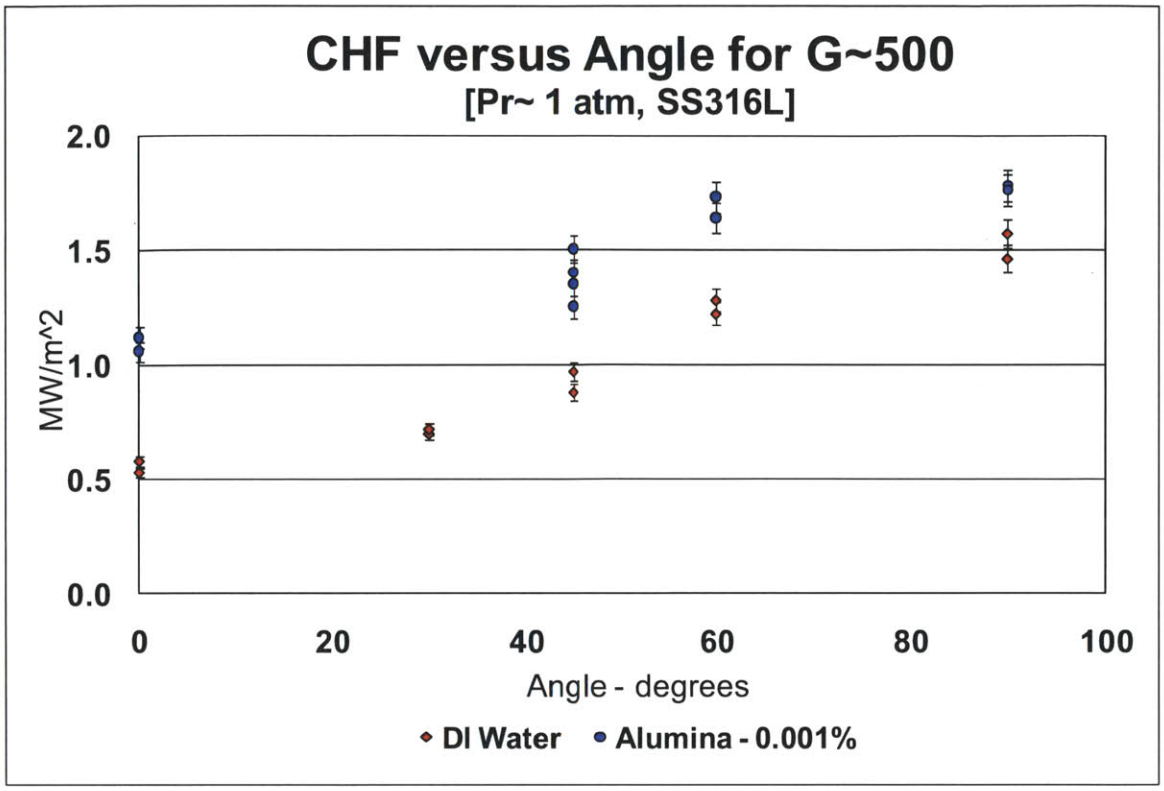

Figure 11-3: CHF versus Downward Facing Angle (G=1,000 kg/m^2-s)

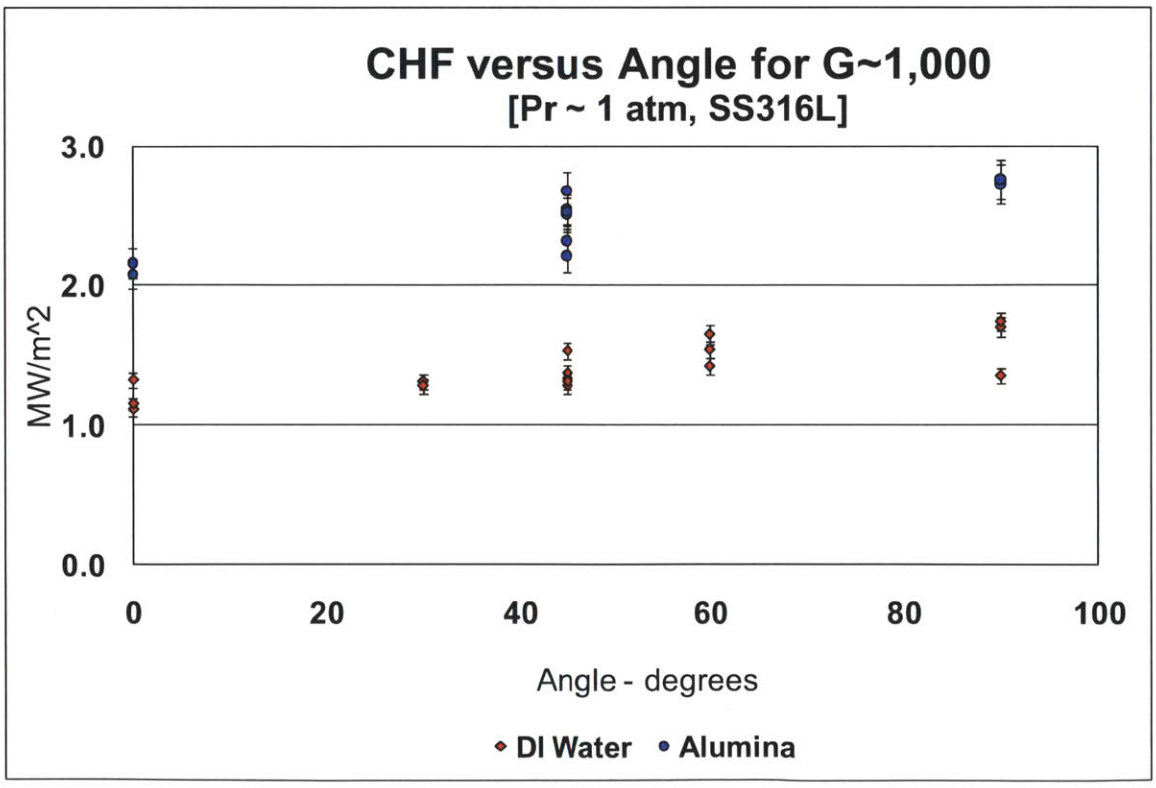

Figure 11-4: CHF versus Downward Facing Angle (G=1,500 kg/m^2-s)

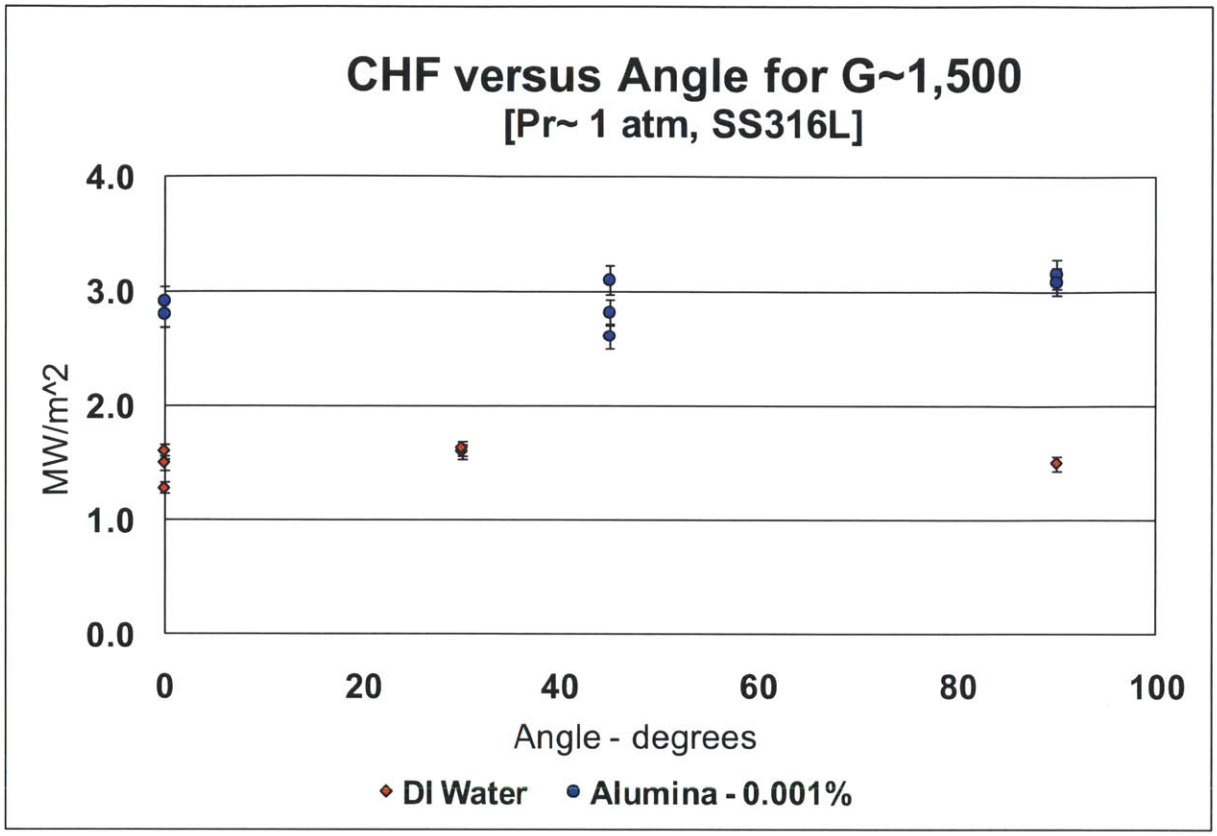

For a given mass flux and pressure, CHF increases as downward facing angle increases. At horizontal (0°), which represents the bottom of the reactor pressure vessel, CHF is a minimum. CHF increases smoothly and fairly linearly to a maximum at vertical (90°). The influence that angle has on CHF diminishes as mass flux increases. For the lowest mass flux of 500 kg/m^2-s the DI water CHF nearly triples from ~0.5 MW/m^2 at horizontal to ~1.5 MW/m^2 for vertical. For the mass flux of 1,000 kg/m^2-s the DI water CHF increases about 60% from ~1.2 MW/m^2 at horizontal to ~1.8 MW/m^2 for vertical. For the highest mass flux of 1500 kg/m^2-s the angular dependence of CHF nearly disappears as momentum dominates buoyancy force. Froude numbers (the ratio of inertia to gravitational forces) for mass fluxes of 500, 1000 and 1500 kg/m^2-s are 1.3, 5.1 and 11.5, respectively.

CHF enhancement exists in all cases for SS316L. For the lowest mass flux the relative CHF enhancement declines with increasing angle from 96% at horizontal to a minimum of about 17%

at vertical. The two (2) higher mass fluxes show little or no CHF enhancement dependence on angle. At mass flux of 1,000 kg/m^2-s, CHF enhancement varies from 78% at horizontal to 94% at 45o then to 72% at vertical inclination angle. For the highest mass flux of 1,500 kg/m^2-s the relative CHF enhancement is ~96% at horizontal and 108% in vertical orientation.

11.2.4 Influence of Pressure on Downward Facing CHF

To visualize CHF and pressure dependence, SS316L data is plotted for mass flux of 1,000 kg/m^2-s and downward facing angle of 45^o (see Figure 11-5). Pressure is at the test section exit.

Figure 11-5: CHF versus Pressure

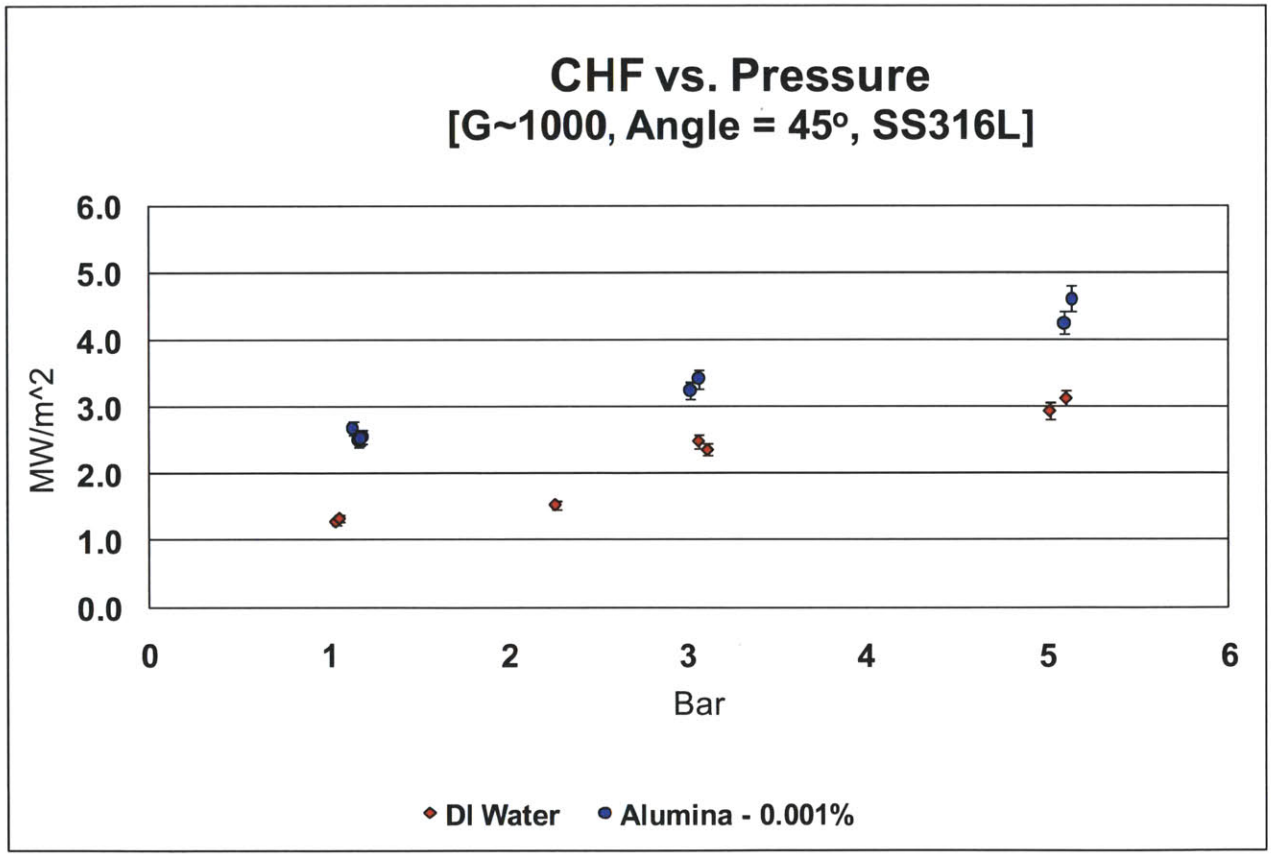

CHF increases with increasing pressure both for water and alumina nanofluid, as would be expected from theory for these modest pressures. Variation is smooth and linear over the range tested for both working fluids. Relative CHF enhancement decreases with increasing pressure, but absolute enhancement is fairly constant. Relative CHF enhancement is the ratio of nanofluid

CHF to DI water CHF of analogous conditions. Absolute is nanofluid CHF less DI water CHF of analogous conditions.

For exit pressure increasing from 1 bar to 5 bar, the relative CHF enhancement declines from 94% to 46%, respectively. Absolute CHF enhancement over the same range remains fairly constant going from ~1.2 MW/m^2 to ~1.4 MW/m^2.

11.2.5 Influence of Boiling Time on Downward Facing CHF

Most experiments involve in excess of 1 ½ hours of boiling during the procedure. To quantify the influence of boiling time, the normal test procedure was modified so to limit heater surface boiling time. This limitation on boiling time was mainly accomplished by utilizing the pre-heater mounted on the loop to provide a larger fraction of the energy during degassing and heat-up to CHF. The heater thermocouples on the back of the sample were monitored to insure that the heater surface temperature stayed below saturation.

Figure 11-6: CHF versus Boiling Time

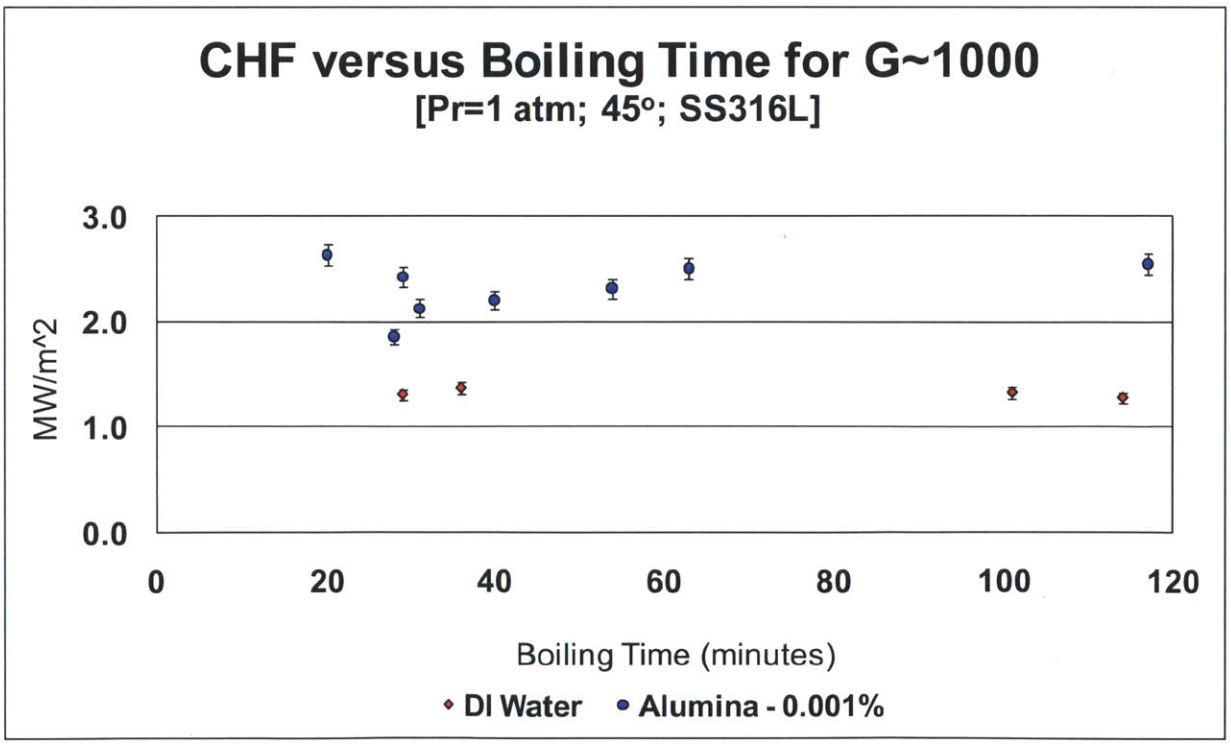

Eight (8) limited boiling tests were run with total boiling times from 20 to 54 minutes (see Figure 11-6). Test conditions where: atmospheric pressure; mass flux equal 1000 kg/m^2-s; downward facing angle of 45°; and SS316L. Six (6) were with alumina 0.001% nanofluid and two (2) with DI water. Operationally it is difficult to reduce the boiling time even further. The data points above 100 minutes are from regular tests previously reported.

The above graph indicates that CHF enhancement is not reduced for the lower boiling times tested, although the reduced boiling times result in larger data scatter. Basically, ½ hour of boiling with alumina 0.001% nanofluid is enough to deposit sufficient nanoparticles onto the surface and enhance CHF. Reduced boiling time for water also had no affect on CHF, as expected.

11.2.6 Influence of Nanofluid Concentration on Downward Facing CHF

To visualize nanofluid CHF dependence on concentration, SS316L data at atmospheric condition is plotted for mass flux of 1,000 kg/m^2-s and downward facing angle of 45° (see Figure 11-7). Only two alumina nanofluid concentrations were CHF tested: 0.001% and 0.01% by volume.

Figure 11-7: CHF versus Nanofluid Concentration

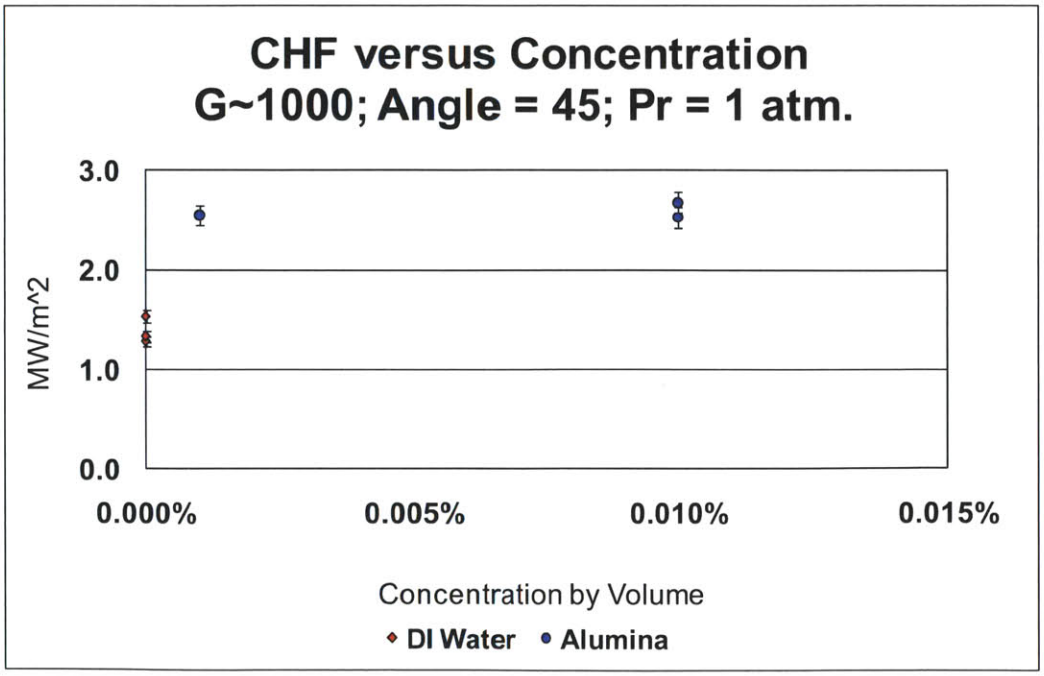

The data indicate that once at least 0.001% by volume of alumina is present in the working fluid, no further CHF enhancement results from increasing concentration by one order of magnitude, 10x.

11.2.7 Influence of Surface Material on Downward Facing CHF

Two surface materials were tested: (1) stainless steel 316L and (2) SA-508. Most experiments were completed with SS316L. Six (6) experiments were completed with SA-508. Four (4) of the SS316L tests had an oxidized surface preparation. Test conditions for SA-508 and oxidized SS316L where: atmospheric pressure; mass flux of 1000 kg/m^2-s; and downward facing angle of 45^o. A bluish tint oxidation of SS316L was achieved by baking a normally prepared surface including sandblasting at 800 ^{o}C for an hour.

Figure 11-8: CHF versus Surface

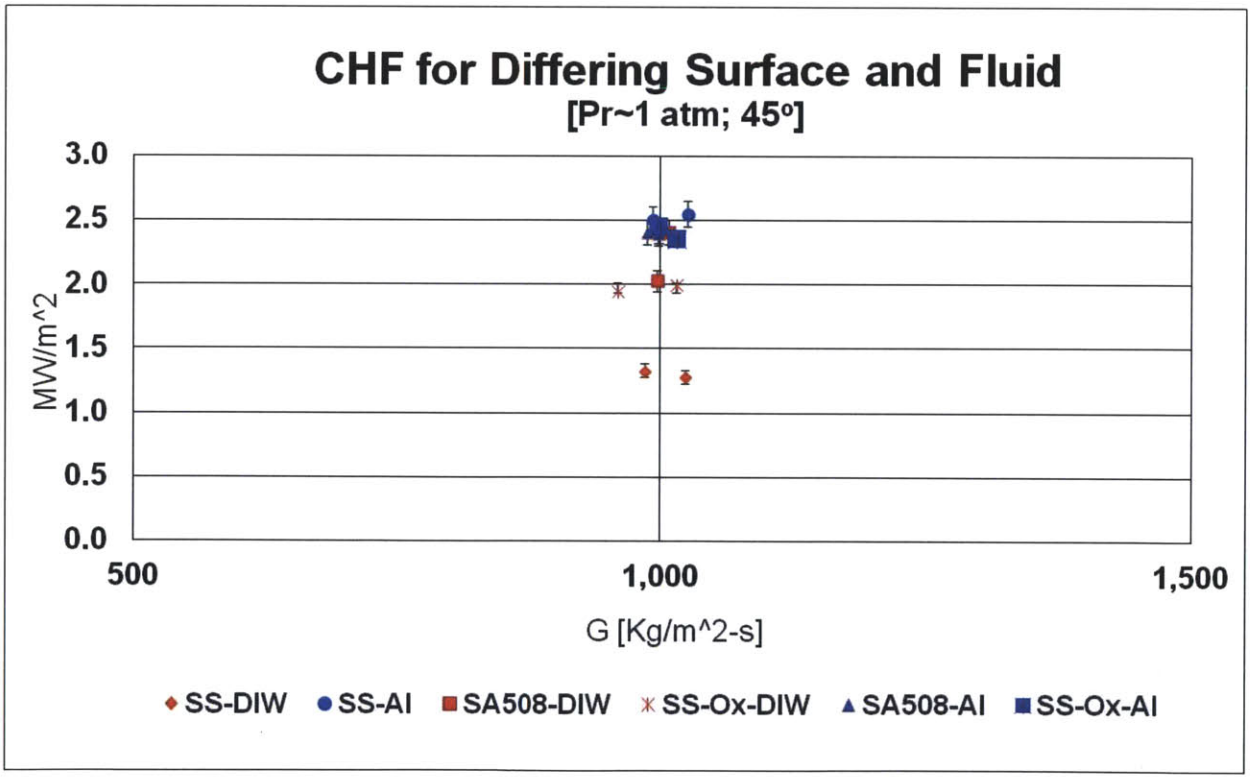

For the SA-508 cases with DI water (3) and alumina at 0.001% (2), the CHF levels are basically the same as SS316L with alumina. Specifically, the SS316L cases with water have an average

CHF of ~1.3 MW/m^2 and ~2.5 MW/m^2 with alumina at 0.001%. This represents a ~94% CHF enhancement. The SA-508 water cases (3) average 2.3 MW/m^2 and 2.4 MW/m^2 if the lowest case is excluded. SA-508 cases (2) with alumina at 0.001% also average 2.4 MW/m^2. These SA-508 CHF results are only 4% less than SS316L with alumina nanofluid, which is within the experimental uncertainty. Additionally, the presence of alumina nanofluid does not improve CHF for SA-508.

These SA-508 results indicate that the heavy oxidation that occurs on the material surface provides CHF enhancement to a similar level as alumina nanofluid on SS316L. Note that the SA-508 oxidation is pervasive, not only coating the flow facing surface, but also the back of the heater and the coupling studs (see Figure 11-9). Consistent with these results, contact angle measurements for SA-508 are similar to SS316L after boiling with alumina nanofluid (see chapter 8). Before the SA-508 CHF test the heater is clean.

Figure 11-9: Photo of SA508 Heaters: CHF Test (left) and Plain (right)

The oxidation seems to dominate the surface and its influence on wettability, roughness, and porosity. Increased roughness could also contribute to the higher CHF. The nanofluid does not seem to further increase these factors or CHF compared to water.

It is likely the joule heating method helps accelerate the rate of oxidation on the SA-508 heater surface. It is well known that electrical potential drives oxidation rates. Voltage drop during boiling are several volts. Potential of only mV are needed for oxidation.

For IVR the question then becomes how much oxidation would be present during the event. Oxidation seems to be a benefit to CHF relative to a clean surface and nanofluid does not lower it. If little or no oxidation is present on the lower head then the nanofluid is likely to increase CHF, though not tested herein. If high oxidation on SA-508 is already present, the alumina would have little or no influence on CHF.

CHF testing of SA-508 with cartridge in contact heating could be used to remove the influence of elevated voltage at the surface fluid interface and will be a recommendation for future work.

To quantify how oxidation impacts CHF on SS316L, four (4) tests were done. These four (4) heaters started with normal preparation and then were baked in a furnace at 800 ^{o}C for one hour (see Figure 11-10). The oxidized SS316L heaters were CHF tested in DI water. The resulting DI water CHF averaged 2 MW/m^2, a value that sits between 1.3 MW/m^2 for normally prepared SS316L in DI water and 2.5 MW/m^2 for normally prepared SS316L with alumina 0.001% nanofluid. The CHF enhancement is ~53% for the oxidized SS316L heater in water compared to 94% for normal SS316L heater in alumina 0.001% nanofluid. Oxidized SS316L was also tested with alumina 0.001%. The resulting average CHF was 2.4 MW/m^2. This represents a 83% enhancement above normally prepared SS316L with DI water and 32% enhancement above the oxidized SS316L with DI water. These measurements support additional CHF enhancement from alumina nanofluid on oxidized or partially oxidized SS316L surfaces approaching values obtained for normally prepared surface with alumina nanofluid.

Figure 11-10: Photo SS316L Heaters: Oxidized Preparation CHF Test (left) and Normal Preparation (right)

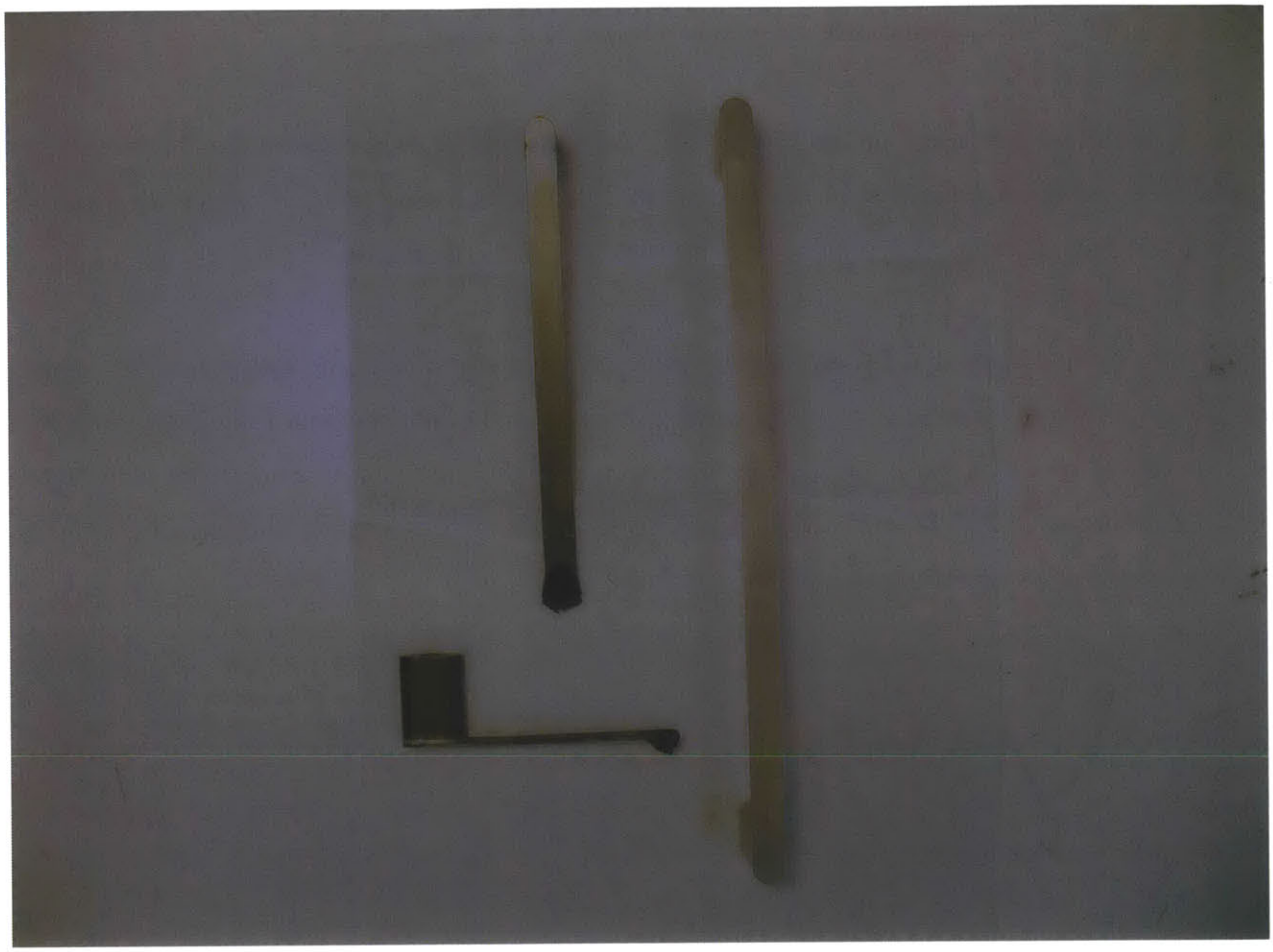

11.3 Visualization

Visualization of the boiling development and CHF is possible with front and back windows designed into the test section (see Figure 6-4: Photo of Test Section Void near CHF Conditions).

11.3.1 Visual Commentary of CHF

CHF is visually identified by the development of an orange dot (> 1,000 °C) on the heater surface. The orange dot starts as a point and spreads in all directions to about 5 cm (2") in length and covering the entire 1 cm width. From first visual identification of the orange dot to sample

failure is less than 5 seconds. If the power is turned off quickly once the orange dot is seen the sample may stay in one piece. Otherwise, the sample will break into two pieces. At very high heat fluxes the sample may break into three pieces; which happened twice.

The location of CHF is nearly always near the flow exit of test section. Specifically, within a couple inches of the heater stud into which the electrode is connected. This section of the test heater has the highest fluid enthalpy. CHF at the top is not always the case with both middle and lower burnout locations occasionally being observed. For nanofluid cases this may be related to how the nanoparticles coated the surface. If in a particular test the higher boiling near the top caused relatively more nanoparticles to deposit compared to lower on the sample, CHF may then occur near this lower region of the heater.

11.3.2 Visualization of Void Fraction

For water-only tests the void fraction development along the heater surface looks like a wedge. The voiding starts right after the entrance heater stud. The maximum void fraction is at the end of the plate portion of the heater. Notably the interface between void and liquid away from the heater is fairly stable and looks like a smooth line that outlines the wedge shape. At CHF the exit void fraction visually is estimated at 70% for all cases tested herein. The precision of this visual observation might be +/- 5%.

It is also noted that the water level in the accumulator near CHF is a couple inches below the midline. This observation can be made by running a finger along the accumulator surface near the condition of CHF. The surface temperature of the accumulator jumps at the water level line. This position represents 40% of the accumulator total volume of 6 liter (1.6 gallons). The 2.4 liter (0.64 gallon) displacement from void implies single phase is achieved within the condenser.

11.4 High Sub-cooling CHF Experiment

One high sub-cooling (T_{sub}=50 °C) experiment was completed with the help of PhD candidate Eric Forrest that takes advantage of the two-phase loop capabilities (see Table 11-5). High speed camera work was completed as part of Eric's studies. Target DI water conditions were atmospheric pressure; mass flux of 1,000 kg/m^2-s; and vertical orientation.

Table 11-5: High Sub-cooling CHF Test Measurements

Description	Condition	Units/notations
Material	SS316L	Sandblast preparation
Fluid	DI Water	Degassing completed
Inclination angle	90	degrees
Pressure	1.0	bar
Mass Flux	1,003	kg/m^2-s
Exit Sub-cooling	50	°C
Exit quality	-0.09	
CHF	5.2	MW/m^2

As with most other CHF tests the location was near the flow exit (top).

12 IVR Studies with Water and Other CHF Correlations

A number of experimental investigations have been completed with associated methods development that relate to IVR and external vessel cooling [89][90]. Studies have covered both general conditions of downward facing surfaces and specific reactor design geometries [91]. Designs that have been analyzed include: Westinghouse AP600 and AP1000, Korean APR1400, and Russian VVER-440.

Three (3) studies are most relevant to IVR:

- University of California, Santa Barbara ("UCSB")
- Penn State University ("PSU"), and
- Sultan Facility, Grenoble, France.

Notably the UCSB work is a primary reference for licensing of the Westinghouse AP600 and AP1000 for beyond design basis IVR accident analysis.

Work done at the Sultan facility in France and the UCSB studied the IVR heat transfer with water utilizing a two-phase flow loop [72]. Other studies, including work at PSU, have utilized pool based natural convection only with both plain and coated surfaces [15]. All three studies addressed angular dependence and sub-cooling dependence of CHF [92]. Pressures studied were generally low (1-2 atmospheres), though Sultan work covered up to 5 bar [17]. From some of these experimental studies CHF correlations were developed are described in the flowing section.

In the literature numerous studies can be found that apply to portions of the IVR conditions including channels and flat heaters [93][94][95][96][97][98][99][100][101][102][103] [104][105] [106][107][108]. Two described herein are: 2006 lookup table and Sudo.

Comparisons are made between these five (5) studies and herein measured CHF data for DI water.

12.1 UCSB

The experimental apparatus built at UCSB was a two phase flow loop that emulated the flow path along the outer reactor vessel (see Figure 12-1). The flow was natural circulation (see Figure 12-2) [109]. Two series of experiments became part of the licensing for Westinghouse designs: Configuration I-III for the AP600 and Configuration V for the AP1000. Due to geometry changes for the AP1000 particularly in the gap region and higher power the expected volumetric flow rate and expected CHF are higher for the AP1000 compared to the AP600.

Figure 12-1: Schematic of UCSB ULPU-2000 for AP600 Flow Loop.

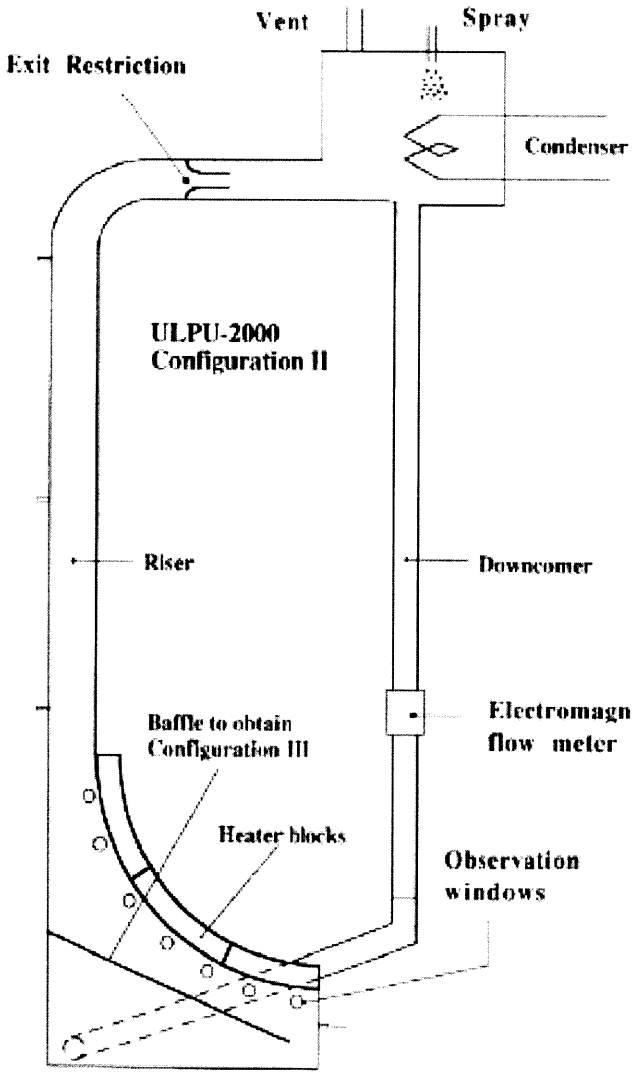

Figure 12-2: Schematic of UCSB ULPU-2400 for AP1000 Flow Loop.

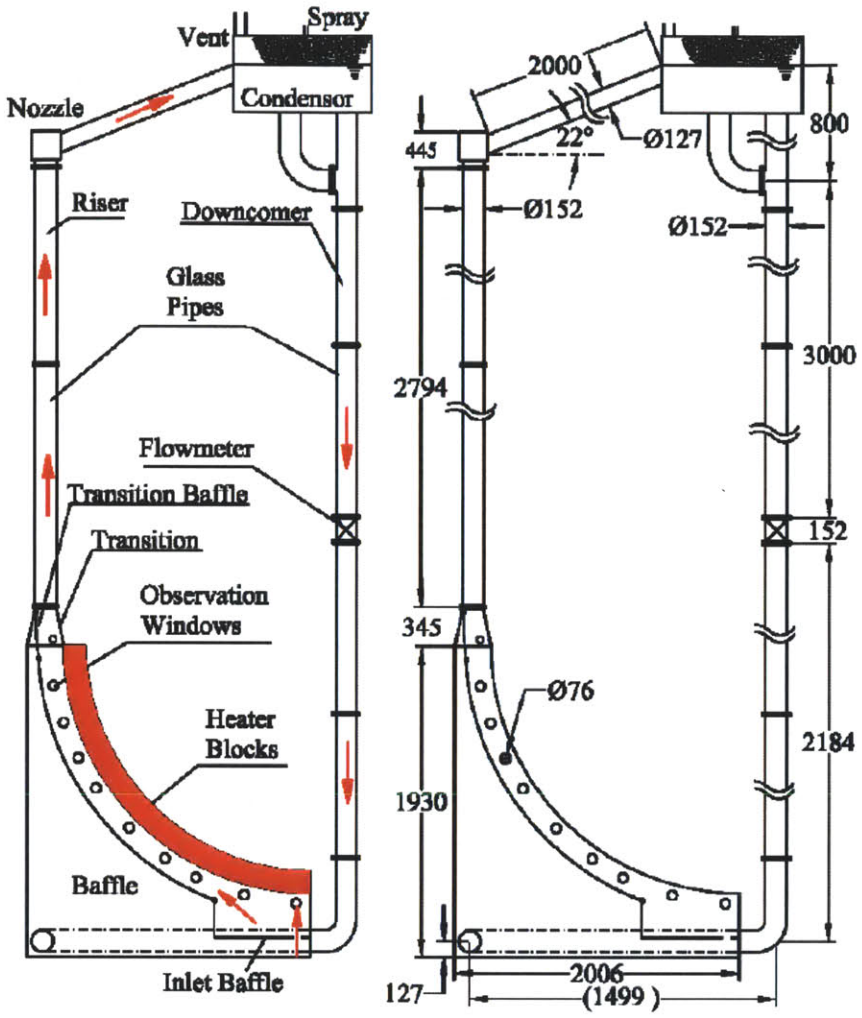

Flow traveled along a quarter-circle with ~2 m radius representing the bottom of the vessel with heat from above. The channel width along the heated area was 15.24 cm. Next flow travelled up a riser (~4m). From the riser flow passed through a fitting designed to have flow resistance similar to the AP1000. The circuit then passed the two-phase water to a condenser. Pressure within the condenser was atmospheric. Out of the condenser the flow travelled a down to the bottom of the apparatus to complete the loop.

Heat along the bottom was provided by cartridges inserted to copper blocks. The loop was instrumented with temperature, pressure and flow measurement devices.

The AP600 configurations had a flow gap of 6" or more along the lower surface. The associated mass flux was approximately 340 kg/m^2-s near the top of the heated length. The resulting CHF data was correlated as a function of angle for the AP600 [5].

$$q''_{chf}(\theta) = 490 + 30.2 \cdot \theta - 0.888 \cdot \theta^2 + 1..35 \cdot 10^{-3} \cdot \theta^3 - 6.65 \cdot 10^{-5} \cdot \theta^4 \qquad \text{Eq. 5.6}$$

Where:

θ	=	Inclination angle (vertical – 90°)
q"chf(θ)	=	Critical heat flux [kW/m^2]

Experimental results for water at atmospheric pressure with mass flux of 500 kg/m^2-s show good agreement to UCSB correlation (see Figure 12-3). CHF levels and trends are highly comparable. For the eight (8) cases compared the standard deviation was 14%.

Figure 12-3: Graph of UCSB AP600 Correlation and G=500 kg/m^2-s CHF Data for water at Atmospheric Conditions

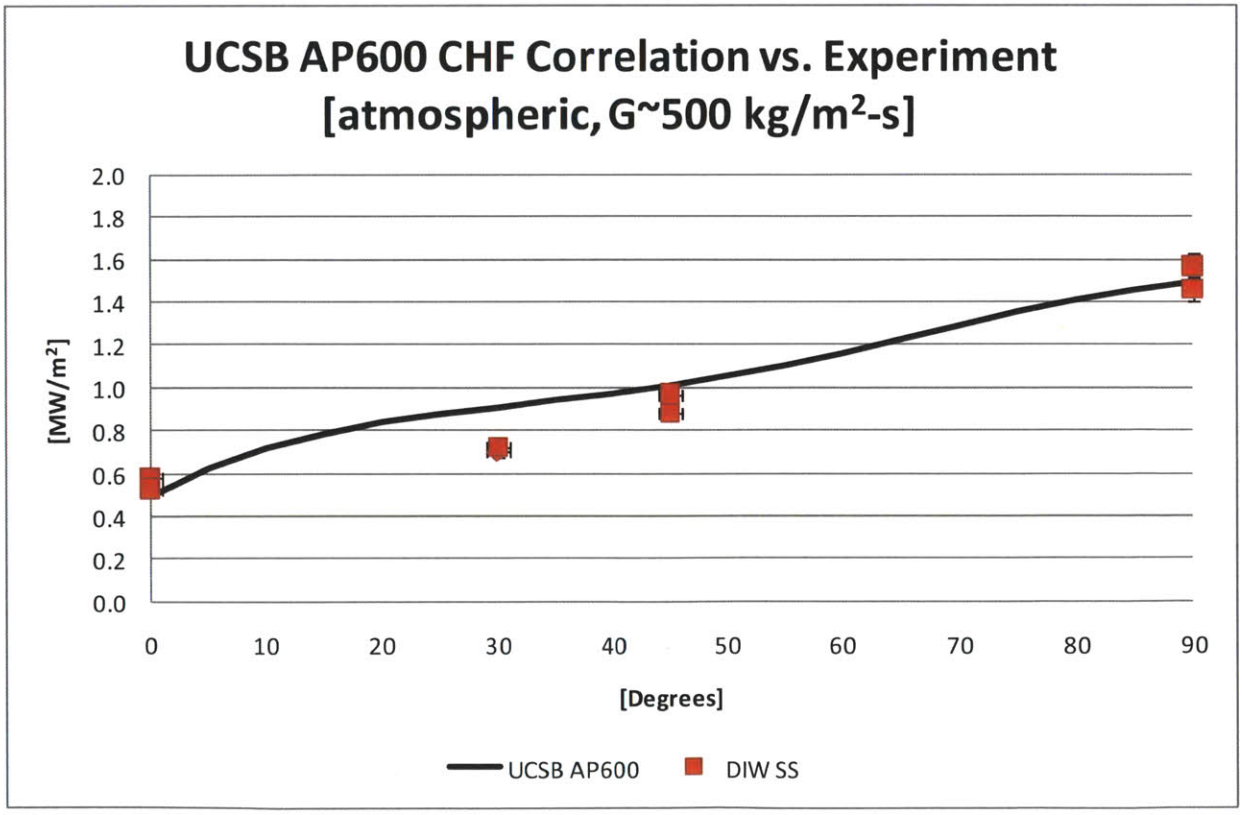

KSNP analyzed the UCSB data and also developed a correlation [110]. No comparison is made.

$$q''_{chf} = 536.5 + 18.997\theta - 0.108\theta^2 - 6.37x10^{-4}\theta^3 + 8.51x10^{-6}\theta^4 \qquad \text{Eq. 12.1}$$

The AP1000 configurations had a flow smaller gap of 7.6 cm (3") along the lower surface and some other improvements to enhance gap flow and thereby accommodate increased power [111]. The associated mass flux near the vertical portion of the lower head is estimated to be ~860 kg/m^2-s. The resulting CHF data from the UCSB Configuration V tests were not correlated. The data is directly compared to herein measurement of CHF.

Again, experimental results for water show good agreement to UCSB AP1000 CHF data (see Figure 12-4). Note that data is compared and to the 1000 kg/m^2-s mass flux data is compared. For the SS316L data the CHF levels and trends are comparable. For the SA-508 and SS316L with an oxidized surface the 45° data point are significantly higher than UCSB and SS316L.

Figure 12-4: Graph of UCSB AP1000 CHF Data and DIW CHF Data for water at Atmospheric Conditions, G~1,000 kg/m^2-s

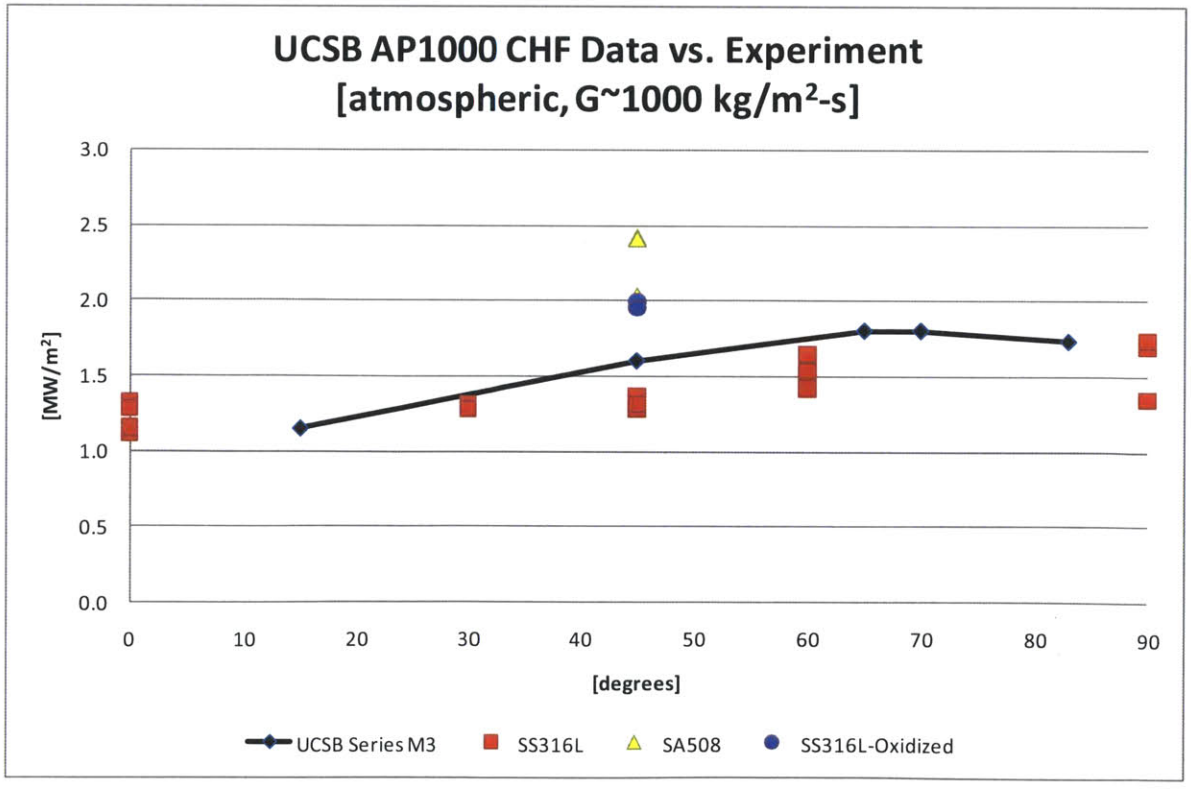

12.2 Sultan Facility

Work done at the Sultan facility in Grenoble, France from 1994 through 1998 is the most analogues to the experimentation herein [17]. The facility had a much larger test section being 4m in length and 15 cm width that varied in downward facing angle [112] [113][114]. Variables studied at Sultan included downward angle, mass flux, quality, pressure and gap size. The loop configuration included a pump, test section, riser, condenser, pressurizer, and downcomer (see Figure 12-5). Fluid is DI water and degassed.

The test heater is 1.5 mm thick and is joule heated. Heating of the fluid on one side is from above. All other sides are insulated by ceramics. CHF is identified by temperature excursion.

Figure 12-5: Schematic of Sultan Facility

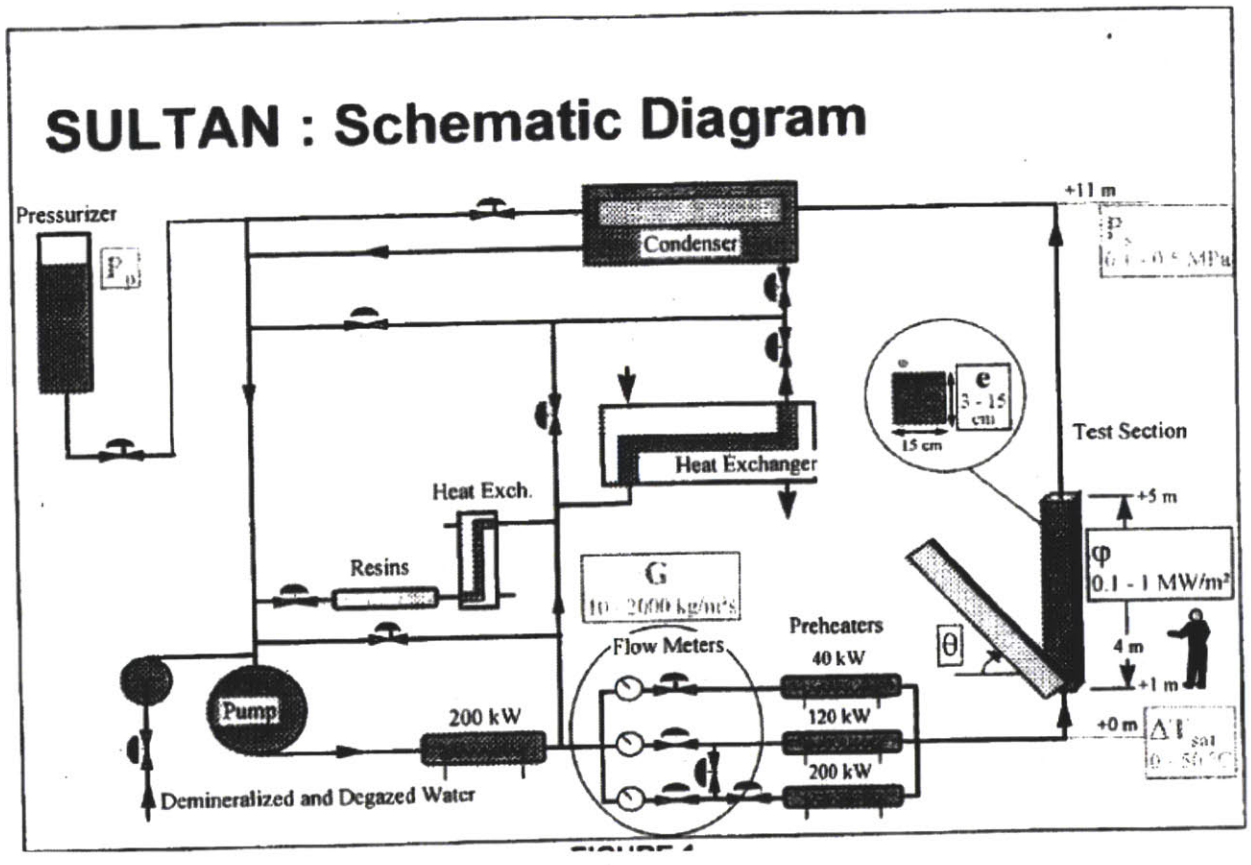

The matrix of CHF experiments completed covered a wide range of conditions (see Table 12-1). Some 191 CHF data points were obtained.

Table 12-1: Sultan Range of Conditions Tested

Pressure:	0.1 – 0.5	MPa
Mass Flux:	10 – 5000	kg/m^2-s
Angle:	10^o – 90^o	
Sub-cooling:	0 – 50	^{o}C
Gap size:	3 – 15	cm
Heat Flux:	0.1 – 2	MW/m^2

The Sultan campaign for analyzing CHF for IVR supported the development of a correlation. Note that the pressure locally includes a hydraulic head for the riser.

$$q''_{chf}(\theta) = A0 + A1 \cdot X + A2 \cdot X^2 + A3 \cdot \Theta + A4 \cdot \Theta^2 \qquad \text{Eq. 12.2}$$

Where:

Θ	=	$\sin(\theta)$
θ	=	Inclination angle (degrees vertical – 90^o)
X	=	local thermodynamic quality
E	=	gap size (m)
q"chf(θ)	=	Critical heat flux [MW/m^2]

$$A0 = b0 + b1 \cdot E \cdot \ln(G) + \frac{b2}{P^2} + b3 \cdot G + b4 \cdot \frac{E}{P} + b5 \cdot E/P^2 + b4 \cdot \frac{E}{P} + b6 \cdot P \cdot \ln(G)^2$$

$$A1 = b7 \cdot \ln(G)^2 + b8 \cdot E \cdot \ln(G)$$

$$A2 = b9 \cdot E$$

$$A3 = b10 \cdot \ln(G)^2 + b11 \cdot E \cdot P + b12 \cdot X \cdot \ln(G)$$

$$A4 = b13 \cdot P + b14 \cdot \ln(G) + b15 \cdot X + b16 \cdot E$$

b0 = 0.65444	b4 = 1.36899	b8 = -4.49425	b12 = 0.855759	b16 = 2.2236
b1 = -1.2018	b5 = -0.077415	b9 = 9.28489	b13 = -1.74177	
b2 = -0.008388	b6 = 0.024967	b10 = -0.0066169	b14 = 0.182895	
b3 = 0.000179	b7 = -0.086511	b11 = 11.62546	b15 = -1.8898	

For the AP600 the expected conditions are: mass flux of 340 kg/m^2-s, with gap of 15.24 cm (6"). For the AP1000 the expected conditions are: mass flux of 860, with gap of 7.62 cm (3"). Comparison is made to DI water experiments completed herein is compared to 500 kg/m^2-s data and 1000 kg/m^2-s data.

For the AP600 related conditions the agreement is very good (see Figure 12-6). For the AP1000 related conditions the SULTAN CHF is lower than measured herein, thought improves with increasing angle (see Figure 12-7).

Figure 12-6: Graph for AP600 CHF Sultan Prediction and DI Water Data - 500 kg/m^2-s

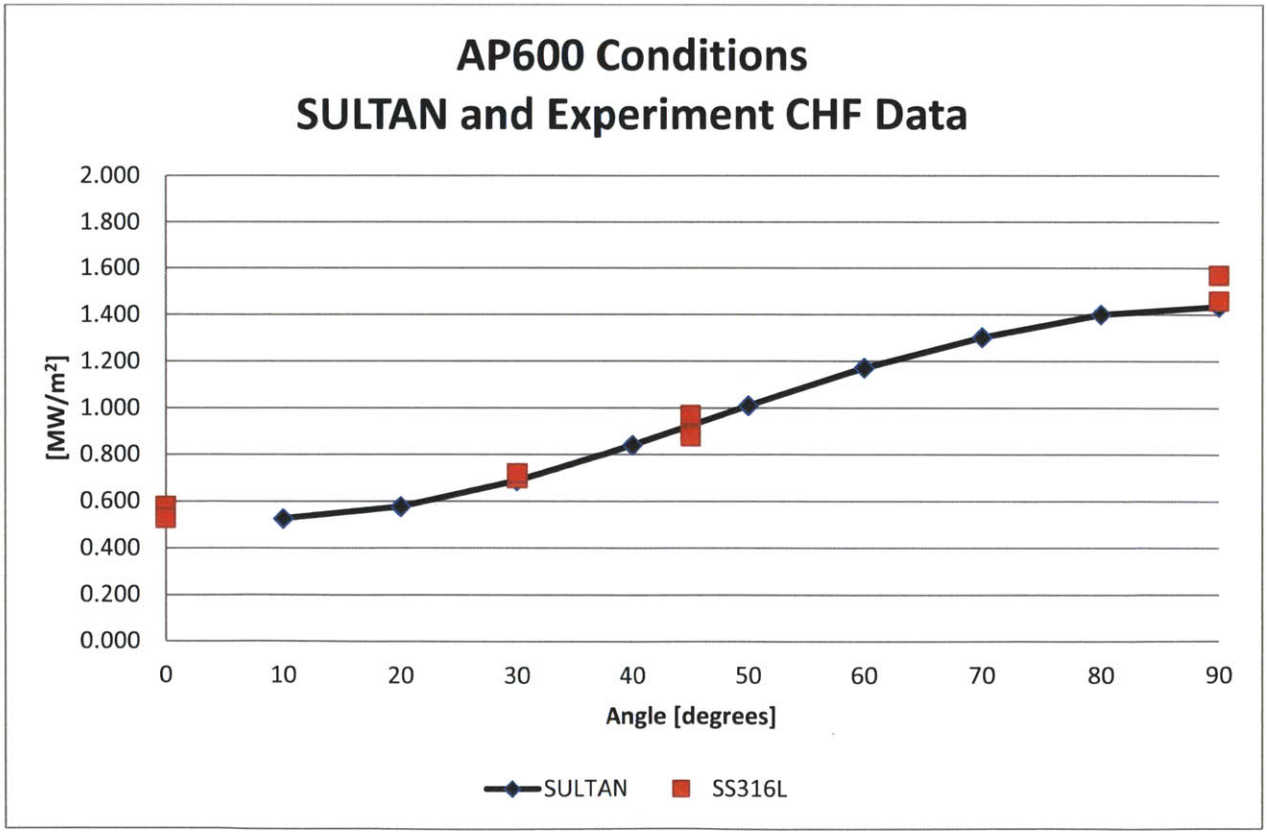

Figure 12-7: Graph for AP1000 CHF Sultan Prediction and DI Water Data - 1000 kg/m^2-s

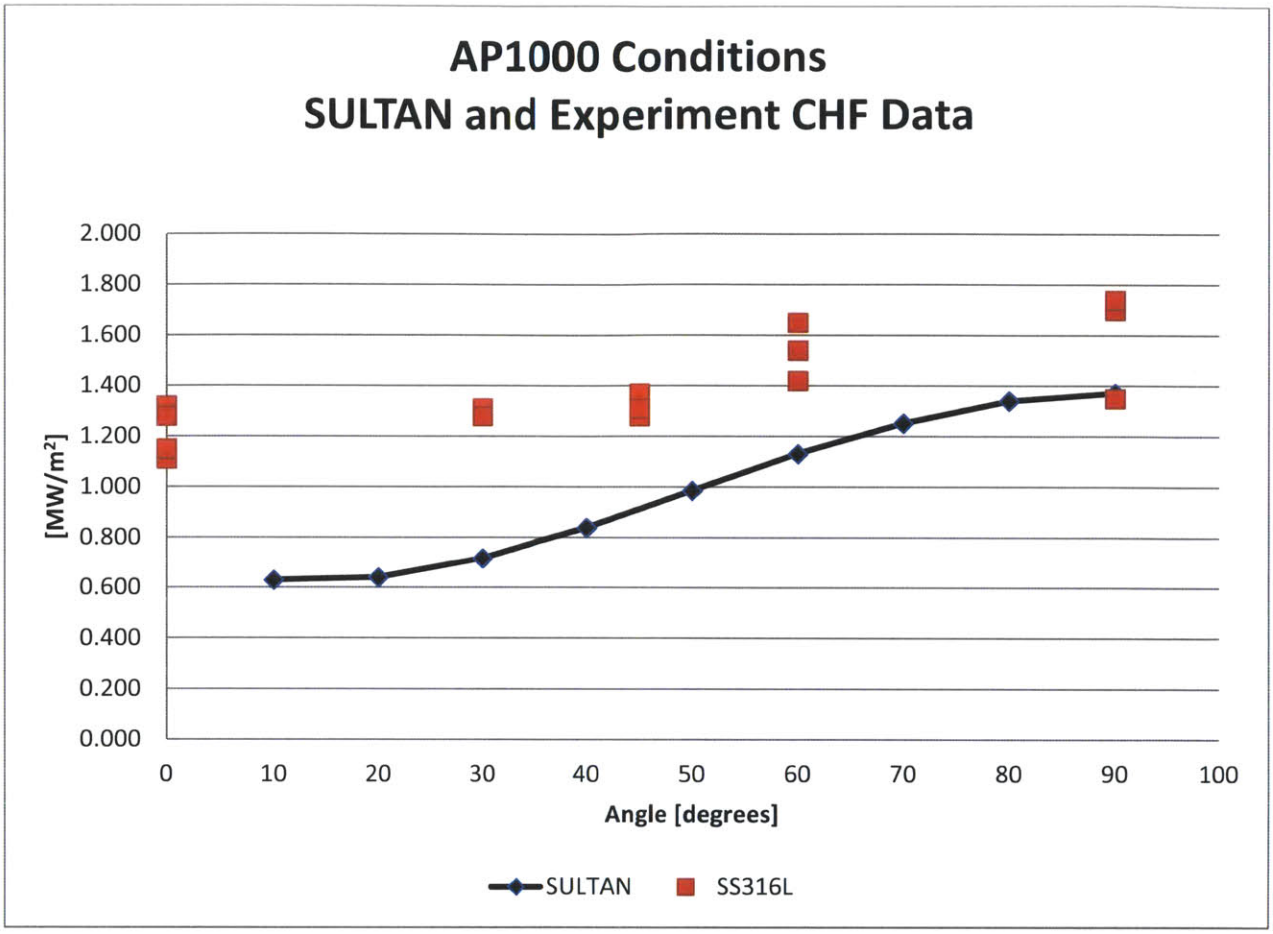

Note that the reason that CHF at 90° is basically the same as for the AP600 is that in the SULTAN correlation the reduced gap size seems to offset the impact of higher mass flux.

12.3 PSU

Research competed at PSU and lead by Dr. Cheong was exclusively natural circulation with no pump involved [115]. In this work a scale of a reactor vessel lower hemisphere was built, subscale boundary layer boiling ("SBLB") facility (see Figure 12-8). The scaled vessel was then submerged into a tank of water. Heating water provided by internal cartridge heaters. Some tests also included gap geometry along the vessel to enhance natural circulation flow. Both quenching and heat-up CHF tests were completed. Mass flow rates along the hemisphere were

not reported. Instrumentation and analysis identified local CHF level, CHF location (angle), pressure, and fluid temperature.

Figure 12-8: Schematic of PSU SBLB Facility

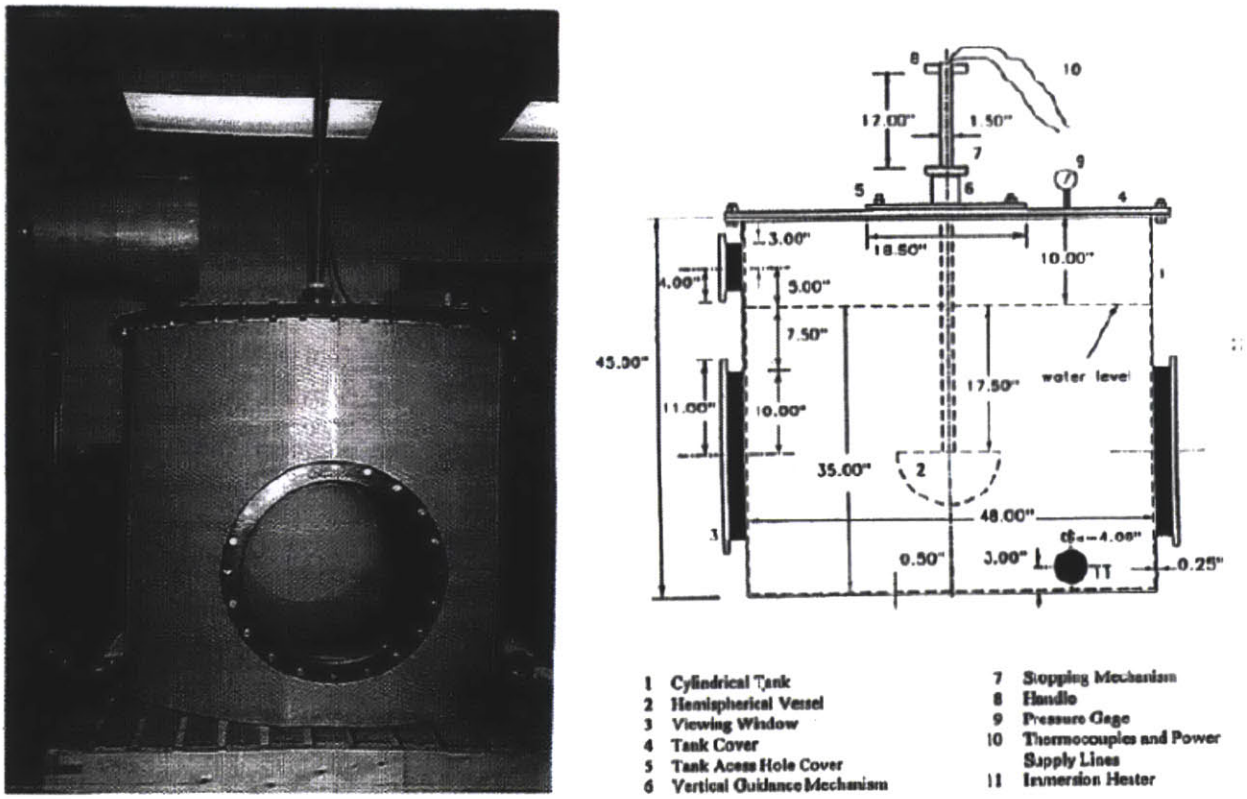

The reactor geometries of interest for this study were the Westinghouse AP600 [115][116] [117][118] and the Korean APR1400 [119][120][121]. A CHF correlation was developed that has angle and quality as independent variables.

$$q''_{chf}(\theta) = 0.4 \cdot (1 + (0.021 \cdot \theta) - (0.007 \cdot \theta)^2) \cdot (1 + 0..036 \cdot T_{sub}) \qquad \text{Eq. 12.3}$$

Where:

θ	=	Inclination angle
T_{sub}	=	Bulk fluid sub-cooling [°C]
q"chf(θ)	=	Critical heat flux [kW/m^2]

Due to the expected low mass flux involved, the comparison to experiments completed herein is with the 500 kg/m^2-s (see Figure 12-9). The eight (8) DI water only cases having mass flux of approximately 500 kg/m^2-s all plot above the PSU correlation. The difference is greatest at the vertical position. The CHF trend and difference at angles of 45° and lower are similar. The likely source of the higher test CHF data is higher mass flux compared to PSU.

Figure 12-9: Graph Comparing PSU Correlation to DIW CHF Data with G~500 kg/m^2-s and atmospheric pressure

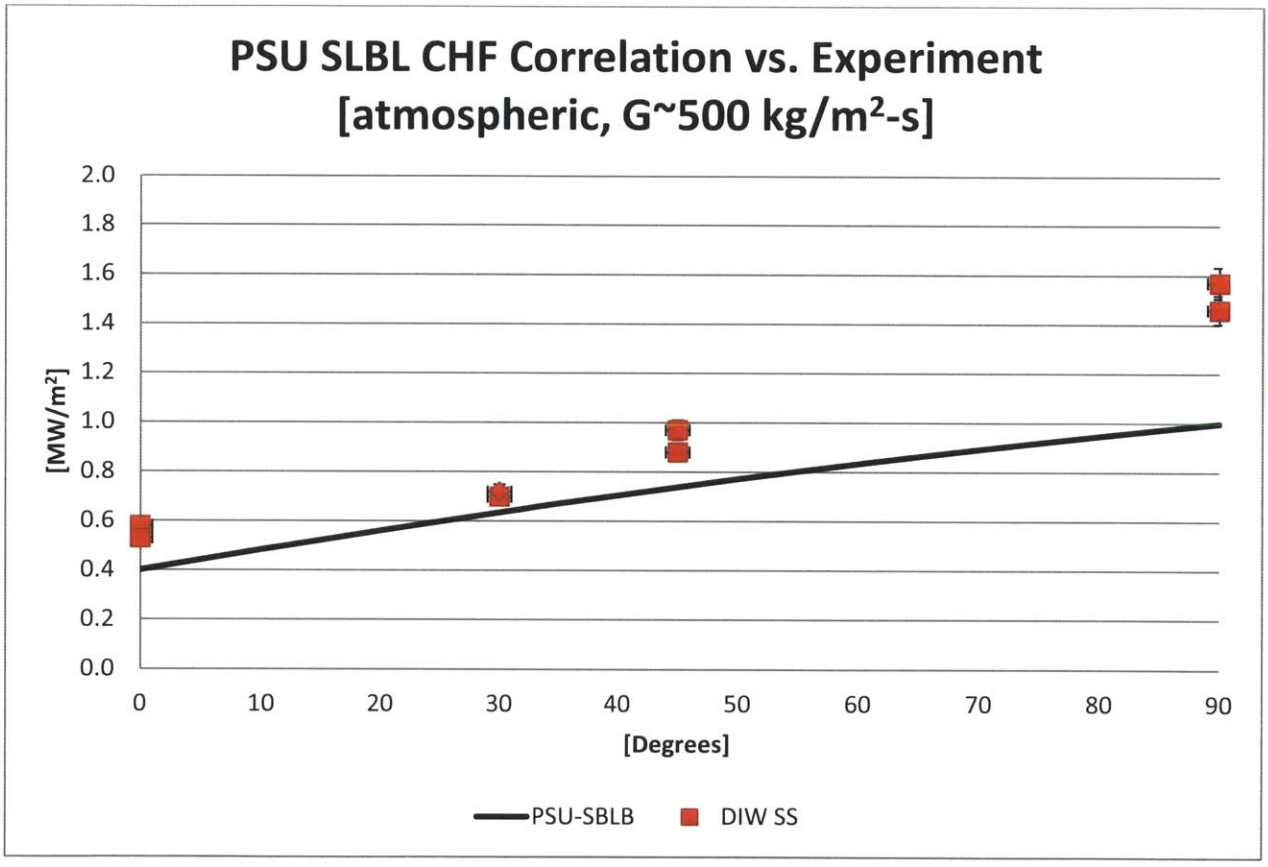

12.4 Sudo CHF Correlation

Sudo developed a correlation relevant for vertical plate heating in flow boiling for rectangular channels [122]. Data from eight (8) studies make up the database with single side heating and two sided heating included. The approach splits flow into three mass flux regions: I-high, II-

medium, and III-low. Geometric and flow conditions are first used to determine which flow region is applicable. Then an associated CHF correlation is used. Note the methodology addresses both up-flow and down-flow, but only up-flow is presented here. A MATLAB program with script name "Sudo_CHF_corr.m" has been written (see Appendix A).

Table 12-2: Sudo Range of Data Included

Pressure:	0.1 – 4.0	MPa
Mass Flux:	-25,800 – +6250	kg/m^2-s
Angle:	90°	vertical only
Sub-cooling:	1 – 73	°C
Heat Flux:	0.1 – 19	MW/m^2

The boundary, G_1^*, between high flow (Region I) and medium flow (Region II) is determined with the flowing relation.

$$G_1^* = \left(\frac{0.005}{\frac{A}{A_H} \cdot \Delta T_{SUB,in}^*} \right)^{\frac{1}{0.389}} \qquad \text{Eq. 12.4}$$

Where:

A = Flow area [m^2]

A_H = Heated area [m^2]

$T_{SUB,in}^* = \left(\frac{C_p \cdot (T_{sat} - T_{in})}{h_{fg}} \right)$

Cp = specific heat of liquid [J/kg-K]

T_{sat} = saturation temperature [K]

T_{in} = inlet temperature [K]

h_{fg} = latent heat of evaporation [J/kg]

The boundary, G_2^*, between low flow (Region III) and medium flow (Region II) is determined with the flowing relation.

$$G_2^* = \left(140 \cdot \frac{A}{A_H} \cdot \frac{\sqrt{W/\lambda}}{\left(1+\left(\frac{\rho_g}{\rho_l}\right)^{1/4}\right)^2} \right)^{\frac{1}{0.661}} \quad \text{Eq. 12.5}$$

Where:

W = Width of channel [m]

g = gravitational acceleration constant [m/s^2]

ρl = liquid density [kg/m^3]

ρ_g = vapor density [kg/m^3]

σ = surface tension [N/m]

$$\lambda = \left(\frac{\sigma}{(\rho_l - \rho_g)\cdot g}\right)^{\frac{1}{2}}$$ characteristic length [m]

These two boundaries are converted from dimensionless mass flux, G*, to dimensional mass flux.

$$G_r = G_r^* \cdot \sqrt{\lambda \cdot g \cdot \rho_g \cdot (\rho_l - \rho_g)} \quad \text{Eq. 12.6}$$

Where:

r = region boundary 1 or 2

G = mass flux [kg/m^2-s]

If mass flux, G, is greater than G_2 then the case lies in region 1 (high) and the dimensionless CHF correlation is as follows.

$$q_{CHF}^* = 0.005 \cdot G_r^{*0.661} \cdot \left(\frac{1+\frac{5000}{G_r^*}\cdot T_{SUB,in}^*}{1+25\cdot G_r^{*-1.389}\cdot\frac{A}{A_H}} \right) \quad \text{Eq. 12.7}$$

If mass flux, G, is less than or equal to G_2 and greater than G_1 then the case lies in region II (medium) and the dimensionless CHF correlation is as follows.

$$q^*_{CHF} = 0.005 \cdot G_r^{*0.661} \qquad \text{Eq. 12.8}$$

If mass flux, G, is less than or equal to G_1 then the case lies in region I (low) and the dimensionless CHF correlation is as follows.

$$q^*_{CHF} = 0.7 \cdot \frac{A}{A_H} \cdot \frac{\sqrt{W/\lambda}}{\left(1+\left(\frac{\rho_g}{\rho_l}\right)^{1/4}\right)^2} \qquad \text{Eq. 12.9}$$

Lastly, the dimensionless is converted to dimensional CHF.

$$q_{CHF} = q^*_{CHF} \cdot h_{fg} \cdot \sqrt{\lambda \cdot g \cdot \rho_g \cdot (\rho_l - \rho_g)} \qquad \text{Eq. 12.10}$$

Where

q_{chf} = Critical heat flux [W/m^2]

All water only cases in vertical orientation are compared to Sudo correlation. Graphically, the vertical water only data compares well to the Sudo prediction (see Figure 12-10). The average difference and standard deviation are 0.5% and 12.8%, respectively.

Figure 12-10: Graph of Water Only, Vertical CHF and Sudo Prediction

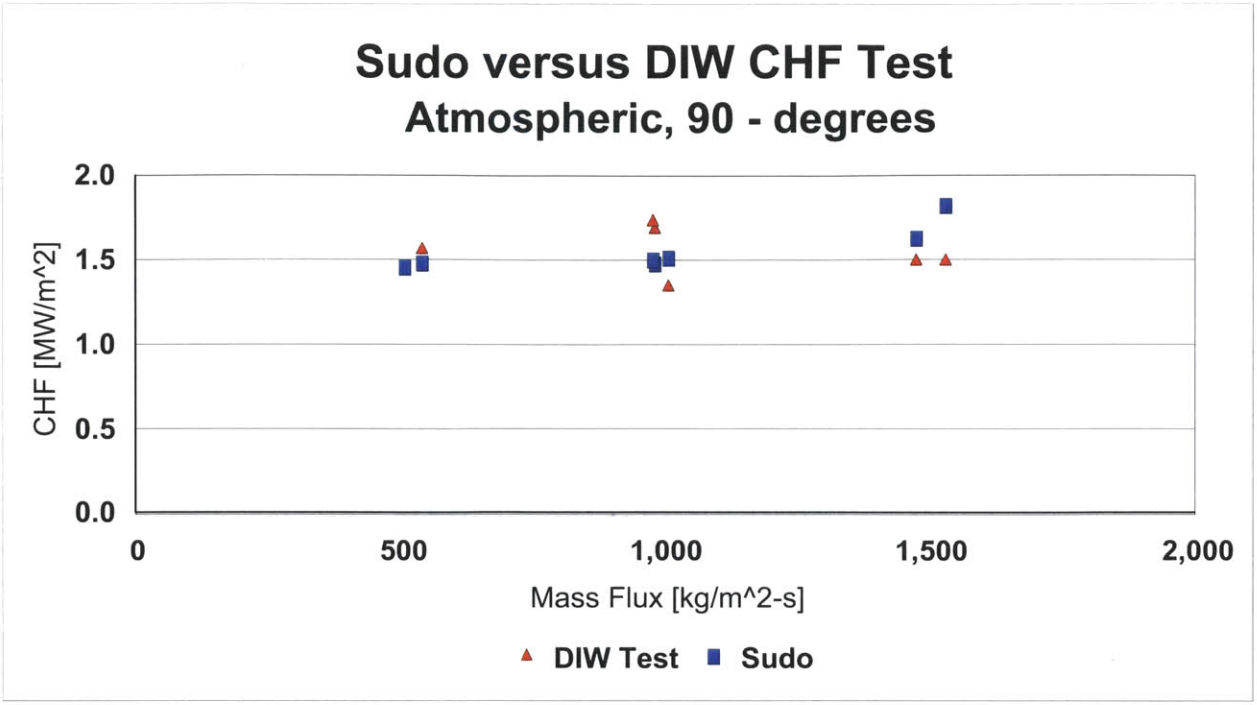

12.5 2006 CHF Lookup Table

CHF lookup table for 2006 [123] was an update from the 1995 version [124]. The data is relevant for water, vertical tube heating, and flow boiling. The data is presented in tabular form for tube with 8mm inner diameter. The parameters for variation are pressure, quality and mass flux. A complimentary method to make comparison to other geometries was also developed that utilizes the hydraulic diameter concept [125].

$$q''_{CHF} = q''_{CHF,8mm} \cdot \left(\frac{D_h}{0.008}\right)^{-1/2} \qquad \text{Eq. 12.11}$$

Where

D_h = $4*A_f/P_w$ [m]

A_f = Flow area [m^2]

P_w = Wetted perimeter [m]

Tables are used for interpolation for the condition of interest. A MATLAB program with script name "GLD_CHF_2006_Lookup_Program.m" has been written to perform the linear regressions (see Appendix A). All water only cases in vertical orientation are compared to adjusted 2006 Lookup. Graphically, the vertical and water only data does not compares well to the adjusted 2006 CHF lookup prediction (see Figure 12-11). The average difference is 28% with a maximum of 41%.

Figure 12-11: Graph of Water Only, Vertical CHF and Lookup Prediction

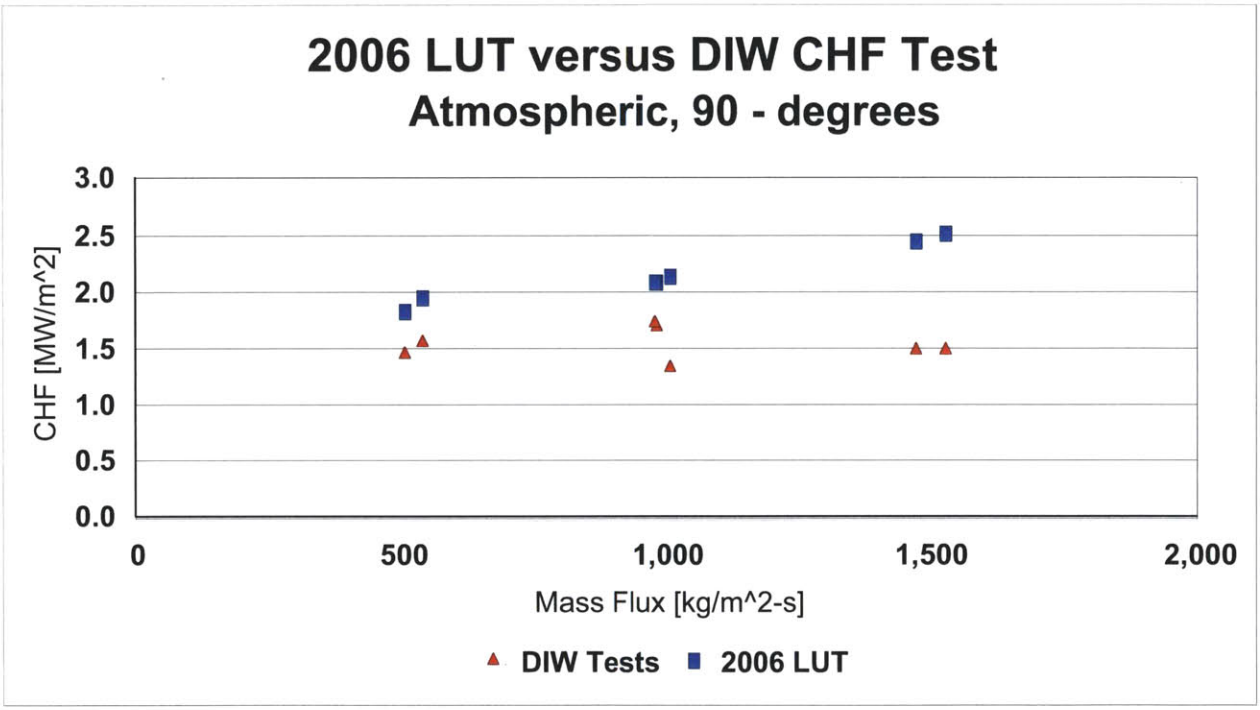

This significant over-prediction of CHF by 2006 Lookup data was also noted by the group working at the Sultan facility [17]. The primary factors are the fact that tube data has complete circumferential heating compared to single wall heating of the test section channel with the expected "cold wall effect".

13 RELAP Model

RELAP5 was used to model the flow along the gap outside of the reactor vessel, at saturated conditions, for the IVR scenario. The reference geometry is that of the Westinghouse AP1000 [126]. Specifically, the gap between the reactor vessel outer wall and the thermal insulation was modeled. The CHF correlations in the RELAP code were modified with multipliers that are a result of the herein experimentation. The objective was to determine CHF margin as a function of angle along the lower reactor vessel and identify minimum margin to CHF during the IVR.

There are several versions of RELAP5, developed for different applications. The code version utilized is of RELAP5 Mod 3.3, often called the NRC version. This version was chosen because it was validated for low pressure conditions, like that anticipated during IVR.

Comparison is made between: (1) water based modification of RELAP CHF correlation from experiment, (2) nanofluid modification of RELAP CHF correlation from experiment, and (3) AP1000 NRC licensing accepted CHF data. The RELAP CHF correlation method is the 1986 Groeneveld look-up table and is the default selection [127].

The model geometry includes: vessel lower head, vessel main body, vessel nozzle gallery, gap region between vessel and thermal insulation, and containment (see Figure 13-1). Natural circulation loop closure is modeled by boundary conditions. The top of the RELAP model represents the containment, with IVR expected conditions (~2 hours) of ~1.5 bar pressure and saturation temperature. The bottom represents the bottom of the reactor cavity, at the same temperature as the containment and pressure equal to containment pressure plus hydraulic head (~2.1 bar).

Overall, subcritical decay heat enters the problem from the corium surface. This heat conducts through the vessel and into the working fluid. The buoyancy force drives the natural circulation of the fluid. At the liquid interface with containment atmosphere vapor mixes with air. The humid air is expected to condense on the steel shell of the containment given normal weather conditions. The outer surface of the steel shell has a thin film of water running down its surface

which evaporates into the surrounding environment and is the final heat sink (see Figure 5-6: AP1000 Containment Cooling Schematic). The condensate returns to the natural circulation flow path.

Figure 13-1: Simplified Schematic for RELAP Model

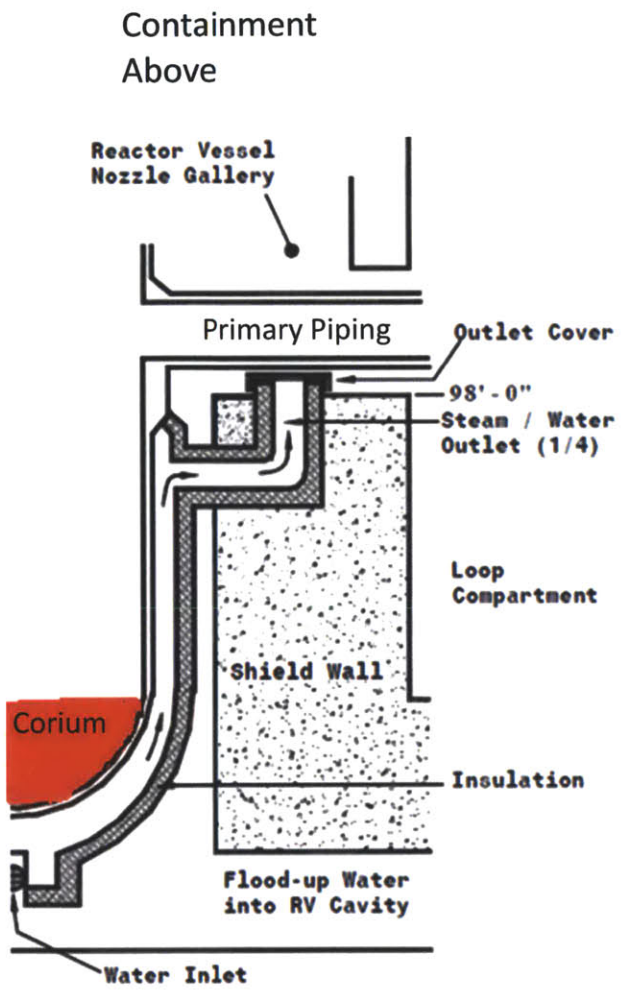

Factors that play into determining the location where CHF may occur during IVR include: (1) downward facing angle increasing from horizontal at the vessel bottom to vertical at the top of the lower cap, (2) the fluid velocity decreasing along the vessel lower hemisphere due to flow area increasing given natural circulation, (3) quality increasing along the vessel lower cap as energy is added and boiling occurs, (4) pressure decreasing along the vessel from bottom to top due to declining gravitational head, form losses, and frictional drop, and (5) heat flux along the vessel surface is expected to increase with angle due to thermal stratification of corium, crust

development along the lower portion of the corium and possible focusing of heat flux at the top of the corium due to light metal stratification [5].

The model presumes complete corium formation (see Table 13-1). The time from accident initiation at full power to corium formation is assumed to be two (2) hours (see Chapter 5). Minimum CHF margin occurs at this time because the decay power declines with time.

Table 13-1: List of Assumptions for RELAP Model of IVR

Corium Development	2	Hours
Decay Power (t=2Hrs)	28.6	MW
Containment Pressure	1.5	Atmosphere
Containment Temperature	111.6	^{o}C
Inlet Pressure at bottom of vessel	2.07	Atmosphere
Inlet Temperature	111.6	^{o}C
Corium Surface Heat Flux Shape	NRC licensing q"(θ)	kW/m^2
Radial symmetry	1:89 scale	
Heat Flux Profile	q"(θ)/Power	NRC licensing/UCSB
All heat through vessel lower head	No axial conduction above corium	Conservative for CHF
Thermal insulation	adiabatic	Conservative for CHF

Note that at the bottom of the vessel the heat flux is fully downward and has a significantly lower CHF. Other factors including higher pressure, lower quality, and lower expected heat flux tend to lower the possibility of CHF. Conversely, heat flux is expected to be highest near the top of the corium within the lower vessel cap along with decreasing pressure and increasing quality. At the same location vertical orientation contributes to higher CHF.

The outer surface of the lower vessel cap is defined with a heat flux boundary condition representing the decay heat leaving the corium. All of the energy is assumed to leave the lower vessel cap and enter the working fluid. This is conservative because even though only steam would be above the corium within the vessel, some amount of heat would transfer out of the vessel via mass transfer of the steam out of the vessel, thermal radiation heat transfer to the upper vessel, or conduction though the upper portions of the vessel. Axial conduction from the lower cap to the upper vessel shell is not modeled. The decay heat amount is ultimately removed from the system via the containment shell to the environment.

The surface flux profile assumption is that used in the NRC licensing submittal for the AP1000 [61]. The heat flux increases along the lower vessel head from a minimum of 0.2 MW/m^2 at the bottom to 1.4 MW/m^2 at the top segment of the corium (see Figure 5-12: Base Case Corium Heat Flux Profile for the AP1000). The flux level remains at this constant level across the region that represents the light metal layer "focus effect" about the corium. This heat flux shape is normalized and applied to the decay power at 2 hours, 28.6 MW.

The free surface liquid level is at the level of the primary loop nozzles. The vapor then mixes with the air and vapor environment above. Condensation occurs along the containment surface. The condensate flows down and is directed back to the bottom of the pressure vessel. Above the water line a single volume represents the containment.

Experimental studies at UCSB were a primary contributor to the IVR licensing analyses for the AP1000 and AP600. Results of this work together with supporting studies quantified: expected volumetric flow rates, conditions of pressure and temperature, and CHF margin. Details of the experimental facility are described in Chapter 12 and generally are full scale axially. The specific geometry for the AP1000 and NRC accepted CHF data are a result of the Configuration V series of experiments [72].

13.1 Westinghouse AP1000 IVR Modeling with RELAP

Details of the Westinghouse AP1000 Advanced Nuclear Plant found in the literature give details of the geometry [128][129] and materials and properties [130][131] relevant to the flow gap are used to develop RELAP input. A pie slice, 1:89th, is modeled based on vessel perimeter for the cylinder portion. The input deck can be found in Appendix D and contains all geometric data.

Seven (7) hydraulic components with thirty-one (31) volumetric nodes specify the flow from below the reactor vessel, up the gap, and into the containment (see Figure 13-2). Boundary conditions at top and bottom model the closed natural circulation loop. An eighteen (18) node

heat structure source specifies the heat flux along the lower surface of the reactor vessel (5° each). The heat transfer area from the heat structure to the hydrodynamic volume is assumed rectangular. Heated surface and flow area increase along the lower hemisphere with a 7.62 cm (3") gap. Ten (10) equal size nodes model the vertical riser portion along the vessel cylinder to the nozzle gallery. The nozzle gallery is modeled as a separate volume with associated frictional losses.

Table 13-2: List of Key Parameters Used in RELAP Modeling of AP1000 IVR and Validation

Parameter	Value	Source
Radius of Lower Head	2.16 m	drawing
Height to water line	6.14 m	UCSB Configuration V
Gap width (3") along lower head	7.62 cm	UCSB Configuration V
Volumetric Flow Rate	14,500 to 15,000 GPM	UCSB & AP1000 FSER
Pressure Drop - lower head	0.167 bar	UCSB Configuration V
Pressure Drop - riser	0.285 bar	UCSB Configuration V
Pressure Drop – nozzle gallery	0.127 bar	UCSB Configuration V

To validate the RELAP model, comparison of pressure drop data, volumetric flow rate, exit quality, and exit void fraction are analyzed. The UCSB study provides pressure drop data for segments of their facility including: from flow inlet to the end of the curved heated length, riser length, and from the riser to the condenser that represents the containment. Note that RELAP cases for comparison to UCSB data were done with containment volume at atmospheric pressure to match the experiment conditions.

Figure 13-2: Schematic of RELAP Nodal Diagram

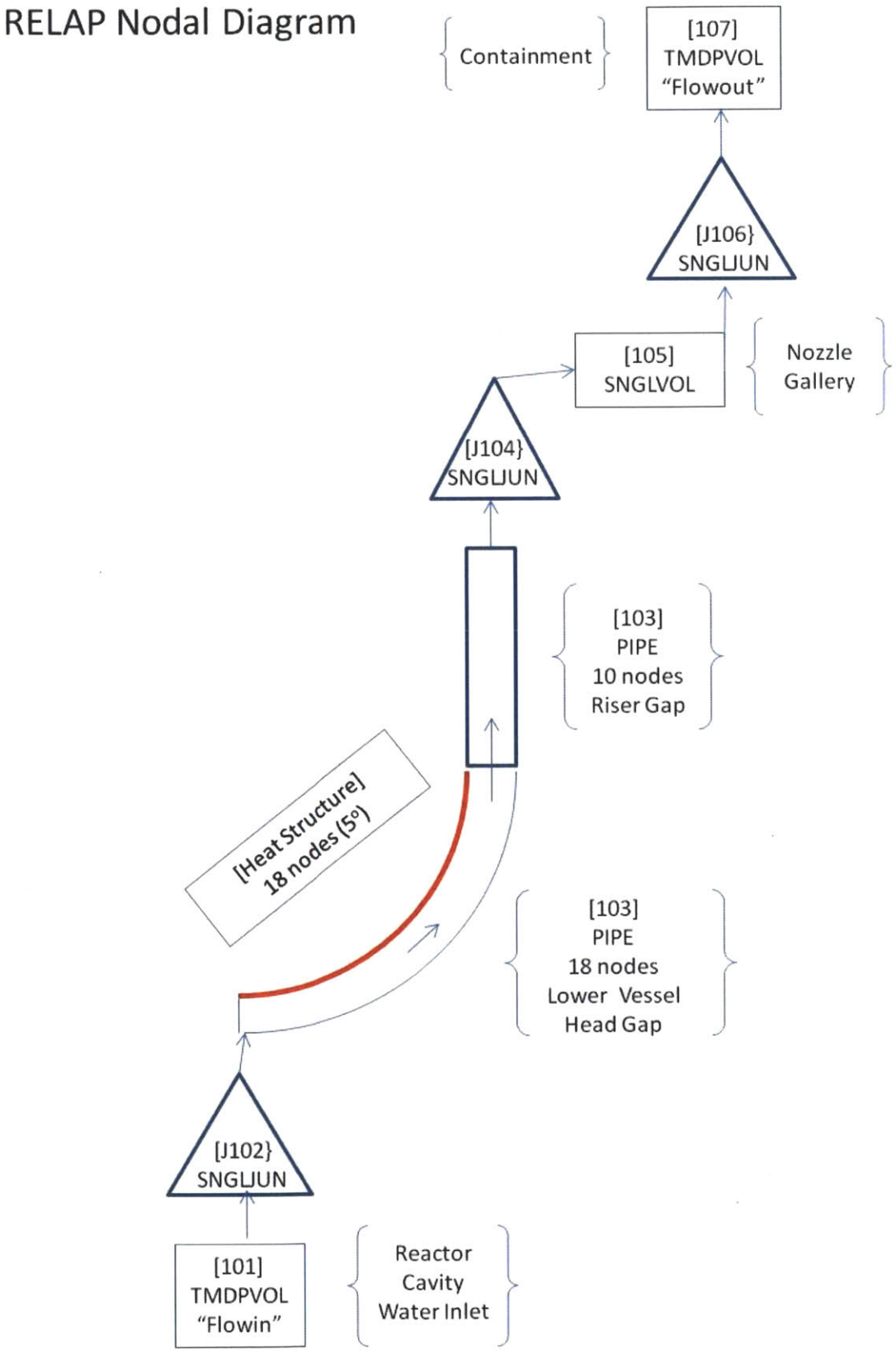

13.2 Results of RELAP Model of IVR

The RELAP model was first compared to UCSB pressure data. Loss coefficients were selected to match the losses measured in the nozzle galley region linking the riser portion to the containment. To accomplish this comparison to UCSB experiment data, the mass flux was set a boundary condition.

Comparisons are made between the UCSB experimental facility and RELAP results: flow rate, pressure profile, and exit void fraction. First, the scaled up total gap volumetric flow rate from RELAP is 883 kg/s (14,612 GPM) and compares to UCSB's value of ~876 kg/s (~14,500 GPM).

Next pressures at five locations along the flow path are compared: top of the heated region, riser mid-point, riser exit, riser exit, and nozzle gallery exit (see Table 2-1). Note that the RELAP boundary conditions are set to the UCSB reported values.

Table 13-3: Pressure Drop Comparison between UCSB Configuration V and RELAP

UCSB Label		UCSB Pressure Drop mH2O	UCSB Exit Absolute Bar	RELAP Exit Absolute Bar	diff Bar	%
	Entrance		1.593	1.593	0.000	0.0%
P12	heated channel	1.70	1.426	1.403	0.023	1.6%
P23	riser - lower	1.70	1.259	1.283	-0.024	-1.9%
P34	riser - upper	1.20	1.142	1.143	-0.001	-0.1%
P45	riser - exit	1.00	1.044	1.046	-0.002	-0.2%
P56	Nozzle gallery	0.30	1.014	1.014	0.000	0.0%

Void fraction calculated in RELAP at the nozzle gallery is 72% and compares to UCSB estimate of 61%. This is similar to 70% visual observations made from herein described experimentation.

With the nozzle gallery loss coefficients, the RELAP model was modified to allow free determination of mass flow rate. Next, all other form losses were removed and the entrance form loss adjusted until the RELAP calculated mass flow rate matched UCSB.

Lastly, these form loss coefficients were used in IVR conditions of interest. IVR containment pressure at 2 hours is expected to be ~1.5 atmospheres. Saturation temperature (111.6 °C) is assumed for both containment volume and the bottom of the reactor vessel. The RELAP case then has an entrance pressure of 2.07 atmospheres.

The resulting mass flow rate for expected IVR conditions for the RELAP model is 10.1 kg/s and translates to 899 kg/s [15,059 GPM] for the AP1000 (see Table 13-4).

Table 13-4: RELAP Nodal Summary of Thermal Hydraulic Parameters for IVR Conditions

Total Node	Volume	Node	Angle [degrees]	Pressure [Pa]	Heat Flux [W/m^2]	Mass Flow Rate [kg/s]	Mass Flux [kg/m^2-s]	X_e	Void
1	101	1	90	2.09730E+005	0	10.1	0	-0.019	0.00
2	103	1	5	1.90635E+005	1.37300E+005	10.1	2,526	-0.014	0.00
3		2	10	1.90244E+005	2.41203E+005	10.1	2,526	-0.013	0.00
4		3	15	1.89702E+005	2.30310E+005	10.1	2,526	-0.013	0.00
5		4	20	1.89013E+005	3.24527E+005	10.1	2,526	-0.013	0.00
6		5	25	1.89334E+005	2.59622E+005	10.1	2,062	-0.013	0.00
7		6	30	1.89086E+005	2.95247E+005	10.1	1,742	-0.013	0.00
8		7	35	1.88491E+005	3.36118E+005	10.1	1,508	-0.012	0.00
9		8	40	1.87628E+005	4.18177E+005	10.1	1,347	-0.012	0.00
10		9	45	1.86571E+005	5.52031E+005	10.1	1,232	-0.011	0.00
11		10	50	1.85376E+005	7.32483E+005	10.1	1,135	-0.010	0.00
12		11	55	1.84051E+005	9.00279E+005	10.1	1,064	-0.008	0.00
13		12	60	1.82645E+005	1.00308E+006	10.1	1,001	-0.007	0.04
14		13	65	1.81192E+005	1.09194E+006	10.1	962	-0.005	0.12
15		14	70	1.79817E+005	1.19218E+006	10.1	927	-0.003	0.28
16		15	75	1.78554E+005	1.30285E+006	10.1	902	-0.001	0.42
17		16	80	1.77415E+005	1.41517E+006	10.1	886	0.001	0.52
18		17	85	1.76387E+005	1.52186E+006	10.1	871	0.003	0.60
19		18	90	1.75433E+005	1.68381E+006	10.1	871	0.006	0.67
20		19	90	1.74996E+005	0	10.1	554	0.006	0.63
21		20	90	1.73939E+005	0	10.1	554	0.006	0.62
22		21	90	1.72813E+005	0	10.1	554	0.007	0.63
23		22	90	1.71685E+005	0	10.1	554	0.007	0.63
24		23	90	1.70560E+005	0	10.1	554	0.007	0.63

25		24	90	1.69439E+005	0	10.1	554	0.008	0.63
26		25	90	1.68324E+005	0	10.1	554	0.008	0.63
27		26	90	1.67218E+005	0	10.1	554	0.009	0.64
28		27	90	1.66121E+005	0	10.1	554	0.009	0.64
29		28	90	1.65022E+005	0	10.1	554	0.009	0.63
							796		
30	105	1	22	1.54037E+005	0	10.1	796	0.013	0.67
31	107	1	90	1.51418E+005	0	10.1	0	-0.000	0.00

Results of the RELAP modeling of IVR indicate that the minimum ratio of CHF to surface heat flux occurs near the top of the lower vessel cap where corium and light metal meet (see Table 13-5). This is primarily driven by the high surface heat flux, decreasing mass flux, and higher local quality at this region. For SS316L water only case CHF seems likely at the top of the heated section with a CHF ratio of 0.9 implied -10% CHF margin (see Figure 13-3). For SS316L with alumna 0.001% nanofluid CHF margin is improved to 60% with no threat of CHF (see Figure 13-4). For SA-508 in water or with alumina CHF margin is similar to the SS316L with alumina with little threat for CHF (see Figure 13-5).

Table 13-5: Minimum CHF Margin for IVR

Material	Fluid	CHF Ratio	CHF Margin	Angle
SS316L	DI Water	0.9	-10%	90°
SS316L	Alumina 0.001%	1.6	+60%	90°
SA-508	DI Water	4.0	+300%	45° one point

Note that experimental CHF values are at saturation, χ_e =0.0. CHF is generally inversely dependent on quality. Using experimentally based CHF is conservative because the qualities are in the lower head region are negative and approaching zero. Exit quality of ~0.013 is at the top of the natural circulation flow channel as it enters the containment where pressure is the lowest.

Figure 13-3: SS316L DIW CHF Margin

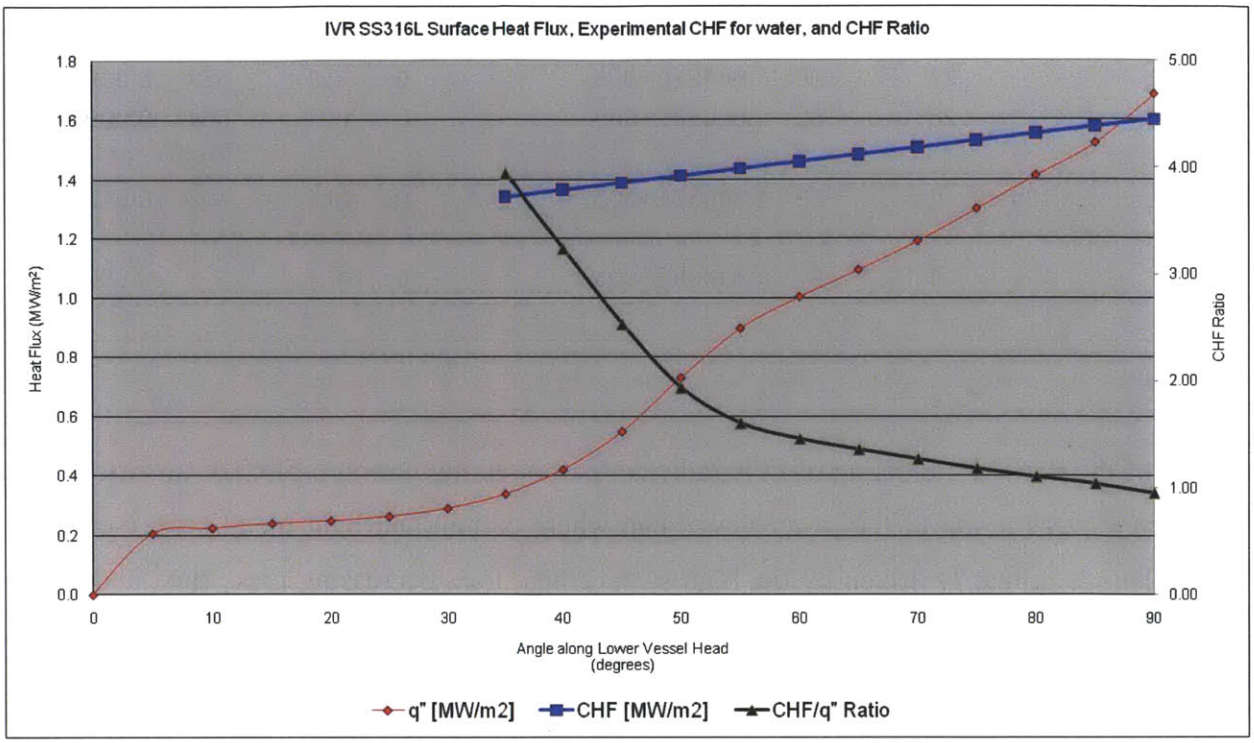

Figure 13-4: SS316L with Alumina 0.001% Nanofluid CHF Margin

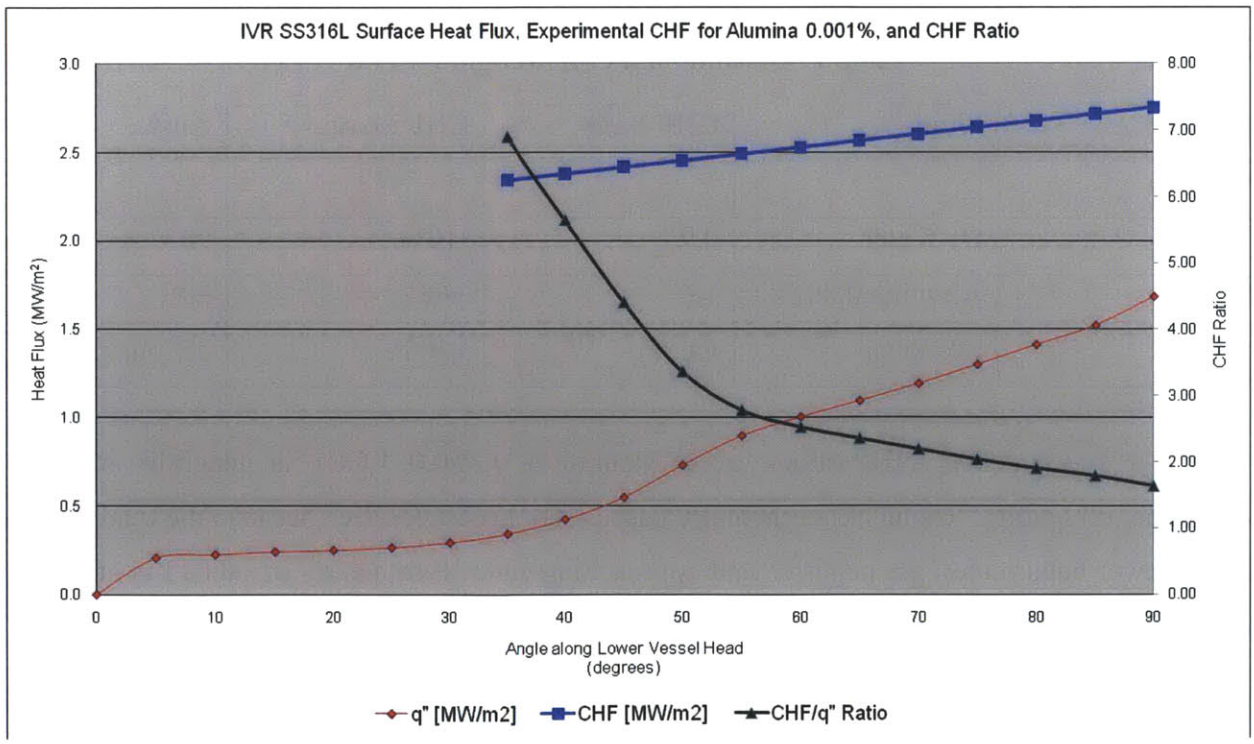

Figure 13-5: SA508 with DIW or Alumina 0.001% Nanofluid CHF Margin

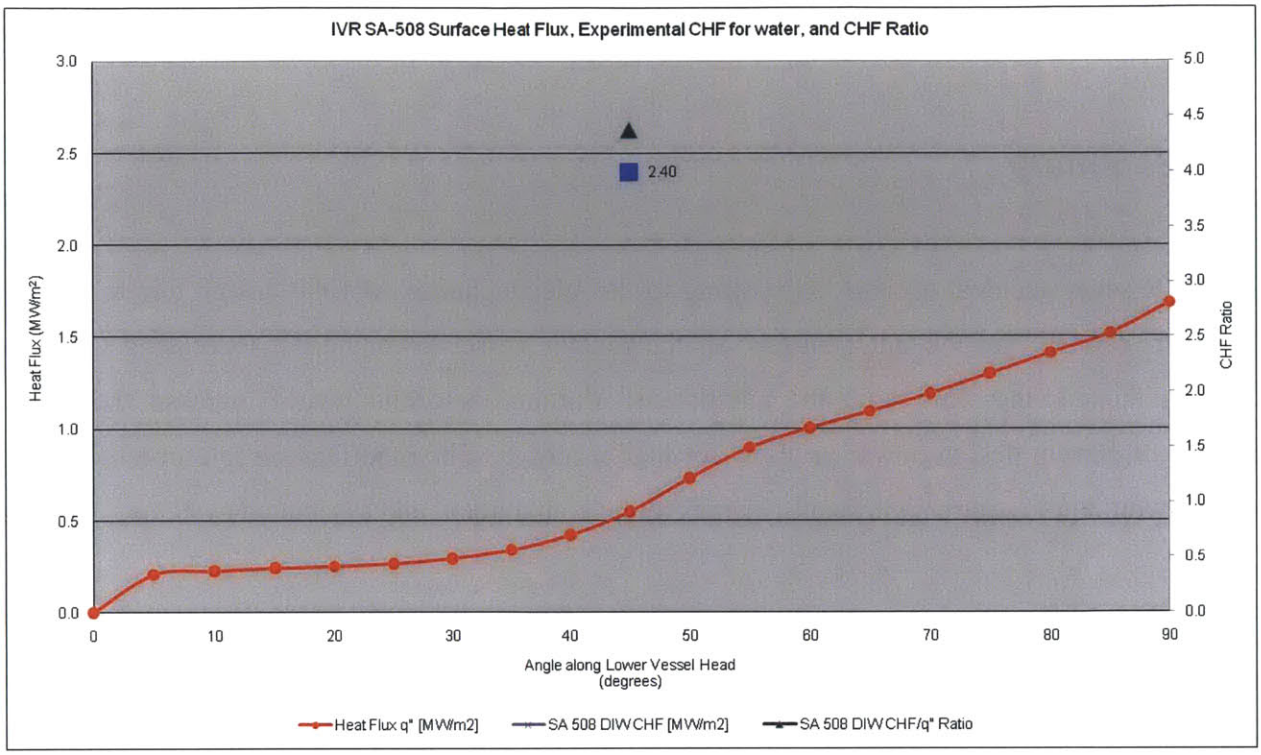

Figure 13-6: UCSB Configuration V CHF Margin

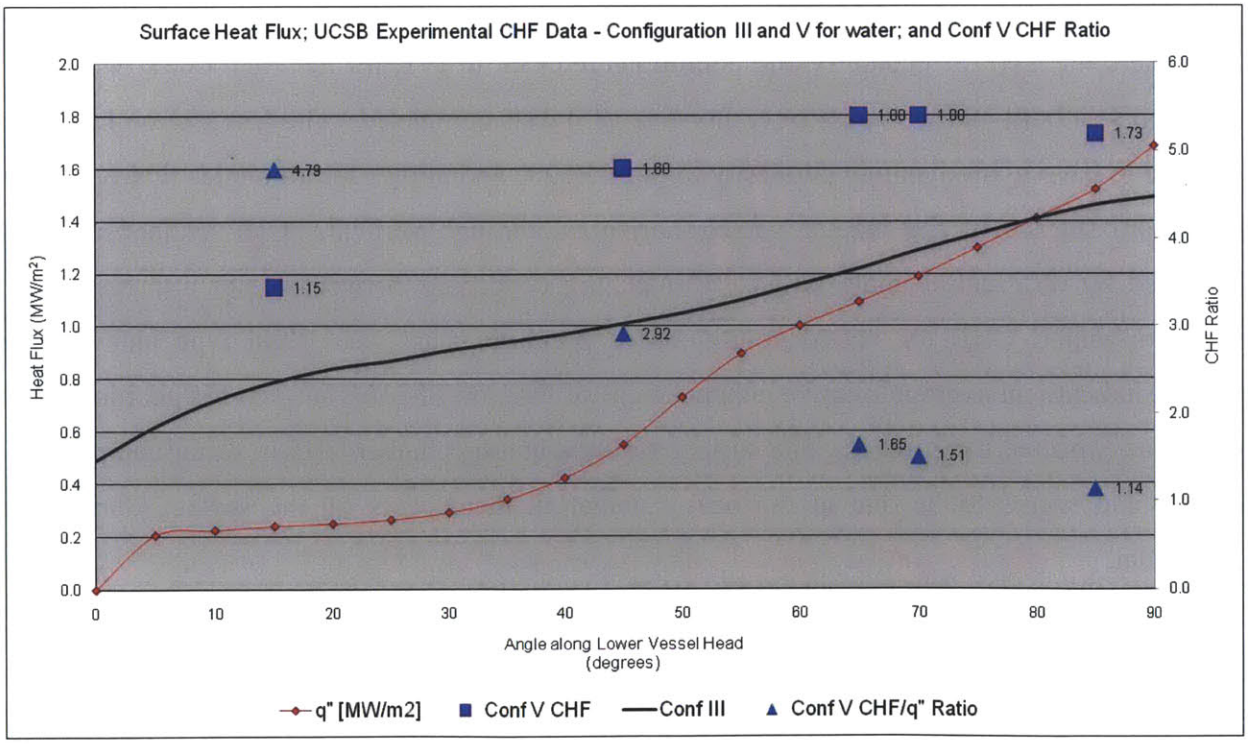

14 Summary, Conclusions, Major Contributions, and Future Work

14.1 Summary

The IVR sever accident scenario is limiting to the Westinghouse AP1000 design due to critical heat flux ("CHF") at the outer surface of the reactor vessel lower head. Increasing CHF by altering the cooling fluid with the addition of alumina nanofluid would increase the safety margin of current design power or allow for higher power. The modification to current licensed design would not require significant changes to the containment and associated systems.

Research at MIT and other institutions have demonstrated that CHF of water on a heated metal surface can be increased from 30% to 200% with the introduction of alumina nanoparticles at low concentrations. Previous research has measured enhanced CHF in both pool boiling (metallic sphere, rod and flat plate facing upward geometries) and forced convective boiling (tube geometry with sub-cooled and saturated fluid conditions).

To measure the CHF of geometry and conditions relevant to IVR for the AP1000, a two-phase flow loop was built and in excess of eighty-five (85) tests completed. The test section has been designed to have hydrodynamic similarity to the AP1000 and allows for all angles that represent the bottom surface of the reactor vessel, horizontal through vertical. CHF enhancement is quantified by differential analysis closely matching conditions between water and nanofluid. Herein measured CHF for varied conditions of pressure, mass flux, fluid type and surface material indicate an average relative enhancement of 70% on SS316L surface for geometry and conditions expected for IVR. SA-508 surface resulted in much higher CHF in water compared to SS316L and seems to be due to the heavy oxidation that occurs on the surface during the experiment.

Conceptual design implementation could involve storage tanks of high concentration nanofluids be installed in containment. Once IVR scenario has initiated with flooding of the vessel support

cavity with water from the IRWST, the alumina nanofluids would be released and allowed to mix as the natural circulation flow sets up along the gap between the vessel and the insulation mounted to the concrete wall on the vessel cavity. The slow heat-up and boiling allows plating of nanoparticles onto the surface. It is this deposition of nanoparticles that enhances CHF.

14.2 Conclusions

Eleven (11) conclusions are made as a result of this experimental study of the affect alumina and water based nanofluids have on CHF in IVR conditions for the AP1000.

(1) - Introduction of alumina nanofluids at 0.001% concentration by volume can increase CHF on average by 70% for IVR conditions tested relative to water only for SS316L surface. Increases in CHF with alumina nanofluid compared to water for similar conditions ranged from 17% to 108%. CHF enhancement on SS316L was measured for all angles, pressures, and mass fluxes.

(2) - Increasing alumina concentration by a factor of ten (10) to 0.01% by volume has no additional CHF enhancement.

(3) - SA-508 has about the same CHF, 2.4 MW/m^2, as SS316L with alumina nanofluid, 2.5 MW/m^2 for conditions tested. This higher CHF level is greater than studies completed by UCSB, Sultan and PSU that support the AP1000 licensing. It is the heavy oxidation that improves wettability on SA-508 and would need to be present on the lower vessel head at the time of IVR. No additional CHF enhancement was measured on SA-508 with alumina nanofluid with 0.001% concentration by volume.

(4) - Oxidized SS316L has enhanced CHF, 2.0 MW/m^2, relative to normally prepared SS316L with DI water, 1.3 MW/m^2, for conditions tested. Additional CHF enhancement was measured, 2.4 MW/m^2, on oxidized SS316L with alumina nanofluid with 0.001% concentration by volume nearly matching the normally prepared SS316L with alumina for the same conditions of 2.5 MW/m^2.

(5) - The CHF relative enhancement does not depend on downward facing angle for mass flux above 1,000 kg/m^2-s. CHF and CHF relative enhancement are more sensitive

to downward facing angle at the lower mass flux, 500 kg/m^2-s, for both water and nanofluids. The CHF for 500 kg/m^{2}s mass flux of water increases by 3x as inclination angle increases from 0° to 90°. The CHF level for 1000 kg/m^{2}s mass flux of water increases by ~50% as inclination angle increases from 0° to 90°. The CHF level for the 1500 kg/m^{2}s mass flux of water does not increase as inclination angle increases from 0° to 90° (see Figure 23.3).

(6) - For a given mass flux, CHF increase is basically linear with angle with a positive slope from downward facing horizontal (0°) to vertical (90°). The slope declines with increasing mass flux and nearly disappears at mass flux of 1500 kg/m^2-s.

(7) – CHF void fraction in test preformed herein is nearly always ~70%. This conclusion is based solely on visual observation of CHF through the windows of the test section.

(8) - Increased local pressure increases CHF for tested conditions with consistent CHF enhancement with alumina nanofluid.

(9) - Boiling time of 30 minutes is all the time needed to obtain CHF enhancement. Basically it takes only about 1/2 hour of vigorous boiling to deposit nanoparticles onto the surface in sufficient amount to have meaningful CHF enhancement.

(10) - CHF for IVR is most likely to occur at the top of the corium. This is primarily due to stratification within the corium driving higher surface heat flux as the distance from the corium bottom increases. Focus effect of a metal layer at the top of the corium would also support the conclusion that the highest vessel surface heat flux will be at the top of the corium. Additionally, with natural circulation driving upward flow along the vessel surface the cooling fluid quality will continuously increase along the travel path along the vessel bottom head.

(11) - Low concentration alumina nanofluid does not lower CHF in any condition tested.

14.3 List of Major Contributions

A list of major contributions of this work includes:

(1) - To measure the CHF of geometry and conditions relevant to IVR for the AP1000, a two-phase flow loop was built.

a. Generated large set (> 80 tests) of CHF data for water and alumina nanofluid with emphasis on the effects of mass flux, angle, and pressure.

b. Loop includes pumping power, joule energy, pressure control and heat sink capability.

c. Facility easily can accommodate new test sections with 1" NPT coupling.

(2) - An Agilent and LabVIEW control and data system was implemented that allowed safe operation from a chair and could have been made to operate remotely.

a. Instrumentation for bulk temperature, pressure, flow, current and voltage are incorporated and can readily expanded.

b. Allows for on-the-fly MATLAB calculation of two-phase parameters of interest.

c. Steam table functions have been incorporated.

(3) - The test section has been designed to have hydrodynamic similarity to the AP1000 and allows for all angles that represent the bottom surface of the reactor vessel, horizontal through vertical.

(4) - CHF enhancement is quantified by differential analysis closely matching conditions between water and nanofluid.

a. Herein measured CHF for varied conditions of pressure, mass flux, fluid type and surface material indicate an average relative enhancement of 70% on SS316L surface for geometry and conditions expected for IVR.

b. No identified previous experimental research has tested CHF with alumina nanofluid in IVR relevant conditions.

c. SA-508 surface resulted in much higher CHF in water [2.4 MW/m^2] compared to SS316L [1.3 MW/m^2].

i. seems to be due to the heavy oxidation that occurs on the surface during the experiment

ii. did not benefit from alumina nanofluid.

iii. Similar to SS316L with alumina nanofluid [2.5 MW/m^2]

d. CHF margin for the AP1000 has been estimated and compared to licensing.
   i. RELAP model
   ii. CHF modification with results of experimental data.

14.4 Recommendations for Future Work

To further the understanding of the influence that nanofluids have on CHF in IVR conditions for the AP1000, improve the acceptance of conclusions made herein, and to reduce operational challenges, ten (10) recommendations are made for future work.

(1) - More cases within the IVR ranges of interest could be done to add statistical strength to the conclusions by those who may want to use the results for design of nuclear plants that utilize IVR sever accident strategy.

(2) - Experiments should be conducted to determine the impact that chemistry expected to be found in the working fluid during IVR might have on CHF. Example chemicals that may be present include boron and tri-sodium phosphate. If these or other chemicals impact the deposition of alumina nanoparticles onto vessel surface the CHF may be affected. The presence of these other chemical may also alter wettability even with the same amount of alumina present at the surface.

(3) - Tests should be designed to quantify the boiling time needed to set up the nanoparticle deposits on the surface. It is observed from the work herein that only 30 minutes of boiling is sufficient to achieve significant CHF enhancement. The minimum time needed is likely less. Some changes may be need to the test procedure and loop to get boiling times to below fifteen (15) minutes. For example only use the pre-heater to bring the system temperature to near saturation. Then only use the test heater for the last steps to CHF.

(4) - Add local pressure of two (2) bar to the future test matrix. This will support characterization of the dependence of CHF in IVR conditions as a function of pressure. The current experimental matrix tested 1, 3, and 5 atmospheres. Though, one test was

done at ~ 2 bar. Much of the IVR event post corium formation has containment pressure of 2 bar or less plus an additional 0.5 bar for hydraulic head to the lower vessel head.

(5) - In order to gain confidence that the test heater surface finish, as close as possible, matches the AP1000. A suggestion might be to send a prepared but unused heater to Westinghouse for analysis to confirm similarity.

(6) - Reactor vessel surface aging should be examined to determine if any aging effects, over plant life (40+ year), change the lower vessel head surface.

(7) - To improve the uncertainty related to flow, use of non-invasive flow measurement would improve the system by lowering flow resistance and maintenance.

(8) - To better understand SA-508 for IVR the influence of heating on surface oxidation should be studied. It is the oxidation that provides higher wettability and CHF that SS316L in water. If the electrical potential at the surface because of joule heating method is accelerating oxidation, the actual reactor vessel surface may not see the same CHF benefit. Cartridge heating could be used to determine oxidation levels and CHF without the electric potential that resistive heating carries.

(9) - The reactor vessel to insulation gap will be subject to high gamma radiation from corium decay heat. The influence of gamma on alumina deposition in IVR flow conditions should also be studied.

(10) – Tests should be done without steps to remove non-condensable gases from the working fluid to determine the impact on CHF. In an actual IVR event the reactor vessel cavity is going to have some amount of non-condensable gas in the water.

As a final note regarding the available loop test facility: any test section that can couple to 1" NPT can be mounted in any angle. High temperature pump provides flow, DC power supplies can provide heating, accumulator with gas system can set pressure, the heat exchanger can remove heat, and an adaptable LabVIEW data acquisition system can capture data and provide control. The system is designed for 150 psi, but can easily increase with a few upgraded components.

Appendix A: MATLAB Scripts

A-1: Test Section Exit Quality

```
% ************************************************************************
% *****              2-Phase Analysis of Test Section                  *****
% *****          Calculation of Exit Quality of Test Section           *****
% *****                                                                *****
% *****                   BY: GREGORY L. DEWITT                        *****
% *****                       August 31, 2011                          *****
% *****                 Test_Section_Exit_Quality.m                    *****
% ************************************************************************
%
% ************************************************************************
% *****                 INITIALIZATION SECTION                         *****
% ************************************************************************
%
clear variable
%
% set path to find data
%
path('c:\documents and settings\gdewitt\my
documents\mit\thesis\vessel_ht\calculations\', path) ; % MIT computer
%path('c:\documents and settings\greg\my documents\\gldfiles\mit\thesis\',
path) ; % home computer
%
% ************************************************************************
% *****                 INPUT SECTION                                  *****
% ************************************************************************
% ****                Operating Conditons                              ****
% ************************************************************************
%
disp('                      MODELING TEST SECTION')
disp('         Determination of Equilibrium Quality at Exit')
disp(' ')
disp('START NEW CASE')
disp(' ')
%
Q_flux = input('Power to Sample (MW/m^2)= ') ;
disp(' ')
%
Q_flux = Q_flux * 1000000 ; % convert to [Watts/m^2]
%
Pr_in = input('Pressure at Entrance (MPa)= ') ;
disp(' ')
%
Pr_out = input('Pressure at Exit (MPa)= ') ;
disp(' ')
%
T_in = input('Inlet water temperature (C)= ') ;
disp(' ')
%
T_out = input('Outlet fluid temperature (C)= ') ;
disp(' ')
```

```
%
G = input('Mass Flux in Test Section (Kg/m^2-s)= ') ;
disp(' ')
%
% ************************************************************************
% ****                  Constants                                     ****
% ************************************************************************
%
g = 9.81 ;                      % gravity [m/s^2]
%
% ************************************************************************
% ****                  Geometry Input                                ****
% ************************************************************************
%
s = 0.020  ;                    % side [m]
w = 0.0143 ;                    % width [m]
%
heated_l = 0.20 ;               % heated length [m]
%                                 End studs assumed unheated
heated_w = 0.01 ;               % heated width [m]
%
A_flow = s * w ;                % flow area [m^2]
%
P_w = 2 * ( s + w )          ; % wetted perimeter [m]
%
D_e = ( 4 * A_flow ) / P_w ; % equivalent hytraulic diameter [m]
%
A_heated = heated_l * heated_w ; % [m^2]
%
% ************************************************************************
% ****              Water & Steam properties                          ****
% ************************************************************************
%
T_sat_in  = Ts(Pr_in *10) ;         % [C] at entrance
if T_in < T_sat_in
    text = sprintf('Subcooling at Entrance [C] = %6.2f',T_sat_in-T_in) ;
    disp(text)
    disp(' ')
end
%
T_sat_out = Ts(Pr_out*10) ;         % [C] at exit
%
if T_out < T_sat_out
    text = sprintf('Subcooling at Exit [C] = %6.2f',T_sat_out-T_out) ;
    disp(text)
    disp(' ')
else
    text = sprintf('Saturated at Exit') ;
    disp(text)
    disp(' ')
end
%
T_avg = (T_in + T_out) /2 ;     % [C] Average temperature in test section
%
rho_f = 1 / vf(T_in) ; % density of saturated liquid [Kg/m^3]
rho_g = 1 / vg(T_in) ; % density of saturated vapor  [Kg/m^3]
%
```

```
mu_f  = muf(T_in) ;     % [Pa-s]
mu_g  = mug(T_in) ;     % [Pa-s]
%
surf_tension = sigma(T_in) ;  % surface tension [N/m]
%
h_f_in  = hf(T_in)      * 1000 ; % entrance saturated fluid enthalpy [J/Kg]
h_f_out = hf(T_sat_out) * 1000 ; % exit saturated fluid enthalpy [J/Kg]
%
h_g_out  = hg(T_sat_out)  * 1000 ; % exit saturated vapor enthalpy [J/Kg]
h_fg_out = hfg(T_sat_out) * 1000 ; % exit heat of vaporization [J/Kg]
%
Cp_f = Cpf(T_avg) * 1000;      % [J/Kg-C]
%
% ************************************************************************
% ****             Calculate Exit Thermodynamic Enthalpy x_e           ****
% ************************************************************************
%
m_rate = G * A_flow ;   % [Kg/s]
%
Q = Q_flux * A_heated ; % [Watts]
%
h_out = Q/m_rate + h_f_in ; % [J/Kg]
%
x_e = (h_out - h_f_out) / h_fg_out ;
%
text = sprintf('Equilibrium Quality at Exit = %6.3f',x_e) ;
disp(text)
disp(' ')
%
% ************************************************************************
% ****                          END OF PROGRAM                          *****
% ************************************************************************
```

A-2: 2006 Lookup Table CHF

```
% ************************************************************************
% *****        2006 CHF Lookup Interpolation Routine        ***************
% *****             BY: GREGORY L. DEWITT                   ***************
% *****                   August 2011                       ***************
% *****              GLD_CHF_2006_Lookup_Program.m          ***************
% ************************************************************************
% *****     This program uses linear interpolation to determine       *****
% *****     determine CHF from 2006 Lookup Table.                     *****
% *****     Routine will also adjust for hydraulic Diameter           *****
% *****                                                               *****
% *****     Test Section & Tube Geometry                              *****
% ************************************************************************
% *****     Ranges covered in input table.                            *****
% *****     Pr    = [ 100, 1000 KPa ]                                 *****
% *****     G     = [ 300, 2000 Kg/m^2-s]                             *****
% *****     X_eq = [ -.05 , 0.5 ]                                     *****
% ************************************************************************
%
clear variables
%
% set path to find data
%
path('c:\documents and settings\gdewitt\my
documents\mit\thesis\vessel_ht\calculations\', path) ; % MIT computer
%
% ************************************************************************
% *****                  INPUT SECTION                            *****
% ************************************************************************
%
% ****                 Geometry Input of Test Section                ****
%
width     = 1.43 ;              % [cm]
gap       = 2.0  ;              % [cm]
flow_area = width * gap ;       % [cm]
P_w       = (width + gap) * 2 ; % [cm] Wetted Perimeter
%
hyd_diameter = 4 * flow_area / P_w ; % [cm] hydraulic diameter
%
ref_diameter = 0.8 ;            % [cm] 2006 reference tube ID is 8 mm
%
% ****               End Geometry Input of Test Section             ****
%
disp('                    Interpolation CHF 2006 Table Lookup')
disp(' ')
%
Geo_type = input('Geometry [Test Section = 1 (default); Tube = 2] = ') ; %
flow geometry
disp(' ')
%
G_chf = input('Input Fluid Mass Flux [min = 300; max = 2000] (Kg/m^2-s) = ')
; % mass flux
disp(' ')
%
```

```
Pr_chf = input('Input Pressure [min = 100; max = 1000] (KPa) = ') ;        %
CHF pressure
disp(' ')
%
X_eq_chf = input('Input the equilibrium quality at point of CHF [min = -0.05;
max = +0.05] = ') ;
disp(' ')
%
if Geo_type == 2
    %
    hyd_diameter = input('Enter Tube Wetted Diameter (cm) = ') ; % mass flux
    %
    disp(' ')
    %
end
%
% ****       Read The 2006 CHF Lookup Table Array                          ****
% ****       CHF_2006_array(Pr, G, X_eq, CHF)                              ****
%
input_file_name = 'CHF_TABLE_LOOKUP_2006.xls' ;
%
CHF_2006_array = xlsread(input_file_name) ; %
%
num_chf_records = length(CHF_2006_array) ; % number of records in CHF array
%
% ***************************************************************************
% *****                  END INPUT SECTION                                  *****
% ***************************************************************************
%
% ***************************************************************************
% ***** This section reduces the CHF array by eliminating records      *****
% ***** that are not in range                                          *****
% ***************************************************************************
%
% ***** Pressure lookup range
%
Pr_min = 100  ; % table lookup minimum pressure (default)
Pr_max = 300  ; % table lookup minimum pressure (default)
%
if Pr_chf >= 500
    %
    Pr_min = 500  ; % table lookup minimum pressure
    Pr_max = 1000 ; % table lookup maximum pressure
    %
elseif Pr_chf >= 300 && Pr_chf < 500
    %
    Pr_min = 300 ; % table lookup minimum pressure
    Pr_max = 500 ; % table lookup maximum pressure
    %
end
%
% ***** Mass Flux lookup range
%
G_min = 300  ; % table lookup minimum mass flux (default)
G_max = 500  ; % table lookup minimum mass flux (default)
%
if G_chf >= 1500
```

```
    %
    G_min = 1500  ; % table lookup minimum G
    G_max = 2000  ; % table lookup maximum G
    %
elseif G_chf >= 1000 && G_chf < 1500
    %
    G_min = 1000 ; % table lookup minimum G
    G_max = 1500 ; % table lookup maximum G
    %
elseif G_chf >= 750 && G_chf < 1000
    %
    G_min = 750  ; % table lookup minimum G
    G_max = 1000 ; % table lookup maximum G
    %
elseif G_chf >= 500 && G_chf < 750
    %
    G_min = 500  ; % table lookup minimum G
    G_max = 750  ; % table lookup maximum G
    %
end
%
% ***** Equilibrium CHF quality lookup range                              *****
%
X_eq_min = -.05  ; % table lookup minimum mass flux (default)
X_eq_max = 0     ; % table lookup minimum mass flux (default)
%
if X_eq_chf > 0
    %
    X_eq_min = 0.00  ; % table lookup minimum X_eq
    X_eq_max = 0.05  ; % table lookup maximum X_eq
    %
end
%
n = 0 ;  % Index variable
%
for i = 1 : num_chf_records
    %
    if CHF_2006_array(i,1) >= Pr_min && CHF_2006_array(i,1) <= Pr_max
        %
        if CHF_2006_array(i,2) >= G_min && CHF_2006_array(i,2) <= G_max
            %
            if CHF_2006_array(i,3) >= X_eq_min && CHF_2006_array(i,3) <=
X_eq_max ;
                %
                n = n + 1 ;
                %
                CHF_2006_array_reduced(n,1) = CHF_2006_array(i,1) ;
                CHF_2006_array_reduced(n,2) = CHF_2006_array(i,2) ;
                CHF_2006_array_reduced(n,3) = CHF_2006_array(i,3) ;
                CHF_2006_array_reduced(n,4) = CHF_2006_array(i,4) ;
                %
            end
        end
    end
    %
end
%
```

```
% ************************************************************************
% *****            END CHF ARRAY REDUCTION                              *****
% ************************************************************************
%
% *****  Interpolation on Pressure                                      *****
%
pair_incr = length(CHF_2006_array_reduced) / 2 ;    % records between pairs
%
for i = 1 : pair_incr
    %
    Pr_interp_ratio = (Pr_chf - Pr_min) / (Pr_max - Pr_min) ;
    %
    CHF_Pr_interp(i,1) = Pr_chf ;                          % Press
    CHF_Pr_interp(i,2) = CHF_2006_array_reduced(i,2) ;     % G
    CHF_Pr_interp(i,3) = CHF_2006_array_reduced(i,3) ;     % X_eq
    %
    CHF_Pr_interp(i,4) = CHF_2006_array_reduced(i + pair_incr,4) -
CHF_2006_array_reduced(i,4) ;
    CHF_Pr_interp(i,4) = CHF_Pr_interp(i,4) * Pr_interp_ratio ;
    CHF_Pr_interp(i,4) = CHF_Pr_interp(i,4) + CHF_2006_array_reduced(i,4) ;
    %
end
%
% *****  Mass Flux [G] Interpolation                                    *****
%
pair_incr = length(CHF_Pr_interp) / 2 ;            % records between pairs
%
for i = 1 : pair_incr
    %
    G_interp_ratio = (G_chf - G_min) / (G_max - G_min) ;
    %
    CHF_G_interp(i,1) = Pr_chf ;                          % Press
    CHF_G_interp(i,2) = G_chf ;                           % G
    CHF_G_interp(i,3) = CHF_Pr_interp(i,3) ;              % X_eq
    %
    CHF_G_interp(i,4) = CHF_Pr_interp(i+pair_incr,4) - CHF_Pr_interp(i,4) ;
    CHF_G_interp(i,4) = CHF_G_interp(i,4) * G_interp_ratio ;
    CHF_G_interp(i,4) = CHF_G_interp(i,4) + CHF_Pr_interp(i,4) ;
    %
end
%
% *****  Quality [X_eq] Interpolation                                   *****
%
X_interp_ratio = (X_eq_chf - X_eq_min) / (X_eq_max - X_eq_min) ;
%
CHF_final(1,1) = Pr_chf   ;                          % Press
CHF_final(1,2) = G_chf    ;                          % G
CHF_final(1,3) = X_eq_chf ;                          % X_eq
%
CHF_final(1,4) = CHF_G_interp(2,4) - CHF_G_interp(1,4) ;
CHF_final(1,4) = CHF_final(1,4) * X_interp_ratio + CHF_G_interp(1,4) ;
%
% ************************************************************************
% *****                  END of interpolation                          *****
% ************************************************************************
%
```

```
text = sprintf('Interpolated CHF value from 2006 table [KW/m^2) =
%6.0f',CHF_final(1,4)) ;
disp(text)
disp(' ')
%
% ************************************************************************
% *****              Adjustment of CHF for hydrualic diameter          *****
% *****                 3 mm < D < 25 mm                               *****
% ************************************************************************
%
CHF_adj = CHF_final(1,4) * ((hyd_diameter / ref_diameter)^(-0.5)) ;
%
text = sprintf('Adjusted CHF value for hydraulic diameter [KW/m^2) =
%6.0f',CHF_adj) ;
disp(text)
disp(' ')
%
% ************************************************************************
% *****                          END PROGRAM                           *****
% ************************************************************************
```

A-3: Zuber/Dhir CHF Correlation

```
% ************************************************************************
% ****          file:      Zuber_Dhir_CHF.m                             ****
% ****            by:      Gregory L. DeWitt                            ****
% ****          date:      August 31, 2011                              ****
% ************************************************************************
% ****    references:      Fundamentals of Heat Transfer - page 629     ****
% ****                     Dhir - Hydrodynamic prediction of peak and   ****
% ****                     pool boiling heat fluxes from finite bodies  ****
% ************************************************************************
% ****         Notes:      Pool Boiling                                 ****
% ****                     Flat heater                                  ****
% ****                     Bulk fluid properties at T_sat               ****
% ****                     Includes Dhir modification for               ****
% ****                     flat plates oriented vertically              ****
% ************************************************************************
%
clear variables
%
% set path to find data-
%
path('c:\documents and settings\gdewitt\my
documents\mit\thesis\vessel_ht\calculations\', path) ; % MIT computer
%
% ************************************************************************
% ****                   GEOMETRY INPUT SECTION                       ****
% ************************************************************************
%
s     = 0.02   ;   % [m] side gap of flow channel
w     = 0.0143 ;   % [m] width of flow channel
w_h   = 0.01   ;   % [m] width of heater
L_h   = 0.20   ;   % [m] heated length of heater - studs assumed not heated
%
% ************************************************************************
% ****                      USER INPUT SECTION                        ****
% ************************************************************************
%
disp('       Zuber CHF Correlation for Pool Boiling with Dhir Adjustments')
disp(' ')
%
Pr = input('Input Pressure (Bar) = ') ;       % CHF pressure
disp(' ')
%
Orientation = input('Input Heater Orientation (F=Flat Facing Up; V=Vertical)
',’s') ;
disp(' ')
%
% ************************************************************************
% ****                    Property Data                               ****
% ************************************************************************
%
T_sat = Ts(Pr)         ;     % saturation temperature (C)
rho_f = 1 / vf(T_sat) ;     % liquid density (kg/m^3)
rho_g = 1 / vg(T_sat) ;     % vapor density (kg/m^3)
```

```
sigm  = sigma(T_sat)  ;     % surface tension (N/m)
h_fg  = hfg(T_sat)    ;     % heat of vaporazation [KJ/Kg-C]
%
% ************************************************************************
% ****                    Constants                                   ****
% ************************************************************************
%
g = 9.81 ; % gravitational acceleration [m/s^2]
%
C_zuber = pi / 24 ;     % Zuber constant
C       = C_zuber ;     % default constant is zuber
C_dhir  = 0.149   ;     % Dhir constant
%
Heater_size = 'Large'; % Default Large
%
if Orientation == 'F'
    %
    Constant = input('Which constant (1 = "Zuber = 0.131", 2 = "Dhir =
0.149")? ') ; % lead constant
    disp(' ')
    %
    if Constant == 1
        %
        C = C_zuber
        %
    elseif Constant == 2
        %
        C = C_dhir
    end
end
%
% ************************************************************************
% ****                    GEOMETRY SECTION                            ****
% ****                Square Channel with one heated side             ****
% ************************************************************************
%
A_flow   = s * w       ;       % flow area
P_w      = 2 * (s + w) ;       % wetted perimeter
A_heated = w_h * L_h   ;       % [m^2]
%
D_h      = 4 * A_flow / P_w ;  % [m]
%
if Orientation == 'F'
    %
    L_c = w * ( g * (rho_f - rho_g)/sigm)^0.5 ; % characteristic length
    %
elseif Orientation == 'V'
    %
    L_c = L_h * ( g * (rho_f - rho_g)/sigm)^0.5 ; % characteristic length
    %
    if L_c > 6   % determine correction for heater size for vertical
        %
        Heater_size = 'Large' ;
    else
        %
        Heater_size = 'Small' ;
    end
```

```
    %
end
%
% ************************************************************************
% ****              END GEOMETRY SECTION                                ****
% ************************************************************************
%
% ************************************************************************
% ****                        Zuber Correlation                         ****
% ************************************************************************
%
q_flux_chf = (sigm * g * (rho_f - rho_g)/(rho_g^2))^(1/4) ;
q_flux_chf = q_flux_chf * C * h_fg * rho_g ;                % [KW/m^2]
q_flux_chf = q_flux_chf / 1000 ;                            % [MW/m^2]
%
if Orientation == 'V'  % For vertical cases
    %
    if Heater_size == 'Large'
        %
        q_flux_chf = q_flux_chf * 0.9 ; % large vertical one-side insulated
        %
    else
        %
        q_flux_chf = q_flux_chf * 1.4 / (L_c^0.25) ; % small vertical one-
side insulated
        %
    end
end % End vertical cases
%
% ************************************************************************
% ****                             PRINT                                ****
% ************************************************************************
%
text = sprintf('Saturation Temperature [C] = %6.2f',T_sat) ;
disp(text)
disp(' ')
%
text = sprintf('CHF [MW/m^2] = %6.2f',q_flux_chf) ;
disp(text)
disp(' ')
%
% ************************************************************************
% ****                              END                                 ****
% ************************************************************************
%
```

A-4: Sudo CHF Correlation

```
% ************************************************************************
% ****          file:      Sudo_CHF_corr.m                              ****
% ****            by:      Gregory L. DeWitt                            ****
% ****          date:      August 25, 2011                              ****
% ************************************************************************
% ****     reference:      A New CHF Correlation Scheme Proposed for     ****
% ****                     Vertical Rectangular Channels Heated From     ****
% ****                     Both Sides in Nuclear Research Reactors       ****
% ****                                                                   ****
% ****         Notes:      Flow Boiling                                  ****
% ****                     Pregrammed for Upflow only                    ****
% ****                                                                   ****
% ****                     Program uses water for properties             ****
% ************************************************************************
%
clear variables
%
% set path to find data
%
path('c:\documents and settings\gdewitt\my
documents\mit\thesis\vessel_ht\calculations\', path) ; % MIT computer
%
% ************************************************************************
% ****                  GEOMETRY INPUT SECTION                        ****
% ************************************************************************
%
s     = 0.02   ;    % [m] side gap of flow channel
w     = 0.0143 ;    % [m] width of flow channel
w_h   = 0.01   ;    % [m] width of heater
L_h   = 0.20   ;    % [m] length of heater - stubs assumed unheated
%
% ************************************************************************
% ****                      New Case Loop                                ****
% ************************************************************************
%
new_case = 1 ;                  % set loop variable to (1=Yes; 0=No)
%
while new_case == 1 ;
    %
    % ********************************************************************
    % ****                     USER INPUT SECTION                       ****
    % ********************************************************************
    %
    disp('                   Sudo CHF Correlation Scheme for Flow Boiling')
    disp(' ')
    %
    Pr = input('Input Local Pressure (Bar) = ') ;                % CHF
pressure
    disp(' ')

    %
    % ********************************************************************
    % ****                   Property Data                               ****
    % ********************************************************************
```

```
%
T_sat = Ts(Pr) ;            % saturation temperature (C)
rho_f = 1 / vf(T_sat) ;     % liquid density (kg/m^3)
rho_v = 1 / vg(T_sat) ;     % vapor density (kg/m^3)
sigm  = sigma(T_sat)  ;     % surface tension (N/m)
h_fg  = hfg(T_sat)*1000 ;   % heat of vaporazation [J/Kg-C]
Cp    = Cpf(T_sat)*1000 ;   % Specific heat fluid [J/Kg-C]
%
text = sprintf('Local Saturation Temperature [C] = %6.2f',T_sat) ;
disp(text)
disp(' ')
%
G = input('Input Local Mass Flux (Kg/m^2-s) = ') ;           % Mass Flux
disp(' ')
%
T_in = input('Input Fluid Temperature at Entrance (C) = ') ; % Fluid Temp
disp(' ')
%
% ************************************************************************
% ****                    Constants                                   ****
% ************************************************************************
%
g = 9.81 ;                              % gravitational acceleration
[m/s^2]
%
% ************************************************************************
% ****                     GEOMETRY SECTION                           ****
% ****                  Square Channel with one heated side           ****
% ************************************************************************
%
A_flow   = s * w       ;       % flow area
%
P_w      = 2 * (s + w) ;       % wetted perimeter
%
A_heated = w_h * L_h   ;       % [m^2]
%
D_h      = 4 * A_flow / P_w ;  % [m]
%
% ************************************************************************
% ****                END GEOMETRY SECTION                            ****
% ************************************************************************
%
% ************************************************************************
% ****                Sudo Method for CHF Correlation                 ****
% ************************************************************************
% ****              Determine flow Region boundaries                  ****
% ****                                                                ****
% ****              Region I   - High Mass Flux                       ****
% ****              Region II  - Medium Mass Flux                     ****
% ****              Region III - Low Mass Flux                        ****
% ************************************************************************
%
T_sub_in = T_sat - T_in ;              % inlet subcooling
T_S_sub_in = Cp * T_sub_in / h_fg ;    % dimensionless inlet subcooling
%
Lambda = (sigm / (g * (rho_f - rho_v)))^(0.5) ; % characteristic length
[m]
```

```
%
% ****       Determine Region I to II boundary                    ****
%
G_S_1 = (A_flow/A_heated) * T_S_sub_in ;
G_S_1 = (0.005/G_S_1)^(1 / 0.389) ;
%
G_1 = Lambda * g * rho_v * (rho_f - rho_v) ;
G_1 = G_S_1 * (G_1^(0.5)) ;                  % Region I to II boundary
%
% ****       Determine Region II to III boundary                  ****
%
G_S_2 = (( w / Lambda)^0.5) / ((1 + ((rho_v/rho_f)^0.25))^2) ;
G_S_2 = G_S_2 * 140 * (A_flow/A_heated) ;
G_S_2 = G_S_2 ^(1 / 0.611) ;                 % Region II to III boundary
%
G_2 = Lambda * g * rho_v * (rho_f - rho_v) ;
G_2 = G_S_2 * (G_2^(0.5)) ;                  % Region II to III boundary
%
text = sprintf('Mass Flux Boundary Region I - II [Kg/m^2-s] = %6.2f',G_1)
;
disp(text)
disp(' ')
%
text = sprintf('Mass Flux Boundary Region II - III [Kg/m^2-s] =
%6.2f',G_2) ;
disp(text)
disp(' ')
%
if G <= G_2                  % Region III
    %
    Region = 3 ;
    %
    text = sprintf('Mass Flux is Region III (LOW) ') ;
    disp(text)
    disp(' ')
    %
elseif G <= G_1              % Region II
    %
    Region = 2 ;
    %
    text = sprintf('Mass Flux is Region II (MEDIUM) ') ;
    disp(text)
    disp(' ')
    %
else                         % Region I
    %
    Region = 1 ;
    %
    text = sprintf('Mass Flux is Region I (HIGH) ') ;
    disp(text)
    disp(' ')
    %
end
%
% ****          Determine dimensionless mass flux                 ****
%
G_S = Lambda * g * rho_v * (rho_f - rho_v) ;
```

```
    G_S = G / (G_S^(0.5)) ;                          % Mass Flux dimensionless
    %
    % ************************************************************************
    % ****                          Region I CHF                              ****
    % ************************************************************************
    %
    if Region == 1
        %
        q_S_chf_4 = 1 + ((5000 / G_S) * T_S_sub_in ) ;
        q_S_chf_4 = q_S_chf_4 / ( 1 + (25 * (G_S^-1.389) *(A_heated/A_flow)))
;
        q_S_chf_4 = q_S_chf_4 * 0.005 * (G_S^0.611) ;
        %
        q_chf = q_S_chf_4 * h_fg * ((Lambda *g* rho_v * (rho_f -
rho_v))^0.5);
        %
    end
    %
    % ************************************************************************
    % ****                          Region II CHF                             ****
    % ************************************************************************
    %
    if Region == 2
        %
        q_S_chf_1 = 0.005 * (G_S^0.611) ;
        %
        q_chf = q_S_chf_1 * h_fg * ((Lambda *g* rho_v * (rho_f -
rho_v))^0.5);
        %
    end
    %
    % ************************************************************************
    % ****                          Region III CHF                            ****
    % ************************************************************************
    %
    if Region == 3
        %
        q_S_chf_3 = (( w / Lambda)^0.5) / ((1 + ((rho_v/rho_f)^0.25))^2) ;
        q_S_chf_3 = q_S_chf_3 * 0.7 * (A_flow/A_heated)  ;
        %
        q_chf = q_S_chf_3 * h_fg * ((Lambda *g* rho_v * (rho_f - rho_v))^0.5)
;
        %
    end
    %
    q_chf = q_chf / 1000000 ;           % convert to MW/m2
    %
    text = sprintf('Critical Heat Flux [MW/m^2] = %6.2f',q_chf) ;
    disp(text)
    disp(' ')
    %
    new_case = input('Do another case (1 = Yes, 0 = No) ? ') ;  % new case
    disp(' ')
    %
end   % End while loop for new case
%
% ************************************************************************
```

```
%  ****                                END                                    ****
%  ***************************************************************************
%
```

A-5: Sultan CHF Correlation

```
% ************************************************************************
% ****          file:      Sultan_CHF_corr.m                          ****
% ****            by:      Gregory L. DeWitt                          ****
% ****          date:      August 31, 2011                            ****
% ************************************************************************
% ****     reference:      Reactor Vessel External Cooling for Corum   ****
% ****                     Retention SULTAN Experimental Program and   ****
% ****                     Modelling with CATHARE Code                 ****
% ****                     S. Rouge 1998                               ****
% ****                                                                 ****
% ****         Notes:      Flow Boiling                                ****
% ****                     Cover pressure is 6m above vertical outlet  ****
% ****                     Program uses water for properties           ****
% ************************************************************************
% ****       Appllicability Ranges:                                    ****
% ****                       Pressure [ 0.1 - 0.5 MPa]                 ****
% ****                       Angle    [ 10 - 90 degrees]               ****
% ****                       Mass Flux [ 10 - 5,000 Kg/m^2-s]          ****
% ************************************************************************
%
clear variables
%
% set path to find data
%
path('c:\documents and settings\gdewitt\my
documents\mit\thesis\vessel_ht\calculations\', path) ; % MIT computer
%
% ************************************************************************
% ****                  TEST SECTION GEOMETRY INPUT SECTION            ****
% ************************************************************************
%
s     = 0.02   ;   % [m] side gap of flow channel
w     = 0.0143 ;   % [m] width of flow channel
w_h   = 0.01   ;   % [m] width of heater
L_h   = 0.20   ;   % [m] length of heater - stubs assumed unheated
%
% ************************************************************************
% ****                   GEOMETRY SECTION                              ****
% ****                Square Channel with one heated side              ****
% ************************************************************************
%
A_flow   = s * w       ;       % flow area
%
P_w      = 2 * (s + w) ;       % wetted perimeter
%
A_heated = w_h * L_h   ;       % [m^2]
%
D_h      = 4 * A_flow / P_w ;  % [m]
%
% ************************************************************************
% ****              END TEST SECTION GEOMETRY SECTION                  ****
% ************************************************************************
% ************************************************************************
% ****                  SULTAN GEOMETRY INPUT SECTION                  ****
```

```
% ************************************************************************
%
sultan_riser_L = 6 ; % [m] length of riser - test section to free surface
%                       vertical
%
% ************************************************************************
% ****                        New Case Loop                             ****
% ************************************************************************
%
new_case = 1 ;                  % set loop variable to (1=Yes; 0=No)
%
while new_case == 1 ;
    %
    % ********************************************************************
    % ****                    USER INPUT SECTION                        ****
    % ********************************************************************
    %
    disp('                    Sultan CHF Correlation for Flow Boiling')
    disp(' ')
    %
    gap = input('Input Gap Size (m) = ') ;
    disp(' ')
    %
    P = input('Input Test Section Local Pressure (MPa) = ') ; %CHF pressure
    disp(' ')
    %
    x = input('Input Local thermodynamic quality = ') ;  % exit quality
    disp(' ')
    %
    void = input('Input Void Fraction = ') ;  % exit void fraction
    disp(' ')
    %
    angle = input('Input Angle from Horizontal (degrees) (min=10, max=90) =
') ; % TS angle
    disp(' ')
    %
    G = input('Input Local Mass Flux (Kg/m^2-s) = ') ;          % Mass Flux
    disp(' ')
    %
    angle_rad = (angle/360)*2*pi ;             % convert degrees to radians
    %
    % ********************************************************************
    % ****                   Property Data                              ****
    % ********************************************************************
    %
    T_sat = Ts(P*10) ;          % saturation temperature (C)
    rho_f = 1 / vf(T_sat) ;     % liquid density (kg/m^3)
    rho_v = 1 / vg(T_sat) ;     % vapor density (kg/m^3)
    sigm  = sigma(T_sat)  ;     % surface tension (N/m)
    h_fg  = hfg(T_sat)*1000 ;   % heat of vaporazation [J/Kg-C]
    Cp    = Cpf(T_sat)*1000 ;   % Specific heat fluid [J/Kg-C]
    %
    text = sprintf('Local Saturation Temperature [C] = %6.2f',T_sat) ;
    disp(text)
    disp(' ')
    %
    % ********************************************************************
```

```
% ****                    Constants                                    ****
% ***************************************************************************
%
g = 9.81 ;                              % gravitational acceleration [m/s^2]
%
% ****    Sultan Correlation Constants                                  ****
%
b0  =  0.65444   ;
b1  = -1.2018    ;
b2  = -0.008388  ;
b3  =  0.000179  ;
b4  =  1.36899   ;
b5  = -0.077415  ;
b6  =  0.024967  ;
b7  = -0.086511  ;
b8  = -4.49425   ;
b9  =  9.28489   ;
b10 = -0.0066169 ;
b11 = 11.62546   ;
b12 =  0.855759  ;
b13 = -1.74177   ;
b14 =  0.182895  ;
b15 = -1.8898    ;
b16 =  2.2636    ;
%
% ***************************************************************************
% ****              Sultan CHF Correlation                               ****
% ***************************************************************************
% ****   Adjust pressure for riser in SULTAN facility                    ****
% ***************************************************************************
% ****   Determine void fraction for SULTAN riser from Test              ****
% ****   Outlet Quality                                                  ****
% ***************************************************************************
%
if x <= 0
    %
    sult_riser_void = void ;
    %
else
    sult_riser_void = void ;
end
%
sult_riser_den = sult_riser_void * rho_v ;
sult_riser_den = sult_riser_den + (1 - sult_riser_void) * rho_f ;
%
P_sultan = P - (sult_riser_den * g * sultan_riser_L)/1000000  ;
%                       subtract SULTAN riser hydraulic dead from test
%                       section measured exit pressure to get cover
%                       pressure [MPa]
%
A0 = b0 + (b1*gap*log(G)) + (b2/(P_sultan^2)) + (b3*G) +
(b4*gap/P_sultan) ;
A0 = A0 + (b5*gap/(P_sultan^2))  + (b6*P*(log(G)^2))    ;
%
A1 = b7*(log(G)^2) + b8*gap*log(G) ;
%
A2 = b9 * gap ;
```

```
    %
    A3 = b10*(log(G)^2) + b11*gap*P + b12*x*log(G) ;
    %
    A4 = b13*P + b14*log(G) + b15*x + b16*gap ;
    %
    q_chf = A0 + A1*x + A2*(x^2) ;
    q_chf = q_chf + A3*sin(angle_rad) + A4*(sin(angle_rad)^2) ;
    %
    text = sprintf('Sultan Riser Void Fraciton = %6.2f',sult_riser_void) ;
    disp(text)
    disp(' ')
    %
    text = sprintf('Pressure + Sultan Riser Head [MPa] = %6.2f',P_sultan) ;
    disp(text)
    disp(' ')
    %
    text = sprintf('Critical Heat Flux [MW/m^2] = %6.2f',q_chf) ;
    disp(text)
    disp(' ')
    %
    new_case = input('Do another case (1 = Yes, 0 = No) ? ') ;  % new case
    disp(' ')
    %
end   % End while loop for new case
%
% ************************************************************************
% ****                          END                                   ****
% ************************************************************************
```

A-7: Steam Table Functions

```
function [Cpf]=Cpf(T)
  %fluid specific heat [kJ/kg*C] at T [celsius]

 Tsat=[0:10:370,374.15];
  %saturation temperature in celsius


Cpliq=[4.218,4.194,4.182,4.179,4.179,4.181,4.185,4.191,4.198,4.207,4.218,4.23
0,4.244,4.262,4.282,4.306,4.334,4.366,4.403,4.446,4.494,4.550,4.613,4.685,4.7
69,4.866,4.985,5.134,5.307,5.520,5.794,6.143,6.604,7.241,8.225,10.07,15,55,1e
6];
 %liquid specific heat [kJ/kg*C] at T [celsius]

Cpf=interp1(Tsat,Cpliq,T);

function [Cpg]=Cpg(T)
  %gas specific heat [kJ/kg*C] at T [celsius]

 Tsat=[0:10:370,374.15];
  %saturation temperature in celsius


Cpvap=[1.863,1.870,1.880,1.890,1.900,1.912,1.924,1.946,1.970,1.999,2.034,2.07
6,2.125,2.180,2.245,2.320,2.406,2.504,2.615,2.741,2.883,3.043,3.223,3.426,3.6
56,3.918,4.221,4.575,4.996,5.509,6.148,6.968,8.060,9.580,11.87,15.8,27.0,107.
0,1e5];
 %vapor specific heat [kJ/kg*C] at T [celsius]

Cpg=interp1(Tsat,Cpvap,T);

function [hf]=hf(T)
  %liquid enthalpy [kJ/kg] at T [celsius]

 Tsat=[0:10:370,374.15];
  %saturation temperature in celsius


hliq=[0.000611,41.99,83.86,125.66,167.47,209.3,251.1,293.0,334.9,376.9,419.1,
461.3,503.7,546.3,589.1,632.2,675.5,719.1,763.1,807.5,852.4,897.7,943.7,990.3
,1037.6,1085.8,1135.0,1185.2,1236.8,1290,1345,1402,1462,1526,1596,1672,1762,1
892,2095];
 %liquid saturation enthalpy in kJ/kg

hf=interp1(Tsat,hliq,T);

function [hfg]=hfg(T)
  %evaporation enthalpy [kJ/kg] at T [celsius]

 Tsat=[0:10:370,374.15];
  %saturation temperature in celsius
```

```
hvap=[2501,2519,2538,2556,2574,2592,2609,2626,2643,2660,2676,2691,2706,2720,2
734,2747,2758,2769,2778,2786,2793,2798,2802,2803,2803,2801,2796,2790,2780,276
6,2749,2727,2700,2666,2623,2565,2481,2331,2095];
 %vapor saturation enthalpy in kJ/kg


hliq=[0.000611,41.99,83.86,125.66,167.47,209.3,251.1,293.0,334.9,376.9,419.1,
461.3,503.7,546.3,589.1,632.2,675.5,719.1,763.1,807.5,852.4,897.7,943.7,990.3
,1037.6,1085.8,1135.0,1185.2,1236.8,1290,1345,1402,1462,1526,1596,1672,1762,1
892,2095];
 %liquid saturation enthalpy in kJ/kg

deltah=hvap-hliq;

hfg=interp1(Tsat,deltah,T);

function [hg]=hg(T)
  %gas saturation enthalpy [kJ/kg] at T [celsius]

 Tsat=[0:10:370,374.15];
  %saturation temperature in celsius


hvap=[2501,2519,2538,2556,2574,2592,2609,2626,2643,2660,2676,2691,2706,2720,2
734,2747,2758,2769,2778,2786,2793,2798,2802,2803,2803,2801,2796,2790,2780,276
6,2749,2727,2700,2666,2623,2565,2481,2331,2095];
 %vapor saturation enthalpy in kJ/kg

hg=interp1(Tsat,hvap,T);

function [Kf]=Kf(T)
  %fluid thermal conductivity [W/m*C] at T [celsius]

 Tsat=[0:10:370,374.15];
  %saturation temperature in celsius


Kliq=[0.569,0.587,0.603,0.618,0.631,0.643,0.653,0.662,0.670,0.676,0.681,0.684
,0.687,0.688,0.688,0.687,0.684,0.681,0.677,0.671,0.664,0.657,0.648,0.639,0.62
8,0.616,0.603,0.589,0.574,0.558,0.541,0.523,0.503,0.482,0.460,0.434,0.397,0.3
40,0.240];

Kf=interp1(Tsat,Kliq,T);

function [Kg]=Kg(T)
  %gas thermal conductivity [W/m*C] at T [celsius]

 Tsat=[0:10:370,374.15];
  %saturation temperature in celsius

 Kvap=1e-
3*[17.6,18.2,18.8,19.5,20.2,20.9,21.6,22.4,23.2,24.0,24.9,25.8,26.7,27.8,28.9
```

```
,30.0,31.3,32.6,34.1,35.7,37.4,39.4,41.5,43.9,46.5,49.5,52.8,56.6,60.9,66.0,7
1.9,79.1,87.8,99.0,114,134,162,199,240];

Kg=interp1(Tsat,Kvap,T);

function [muf]=muf(T)
  %fluid dynamic viscosity [Ns/m^2] at T [celsius]

 Tsat=[0:10:370,374.15];
  %saturation temperature in celsius

 muliq=1e-
6*[1786,1304,1002,798.3,653.9,547.8,467.3,404.8,355.4,315.6,283.1,254.8,231.0
,210.9,194.1,179.8,167.7,157.4,148.5,140.7,133.9,127.9,122.4,117.5,112.9,108.
7,104.8,101.1,97.5,94.1,90.7,87.2,83.5,79.5,75.4,69.4,62.1,51.8,41.4];

muf=interp1(Tsat,muliq,T);

function [mug]=mug(T)
  %gas dynamic viscosity [Ns/m^2] at T [celsius]

 Tsat=[0:10:370,374.15];
  %saturation temperature in celsius

 muvap=1e-
6*[8.105,8.504,8.903,9.305,9.701,10.10,10.50,10.89,11.29,11.67,12.06,12.45,12
.83,13.20,13.57,13.94,14.30,14.66,15.02,15.37,15.72,16.07,16.42,16.78,17.14,1
7.51,17.90,18.31,18.74,19.21,19.73,20.30,20.95,21.70,22.70,24.15,26.45,30.6,4
1.4];

mug=interp1(Tsat,muvap,T);

function [Ps]=Ps(T)
%yields the saturation pressure P [bar] at temperature [celsius]

Tsat=[0:10:370,374.15];
 %saturation temperature in celsius

Psat=[0.006112,0.012271,0.023368,0.042418,0.073750,0.12335,0.19919,0.31161,0.
47358,0.70109,1.01325,1.4327,1.9854,2.7011,3.6136,4.7597,6.1804,7.9202,10.027
,12.553,15.550,19.080,23.202,27.979,33.480,39.776,46.941,55.052,64.191,74.449
,85.917,98.694,112.89,128.64,146.08,165.37,186.74,210.53,221.2];
 %saturation pressure in bar

Ps=interp1(Tsat,Psat,T);

function [sf]=sf(T)
  %fluid specific entropy [kJ/kg*K] at T [celsius]

 Tsat=[0:10:300,320,340,360,374.15];
  %saturation temperature in celsius


sliq=[0,0.151,0.2966,0.4369,0.5725,0.7038,0.8312,0.9549,1.0753,1.1925,1.3069,
```

```
1.4185,1.5276,1.6344,1.7391,1.8418,1.9427,2.0419,2.1396,2.2359,2.3309,2.4248,
2.5178,2.6099,2.7015,2.7927,2.8838,2.9751,3.0668,3.1594,3.2534,3.448,3.6594,3
.9147,4.4298];
  %saturated liquid specific entropy in kJ/kg*K

sf=interp1(Tsat,sliq,T);

function [sg]=sg(T)
  %vapor specific entropy [kJ/kg*K] at T [celsius]

 Tsat=[0:10:300,320,340,360,374.15];
  %saturation temperature in celsius


svap=[9.1562,8.9008,8.6672,8.4533,8.2570,8.0763,7.9096,7.7553,7.6122,7.4791,7
.3549,7.2387,7.1296,7.0269,6.9299,6.8379,6.7502,6.6663,6.5857,6.5079,6.4323,6
.3585,6.2861,6.2146,6.1437,6.0730,6.0019,5.9301,5.8571,5.7821,5.7045,5.5362,5
.3357,5.0526,4.4298];
  %saturated vapor specific entropy in kJ/kg*K

sg=interp1(Tsat,svap,T);


function [sigma]=sigma(T)
  %surface tension [N/m] at T [celsius]

 Tsat=[0:10:370,374.15];
  %saturation temperature in celsius

 surftens=1e-
3*[75.6,74.24,72.78,71.23,69.61,67.93,66.19,64.40,62.57,60.69,58.78,56.83,54.
85,52.83,50.79,48.70,46.59,44.44,42.26,40.05,37.81,35.53,33.23,30.90,28.56,26
.19,23.82,21.44,19.07,16.71,14.39,12.11,9.89,7.75,5.71,3.79,2.03,0.47,0];

sigma=interp1(Tsat,surftens,T);

function [Ts]=Ts(P)
%yields the saturation temperature [celsius] at pressure P [bar]

Tsat=[0:10:370,374.15];
 %saturation temperature in celsius

Psat=[0.006112,0.012271,0.023368,0.042418,0.073750,0.12335,0.19919,0.31161,0.
47358,0.70109,1.01325,1.4327,1.9854,2.7011,3.6136,4.7597,6.1804,7.9202,10.027
,12.553,15.550,19.080,23.202,27.979,33.480,39.776,46.941,55.052,64.191,74.449
,85.917,98.694,112.89,128.64,146.08,165.37,186.74,210.53,221.2];
 %saturation pressure in bar

Ts=interp1(Psat,Tsat,P);

function [uf]=uf(T)
  %liquid specific internal energy [kJ/kg] at T [celsius]

 Tsat=[0:10:370,374.15];
```

```
  %saturation temperature in celsius


hliq=[0.000611,41.99,83.86,125.66,167.47,209.3,251.1,293.0,334.9,376.9,419.1,
461.3,503.7,546.3,589.1,632.2,675.5,719.1,763.1,807.5,852.4,897.7,943.7,990.3
,1037.6,1085.8,1135.0,1185.2,1236.8,1290,1345,1402,1462,1526,1596,1672,1762,1
892,2095];
  vliq=1e-
3*[1.0002,1.0004,1.0018,1.0044,1.0079,1.0121,1.0171,1.0228,1.0290,1.0359,1.04
35,1.0515,1.0603,1.0697,1.0798,1.0906,1.1021,1.1144,1.1275,1.1415,1.1565,1.17
26,1.1900,1.2087,1.2291,1.2512,1.2755,1.3023,1.3321,1.3655,1.4036,1.4475,1.49
92,1.562,1.639,1.741,1.894,2.22,3.17];

Psat=[0.006112,0.012271,0.023368,0.042418,0.073750,0.12335,0.19919,0.31161,0.
47358,0.70109,1.01325,1.4327,1.9854,2.7011,3.6136,4.7597,6.1804,7.9202,10.027
,12.553,15.550,19.080,23.202,27.979,33.480,39.776,46.941,55.052,64.191,74.449
,85.917,98.694,112.89,128.64,146.08,165.37,186.74,210.53,221.2];
  uliq=hliq-(1e5*Psat.*vliq)/1e3;
 %liquid saturation internal energy in kJ/kg

uf=interp1(Tsat,uliq,T);

function [ug]=ug(T)
  %vapor specific internal energy [kJ/kg] at T [celsius]

 Tsat=[0:10:370,374.15];
  %saturation temperature in celsius


hvap=[2501,2519,2538,2556,2574,2592,2609,2626,2643,2660,2676,2691,2706,2720,2
734,2747,2758,2769,2778,2786,2793,2798,2802,2803,2803,2801,2796,2790,2780,276
6,2749,2727,2700,2666,2623,2565,2481,2331,2095];

vvap=[206.146,106.422,57.836,32.929,19.546,12.045,7.6776,5.0453,3.4083,2.3609
,1.6730,1.2101,0.89171,0.66832,.50866,.39257,.30685,.24262,.19385,.15635,.127
19,.104265,.086062,.071472,.059674,.05056,.042149,.035599,.030133,.025537,.02
1643,.018316,.015451,.012967,.010779,.008805,.006943,.00493,.00317];%

Psat=[0.006112,0.012271,0.023368,0.042418,0.073750,0.12335,0.19919,0.31161,0.
47358,0.70109,1.01325,1.4327,1.9854,2.7011,3.6136,4.7597,6.1804,7.9202,10.027
,12.553,15.550,19.080,23.202,27.979,33.480,39.776,46.941,55.052,64.191,74.449
,85.917,98.694,112.89,128.64,146.08,165.37,186.74,210.53,221.2];
  uvap=hvap-(1e5*Psat.*vvap)/1e3;
 %vapor saturation internal energy in kJ/kg

ug=interp1(Tsat,uvap,T);

function [vf]=vf(T)
  %fluid specific volume [m^3/kg] at T [celsius]

 Tsat=[0:10:370,374.15];
  %saturation temperature in celsius

 vliq=1e-
3*[1.0002,1.0004,1.0018,1.0044,1.0079,1.0121,1.0171,1.0228,1.0290,1.0359,1.04
```

```
35,1.0515,1.0603,1.0697,1.0798,1.0906,1.1021,1.1144,1.1275,1.1415,1.1565,1.17
26,1.1900,1.2087,1.2291,1.2512,1.2755,1.3023,1.3321,1.3655,1.4036,1.4475,1.49
92,1.562,1.639,1.741,1.894,2.22,3.17];
  %saturated liquid specific volume in m^3/kg

vf=interp1(Tsat,vliq,T);

function [vg]=vg(T)
  %gas specific volume [m^3/kg] at T [celsius]

 Tsat=[0:10:370,374.15];
  %saturation temperature in celsius


vvap=[206.146,106.422,57.836,32.929,19.546,12.045,7.6776,5.0453,3.4083,2.3609
,1.6730,1.2101,0.89171,0.66832,.50866,.39257,.30685,.24262,.19385,.15635,.127
19,.104265,.086062,.071472,.059674,.05056,.042149,.035599,.030133,.025537,.02
1643,.018316,.015451,.012967,.010779,.008805,.006943,.00493,.00317];%
  %saturated vapor specific volume in m^3/kg

vg=interp1(Tsat,vvap,T);
```

Appendix B: LabVIEW Front and Back Panel Programming

LabVIEW: GLD CHF Loop (Mod 3).vi

FRONT PANEL – 1ST PLANE TOP

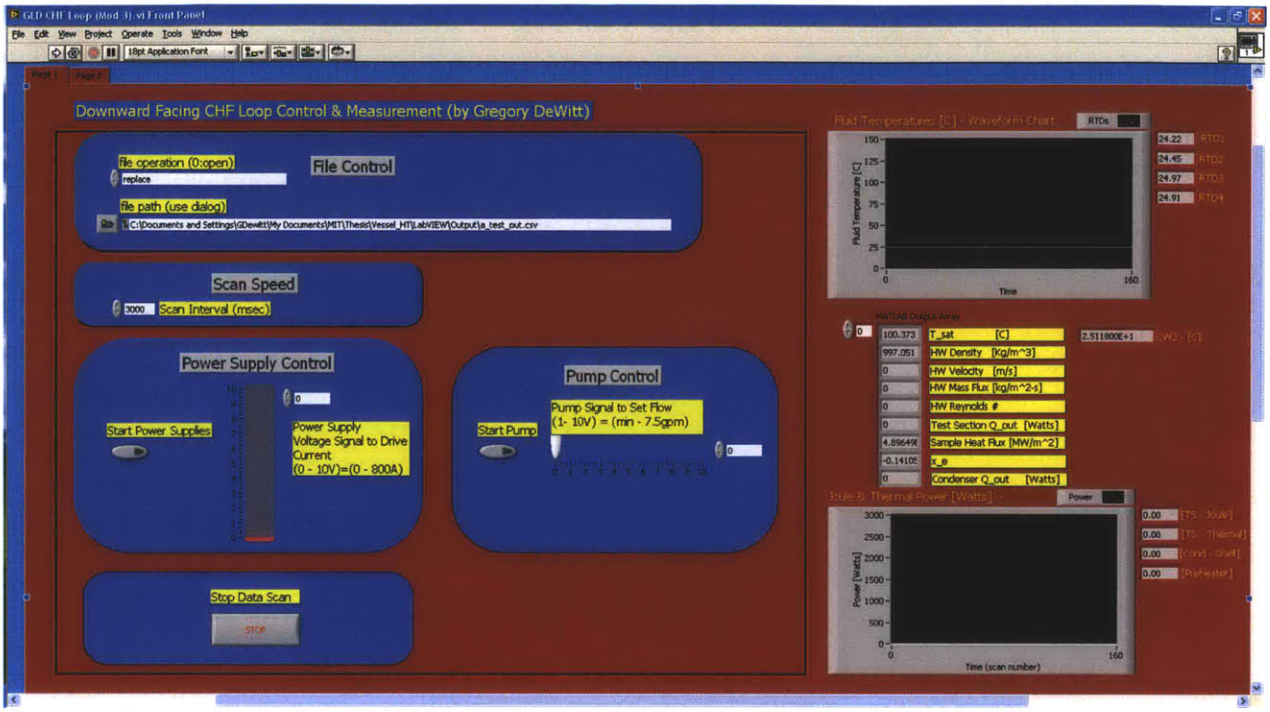

FRONT PANEL – 1ST PLANE BOTTOM

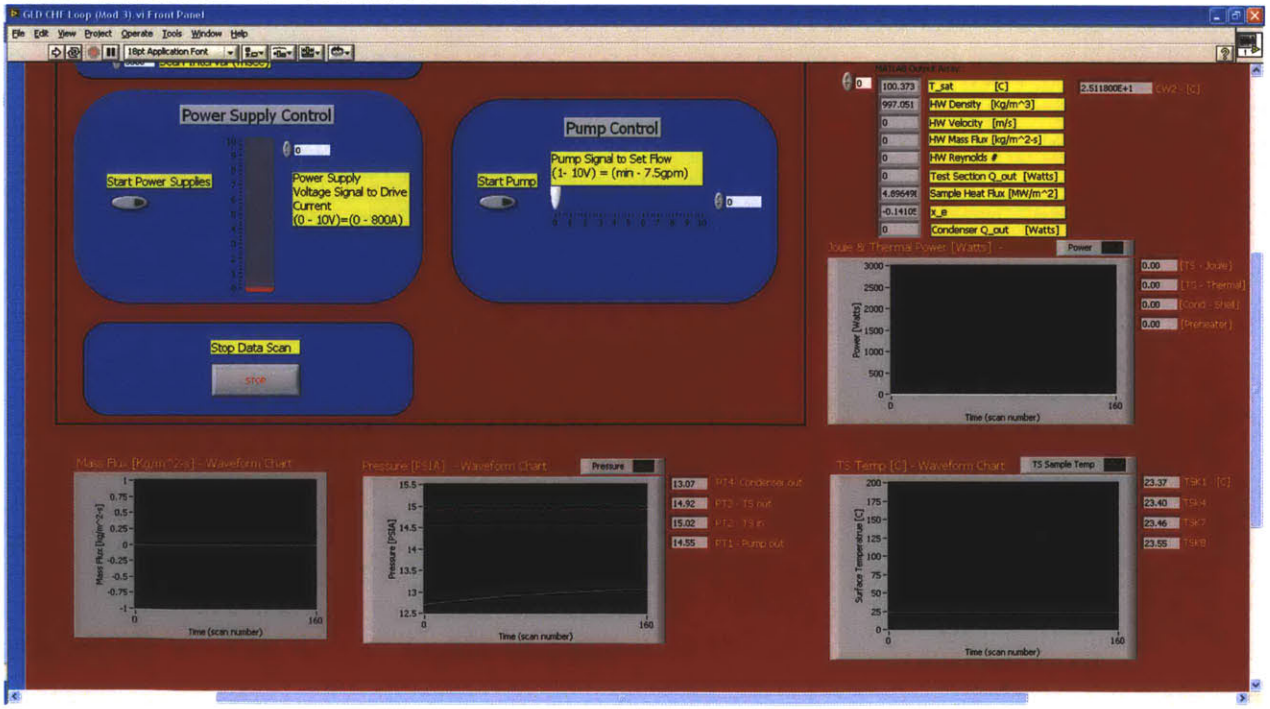

FRONT PANEL – 2nd PLANE TOP

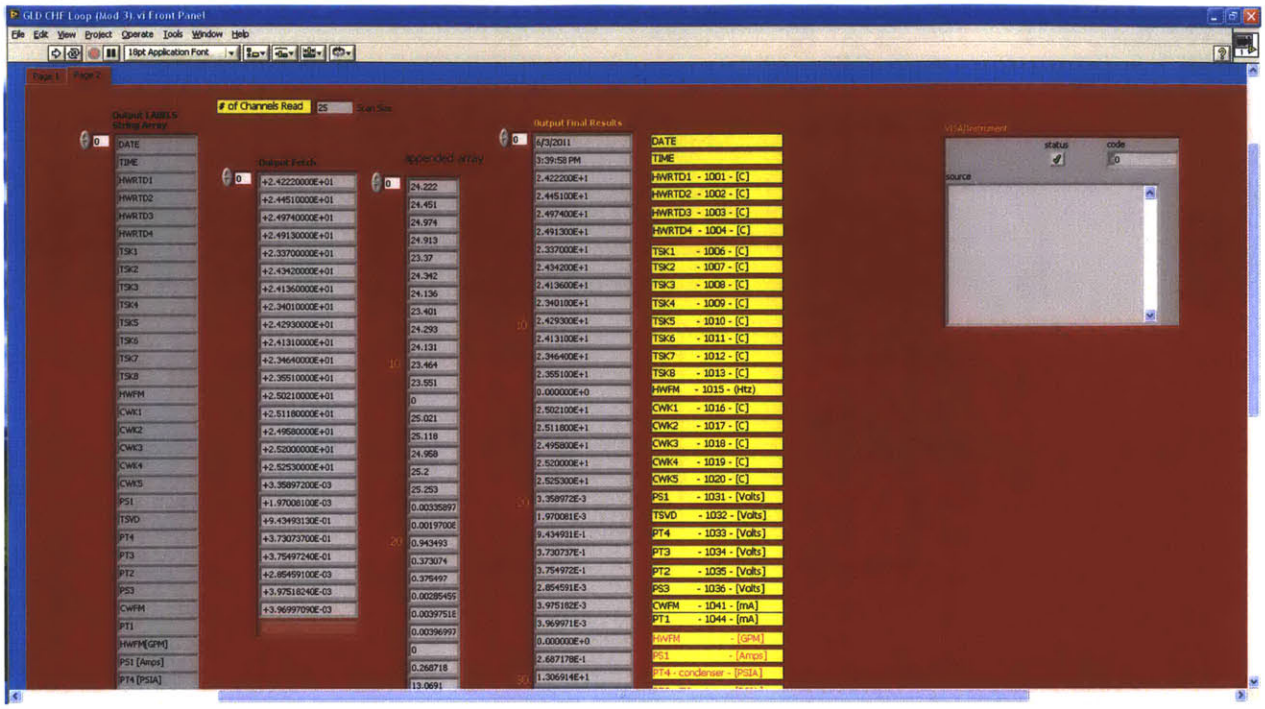

FRONT PANEL – 2nd PLANE BOTTTOM

BACK PANEL #1

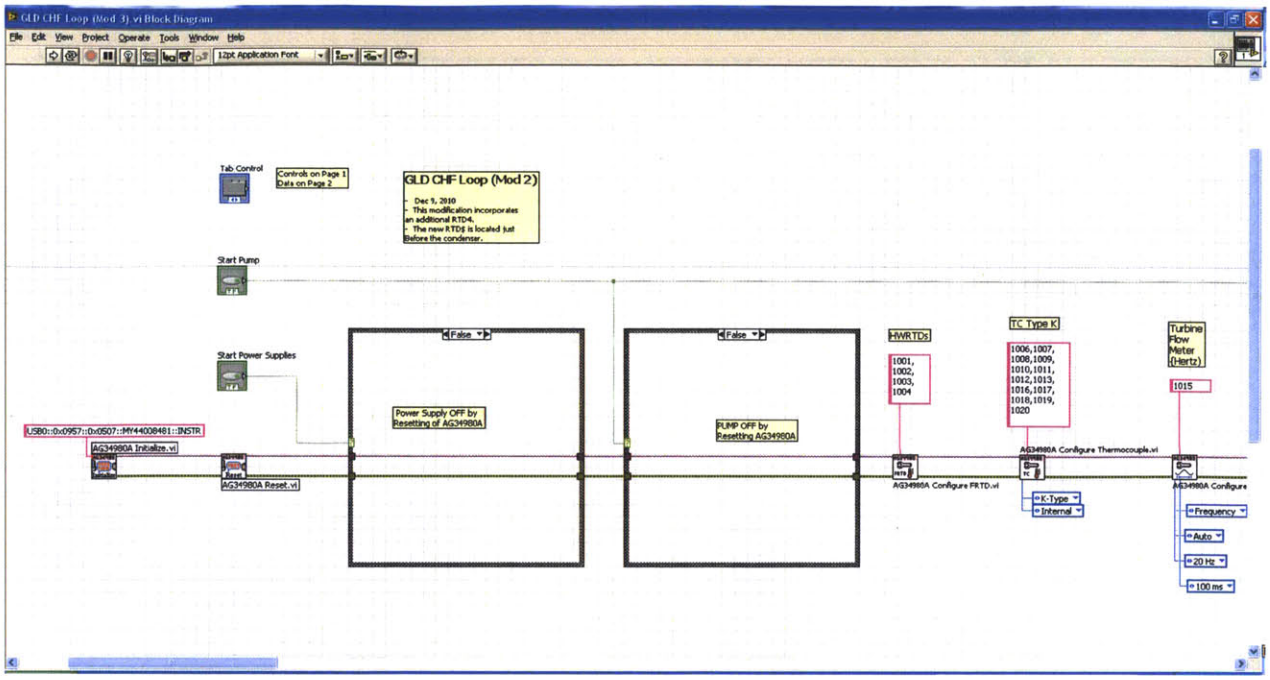

BACK PANEL #2

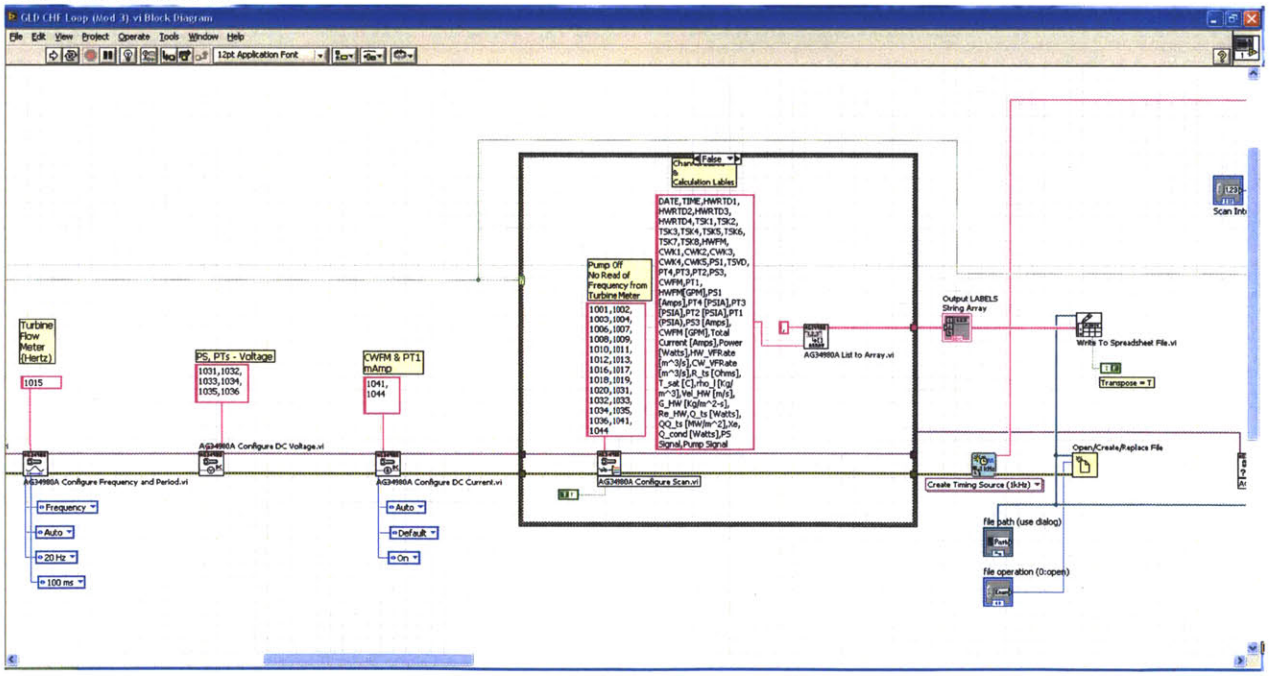

BACK PANEL #3

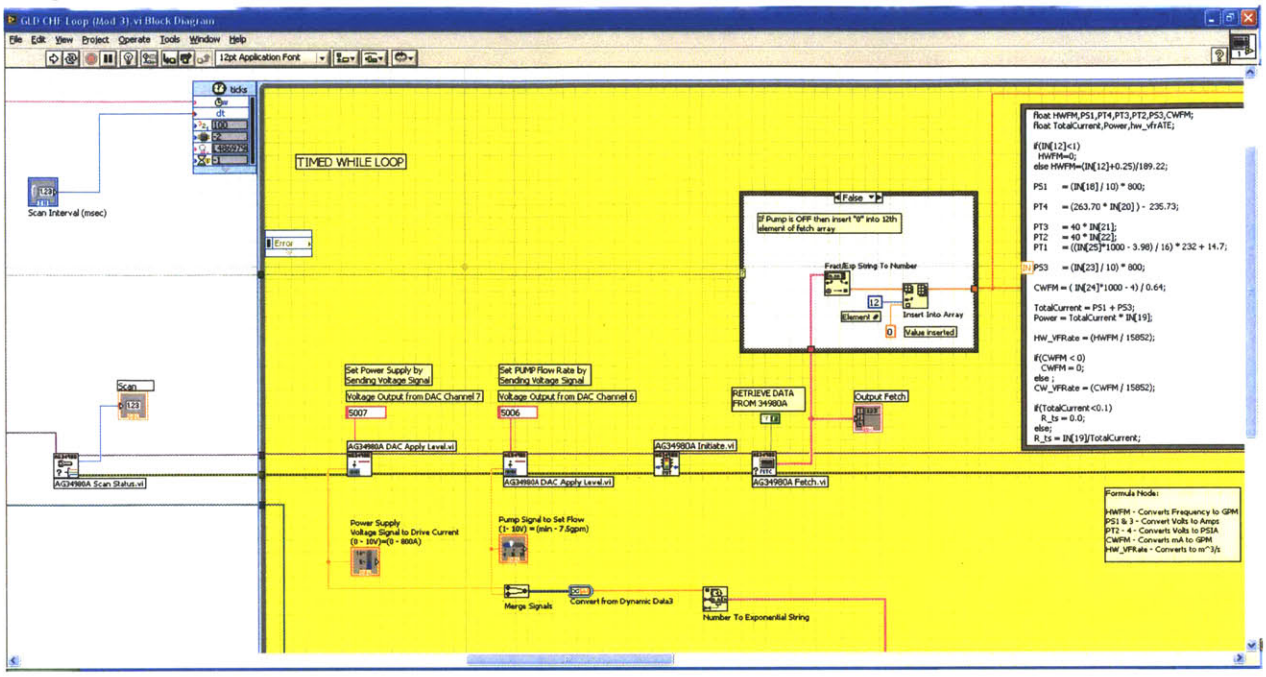

BACK PANEL #4

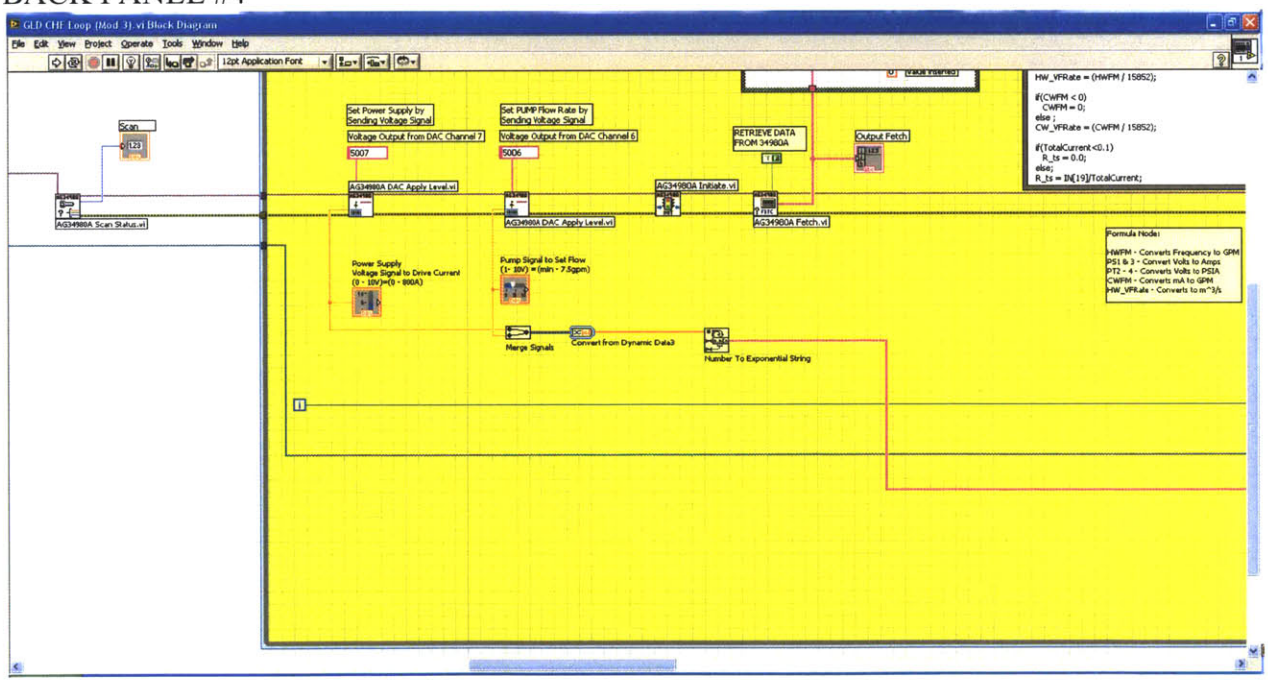

BACK PANEL #5

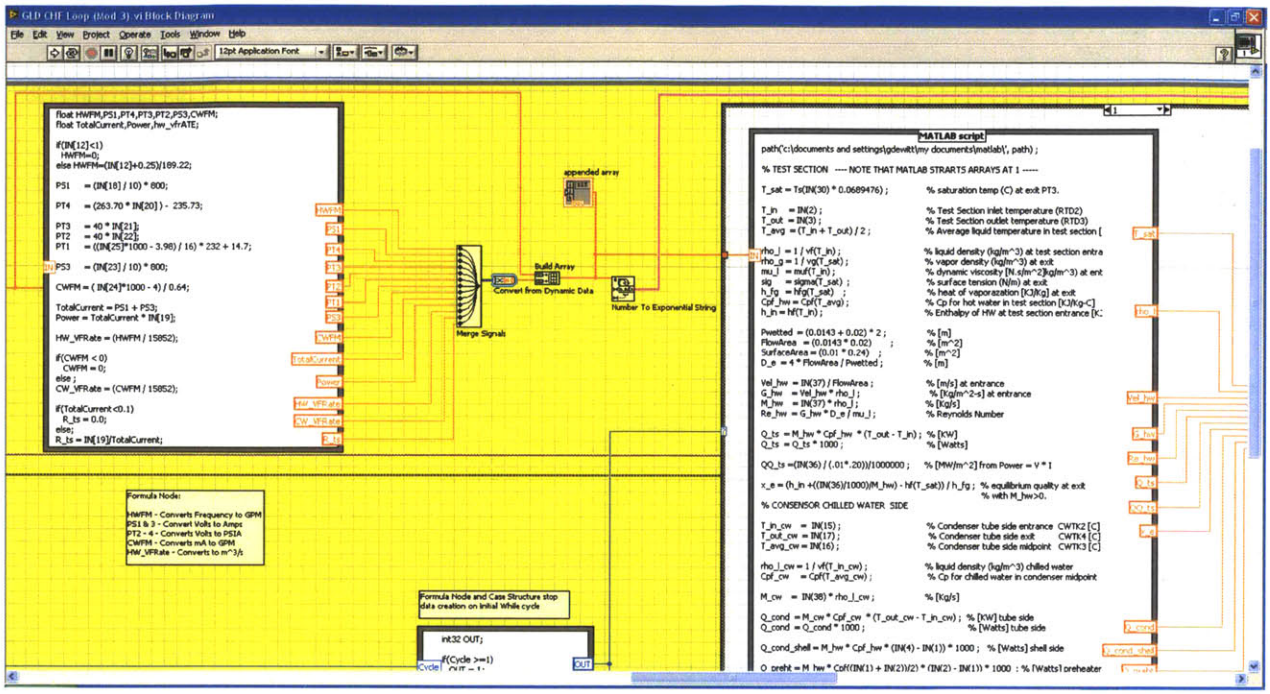

BACK PANEL #6

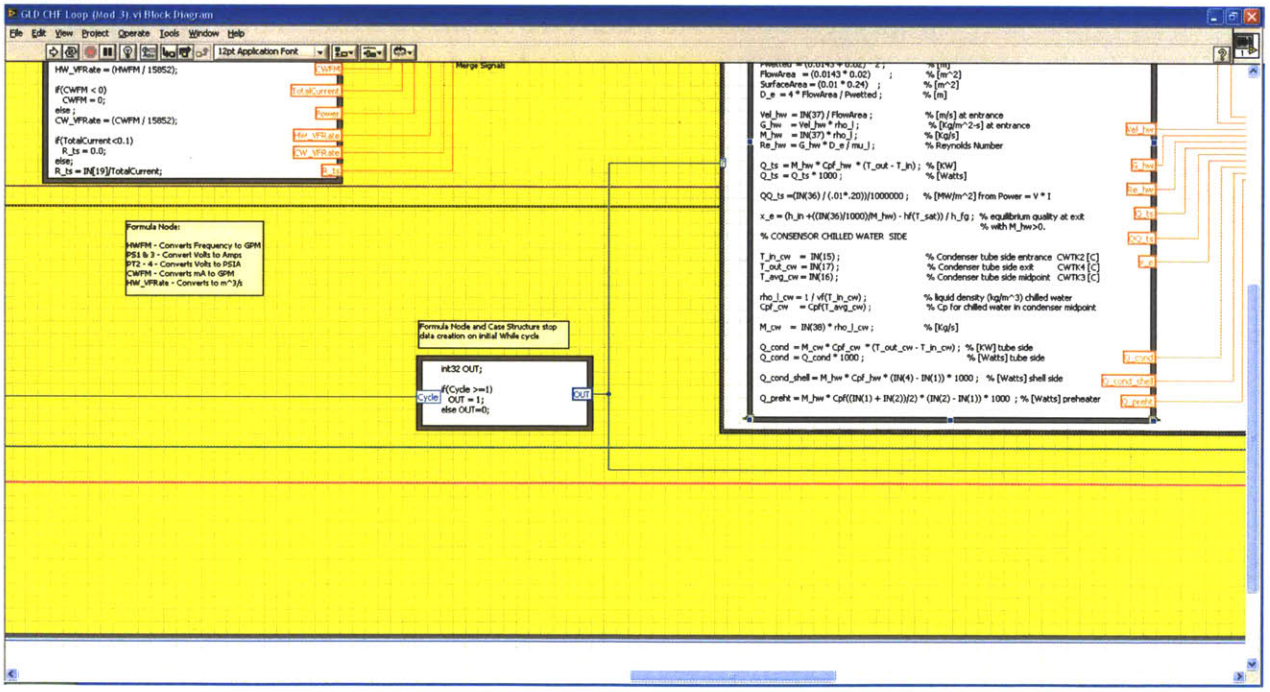

BACK PANEL #7

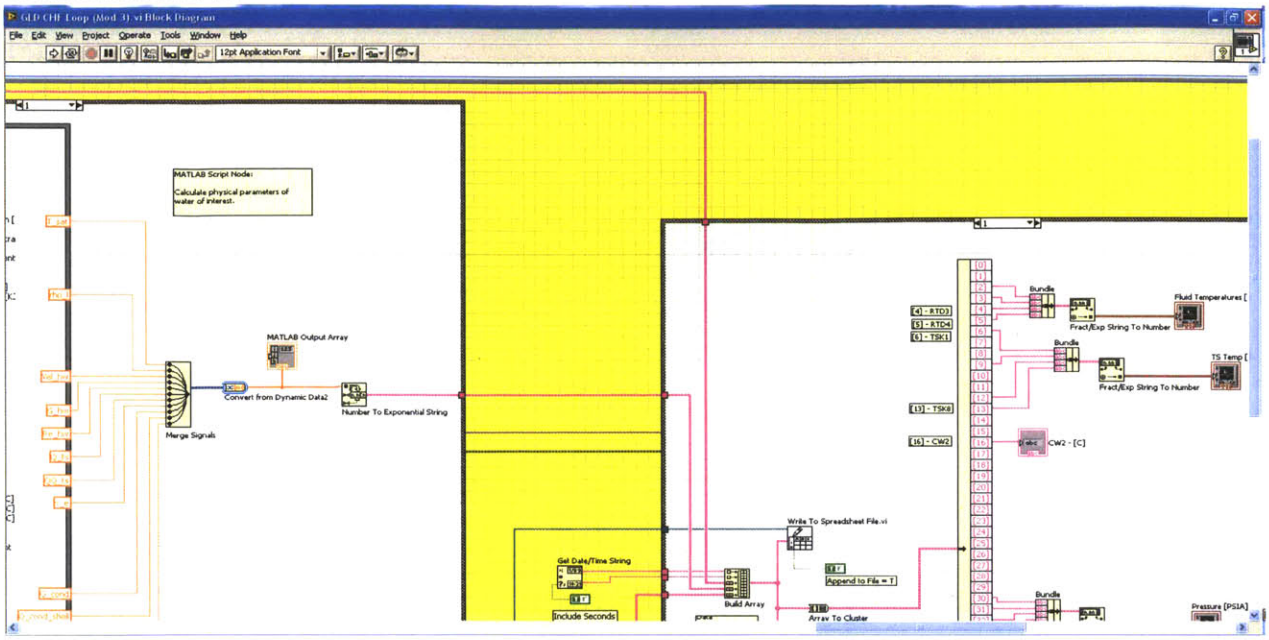

BACK PANEL #8

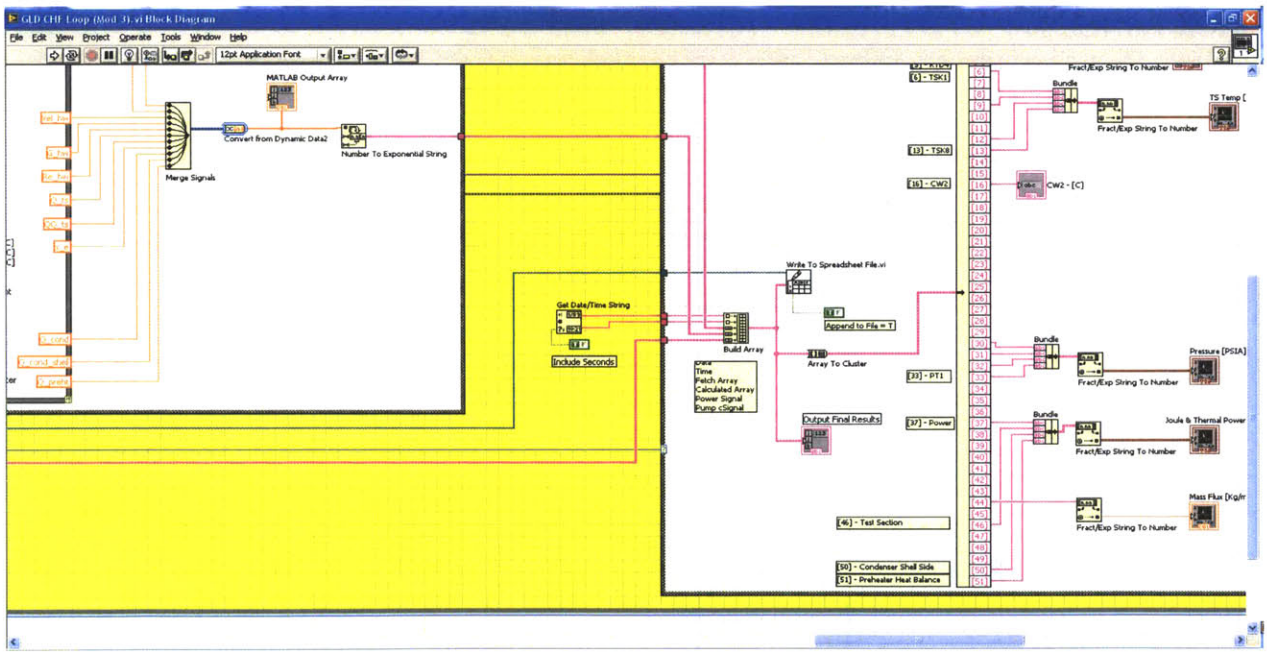

BACK PANEL #9

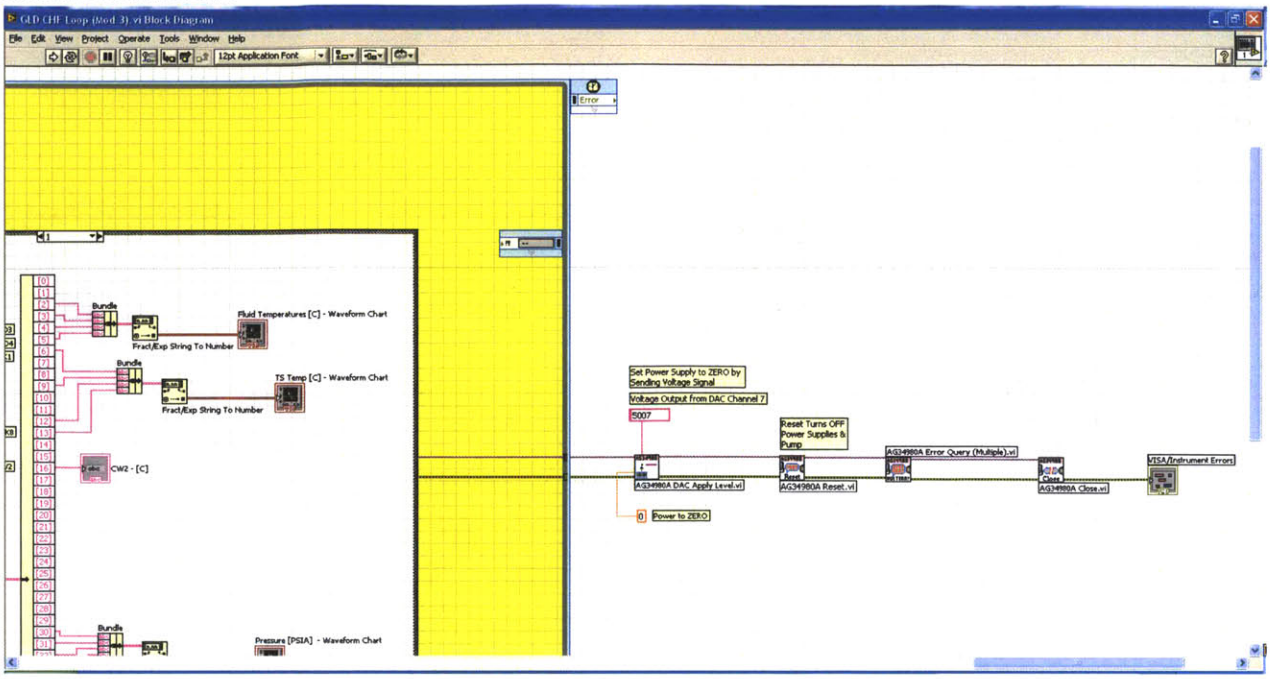

BACK PANEL #10

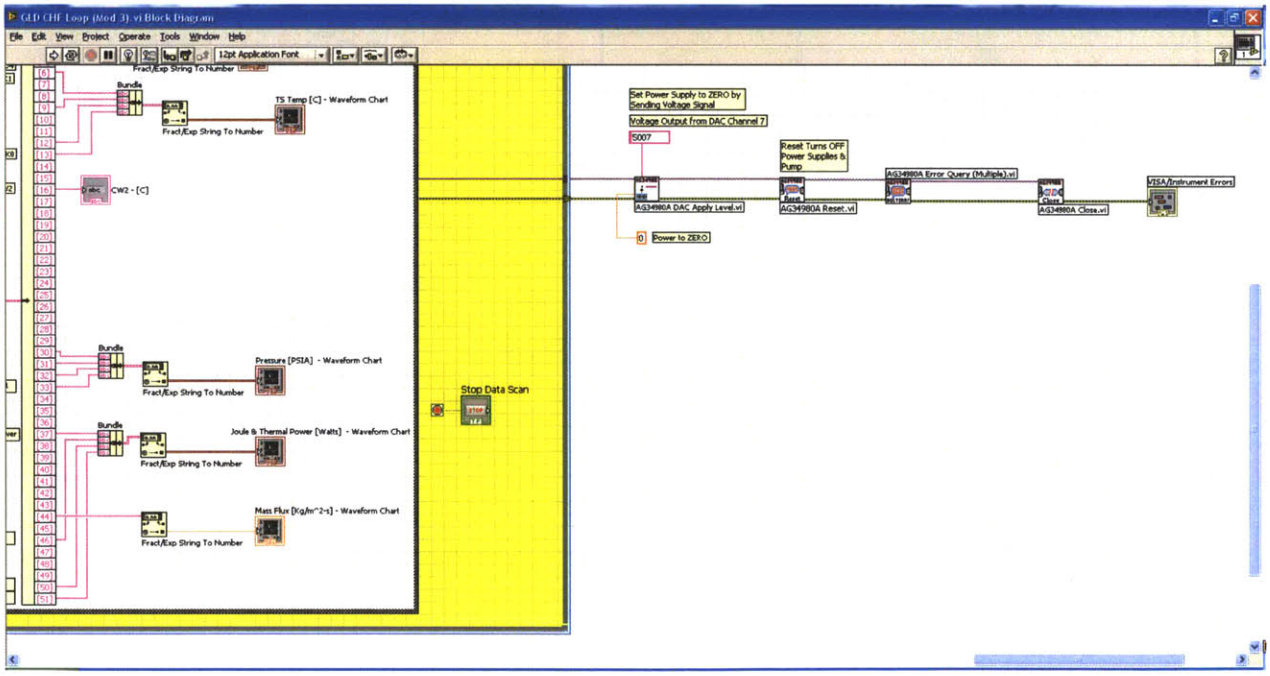

Appendix C: Experimental Procedure

TEST PROCEDURE

Investigation Downward Facing CHF with Water-based Nanofluids for IVR Applications

July 24, 2011

A) TEST SAMPLE PREPARATION

a. Clean surface with acetone & DI water
b. Sand blast surface (3 – 5 sweeps)
c. Re-clean surface with acetone & water
d. Clean MACOR insulator surface with water.
e. Polish copper studs and coupling blocks with steel wool
f. Mount test sample onto MACOR insulator and heat to 110 °C for ~15 minutes.
g. Screwing on copper studs

    i. Replace O-rings, if necessary

h. Install into test section
i. Measure angle of inclination

B) STARTING CONFIGUATION

a. Electric Power - Off

    i. Power supply "A" & "B" wall electrical box - OFF – levers down
    ii. Pump wall electrical box - OFF – lever down
    iii. Computer - OFF
    iv. Agilent DAS - OFF
    v. Control box AC supply – off – green light OFF
    vi. Suction pump – OFF
    vii. 2 kW pre-heater – OFF
    viii. DO probe NOT mounted.

b. Valves - closed

    i. Chilled Water ("CW")

        1. Ball valves (6) – closed
        2. 1" gate valve – closed
        3. Needle valve – closed

ii. Loop

1. Ball valves (4) – closed
2. Needle valve – closed

iii. Nitrogen Gas Line ("NGL")

1. Open all fittings and blow lines clear.
2. Weekly remove accumulator and check that balloon is clear of water.
3. Ball valve near regulator – closed
4. Four-way valve – open

    a. NGL are now atmospheric

5. Nitrogen tank valve – closed
6. Regulator valve – open

c. Record general conditions

i. Room temperature
ii. Weather conditions

C) WORKING FLUID

a. Drain and dispose of old fluid

i. Use gloves when handling nanofluids
ii. Open needle valve - top of loop
iii. Fill/drain tank – place on floor
iv. Open drain ball valve
v. Loosen priming screw on pump
vi. Close drain ball valve once flow to tank has stopped
vii. Open drain screw at bottom of pump for any residual fluid and add to tank
viii. Dispose of old fluid as per Green Lab procedure
ix. Tighten priming screw and drain screw on pump

b. Fill loop with fluid

i. Add ~11 liters of fluid to fill tank
    1. If alumina nanofluid then used
        a. If 0.001% then 10.6L DI Water plus 1.4ml Nyacol 20% by weight
        b. If 0.01% then 10.6L DI Water plus 14ml Nyacol 20% by weight

ii. Insert 1 kW cartridge heater into fill tank
    1. 1 kW Cartridge heater – ON
    2. Raise fluid temperature to ~60 °C to 70 °C
iii. Connect suction line to loop
iv. Cartridge heater – OFF
v. Plug DO probe mount with rubber stopper.
vi. Open ball valves on loop, except drain/fill ball valve.
vii. Turn on suction pump

    1. wait until ~ -30" Hg on both suction pump gauge and loop gauge near accumulator
    2. close needle valve

viii. Suction pump – off
ix. Open fill and drain ball valve.
x. Close drain ball valve once flow from tank has stopped.
xi. If fluid is not up to DO probe then:
    1. Check that about 1 liter of fluid remains in tank
    2. Put cover on fill tank
    3. Add about 5 to 10 psi of Nitrogen gas above remaining fluid
    4. Slowly open fill ball valve and watch fluid go above the flow meter before the DO probe stand.
    5. Close fill valve.
xii. Disconnect suction line from loop
xiii. Lift stopper on top of DO probe stand.

    1. pressure gauge on loop should = 0 psi.
    2. loop should be water solid

xiv. CHECK FOR LEAKS

D) **POWER ON**

a. Pump electric box on wall – lever up – ON
b. Power supplies – "A & B" – levers up – ON

    i. PS1 - switch up
        1. press reset button
    ii. PS3 – switch up
        1. pres reset button
    iii. Fans should be running

c. Computer – on
d. Agilent DAS – on
e. Control box – on – green light on

f. Start LabVIEW
g. Check measurement devices are functioning

    i. Chilled Water vortex flow meter

        1. Open all chilled water valves
        2. Note maximum flow
            a. visual reading
            b. digital output
        3. Close ball valve above condenser (CW GPM = 0)

    ii. Loop turbine flow meter

        1. Set pump flow rate to target mass flux
        2. Note digital readout

    iii. RTDs (4) – loop fluid temperature
        1. Check with Ice or flow with no heat added
        2. Record initial readings
    iv. Test section K-type thermocouples (up to 8)
    v. Chilled water K-type thermocouples (5)
    vi. Pressure transducers (4)
        1. While loop is empty record
    vii. Current (2)
    viii. Voltage Drop - Test section

E) DE-GASING OF FLUID

a. Attach green degassing line to loop needle valve
b. Submerge burping line into fill/drain tank below remaining fluid level.
c. Set test section power such that nucleate sub-cooled boiling can be seen on the test section surface
d. Wait until bulk fluid temperature ~ 60 ^{o}C
e. On 10 minute intervals open needle valve slowly until gas bubbles into de-gassing bucket stops
f. Take Dissolved Oxygen measurement ("DO")
g. Repeat steps (e – f) until DO measurement. = 4.0 ppm

F) SET PRESSURE IN ACCUMULATOR

a. Atmospheric pressure – leave gas line open at four way valve next to gas bottle regulator.
b. Above atmospheric pressure

i. Ball valve connecting NGL to fill tank – closed
ii. NGL purge valve - closed
iii. Ball valve next to regulator – closed
iv. Backpressure regulator valve – set valve
v. Gas bottle regulator –set target pressure.
vi. Open ball valve next to regulator.
vii. Check visual reading on top of accumulator once gas feed has stopped

G) HEATUP TO SATURATION

a. Increase flow rate to target mass flux
b. Set test section power to about 65% of expected CHF value
c. Target RTD1 = 2 – 3 °C below saturation

i. Condenser exit
ii. Protect pump from cavitations
iii. Chilled Water flow - increase as needed

1. close 1" gate valve
2. open ball valve above condenser
3. adjust needle valve near gate valve

d. Reduce power to 0.25 MW/m^2 at any sign of cavitations
e. Monitor target mass flux

H) CHF DETERMINATION

a. Set loop flow rate for CHF experiment
b. Set Power = 65% of expected CHF

c. Stepwise increases of ~0.1 MW/m^2
d. 2 minute intervals or longer
e. Adjust CW flow with needle valve to maintain bulk fluid temperature entering pump (RTD1 = T_sat – 2 C)
f. Test Section exit bulk (RTD3 = T_sat)
g. Monitor loop pressure
h. Repeat (c-g) until CHF (Orange dot)

i. Hit stop button on LabVIEW control panel
    1. Power supply and pump are now OFF

ii. If necessary hit Red panic button on control box

1. Power supplies are now OFF
2. Pump still ON

iii. Turn of pre-heater
iv. Power Supply electric box levers on wall – DOWN – OFF
v. Power Supply ON/OFF switches – DOWN - OFF

I) COOLDOWN

a. Chilled Water open
b. Restart pump at minimum via LabVIEW
    i. Be sure to change filename so to no overlay test data
c. Pump OFF after fluid temperature RTD3 < 20 °C

    i. Electric box on wall – Lever down – OFF

d. All CW ball valves closed
e. Turn off Agilent DAS after data is saved
f. Turn off Computer
g. Disconnect Locomotive Cables from Test Section
h. Remove copper connector blocks from Test Section

J) DISASSEMBLE

a. Remove DO probe
b. Drain loop of working fluid
    i. Open needle valve used for vacuum and degassing line
    ii. Using wooden block, raise flex line to above lower span of loop
    iii. Open valve between loop and drain tank
    iv. Remove priming screw from pump once most of fluid has left the system
    v. Close valve between loop and drain tank
    vi. More fluid can be removed by opening drain screw at bottom of pump into a glass beaker.
    vii. Replace pump screws once fluid is removed.
c. Remove locomotive cables from copper blocks
d. Remove safety bar between copper blocks
e. Remove copper blocks
f. Unscrew and remove back to test section
g. Lift out MACOR
h. Unscrew copper studs
i. Carefully remove test heater
    i. Store test heater in zip-lock bag
    ii. Label
j. Inspect MACOR for defects
k. Clean MACOR with water

Appendix D: RELAP5 Input Deck for AP1000 IVR

```
= GLD RELAP5 Mod 3.3 Input Deck for Downward Facing AP1000 IVR CHF
*
*******************************************************************************
* Gregory L. DeWIttt - PhD candidate MIT Nuclear Science and Engineering      *
*******************************************************************************
* Modification Date:  August 18, 2011                                         *
*                                                                             *
* TMDPVOL -> SNGLJUN -> PIPE -> SNGLJUN -> SNGLVOL -> SNGLJUN ->TMDPVOL       *
*                                                                             *
* This model uses TMDPVOL to set the boundary pressures.                      *
* Pressures set as expected during IVR at 2 hours (1.5 atm in containment)    *
* Bottom: Pr = 2.07 atm & T=111.6 C                                           *
* Top:    Pr = 1.5  atm & T=111.6 C                                           *
* RELAP is free to calculate Mass Flow rate.                                  *
*******************************************************************************
* In this case top and one bottom loss coefficients are used. None between.   *
*******************************************************************************
*    Model Options Section                                                    *
*******************************************************************************
* Problem Type Card ***********************************************************
*
*   Type      State
*
100   new       stdy-st    * for [steady state: stdy-st] [transient: transnt]
*
* Input check or run option card **********************************************
*
101 run
*
*   Input   Output
*   units   units
*
102  si      si
*
*******************************************************************************
*      Time Step Control Section                                              *
*******************************************************************************
*  End     Minimum     Maximum     Control   Minor   Major   Restart
*  time    time step   time step   Options   Edit    Edit    Freq.
*  (sec)   (sec)       (sec)       (ssdtt)   Freq.   Freq.
*
201  1000.0   1.0e-7      0.01        00003     100     50000    50000
*
*******************************************************************************
*      Hydrodynamic Component Section {CCCXXNN}                               *
*******************************************************************************
* START TMDPLVOL [101] represents IVR inflow at bottom of vessel cavity       *
*******************************************************************************
* Used to set a pressure boundary conditions of 1.57 atmospheres & T=100 C    *
*******************************************************************************
*
*          Component    Component
```

```
*         name        type
*
1010000     "Flowin"    tmdpvol
*
*
1010101  100.0       * arbitrary flow area    [m^2]
1010102   0.0       * length - calculated    [m]
1010103  100.0       * volume - large         [m^3]
1010104   0.0       * azimuthal angle        [degrees]
1010105   0.0       * inclination angle - up [degrees]
1010106   0.0       * elevation change       [m]
1010107   0.0       * wall roughness         [m]
1010108   0.0       * D_e - calculated       [m]
1010109   0000010   * "tlpvbfe" - no wall friction
*
*       TMDPVOL
*       Control  Table
*       Word     Trip
*       {ebt}
*
1010200   003     0   * TMDPVOL conrol word - set pressure and temperature
*
*       Search   Pressure  Temperature
*       Variable [Pa]     [K]
*
1010201   -1.0     159280.0  373.15     * Pr=1.57 atm & T=100 C
*
*******************************************************************************
* END TMDPLVOL [101] represents IVR inflow at bottom of vessel cavity          *
*******************************************************************************
*******************************************************************************
* START SNGLJUN [J102] from inlet volume [101] to gap pipe [103]               *
*******************************************************************************
*
*       Component    Component
*       name         type
*
1020000  "j102"       sngljun       * D=3" UCSB
*                                     vertical flow
*
*       From     To       Flow    Foward Reverse
*       TMDPVOL  PIPE     Area    Loss   Loss
*       [101]    [103]    [m^2]   Coef.  Coef.  "jefvcahs"
*
1020101   101010000 103000000 0.00456 0.0    0.0     01000000    * 3" diameter
*
*       Search   Liquid  Vapor  Inferface
*       Variable Flow    Flow   Velocity
*                [kg/s]  [kg/s] [m/s]
*
1020201   1        9.8     0.0    0.0          * junction initial conditions
*
*******************************************************************************
* END   SNGLJUN [J102] from inlet volume [101] to pipe [103]                   *
*******************************************************************************
*******************************************************************************
```

```
* START PIPE [103] from [102] Junction to [104] exit Junction                    *
*********************************************************************************
* This pipe represents the gap along the pressure vessel.  This includes the     *
* lower head and the riser length along the cylinder portion of the vessel.      *
*********************************************************************************
* To model analogus to UCSB geometry the lower head is a rectangular channel     *
* and the riser is a 6" tube.                                                    *
*********************************************************************************
*
*       Component    Component
*       name         type
*
1030000  "gap103"     pipe
*
*       # of
*       cells
*
1030001  28          * 28 volumes used to model the gap entrance to exit
*                    18 along lower head representing 5 degrees each
*                   +10 along the vertical portion of the gap before the
*                    exit junction [104].
*                    The lower gap along the vessel lower head is modeled as
*                    a rectagular channel.
*                    The vertical riser region is modeled as a pipe.
*
********    X-directional (horizontal) data for pipe [103]    ****************
*
*       flow
*       x-area       pipe
*       [m^2]        vol#
*                     * rectangular channel -horizontal to vertical
1030101  0.0040       1     * inlet region
1030102  0.0040       2     * inlet region
1030103  0.0040       3     * inlet region
1030104  0.0040       4     * varied x 3" gap - beginning of gap - 20 degrees
1030105  0.0049       5     * varied x 3" gap
1030106  0.0058       6     * varied x 3" gap
1030107  0.0067       7     * varied x 3" gap
1030108  0.0075       8     * varied x 3" gap
1030109  0.0082       9     * varied x 3" gap
1030110  0.0089       10    * varied x 3" gap
1030111  0.0095       11    * varied x 3" gap
1030112  0.0101       12    * varied x 3" gap
1030113  0.0105       13    * varied x 3" gap
1030114  0.0109       14    * varied x 3" gap
1030115  0.0112       15    * varied x 3" gap
1030116  0.0114       16    * varied x 3" gap
1030117  0.0116       17    * varied x 3" gap
1030118  0.0116       18    * 6"x3" rectangular channel -horizontal to vertical
1030119  0.0182415    28    * 6" tube - vertical
*
*       x-length     vol#
*       [m]
*
1030301  0.1885       18    * Lower hemishere - LH/18 where LH=(2*pi*2.16m)/4
1030302  0.3152       28    * Riser - L/10 where L = 3.152m
```

```
*
*       volume      vol#
*       [m^2]
*
1030401  0.0         28    * Zero entered - volume internal calculation
*
*       vert-angle  vol#
*
1030601   5.0        1     * volume  1 - bottom of lower head gap
1030602  10.0        2
1030603  15.0        3
1030604  20.0        4
1030605  25.0        5
1030606  30.0        6
1030607  35.0        7
1030608  40.0        8
1030609  45.0        9
1030610  50.0        10
1030611  55.0        11
1030612  60.0        12
1030613  65.0        13
1030614  70.0        14
1030615  75.0        15
1030616  80.0        16
1030617  85.0        17
1030618  90.0        18    * volume  18 - vertical lower head gap
1030619  90.0        28    * volume  19 - 28 vertical riser gap
*
*       x-wall fric  xhd     vol#
*       [m]          [m]          * 0.0 -> xhd = 2 * (Af/Pi)^0.5
*
1030801  4.57e-5     0.0     18    * steel finish - lower gap
1030802  4.57e-5     0.0     28    * steel finish - riser
*
*       Loss coef Loss Coef
*       A_f       A_r       Junc#
*
1030901  0.0        0.0       18   * lower head gap
1030902  5.0        5.0       19   * transitions from lower head to riser
1030903  4.0        4.0       26   * riser - match UCSB dP
1030904  5.0        5.0       27   * riser exit
*
*
*       x-flags     vol#
*       {tlpvbfe}
*
1031001  0000000     28          * all volumes of gap pipe [103]
*
*       x-flags     vol#
*       {jefvcahs}
*
1031101  01000000    27          * junction control flags all gap pipe [103]
*
*       Control
*       Word        Pressure  Temperature          Volume
*       {ebt}       [Pa]      [K]        W-4 W-5 W-6  Number
```

```
*
1031201  003        158900.0  373.15    0.0 0.0 0.0  1
1031202  003        158500.0  373.15    0.0 0.0 0.0  2
1031203  003        158000.0  373.15    0.0 0.0 0.0  3
1031204  003        157300.0  373.15    0.0 0.0 0.0  4
1031205  003        157200.0  373.15    0.0 0.0 0.0  5
1031206  003        157100.0  373.15    0.0 0.0 0.0  6
1031207  003        156600.0  373.15    0.0 0.0 0.0  7
1031208  003        155700.0  373.15    0.0 0.0 0.0  8
1031209  003        154700.0  373.15    0.0 0.0 0.0  9
1031210  003        153500.0  373.15    0.0 0.0 0.0  10
1031211  003        152100.0  373.15    0.0 0.0 0.0  11
1031212  003        151000.0  373.15    0.0 0.0 0.0  12
1031213  003        149000.0  373.15    0.0 0.0 0.0  13
1031214  003        148000.0  373.15    0.0 0.0 0.0  14
1031215  003        146000.0  373.15    0.0 0.0 0.0  15
1031216  003        144000.0  373.15    0.0 0.0 0.0  16
1031217  003        143000.0  373.15    0.0 0.0 0.0  17
1031218  003        141000.0  373.15    0.0 0.0 0.0  18
1031219  003        140000.0  373.15    0.0 0.0 0.0  19
1031220  003        137000.0  373.15    0.0 0.0 0.0  20
1031221  003        134000.0  373.15    0.0 0.0 0.0  21
1031222  003        131000.0  373.15    0.0 0.0 0.0  22
1031223  003        128000.0  373.15    0.0 0.0 0.0  23
1031224  003        125000.0  373.15    0.0 0.0 0.0  24
1031225  003        122000.0  373.15    0.0 0.0 0.0  25
1031226  003        120000.0  373.15    0.0 0.0 0.0  26
1031227  003        117000.0  373.15    0.0 0.0 0.0  27
1031228  003        114000.0  373.15    0.0 0.0 0.0  28
*
*       Control
*       Flag
*
1031300  1
*
*       Initial     Initial
*       Liquid      Vapor     Interface
*       Mass Flow   Mass Flow Velocity   Junction
*       Rate        Rate
*       [kg/s]      [m/s]     [m/s]      Number
*
1031301  9.8        0.0       0.0        27  * initial mass flow rates
*
*******************************************************************************
********        END x-directional data for gap pipe [103]                 **********
*******************************************************************************
*******************************************************************************
*********       END - PIPE [103] data                                     **********
*******************************************************************************
*
*******************************************************************************
* START SNGLJUN [J104] from gap pipe [103] to exit volume [105]                 *
*******************************************************************************
*
*       Component     Component
*       name          type
```

```
*
1040000  "j104"       sngljun       * tube D=6" - reduced area
*
1040101  103010000    * From gap pipe outlet  [103]
1040102  105000000    * To exit volume inlet  [105]
1040103  0.0126677    * flow area = pi/4*(D^2) [m^2]
1040104  9.0         * Forward loss coefficient - match UCSB dP
1040105  9.0         * Reverse loss coefficient - match UCSB dP
1040106  01000000     * "jefvcahs"
*
*       Control Liquid  Vapor  Inferface
*       flag   Flow   Flow   Velocity
*              [kg/s]  [kg/s] [m/s]
*
1040201  1      9.7    0.1    0.0          * junction initial conditions
*
*******************************************************************************
* END  Junction [J104] from gap pipe exit [103] to exit volume [105]           *
*      This volume represents the primary piping gallary with losses.         *
*      UCSB models as 22 degree incline with flow restriction.                *
*******************************************************************************
*******************************************************************************
* START SNGLVOL [105] from junction [104]                                     *
*******************************************************************************
*
*       Component    Component
*       name         type
*
1050000  "105"       sngljun       * [105]
*
1050101  0.0127       * flow area                    [m^2]
1050102  2.0         * Length set to zero after initialization [m]
1050103  0.0         * Volume                       [m^3]
1050104  0.0         * Azimuthal angle x-y plane
1050105  22.0         * Inclination angle - riser to condenser  [degrees]
1050106  0.8         * Elevation change - riser to condensor   [m]
1050107  4.57e-5      * Wall roughness - steel              [m]
1050108  0.127       * Hydraulic diameter - 5"             [m]
1050109  0000000      * Volume conrol flags {tlpvbfe}
*
*       Control
*       Word    Pressure Temperature
*       {ebt}   [Pa]    [K]
*
1050200   003    104000.0 373.15 * conrol word - set pressure and temperature
*
*******************************************************************************
* START SNGLJUN [J106] from exit volume [105] to TMDPVOL [107]                *
*******************************************************************************
*
*       Component    Component
*       name         type
*
1060000  "j106"       sngljun       * tube D=6" - reduced area
*
1060101  105010000    * From gap pipe outlet  [103]
```

```
1060102  107000000    * To exit volume inlet  [105]
1060103  0.0127       * flow area = pi/4*(D^2) [m^2]
1060104  2.00         * Forward loss coefficient
1060105  2.00         * Reverse loss coefficient
1060106  01000000     * "jefvcahs"
*
*       Control Liquid  Vapor  Inferface
*       flag   Flow    Flow   Velocity
*              [kg/s]  [kg/s] [m/s]
*
1060201  1      9.7    0.1    0.0          * junction initial conditions
*
*******************************************************************************
* END   Junction [J106] from exit volume [105] to TMDPVOL [107]                *
*******************************************************************************
*
*******************************************************************************
* START TMDPVOL [107] from junction [106]                                      *
*******************************************************************************
* Used to set a pressure boundary conditions of 1 atmosphere & T=100 C         *
*******************************************************************************
*
*       Component    Component
*       name         type
*
1070000  "Flowout"    tmdpvol       * [107]
*
1070101  100.0        * flow area                    [m^2]
1070102  0.0          * Length set to zero after initialization [m]
1070103  100.0        * Volume set as large          [m^3]
1070104  0.0          * Azimuthal angle x-y plane
1070105  0.0          * Inclination angle - riser to condenser  [degrees]
1070106  0.0          * Elevation change - riser to condensor   [m]
1070107  0.0          * Wall roughness - steel       [m]
1070108  0.0          * Hydraulic diameter computed  [m]
1070109  0000010      * Volume conrol flags {tlpvbfe}
*
*       TMDPVOL
*       Control  Table
*       Word     Trip
*       {ebt}
*
1070200  003    0    * TMDPVOL conrol word - set pressure and quality
*
*       Search   Pressure   Temperature
*       Variable [Pa]      [K]
*
1070201  -1.0     101418.0  373.15      * Pr=1.0 atm & T=100 C
*
*******************************************************************************
* END   TMDPVOL [107] from junction exit [106]                                 *
*******************************************************************************
*******************************************************************************
* END   Hydrodynamic Component Section {CCCXXNN}                               *
*******************************************************************************
* START HEAT STRUCTURE - Vessel lower head outer wall                          *
```

```
* LEFT is in contact with water.                                    *
**************************************************************************
*
*       Number     Radial  Geometry       Initial     Left      Reflood
*       of heat    Mesh    Type           Steady-state Boundary  Flag
*       Structures Points  (1=rectangular) Flag        Coordinate (0=off)
*
11031000 18        2       1              1           0.0       0
*
*       Mesh       Mesh
*       Location   Format
*       Flag       Flag
*
11031100 0         1
*
*       Number     Right
*       of         Coordinate
*       intervals  [m]
*
11031101 1         0.01       * arbitray = 1 cm
*
*       Composition Interval
*       number     Number
*       (C-STEEL)
*
11031201 12        1
*
*       Source     Mesh
*       value Q    Interval#
*
11031301 1.0       1
*
*       temp       mesh point#
*
11031401 375.      2
*
**************************************************************************
****    Heated Surface Area = 0.1885m * varied  = varied  m^2 per node                ****
****    Heated Surface Area = 0.1885m * 0.1524m = 0.028727m^2 per node [18]           ****
**************************************************************************
*
*       Boundary          Boundary   Surface Surface  Heat
*       Condition Increment Condition Area    Area     Structure
*       Left              Type       Code    [m^2]    Number
*
11031501 103010000 10000    130       0       0.0013   1    * lower head
11031502 103020000 10000    130       0       0.0037   2    * lower head
11031503 103030000 10000    130       0       0.0062   3    * lower head
11031504 103040000 10000    130       0       0.0066   4    * lower head
11031505 103050000 10000    130       0       0.0110   5    * lower head
11031506 103060000 10000    130       0       0.0133   6    * lower head
11031507 103070000 10000    130       0       0.0154   7    * lower head
11031508 103080000 10000    130       0       0.0175   8    * lower head
11031509 103090000 10000    130       0       0.0194   9    * lower head
11031510 103100000 10000    130       0       0.0212   10    * lower head
11031511 103110000 10000    130       0       0.0228   11    * lower head
```

```
11031512 103120000 10000    130      0     0.0242  12   * lower head
11031513 103130000 10000    130      0     0.0255  13   * lower head
11031514 103140000 10000    130      0     0.0265  14   * lower head
11031515 103150000 10000    130      0     0.0274  15   * lower head
11031516 103160000 10000    130      0     0.0280  16   * lower head
11031517 103170000 10000    130      0     0.0285  17   * lower head
11031518 103180000 10000    130      0     0.028727 18   * lower head
*
*       Boundary          Boundary   Surface Surface  Heat
*       Condition  Increment Condition  Area    Area     Structure
*       Right              Type      Code    [m^2]    Number
*
11031601 0         0       0         0       0.0013   1    * lower head
11031602 0         0       0         0       0.0037   2    * lower head
11031603 0         0       0         0       0.0062   3    * lower head
11031604 0         0       0         0       0.0066   4    * lower head
11031605 0         0       0         0       0.0110   5    * lower head
11031606 0         0       0         0       0.0133   6    * lower head
11031607 0         0       0         0       0.0154   7    * lower head
11031608 0         0       0         0       0.0175   8    * lower head
11031609 0         0       0         0       0.0194   9    * lower head
11031610 0         0       0         0       0.0212   10    * lower head
11031611 0         0       0         0       0.0228   11    * lower head
11031612 0         0       0         0       0.0242   12    * lower head
11031613 0         0       0         0       0.0255   13    * lower head
11031614 0         0       0         0       0.0265   14    * lower head
11031615 0         0       0         0       0.0274   15    * lower head
11031616 0         0       0         0       0.0280   16    * lower head
11031617 0         0       0         0       0.0285   17    * lower head
11031618 0         0       0         0       0.028727 18    * lower head
*
*********************************************************************************
*********************     POWER PROFILE (18 NODES)          *********************
*********************     UCSB                              *********************
*********************************************************************************
*       Power             Direct     Direct
*       Source  Source    Moderator  Moderator
*       Type    Multiplier Heating   Heating    Heat
*       (Table)           Multiplier Multiplier Structure
*                  Left     Right      Number
*
11031701 10        0.01     0.         0.         1
11031702 10        0.05     0.         0.         2
11031703 10        0.08     0.         0.         3
11031704 10        0.12     0.         0.         4
11031705 10        0.16     0.         0.         5
11031706 10        0.22     0.         0.         6
11031707 10        0.29     0.         0.         7
11031708 10        0.41     0.         0.         8
11031709 10        0.60     0.         0.         9
11031710 10        0.87     0.         0.         10
11031711 10        1.15     0.         0.         11
11031712 10        1.36     0.         0.         12
11031713 10        1.56     0.         0.         13
11031714 10        1.77     0.         0.         14
11031715 10        2.00     0.         0.         15
```

```
11031716 10      2.22     0.       0.       16
11031717 10      2.43     0.       0.       17
11031718 10      2.71     0.       0.       18
*
*       Format
*
11031800 1     * 12 word format for addtional right boundary options
*
*       Heat
*       Transfer              Grid   Grid
*       Hydraulic Heated  Heated  Spacer  Spacer
*       Diameter  length  length  length  length
*       4*Af/Ph   forward reverse forward reverse  * Dheated = 0.3048m for all
*       [m]       [m]     [m]     [m]     [m]    [ff - modify CHF correlation]
*
*       hd        hl      rhl     gl      rgl    Kg0 rKg LBF NCL pdr ff  hd#
11031801  0.3048    10.0    10.0    0.0     0.0    0.0 0.0 1.0 0.0 0.0 10.0 18
*
*******************************************************************************
* END HEAT STRUCTURE - Vessel lower head outer wall                            *
*******************************************************************************
* START Heat Structure Thermal Property Data - Carbon Steel SA508              *
*******************************************************************************
*
*       Material   k-tc    Cp
*       Type       Format  Format
*
20101200  tbl/fctn   1      1
*
*       k-tc
*       [W/m-C]
*
20101201  40.0       * thermal conductivity constant SA508
*
*       Cp
*       [J/m^3-C]
*
20101251  4.0e6      * heat capacity constant SA508
*
*
*******************************************************************************
* END Heat Structure Thermal Property Data                                     *
*******************************************************************************
*******************************************************************************
* START General Table Data 202TTTNN where TTT=table#                           *
*******************************************************************************
*
* Start - Table 100 - Heat Structure - Right Side
*
*       Table
*       Type
*
20210000  temp       * temperature vs time
*
*       time      temperature
*       [s]       [K]
```

```
*
20210001  0.0       430.
20210002  100000.0  430.
*
* End - Table 100
*******************************************************************************
*
* Start - Table 10 - table of time and core power
*
*crdno    name    trip  factor
*              (none) (none)
*
20201000  power   0
*
* RELAP IVR Power = 0.321 MW --> 28.6MW Decay Heat/ 89 scaling
*
*crdno    time     watts
*        (sec)    (watts)
*
20201001        0.0  17849.     * 17.8 kW per heat structure node
20201002  1000000.0  17849.     * 17.8 kW per heat structure node
*
* End - Table 10
*******************************************************************************
* END General Table Data 202TTTNN where TTT=table#                             *
*******************************************************************************
*
* START Control Variables: Power from the hot loop in kW
*
*       Name     Type  Scaling   Initial Initial
*                 Factor   Value   Value Control
*                            Flag
*
20510300 hotpower  sum  1.0e-03  0.0     1   * computer initial condition
*
*           A0   A1  V1     parameter   A2   V2      parameter
20510301  0.0   1.0  q      103010000   1.0  q      103020000
20510302        1.0  q      103030000   1.0  q      103040000
20510303        1.0  q      103050000   1.0  q      103060000
20510304        1.0  q      103070000   1.0  q      103080000
20510305        1.0  q      103090000   1.0  q      103100000
20510306        1.0  q      103110000   1.0  q      103120000
20510307        1.0  q      103130000   1.0  q      103140000
20510308        1.0  q      103150000   1.0  q      103160000
20510309        1.0  q      103170000   1.0  q      103180000
*
* END Control Variable to calculate Power in kW
*******************************************************************************
**************       END RELAP MODEL - Base Deck          ***********************
*******************************************************************************
*
*******************************************************************************
* START Replacement Cards                                                      *
*******************************************************************************
*
100  new      transnt     *  for [steady state: stdy-st] [transient: transnt]
```

```
*
*  End     Minimum     Maximum      Control    Minor    Major    Restart
*  time    time step   time step    Options    Edit     Edit     Freq.
*  (sec)   (sec)       (sec)        (ssdtt)    Freq.    Freq.
*
*201  500.0    1.0e-9      1.25e-4      00023     100      500000    50000
*
1010201  -1.0     209730.0  384.78    * Pr=2.07 atm & T=111.6 C
*
*       From     To       Flow    Foward Reverse
*       TMDPVOL  PIPE     Area    Loss   Loss
*       [101]    [103]    [m^2]   Coef.  Coef.  "jefvcahs"
*
1020101  101010000 103000000 0.00456 6.0    6.0    01000000    * 3" diameter
*
******* ZERO OUT LOSS COEF  ************************************************
*       Loss coef Loss Coef
*       A_f      A_r      Junc#
*
1030901  0.0      0.0      18    * lower head gap
1030902  0.0      0.0      19    * transitions from lower head to riser
1030903  0.0      0.0      26    * riser - match UCSB dP
1030904  0.0      0.0      27    * riser exit
*
*1040104  9.0          * Forward loss coefficient - match UCSB dP
*1040105  9.0          * Reverse loss coefficient - match UCSB dP
*
1060104  1.8         * Forward loss coefficient
1060105  1.8         * Reverse loss coefficient
*
*       hd       hl      rhl     gl      rgl     Kg0 rKg LBF NCL pdr ff  hd#
11031801 0.3048   10.0    10.0    0.0     0.0     0.0 0.0 1.0 0.0 0.0 10.0 18
*
*       Search   Pressure  Temperature
*       Variable [Pa]      [K]
*
1070201  -1.0     151418.0  384.78     * Pr=1.5 atm & T=111.6 C
*
* RELAP IVR Power = 0.321 MW --> 28.6MW Decay Heat/ 89 scaling
*
*crdno    time      watts
*         (sec)     (watts)
*
*20201001        0.0  17849.     * 17.849 kW per heat structure node
*20201002  1000000.0  17849.     * 17.849 kW per heat structure node
*
*******************************************************************************
* END Replacement Cards                                                       *
*******************************************************************************
*
. ************  END OF INPUT DECK
```

References

[1] J. Scobel, T. Theofanous, L. Conway, "In-Vessel Retention of Molten Core Debris in the Westinghouse AP1000 Advanced Passive PWR", American Nuclear Society, International Congress on Advances in Nuclear Power Plants, Hollywood, Florida, June 9-13, 2002.

[2] A. Chupin, L.W. Hu, J. Buongiorno, "Application of nanofluids to enhance LWR accidents management in in-vessel retention and emergency core cooling systems", Proceedings of ICAPP '08, Anaheim, California USA, Paper 8043, June 8-12, 2008.

[3] T. Theofanous, C. Liu, S. Angelini, "Experience From the First Two Integrated Approaches in In-vessel Retention Through External Cooling", Proceedings of Workshop on Large Molten Pool Heat Transfer, Grenoble, France, March 9-11, 1994, Pages 45-76.

[4] Westinghouse, "UK AP1000 Probabilistic Risk Assessment – Chapter 39: In-Vessel Retention of Molten Core Debris". Revision 0.

[5] T. Theofanous, C. Lui, S. Additon, S. Angelini, O. Kymalainen, T. Salmassi, "In-vessel Coolability and Retention of a Core Melt". Nuclear Engineering and Design, 169, 1-48, 1997.

[6] J. Rempe, K. Suh, F. Cheung, S. Kim, "In-Vessel Retention of Molten Corium: Lesson Learned and Outstanding Issues", Nuclear Technology, Vol. 161, pages 210-267, March 2008.

[7] R. Hannink, "Investigation of the use of nanofluids to enhance the In-Vessel Retention capabilities of Advanced Light Water Reactors", S.M. Thesis, Nuclear Science and Engineering Department, MIT, (2007).

[8] J. Buongiorno, L.W. Hu, "Nanofluid Heat Transfer Enhancement for Nuclear Reactor Applications", Journal of Energy and Power Engineering, Vol. 4, No. 6 (Serial No. 31), June 2010.

[9] T. Lucas, "Study of Chemistry and Irradiation Effects on Nanofluids to be used in Light Water Reactor Accident Cooling", S.M. Thesis, Nuclear Science and Engineering Department, MIT, January 2008.

[10] R. Hannink, J. Buongiorno, L. Hu, G. Apostolakas, June 2007, "Using Nanofluids to Enhance the Capability of In-Vessel Retention of Fuel Following Severe Reactor Accidents", MIT CANES, MIT-ANP-TR-116, Nuclear Science and Engineering Department, MIT.

[11] J. Buongiorno, L.W. Hu, "Nanofluids for Enhanced Economics and Safety of Nuclear Reactors", Presentation at University Park Hotel at MIT, Cambridge, MA, November 29, 2007.

[12] J. Buongiorno, L. W. Hu, S. J. Kim, R. Hannink, B. Truong, E. Forrest, "Nanofluids for enhanced Economics and Safety of Nuclear Reactors: an Evaluation of the Potential Features, Issues and Research Gaps", *Nuclear Technology*, Vol. 162,80-91, 2008.

[13] B. Truong, L-w. Hu, J. Buongiorno, June 2008, "Optimizing Critical Heat Flux Enhancement Through Nanoparticle -Based Surface Modifications", International Congress on Advances in Nuclear Power Plants (ICAPP), Anaheim, CA.

[14] S. J. Kim, "Subcooled Flow Boiling Heat Transfer and Critical Heat Flux in Water-Based Nanofluids at Low Pressure", *PhD Thesis*, Nuclear Science and Engineering Department, MIT, March 2009.

[15] J. Yang, M.B. Dizon, F.B. Cheung, J.L. Rempe, K.Y. Suh, S.B. Kim, "CHF enhancement by vessel coating for external reactor vessel cooling", Nuclear Engineering and Design, Vol. 236 (2006), 1089-1098.

[16] J. Buongiorno, L.W. Hu, G. Apostolakis, R. Hannink, T. Lucas, A. Chupin, "A feasibility assessment of the use of nanofluids to enhance the in-vessel retention capability in light-water reactors", Nuclear Engineering and Design, Vo. 239, Issue 5, May 2009, pages 941-948.

[17] S. Rouge, 1997, "SULTAN Test Facility for Large-Scale Vessel Coolability in Natural Convection at Low Pressure", Nuclear Engineering and Design, ISSN 0029-5493, Vol. 169, pages 185-195.

[18] W. Williams, "Experimental and Theoretical Investigation of Transport Phenomena in Nanoparticle Colloids (Nanofluids)", PhD Thesis, Nuclear Science and Engineering Department, MIT, (2006).

[19] A. Chupin, "Nanofluids to Enhance Accidents Management", INSTN report, August 2007.

[20] J. Buongiorno, "Convective Transport in Nanofluids", Journal of Heat Transfer, Vol. 128, pages 240-251, March 2006.

[21] V. Carey, Liquid-Vapor Phase-Change Phenomena, Second Edition, Taylor & Francis, 2008, ISBN 978-59169-035-1.

[22] M.N. Golubovic, H.D.M. Hettiarachchi, W.M. Worek, W.J. Minkowycz, September 2007, "Nanofluids and Critical Heat Flux, Experimental and Analytical Study", Applied Thermal Engineering, Volume 29, Issue 7, May 2009, Pages 1281-1288.

[23] H. Kim, J. Kim, M. Kim, 2006, "Experimental study on CHF characteristics of water-TiO_2 nano-fluids", *Nuclear Engineering and Technology*, Vol. 38, No. 1.

[24] S. You, J. Kim, K. Kim, "Effect of nanoparticles on critical heat flux of water in pool boiling heat transfer", Applied Physics Letters, Vol. 83, No. 16, October 20, 2003

[25] H. Kim, J. Kim, M. Kim, 2007, "Experimental study on the characteristics and mechanism of pool boiling CHF enhancement using nano-fluids", *ECI International Conference on Boiling Heat Transfer*, Spoleto, 7-12 May.

[26] G. Moreno, "Investigation of Pool Boiling Heat Transfer with Nanofluids", M.S. Thesis, University of Texas at Arlington, Department of Mechanical Engineering, December 2005.

[27] S.J. Kim, T. McKrell, J. Boungiorno, L.W. Hu, "Subcooled Flow Boiling Heat Transfer of Dilute Alumina, Zinc Oxide, and Diamond Nanofluids at Atmospheric Pressure", Nuclear Science and Engineering, Vol. 240, 1186, (2010).

[28] J. Jackson, B. Borgmeyer, C. Wilson, P. Cheng, J. Bryan, "Characteristics of Nucleate Boiling with Gold Nanoparticles in Water", Proceedings of IMECE2006, November 5-10, Chicago, Illinois, USA, 2006.

[29] H. Xie, L. Chen, Y. Li, W. Yu, "Thermal Transport Properties of Nanofluids Containing Carbon Nanotubes", Proceedings of the Sixth International ASME Conference on Nanochannels, Microchannels and Minichannels, Darmstadt, Germany, June 23-25, 2008.

[30] H. Park, D. Shiferaw, B. Sehgal, D. Kim, M. Muhammed "Film Boiling on a High Temperature Sphere in Nanofluid", Proceedings of the 2004 ASMA Heat Transfer/Fluids Engineering Summer Conference, Charlotte, North Carolina, USA, July 11-15, 2004.

[31] H. Kim, G. DeWitt, T. McKrell, J. Buongiorno, L-w. Hu, "On the Quenching of Steel and Zircaloy Spheres in Water-Based Nanofluids with Alumina, Silica and Diamond Nanoparticles", *International Journal of Multiphase Flow*, 2009.

[32] H. Kim, T. McKrell, J. Buongiorno, L. W. Hu, "Nanoparticle Deposition Effects on the Minimum Heat Flux Point and Quench Front Speed during Quenching of Rodlets and Spheres in Water-based Alumina Nanofluids", InternationalJournal of Heat and Mass Transfer, 53, pages 1542-1553, 2010.

[33] I. Bang, "Effects of Nanoparticles on Single Rod Quenching", Sixth Japan-Korea Symposium on Nuclear Thermal Hydraulics and Safety, Okinawa, Japan, November 24-27, 2008.

[34] C. Gerardi, "Investigation of the Pool Boiling Heat Transfer Enhancement of Nano-Engineered Fluids by means of High-Speed Infrared Thermography", PhD Thesis, Nuclear Science and Engineering Department, MIT, (2009).

[35] S. J. Kim, T. McKrell, J. Buongiorno, L. W. Hu, 2007, "Alumina nanoparticles enhance the flow critical heat flux of water at low pressure", *J. Heat Transfer*, Vol. 129, Issue 12.

[36] B. Truong, "Critical Heat Flux Enhancement via Surface Modification Using Colloidal Dispersions of Nanoparticles (Nanofluids)", M.S. Thesis, MIT, 2008.

[37] B. Truong, L.W. Hu, J. Buongiorno, T. McKrell, "Subcooled Flow Boiling Critical Heat Flux Enhancement of Alumina Nanoparticle Pre-coated Tubing" Proceedings of ECI International Conference on Boiling Heat Transfer, Florianopolis, Brazil, May 3-7, 2009.

[38] B. Truong, L.W. Hu, J. Buongiorno, T. McKrell, "Alumina Nanoparticle Pre-coated Tubing Enhanced Subcooled Flow Boiling Critical Heat Flux", Proceedings of the ASME 2009 2nd

Micro/Nanoscale Heat and Mass Transfer International Conference, December 18-21, 2009, Shanghai, China.

[39] B. Truong, "Effects of Surface Parameters on Boiling Heat Transfer Phenomena", *PhD Thesis*, Nuclear Science and Engineering Department, MIT, May 2011.

[40] J.H. Kim, K.H. Kim, S.M. You, November 2004, "Pool Boiling Heat Transfer in Saturated Nanofluids", Proceeding of 2004 ASME International Mechanical Engineering Congress and Exposition, Anaheim, CA.

[41] Y. Jeong, M. Sarwar, S. Chang, "Flow boiling CHF enhancement with surfactant solutions under atmospheric pressure", International Journal of Heat and Mass Transfer, 51, (2008), 1913-1919.

[42] J. Lee, Y. Jeong, S. Chang, "Experimental study on the CHF enhancement in flow boiling system with TSP and boric acid solutions under atmospheric pressure", Transactions of the American Nuclear Society, 901-902, November 2009.

[43] P. Trang, T. Kim, S. Chang, "An application of zeta potential method for the selection of nano-fluids to enhance IVR capability", Transactions of the Korean Nuclear Society Spring Meeting, Jeju, Korea, May 22, 2009, pages 559-560.

[44] R. Kathiravan, R. Kumar, A. Gupta, R. Chandra, "Characterization and Pool Boiling Heat Transfer Studies of Nanofluids", Journal of Heat Transfer, Vol. 131, Issue 8, (8 pages), August 2009.

[45] S. Kwark, R. Kumar, G. Moreno, J. Yoo, S. You, "Pool Boiling Characteristics of Low Concentration Nanofluids", International Journal of Heat and Mass Transfer, Vol. 53, Issues 5-6, February 2010, pages 972-981.

[46] S. Das, S. Choi, H. Patel, "Heat Transfer in Nanofluids – A Review", Heat Transfer Engineering, Vol. 27, Number 10, pages 3-19, (2006).

[47] J. Buongiorno, D. Venerus, N. Prabhat, T. McKrell, J. Townsand, et. al., "A Benchmark Study on the Thermal Conductivity of Nanofluids", Journal of Applied Physics, Vol. 106, Issue 9, 2009.

[48] S. Kabelac, K. Anoop, "Experimental Convective Heat Transfer with Nanofluids", Proceedings of the Sixth International ASME Conference on Nanochannels, Microchannels and Minichannels, Darmstadt, Germany, June 23-25, 2008.

[49] K. Kurowska, G. Dzido, A. Gierczycki, A. Jarzebski, "Experimental Investigation of Heat Transfer to Nanofluids", Proceedings of the Sixth International ASME Conference on Nanochannels, Microchannels and Minichannels, Darmstadt, Germany, June 23-25, 2008.

[50] A. Falahatpisheh, O. Abouali, "Free Convection of Nanfluid in Vertical Annuli", Proceedings of the Sixth International ASME Conference on Nanochannels, Microchannels and Minichannels, Darmstadt, Germany, June 23-25, 2008.

[51] P. Vaziee, O. Abouali, "Numerical Study of Forced Convection of Nanofluids in a Microchannel Heat Sink, Proceedings of the Sixth International ASME Conference on Nanochannels, Microchannels and Minichannels, Darmstadt, Germany, June 23-25, 2008.

[52] S. J. Kim, I. C. Bang, J. Buongiorno, L. W. Hu, 2006, "Effects of nanoparticle deposition on surface wettability influencing boiling heat transfer in nanofluids", *Applied Physics Letters*, Vol. 89, 153107.

[53] S. Kim, I. Bang, J. Buongiorno, L. Hu, "Surface wettability change during pool boiling of nanofluids and its effect on critical heat flux", International Journal of Heat and Mass Transfer, Vol. 50, Pages 4105-4116, 2007.

[54] E. Forrest, "Nanoscale Modification of Key Surface Parameters to Augment Pool Boiling Heat Transfer and Critical Heat Flux in Water and Dielectric Fluids", S.M. Thesis, Nuclear Science and Engineering Department, MIT, June 2009.

[55] A. Zoubir, B. Tidjani, S. Youcef, "Comparison of correlations for predicting critical heat flux for uniformly heated vertical porous coated tubes at low pressure", Nuclear Engineering and Design, Vol. 240, Issue 1, January 2010, pages 71-75.

[56] D. Schroeder-Richter, S. Yildiz, G. Bartsch, "Effects of Porous Coating on Critical Heat Flux", International Communications in Heat and Mass Transfer, Vo. 23, No. 4, pages 463-471, 1996.

[57] D. Min, G. Hwang, Y. Usta, O. Cora, M. Koc, M. Kaviany, "2-D and 3-D modulated porous coatings for enhanced pool boiling", International Journal of Heat and Mass Transfer, Vol. 52, (2009), pages 2607-2613.

[58] F. Ramstorfer, H, Steiner, G. Brenn, C. Lormann, F. Rammer, "Subcooled Boiling Flow Heat Transfer from Plain and Enhanced Surfaces in Automotive Applications", Journal of Heat Transfer, Vol. 130, January 2008.

[59] B. Jones, S. Garimella, "Surface Roughness Effects on Flow Boiling in Microchannels", Journal of Thermal Science and Engineering Applications, Vol. 1, December 2009.

[60] S. Kim, et.al., "Experimental Investigation of Critical Heat Flux Enhanced by Micro/Nanoscale Surface Modification in Pool Boiling", Proceedings of the Sixth International ASME Conference on Nanochannels, Microchannels and Minichannels, Darmstadt, Germany, June 23-25, 2008.

[61] "Westinghouse AP1000 Design Control Document", Revision 16 (Public Version), U.S. NRC, May 26, 2007.

[62] N. Kolev, Multiphase Flow Dynamics 4: Nuclear Thermal Hydraulics, Springer, 2009, ISBN: 978-3-540-92917-8.

[63] T. Theofanous, S. Angelini, "Natural convection for in-vessel retention at prototypic Rayleigh numbers", Nuclear Engineering and Design, Vo. 200, (2000), Pages 1-9.

[64] Y. Zhang, S. Qiu, G. Su, W. Tian, "Analysis of safety margin of in-vessel retention for AP1000", Nuclear Engineering and Design, 240, pages 2023-2033, 2010.

[65] L. Tong, J. Weisman, Thermal Analysis of Pressurized Water Reactors, third edition, American Nuclear Society, ISBN 0-89448-038-3, 1996.

[66] R. Knief, Nuclear Engineering: Theory and Technology of Commercial Nuclear Power, second edition, American Nuclear Society, ISBN 0-89448-458-3, 2008.

[67] T. Theofanous, S. Oh, J. Scobel, "In-Vessel Retention Technology Development and Use for Advanced PWR Designs in the USA and Korea", International Nuclear Energy Research Initiative, 2002-022-K (I), 2004.

[68] K. Kang, R. Park, K. Koo, S. Kim, H. Kim, "Experimental Investigation on In-Vessel Corium Retention through Inherent Gap Cooling Mechanisms", Journal of Nuclear Science and Technology, Vol. 43, No. 12, p. 1490-1500, (2006).

[69] J. Rempe, D. Knudson, "High temperature thermal properties for metals used in LWR vessels", Journal of Nuclear Materials, Vol. 372, pages 350-357, (2008).

[70] T. Theofanous, S. Syri, "The coolability limits of a pressure vessel lower head", Nuclear Engineering and Design, Vol. 169, (1997), pages 59-76.

[71] G. Hart, Multidimensional Analysis: Algebras and Systems for Science and Engineering, Springer-Verlag, ISBN: 0-387-94417-6, 1995.

[72] T-N. Dinh, J. Tu, T. Salmassi, T. Theofanous, "Limits of Coolability in the AP1000 Related ULPU-2400 Configuration V Facility", University of California, Santa Barbara, CRSS-03/06, June 30, 2003.

[73] F. Incropera, D. DeWitt, T. Bergman, A. Lavine, Fundamentals of Heat and Mass Transfer, second edition, John Wiley & Sons, ISBN 978-0-471-45728-2, 2007.

[74] Richard Wright, Westinghouse, Email communication to J. Buongiorno, June 14, 2011.

[75] J. Collier, J. Thome, Convective Boiling and Condensation, third edition, Oxford University Press, ISBN 0-19-856296-9, 1996.

[76] N. Todreas, M. Kazimi, Nuclear Systems I: Thermal Hydraulic Fundamentals, Taylor & Francis, ISBN 13 978-1-56032-051-7, 1990.

[77] L. Tong, Y. Tang, Boiling Heat Transfer and Two-Phase Flow, Second Edition, Taylor & Francis, 1997, ISBN: 1-56032-485-6.

[78] E. Forrest, L. Hu, T. McKrell, J. Buongiorno, Y. Ostrovsky, Pressure Effects on the Pool Boiling of the Fluorinated Ketone $C_2F_5C(O)CF(CF_3)_2$, ITHERM, ISBN 978-1-4244-5343-6, Las Vegas, June 2-5, 2010.

[79] T. Conboy, "Assessment of Helical-Cruciform Fuel Rods for High Power Density LWRs", *PhD Thesis*, Nuclear Science and Engineering Department, MIT, April 2010.

[80] Richard Wright, Westinghouse, Email communication to Prof. Ballinger, April 12, 2010.

[81] British Stainless Steel Association, "Elevated temperature physical properties of stainless steel", online report, www.bssa.org.uk/topics.php?article=139.

[82] P. Bevington, D. Robinson, Data Reduction and Error Analysis, third edition, McGraw-Hill Publishing, ISBN-13: 978-0-07-247227-1, 2003.

[83] N. Todreas, M. Kazimi, Nuclear Systems II: Elements of Thermal Hydraulic Design, Taylor & Francis, ISBN 1-56032-079-6, 2001.

[84] A. Mills, Heat Transfer, second edition, Prentice Hall, ISBN 0-13-947624-5, 1999.

[85] Richard Wright, Westinghouse, Email communication to J. Buongiorno, May 3, 2010.

[86] B. Forrest, E. Forrest, L.W. Hu, T. McKrell, J. Buongiorno, "Measurement of Contact Angles on Smooth and Practical Boiling Surfaces", MIT Nuclear Reactor Laboratory, Cambridge, Massachusetts, August 10, 2009.

[87] S. Zhou, R. Ni, "Measurement of specific heat capacity of water-based Al_2O_3 nanofluid", Applied Physics Letters, 92, 093123, (2008).

[88] S. Ross, "Peirce's criterion for the elimination of suspect experimental data", Journal of Engineering Technology, Fall 2003.

[89] T.G. Theofanous, S. Syri, T. Salmassi, O. Kymalainen, H. Tuomisto, March 1994, "Critical Heat Flux Through Curved, Downward Facing Thick Walls", Nuclear Engineering and Design 151 (1994) 247-258.

[90] D.L. Knudson, J.L. Rempe, "In-Vessel Modeling Capabilites of SCDAP/RELAP5-3D", Proceedings of ICONE10, paper 22754, Arlington, VA, April 14-18, 2002..

[91] H. Merte Jr., R.B. Keller, B.J. Kirby, 1997, "Effects of Heater Surface Orientation on the Critical Heat Flux-I. An Experimental Evaluation of Models for Subcooled Pool Boiling", International Journal of Heat and Mass Transfer, Vol. 40, No. 17, pp. 4007-4019.

[92] H. Ohtake, Y. Koizumi, 2004, "Study on Ex-Vessel Cooling of Reactor Pressure Vessel (Model Analysis of Critical Heat Flux on Inclined Plate and Hemisphere Facing Downward)", JSME International Journal, Series B, Vol. 47, No. 2.

[93] B. Yucel, S. Kakac, "Forced Flow Boiling and Burnout in Rectangular Channels", papers presented at the International Heat Transfer Conference, Vol. 1, (1978), 387-392.

[94] J. Galloway, I. Mudawar, "CHF mechanism in flow boiling from a short heated wall-I. Examination of near-wall conditions with the aid of photomicrography and high-speed video imaging", International Journal of Heat and Mass Transfer, Vol. 36, No. 10, pp. 2511-2526, (1993).

[95] M. Kureta, H. Akimoto, "Critical heat flux correlation for subcooled boiling flow in narrow channels", International Journal of Heat and Mass Transfer, Vol. 45, 4107-4115, (2002).

[96] J. Zhao, Y. Lu, J. Li, "CHF on Cylinders-Revisit of Influences of Subcooling and Cylinder Diameter", ECI International Conference of Boiling Heat Transfer, Brazil, May 3-7, 2009.

[97] R. Boyd, "Local Heat Transfer and CHF for Subcooled Flow Boiling", Department of Mechanical Engineering, Prairie View A&M, Report to DOE, DE-FG03-92ER54189, 1998.

[98] Y.H. Kim, S.J. Kim, J.J. Kim, S.W. Noh, K.Y. Suh, J.L. Rempe, F.B. Cheung, S.B. Kim, "Visualization of boiling phenomena in inclined rectangular gap", International Journal of Multiphase Flow, Vol. 31, (2005), 618-642.

[99] Y. H. Kim, S. J. Kim, K. Y. Suh, J. L. Rempe, F. B. Cheung, S. B. Kim, "Internal Vessel Cooling Feasibility Attributed by Critical Heat Flux in Inclined Rectangular Gap", Nuclear Technology, Vol. 154, April 2006, pages 13-40.

[100] H. Zhang, I. Mudawar, M. Hasan, "Experimental assessment of the effects of body force, surface tension force, and inertia on flow boiling CHF", International Journal of Heat and Mass Transfer, 45, (2002), 4079-4095.

[101] M. Kashinath, "Parameters Affecting Critical Heat Flux of Nanofluids: Heater Size, Pressure, Orientation and Anti-Freeze Addition", M.S. Thesis, University of Texas at Arlington, Department of Mechanical Engineering, August 2006.

[102] S. Kandlikar, "A Theoretical Model to Predict Pool Boiling CHF Incorporating Effects of Contact Angle and Orientation", Journal of Heat Transfer, Vol. 123, 1071-1079, December 2001.

[103] J. Lienhard, V. Dhir, "Hydrodynamic Prediction of Peak Pool-boiling Heat Fluxes from Finite Bodies", Journal of Heat Transfer, Vol. 95, 152-158, 1973.

[104] T. Bui, V. Dhir, "Transition Boiling Heat Transfer on Vertical Surface", Journal of Heat Transfer, Vol. 107, Issue 4, 756-763, November 1985.

[105] V. Dhir, "Boiling Heat Transfer", Annual Review of Fluid Mechanics, Vol. 30, pages 365-401, 1998.

[106] J. Lienhard IV, J. Lienhard V, A Heat Transfer Text Book, third edition, Phlogiston Press, (2006).

[107] H. Zhang, I. Mudawar, M. Hasen, "Experimental and theoretical study of orientation effects on flow boiling CHF", International Journal of Heat and Mass Transfer, Vol. 45, Pages 4463-4477, (2002).

[108] I. Mudawar, D. Maddox, "Critical Heat Flux in subcooled flow boiling of fluorocarbon liquid on a simulated electronic chip in a vertical rectangular channel", International Journal of Heat and Mass Transfer, Vol. 32, No. 2, pages 379-394, 1989.

[109] T. Dinh, J. Tu, T. Salmassi, T. Theofanous, "Limits of Coolability in the AP1000-Related ULPU-2400 Configuration V Facility", NURETH-10, Seoul, Korea, Paper G00407, October 5-9, 2003.

[110] J. H. Park, Y. H. Jeong, W. P. Baek, S. H. Chang, "An assessment methodology for in-vessel corium retention by external reactor vessel cooling during severe accidents in PWRs", Annals of Nuclear Energy, Vol. 28, (2001), pages 1237-1250.

[111] T. Theofanous, J. Tu, T. Salmassi, T. Dinh, "Quantification of Limits of Coolability in ULPU-2000 Configuration IV", University of California, Santa Barbara, May 23, 2002.

[112] S. Rouge, D. Geffraye, "Reactor Vessel External Cooling for Corium Retention SULTAN Experimental Program and Modeling with CATHARE Code", Workshop on in-vessel core debris retention and coolability, Garching, Germany, 3-6 March, 1998.

[113] M. Caira, G. Caruso, A. Naviglio, "A Correlation to Predict CHF in Subcooled Flow Boiling", International Communications in Heat and Mass Transfer, Vol. 22, No. 1, pages 35-45, 1995.

[114] M. Caira, G. Caruso, A. Naviglio, S. Rouge, "CHF Prediction for Sloping Surfaces", NUTHOS-5, Beijing, China, April 14-18, 1997.

[115] F. B. Cheung, K. H. Haddad, Y. C. Liu, "Critical Heat Flux (CHF) Phenomenon on a Downward Facing Curved Surface", U.S. Nuclear Regulatory Commission, NUREG/CR-6507, June 1997.

[116] J. Yang, F. Cheung, J. Rempe, K. Suh, S. Kim, "Correlations of Nucleate Boiling Heat Transfer and Critical Heat Flux for External Reactor Vessel Cooling", Proceeding of HT2005, 2005 ASME Summer Heat Transfer Conference, July 17-22, 2005, San Francisco, California, HT 2005-72334.

[117] J. Yang, F. Cheung, J. Rempe, K. Suh, S. Kim, "Critical Heat Flux for Downward-Facing Boiling on a Coated Hemispherical Vessel Surrounded by an Insulation Structure", Proceeding of ICAPP '05, Seoul, Korea, May 15-19, 2005, Paper 5321.

[118] F. Cheung, J. Yang, M. Dixon, J. Rempe, K. Suh, S. Kim, "On the Enhancement of External Reactor Vessel Cooling of High-Power Reactors", NURETH-10, Paper G00403, Seoul, Korea, October 5-9, 2003.

[119] Y. H. Jeong, S. H. Chang, "CHF Experiments on the Reactor Vessel Wall using 2-D Slice Test Section", NURETH-10, paper G00314, Seoul, Korea, October 5-9, 2003.

[120] Y. Jeong, W. Baek, S. Chang, "CHF Experiments for IVR-EVC using 2-D Slice Test Section", Proceedings of the Korean Nuclear Society Spring Meeting, Kwangju, Korea, May 2002.

[121] J. Hwang, K. Suh, "Optimized Design for Critical Heat Flux Experiment Using Downward-Facing Hemisphere", Transactions of the American Nuclear Society, Vol. 100, pages 771-712, 2009.

[122] Y. Sudo, M. Kaminaga, "A New CHF Correlation Scheme Proposed for Vertical Rectangular Channels Heated from Both Sides in Nuclear Research Reactors", Journal of Heat Transfer, Vol. 115, May 1993, 426-434.

[123] D.C. Groeneveld, et.al., "The 2006 CHF look-up table", Nuclear Engineering and Design, 237, (2007), 1909-1922.

[124] D.C. Groeneveld, et.al., "The 1995 look-up table for critical heat flux in tubes", Nuclear Engineering and Design, 163, (1996), 1-23.

[125] A. Tanase, et.al.,"Diameter effect on critical heat flux", Nuclear Engineering and Design, 239, (2009), 289-294.

[126] W. Cummins, M. Corletti, T. Schulz, "Westinghouse AP1000 Advanced Passive Plant", Proceeding of ICAPP '03, Cordoba, Spain, May 4-7, 2003, Paper 3235.

[127] "RELAP5 Mod 3.3 Code Manuals Volumes I – V", U.S. NRC, NUREG/CR-5535 Rev. 1, December 2001.

[128] Westinghouse Electric Co., LLC, "The Westinghouse AP1000 Advanced Nuclear Plant – Plant Description", 2003.

[129] A. Sterdis, Westinghouse Electric Co., LLC, "AP1000 Regulatory Overview", presentation slides.

[130] V. Shah, P. MacDonald, "Aging and Life Extension of Major Light Water Reactor Components", Elsevier, 1993.

[131] R. Sterne, L. Steele, "Steels for Commercial Nuclear Power Reactor Pressure Vessels", Nuclear Engineering and Design, Vol. 10, pages 259-307, 1969.